SYNTHESIS AND CHARACTERISATION OF CARBON-BASED ADSORBENTS FROM SOME LIGNO-CELLULOSE AGRICULTURAL RESIDUES AND THEIR APPLICATION IN THE REMOVAL OF CADMIUM (II) AND LEAD (II) IONS FROM AQUEOUS SYSTEMS

A Thesis Submitted to the University of Manchester for the Degree of

Doctor of Philosophy in the Faculty of Engineering and Physical Sciences.

2016

EDIDIONG DIANABASI ASUQUO

SCHOOL OF CHEMICAL ENGINEERING AND ANALYTICAL SCIENCE

List of Contents

List of Tables

Chapter Seven

Chapter Eight

Chapter Nine

Chapter Ten

List of Figures

Chapter Five

Chapter Six

Chapter Seven

Chapter Eight

Chapter Nine

Chapter Ten

List of Appendices

List of Symbols

Å	Angstrom
a_m	The cross-sectional area occupied by each nitrogen molecule (0.162 nm^2)
K_L	The sorption equilibrium constant (L.mg^{-1})
C_o	Initial concentration
C_t	Concentration at time
C_e	Concentration at equilibrium time
d	The inter planar spacing generating the diffraction
D	Diffusion coefficient
K_F	Freundlich isotherm parameter
M	The weight of the sample
N	Freundlich isotherm constant
n_a	Avogadro's constant
N_A	Avogadro's number
P	Absolute pressure
P_o	The Saturation pressure
qe	Adsorption Capacity (mg.g^{-1})
q_{max}	The maximum adsorption capacity (mg.g^{-1})
$qe,_{cal}$	The equilibrium capacity obtained from the isotherm model,
$qe,_{exp.}$	The equilibrium capacity obtained from experiment
$qe,_{av}$	The average $q_{e,exp}$.
r^2	Coefficient of determination
R	Gas constant
t	Time
T	Absolute temperature
V_a	The adsorbed volume
V_m	The monolayer volume
V_L	Molar volume of nitrogen gas
X	Displacement of a particle along a given axis
ʎ	Wavelength of the X-Ray
θ	The angle of diffraction

ABSTRACT

Adsorption using activated carbon has become an important separation process applied in industrial wastewater treatment. Presently, the need to reduce the cost of this process has driven the search for low cost adsorbents such as those obtained from agricultural by-products in effluent treatment especially in developing countries. In this study, seven agricultural residues were investigated as adsorbents for the removal of cadmium(II) and lead(II) ions from aqueous systems using a batch sorption. The residues were: oil palm fruit fibre (OPFS), cocoa pod (CCPS), coconut shell fibre (CNFS) plantain peel residue (PTHS) cocoyam peel (CCYBS), sweet potato peel (PTPS) and white yam peel (YTBS). These residues were further subjected to hydrothermal carbonisation at $200^{\circ}C$ & $170^{\circ}C$, carbonisation at $400^{\circ}C$ in limited air, pyrolysis at $700^{\circ}C$ in N_2 and chemical activation using K_2CO_3 and Na_2CO_3 in N_2 to develop a number of carbon adsorbents that improve their sorption capabilities. Adsorbent characterisation studies included: functional group analysis; BET surface area; morphology, thermal degradation profile, zeta potential and chemical composition. The pHpzc was used to determine the most favourable pH for sorption and this was 6.5 for the residues and 7 for the prepared adsorbents. The results show that the BET surface area of the adsorbents did influence the rate of uptake of the two metal ions. The kinetics of sorption showed a two-stage profile for all adsorbents- initial uptake time was 180 minutes (residues) and 30-60 minutes for the other adsorbents. Sorption kinetics indicated that for Cd(II) ion sorption, optimum uptake was obtained using the CNFS; CNFS-HTC 200; CCPPCA and CNFKCA adsorbents, while for Pb(II) ion this was observed for the OPFS; CNFS-HTC; YTBPCA and CNFNCA adsorbents. Kinetic modelling indicated that the pseudo-first order (PFO) model described the sorption better than the pseudo second order (PSO) for both ions implying that the rate limiting step of sorption depends on concentration. Equilibrium isotherm modelling for metal ion sorption for the unmodified residues; Na_2CO_3 activated adsorbents and a commercial activated carbon (CGAC) was also studied from which the Langmuir isotherm parameter (q_{max}) to rank their adsorption capacities. The results obtained showed that the CCPNCA was the best adsorbent for Cd(II) ion removal with a q_{max} value of 29.4 mgg^{-1}, while for Pb(II) ion, the CCYBNCA adsorbent was the best with an optimum q_{max} value of 41.9 mgg^{-1}.These values were higher than those of the CGAC adsorbent used to benchmark this sorption study which were; 20.3 mgg^{-1} and 27.2 mgg^{-1} for Cd(II) and Pb(II) ions respectively. Finally, spent adsorbent ash stabilization using polymer encapsulation was successful carried out as leached samples after 60 days showed no leaching of the two ions.

DECLARATION

No portion of the work referred to in this thesis has been submitted in support of an application for another degree or qualification of this or any other University or other institute of learning.

Edidiong Dianabasi Asuquo

Manchester, 2016

COPYRIGHT STATEMENT

i.   The author of this thesis (including any appendices and/or schedules to this thesis) owns certain copyright or related rights in it (the "Copyright") and he has given The University of Manchester certain rights to use such Copyright, including for administrative purposes.

ii.   Copies of this thesis, either in full or in extracts and whether in hard or electronic copy, maybe made only in accordance with the Copyright, Designs and Patents Act 1988 (as amended) and regulations issued under it or, where appropriate, in accordance with licensing agreements which the University has from time to time. This page must form part of any such copies made.

iii.   The ownership of certain Copyright, patents, designs, trademarks and other intellectual property (the "Intellectual Property") and any reproductions of copyright works in the thesis, for example graphs and tables ("Reproductions"), which may be described in this thesis, may not be owned by the author and may be owned by third parties. Such Intellectual Property and Reproductions cannot and must not be made available for use without the prior written permission of the owner(s) of the relevant Intellectual Property and/or Reproductions.

iv.   Further information on the conditions under which disclosure, publication and commercialisation of this thesis, the Copyright and any Intellectual Property and/or Reproductions described in it may take place is available in the University IP Policy (see http://www.campus.manchester.ac.uk/medialibrary/policies/intellectualproperty.pdf.), in any relevant Thesis restriction declarations deposited in the University Library, The http://www.manchester.ac.uk/library/aboutus/regulations) and in The University's policy on presentation of thesis.

DEDICATION

I dedicate this work to the memory of my father who made me appreciate the value of education and left this world in the year of our Lord 2011 and my mother who has borne so much to make us achieve our life goals.

ACKNOWLEDGMENTS

CHAPTER ONE

INTRODUCTION

CHAPTER ONE

1.0 Introduction

This chapter sets the basis of the study with a general background, followed by a description of heavy metal pollution in wastewater and an overview of wastewater treatment in developing countries. The last section presents a problem statement of the thesis, the objectives and significance of the study as well as an outline of the subsequent chapters of the thesis.

1.1 Background

The advent of industrialization and the increasing rate of consumption in our society has brought with it increased levels of industrial pollution resulting in a significant level of ecosystem destruction with high pollutant concentrations. This has led to increased concentrations of various pollutants such as heavy metals and organic compounds in water resources raising global concern on the threat posed by industrial activities on the environment (Park *et al*., 2006). In Africa, the abundant deposit of mineral resources has led to an increase in mining activities which is often associated with negative environmental consequences such as metal pollution and contamination of water and land resources. A number of incidences of associated with heavy metal pollution has been reported in some countries in Africa such as mercury in Algeria, arsenic in Namibia and South Africa, tin in Nigeria and copper in Zambia (Fasinu and Orisakwe, 2013; Alo and Olanipekun, 2010). Specific heavy metal ion pollution case studies have also been documented in literature, for example, high concentrations of lead(II) (62-143mgkg^{-1}) have been reported in some top soil samples obtained in the vicinity of an Industrial estate (Ikeja industrial estate) in Nigeria (Fakayode and Onianwa, 2002). In addition, the discharge of industrial and municipal wastewater onto land and surface water bodies can lead to contamination of surface and groundwater thereby making the management of water resources more complex and posing a threat to the health of human population (Hashem, 2007). It has been reported recently that high concentrations of lead(II) and cadmium(II) ions up to 297.0 and 4.0 mgkg^{-1} respectively which were associated with anthropogenic activities were recorded in Nador Lagoon sediment in Morocco (Bloundi *et al*, 2009). This scenario accounts for the exponential deterioration in the quality of water resources in

many countries around the world especially in developing countries and it is expected to worsen over the coming decades especially with the increase in population growth, higher economic growth and industrialization, agricultural activities as well as the changing geological and environmental conditions (Olade, 1987; Ali and Gupta, 2007).

The most common heavy metal ions associated with these industrial activities include; cadmium, nickel, chromium, mercury, copper, lead, zinc, and the metalloid arsenic amongst others. These metals are persistent and non-bio-degradable in the environment and hence accumulate in living organisms resulting in toxic effects that could result in biochemical disorders and diseases (Bailey *et al*., 1999). The organic pollutants often include pesticides, polynuclear aromatic hydrocarbons (PAHs), polychlorinated biphenyls (PCBs), phenol, benzene, xylene and their derivatives in addition to dye compounds and residues (Obute *et al.,* 2004; Osuji *et al*.,2006). Some of these chemical compounds are not only toxic but are also known to be carcinogenic in nature (Ali and Gupta, 2007; Nayak *et al*., 2007; Yamasaki *et al*., 2006) thus complicating water pollution problems. It is thus fair to say that the complexity of water pollution from industrial effluents, the diversity of the pollutant sources and the global nature of its impacts have exacerbated water pollution concerns and prioritized it as a major global environmental problem hence the need for a concerted effort to address this threat towards salvaging water sources worldwide, protecting life forms and enabling sustainable industrial activities (Ajimal *et al*., 2003). According to Fasinu and Orisakwe, (2013), the increased risk the problem poses in developing countries such as Nigeria is due to the poor regulatory environment and the level of population awareness on the problems associated with these heavy metal ions and their sources within their locality. Hence, insight into the nature of these heavy metal pollutants is crucial for proper understanding of their speciation and toxicity.

1.2 Heavy metal pollutants in wastewater

A large proportion of water pollutants that affect our environment results from industrial activities and their ever increasing nature have led to the present state of our global environment. This is because of the huge chemical input associated with these processes and the inefficient resource utilization of the input components leads to huge generation of waste streams that require disposal into the environment. For example, in Nigeria a number of metal contamination incidences of natural rivers have been reported in areas where large industrial plants such as refineries are located (Yabe *et al.,* 2010). The contamination of the Bonny/New Calabar River Estuary in the Niger Delta by some heavy

metal ions such as lead(Pb), cadmium(Cd), copper (Cu), zinc(Zn), vanadium(V) and chromium(Cr) has been attributed primarily to pollution activities arising industrial activities from an oil refinery, as the rivers receives effluents from Port Harcourt Refinery and other oil related activities (Chindah *et al.,* 2004). In a related study, elevated levels (mgL^{-1}) of Pb (0.025–0.064), Cd (0.01– 0.11), Cr (0.03–0.081) and Ni (0.03–0.09) recorded in the Ijana River were mainly attributed to Warri oil refinery discharges (Emoyan *et al.,* 2006). In another study, high concentrations (mgL^{-1}) of Pb(2.57) and Cd(0.39) were recorded in the Warri River following dredging of an oil well access canal as compared to the trace levels recorded prior to dredging (Ohimain *et al.,* 2008).

The low efficiency of the treatment processes used in these industrial sites for the treatment of industrial effluents further increases the pollutant load in treated discharged effluents. Thus, wastewater from these industrial activities is mostly contaminated with organic and inorganic pollutants amongst which are heavy metal ions, phosphates, sulphates, organic and hydrocarbon compounds. These compounds are known as priority pollutants in many waste streams such as those originating from industrial activities relating to petroleum production, refining and petrochemicals, pulp and paper manufacture, battery manufacture, tanneries, paint and pigment industries, fertilizer, herbicide and pesticide industries as well as mining and metallurgical plants (Pamukoglu and Kargi, 2007; Ho and Ofomaja, 2006; Osuji and Uwakwe, 2006; Otokunefor *et al.,* 2005; Bailey *et al.*, 1999). However, for the purpose of this research we will focus our attention on heavy metal pollutants.

"Heavy metals" is a collective term used to describe metallic or metalloid elements that have relative high atomic densities (atomic densities greater than $3.5g/cm^3$ and up to $7g/cm^3$) (Appenroth, 2010). However, that definition has become a centre of debate in the realm of science in recent years. According to Lenntech (2004) "the term heavy metals" refers to any metallic chemical element that has a relatively high density and is toxic or poisonous at low concentrations. Such as mercury (Hg), cadmium (Cd), arsenic (As), chromium (Cr), thallium (Tl) and lead (Pb)". Most of these ions are also toxic even at low concentrations and there has been a general assumption that associates heavy metal with toxicity and Duruibe *et al.,* (2007) observed that being a heavy metal is mainly due to chemical properties and less association with density. This idea was also proposed by Duffus (2002) in a review commissioned by the International Union of Pure and Applied Chemistry (IUPAC) in which he suggested that the idea of defining "heavy metals on the basis of density should be abandoned as it leads to more confusion. However for the

purpose of this study we will use the term "heavy metals" loosely and we will define heavy metal pollutants as a group of water pollutants that have been reported to cause toxic incidences when taken up into animal and plant tissues and these heavy metal pollutants will include; zinc (Zn), nickel (Ni), mercury (Hg), cadmium (Cd), arsenic (As), chromium (Cr), lead (Pb) and copper (Cu). Due to their chemical implications relating to toxicity the term "toxic heavy metals" will be used and assumed in this study. The Dangerous Substances Directive of the European Union (76/464/EEC) and its amended directive (2006/11/EC) define dangerous chemicals as those which are toxic, persistent and / or bioaccumulative. Heavy metals are amongst the chemicals described in these directives, as they cannot be broken down and therefore persist in the environment. Unlike many organic pollutants, which eventually degrade to carbon dioxide and water, heavy metals tend to accumulate in the environment, especially in lakes, estuarine or marine sediments. These metals can also be transported from one environment compartment to another thereby extending the boundaries of their toxic and polluting effect (APIS, 2014).

A number of elements classified as heavy metals are essential in the physiological development and functioning of cells in humans at low concentrations, however there may lead to a number of toxicity related implications when their concentrations are increased. Copper is an essential trace metal for human metabolism but an excessive concentration may lead to conditions such as vomiting, cramps, liver damage, Wilson disease, insomnia and convulsions (Paulino *et al.,* 2006; Kurniawan *et al.,* 2006; Nurchi and Villaescusa, 2008; Adekunle *et al.,* 2014). Zinc is an important micronutrient for human physiological functions like copper as it regulates a number of cellular biochemical processes but at high concentrations it can result in skin irritations, stomach cramps, vomiting, anaemia, lethargy, seizures and ataxia (Kurniawan *et al.,* 2006; Oyaro *et al.,* 2007; O'Connell *et al.,* 2008; Adekunle *et al.,* 2014). Chromium exists in two stable oxidation states; chromium (III)-{Cr (III)} and chromium (VI)-{Cr (VI)} with contrasting toxicities. While chromium (III) is essential in human nutrition (in glucose metabolism), chromium (VI) is known to be very toxic at high concentrations resulting in nausea, diarrhoea, vomiting and lung cancer (Nomanbhay and Palanisamy, 2005; Kurniawan *et al.,* 2006). At high concentrations lead is known to cause encephalopathy, cognitive impairment, kidney and liver damage, anaemia and toxicity to the reproductive system (Pagliuca and Mufti, 1990; O'Connell *et al.,* 2008; Adekunle *et al.,* 2014). Mercury at high concentrations in humans can result in the impairment of pulmonary and kidney functions, chest pain as well as a number of developmental disabilities and neurobehavioural disorders such as dyslexia, attention

deficit hyperactivity disorder and intellectual retardation (Weiss and Landrigan, 2000; Namasivayam and Kadirvelu, 1999; O'Connell *et al.,* 2008; Adekunle *et al.,* 2014). Cadmium at high concentrations is associated with nephrotoxic effects, kidney dysfunction and bone damage (Kurniawan *et al.,* 2006; O'Connell *et al.,* 2008; Adekunle *et al.,* 2014). Nickel at high concentrations is known to cause skin dermatitis, nausea, lung and kidney damage, renal edema, pulmonary fibrosis, chronic asthma and coughing (Akhtar *et al.,* 2004; Kurniawan *et al.,* 2006). Arsenic toxicity has been reported to cause skin, lung, bladder and kidney cancer, neurological disorders and nausea (Hughes, 2002; Mohan and Pittman, 2007).

These heavy metals have various routes of exposure and due to industrial development in recent decades; their main source of input into the environment has been from industrial activities which leads to challenges in their reduction and remediation. Since these heavy metals possess diverse toxicity and are not biodegradable, their toxic impact may develop over a long period of time as is the case in closed mines or mining sites that have fallen into disrepair and abandoned. This may lead to a variety of chemical speciation of these heavy metals in the soil, air and water environments and with different routes of exposure their toxic implications are magnified over a long time due to their long half-lives (Nurchi and Villaescusa, 2008).

Two common toxic heavy metals are considered in this study and these are cadmium(II) and lead(II). The choice of two is based on reported incidences involving these metals in literature and in the developing country of interest (Nigeria) in this study. Lead(II) and cadmium(II) ions have been reported in high concentrations in the blood of a number of people residing in the South-West, South-East and South-South of Nigeria and these regions are known to have high concentration of industries. In a study of the blood serum, liver and kidney function tests of paint factory workers in Nkpor, Nigeria by Orisakwe *et al.,* (2007), it was observed that there was occupational exposure to lead(II) and cadmium(II) as the concentrations of the blood lead (BPb) and serum cadmium in the workers were higher {13μgdL^{-1}(Cd) and 39μgdL^{-1} (Pb)} than those in the control sample {(9μgd L^{-1}(Cd) and 17μgd L^{-1} (Pb)} who were not exposed to these paints. Thus, these two toxic metals have been reported to be of more public health importance in Nigeria in recent times. Lead (II) ion exposure has also been identified as a risk factor for chronic kidney disease (CKD) in Nigeria (Orisakwe, 2014). In another study, the amounts of heavy metal ions in some pharmaceutical effluents from companies in Lagos, Nigeria were monitored from their point of discharge into the environment. A high concentration of nickel(II), lead(II) and cadmium(II)

ions were reported and these were above the WHO and USEPA permissible standards (Anyakora *et al.,* 2011). This study gives an indication of the risk posed by poorly treated effluents from industrial activities that is prevalent in Nigeria and has grave consequences on the health and environment of the country.

1.2.1 Cadmium

Cadmium is released into the environment in a variety of ways such as tobacco smoking, mining, smelting and refining of non-ferrous metals; fossil fuel combustion, incineration of municipal waste (especially cadmium-containing batteries and plastics), manufacture of phosphate fertilizers, recycling of cadmium-plated steel scrap as well as electric and electronic waste. On release, cadmium can be carried and deposited on areas different from the sources of emission by means of long-range atmospheric transport (WHO, 2010). Cadmium has had considerable pollutant impact in the environment due to its toxicity and its diverse means of entry into the environment (Benaissa, 2006). Its release into the environment is mainly through waste streams of electroplating, smelting, alloy manufacture, pigments, mining and refining processes. Vegetable and grain components as well as inhalation of cadmium particles from cigarette smoke are also exposure routes of cadmium in the general population that has been reported (Kazantzis, 2004) with the risk from water sources also identified as a potential route (ATSDR, 2008).

Cadmium is an element with no known positive biological function on humans and is one of the most serious environmental pollutants especially in the vicinity of smelters. It has a high affinity for sulfhydryl (-SH) groups of proteins for which it competes with Zn(II) in biological systems. It binds to the bases of DNA with little apparent affinity for a specific nucleotide and can induce single strand breaks. It is thus mutagenic and carcinogenic (Hill, 1984). Tobacco is a major source of cadmium as the tobacco plants selectively accumulate cadmium from the soil. An estimated 1.7 µg of cadmium per cigarette is the amount a smoker is exposed, this has been established in studies wherein blood levels of Cd in smokers are significantly higher than those of non-smokers (Mannino *et al.,* 2004; Joseph, 2009). The general population that are non-smokers are mainly exposed to cadmium mainly from food sources. The daily adult intake of cadmium is estimated to be approximately 30 µg, with the largest contribution coming from grain cereal products, potatoes and other vegetables (ATSDR, 2008). Certain crustaceans such as crab have been found to have high cadmium content (30-50ppm) (Schwartz and Reis, 2000). The food crop component route of cadmium exposure are caused by the release of cadmium into the

environment via a variety of industrial and agricultural sources such as fertilizer and sewage sludge to agricultural land, atmospheric emission from cadmium smelter plants and the disposal of cadmium containing wastewater from industries that produce cadmium containing products such as batteries, glass and plastics (TEFLON) (Kazantzis, 2004; Schwartz and Reis, 2000; Joseph, 2009).

The toxic effects of cadmium exposure can be classified as chronic or acute. In man cadmium toxicity can cause kidney damage and it has been known to affect aquatic organisms even in low concentrations. Exposure to high levels of cadmium over short periods of time leads to nausea, vomiting and cramps. Inhalation of cadmium fumes can produce acute pneumonitis and pulmonary edema. Chronic exposure can result in kidney damage (renal tubular disease) (Kamrin and Leader, 1997). Chronic cadmium toxicity also results in chronic obstructive pulmonary disease, bone fragility, and emphysema. Ingested cadmium is carcinogenic in animals, but such carcinogenicity has not been confirmed in humans. In acute cadmium poisoning by ingestion, irritation of the gastrointestinal tract is the major toxic effect causing nausea and abdominal cramps. Furthermore, cadmium interferes with zinc and copper metabolism and it is capable of accumulating in food chains and such accumulation depends on certain factors such as low pH and high temperature. Cadmium uptake is irreversible and its excretion only occurs slowly due to its long half-life (Joseph, 2009).

The toxic implications of cadmium in the environment has made the US Environmental protection Agency (USEPA) to set the level of cadmium in drinking water to 0.002 mg/L below which there is no known risk, this is known as the maximum contamination level goal (MCLG) (US EPA, 2013). In line with this, the World Health Organisation (WHO) maximum permissible limit for cadmium in drinking water is set at 0.003 mgL^{-1} (WHO, 2010). The maximum limit for cadmium in discharged effluent set by the Standard Organisation of Nigeria (SON) for industries is set at 0.003 mgL^{-1}(Ipeaiyeda and Onianwan, 2011). However, the enforcement of standards by regulatory bodies is a fundamental issue and for a developing country like Nigeria the monitoring of industrial discharged effluents is poorly carried out leading to the discharge of heavy metal polluted effluents in land and water resources. This has led to the presence of heavy metal ions in a number of Nigerian rivers at concentrations above the international permissible levels (Ekiye and Zejiao, 2010). In Nigeria, high levels of cadmium(II) ions have been reported in the soils within an abandoned steel plant in Akwa Ibom, Nigeria. In the study, soil

analysis within the plant and a control site were evaluated and the results revealed that the levels of cadmium(II) and lead(II) and other trace metals in the soils within the abandoned steel plant were generally higher than those in the control site. This gave an indication that the activities of steel production and associated manufacturing processes which took place when the industry was operational, contributed to the observed higher levels of trace metals in the industrial environment (Udosen *et al*, 2012). Furthermore, cadmium often enters many chemical and biological processes such as photosynthesis and translocation through repeated application of certain phosphate fertilizers and from contaminated soils and water sources (Udosen *et al.,* 1990). Hence agricultural lands and water bodies around industrial plants that process cadmium related products are prone to the risk of cadmium uptake into food crops. Therefore, there is need to remove this heavy metal from aqueous streams and effluents of industrial areas before their discharge into land and water resources in Nigeria.

1.2.2 Lead

Lead has applications in a variety of sectors that cut across human life such as the construction and building industry where it is used as a component of metal alloys and in the nuclear industry as a radiation shield. Its application is also relevant in the electroplating industry, textile industry, metal processing and finishing, as solders with tin (Sn), fusible alloys, storage batteries (lead-acid car battery), explosive materials, photographic materials and fuel additives (ATSDR, 2010; Tong *et al*, 2000). Lead pigments are used in a variety of applications like chromate for road markings and oxides for glass and chemicals. Lead is also used as an additive in polyvinyl chloride plastic stabilizers (Greenwood and Earnshaw, 2006). Human exposure to lead ions can be from lead dust which originates from the degradation of lead paints and other routes including drinking contaminated water from lead pipes. Due to accumulation of lead in the environment from anthropogenic sources, human exposure to lead ions has become a problem in the society in both developing and developed countries.

The form of lead(II) ions also affects the rate of absorption as the human body is known to absorb organic lead faster than inorganic lead. It is a heavy metal poison that affects the functioning of the blood, liver, kidney and brain of the human being (Tong *et al.*, 2000). It is known as a large cation especially prone to react with sulfhydryl (-SH) groups in proteins in a manner similar to cadmium(II) ions. It acts by complexing with oxo-groups in enzymes affecting virtually all steps in the process of heme-synthesis and porphyrin metabolism (ATSDR, 2010; Greenwood and Earnshaw, 2006). Lead is known to inhibit

two enzymes whose catalytic function is essential for biosynthesis of heme, since this impairs the production of haemoglobin, oxygen starvation and anaemia may result from elevated blood lead levels. For one enzyme, δ-aminolevulinic acid dehydrase, evidence indicates that current levels of environmental lead contamination are sufficient to produce inhibition and that there are no safety threshold for lead. It has also been suggested that blood lead levels may be associated with biochemical abnormalities in children's brains because of the direct relationship between the activities of the blood and brain enzymes (Goyer, 1993). Typical symptoms of lead poisoning are cholic, anaemia, headaches, and convulsions, chronic nephritis of kidneys, brain damage and central nervous system disorders. This may account for increased hyper-activity and delinquent behaviour among children and adults leading to adverse social consequences (Goyer, 1993). The most serious adverse effects of lead - mental retardation and learning problems occur in young children subjected to chronic exposure, most often through ingestion of lead paints. Children with iron and calcium deficiencies absorb more lead and may suffer greater adverse effects (Kamrin and Leader, 1997; 2012). The principal effect of lead on adults is also neurological. The initial symptoms include nausea, vomiting, and joint pain, and at higher exposure levels may progress to toxic psychosis. Lead can also cause a variety of other effects such as hypertension, anaemia, kidney damage, and digestive problems. Lead acetate and lead phosphate are carcinogenic to animals and it is possible that similar effects can occur in humans (Kamrin and Leader, 1997; 2012).

Due to the toxic implications of lead in the environment and especially drinking water sources, the US Environmental protection Agency has set a zero level of lead in drinking water of which there is no known risk (MCLG- maximum contamination level goal) (Swiatkowsk *et al.,* 2004, US EPA, 2013). The USEPA discharge limit for lead(II) in effluents is 0.003 mgL^{-1}, while the limit for discharged effluents into aquatic water by the World Health Organisation (WHO) and the Standard Organisation of Nigeria (SON) is 0.01 mgL^{-1}(Ipeaiyeda and Onianwan, 2011). The existence of these regulatory standards for lead(II) and cadmium(II) ions as well as other heavy metal ions indicates the global awareness of regulatory bodies on the impact of these heavy metals on man and the environment. However, the increasing pollution of natural water bodies in developing countries with industrial waste and poor enforcement especially in developing countries and has resulted in an increased number of pollution incidences associated with these heavy metals (Awoyale *et al.,* 2013).

1.3 Wastewater treatment in developing countries

The extent of industrialization in the developing economies of the world has increased in recent years due to the desire to improve the society and economy to standards obtained in the developed countries. This drive is further increased as the developing countries serve as sources of raw materials for the developed economies' technologies, mainly because the developing countries are rich in resources and their level of technological advancement is limited to basic raw materials conversion into forms required for export. This basic raw material conversion process is often associated with high levels of pollutant load resulting in their discharge into the environment without adequate treatment. The transformation processes involved in mineral ore exploitation generate metal by-products and waste that are high in a variety of mineral pollutants such as metals ions. Waste mines and unmanaged ore extraction sites are often sources of pollution especially from surface run-off from these unmonitored mine sites (acid mine drainage). For example, it has been reported that slag from a smelting plant contained high levels of lead which polluted the soil around a dumpsite, in Ota, Nigeria (Adie and Osibanjo, 2009). These poor waste management practices are also associated with a number of mineral extraction sites in Nigeria thereby leading to the disposal of waste ores indiscriminately due to the poor level of enforcement of emission standards (Ekiye and Zejiao, 2010).

Furthermore, as the exploitation of mineral resources in the developing countries is the basis of their growth, the level of pollution associated with these processes is bound to increase as resource exploitation increases to feed advanced technologies in developed countries. A key component of the resource exploitation and transformation process is the generation of wastewater which is a major carrier of pollutant load. In many instances, heavy metals are major components of these wastewater streams and their disposal or treatment (if it exists) often does not eliminate these pollutants before their final discharge into the environment through streams, rivers and land resources. This is as a consequence of the rudimentary nature or non-existence of appropriate wastewater treatment technologies for specific pollutants such as heavy metals in these developing countries.

The aforementioned scenario is a true illustration of the practice applicable in Nigeria - the developing country of interest in this thesis. This shortcoming has led to pollution of a large number of rivers, streams and land by poorly treated wastewater effluents as previously reported (Ekiye and Zejiao, 2010; Awoyale *et al.,* 2013). An analysis of untreated effluents collected from an industrial layout in Nigeria for sorption studies

showed a high amount of metal concentration for four elements: Pb(II) ion, Ni(II) ion, Cd(II) ion and Cr(III) ion. The industrial effluents were subjected to adsorption using three adsorbents (unmodified oil palm fibre (UOPF) and mercaptoacetic acid modified oil palm fibres (0.5MOPF 1.0MOPF) and the study was carried out to test the efficiency of the adsorbents for the removal of various metal ions in an industrial wastewater effluent where the metal pollutants exist in a mixed metal system (Asuquo, 2005). Also in a recent study, heavy metal contamination of two Nigerian water supply schemes was detected and the prominent metal ion concentrations that exceeded WHO standards were chromium, cadmium, lead, manganese and cobalt. This was associated with contaminated dam water and ineffective treatment (Etchie *et al.,* 2013). In a similar study, Ipeaiyeda and Onianwan, (2011) have reported on the water pollution of the Alaro river associated with some heavy metals discharged from the effluents of two food and beverage companies in Ibadan, Nigeria. Their study was based on analysis of two sampling points upstream and downstream the river channel over the months of January 2003 and December 2007. The results of their study showed that the concentration of Zn, Ni, Cr, Cd and Pb in the effluents and river were high and the effluents contained contaminants with levels that exceeded the effluent guidelines of the WHO, USEPA and Standard Organisation of Nigeria for effluent discharge.

Based on the above scenario and in line with the current trends in the global environment, a sustainable approach is thus desirable to facilitate an efficient process that will help in reducing the levels of pollution associated with mineral exploitation practices in developing countries. Thus, there is need for adequate and efficient wastewater treatment technologies that are not only cost effective but also efficient and feasible within the constraints of technological development in these developing countries. The feasibility of these technologies will depend on the use of locally available raw materials as well as appropriate technologies that can be implemented and maintained locally in the environment of interest (Ademiluyi *et al*., 2009). In Nigeria, the treatment of wastewater from industrial sources is not a very developed process or technology and not enough priority is given to the source, content and location of disposal of wastewater by the regulatory agencies. The regulatory agencies standard in this developing country is neither as robust nor enforced as is the case of developed countries. In addition, the developing countries have pristine environments that must be preserved as the drive for industrialization expands which supports the need for the type of environmental standards obtainable in developed countries like Europe and United States of America where

constant monitoring of natural water resources is practiced (Sabo *et al*., 2013; Ayenimo *et al*., 2005). Thus, the design of materials to apply under this new regulatory regime should be carried out with a supporting cost performance structure that will not hinder development in these low income or less developed countries with emphasis on feasible technologies that can be applied locally.

1.4 Statement of problem

Industrial water pollution has had great impact on our society due to the ecological disharmony and health hazards arising from their occurrence (Karnitz *et al*., 2007). This situation is of concern today because of the acute and chronic toxicity risk associated with certain water pollutants especially heavy metal ions even at low concentrations (mgL^{-1}) due to their tendency to bio-accumulate and their long half-lives in biological systems. Some of these pollutants have the potential of moving through the food chain thereby causing toxic incidences amongst flora and fauna both in the aquatic and terrestrial environments (Li and Bai, 2006). For example, some of these metals pollutants such as nickel, cadmium, mercury and lead have bio-concentration factors in marine organisms and are highly toxic with no known natural biological function. An obvious route of these metals into the food chain is through water sediments via filter feeders. Many heavy metals are retained in the organisms as a simple ion, others particularly cadmium and mercury can be converted into covalent organo-metallic compounds and these will preferably accumulate in fatty tissues of the host organism (Horsfall and Spiff, 2005).

One of the most serious consequences of the persistence of heavy metals is the biological concentration of the metals in food chains (bio-magnification). This process could lead to an increase in the level of metals in the upper members of the food chain which can reach values many times higher than those found in air or water. A consequence of this is that some plants or animals become health hazards when used as food and human beings have been reported to have a tendency to accumulate metals as shown by the long half-life (t ½) of some metals in the body (1460 days for lead and 200 days for cadmium) (Ademoroti, 1996). The bio-accumulation of metals has led to outbreaks of metal poisoning in many countries. The Minamata disease was caused by the outbreak of methyl mercury (CH$_3$Hg) poisoning in a river. Here the Chisso Chemical Company constructed a Chemical plant for production of plastics which used organo-mercury as catalyst in the production of acetaldehyde. Each year, a small quantity of chloro-methylmercury (II) was discharged into the Minamata River and adjacent Yatsushiro bay. In 1953, the inhabitants of the area

that ate fish from Minamata River over a period of time developed serious illness. The consumed fishes had concentrations of methyl-mercury up to 15 – 20 mgL^{-1} which was magnified with an increase in the quantity of fish consumed (bio-concentration and bio-magnification). The result was an accumulation of mercury in the brains and liver of these victims. They became crippled, mentally deranged, deformed and most of them finally died (Ademoroti, 1996). The magnification of mercury ions along the food chain was implicated in the mercury toxicity of the inhabitants of the area and the disease was termed "Minamata disease" due to the alkyl-mercury poisoning from sea foods polluted by the industrial waste in Minamata bay in Japan (Kondo, 2000). Also, the outbreak of the multiple bone fracture disease along the Jinzu river basin in Japan called the "itai-itai" disease was due to pollution of the river by cadmium sludge dumped from a zinc mine. This high cadmium concentration was taken up in the soil by rice plants and the cadmium concentration in the harvested rice was found to be about 0.68 mg kg^{-1} compared to the threshold limit value (TLV) of 0.16 mg kg^{-1} (Kazantis, 2004). These reported incidences increased the level of understanding of the toxic implications of discharging pollutant laden wastewater into water reservoirs. Presently, these activities still persist and have been reported in various countries' of the world and concerns have been raised and efforts are being made to eliminate these man-made disasters. However, the cost of wastewater treatment is an obvious obstacle to the elimination of these toxic metal ions in discharged effluents. Heavy metals enter water bodies through a variety of sources such as:

➢ Direct discharge of industrial and consumer waste
➢ Percolation of contaminated soil
➢ Leaching of wastes from landfills

All these routes lead to the release of heavy metals into streams, lakes, rivers and groundwater. Human exposure to heavy metals can occur through the food chain, drinking water, air or absorption through the skin as indicated in Figure 1.1 (Benavente, 2008).
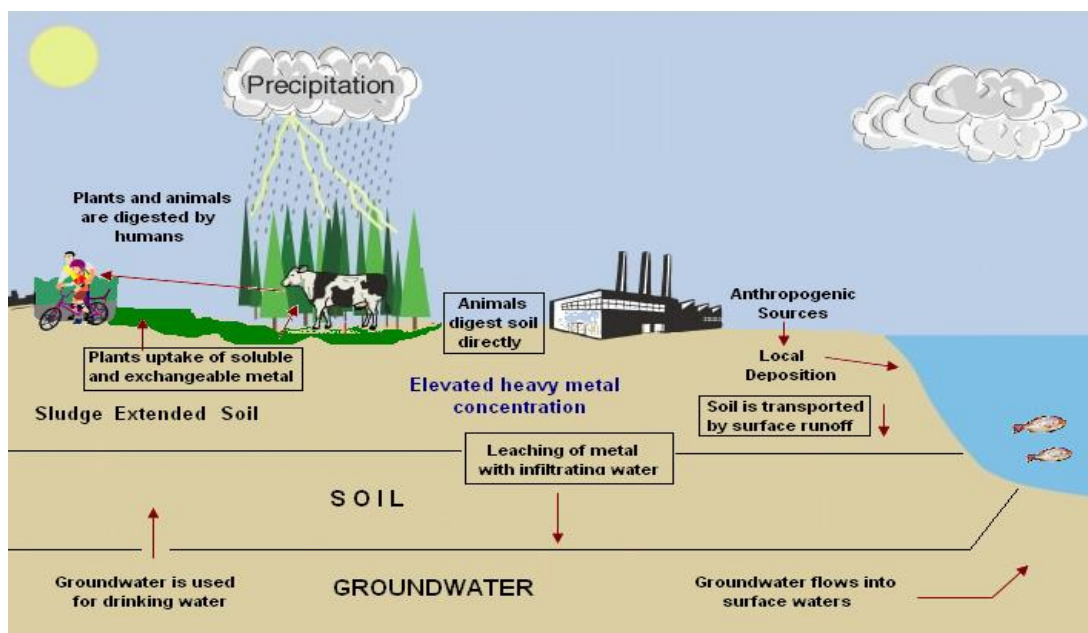
Figure 1.1 : Heavy Metal Cycle through the Food Chain (Benavente, 2008)

Other incidences of metal poisoning have also been reported for lead, cadmium, arsenic and bismuth in a number of countries. Due to these problems, it is necessary for industrial effluents in a developing country like Nigeria to be treated and the toxic metal ion concentrations reduced to regulatory acceptable levels before the wastewater is discharged into receiving water bodies by companies in the country to guard against toxic metal pollution. Some of the industries that generate effluents with heavy metals contamination in Nigeria are presented in Table 1.1.

Table 1.1: Toxic heavy metals generated from industries in Nigeria.

Industries	Toxic metals
Electroplating	Cr, Zn, Cd, Cu, and Ni
Metallurgical	Cd, Cu, Zn and Pb
Chlor-Alkali	Hg
Fertilizer	Cr, Cd
Dyes and Pigment	Cd, Pb, Ti

Ademoroti, (1996)

Different industrial activities generate different types of pollutant resulting in complex chemical contaminants in industrial wastewaters that pose treatment problems. In Nigeria,

effluents/industrial wastewaters receive inadequate or in some cases no treatment before discharge into water reservoirs. It has been reported that industrial and domestic effluents discharged into River Delimi in Jos, Nigeria which is used for extensive irrigation in the area has raised the concentrations of cadmium and copper ions above the limit recommended for irrigation water by the Food and Agricultural Organisation (FAO)(Sabo *et al.,* 2013). In another study, the Niger Delta region in Nigeria has been reported to have witnessed an increased amount of metal pollutants in recent years due to the industrialisation activities that have taken place within the area (Ayenimo *et al.,* 2005). This prevailing situation has been associated to the cost of waste treatment technologies and the low level of enforcement of environmental regulations by the Federal Environmental Protection Agency (FEPA) (Amuda *et al.,* 2007).

The implication of this is a series of environmental problems arising from the toxicity associated with these effluents from the industries in different parts of the country and some of them have affected the groundwater resources in different regions. Presently, there are still large parts of Nigeria without access to treated public water supply and these areas depend on groundwater and river water for domestic and irrigation purposes (Ipeaiyeda and Onianwan, 2011). However these surface and ground water resources have become polluted in the country due to pollution activities. According to Vivien *et al.,* (2012) increased industrialization and population growth in Nigeria has led to numerous incidences of water pollution and some heavy metal ions are also amongst these pollutants. These incidences are more prevalent as the municipal drains of Nigeria carry untreated industrial and municipal effluents across many cities in the country. These drains are often washed off by storm water run-off when it rains leading to the discharge of these toxic compounds into canals and rivers thereby polluting these freshwater sources. These untreated industrial and municipal wastes are toxic in waters used for irrigation, drinking and sustenance of aquatic life as they contain heavy metals as well as biological contaminations. The drainage run-offs are known to cause both surface and groundwater contamination especially in areas where surface water is used to irrigate crops posing significant risks to public health in the country. It is therefore fundamental that industrial wastewater be treated properly to remove these metallic, non-metallic, organic and hydrocarbon compounds before their discharge into water bodies as this will help reduce the pollutant load that enters the natural cycle and affect both flora and fauna (Mohanty *et al*., 2006).

The need for efficient wastewater treatment facilities is therefore essential to enable treatment of industrial effluents in countries like Nigeria. At present, conventional wastewater treatment processes like chemical precipitation, coagulation, oxidation-reduction, reverse-osmosis, ion-exchange and electrodialysis are employed for the treatment of wastewater in the country. For refinery wastewater treatment, physiochemical and mechanical techniques have been employed in addition to biological treatment carried out in integrated activated sludge treatment units (Saien and Nejati, 2007). However, these treatment processes have been observed to be ineffective for the treatment of aromatic fractions of hydrocarbons and heavy metals (from catalyst) which often form part of refinery wastewater. The resistance posed by these chemical compounds to these treatment methods have necessitated further advanced methods of treating waste streams that would ensure that the effluents meet regulatory discharge standards and also allow for recycling of the wastewater for use in the plant cooling processes to enhance water utilization efficiency. Previous works have studied the application of industrial and agricultural wastes as adsorbents in the removal of some heavy metal ions and dyes from wastewater (Vaghetti *et al.,* 2009). This is in line with the desire to design efficient and cost effective treatment processes using waste products and evaluate the various adsorption performance parameters that influence the efficiency of the process.

In Nigeria, the high cost of efficient wastewater treatment is also a major problem and this is because most of the materials and technology necessary for efficient wastewater treatment are imported making them out of reach for the small-scale industries that operate in these areas. Activated carbon adsorbents, which are commonly used for effluent treatment is imported from Europe and Asian countries such as Thailand and Malaysia (Adewumi, 2009). Since this is a product that is used in many sectors in the economy, the demand is often higher than the supply which further increases the cost. Due to the high operating cost for effluent treatment in these circumstances, most of the small scale companies are therefore not able to properly treat their effluent before discharge into natural water bodies, thereby resulting in more poorly treated effluents being discharged into land and water environments (rivers and streams). Furthermore, in some instances, small scale enterprises play a large role in discharging toxic substances into the environment because some of these operations are carried out in the informal economy; and there are limited financial resources to execute best practices of wastewater treatment (Blacksmith Institute, 2012).

Thus, the prospect of utilising materials that are readily available at a low cost for the effective treatment of industrial wastewater from these small scale industries will be highly welcomed. This will help in reducing the amount of toxic pollutants discharged into the environment and minimise the pollutant load on the environment. This is the purpose of this study, which will involve the utilization of agricultural by-products often considered as waste in it raw and modified forms to remove Cd(II) and Pb(II) ions from aqueous systems.

1.5 Objectives and Significance of Study

The objectives of this study will be set out under this section as well as the significance of the study in the context of study area.

1.5.1 Objectives of the Study

This work sets out to examine the efficiency of using some agricultural residues namely oil palm fruit fibre, coconut shell fibre, cocoa pod, plantain husk, cocoyam peel, sweet potato peel and white yam peel for the treatment of wastewater containing two heavy metals-Cd(II) and Pb(II) ions. The goal was to optimize laboratory conditions for the production and characterisation of the different adsorbents, while employing adsorption modelling parameters to select optimum adsorbents and sorption conditions in a batch mode for the two ions. The research was designed to achieve the following objectives:

➢ Conversion of a number of agricultural residues into adsorbents for metal ion removal from aqueous systems.

➢ Investigation of the effect of the different adsorption parameters such as contact time, pH, initial concentration and adsorbent dose on the sorption of Cd(II) and Pb(II) ions using the unmodified residue adsorbents.

➢ Preparation of new adsorbents from the agricultural residues using hydrothermal carbonisation, carbonisation, pyrolysis and chemical activation procedures.

➢ Characterisation of the different adsorbents to determine the physical and chemical properties useful in adsorbent selection process.

➢ Investigation of the kinetics of Cd (II) and Pb (II) ion removal using the new adsorbents and the modelling of the kinetics of metal ion sorption using these adsorbents and a comparison of their performance with a commercial activated carbon.

➢ Determination of the equilibrium modelling parameters for the sorption of Cd (II) and Pb (II) metal ions using selected adsorbents and a comparison of their performance with a commercial activated carbon.

➢ Investigation of procedure for spent adsorbent stabilization

1.5.2 Significance of Study

The advancement in developing countries has expanded industrial activities with a consequent increase in pollution of the natural environment. Most of these countries do not comply with environmental and waste management regulations leading to indiscriminate pollution of air, water and land resources. This practice is often blamed on the high cost of waste management. One area where this is very pronounced is industrial wastewater treatment where heavy metal compounds, organic compounds, dyes and other chemical pollutants are discharged into water bodies without proper treatment to reduce their concentrations. The high cost of importing materials for wastewater treatment such as activated carbon is one of the reasons attributed to this negligence. Commercially activated carbon is generally obtained from activation of coal or lignite. Coal and Lignite are important fossil resources used for energy applications and they are very expensive. This cost is reflected in the price of the activated carbon which is mainly manufactured from coal and lignite (Unur, 2013). Based on this high cost, its utilization for wastewater treatment is not sustainable in developing countries like Nigeria considering the large volumes of polluted waste streams generated and the large scale of the required treatment process to handle these waste streams; a situation that has limited the treatment of wastewater effluents in the Country.

The use of biomass has been proposed as a potential solution to this waste management problem (Bhatnagar and Sillanpaa, 2010; Ma and Zhu, 2006). This is because most developing countries have tropical plants as their prominent crops with a rich supply of residues often disposed either by composting or burning. The abundance of these tropical plants has ignited interest into the use of their residues (obtained after harvesting and utilization) as adsorbents for the treatment of wastewater. In line with the shift towards the use of biomass as a renewable substitute precursor for activated carbon type material, this work examines the potential of transforming Nigeria's abundant agricultural residues like oil palm fruit fibre, coconut shell fibre, cocoa pod, plantain husk, cocoyam peel, sweet potato peel and white yam peel into useful products that can be utilized in wastewater

pollution remediation. These residues are by-products of food and industrial crops cultivation and harvesting in Nigeria and have low value but are generated in large quantities. For example in 2004 about 22 million metric tons of yam residue was produced in Nigeria using the processing residue-to-product ratio (Sokan-Adeaga and Ana, 2015). These materials presently are viewed as waste and pose disposal challenges in many towns and cities in the country. The present practice involves burning these residues or leaving them to decompose both of which lead to pollution of the environment (Jekayinfa and Omisakin, 2005; Oladeji, 2011). Thus, this work is designed to provide an environmentally friendly outlet for the utilization of these materials for pollution remediation. This will enable the treatment of the target pollutants, Cd(II) and Pb(II) ions which are present in effluents discharged from refineries, petrochemical plants and metal ore mining industries which make up a large percentage of the country's industrial and manufacturing sector. There is, however, no mechanism other than trial and error for the selection of these residues as potential cheap adsorbents.

The study also sets to examine a number of protocols for the conversion of these agricultural residues into useful adsorbents while evaluating the efficiency of these processes and the impact of the modifications on the effectiveness of the material towards the target pollutants. This integrated approach using raw residue, hydrothermal carbonized adsorbents, carbonized adsorbent, and pyrolysed adsorbents for the removal of Cd(II) and Pb(II) ions from aqueous system presents a platform that the material-structure and application properties will be examined for these groups of residues with respect to their adsorption potential. This approach is a crucial component of the study that will facilitate the development of insight into the structure-property relationship of the prepared adsorbents with a suite of physical and chemical characterization techniques that highlights the capability of each material or modified material being utilized. These techniques will also give significant information on the material prepared within this study and will be used to choose the appropriate conditions for the application of the adsorbents to optimize metal ion uptake. The determination of isotherm and kinetic modelling parameters for the adsorption of the heavy metal pollutants will be used to quantify the effectiveness of the adsorbents using a non-linear optimization procedure. This will prevent the inherent limitation associated with the conventional linearization technique thus providing a basis for the design of processes that will be effective in the removal of heavy metal ions.

The study reported in this thesis would thus yield a set of representative characterisation that can be used to evaluate appropriate residues in order to deal with the pollution

incidences relating to metals ions in Nigeria. It will evaluate some residues that are specific to the areas in question and the information obtained here would help in building a library of materials that can be used as adsorbents in the country thereby helping to contribute to sustainable environmental practices through improving water resource management, waste management practices and public health.

1.6 Thesis Outline

The rest of this thesis is divided into ten chapters each of which describes one component of the study.

Chapter two presents a review of related literature. It is divided into five sections. The first section gives a brief explanation of the theory of adsorption process. The second section presents a general description of the treatment technologies for wastewater and their application levels and limitations. The third presents a review of the selected materials that have been used in metal ion removal from wastewater and the factors that affect process efficiency as well as the techniques used in adsorption modelling. The fourth section examines the agricultural residues that will be used for study.

Chapter three examines the characterisation techniques used to evaluate the different agricultural residues and modified adsorbents developed in this study. A general description of the equipment and the protocols used in the characterisation and the type of information obtained from them is also presented. It also presents information of the instrumentation used to determine the metal ion concentrations before and after adsorption.

Chapter four describes the experimental methods used in the study. This Chapter is divided into three sections. The first section describes the collection and preparation of the different adsorbents used in the study. The second section gives information on the procedures used in the characterisation of the adsorbents. The third section describes the methods used in carrying out equilibrium batch adsorption for all the adsorbents for Cd(II) ion and Pb(II) ion removal as well as measures to ensure spent adsorbent stabilization prior to disposal.

Chapter five discusses the results for characterization and experimental studies using the agricultural residue adsorbents. This includes the equilibrium and kinetics batch adsorption modelling of Cd(II) and Pb(II) ions from aqueous solution using the raw residue adsorbents prepared in the study.

Chapter six deals with the characterisation of the hydrothermal adsorbents developed in the study. It also presents a discussion on the kinetic sorption studies for the two metals-Cd(II)

and Pb(II) ions using the hydrothermally carbonised adsorbents. The modelling of the kinetics of the sorption of the two metal ions is also discussed.

Chapter seven relates the characteristics features of the carbonised and pyrolysed adsorbents as well as the kinetics of Cd(II) and Pb(II) ion sorption from aqueous solutions using these adsorbents. An evaluation of the modelling of the kinetics of Cd(II) and Pb(II) ions is also reported here.

Chapter eight reports on the characterisation of the two chemically activated carbon adsorbents developed. It also includes the discussion of the equilibrium modelling of Cd(II) and Pb(II) ions sorption from aqueous solutions carried out using one of the chemically activated adsorbents. The kinetics of metal ion sorption using the two sets chemically activated adsorbents and its modelling is also discussed here.

Chapter nine details the characterisation and sorption processes carried out using a commercially available activated carbon adsorbent. The study discusses equilibrium and kinetic sorption studies for this commercial adsorbent using a number of models.

Chapter ten examines the mechanism of sorption using a number of characterisation results obtained for Cd(II) and Pb(II) ions with some of the adsorbents developed in this study. The chapter also includes discussions on the ranking and comparison of these adsorbents and the implication of the ranking of the prepared adsorbents and the commercially activated carbon adsorbent. Adsorption disposal studies carried out using number of spent adsorbents is also discussed in this chapter.

Finally, chapter eleven gives the conclusion and recommendations of the work.

CHAPTER TWO

LITERATURE REVIEW

CHAPTER TWO

2.0 Literature review

This chapter presents a review of related literature for the study. It is divided into four sections. The first section gives a brief explanation on the theory of adsorption process; the second presents a general description of the treatment technologies for wastewater and their application levels and limitations. The third presents a review of the selected materials that have been used in metal ion removal from wastewater and the factors that affect process efficiency. The last section examines the agricultural resides that will be used for the study.

2.1 Adsorption

Adsorption is the thermodynamic property of an interface between two immiscible phases (solid, liquid or gas) which attracts and concentrates components of either phase or both phases as an adsorbed interfacial film. Gases may adsorb unto solids or liquids, and solutes may adsorb at liquid-vapour, liquid-liquid, liquid-solid and solid-solid interfaces. Adsorption therefore is the term used to describe the tendency of molecules from an ambient fluid phase to adhere to the surface of a solid. This property of matter has its origin from the attractive forces between molecules. It can be said to be a process in which a fluid (adsorbate) is brought in contact with a solid (adsorbent), which selectively takes up one or more of the components in the fluid (Lydersen and Dahlq, 1992).

Due to the abnormal condition of atoms at the surface of a solid or liquid compared with atoms in the bulk, the surface of a solid or liquid is a "seat of free energy". Thus the process of adsorption in which atoms or molecules become attached to the surface lowers the free energy of the surface. For example, the adsorption of detergent molecules at liquid surfaces lowers the surface tension of the liquid (Sharp, 1990). During adsorption process, atoms, ions or molecules in a gas or liquid diffuse towards the surface of a solid (adsorbent), wherein they are held by weak intermolecular forces that exist at the surface or they bond with the solid surface. The goal in adsorption process is to design a material that has a very large surface area for adsorption per unit volume and highly porous solid particles with small-diameter in interconnected are often used (Seader *et al.,* 2011).

Some common adsorbents include activated carbon, silica gel, activated alumina, zeolites-molecular sieve (alumino-silicates), macro porous polymers and polymeric resins. These adsorbents are used in various applications however most of the important applications of these adsorbents depend on their selectivity which is the difference in the affinity of the surface for different components. As a result of this selectivity, these adsorbents at least in principle offer a relatively straightforward means of purification (removal of an undesirable trace component from a fluid mixture) and a potentially useful means of bulk separations (Duong, 1998). Various factors influence the rate of adsorption on different surfaces and these include temperature, pressure, surface area, concentration of adsorbate, nature of adsorbent and pH (Puri *et al.*, 2002).

2.1.1 Types of adsorption

Adsorption is an equilibrium phenomenon studied for the light it throws on the properties of solid surface and the fluids adsorbed there on. The process of adsorption may be classified into two depending on the nature of the forces acting on the surface. These are physical adsorption (physisorption or van der Waals adsorption) and chemical adsorption (chemisorption or activated adsorption).

2.1.1.1 Physical adsorption

This type of adsorption is one in which the forces operating are physical in nature (van der Waals force) and the adsorption is relatively weak. The forces involved are intermolecular forces because there is no significant distribution of electron density in either the molecule or the substrate surface. The concept is that the forces holding the adsorbed molecule (adsorbate) to the surface of the solid (adsorbent) may be analogous either to the van der Waals attractive forces operative between molecules within a liquid in physical adsorption and the resulting adsorption is similar to condensation, which is exothermic being accompanied by a release of heat (Seader *et al.,* 2011). The heat of adsorption here can be less than or greater than the heat of vaporisation, which may change depending on the extent of adsorption. The heat enthalpy ΔH_{ads} when it occurs is presumed to be less than 40 kJmol^{-1} (Laidler and Meiser, 1982). Physical adsorption occurs rapidly and the molecules are attracted to all points on the surface and are limited only by the number that can squeeze into each layer. The adsorbed molecules on the surface may be a monomolecular (unimolecular) layer, two, three or more layers thick (multimolecular). If the layer is unimolecular, it is reversible; if multimolecular, such that capillary pores are filled, hysteresis may occur (Seader *et al.,* 2011; Bowen, 1991). Sometimes in physical

adsorption, the van der Waals type forces (induced-dipole-dipole interactions) are supplemented in many ways by electrostatic contributions from field gradient- dipole or quadruple interactions (Ruthven, 1991).

2.1.1.2 Chemical adsorption

Adsorption is not always a physical phenomenon. It may well be a chemical process involving chemical interaction between the surface atoms of the adsorbent and the atoms of the adsorbate. This type of adsorption is known as chemical adsorption (chemisorption) and involves the formation of chemical bonds between the adsorbent and adsorbate in a monolayer; this is often accompanied with a release of heat, the magnitude of which is larger than the heat of vaporisation (Seader *et al.,* 2011. For example, oxygen is chemisorbed by carbon and hydrogen is chemisorbed by nickel under suitable conditions. In each case, a stable surface compound, frequently called a surface complex results (Puri *et al.*, 2002).

Also in chemisorption, there is significant electron transfer, equivalent to the formation of a chemical bond between the sorbate and the sorbent. Such interactions are both stronger and more specific than the forces of physical adsorption and are obviously limited to monolayer coverage. Chemisorption is frequently associated with an appreciable activated energy and may therefore be a relatively slow process. For this reason chemisorption is often referred to as "activated adsorption".

2.1.2 Adsorption process and mechanism

The adsorption process in porous materials such as activated carbon type materials takes place in the pores of the adsorbent. The size of the pores in an adsorbent affects the type of transport mechanism or activity that takes place on the adsorbent surface. The classifications of these pores are as follows (Sing, 1982):

1. Micropores (pore size < 2 nm),
2. Mesopores (2 nm ≤ pore size ≤ 50 nm),
3. Macropores (pore size > 50 nm)

These pores are illustrated in Figure 2.1 and it indicates the presence of 3 pores in the particle.
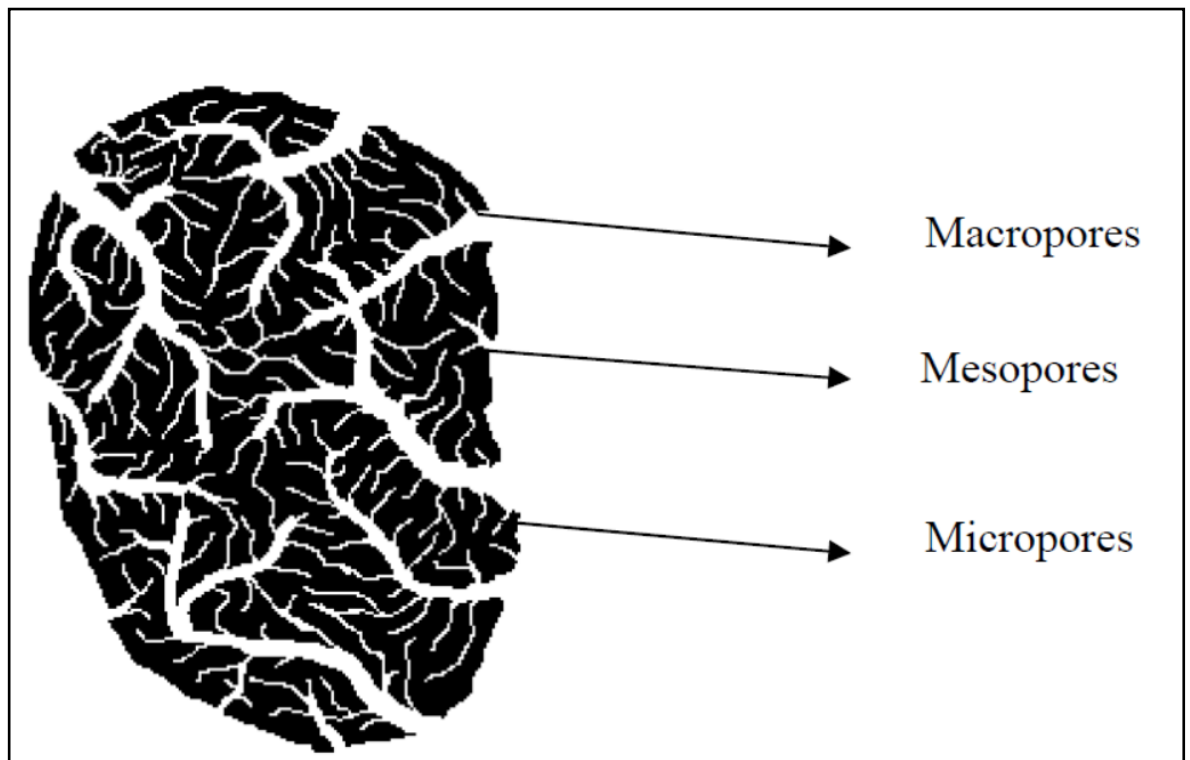
Figure 2.1: Schematic representation of the pores in activated carbon particle (Wu, 2004).

The activated carbon is a model often used to show the transport and network in porous adsorbents as shown in Fig 2.1& 2.2. When activated carbon adsorbents are used for the removal of contaminated molecules, the adsorption of these molecules is facilitated by the type of pore network present. There are three types of pores present in an activated carbon adsorbent as previously mentioned namely; macropores, mesopores and micropores and these all influence the process of contaminant transport and adsorption based on their pore dimensions (Fig 2.2).The macropores are the first transport pathway through which the adsorbate molecules migrate to the mesopores. From the mesopores, the adsorbate particle then enters the micropore wherein the surface adsorption takes place (Wu, 2004; Sushrut Chemicals, 2006).
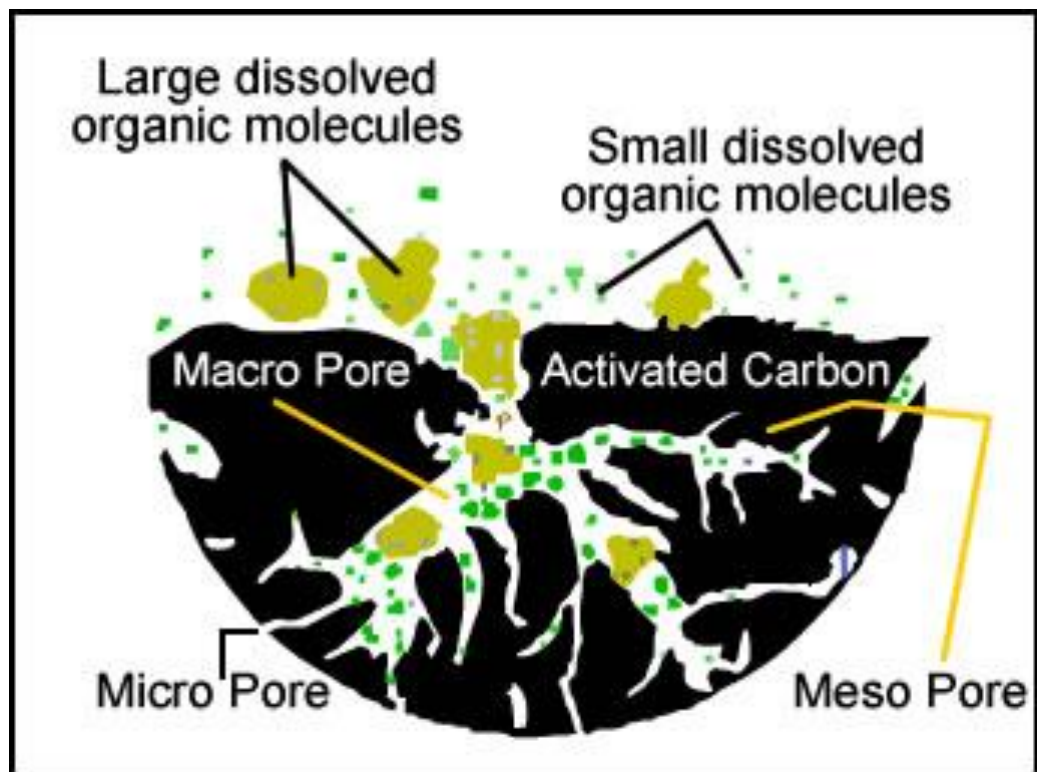
Fig. 2.2: Types of pores for transport and adsorption on activated carbon (Sushrut Chemicals, 2006)

1. The process by which adsorption on the adsorbent takes place can be divided into four elementary steps and these are: Bulk solution transport,
2. Film diffusion transport,
3. Pore transport and
4. Adsorption.

The movement of the material to be absorbed through the bulk liquid to the boundary layer of fixed film of liquid surrounding the adsorbent, typically by advection and dispersion is described as *bulk solution transport*. While *film diffusion transport,* involves the transport by diffusion of the material through the liquid film to the entrance of the pores of the adsorbent. *Pore transport* on the other hand involves the transport of the material to be absorbed through the pores by a combination of molecular diffusion through the pore and/or by diffusion along the surface of the adsorbent. After the transport of the material has taken place, *adsorption* can then occur (Wu, 2004).

Since adsorption rate is limited by diffusion, variables that influence diffusion have significant effect on adsorption rate. For example, a higher concentration gradient across the surface of the adsorbent will increase the rate of adsorption (Naraine, 1998). The rate at which sorption occurs can be very important during the removal of contaminants from

wastewater. Thus it can be stated that the mechanism of adsorption is by diffusion first of the adsorbate to the adsorbent surface. For most purposes, the adsorption of the adsorbate molecule at the site on the internal surface occurs almost instantaneously, so it has little effect on the rate of the overall reaction. The transfer of the adsorbate from the bulk liquid to the surface layer of fluid around a particle can occur rather slowly, but in most treatment systems, this is encouraged by the constant movement of fluid past the surface (Naraine, 1998). However, when the diffusion of the adsorbate through or across the surface adsorbent occurs slowly, this diffusion usually limits the rate of adsorption. Since the rate of adsorption is usually limited by diffusion, it is influenced by the same variables which affect diffusion rate. The concentration gradient of the solute across the surface of the adsorbent also has a large effect on the rate, as does the temperature of the system (Naraine, 1998).

2.2 Industrial wastewater treatment technologies

Industrial wastewater treatment deals with a variety of processes that are used to treat the complex effluents produced in industrial plants. The different characteristics of industrial wastewater amongst industries further increases the challenge posed on treatment methods. This is because the aggregate composition of wastewater depends on the nature of water utilization. These effluents do not only have collective properties such as the amount of suspended solids and biochemical oxygen demand but also possess specific components such as organic and inorganic compounds which vary in concentration, volume and composition (Sonune and Ghate, 2004).

The volume of wastewaters are usually high and they mainly come from industries such as petroleum refining and petrochemical production plants, paper and fibre plants, chemical and fertilizer plants as well as pharmaceutical industries. In these plants, large quantities of water are used for the various production processes and hence a high volume of wastewater is therefore generated. These wastewaters contain organic and dissolved inorganic compounds from raw materials and also residual chemicals that are used in production processes which are not incorporated into the final products (Reeves, 2000; Alva-Argaz *et al*., 2007; Coelho *et al*., 2006). Some of the chemical components of these industrial effluents are compounds which are resistant to bio-degradation while others not only increase the oxygen demand in water streams if discharged but are even detrimental to effluent treatment processes, for example high concentrations of nickel in wastewater (concentrations of 15 mg dm^{-3}) is toxic to activated sludge bacteria. Hence, the presence of

nickel may interfere significantly with the operation of anaerobic digesters used in most wastewater treatment plants (Cuenot *et al.*, 2005; O'Connell *et al.*, 2006). Since industrial effluents have complex characteristics, conventional wastewater technologies which constitute physical, chemical and biological processes are deployed to treat these effluents. These treatment levels include primary, secondary and tertiary and or advanced wastewater treatment (Sonure and Ghate, 2004).

2.2.1 Primary and secondary wastewater treatment processes

Industrial wastewater treatment processes involves primary, secondary and advanced processes with each process tailor-made for removal of specific pollutants.

Primary treatment which utilises physical processes like sedimentation and flotation is designed to remove organic and inorganic solids. It acts as a precursor for secondary treatment and is aimed at producing a liquid effluent suitable for downstream biological treatment whereby it separates out solids as a sludge that can be conveniently and economically treated before ultimate disposal. The effluent from primary treatment contains a large amount of organic matter and is characterized by a relatively high biological oxygen demand (BOD) (Liu, 2014).

The treatment requirements include removal of 20% organic matter (measured as BODs) and 50% suspended solids (SS) according to the European Union criteria (Rusten and Odegaad, 2006; Sonune and Ghate, 2004). Since current effluent and water quality standards require a higher removal efficiency of organics from wastewater than what is obtained through primary treatment, a secondary treatment is used to achieve this goal. This secondary treatment step involves biological wastewater treatment in a controlled environment using a variety of microorganism (Sonune and Ghate, 2004).

The *secondary* biological treatment process has many forms in which the more common types are variations of either the fixed film processes or the suspended growth. In both cases, microorganisms come in contact with suspended and dissolved organic wastes. The most commonly used processes are the activated sludge, surface impoundment (lagoon), sequencing batch reactor (SBR) and anaerobic suspended growth (Guyer, 1998). Primary and secondary treatment processes have been reported to have the capacity to remove about 85 percent of the BOD and suspended solids in effluents. However, these two processes have been proven to be insufficient in completely removing pollutants to ensure that treated wastewater is adequate for discharge into receiving water bodies or reuse in

industrial plants processes such as cooling. Therefore, advanced treatment processes have been designed to remove the pollutants that primary and secondary treatment could not eliminate (Sonure and Ghate, 2004; Guyer, 1998). Advanced wastewater treatment technology is therefore targeted towards the following (Sonure and Ghate, 2004):

- ➢ Removal of additional organic and suspended solids

- ➢ Removal of nutrient removal (nitrates, phosphates)

- ➢ Removal of toxic materials such as heavy metal ions and non-biodegradable organic species).

2.2.2   Water   quality   and   advanced   wastewater   treatment technologies

Water quality standards have become more stringent in many countries as a result of the environmental implications of surface and groundwater contamination by inorganic and organic pollutants. These regulations on environmental standards for industrial wastewater are used to establish quality requirements that will protect the environment (Chojnacka *et al*., 2004). This poses a great challenge as increase in environmental regulation necessitates the treatment of industrial wastewater efficiently before disposal. For example, with the introduction of the European water framework directive in 2000 (2000/60/EC) regulatory authorities within the European Union (EU) are now obligated to ensure that the stringent discharge limits are complied with by industries regarding the disposal effluents loaded with heavy metals, organic and hydrocarbon compounds (Miska *et al*., 2006).

Therefore, these industrial effluents need processes that will ensure the simultaneous removal of these pollutants so that their disposal concentration may meet the water quality guidelines set by environmental laws. This makes it mandatory for industries to design more efficient wastewater treatment technologies for the removal of toxic pollutants from effluent streams before disposal into natural reservoir (Chojnacka *et al*., 2004; Shang and Reedijk, 1984; Niu *et al*., 2007). Presently, a high interest has been generated in the chemical and petrochemical industries towards improvement of wastewater management through introduction of water recycling technologies within production processes (Bagajewicz, 2000). In this regard, a variety of advanced wastewater treatment technologies have been developed and used to treat industrial effluents. These advanced wastewater techniques include; evaporation, chemical precipitation,

coagulation/flocculation, electrolysis, electrochemical deposition/cementation, oxidation-reduction, membrane processes (nanofiltration, reverse osmosis, ultra-filtration and electrodialysis), ion-exchange and activated carbon adsorption (Mohan and Pittman, 2007; Sonune and Ghate, 2004). However, the choice of an advanced wastewater treatment technology by industries may depend on its technical and economic feasibility which is a function of certain factors. Some of these include the cost implication of the process, level of clean-up required, pollutant type, composition and concentration, selectivity and efficiency of the process for target effluent streams, environmental friendliness of process, nature of disposal of resulting generated waste product as well as the nature and complexity of its operation (Pavasant *et al*., 2006).

2.2.3. Limitations of advanced wastewater treatment technologies in developing countries

The nature and impacts of pollutants on the environment has made wastewater treatment a dynamic area of a wide number of technology applications, however most of the conventional advanced wastewater technologies have inherent limitations that reduce its wide use in small scale industrial plants and these problems have reduced their application in many developing nations such as Nigeria. Chemical precipitation is one method of wastewater treatment that is used to remove metal ions using the changes in pH to carry out the separation process. Metal ion precipitation is a type of heterogeneous equilibrium, where separation involves more than one phase (Kellner *et al*., 2004). One of the most widely used process in this technique where economic recovery of the metal is not a consideration is the lime treatment. However, it does not provide complete recovery as precipitation may be incomplete in heavy metals such as cadmium, lead and mercury (Dean *et al.,* 1972). A fundamental problem that arises with the use of chemical precipitation is the generation of toxic sludge which further imposes a safe disposal problem thereby increasing the cost of the process and their application in a developing economy may not be financially sustainable. In addition, metal hydroxide precipitation may be hindered by the presence of complex ligands in the industrial wastewater. This invariably results in residual metal concentration thereby limiting its efficiency (Weng, 2002; Arvanitoyannis *et al*., 2006).

Oxidation methods are useful for organic carbon removal but their application is mainly efficient in wastewater with very low concentration of organic compounds. This necessitates a dilution process to be used prior to treatment therefore increasing plant cost

(Sun and Xu, 1997; Tarawou and Horsfall, 2007). Ion-exchange, reverse osmosis, electrodialysis and electrolysis are not economically feasible in most industries especially in developing countries due to a high operational cost associated with these technologies (Ali and Gupta, 2007; Nomanbhay and Palanisamy, 2005). Furthermore, the cost effectiveness of these processes and their practical application is mainly in high strength wastewater but are ineffective when the pollutant concentration is in the range of $10 - 100$ mg L^{-1} (Volesky, 1990).

Due to the limitations of these processes, adsorption technology has been explored as an efficient method of wastewater treatment due to the ease of its operation and wide range of pollutants it can be applied to remove. This area of wastewater research has expanded in recent years due to its efficiency, ease of operation and the different pollutant species it can be applied to (Ali and Gupta, 2007). The most common adsorbent used in adsorption technology in wastewater treatment is the application of activated carbon for pollutant removal.

Commercial activated carbon adsorption is very efficient for the removal of both organic and inorganic pollutants such as heavy metal ions, dyes and hydrocarbon compounds from industrial wastewater. It has also been recommended by the USEPA as one of the Best Available Technologies (BAT) in the removal of organic compounds. Activated carbon is perhaps the best broad-spectrum technology available at present and as a consequence, the utilisation of activated carbon in water treatment has increased throughout the world due to its efficiency (Dabrowski, 2001). Nonetheless, the cost implication of using this technology limits its application due to the variety of its other applications in the chemical industry. This vast market demand for activated carbon has made it a very expensive material for wastewater treatment thereby reducing its attractiveness especially to small scale industries (Ioannidou and Zabaniotou, 2007; Babel and Kurniawan, 2003a). Moreover, the problems associated with the regeneration of the spent activated carbon and the carbon loss in the waste sludge restricts its application in many industries (Sud *et al.*, 2008; Bhattacharyya and Sharma, 2005).

2.2.4 Cost implication of activated carbon technology in developing countries

The widespread use of activated carbon as a universal adsorbent for the removal of pollutants from wastewater via adsorption technology has also been appreciated in

developing countries. However, the relative high cost of commercial activated carbon has limited its use in many developing economies. In Nigeria, there is a high demand for activated carbon, especially from the growing packaged water industries (PWI) that produce treated water in plastic materials and bottles. This has led an increase in the cost as these activated carbon materials are imported in the countries from Asia such as Thailand and Malaysia (Adewumi, 2009). Activated carbon cost varies based on its precusors and type of manufacturing process. Since this material is imported into the country, it would require a huge capital outlay for small and medium enterprises (SMEs) based industries to use this adsorbent for their effluent treatment processes because as at 2012, the cost of activated carbon imported into Nigeria was USD 450ton^{-1}(Olafadehan *et al.,* 2012). Presently, the cost of a ton of activated carbon varies from USD1160ton^{-1} to USD2668ton^{-1} (EPS, 2015). Thus, the high cost of activated carbon in addition to the associated capital outlay for effluent treatment equipment is often presented by SMEs as the reason for their investment in treatment processes for their effluents before discharge in land and water resources.

In view of this, many attempts have been made to develop low cost adsorbents as well as produce activated by utilizing naturally occurring low cost materials for the removal of trace contaminants from wastewater (Bhatnagar and Sillanpaa, 2010; Ma and Zhu, 2006). This is to ensure the incorporation of sustainability principles with respect to the cost, performance and technological requirement of wastewater treatment processes in developing countries. It would also increase the adoption of the technology to treat industrial wastewater and reduce the incidence of disposing untreated wastewaters into natural water bodies especially due to the high cost and feasibility of the available treatment processes (Ho and Ofomaja, 2005; Bhatnagar and Sillanpaa, 2010).

In developing countries, domestic and municipal waste, brewery bio-based waste products, industrial wastes and agricultural wastes are some of the materials investigated as low cost adsorbents and agricultural residue make up a large proportion of these materials investigated (Ho and Ofomaja, 2005). The application of these agricultural wastes as low cost precursors for the manufacture of locally available low cost carbon adsorbents is based on the composition of these residues which are readily available. These agricultural waste materials have high organic (carbon) content and low inorganic content making them easily activated for use as adsorbents (Bhatnagar and Sillanpaa, 2010). This is most often the primary aim of the extensive studies that have been carried out on a wide variety of

locally available biomass materials for use as adsorbents in developing countries one of which is Nigeria (Horsfall and Spiff, 2005; Opeolu *et al.,* 2009).

2.3 Wastewater treatment using low-cost adsorbents

Adsorption technology has become a frontline process for advanced wastewater treatment in recent years. It has some advantages over the conventional advanced treatment processes for wastewater and these include (Mohanty *et al*., 2006):

- ➢ Removal of both organic and inorganic components at very low concentrations
- ➢ Easy and safe process to operate
- ➢ Economical process as it requires low capital cost and the abundance of low-cost materials as adsorbents
- ➢ Batch and continuous process equipment can be utilized.
- ➢ Eliminates the need for sludge-handling processes

Moreover, the wide application range of adsorption processes means it can be applied for the removal of soluble and insoluble contaminants as well as biological pollutants. It can also be fine-tuned in industrial applications using columns and contractors filled with sorbents which can give a removal efficiency of 90 – 99% (Ali and Gupta, 2007). The availability of low-cost materials such as natural materials and certain waste materials form industrial and agricultural activities further improves the cost effectiveness of this technology as the materials can be disposed after use, thereby removing the need for expensive regeneration processes. Also, some of these materials can be utilized as adsorbents with little processing (Bailey *et al*., 1999; Kurniawan *et al*., 2006).

Thus, the trend in today's society points towards the need for utilization of various industrial and agricultural by-products in efficient processes. The route for application of these residues in wastewater treatment will significantly minimize the environmental problems associated with their presence and accumulation which often imposes disposal problems. For instance, it has been reported that cellulose and hemi-cellulose alone comprise about 60% of the dry weight of municipal solid waste (MSW) that are now required to be diverted from landfill sites in accordance to the EU landfill directive (99/31/EC). These agricultural wastes that are components of MSW will therefore have better utility if they are used as adsorbents for wastewater (Karnitz *et al*., 2007; Slack *et al*., 2005).

In addition, the by-products of industrial processes such as fly ash from power generating stations also have the potential of being efficient adsorbents in wastewater treatment. The need to use these materials as alternative feedstock for adsorbent manufacture comes from their inherent structure and composition which make them suitable as adsorbents. The functional groups on these materials increases their capacity of aiding the removal of ions or chemical moieties from wastewater and their structural features helps in their manner of deployment and removal from aqueous and non-aqueous solutions as well as their separation. Their application also reduces the cost implications of wastewater treatment and the environmental burden these waste materials would have impacted on the ecosystem if this route of recycling was not explored. Some of the naturally occurring materials which have featured in the range of materials suitable as adsorbents for wastewater treatment applications include clay and zeolites, cellulosic based materials (mainly from plant or agricultural waste), chitin/chitosan from fishery waste and combustion residue (fly ash) from power stations (Liu, 2014).

2.3.1 Chitin and chitosan

Studies have been reported on the use of certain natural materials for heavy metal removal from wastewater. Chitin and chitosan are two of these natural abundant materials. They are mainly obtained from the fishery industries and have been applied as low-cost sorbents in the environment. Chitin is a cationic biopolymer, a polyaminosaccharide and contains 2-acetamido-2-deoxy-β-D-glucose units (N-acetylglucan) through a β (1–4) linkage with a molecular formula ($C_8H_{13}NO_5$). It is a material that is insoluble in most ordinary solvents such as water, acetone, dilute acids and alcohols and in this chemical state chitin has limited applications. This chitin form is transformed by the reaction with a strong alkaline (a process called deacetylation of chitin) which produces poly-D-glucosamine, containing 2-acetamido-2-deoxy-β-D-glucose-(N-acetylglucosamine (chitosan) as indicated in Figure 2.3. Thus chitosan is slightly soluble at low pH values (Chandumpai *et al*., 2004; Kalut, 2008, Benavente, 2008).

The structure of chitin can also be regarded as cellulose with hydroxyl at position C-2 replaced by an acetamido group (Crini, 2005). It is the second most abundant material in nature (with the first being cellulose) and is found in the exoskeleton of crabs, shrimps, lobster and other crustaceans. It can be isolated by treating the shells of crabs, lobsters, shrimps and other crustaceans with strong acids for decalcification which is then followed with treatment with strong bases for deproteinization (Bailey *et al*., 1999). Chitosan on the

other hand is a partially acetylated glucosamine and a principal fibrillar biopolymer found in the cell wall of some fungi such as *Mucorales* strains but today it is mainly obtained from the deacetylation of chitin (Onsoyen and Skaugrud, 1990; Wu *et al*., 2000).

The physical and chemical properties of chitin and chitosan are different and these are governed by three variables; source of raw material, molecular weight and degree of deacetylation (Chandumpai *et al*., 2004). The fishery waste materials are abundantly available and serve as a source of chitosan which is the deacetylated derivative of chitin also called glucosamine which has a high content of functional amine groups ($-NH_2$). It is reported to have excellent metal-binding capacities even more than chitin due to the high amount of amino and hydroxyl functional groups. In addition, since it can be obtained from a readily available fishery waste, it can therefore be obtained at a low-cost (Bailey *et al*., 1999; Babel and Kurniawan, 2003a).

These two naturally occurring materials are effective in pollutant removal for dyes and metal ions but their sensitivity to the pH variation can cause them to dissolve or form gels thereby limiting their applications under conditions with varying pH values. Due to this property, cross-linking of chitin and chitosan with a variety of cross-linking agents is carried out to improve their stability in acidic and basic solutions, improve its mechanical properties as well as improve their performance as adsorbents (Chiou *et al*., 2004).

Chitosan is also used to coat a variety of adsorbents and applied in wastewater treatment for dye and metal ion removal. A chitosan coated acid treated oil palm shell charcoal (AOPSC) adsorbent has been studied for the removal of Cr (VI) from wastewater (Nomanbhay and Palanisamy, 2005). In the study, the chitosan loading on the AOPSC support was about 21% by weight. The adsorption capacity of the composite biosorbent was evaluated at 25°C and the Langmuir isotherm model was used to fit the experimental data. The uptake capacity from the study was 154 mg Crg^{-1} and adsorbent was regenerated using NaOH. The mechanism of uptake of Cr (VI) was found to be ionic interactions and complexation.
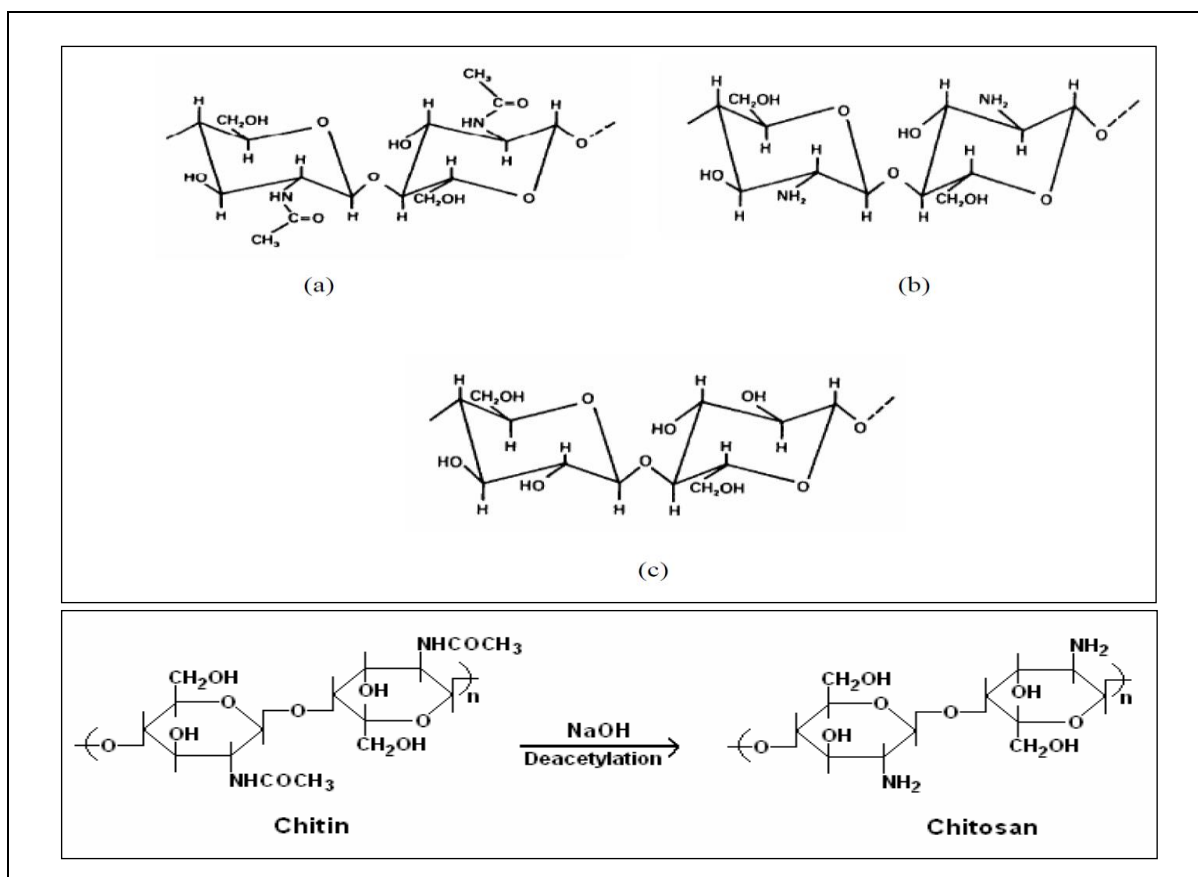
Figure 2.3: Chemical Deacetylation of Chitin to produce Chitosan and structures of chitin(a), chitosan(b) and cellulose(c) (Kalut, 2008; Benavente, 2008)

In another study, an evaluation of the removal of Cu(II) ions and a commercial reactive dye (RR222) was carried out using two types of chitosan materials (flake and bead) that were prepared from three fishery waste materials (shrimp, lobster shells and crab) at 30°C. The two chitosan types exhibited similar adsorption capacity for Cu(II) ion while for the reactive dye the bead chitosan had a better capacity than the flake type chitosan (Wu *et al.,* 2000). In a similar study on the removal of Cr (VI) reported by Babel and Kurniawan (2004) chitosan was used to coat coconut shell activated carbon (CSC) and sulphuric acid modified coconut shell activated carbon adsorbents used for the removal of Cr (VI) from synthetic wastewater. In the study, the chitosan modification of the two adsorbents (coconut shell charcoal coated with chitosan (CSCCCC) and sulphuric acid modified

coconut shell charcoal coated with chitosan (sulphuric acid CSCCCC) were observed to improve the removal capacity of the adsorbents when compared with the unmodified coconut shell activated carbon (CSC) adsorbent. For an adsorbate concentration of 5 to 25mgL^{-1}, the adsorption capacity for Cr (VI) of the sulphuric acid treated coconut shell charcoal coated with chitosan (sulphuric acid CSCCCC) was 8.94mgg^{-1}, while that of the coconut shell charcoal coated with chitosan (CSCCCC) was 3.65mgg^{-1}.

From the above reported studies it has been observed that the ability of chitosan to remove metals depends on variables such as amino group content, affinity for water, degree of polymerisation and deacetylation and the distribution of acetyl groups along the polymer chain (Onsoyen and Skaugrud, 1990). However, due to their stability in adsorbate solutions over a range of pH they are best suited as modification materials with more stable adsorbents as in the development of activated carbon based composite adsorbents or other types of composite adsorbents(Deliyanni *et al.,* 2015).

2.3.2 Zeolite and clay materials

Zeolites are microporous crystalline aluminosilicates with cages and channels of molecular size ranging from about 2 – 15Å in diameter. Their framework is made up of a structural assembly of SiO$_4$ and AlO$_4$ tetrahedra and is joined together at a variety of regular arrangements via the sharing of oxygen atoms (Si-O-Al). The nature of the structural arrangement forms an open crystal lattice containing pores of molecular dimensions into which guest molecules can penetrate. In zeolites, the micro pore structure is determined by the crystal lattice which is precisely uniform with no distribution of pore size. This property is what distinguishes zeolites from other traditional microporous adsorbents (Ruthven, 1991). Clays are finely divided (< 2 μm diameter) crystalline silicates which are often classified as phyllosilicates and are often layered materials where a layer is composed of silicon–oxygen tetrahedra sheets and aluminium–oxygen or magnesium–hydroxyl octahedral sheets (VanLoon and Duffy, 2010).

There are about 40 naturally abundant zeolites and about 100 synthetic ones have been developed. The application of zeolites for metal ion removal from aqueous or wastewater systems mainly involves an ion-exchange mechanism between the guest ion in the zeolite structure and the metal ion of interest to be removed. Zeolites have over the years been used for water purification in urban and industrial residual waters and these zeolite materials have important properties such as individual micro-pores, high surface area and

the presence of multiple channels which make them effective in their applications (Padervand and Gholami, 2013).

Zeolite materials have been used in treating contaminated wastewater, a number of which have been reported and the material showed great promise as it had ion-exchange capacity especially for heavy metal ions. The sorption of Cr (III), Ni (II), Zn (II), Cu (II) and Cd (II) has been reported using natural zeolite (clinoptilolite) (Alvarez-Ayuso et al., 2003). The sorption of Cr (VI) from a simulated wastewater system has been reported using natural zeolite (Babel and Kurniawan, 2003b). Two pure forms of zeolite materials (A and X) were synthesized using a two-stage hydrothermal treatment by Chunfeng et al., (2009) and used to remove Cu and Zn ions and the results indicates that zeolite A had a higher capacity than zeolite X for both metal ions. Fly ash has been used to synthesize Faujasite-Na zeolites at $80^{\circ}C$ for the removal of nickel ion from wastewater and in this study the maximum adsorption of the metal ion was obtained at pH6 (Harja et al., 2012).

Clay minerals have been reported to have high loading capacities due to its high surface area and ion-exchange capacity which is as a result of the net negative charge on the structure of the fine-grain silicate materials making it capable of attracting cations such as heavy metals (Bailey et al., 1999; Babel and Kurniawan, 2003a). Different classes of clay such as montmorillonite, kaolinite and bentonite have been used to remove heavy metal ions and dyes. Spent activated clay has been used in the removal of methylene blue from aqueous solution (Weng and Pan, 2007). Kaolinite has also been used for the removal of Ni (II), Cu (II), Co (II) and Mn (II) from aqueous solutions (Yavuz et al., 2003; Kurniawan et al., 2006). The effect of pH on the removal of some metal ions such as Cd, Cr, Cu, Pb, Zn, Mn and Ni was carried out using Na-montmorillonite and the results indicated that the clay material had a good adsorption capacity for these metals and the pH variations had significant influence on the metal ion concentrations of Cu, Pb, and Cd adsorbed (Zhao et al., 2011; Abollino et al., 2003). Furthermore, in a recent study by Alhawas et al., (2013) two natural clay deposits were used to remove Ni (II) ion from wastewater and it was observed that the clay with a higher cation exchange capacity had the higher adsorption capacity and the adsorption process was modelled using Langmuir and Freundlich isotherms.

2.3.3 Industrial by-products adsorbents

A number of by-products from industrial manufacturing have been used as adsorbents for the removal of metal ions. These industrial processing by-products that have been used as

low-cost sorbents; these include fly-ash, synthetic iron oxides, red mud, lignite, blast-furnace slag and activated slag. These materials have been explored to determine their capacity as wastewater treatment sorbents (Babel and Kurniawan, 2003a; Kurniawan *et al*., 2006). Red mud has been used for Ni(II) removal from simulated wastewater (Zouboulis and Kydros, 1993), while iron and steel slags were studied for their removal capacity for Cu(II) and Pb(II) (Feng *et al*., 2004). Balkaya and Cesur (2008) have reported on the adsorption of cadmium ions from aqueous solution using phosphogypsum-a waste material obtained from the wet process manufacture of phosphoric acid. The waste material was pre-conditioned with lime prior to its use for sorption studies. In the study, the effect of initial adsorbate pH on the sorption of Cd(II) ions by the phosphogypsum was investigated and the results indicated that Cd(II)ion adsorption was dependent on the adsorbate pH with maximum removal obtained in the pH range of 9.5 to 11.5. In addition, the sorption system was modelled using the Freundlich and Langmuir isotherms and the adsorption process fitted better with the Freundlich isotherm. The maximum adsorption capacity of the lime pre-conditioned phosphogypsum was $131 mgg^{-1}$.

The influence of pH value and dose of adsorbent on the adsorption of Cd (II) and Pb (II) onto natural and synthetic goethite has also been studied by Abdus-Salam and Adekola (2005). In this study, it was observed that both synthetic and natural goethite had similar adsorption behaviour with the synthetic goethite slightly higher and the sorption of Pb (II) ion on the natural goethite increased with increasing pH value from 3 to 5 with 99% sorption. Increasing the dose had no effect on the sorption of Pb (II) using the natural goethite. Nano structured goethite was synthesized at pH 3 and used to remove Pb(II), Cd(II), Cu(II) and Co(II) from single and binary aqueous solutions by Mohapatra *et al*., (2010). Experimental maximum loading capacity obtained for Pb(II), Co(II), Cd(II) and Cu(II) were; 109.2, 86.6, 29.15 and 37.25 mgg^{-1} of goethite from single metal solutions of initial concentrations of 500, 500, 300 and 300 mgL^{-1} respectively. Pb(II) loading capacity increased in the presence of Cd(II) or Co(II), while it decreased in the presence of Cu (II) at Pb(II) initial concentration of 500 mgL^{-1}. An increase in the overall metal uptake capacities were obtained for Pb(II) – Cd(II) and Pb(II) – Co(II) systems whereas a decrease in capacity was observed for the Pb(II) – Cu(II) binary system.

Synthetic Al_2O_3 has been used to remove cadmium from aqueous solutions; the kinetic modelling studies indicated that sorption proceeded via through pseudo-second order kinetics. The kinetic studies also indicated that cadmium sorption on the aluminium oxide was a two-step process, with an initial rapid sorption on the external surface followed by a

slow intra-particle diffusion in the interior adsorbent (Sen and Sarzali, 2008). Khan *et al.,* (2015) have also reported on the equilibrium uptake, isotherm and kinetic studies of Cd(II) ion adsorption from aqueous solution using oxide activated red mud and the optimized adsorption parameters for Cd(II) ion removal were; pH 6, a dose of 6 gL^{-1}, initial metal ion concentration of 400 μgL^{-1}, temperature of $27^{\circ}C$ and duration of 90 minutes.

2.3.4 Activated Carbon

Activated carbon is a crude form of graphite with a random or amorphous structure, which is highly porous, exhibiting a broad range of pore sizes, from visible cracks, crevices and slits of molecular dimension. It is the name given to a group of carbon materials that are synthesized by processes that involve the partial oxidation of a number of materials such as wood, coconut shells, coal, lignite, peat, petroleum residues. The quality depends on the nature of the precursors and operating transformation conditions. The choice of activated carbon precursors also depends on the cost of the starting material, availability, purity and type of intended application (Mohan and Pittman, 2007). It is the product of the thermal decomposition of any carbonaceous material that is accompanied by activation which can be via steam, carbon dioxide or any other chemicals at elevated temperature (700 – $1100^{\circ}C$). The essence of the activation process is to open the pores of the material by aiding the removal of tarring carbonisation products that are formed during carbonisation. The structural features of activated carbon consist of elementary micro-crystallites of graphite which are stacked together in random orientation and the micropores in the structures are from the spaces between crystals (Ruthven, 1991; Seader *et al.,* 2011).

The chemical nature of the surface of activated carbon depends on the mode of preparation of the activated carbon. Since activated carbon is produced from oxygen rich compounds, the functional groups often have oxygen atoms. In addition, oxygen functional groups which are either acidic or basic can be introduced during preparation process with oxidizing agents such as hydrogen peroxide or removed by exposure to vacuum and high temperature. Activated carbon as an adsorbent is a complex and versatile material used in a wide variety of industries. It is a very important adsorbent in wastewater treatment due to its extremely high surface area, micro-porous structure and a high degree of surface reactivity (Duong, 1998; Mohan and Pittman, 2007). Activated carbon can be produced in two forms based on the type of application required, granular activated carbon (GAC) that is made up of different granules of varying sizes of activated carbon or powdered activated carbon (PAC) obtained by the complete grinding of the activated carbon into a uniform

powered particle size distribution. Granular activated carbon has been used as an effective treatment technology for the removal of organic compounds from drinking water. In addition, it also has also been used for the removal of heavy metals such as Cd, Cr, Hg, Cu, Pb, Ni, and V from water and in water purification processes. Hence, activated carbons are now being used at a larger scale than ever before (Dabrowski, 2001).

Activated carbons that are effective adsorbents in the treatment of industrial wastewater are commercially obtained from bituminous or lignite coal but recently the reduction in availability of coal in addition to their environmental impacts has made it imperative that cheaper alternatives are developed with less environmental load (Qureshi *et al*., 2008). Activated carbon can be synthesized through two modes: physical and chemical activation and these processes refine the pore structure of the resulting activated carbons. During the activation process, the spaces between the elementary crystallite of the precursor material are cleared by the removal of the less organised loosely bound carbonaceous material. The pore structure of the activated carbon is thereby developed and this imparts a porous network onto the material.

The physical activation process is usually carried out via two stages, the first being the carbonization and the second being the activation. The physical activation process involves the carbonisation of the precursor at $500 - 600^{\circ}$C to drive out the bulk of the volatile matter. Hydrogen, oxygen and non-carbon materials are removed and this is followed by a partial gasification process using steam or carbon dioxide for the mild oxidation of the carbonaceous matter at $800 - 1000^{\circ}$C. The partial oxidation of the carbon surface during this process develops surface functional groups on the activated carbon and large pores are developed in the carbon structure (Mohan and Pittman, 2007; Danish *et al*., 2011). The physical activation process being a two-step synthesis route has a high demand for energy and gas to drive the carbonisation and activation steps and to reduce this high energy consumption in the production of activated carbon, a chemical activation step is used.

The chemical activation process is designed to combine both carbonisation and activation steps into a single thermal process. In chemical activation, there is an incorporation of chemical species into the carbon structure to influence the development of pores. Chemical compounds such as zinc chloride ($ZnCl_2$), sulphuric acid (H_2SO_4), potassium hydroxide (KOH), sodium hydroxide (NaOH) and phosphoric acid (H_3PO_4) are initially used to impregnate the precursor material. This impregnated precursor is then subjected to thermal treatment and the temperature of chemical activation used can be between $200 - 800^{\circ}$C and

leads to activated carbon with well-developed mesoporous and microporous structure depending on the nature of the material, temperature, heating rate, chemical activating agent and atmosphere of synthesis (Mohan and Pittman, 2007; Danish *et al*., 2011).

Chemical activation has some important advantages over physical activation. These include:

- The lower temperature at which activation is carried out and the fact that chemical activation can be carried out in single carbonisation-activation process after impregnation in contrast to physical activation which requires a 2-step process of carbonisation and activation with different temperature regimes. Thus, chemical activation has shorter treatment times (Hirunpraditkoon *et al.*, 2011).

- The second advantage of chemical activation is that the global yield of the activated carbon from this process tends to be greater since burn-off is lower under this regime (Sahu *et al.,* 2010).

- Another advantage is that activated carbon obtained by chemical activation exhibits a larger surface area and better developed mesoporosity than that obtained via physical activation (Sricharoenchaikul *et al*, 2008).

The type of activation process that a precursor material is subjected to will determine the performance capacity of the carbon material synthesized due to the influence of the activation process regime on the structure and chemical characteristics of the resulting activated carbon. When an activated carbon is prepared from a carbon rich precursor material, its resulting characteristics that are significant as an adsorbent is determined by the nature of the porous structure developed within the material and its chemical structure. Thus, the synthesis of activated carbon involves the balancing of these synthesis variables such as impregnation ratio, activation time, activation temperature to obtain the desired characteristics in the output carbon and the process gets complex when there are many desired characteristics such as high surface area, considerable porosity (pore size and pore volume) and high bulk density (Sahu *et al.,* 2010).

Another variable that has to be considered is the optimisation of yield of activated carbon at lower energy and operating cost. The developed porous structure of the activated carbon will influence the adsorption capacity the adsorbent possesses while the nature of its interaction with different types of adsorbates (polar, non-polar, organic or inorganic) will depend on the chemical structure within the carbon material (Selomulya *et al.,* 1999). The surface oxygen groups on the activated carbon surface can be controlled using suitable

oxidizing agents and thermal treatment. Some of these functional groups present on the activated carbon are carbonyl, phenolic and lactonic groups (Toles *et al.,* 1999; Rao *et al.,* 2010b). Due to the chemical composition of waste materials from agricultural activities and their natural abundance, these materials have been used as adsorbents for water purification a substitutes for activated carbon (Rao *et al.,* 2010a; Rao *et al.,* 2010b).

2.4 Agricultural waste adsorbents used for wastewater treatment

The utilization of natural materials such as zeolites, clay, chitin/chitosan and industrial by-products like fly-ash has received considerable attention for wastewater treatment. However based on the context of availability, cost implications, versatility and removal efficiency, agricultural by-products and wastes have generated more research interest for wastewater treatment in recent years. This is due to their abundance and ease of transformation into adsorbents as the residues can be used with further processing depending on the nature of the material as well as their local availability and ease of utilization (Kurniawan *et al.,* 2006). Agricultural by-products have also been used because of the potential of reusing waste materials in the detoxification of wastewaters which fit the *renewable and low cost* expectation of the materials to replace the current costly conventional wastewater treatment technologies (Taty-Costodes *et al*., 2005; Nurchi and Villaescusa, 2007).

Agricultural product processing often yields a large amount of by-products which are generally considered to be of low value. Some of these by-products are disposed as waste and constitute a component of bio-degradable waste presently sent to landfills while other by-products are used as a source of fuel or animal feed (Mohan and Pittman, 2007). Recent studies have shown that these low-value agricultural by-products intrinsically have the capacity to be used for pollutant removal in wastewater treatment in their pure or modified forms (Bailey *et al*., 1999; Kurniawan *et al*., 2006). However, there are three fundamental issue s that have to be addressed significantly in the research into the utilisation of low cost residues or waste agricultural materials in the removal of pollutants from wastewater.

The first is the process of selecting viable residues as effective adsorbents from an abundant pool of low cost residues in the environment. The approach of this screening process is often time consuming as individual candidate residues have to be assessed using a batch adsorption process. The identification and confirmation of the specific mechanism

of pollutant removal using these low cost adsorbents is the second issue that is critical in the application of low cost adsorbent technology. This is of great importance as the current body of knowledge on the mechanism/mechanisms that metal ion removal proceeds is limited and insight into the reactions that occur in this technique is not extensive (Yeneneh *et al.*, 2011). The third issue is the scale of application and cost of this technology as majority of the adsorbent testing using metal ions occurring presently is based on batch scale studies. The issue of the scale of deployment of this technology is a crucial factor as batch scale adsorption studies have to be upgraded to column and continuous systems and evaluated before an industrial application of the adsorbent in the technology can be applied.

A variety of factors also come into play when a scale up of a batch process is carried out including separation after adsorption, regeneration process and re-use of the adsorbent under consideration (Nascimento *et al.,* 2012). These variables become complex when the industrial scale up of a successful batch adsorption is carried out and contributes to significant high cost and complexities that come into play at this stage of the application of these low cost adsorbents. A fundamental understanding of the nature and composition of the agricultural residues is an important factor if success in their utilisation as adsorbents is to be achieved. Hence, information on the characterisation of residue materials such as agricultural residue and other type of biomass would aid in giving insight into these materials so that their structure-property relationship can be exploited in adsorption applications. Thus, in this work a number of physical and chemical characterisation procedures would be used to evaluate the different adsorbents synthesized and utilized in the removal of Cd(II) and Pb(II) ions from aqueous systems. This will be designed to seek insight into some of the properties of these materials and how they influence adsorption performance in a liquid phase system.

2.4.1 Composition of agricultural adsorbents

These agricultural by-products are mainly composed of cellulose, hemi-cellulose and lignin and these components are varied due to the nature of the residue. Cellulose is a polydisperse biopolymer. The basic monomeric unit of cellulose is D-glucose (anhydroglupyranose) linked by β-1, 4-glycosidic bonds. The presence of the hydrogen bonds and van der Waal's forces couples the adjacent cellulose polymer chains and determines the crystalline structure of cellulose giving the plant materials structural strength. Hemi-cellulose is a highly branched polymer composed primarily of five-carbon

sugars (polysaccharides) and is mainly found in the cell walls of plants (Varshney and Naithani, 2011). Lignin is a natural polymer of 3 different phenyl propane units, namely coniferyl alcohol (G), sinapyl alcohol (S) and p-coumaryl alcohol (H) linked primarily by ether bonds which acts as a binder for cellulose. The structure of lignin is found to depend on the nature of the plant material and this is presented by differences concerning its monolignol composition (Percival-Zhang, 2008). The structures of these three components of agricultural products are shown in Figure 2.4.
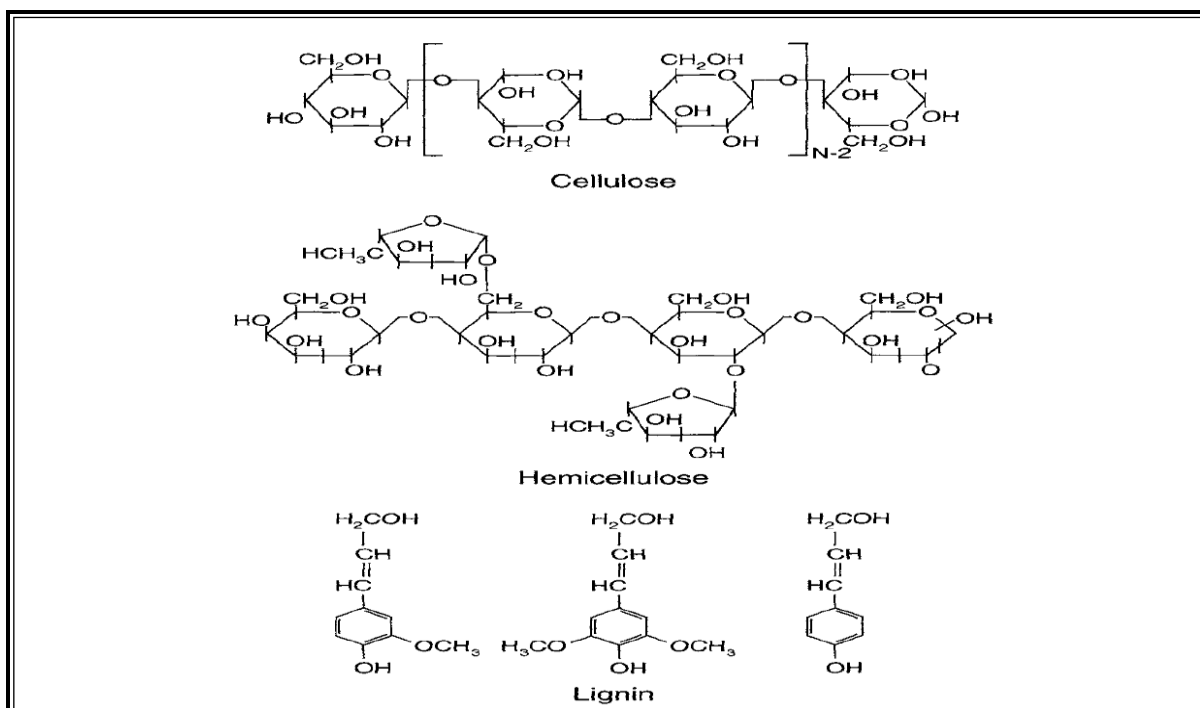
Figure 2.4: Chemical Structures of cellulose, lignin and hemicellulose (Jagtoyen and Derbyshire (1998)

Some other constituents include extractives, lipids, proteins, simple sugars, alcohols, starch, waxes, aldehydes, ketones, carboxylic, phenolic and ether groups, water and hydrocarbons species (Bailey *et al*., 1999). These chemical functional groups provide these agricultural residues with the capacity to bind pollutants especially heavy metal ions via the replacement of hydrogen ions for metal ion in solution, electrostatic interaction, sequestration or by complexation. These interactions enable the agricultural residues to have the capacity to remove organic compounds, metal ions and hydrocarbons from wastewater (Ofomaja and Ho, 2007; Demirbas, 2007; Sud *et al*., 2008).

The compositions of the cell walls of different plants are composed of primary and secondary wall wherein the primary wall is composed of polysaccharides in addition to small quantities of structural glycoproteins and phenolic esters. This is what surrounds

growing and dividing plant cells and thereby provides mechanical strength. The secondary wall is a thicker and stronger wall which is composed of cellulose, hemicellulose and lignin (Sciban *et al.,* 2013). These polymeric plant components form the majority of the structural nature of agricultural residues which are commonly used as adsorbents in pollutant removal from wastewater. An understanding of the implications of the different components of lignocellulosic materials and their role in metal ion sorption is important. According to Aziz *et al.,* (2002) cellulose contains crystalline and amorphous regions and these structural features of cellulose determine its chemical characteristics especially in lignocellulosic materials such as plant residues. These two regions in cellulose influence its properties such as :(Aziz *et al.,* 2002)

1. The degree of swelling by water
2. Crystallinity
3. Presence of specific functional groups (Aziz *et al.,* 2002).

Even though cellulose has the above characteristics, its sorption capacity is low as cotton with high cellulose content shows very low sorption capacity (Han, 1999). Thus, the high sorption capacity of lignocellulosic materials is not due to only cellulose but also lignin, hemicellulose, and extractives. Lignin, as a highly branched polymer attached with polysaccharides, is composed of phenyl propane-based monomeric units linked together by several types of ether linkages and also various kinds of carbon-carbon bonds (Aziz *et al.,* 2002). The general high sorption capacity of non-woods can be attributed to syringly lignin. Guaiacyl lignin is found in softwoods and a mixture of syringl and guaiacyl lignin in hardwoods (Han, 1999).

According to Han (1999), two assumptions can be made about the relationship of lignin to sorption capacity. The first is that the lower the lignin contents, the higher the sorption capacity and low lignin content represents low density and easy accessibility of ions to active sites. Hemicellulose is a group of heterogeneous polysaccharides; hemicellulose takes the form of galactoglucomannan, arabinoglucoronaxylan and arabinogalactan. Mannose, with an axial hydroxyl group at C-2 and galactose, with an axial hydroxyl group on C4 can provide active sites for ion exchange. Hemicellulose is chemically less stable than cellulose and some hardwoods like aspen, with high hemicellulose content show high sorption capacity (Han, 1999). Extractives can be regarded as plant constituents and can be identified as fats, phenolics and resin. These extractives provide carbonyl and hydroxyl groups which contribute to ion-exchange. Thus, it can be said that cellulose and lignin

make minimum contributions to ion-exchange while hemicellulose and extractives are the major players in ion-exchange mechanism which is the principle involved in sorption of metals on lignocellulosic materials (Han, 1999).

Thus, the ability of lignocellulosic materials to remove metal ions is based on the nature of the lignocellulosic surface. However, the mechanism of this process is complex as it involves different types of interactions such as cation exchange, complexation, surface adsorption and precipitation (Ahmad *et al.,* 2014; Ding *et al.,* 2014). The cations (metal ions) are thought to be attracted to the negatively charged active sites throughout the lignocellulosic materials and it is presumed that hydroxyl and carbonyl groups are the main suppliers of active sites as their participation has been inferred from evidence from infra-red spectroscopy of adsorbents after metal ion sorption with decrease in the position of the O-H bands on the metal ion loaded adsorbent (Kim *et al.,* 2013). These groups are abundant in lignocellulosic, yet they are tightly bonded to each other in cellulose and lignin and thus are not available unless hydrogen bonding is broken through chemical modification, hence the low loading associated with most raw lignocellulosic residues (Han, 1999). This makes it important that different approaches be examined to design the optimum method of modifying lignocellulosic material to increase its adsorption performance. Hence, in this study a number of modification regimes would be explored to convert lignocellulosic residues obtained from agricultural by-products into carbon based adsorbents for the removal of Cd(II) and Pb(II) ions from aqueous systems.

2.4.2 Mechanism of adsorption in agricultural adsorbents

Some agricultural adsorbents are non-selective and bind to a wide range of metals while others are specific depending on the chemical composition of the target metal ion. The multiple constituents of agricultural waste materials such as; cellulose, hemi-cellulose, lignin, extractives, lipids, proteins, simple sugars, starches, water, hydrocarbons and mineral elements contain the functional groups that are used in pollutant binding and removal from wastewater. Sorption of pollutants proceeds via two mechanisms: physisorption and chemisorption. Physisorption is an exothermic phenomenon and involves weak van der Waals interaction which induces adsorption with no bond formation. Chemisorption on the other hand involves bond formation through changes in electronic and molecular distributions between the adsorbate and adsorbent (Perez *et al*., 2006). Other mechanisms also influence sorption and some of these are complexation, ion-exchange, chelation, entrapment in inter and intra-fibrillar capillaries and spaces of the

structural adsorbent network. These mechanisms differ quantitatively and qualitatively based on the type of species in solution and the type and degree of processing of the sorbents (Qaiser *et al*., 2007; Basso *et al*., 2002; Sud *et al*., 2008; Villaescusa *et al*., 2004).

The evaluation of adsorption studies to discriminate the mechanism of sorption involves utilisation of kinetic and isotherm studies to provide insight onto how a pollutant is bound within the adsorbent surface (Crini, 2005). One of the most important aspects of the understanding the mechanism of adsorption is the ability to predict the rate-limiting step in an adsorption. For a solid-liquid sorption process, the adsorbate transfer is mainly characterised by either external mass transfer (boundary layer diffusion) or Intraparticle diffusion or both. The dynamics of the sorption process can be described by the following steps (Acharya *et al.,* 2009; Senthilkumar *et al.,* 2012);

➢ The movement of adsorbate molecules from the bulk of the solution to the external surface of the adsorbent (film diffusion)

➢ Adsorbate molecules move through the interior of the adsorbent particles (particle diffusion)

➢ Sorption of the adsorbate on the interior surface of the pores and capillary spaces of the adsorbent (sorption)

Agricultural adsorbents have complex constituents on their surface and due to the heterogeneous nature of these adsorbent matrix, the mechanism of metal ion sorption is not due to only a single interaction but a mixture of different forces that operate at the surface of the adsorbent. These complex interactions are also known to be affected by the diverse conditions under which the adsorbents operate in solution such as pH, presence of different types of ligands and the ionization effect of the different functional groups in aqueous environment (Crini, 2005). Analysis of literature indicates that the following forces may be in operation simultaneously or in series during adsorbent metal ion interaction depending on the chemical composition, adsorbate environment and nature of adsorbate. These interactions include ion-exchange, complexation, coordination/chelation, electrostatic interactions, acid-base interactions, hydrogen bonding, hydrophobic interaction, physical adsorption as well as precipitation (Crini, 2005).

To elucidate the exact mechanisms that govern metal ion or pollutant removal from aqueous solution or wastewater systems, Rao *et al.,* (2010b) suggest that appropriate characterisation of the adsorbent surface; structure and chemical composition should be carried out before and after adsorption to give insight into the nature of changes that have

occurred during the sorption process. These characterisation techniques may include; surface area, pore size, porosity, pHpzc (pH point of zero charge) of these modified adsorbents. Morphology changes in the adsorbent surface can be examined using scanning electron microscopy (SEM). In addition, spectroscopic techniques such as Fourier-transform infra-red (FT-IR), solid-state nuclear magnetic resonance (NMR), X-ray photoelectron spectroscopy (XPS), X-ray energy dispersive spectroscopy (EDAX), X-ray diffraction (XRD), X-ray absorption near edge structure spectroscopy (XANES) and extended X-ray fine structure (EXAFS) can be used to characterize the chemical composition and structure of the adsorbents (Rao, 2010b). However, some of these techniques may not be used in characterisation studies of adsorbents due to their non-availability and cost implications.

Thus, this study is also designed to use a number of physical and chemical characterisation techniques for the determination of the properties of the adsorbents developed in this work for liquid phase Cd(II) and Pb(II) ions sorption. These techniques would be used to elucidate some important features of adsorbents that can be used to explain performance thereby providing information that is valuable in adsorbent optimization and scale-up.

2.4.3 Types of agricultural wastes adsorbents used for adsorption

Different types of agricultural wastes have been used in the removal of heavy metal ions including Cd (II) and Pb(II) ions from wastewater and the nature of the material may be influenced by chemical or thermal processes used to improve its performance even though the raw waste materials are used in some processes with some degree of efficiency. The different groups of materials produced from agricultural residue are examined hereafter and they include: unmodified, chemically modified, thermally modified, hydrothermally carbonised agricultural waste adsorbents and activated carbon adsorbents.

2.4.4 Unmodified agricultural waste adsorbents

A range of unmodified agricultural by-products have been reported in literature as adsorbents and have been used for removal of metal ions from aqueous solutions or wastewater systems. These include tree fern (Ho *et al.*, 2004), cassava waste (Horsfall and Abia, 2003), fluted pumpkin (*Telfairia occidentalis*) (Horsfall and Spiff, 2005), maize cob (Igwe and Abia, 2007), sugarcane bagasse (Lee and Yang, 1997), rice husk (Kurmar and Banduopadhay, 2006) groundnut husk (Dubey and Gopal, 2006) and carrot residues (Nasernejad *et al.*, 2005).

Marshall and Champagne (1995) evaluated by-products of soybean, cottonseed hulls, rice straw and sugar cane bagasse as metal ion adsorbents in aqueous solutions. At an initial metal ion concentration of 100mg/L, soybean and cotton seed hulls were found to adsorb high levels of the heavy metal ions Cr (III), Co (II), Ni (II) and Zn (II) within the range of 95.6-99.7%. In the test of wastewater with environmentally unacceptable concentrations of Zn (II), Cu (II) and Ni (II), the percentage of metal ion adsorbed ranged from 53.4 – 99.8% depending on the particular wastewater and metal ion.

The husk and pods of moringa (*Moringa Oleifera)* an agricultural waste was used to remove Pb (II) ion from an aqueous solution. The adsorption was strongly dependent on pH, adsorbate, adsorbent dose and contact time. Maximum uptake capacity of Pb (II) was high and the experimental data was analysed with the Langmuir and Freundlich models with the Langmuir model representing the sorption process better than the Freundlich model (Nadeem *et al.,* 2006). Rubber (*Hevea Brasiliensis*) leaf powder has also been used to adsorb Pb(II) from aqueous solution and the effect of contact time; temperature and initial ion concentration were studied with the Langmuir isotherm modelling used to analyse the adsorption equilibrium data for Pb(II) (Hanafiah *et al.,* 2006).

A study on the removal of Cu(II), Mn(II) and Pb(II) from aqueous solutions using an agricultural residue adsorbent- pecan nutshell (*Carya illinoensis*) using a batch procedure has been reported by Vaghetti *et al., (*2009).The effect of pH and adsorbent dose on the metal loading capacity of the metal ions were analysed using equilibrium isotherms. From the analysis, the best model for the experimental data was the Sips isotherm. The maximum loading capacities obtained for each metal ion were; 1.35, 1.78 and 0.946 mmol g-^{1} for Cu(II), Mn(II) and Pb(II) respectively.

Some other types of agricultural residues have been applied in pollutant decontamination such as saw dust, barks of trees, stems of plants, shells of nuts, seeds and peels of fruits, peels of tuber crops and other agricultural products (Rao *et al.,* 2010a; Rao *et al.,* 2010b). Boudarhem *et al.,* (2011) have reported their investigations on the use of date tree leaves for the removal of Pb(II) ion from solutions. In their study parameters such as contact time, initial metal ion concentration, adsorbent dose, solution pH, agitation speed, ionic strength and temperature on Pb(II) ion adsorption were evaluated. The maximum removal efficiency for Pb(II) ion was 94% at a pH of 5.8 and initial concentration of 10 mgL^{-1} using 1gL^{-1} of adsorbent, agitation speed of 200 rpm, ionic strength of 0.005M and a temperature of 25$^{°}$C. Ibrahim *et al.,* (2010) in their study on the use of modified soda

lignin extracted from oil palm empty fruit bunches for the removal of Pb(II) ions from aqueous solutions studied the effect of contact time, point of zero charge (pHpzc) and pH of solution, initial metal ion concentration and adsorbent dose. In their study, the amount of Pb(II) ion uptake was found to increase with increase in contact time, pH and initial metal ion concentration.

In a similar study Opeolu *et al.,* 2009 reports on the utilization of maize (*Zea mays*) cob for the removal of Pb (II) ion from aqueous solutions and effluents from paint and battery industries. In the study a synthetic resin (Dowex) was used as a control to evaluate the adsorbent performance. The results of the study using aqueous solutions of Pb(II) indicates that equilibrium sorption for both maize cob and Dowex resin was attained after 2h using $100mgL^{-1}$ of Pb(II) in 25ml of solution at pH 6 using 0.4g of adsorbent and the adsorption rate constants for the maize and Dowex adsorbents were: 7.26×10^{-2} and 7.58×10^{-2} min^{-1} respectively. It was also observed that agitation of the adsorption system at 150 rpm enhanced the sorption for both battery and paint effluents and the optimal adsorbent weight at equilibrium in Pb(II) solution was 16 mgL^{-1}. The percentage removal of Pb(II) by the maize cob adsorbent from the battery effluent was 99% while that of the Dowex resin was 47% and the removal of Pb(II) from the paint effluent were 66% and 28% for the maize cob and Dowex resin respectively.

From the studies reported on the use of unmodified agricultural waste adsorbents for metal ion removal, it is observed that parameters such as pH, contact time, metal ion concentration, temperature, adsorbent dose, agitation speed and ionic strength of adsorbate may influence the adsorption capacity of these lignocellulosic residues. It is also pertinent to observe that some of these studies report on the use of isotherm parameters for the description of the loading capacity of these residues. An observation that can also be made from the reported literature and a large number of studies on adsorption is that some of these studies do not report the loading of the adsorbent using the sorption ''capacity'' qe (loading) term which takes into consideration the amount of adsorbent and volume of the adsorbate and permits universal adsorption capability comparison. Instead what is reported is the percentage of adsorption that depends only on the initial and final concentration of the metal ions in the adsorbate. This percentage adsorption approach does not allow a universal comparison of adsorption capabilities of adsorbents and may also overstate the effectiveness of the adsorbent under consideration. A more appropriate approach as can be observed in some of the reported studies here is the use of the adsorption loading or

sorption capacity relationship "q_e", which gives the amount of the pollutant removed with respect to the volume of the adsorbate and mass of adsorbent.

Furthermore, it is observed that the utilisation of low cost adsorbents from agricultural residues for heavy metal removal from wastewater and aqueous solution is a growing research area but the loading capacity of these low cost adsorbents needs to be improved to ensure a greater scale up and industrial application of these waste adsorbents. Several methods have been applied to improve the loading capacity of the residue adsorbents such as; chemical modification using chemical agents or surfactants, thermal modification, activation (chemical and thermal) and the used of techniques such a microwave heating to improve the rate of carbonisation. A number of these approaches are reviewed in the subsequent sections of this study and will be used to modify the agricultural residues utilized in this work.

2.4.5 Chemically modified agricultural adsorbents

Chemical modification of agricultural residues has been reported as one approach that is used to develop adsorbents with higher equilibration metal ion loading. Here the raw residue is pre-treated with the chemical modifying agent to remove soluble organic compounds, colour and increase the equilibration metal ion loading (Ngah and Hanafiah, 2008). The most common chemicals used as reported in literature include mineral and organic acids (hydrochloric acid, nitric acid, sulphuric acid, citric acid, thioglycollic acid and tartaric acid), base solutions such as sodium hydroxide, calcium hydroxide, and sodium carbonate. Some organic compounds are also used some of which include; formaldehyde, epichlorohydrin and methanol (Adediran *et al.,* 2007).

Some other chemical compounds such as hydrogen peroxide and chelating agents such as ethylene diamminetetraacetic acid (EDTA) and surfactants have been applied as modifying agents. The chemical modified adsorbents often vary in their metal removal efficiency for heavy metal ions from aqueous solutions. Studies have indicated that this modification improves the adsorption capacity of the adsorbents due to incorporation of a higher number of active binding sites, improved ion-exchange properties and the formation of new functional groups that enhance metal uptake (Ngah and Hanafiah, 2008).

Research carried out by Li *et al.*, (2008) on the chemical modification of orange (*citrus sinensis*) peel waste indicates that a variety of chemical modifying agents such as bases (NaOH, NH_4OH and $Ca(OH)_2$) were used to prepare adsorbents for Co(II), Ni(II) ,Zn(II)

and Cd(II) adsorption. The acids also used to prepare adsorbents in the study were; ethanoic acid ($C_2H_4O_2$) and phosphoric acid (H_3PO_4). The characterisation of the adsorbents was carried out using Fourier Transform Infra-red spectroscopy (FT-IR) to identify the functional groups on the chemically modified orange peel adsorbent. The results of the analysis confirmed the presence of a variety of functional groups capable of interacting with the metal ions in solution. The maximum loading of the chemically modified adsorbents when compared with that of the unmodified orange peel showed an increase in loading capacity between of 95 – 97%. The Langmuir and Freundlich isotherm model analysis carried out in the study were also found to fit the experimental data with a regression coefficient $R^2 > 0.95$ for all the metal ions (Li *et al*., 2008).

A range of other studies have been carried out using chemical modified adsorbents, some of which include; citric acid modification of orange peel for removal of lead (II) ions (Xuan *et al.,* 2006); mercapto-acetic acid modification of orange peel for the removal of Cu(II) and Cd(II) from aqueous solution(Liang *et al*., 2009). The effect of these chemical agents on the adsorbent structure is an important point of consideration since the development of porosity has an influence on the transport of the adsorbate onto the adsorbent active sites for adsorption. Thus, it is important to carry out characterisation studies to determine these properties and hence correlate their effect on the adsorbent capacity for metal ion removal.

2.4.6 Thermally modified agricultural adsorbents

Two principal thermal approaches have been used to convert raw lignocellulosic biomass into higher energy density chars. One approach, called torrefaction, involves mild pyrolysis (which is typically in the temperature range of 200 – 600°C) conducted in an inert environment, the other is hydrothermal carbonisation (Hoekman *et al*., 2011; Funke and Ziegler, 2010). Pyrolysis process of biomass yields 3 different types of products. The first being a liquid product called "bio-oil, pyrolysis oil or bio-crude". The second is a non-condensable gas product containing carbon monoxide (CO), carbon dioxide (CO_2), hydrogen (H_2), methanol (CH_4) and higher hydrocarbons which is called "bio-gas" or "pyrolysis gas". The third product is a solid charcoal product that can be sued in a range of applications including use as a soil additive (and in that use is commonly called "biochar") or as a source of energy in the conversion process (Kung *et al.,* 2015).The utilisation of temperature to modify the properties of agricultural residues to produce adsorbents for wastewater treatment is also another approach in the production of adsorbents from waste

materials. Here the thermal modification of the biomass residue may take place at varying temperatures in the absence of air (N_2 atmosphere) or in a limited oxygen environment. Since the main components of the agricultural residues are cellulose, hemicellulose, lignin and inorganic compounds, the treatment often results in the elimination of hemicellulose and cellulose which is thereafter followed by volatilization of lignin if higher temperature is utilised (Rao *et al.,* 2010).

When the components of the residue are subjected to thermal treatment, the increase in temperature initiates reactions on the residue that leads to elimination of the volatile components of the biomass and the transformation products resulting from this treatment is a carbon rich char residue with high mineral content. This material has been explored as adsorbents for the uptake of toxic pollutants from wastewaters and aqueous systems. In a recent study, Srivastava *et al*., (2013) utilised a thermally modified agro waste material (rice husk) to remove Cr(VI) from aqueous solutions. The agro waste material (rice husk) was subjected to thermal treatment in a limited oxygen environment at 650°C for 2h and the resulting adsorbent called calcined rice husk (CRH) was characterised to determine its surface properties using X-ray diffractometry (XRD) and scanning electron microscopy (SEM). The pH point of zero charge (pHpzc) of the CRH adsorbent was 8.82 and it had high silica content. The effect of a number of parameters on the removal of Cr (VI) such as initial metal ion concentration, adsorbent dose, temperature and pH were studied and the removal was observed to decrease with increasing temperature from $25 - 45^{\circ}$C.The pH effect indicated that the removal of Cr(VI) decreased from 67 to 47% on increasing from 2 to 10. An optimum Cr(VI) removal (89%) was achieved at an initial metal ion concentration of 1.69×10^{-6} M, at 25°C and a pH value of 2. Equilibrium isotherm models such as Langmuir, Freundlich and Temkin were used to evaluate the experimental data with the Freundlich model giving the best description of Cr(VI) removal. The study observed that the thermal treatment of the rice husk was effective in increasing the adsorption capacity for Cr(VI).

Research by Guo and Lua, (1998) into the pyrolysis of oil palm stones indicates that the temperature of pyrolysis of lignocellulosic residue and the duration of pyrolysis have significant effect on the yield from the pyrolysis process and the surface area of the resulting carbon rich material. The pyrolysis process facilitated the preparation of high surface area carbon based adsorbents from oil palm stones with high solid density and fixed carbon but with low ash content. The optimum condition of the pyrolysis was 800°C, with a hold time of 3h generating chars that had a BET surface area of 318 m^2g^{-1} and

significant porosities which was verified using scanning electron microscopy (SEM) technique (Guo and Lua, 1998). Thermal treatment of agricultural waste used in this study was classified as carbonisation treatment (200 – 400°C) or pyrolysis treatment (500 – 900°C) and the nature of the surface functional groups will differ depending on the temperature regime being operated. Thus, it will be important that the physical and chemical characteristics of these thermally modified adsorbents are evaluated to determine their contribution to the resulting adsorption capabilities of the adsorbents.

The influence of the environment of thermal modification on the physical and chemical properties of chars obtained for adsorption purposes is one aspect on the use of thermal process to covert waste materials into useful adsorbents that is gaining significant interest amongst researchers. Thus, in this work two different thermal modification environments would be used to evaluate its effect on the properties of adsorbents and their subsequent adsorption potential. The temperature of thermal treatment is also one of the important variables in the modification of materials for use as adsorbents and its effect on the resulting materials (chars) and pollutant uptake efficiency would also be explored using two different temperatures in this study.

2.4.7 Hydrothermal carbonised agricultural adsorbents

Another method of biomass processing is the treatment of the biomass in a hot, pressurized, aqueous environment, this technique has been known for a long time by a variety of nomenclature such as hydrothermal pre-treatment, wet torrefaction, coalification, hot compressed water (HCW) treatment or hydrothermal carbonisation (HTC) (Hoekman *et al*., 2011; Funke and Ziegler, 2010). Hydrothermal carbonisation is a thermo-chemical conversion process of biomass in pressurized water through a variety of hydrolysis, dehydration and decarboxylation processes to yield a solid coal-like product (hydrochar) with liquid and gaseous by-products (Hoekman *et al*., 2011). Hydrothermal carbonization is an exothermic process that reduces the oxygen and hydrogen content of the resulting char by two types of reactions dehydration and decarboxylation. This carbon synthesis procedure is carried out by suspending the biomass in water at saturated water pressure and at temperatures ranging from 150-260 $^\circ$C. The reaction pressure is usually not controlled and is autogenic with the saturated vapour pressure of water (subcritical-water) corresponding to the reaction temperature (Kambo and Dutta, 2015).

The hydrothermal carbonisation process has become an attractive method for the synthesis of carbon rich materials due to its simplicity, low-cost and energy and carbon dioxide

efficiency. It can also be termed a green approach for carbon synthesis since it does not utilise chemicals (Titirici *et al.,* 2007a). This hydrothermal synthesis treatment has become a promising candidate for the development of novel-carbon based materials that have a wide variety of applications in industry and the environment. The utilization of hydrothermal carbonized chars (hydrochar) for a variety of applications such as nutrient for soil, energy storage and as adsorbents is an aspect of biomass utilization that is expanding in the current decade. This area is currently being investigated because of the environmental benefits that may be associated with waste biomass conversion to useful products (Hu *et al.,* 2010; Kambo and Dutta, 2015).

In the hydrothermal carbonisation (HTC) process, the biomass components are broken down and dissolved in the process water in an autogeneous pressure system via a complex cascade of aldol-reactions, cycloadditions, and condensations yielding a solid carbon enriched "hydrochar" with a liquid phase containing unreacted sugars and oligomers that can be used for production of bio-plastics or biofuels (Roman *et al.,* 2013). The HTC process has an advantage over other methods of adsorbent synthesis as it specifically utilises wet biomass and produces tar-free hydrochar that is mainly composed of aliphatic compounds rather than aromatic compounds found in biochars (Titirici *et al.,* 2007a; Islam *et al.,* 2015). Porous carbonaceous materials have been synthesized using hydrothermal carbonization which proceeds at low-temperature conditions generating materials with controllable surface morphology and possess considerable surface functional groups. One particular characteristic of carbonaceous materials synthesised under this condition is the small number of micropores it possesses and the low surface area compared to activated carbon (Hu *et al.,* 2010).

The hydrothermal carbonisation of sunflower stem (SF), walnut shells (WN) and olives stone (OS) at 220°C for 20h has been reported by Roman *et al.,* (2013). These hydrochars were characterised for their textual and chemical characteristics using nitrogen BET adsorption, scanning electron microscopy (SEM), pH point of zero charge analysis and Fourier Transform infrared spectroscopy (FT-IR). The hydrochars had low BET surface areas of ranging from 22-31m^2g^{-1} and their surface was characterised with weakly developed porous structure with acidic surface properties.

An examination of literature on the hydrothermal carbonisation of biomass for production of materials for environmental applications shows a large number of studies on the use of hydrothermal carbonised adsorbents for soil improvement (Fang *et al.,* 2015; Busch *et al.,*

2013) and removal of organic contaminants such as tetracycline (Zhu *et al.,* 2014), methylene blue (Islam *et al.,* 2015; Unur, 2013) with very few studies on the use of hydrothermal adsorbents for removal of metal pollutants. A comparison of the Cu (II) ion adsorption properties of chars produced from pinewood using pyrolysis (700°C) and hydrothermal carbonisation (300°C) has been reported by Liu *et al.,* (2010). The study observed that pyrolysis of the biomass decreased the oxygen containing groups on the char (carboxylic, lactone and phenolic) by 56% while the hydrothermal treated chars had a 95% increase in oxygen containing groups. Both chars had rough surfaces with cavities as observed from scanning electron microscope (SEM) analysis and their BET surface area was 21 and 29m^2g^{-1} for HTC char and pyrolysed char respectively. The mechanism of Cu (II) ion removal was via ion-exchange in the HTC char, while physisorption was the dominant mechanism for the pyrolysis char. Equilibrium isotherm model analysis indicated that the Langmuir isotherm described the experimental data for both chars and the maximum adsorption capacities were 4.46 and 2.75 mgg^{-1} with the HTC char having a higher adsorption capacity than the pyrolysis char.

In another study, an assessment of the removal of uranium (U(VI)) from groundwater using a hydrothermal carbonised switchgrass adsorbent at 300°C has been reported by Kumar *et al.,* (2011). The adsorbent obtained was characterised using thermogravimetric analysis (TGA), FTIR, SEM, XRD and its physicochemical properties indicated that it could be a good adsorbent for uranium. The carbon content of the biochar was observed to increase from 44.6% in the biomass to 70.5%, while its oxygen content decreased from 40-43% in the biomass to 22-23% in the biochar. The SEM images showed that the biochar had an irregular surface and porous structure compared to the biomass, while the FTIR analysis indicated the presence of oxygen-rich functional groups (hydroxyl, phenolic, carboxylic and carbonyl) on the biochar. The TGA showed that the biochar had a thermally stable composition compared to the switchgrass biomass. The kinetics of adsorption of uranium was fast and dependent on pH and the mechanism was strongly related to its pH-dependent aqueous speciation. The Langmuir isotherm was used to model the experimental data and the sorption capacity was 2.12 mgg^{-1}.

These studies on hydrothermal adsorbents indicates that the temperature used to obtain these hydrochars are often very high about 250-350°C and this high temperature would require high energy input for the transformation process. This high energy demand is bound to increase the cost of the hydrothermal carbonisation process and to reduce this load; a low temperature process can be explored as an option. Thus, in this study the

hydrothermal carbonisation of the agricultural residues utilised as adsorbents in the thesis would be carried out at lower temperatures (170 and 200°C). This approach would be used to evaluate the possibility of designing hydrochars with suitable characteristics for metal ion sorption from aqueous systems at lower operating conditions and cost.

Furthermore, one aspect of the hydrothermal process that is still not fully developed is the understanding of the nature of the resulting carbon residue and its properties that can be modified for diverse applications. According to Libra *et al*., (2011) research in hydrothermal carbonization requires more comprehensive characterization of hydrochars to advance the understanding of processes, products and areas of application towards improving processes and reducing pollution. This aspect is crucial as the ability to relate the char properties to their effect in specific applications would enhance their uptake in diverse sectors. In view of this, one aspect of the study reported in this thesis involves the characterization of the resulting biochars obtained from the hydrothermal carbonization of the agricultural residue to gain insight into their properties and how they can affect the adsorption of the two metals ions - lead (II) and cadmium (II) from aqueous solution. This information would be fundamental to the development of "hydrochars" for water treatment applications. Thus, this work will contribute to bridging this knowledge gap by providing useful characterization and adsorbents utilization data wherein this information on some of the residues is not available in literature.

2.4.8 Activated carbon adsorbents from agricultural waste

Agricultural wastes have also been reported as useful feedstock for the preparation of activated carbon used in wastewater treatment for the removal of compounds such as dyes, heavy metal ions and hydrocarbon compounds. These agricultural residues have varied compositions which influence their reactivity in the pyrolysis/activation reactions (Ionnidou and Zabaniotou, 2007). Methylene blue adsorption has been reported on activated carbon produced form coir pith (Kavitha and Namasivyan, 2007) and water weeds (Tarawou and Horsfall, 2007). Coir pith activated carbon has also been used for the removal of reactive dyes in textile wastewater (Santhy and Selvapathy, 2006).

Activated carbons have also been produced from agricultural waste such as coconut shell, palm kernel shell, peanut hull, apricot stone, cherry stones, almond shell and *chrysophyllum albidum* shell and have been used to remove metal ions from aqueous solutions and wastewater (Demirbas *et al*., 2004; Amuda *et al*., 2007; Kurniawan *et al*., 2006). Chemical activated carbon has been prepared from corn cob biomass using K_2CO_3

and H_3PO_4 as activators in a study reported by Sun and Webley, (2011). In the study, it was observed that the optimal activation temperature for producing the largest BET specific surface area and pore volume of the carbon was 800°C for K_2CO_3 activation and 500°C for H_3PO_4 activation. The maximum BET surface areas of 1450 m^2g^{-1} and 1.1 cm^3 for the K_2CO_3 activated carbon and 1069 m^2g^{-1} and 1.0 cm^3 for the H_3PO_4 activated carbon were obtained for the two adsorbents.

Cashew nut shells were converted to activated carbon using potassium hydroxide (KOH) impregnation with carbon dioxide (CO_2) activation. The cashew nut was first of all carbonized in the absence of air and the chars subsequently impregnated with KOH and dried at 120°C. After drying, the chars were carbonised under nitrogen atmosphere up to a temperature of 850°C and held for 150 minutes. After this time interval, the gas was switched to carbon dioxide and activated. The maximum BET surface area for the activated carbon produced was 1026 m^2g^{-1} and this was obtained using the mixture with the KOH/char ratio of 4, while a surface area of 627 m^2g^{-1} was recorded for the activated carbon produced with a KOH/char ratio of 1 indicating that the impregnation ratio has a significant effect on the development of porosity on the activated carbon structure. The adsorption of Cd(II) and Pb(II) ions on the activated carbon had a maximum loading capacity of 28.90 mgg^{-1} for lead(II) ion and 14.29 mgg^{-1} for cadmium(II) ion (Tangjuank *et al.,* 2009).

Steam activation of pyrolysed peanut shell carbon has been studied by Wilson *et al.*, (2006) to obtain prepared activated carbon from peanut. The peanut shell was prepared by carbonisation under nitrogen atmosphere at 800°C for 2 h after which steam was injected into the system to activate the char. Thereafter, the activated char was subjected to thermal oxidation in a furnace under compressed air at 300°C for 4 h. The prepared activated carbons were then evaluated for the adsorption of Cd(II), Cu(II), Pb(II), Zn(II) and Ni(II) and this was compared with the adsorption of these metals using 3 commercial activated carbons (Draco, Norit C Grain and Minotaur). From the results of the adsorption analysis, it was observed that one of the peanut-shell based carbons metal ion sorption efficiencies was greater than two of the commercial activated carbon (Norit C Grain and Draco) but close to the sorption of the Minotaur carbon (Wilson *et al.,* 2006). The study also revealed that peanut shells were a good source of activated carbon with metal sorption properties and can therefore serve as a replacement for coal based commercial carbon.

The studies reported above indicate that the conversion of agricultural materials into activated carbon type materials can be carried out to obtain materials that can be used to replace commercial sourced activated carbon. Chemical activation of the precusors lignocellulosic material prior to thermal treatment has been utilized in a number of studies for the production of activated carbon adsorbents. These adsorbents obtained also possess increased surface and porosity characteristics which are presumed to increase the sorption performance of these materials for toxic pollutants in aqueous systems. Thus in this study, the agricultural residues would be transformed into activated carbon materials using to basic salts to evaluate the effectiveness of this chemical activation procedure on adsorbent performance.

Furthermore, these studies indicate various degrees of efficiency of each of the agricultural waste adsorbents used for the targeted heavy metal ions. However, for an adsorption system to be effective a variety of factors that affect the performance of both adsorbate and adsorbent must be taken into consideration and these factors should be favourable to the system under design. The factors that influence the effectiveness of an adsorbent during sorption studies are discussed in the subsequent section of this work.

2.5 Factors influencing effectiveness of adsorbents in metal ion removal

The efficiency of any adsorbent depends on its selectivity. Adsorbent selectivity is influenced by many factors, which include temperature, nature of adsorbate, nature of adsorbent, particle size or surface area, adsorbate concentration and pH.

2.5.1 Nature of adsorbents

The physical and chemical characteristics of the adsorbent will affect the adsorption process of either metal ions or organic compounds.

2.5.1.1 Physical characteristics

The nature of the absorbent used for adsorption will influence the efficiency of the adsorption process. For instance, an activated carbon with a high concentration of small pores will tend to adsorb smaller molecules due to its pore size. For activated carbon adsorbents, the structure of the material determines its application. In the development of activated carbon adsorbent, the nature of its pore structure will influence its application. The design of mesoporous adsorbents is desirable for liquid-phase applications whereas

microporous adsorbent is required for gas phase applications (Yang, 2003). Other physical characteristics of an adsorbent that may influence its adsorption properties include surface area and bulk density. Since adsorption is a surface phenomenon, the extent of adsorption will be affected by the amount of surface area available for adsorption (Arief *et al*. 2008). Highly porous solids (small particle size) are generally the most effective adsorbents. So for an increase in the rate of adsorption, a high surface area for the adsorbent is very necessary. This can be obtained by reducing the adsorbent into small sizes with the creation of more pores. This is because in smaller particle size adsorbents, there is a greater reduction in internal diffusion and mass transfer limitation thereby leading to the attainment of equilibrium easily thus increasing the probability of attainment of full adsorption capacity and hence improve efficiency. Studies have shown that increase in surface area of adsorbents can lead to an increase the kinetics of adsorption of an adsorbate due to the creation of more pores and micro-capillaries as sites for adsorption (Perez *et al*., 2006).

2.5.1.2 Chemical characteristics

Heavy metal ions have varied levels of attraction to different types of adsorbents due to a wide level of interactions that may occur. The charge on the metal ion, the charge on the anions, the charge on ligands attached can also affect the level of electrostatic interaction with different adsorbents and this may be covalent or ionic in nature. The physicochemical nature of the adsorbent also has an effect on both the rate and capacity of adsorption.

2.5.2 Nature of adsorbate

The nature of an adsorbate (liquid, solid or gaseous) also determines the efficiency of the adsorption process. The adsorption rate from any substance in liquid phase is slower, often by a factor of 10 or more than a gas. Also, the solubility of the adsorbate plays an important role on the amount of the adsorption that can occur. It can also greatly influence the adsorption equilibrium. There is an inverse relationship between the extent of adsorption of an adsorbate and its solubility (Grassi *et al.,* 2012).

2.5.3 pH value of the system

The pH of the reacting solution affects the extent of adsorption because the distribution of surface charge of the adsorbent in solution (this is due to the composition of the adsorbent or the type of synthesis undertaken) thus varying or transforming the functional groups on the adsorbent. The pH value of the adsorbate also affects the rate of adsorption since the

degree of ionization of the species in the adsorbate affects the adsorption. Here, the pH value significantly influences the dissociation site on the surface of the adsorbent and the solution chemistry of the heavy metals such as hydrolysis, complexation, redox reactions and precipitation as well as the speciation of the metal ion available for sorption (Arief *et al*., 2008).

Most adsorbents can be said to be useful with the pH range of $5 - 9$ and some heavy metal ions have different pH at which there is optimum adsorption due to the nature of the metal ion species. In solution some metal ions exist as cations, others as cations with anionic clusters and this can affect their charge. The tendency of metal ions to form hydroxides at higher solution pH also affect the level of adsorption in any particular system and this has to be taken into consideration when the pH form metal sorption is considered (Grassi *et al.,* 2012).

2.5.4 Initial ion concentration

Adsorption can be affected by the concentration gradient of the ions in solution. The driving force, which causes the adsorbate to migrate to the adsorbent surface, is a function of concentration gradient. The initial metal ion concentration may influence the removal efficiency through a combination of factors such as availability of surface functional groups and the ability of these groups to bind metal ions (especially at high concentrations) (Arief *et al*., 2008). It has been reported that the initial metal ion concentration of Zn (II) ion in aqueous solution influences the amount of metal ion removed by both lignite and coconut shell based activated carbon fibre (Shrestha *et al.,* 2013).

2.5.5 Contact time

The extent of adsorption of an adsorbate by an adsorbent is dependent on the rate at which there is contact between the surface of the adsorbent particles and the speed with which the adsorbate diffuses into the adsorbent pores after contact. The time for there to be sufficient contact between the adsorbent and the adsorbate also determines the time at which the adsorbent capacity is complete (equilibrium sorption). The contact time and the time to reach equilibrium sorption varies depending on the nature and size of adsorbent and the adsorbate concentration and polarity (Grassi *et al.,* 2012; Yang, 2003).

2.5.6 Temperature

Depending on the structure and surface functional groups on an adsorbent, temperature has an influence on adsorption to a certain extent. It is known that a temperature change alters the adsorption equilibrium in a specific way determined by the exothermic or endothermic nature of the process. Adsorption is often accompanied by the evolution of heat, so it is an exothermic process; hence the extent of adsorption generally decreases with increasing temperature (Grassi *et al.,* 2012). However, studies have been reported that indicate that temperature increases may result in increase in adsorption capacity. Shen and Duvnjak (2004) reported an increase in the uptake of copper and cadmium ions with increase in temperature, where a more enhanced level of uptake in parallel with temperature rise resembles the nature of a chemisorption mechanism (endothermic process).

2.5.7 Adsorbent dosage

The amount of an adsorbent in solution has an effect on the metal ion uptake. The measurement of the adsorption efficiency is observed to increase when the adsorbent dose increases even though the amount adsorbed per unit mass decreases. In principle, it is assumed that with more adsorbent present, the available adsorption sites of functional groups also increase. This in turn makes the amount of metal ion adsorbed to increase, which brings about an improved efficiency in the process (Arief *et al*., 2008).

The parameters evaluated above are thus known to influence adsorption performance and some of them would be used to assess their effect on the different adsorbents designed and utilized in this work. This will be carried out to determine the conditions that would be effective for optimum adsorbent performance in the removal of two metal ions- cadmium and lead from aqueous solutions using a number of adsorbents synthesized using different approaches.

2.6 Adsorption modelling techniques

Adsorption equilibrium data are commonly reported in the form of an isotherm, which is a curve that describes the processes governing the release/retention or mobility of an adsorbate from an aqueous environment to a solid-phase adsorbent and constant pH and temperature (Foo and Hammed, 2010). The modelling of adsorption process involves the use of a number of equations which describes the relationship between the adsorbent and adsorbates using some assumptions. Adsorption modelling techniques are fundamental in

the description and quantification of the performance of an adsorbent with respect to an adsorbate or a number of adsorbates as it can provide information about the loading ability of the adsorbent for the adsorbate. This technique generates data that can be used to compare the performance of different adsorbents or different adsorbates with respect to a single adsorbent. These modelling techniques are also useful for design purposes as the adsorption loading of each adsorbent can be used to generate parameters for the design of adsorbers. These adsorption isotherms are herein described in the subsequent sections of this work.

2.6.1 Adsorption isotherms

When an adsorbent is in contact with the surrounding fluid of a certain composition, adsorption of the adsorbate onto the adsorbent occurs and after a time interval the adsorbent and adsorbate reach equilibrium at a particular temperature. This gives insight into the concept of adsorbent loading. The maximum possible loading of a sorbate onto an adsorbent is a function of its concentration at a constant temperature and this relationship can be expressed using the following generalized relationship;

$$q_e = f(C_e) \tag{2.1}$$

Where q_e is the amount of sorbate adsorbed at equilibrium (mgg^{-1})

Ce is the equilibrium concentration of the sorbate (mgL^{-1}) and

f can be equated to the phrase "is a function of" (Hubbe *et al*, 2011)

This type of relationship is termed a sorption isotherm which represents equilibrium between the concentration of a solute in solution and its concentration on the sorbent at a given temperature. An adsorption isotherm is one of the methods used for assessing the maximum loading capacity of a given adsorbent. In addition to this, the sorption isotherm is also a useful tool in the prediction of conditions for the operation of reactors and estimation of optimal operating conditions (Hubbe *et al*., 2011). Typically, the mathematical correlation of the adsorption isotherm is usually depicted by graphically expressing the solid-phase concentration against its residual concentration and this serves as an important tool in the modelling analysis, operational design and application of the adsorption system. This is based on the premise that the combination of the physicochemical parameters and the underlying thermodynamic assumptions provides an insight into the adsorption mechanism, surface properties as well as degree of affinity of the adsorbents (Foo and Hameed, 2010). A number of equilibrium isotherm models have

been formulated and applied in the description of the adsorption of metal ions such as the Langmuir, Freundlich, Redilich-Peterson and Duminin-Radushkevich models (Limousin *et al.*, 2007)

2.6.1.1 Langmuir isotherm

The Langmuir isotherm is a common isotherm based on a reaction hypothesis. It was first published by Irving Langmuir in 1918 for fluid adsorbed on adsorbent to describe and quantify sorption on localised adsorption sites. It is an empirical isotherm and it can be used to describe both physical and chemical adsorption, but is only valid for a monolayer adsorption. In addition, it is based on the assumption that the highest adsorption corresponds to a saturated monolayer of adsorbate molecules on the solid surface, that the energy of adsorption is constant and there is no transmigration of adjacent adsorbed molecules (Limousin *et al.*, 2007). The hypotheses of Langmuir model is based on the following assumptions:

1. All the adsorption sites are assumed to be identical, and there is no interaction between the adsorbed molecules.

2. Each site retains a molecule of the given compound.

3. All adsorption is formed via the same system.

4. Maximum adsorption occurs on a monolayer only at the defined sites of the adsorbent and no others (Langmuir, 1918).

The non-linearised form of the Langmuir model can be described as follows in eqn. (2.2)

$$q_e = \frac{q_m K_L C_e}{1 + K_L C_e}$$
(2.2)

Where: q_e is the equilibrium ion uptake (mg g^{-1}), C_e represents the equilibrium concentration (mg L^{-1}), K_L is the sorption equilibrium constant (L mg^{-1}) and q_m *is* the maximum adsorption capacity (q_{max}) (mg g^{-1})(Sari *et al.*,2008).

2.6.1.2 Freundlich isotherm

The Freundlich isotherm is the earliest known relationship describing the non-ideal and reversible adsorption, not restricted to the formation of monolayer. It was published by Freundlich and Küster in 1907 and this empirical model can be been applied to multilayer adsorption, with non-uniform distribution of adsorption heat affinities over the heterogeneous surface (Freundlich, 1906). The empirical isotherm shown in eqn. 2.3 describes the form of the Freundlich sorption isotherm in terms of sorbate concentration.

$$q_e = K_F(C_e)^{1/n} \qquad\qquad (2.3)$$

Where;

K_F (mg g^{-1})(Lmg^{-1})$^{1/n}$ and n are the constants of the Freundlich isotherm related to adsorption capacity and adsorption intensity respectively. K_F is indicative of the relative sorption capacity, whereas 'n' is a measure of the nature and strength of the sorption process and the distribution of active sites. If (n) <1, then the bond energies increase with the surface density. If (n) >1, then the bond energies decrease with the surface density. When n = 1, all surface sites are equivalent (Hubbe *et al*., 2011).

The Temkin isotherm model contains a factor that explicitly takes into account the adsorbent–adsorbate interactions. It is based on the assumption that the heat of adsorption of all the molecules in the layer would decrease linearly with coverage due to adsorbent–adsorbate interactions (Yousef *et al.*, 2011, Ho *et al.* 2002). The adsorption is characterized by a uniform distribution of binding energies, up to some maximum binding energy. The Temkin adsorption isotherm in its non-linear form in eqn. (2.4) as reported by Temkin and Pyzhev (1940) (Yousef *et al.*, 2011).

$$qe = \frac{RT}{b_T} \ \ln(A_T Ce) \qquad\qquad (2.4)$$

where B= (RT/bT) is Temkin constant related to heat of adsorption(Jmol^{-1}), A_T (Lg^{-1}) is the equilibrium binding constant related to maximum binding energy, Ce(mgL^{-1}) is the equilibrium concentration of cadmium ions, R (8.314 JmolK^{-1}) is the universal gas constant, and T (K) is the absolute solution temperature (298K).

A number of studies have reported on the use the of Langmuir and Freundlich isotherm for the description of the adsorption phenomena for the removal of pollutants from wastewater or aqueous solutions using a number of adsorbents. Coconut shell based activated carbon fibre and lignite were used for adsorption of Zn(II) as a function of initial concentration of Zn(II) ion, temperature and contact time in a batch adsorption process. In the study, uptake of Zn (II) ion was found to increase with initial metal ion concentration and temperature with an optimum contact time of 50minutes. Equilibrium isotherm modelling was carried out using the linearised Langmuir, Freundlich and Temkin isotherms with the experimental data fitting best with Langmuir isotherm. The surface monolayer coverage obtained from the Langmuir isotherm constant q_{max} for the coconut shell based activated carbon was 9.43 mgg^{-1} (Shrestha *et al.,* 2013).Khan *et al.,* (2015) have also reported on the equilibrium uptake, isotherm and kinetic studies of Cd(II) ion adsorption from aqueous solution using

oxide activated red mud and the optimized adsorption parameters for Cd(II) ion removal was pH 6, a dose of 6 gL^{-1}, initial metal ion concentration of 400 μgL^{-1}, temperature of 27°C and duration of 90 minutes. The linearised Langmuir and Freundlich isotherm plots were used to model the equilibrium sorption data and a maximum monolayer adsorption capacity of 117μgg^{-1} was obtained from the Langmuir isotherm plot. However, it was reported that the adsorption of Cd(II) ion followed the Freundlich model better than the Langmuir equation.

Investigations into the ability of different forms of pomegranate peel adsorbent to remove Pb(II) and Cu(II) ions from aqueous solutions has been reported by El-Ashtoukhy *et al.,* (2008). The different types of pomegranate peel used were; raw peel (raw), activated carbon from pomegranate peel (AC$_1$) and activated carbon obtained from chemically treated pomegranate peel (AC$_2$ and AC$_3$). Experimental parameters of pH, contact time, adsorbate concentration and dose were examined in a batch adsorption system. Equilibrium modelling of adsorption was carried out using Langmuir, Freundlich and Temkin equations, with the isotherms constructed using isotherm equations based on linear transformation. For Pb(II) ion the order of fit of the isotherms to experimental equilibrium data was Langmuir>Temkin>Freundlich, while for the Cu(II) ion sorption the trend was Freundlich > Temkin > Langmuir.

Ibrahim *et al.,* (2010) in their study on the use of modified soda lignin extracted from oil palm empty fruit bunches for the removal of Pb(II) ions from aqueous solutions studied the effect of contact time, point of zero charge (pHpzc) and pH of solution, initial metal ion concentration and adsorbent dose. In their study, the amount of Pb(II) ion uptake was found to increase with increase in contact time, pH and initial metal ion concentration. The Langmuir, Freundlich and Temkin isotherm models in their linear forms were used to model equilibrium metal ion uptake. The Langmuir isotherm was the best fit to the experimental data confirming a monolayer adsorption capacity of 46.7 mgg^{-1} for Pb(II) at 47°C.

An observation from the described literature is that these studies all apply the Langmuir, Temkin and Freundlich isotherms using a linearization approach for analysis of adsorption isotherm data. However, a critical examination of the isotherm model equations such as the Langmuir, Freundlich and Temkin indicates that these models are non-linear (Rangabhashiyan *et al*., 2014). Linear regression is frequently employed for the description of the adsorption performance and level of fit of experimental adsorption data to the

isotherm model equations and its wide applicability is due to its mathematical simplicity, however the accuracy of an isotherm model is a function of a number of independent parameters such as the assumptions for the equation, the areas of application and the structure of the error parameter (Foo and Hameed, 2010). The linearization approach used in the selected literature examined and in many sorption studies results in the distortion of the value of the error parameter (the r^2 value) used in the discrimination of the fitting or otherwise of experimental data to a model.

Wong *et al*., (2004) observed that since the R^2 factor is based on the square of the difference between the theoretical and experimental data points in an isotherm plot, it will result in higher weighting to the higher C_e value data points when a reciprocal plot is used as is the case during the linearization of the Langmuir and Freundlich equation. This is because the structure of an isotherm equation is often varied during the linearization and this causes some of the assumptions behind the linear regression to be violated, thereby resulting in the distortion of the experimental error. According to Kumar (2006), linear regression assumes that the scatter of points around a line plot follows a Gaussian distribution and that the error distribution (standard deviation) in this scatter of points is the uniform at every value of the liquid-phase residual concentration (x-axis) on the plot. However, when a non-linear equation like the Langmuir and Freundlich isotherms are subject to linearization and the linear forms of the equation plotted, these Gaussian distribution assumptions are violated and the values of the error parameter is distorted resulting in a better r^2 value that gives a better fitting than if the non-linear equation was plotted.

Ncibi *et al.,* (2014) also observed that as the isotherm equations are non-linear equations, their linearization leads to the alteration of the error distribution after transforming the data to a linear form, hence non-linear regression was used in their analysis of five isotherm models for the characterisation of adsorption using *Posidonia oceanica* fibres. In another study by Mane *et al.,* (2007) the linearization of the Langmuir and Freundlich isotherm models was demonstrated to be inappropriate in predicting the goodness of fit for adsorption of green dye from aqueous solutions using bagasse fly ash. Therefore, due to the inherent bias resulting from linearization, isotherm parameters should be determined by using the non-linear forms of the isotherm model and this was the approach that this work was based on.

2.6.2 Adsorption kinetics

The rate at which adsorption occurs in any given system is an important parameter that has implications on the adsorption process. From the kinetic analysis, the adsorbate uptake rate which determines the residence time required for completion of adsorption reaction can be established. The prediction of the rate at which sorption occurs for any given system is an important factor for consideration in adsorption system design since adsorbate residence times and dimensions of reactor systems are controlled by the kinetics of the system (Qiu *et al.,* 2009; Ho and Chiang, 2001). The kinetics of sorption is known to show a large dependence on the physical or chemical characteristics of the sorbent material which also affects the mechanism of sorption. A number of models have been used to characterise these mechanism and these can be grouped into two; adsorption reaction models and adsorption diffusion models. The adsorption reaction models originate from chemical reaction kinetics and are based on the whole process of adsorption, while the adsorption diffusion models take into account the individual steps or stages by which the adsorption process proceeds (Qiu *et al.,* 2009). The adsorption reaction models include: pseudo first order, pseudo second order, elovich and the second order (Ho, 2006; Qiu *et al.,* 2009). While the adsorption diffusion models include: liquid film diffusion, intraparticle diffusion and double exponential models (Qiu *et al.,* 2009). A variety of these kinetic models have been designed to investigate the mechanism of adsorption and a number of these kinetic-based models have been used to describe the reaction order of adsorption based on adsorbate concentration. These include first order and second order models, pseudo-first order and pseudo second order models (Ho, 2006). In this study these two adsorption reactions models will be used to characterise the kinetics of the sorption of the two metal ions investigated in this work.

2.6.2.1 Pseudo first order model

In 1898, Lagergren presented the first order rate equation for the adsorption of ocalic acid and malonic acid onto charcoal to explain the kinetics of adsorption on solid surfaces. In order to distinguish the kinetic processes based on concentration of solution and adsorption capacity of solid, this Lagergren equation is called the pseudo-first order equation (Lagergren, 1898;Ho, 2004a) was the first rate equation developed for sorption in liquid/solid systems and it is based on solid capacity (Ho, *et al.,* 2004). It is one of the most widely used rate equations reported in adsorption kinetic literature.

Assuming that in a solid liquid adsorption system, the adsorption rate was proportional to the number of effective adsorption sites and then the rate of adsorption would be expressed as eqn (2.5):

$$\frac{dq_t}{d_t} = K_1(q_e - q_t)$$ (2.5)

Where; q_e and q_t are the sorption capacities, at equilibrium and at time t, respectively (mg.g^{-1}), while K_1 is the rate constant of the pseudo-first order sorption (Lmin^{-1}). After integration and applying boundary conditions t = 0 to t = t and q_t = 0 to q_t = q_t, the integrated form of eqn (2.5) is expressed as:

$$Log \ (q_e - q_t) = \log(q_e) - \frac{k_1}{2.303}t$$ (2.6)

Equation 2.5 is the linear form of the equation and the most common form of the pseudo first order (PFO) equation reported in literature for the description of sorption. Xuan *et al.,* (2006) used the linear pseudo first order equation to describe the kinetics of Pb(II) biosorption onto pre-treated chemically modified orange peel. Ho *et al.,* (2004) has also reported on the sorption of Pb(II) from aqueous solutions using tree fern adsorbent in which the linear form of the PFO equation was used. However, a number of studies have reported that the linear form of the PFO equation may lead to error propagation in the results due to the transformation of the PFO equation which is in a non-linear form to a linear form thereby implicitly altering the error structure in the determination of the model parameters (Ho, 2004b; Lin and Wang, 2009). The non-linear form of the PFO is given as eqn (2.7) :

$$q_t = q_e(1 - e^{-k_1 t})$$ (2.7)

The non-linear form of the PFO will be used to model the kinetics of sorption of Pb(II) and Cd(II) onto the different adsorbents developed in this study and eqn. 2.7 represents the reversible interaction between the adsorbate and adsorbent and is used for the prediction of the physisorption of the adsorbates onto the adsorbents in the system under consideration.

2.6.2.2 Pseudo second order model

The reaction kinetics of adsorption is the basis of the adsorption reaction models used in kinetic modelling and one of the most commonly used reaction models for the description of the kinetics of adsorption is the pseudo-second order model proposed by Y.S. Ho in Ho, (2006). This model was proposed in an attempt to present the equation that represents the adsorption of divalent metals onto sphagnum moss peat during agitation. An assumption was made that the process may be second-order and that sorption depends on the adsorption capacity of the adsorbent which is associated with the number of available active sites. This pseudo second order kinetics is presumed to proceed via chemisorption which involves valence forces through the sharing or exchange of electrons between the peat and the divalent metal ion as covalent forces (Ho, 2006). In the work of Ho (2006), the adsorbent used was peat which has a number of polar functional groups and these include ketones, phenolic acids and aldehydes. These chemical species on the surface of the peat are active sites that can be interact via chemical bonding. These groups are therefore the sites for the cation exchange capacity of the peat. Based on the above process and according to Coleman *et al,* (1956), the peat–copper reaction may be represented in two different forms as shown in the equations below:

$$2P^- + Cu^{2+} \leftrightarrow CuP_2 \tag{2.8}$$

$$2HP + Cu^{2+} \leftrightarrow CuP_2 + 2H^+ \tag{2.9}$$

Where; P^- and HP are polar sites on the peat surface.

Here the rate of the second order reaction may be dependent on the amount of the divalent metal ions on the surface of the peat at time "t" and the amount of the divalent metal ions adsorbed at equilibrium (Ho and McKay, 2000; Ho, 2006; Qiu *et al.,* 2009). Hence, the rate expressions for the adsorption can be described by eqns. (2.10) and (2.11) as:

$$\frac{d(P)_t}{dt} = K[(P)_0 - (P)t]^2 \tag{2.10}$$

or

$$\frac{d(HP)_t}{dt} = K[(HP)_0 - (HP)t]^2 \tag{2.11}$$

Where $(P)_t$ and $(HP)_t$ are the number of active sites occupied on the peat at time t, and $(P)_0$ and $(HP)_0$ are the number of equilibrium sites available on the peat. Therefore the driving force (q_e-q_t) is proportional to the available fraction of active sites. Thus from the above, the kinetic rate equation can be written as follows (Ho and Chiang, 2001; Ho, 2006):

$$\frac{dqt}{dt} = K_2(qe - qt)^2 \tag{2.12}$$

Where the parameters q_e and q_t are the sorption capacities at equilibrium and at time t, respectively (mgg^{-1}) and K_2 constant is the rate constant of the pseudo-second order sorption $(g\ mg^{-1}\ min^{-1})$.

For the boundary conditions $t = 0$ to $t = t$ and $q_t = 0$ to $q_t = q_t$, the integrated form of eqn. (2.12) becomes:

$$\frac{1}{qe-qt} = \frac{1}{qe} + K_2 \cdot t \tag{2.13}$$

This is the integrated rate law for a pseudo-second order reaction. Eqn. (2.13) can be rearranged to obtain:

$$qt \quad = \frac{t}{\frac{1}{k_2 q_e^2} + \frac{t}{qe}} \tag{2.14}$$

Eqn (2.14) has the linear form:

$$\frac{t}{qt} = \frac{1}{K_2 qe^2} + \frac{1}{qe} t \tag{2.15}$$

Where h $(mg \cdot g^{-1} \cdot min^{-1})$ can be regarded as initial sorption rate as $q_t/t \rightarrow 0$, hence:

$$h = K_2 \cdot qe^2 \tag{2.16}$$

Equation (2.16) can be written as:

$$\frac{t}{qt} = \frac{1}{h} + \frac{1}{qe} t \tag{2.17}$$

Equation (2.17) is the linear form of the pseudo second order equation (PSO) that is commonly reported in literature. The non- linear for of the equation is given by Lin and Wang, (2009) as:

$$qt \quad = \frac{K_2 \cdot qe^2 t}{1 + K_2 qet} \tag{2.18}$$

Equation (2.18) will be used to model the non-linear pseudo second order kinetics for the sorption reported in this work and assumes a stronger interaction between the adsorbate and adsorbent and is used for the prediction of the chemisorption of the adsorbates onto the adsorbents in the system under consideration.

One advantage of using the pseudo second order equation for the modelling of adsorption kinetics is that there is no need to know the equilibrium capacity from the experiments, as this value, the pseudo second order rate constant and the initial adsorption rate can be calculated from the model (Ho, 2006).

The coefficient of determination r^2 is used to test how the experimental kinetic data fits to the pseudo second order kinetic model for the adsorption of heavy metal ions (Ho and Chiang, 2001) and this relationship is given as eqn. 2.19;

$$r^2 = \frac{\sum(qe_{,model} - qe_{,av.})^2}{\sum(qe_{,model} - qe_{,av.})2 + \sum(qe_{,model} - qe_{,exp.})2} \qquad (2.19)$$

Where; $q_{e, model}$ is amount of metal ion on the surface of the adsorbent at any time t (mgg^{-1}) obtained from the pseudo-second order kinetic model.

$q_{e,exp}$ is the amount of the metal ion on the surface of the adsorbent at any time t, (mgg^{-1}) obtained from the experiment and $q_{e,av.}$ is the average of $q_{e, exp}$ (mgg^{-1}) (Ho, 2006).

The fitting of kinetic experimental data with this model is often carried out using linear regression and non-linear regression using numerical optimization by a number of authors in literature. The application of the linear regression approach is used to obtain values for two parameters in the pseudo second order model (k_2 and $q_{e,model}$). This method has some limitations as the transformation of model data required for linearization can result in modifications of error structure, introduction of error into the independent variable therefore leading to the alteration of the weight placed on each data point. This distortion in the error structure will lead to differences in model data between the non-linear and linear techniques in modelling the pseudo second order equation (Ho, 2004b; El-Khaiary *et al*., 2010). Hence, the better option will be the use of the non-linear method as the pseudo second order equation is a non-linear equation and the numerical optimization used to determine parameters will provide a more accurate representation of the model and the parameters within it (El-Khaiary *et al*., 2010). This non-linear approach will be applied for

the modelling of the sorption kinetics of the two metal ions onto the different adsorbents developed in this study. Error parameters are useful in optimization procedures and two error parameters would be used in the non-linear modelling of the kinetics of Cd(II) and Pb(II) ions sorption using the types of adsorbents.

2.7 Agricultural by-products selected for utilization as adsorbents

The agricultural residues selected for examination as potential adsorbents in this study were chosen from the local environment of Akwa Ibom State in Nigeria. 7 residues were selected and all of these are by-products of agricultural processing. Agricultural activities in this area are mainly via subsistence agricultural practices and there is no provision for the reuse or conversion of the residues that arise from them thereby constituting waste that is disposed indiscriminately in the environment. These residues were selected as they are obtained from crops that are used as food sources in the local environment and can be readily obtained in large quantities for scale up purposes. These materials are hereby discussed subsequently in this work.

2.7.1 Oil palm fibre

Oil palm (*Elaeis guineensis*) derives its generic name from Greek *elaia* meaning olive on account of its fruits rich in oil. Its specific name refers to the species area of origin. The centre of origin of oil palm is the Guinea forest of West Africa (FAO, 1997). It is mostly grown within 10 degrees, north or south of the equator. It does grow commercially in latitudes of 17 degrees from the equator, but yields are reduced at such sites. Oil palm, per hectare, is the highest yielding vegetable oil crop in the world producing a number of types of saturated and unsaturated oils; it yields from the mesocarp of the fruitlet, as well as from the kernel (Obahiagbon, 2012). Oil palm is one of the very few perennial crops that are harvested all year round, but there may be slight peaks and troughs in annual production. While in parts of Africa, oil palms are grown in village environs and form a very important part of the human diet, the crop has in the last 50 years developed as one of the largest plantation crops on the planet, with plantations often exceeding 20,000 hectares in size (FOA, 1997).

Elaeis palms are members of a small genus of only two species of palms. One specie occurs in Africa and the other in central and South America. Both species grow in "open" situations; such as streams, and in swamps. The Africa oil palm is native to numerous countries in tropical Africa and is found in southern Nigeria. The fruits and seeds of *Elaeis guineensis* yield two kinds of oil, palm oil from the fleshy covering and palm kernel oil from the kernel bunch nut. *Elaeis guineesis Jacq* is cultivated in Nigeria in the heavy rain forest zones, characterized with a mean maximum temperature of 29-30 °C and a minimum temperature of 22-24°C (Obahiagbon, 2012).The oils are widely employed for nutritious, cosmetic and trade purposes. Extraction of palm oil from the individual fruitlet during processing is mainly carried out using a mechanical press. The by-product of this stage is called the palm press fibre or oil palm fibre. Globally over 154.2 megaton of fresh oil palm fruit are processed for the extraction of oil and this is carried out in the major oil palm producing countries such as Indonesia, Malaysia, Thailand, Singapore, Brazil, Columbia and Nigeria. For every ton of oil palm fruit bunch being sent to the mechanical milling for oil palm extraction and refining, about 0.07 tonnes of palm shell, 0.103 tonnes of palm fruit fibre and 0.102 tonnes of palm kernels are produced as solid wastes (Luangkiattikhun *et al.,* 2008; Pansamut *et al.,* 2003). This by-product is used as ruminants feed and when dried can be used as fuel, it has also been used for composting and as source of organic fertilizer (Otti *et al.,* 2014; Oviasogoie *et al.,* 2013; FAO, 1997).

In Malaysia, the annual production of oil palm fibres amounts to approximately 8 million metric tonnes, which is generally used as fuel (Low *et al.*, 1993). The same is applicable in Nigeria. However, the economic value of oil palm fibre can be improved as it is currently being investigated for its adsorption properties. The chemical composition of oil palm fibre is cellulose (39.9%), hemi-cellulose (28.9%), lignin (20.3%) and ash (3.6%) (Low *et al.*, 1993). Thus, oil palm fibre is a lignocellulosic material. The exchange properties of the oil palm fibre are due to the presence of various carboxylic, phenolic and hydroxyl groups. This material could be a cheap source of sorbent for heavy metals if the sorption capacity is favourable (Low *et al.,* 1993).

2.7.2 Cocoa pod

Cocoa (*Theobroma cacao*) is a perennial crop widely cultivated in Africa, Asia and America. It is a crop of significant economic value as the seeds (beans) are used to produce chocolate and cocoa powder and current production in 2012 stood at 4.05 million metric tonnes (ICO, 2012; Adamafio, 2013). Cocoa is one of the main agricultural export

commodities in Nigeria and the country is the fourth leading exporter of cocoa in the world after Cote d'Ivoire, Indonesia and Ghana. In Nigeria average cocoa beans production between 2000 and 2010 was 389,272 tonnes per year. Cocoa is mainly exported as beans due to processing activities being limited within the country (FAO, 2013). The husk has a high proportion of ash (> 9%), crude fibre (> 20%), hemicellulose (11%), cellulose (35%), lignin (15%), pectin (6%) and some mineral contents which are potassium (3.18%), calcium (0.32%) and phosphorus (0.15%). The mesocarp had the bulk of the crude fibre and cellulose content and the endocarp has about 60% of the pectin (Sobamiwa and Longe, 1994).

Cocoa pod husk is the waste product generated during the processing of the cocoa fruit. The cocoa husk consists of 70 − 75% of the whole weight of the cocoa fruit and hence a large amount of waste is generated from the cocoa fruit harvesting. For instance per tonne of cocoa fruit harvested, there will be between 770 to 750 Kg of waste (Cruz *et al.,* 2012). Presently, pod husks are a waste product of the cocoa industry and present a serious disposal problem. In Indonesia it is disposed at the cocoa plantation area so that after decomposition it can be used as fertilizer for the cocoa tree (Syamsiro *et al.,* 2012). Fresh or dried husk may be used as livestock feed, but the theobromine (3, 7-dimethylxanthine) content restricts the proportion that can be consumed as it exerts detrimental effects on animals at high dietary concentrations and its use has been limited (Cruz *et al.,* 2012; Adamafio, 2013). It is estimated that each ton of dry beans produced from cocoa generated approximately ten tonnes of cocoa pod husk as a by-product and as the world production of cocoa beans was projected to rise from 3.6 million tonnes in 2009/2010 to 3.9 million tonnes in 2010/2011, a sizeable burden of waste is being generated in the cocoa industry and this poses a serious challenge for waste management (Vriesmann *et al.,* 2012). Hence, the need to find alternative outlets for the utilisation of the cocoa pod husk and reduce the associated problems of their disposal.

2.7.3 Coconut shell fibre

The Coconut palm (*Cocos nucifera L.*) is a tropical oil crop that can be found along the coast and interior of almost all tropical countries. It is a source of food, raw materials, wood for different handicrafts and is thought by many to be the "world's most useful plant. Its wide distribution has been favoured by its usefulness as well as by its adaptability to different ecological conditions. In many tropical countries, the coconut fruit is an important part of the daily diet. The Nigerian coconut groove populations are estimated at 13,615

hectare with over 2 million coconut trees (Eziashi and Omamor, 2010). These coconut palms are found mostly in the Southern states along the mangrove and rainforest regions as well as river deltas. It is also found in some marginal areas up to 10°N mostly along the banks of rivers and streams. The largest coconut palm plantation is found in the Badagry local government area of Lagos State located in the South West of Nigeria. More than 80% of these grove populations are of the West African Tall cultivar and their productivity of the coconut is limited naturally as it can hardly sustain up to 260 mature nuts per palm per annum in Nigeria. This has been a source of concern as the copra is needed for vegetable oil for both industrial and domestic uses, and also for other food supplements. The natural location of the embryo within the copra further minimizes the seed production potential (Odewale *et al.,* 2012).

Botanically the coconut fruit is a drupe and it has three layers: exocarp, mesocarp and endocarp. The exocarp and mesocarp make up the *husk* of the coconut. The mesocarp or "shell" thus exposed is the hardest part of the coconut and is composed of fibers called "coir" which have many local and commercial applications (Uwubanmwen *et al.,* 2011). Its main product is the oil extracted from the kernel. The husk and nut provide an important fibre (coconut coir) that has wide application as ropes, carpets and brushes (Ohler, 1999). Coconut coir is the light fluffy material that falls off from the thick mesocarp of the coconut fruit when it is shredded during coir processing. It is composed of cellulose, hemicellulose and extractives such as pectin and tannins. It contains about 35.99% cellulose, 53.5% lignin, and 9% ash (Israel *et al.,* 2011). Some of the fibre from the coconut is often disposed indiscriminately after the coconut has been harvested and constitutes significant waste disposal problems in many regions in Africa. Thus its evaluation as raw material for adsorbent preparation will serve as a source of reducing its environmental burden.

2.7.4 Cocoyam peel

Cocoyam is an important staple food across many developing countries in Africa, Asia and the Pacific. It is very important food crop in Sub-Saharan Africa where the two most commonly cultivated species (*Colocasia esculenta* and *Xanthosoma sagittifolium*) are grown extensively. Cocoyam belongs to the edible aroids (family Araceae) which comprise of underground food crops grown in several tropical countries. The cultivation of cocoyam in many African countries is mainly by small-scale resource farmers with minimal input. These crops play very important roles in the livelihood of rural farmers, who often resort to

cocoyam as an alternative source of food (Onyeka, 2014). The edible aroids contribute an important part to the carbohydrate content of the diet in many regions in developing countries.

Globally, it has an annual production figure of 10 million tonnes per year with Africa accounting for about 70% of global output with Nigeria producing about 3.9 million tonnes in 2013(Adelekan, 2012; FAOSTAT, 2015). The *Colocasia esculenta* specie produces edible starchy storage corms or cormel which are edible although they are less important than other tropical root crops such as yam, cassava and sweet potato, they are still a major staple food in some parts of the tropics and sub-tropics (Duru and Uma, 2003; Opara, 2003). It is an important food crop consumed in the southern part of Nigeria and is cultivated via subsistence farming. The processing of the food crop for domestic consumption involves removing the peel and these peels are disposed as waste or used as animal feed. However, this means of disposal of this waste is not sufficient to account for the amount of peels generated annually and it leads to the accumulation of the cocoyam peels in the environment.

2.7.5 Plantain peel

Plantain (*Musa paradisiaca L.*) is a tropical fruit that constitutes a staple food crop in Central and West Africa together with banana it is said to be the 4th largest fruit crop in the world with an estimated world production of 28 million tonnes with about 72% coming from Africa with Uganda the highest producer with 8 million tonnes in 2013(FAOSTAT, 2015). Over 2.7 million metric tonnes of plantains are produced in Nigeria annually which contributes substantially to the food supply of sub-tropical local populations (Shodehinde and Oboh, 2013; FAOSTAT, 2015). It also constitutes a significant proportion of their food crop. It remains an important staple food, source of revenue, as well as the raw material for industries producing value added products in many parts of Nigeria. Plantain occupies a strategic role in rapid food production, being a perennial crop with a short gestation period (Ayoola, 2011). It is also a major source of carbohydrate for more than 50 million people.

In Nigeria, all stages of the fruit (from immature to overripe) are used as a source of food in one form or the other, the immature fruits are peeled, sliced, dried and made into powder and consumed (Adeolu and Enesi, 2013).The high demand for plantain fruits generates wastes in the form of peels, which are often discarded and sometimes used as animal feed

(Betiku and Ajala, 2014).The peels of the plantain do not have any important use apart from being used as a source of potash in local soap making and animal feed (Babayemi *et al.*, 2010). Plantain peel is composed of cellulose (13.87%); lignin (1.63%); hemicellulose (15.07%), ash (11.73%) (Oladayo, 2010). With the growth in the cultivation of this crop in Nigeria, the disposal of the peels that arise from its consumption becomes a crucial waste management problem as there has been a geometric increase in solid waste associated with is agricultural residue (Babayemi *et al.,* 2010). To reduce the accumulation of this waste material in the environment, its utilisation as a precursor for the production of adsorbents was initiated.

2.7.8 Sweet potato peel

Sweet potato (*Ipomoea batatas L.*) is a crop that is native to tropical America and its one of the major root and tuber crops in the tropical regions of the world and it is widely grown and consumed as staple food in many parts of Africa, Latin America, Asia and the Pacific Islands. Based on the annual production of sweet potato, it is the fifth most important food crop based on fresh-weight basis in developing countries after rice, wheat, maize and cassava (Srinivas, 2009). It is the tenth major crop in world with a global output of about 100 million tonnes per year (UNCTAD, 2012). It is grown in about 114 countries in the world and is ranked among the five most important food crops in over 50 countries. Asia and Africa are the major producing area of the crop with China accounting for about 85% of global production (Srinivas, 2009). Currently it is the third most important crop due to its production output in seven Eastern and Central African countries and fourth in six Southern African countries. It is a perennial plant but is often grown in many areas as an annual crop. Nigeria is second largest producer after China with a reported annual output of 2.83 million tonnes in 2010 (UNCTAD, 2012) and 3.45 million tonnes in 2013 (FAOSTAT, 2015). In Nigeria, sweet potato is grown for both human and animal consumption and it is consumed in the boiled form after it has been peeled (Olagunju *et al.*, 2013 ; Egbe *et al.,* 2012). The peel has no significant application in Nigeria, except that it is mainly used as animal feed though the generation capacity outstrips animal consumption in many areas of the country thereby leading to a waste management problem.

2.7.9 White yam peel

Yams (*Dioscorea spp*) are tropical perennial or annual tuber-bearing and climbing plants with over 600 species out of which six are economically important in terms of food and medicine. It is an important tropical crop and one of the principal tuber crops in Nigeria, grown principally for the carbohydrate they provide and account for about 20% of the daily calorific intake of Nigerians (Aluko and Koya, 2006). Approximately 93% of the world's annual yam production of 37 million tonnes is produced in the "yam belt" of west and central Africa with Nigeria producing about 18.3 million tonnes (Okeoghene *et al,* 2013). In 2013 the global production of yam was about 64 million tonnes with Africa account for 60 million tonnes and Nigeria the largest producer with 40 million tonnes (FAOSTAT, 2015). The most cultivated species of yam in Nigeria are the *Dioscorea rotundata* (white yam), *Dioscorea alata* (water yam) and *Dioscorea cayenesis* (yellow yam) (Amusa *et al.*, 2003). The consumption of this tuber crop leads to generation of large quantities of peel waste that has no significant value except as animal feed and in Nigeria a large percentage of the crop produced is consumed as food thereby generating increasing quantities of waste yam peels. Thus, the identification of an environmentally friendly outlet for the use of the yam peel will contribute to the waste management strategies of the country. This approach is the basis of the utilization of these residues as candidate adsorbents for pollution remediation.

2.8 Summary

An evaluation of the relevant literature that relates to the adsorption of heavy metals has been carried out in this chapter. The concepts in wastewater treatment and advanced wastewater technologies presently deployed and their limitations have also been looked into. The factors that affect the deployment of wastewater treatment technologies in developing countries and the implications that have arisen thereof have also been examined in this chapter. Furthermore, wastewater treatment using low cost materials have been reviewed and the utilisation of activated carbon in heavy metal removal from wastewater systems has been evaluated during this review. A survey of the different types of agricultural residues used in heavy metal removal, their composition and the different treatment processes used to convert these low cost agricultural residues into adsorbents for heavy metal have also been carried out. The different factors that influence the use of

adsorbents for heavy metal removal and the different adsorption modelling techniques used to evaluate the sorption process were also considered towards highlighting their importance in wastewater treatment. Isotherm and kinetic modelling techniques used to quantify the uptake of pollutants during sorption has also been examined. Consideration has been given to two isotherm and two kinetic modelling equations that are widely applied in the evaluation of metal ion sorption. These models were; Langmuir and Freundlich isotherms and pseudo-first order (PFO) and pseudo-second order (PSO) kinetic models. The use of linear and non-linear approaches for the determination of the modelling parameters has also been discussed highlighting the advantages of using the non-linear approach. In addition, the limitations associated with the use of the linearization approach for the determination of the isotherm and kinetic parameters has also examined in light of the study. Finally, the candidate materials to be used as adsorbents and precusors for the development of new adsorbents for Cd(II) and Pb(II) ion sorption have also been evaluated to give insight for their choice as materials for use in this study.

CHAPTER THREE

CHARACTERISATION TECHNIQUES

CHAPTER THREE

3.0 Characterisation techniques

In the preparation and utilisation of adsorbents in this study, a number of modification regimes will be applied to the agricultural residues. Insights into the characteristics of the materials are fundamental as the properties of these adsorbents vary at one stage or the other. Different methods of modification (with different operating conditions) can alter the physical and chemical properties of resulting adsorbents. Therefore, the characterisation of these materials will be important to understand the properties of the adsorbents. This will also give insight into their performance in the adsorption process and help identify optimum conditions of the different adsorbents. A range of characterisation methods were used in this study and details of these characterisation techniques are provided in this chapter.

3.1 Fourier-transform infra-red (FT-IR) spectroscopy

The determination of functional groups on the surface of an adsorbent is essential for the subsequent adsorption processes facilitating the understanding of adsorbent-adsorbate interactions and revealing the associated adsorption mechanisms (Simonescu, 2012). Therefore, FT-IR characterisation of materials was carried out to study the functional groups on the surface of adsorbents.

The infrared (IR) region in the electromagnetic spectrum corresponds to the energy of vibrations and rotations of molecules. If a molecule is subjected to IR radiation whose frequency is equal to that of one of its oscillators, this oscillator will resonate and absorb part of the radiation. The absorption (emission) intensity is given by the transition probability between ground and excited states. However, not all vibrations are observed, only those transitions corresponding to vibrations with variation of the dipole moment are active in the infrared spectrum. The intensity of the infrared band is thus proportional to the square of the change in dipole moments (Davydov, 2003).

Infrared radiation is divided into:

- near (NIR, $\nu = 10,000 - 4,000$ cm^{-1});

- middle (MIR, $\nu = 4,000 - 200$ cm^{-1}) and

- far (FIR, $\nu = 200 - 10$ cm^{-1})

Because some compounds show characteristic absorption/emission in the IR spectral region, they can be analysed qualitatively using FT-IR spectroscopy to determine the functional groups present. These functional groups can also be identified using the fingerprint infra- red adsorption bands (Simonescu, 2012). In the study of processes occurring on surfaces, several forms of infrared spectroscopies are in use including transmission, reflectance, emission and diffuse reflectance infrared spectroscopies. In the diffuse reflectance mode, samples can be measured as loose powders, with the advantages of elimination of the tedious preparations of wafers and the avoidance of diffusion limitations. Diffuse reflectance infrared Fourier transform spectroscopy (also known as DRIFT or DRIFTS) is also suitable for strongly scattering or absorbing particles (Niemantsverdriet, 2007). One of strengths of the infra-red spectroscopy is that it can be used to obtain spectra from a wide range of solids, liquids and gases. The limitation of this approach is that sample preparations are usually required in order to obtain a good spectrum (PerkinElmer, 2005). Another technique used in FT-IR is the attenuated total reflectance (ATR). This technique has revolutionised solid and liquid FT-IR analysis because it does not require sample preparation which often has an effect on the quality of the sample and spectral reproducibility. In the ATR technique an optically dense crystal with high refractive index is used instead of KBr or mineral oil (Nujol) (PerkinElmer, 2005).

3.1.1 Attenuated total reflection (ATR) Fourier Transform-Infra red spectroscopy

In a conventional IR spectrophotometer, a sample IR beam is directed through the sample chamber and measured against a reference beam at each wavelength of the spectrum. The entire spectral region must be scanned slowly to produce good quality spectrum. However, IR spectroscopy has been dramatically improved by the development of the Fourier Transform method in much the same way as NMR has been revolutionized by this method. Fourier transform spectrometers have recently replaced dispersive instruments for most

applications due to their superior speed and sensitivity. They have greatly extended the capabilities of infrared spectroscopy and have been applied to many areas that are very difficult or nearly impossible to analyse by dispersive instruments. Instead of viewing each component frequency sequentially, as in a dispersive IR spectrometer, all frequencies are examined simultaneously in Fourier transform infrared (FTIR) spectroscopy (Sherman-Hsu, 1997).

ATR is said to occur when a beam of radiation enters the crystal from a more-dense (with a higher refractive index) into a less-dense medium (with a lower refractive index). When this happens, the fraction of the incident beam reflected increases as the angle of incidence increases as shown in Figure 3.1. Thus all incident radiation is completely reflected at the interface when the angle of incidence is greater than the critical angle (which is a function of refractive index). The beam then penetrates a very short distance beyond the interface and into the less-dense medium before the complete reflection occurs. This penetration is called the evanescent wave and typically is at a depth of a few micrometres (μm). The intensity is thus reduced (attenuated) by the sample in regions of the IR spectrum where the sample absorbs (Sherman-Hsu, 1997).
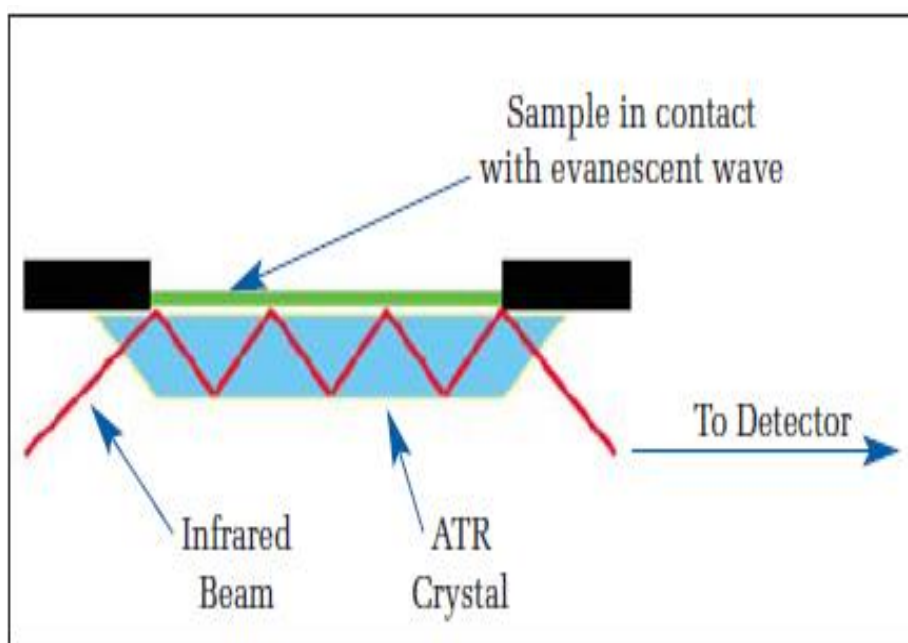
Figure 3.1: Schematic of a multiple Reflection ATR System (PerkinElmer, 2005)

For ATR technique to be successful, the following two requirements must be met:

- The sample must be in direct contact with the ATR crystal because the evanescent wave or bubble only extends beyond the crystal 0.5 μ - 5 μ.

- The refractive index of the crystal must be significantly greater than that of the sample or else internal reflectance will not occur – the light will be transmitted rather than internally reflected in the crystal. Typically, ATR crystals have refractive index values between 2.38 and 4.01 at 2000 cm^{-1} (PerkinElmer, 2005).

The ATR-FT-IR has been used for solid analysis with high precision and reproducibility. Solids are generally best analysed on the single reflection ATR accessories; with a diamond crystal being the preferred choice for most applications because of its robustness and durability. After the crystal area has been cleaned and the background collected, the solid material is placed onto the small crystal area. Experience has shown that ideal results from powder samples have been achieved by placing enough samples to cover the crystal area but the sample height should not be more than a few millimetres (PerkinElmer, 2005).

The performance of an ATR-FTIR spectrometer is dramatically superior to that of conventional instruments. Generally, only a small amount of a sample will produce an excellent spectrum in a fraction of the time with an infrared data station, the computer acquires, processes, stores and retrieves spectral data. The ATR-FT-IR is a very good sampling technique as it provides for a faster sampling, improves sample to sample reproducibility and minimizes user to user spectra variation (Kellner *et al.,* 2004). The ATR-FT-IR technique was used to obtain information on the types of functional groups present in the agricultural residues that may act as active sites for metal ion interaction during adsorption as described in section 4.3.10 of this work and discussed in section 5.9.

3.2 Nitrogen-BET surface area and porosity measurement

The pore characteristics and textual properties of adsorbents are crucial in different applications and in adsorption this information is necessary to give insight into the pore structure of the adsorbent. Most materials used as adsorbents are porous solids and the porosity may either occur naturally or from the preparation methods of the material. For example, during the thermal treatment of materials for the preparation of catalyst, the elimination of the volatile material (burning and/or evaporation) produces cavities that

represent both the result of the solid rearrangement and the exit way of the removed material thereby creating pores in the resultant material (Leofanti *et al.,* 1998). This process also applies in the preparation of adsorbents using thermal or chemical methods. The total surface area is a crucial criterion for solid adsorbents since it determines accessibility of active sites and is thus often related to adsorbent activity. The pore architecture of these adsorbents controls transport phenomena and governs selectivity for materials of interest. Properties, such as pore volume and pore-size distribution, are therefore essential parameters especially in adsorbents such as activated carbon (Storck *et al.*, 1998).

Thus, a typical adsorbent like catalysts contains one or more group of pores whose size and volume depend on their intrinsic properties and preparation method. According to Sing (1982)'s recommendation, the pores are classified depending on their size into macropores, mesopores and micropores. Thus, a typical catalyst contains one or more group of pores whose size and volume depend on preparation method. According to IUPAC (Sing, 1982) recommendations, the pores are classified in different classes depending on their size:

1. Micropores (pore size < 2 nm),

2. Mesopores (2nm <pore size < 50 nm),

3. Macropores (pore size > 50 nm).

The porous structure enables the material to have a total surface much higher than that corresponding to the external one. Some common catalysts have a specific surface area between 10 and 1000 $m^2 g^{-1}$ while their external specific surface area is in the range 0.01 – $10m^2 g^{-1}$. The knowledge of the morphological parameters is very important to understand the catalyst modification during the preparation procedure and gives a feedback useful for modifying the method to obtain the desired results (Leofanti *et al.,* 1998). This process also applies to adsorbents as an understanding of the development of pores during preparation plays a crucial role in determining the types of adsorbent pores are formed. From this information, the adsorbents adsorption capacity and other related parameters of carbon adsorbents can be obtained from different types of adsorption measurements used to generate adsorption isotherms (Menendez-Diaz and Martin-Gullon, 2006). These adsorption isotherms can be used to analyse the pore size distribution, surface area, pore volume, fluid-wall interaction strength, and other properties of adsorbents (Naumov, 2009). Liquid nitrogen adsorption at its boiling temperature (77 K) and atmospheric pressure represents the most widely used technique to determine surface area and to

characterize its porous texture. The nitrogen adsorption at 77 K allows the determination of the following:

1. Total surface of the solid (BET method)

2. Total surface, external to micropores (t-plot or Y, plot method)

3. Mesopore surface distribution vs. their size (BJH method)

4. Micropore volume (t-plot or α_s, plot method)

5. Mesopore volume and volume distribution vs. their size (Gurvitsch and BJH methods) (Leofanti *et al* ., 1998)

The starting point is the determination of the adsorption isotherm which is the volume of nitrogen adsorbed against its partial pressure. Isotherm shape depends on the solid porous texture. According to IUPAC classification, six types can be distinguished but only four are usually found in adsorbent characterization. Listed below are a summary of the six types of isotherms with their characteristics shown in Figure 3.2 (Sing, 1982; Sing, 2001).

Microporous solids (type I): The type I isotherm adsorption takes place at very low relative pressures because of strong interaction between pore walls and adsorbate. The completion of filling often requires higher pressure which is favoured by the interaction between adsorbed molecules. In this case, pore filling takes place without capillary condensation in the low relative pressure region (< 0.3). This way the process is indistinguishable from the monolayer formation process. Once micropores are filled, the adsorption continues on the external surface, following the behaviour described for macro or mesoporous solids. Typical examples of microporous solids are active carbons, zeolites and zeolite-like crystalline solids (Sing, 1982; Leofanti *et al.,* 1998)

Macroporous solids (type II): At low relative pressure, formation of a monolayer of adsorbed molecules is the prevailing process, while at high relative pressure a multilayer adsorption takes place. The adsorbate thickness progressively increases until condensation pressure has been reached. The pressure of first monolayer formation is lower if the interaction between adsorbate and adsorbent is stronger, but monolayer and multilayer formation processes are always overlapped (Sing, 1982; Leofanti *et al.,* 1998).). This isotherm is observed in non-porous powders or powders with pore diameters that are larger than 2nm and in this the point of inflection occurs near the completion of the first adsorbed layer (Leddy, 2012; Lowell and Shields, 1991).

The reversible *Type III* isotherm is convex to the P/P_0 axis over its entire range and therefore does not exhibit a point of inflection-B. It is characterised by heats of adsorption that are less than the heat of liquefaction. The adsorption is observed to proceed as the adsorbate interaction with the adsorbed layer is greater than the interaction with the adsorbent surface (Leddy, 2012). This type of isotherm is not common but can be found in the adsorption of water-vapour on pure non-porous carbon.

Mesoporous solids (type IV): For this isotherm at low relative pressures the process does not differ from what happens in macroporous solids. At high relative pressures the adsorption in mesopores leads to multilayer formation until at a pressure dependent on Kelvin-type rules (larger mesopore = higher pressure), condensation takes place giving a sharp adsorption volume increase. As mesopores are filled adsorption continues on the low external surface. Most oxides used as carriers, catalysts and adsorbents with pores in the mesopores range belong to this class of materials.

The type *V* isotherm is an uncommon one and is related to the Type II isotherm because the adsorbent-adsorbate interaction is weak but can be obtained in some porous adsorbents (Sing, 1982; Sing, 1985; Leofanti *et al.,* 1998; Naumov, 2009). It has also been observed to show strong interaction between adsorbates and powders containing pores in the range 1.5-100nm (Lowell and Shields, 1991).

Uniform ultramicroporous solids (type VI): Here, the pressure at which adsorption takes place depends on surface-adsorbate interaction. If the solid is energetically uniform, the whole process happens at a well-defined pressure. If the surface contains few groups of energetically uniform sites, a stepped isotherm must be expected, each step corresponding to the adsorption on one group of sites. Since all the catalyst surfaces are widely heterogeneous, this behaviour has never been observed. Stepped-like isotherms have been obtained only in the case of well-crystallized zeolites like X (one-step corresponding to cavities filling) or silicate (two steps, corresponding, respectively, to channel filling and to an adsorbent- adsorbate transition) (Sing, 1982; Leofanti *et al.,* 1998).
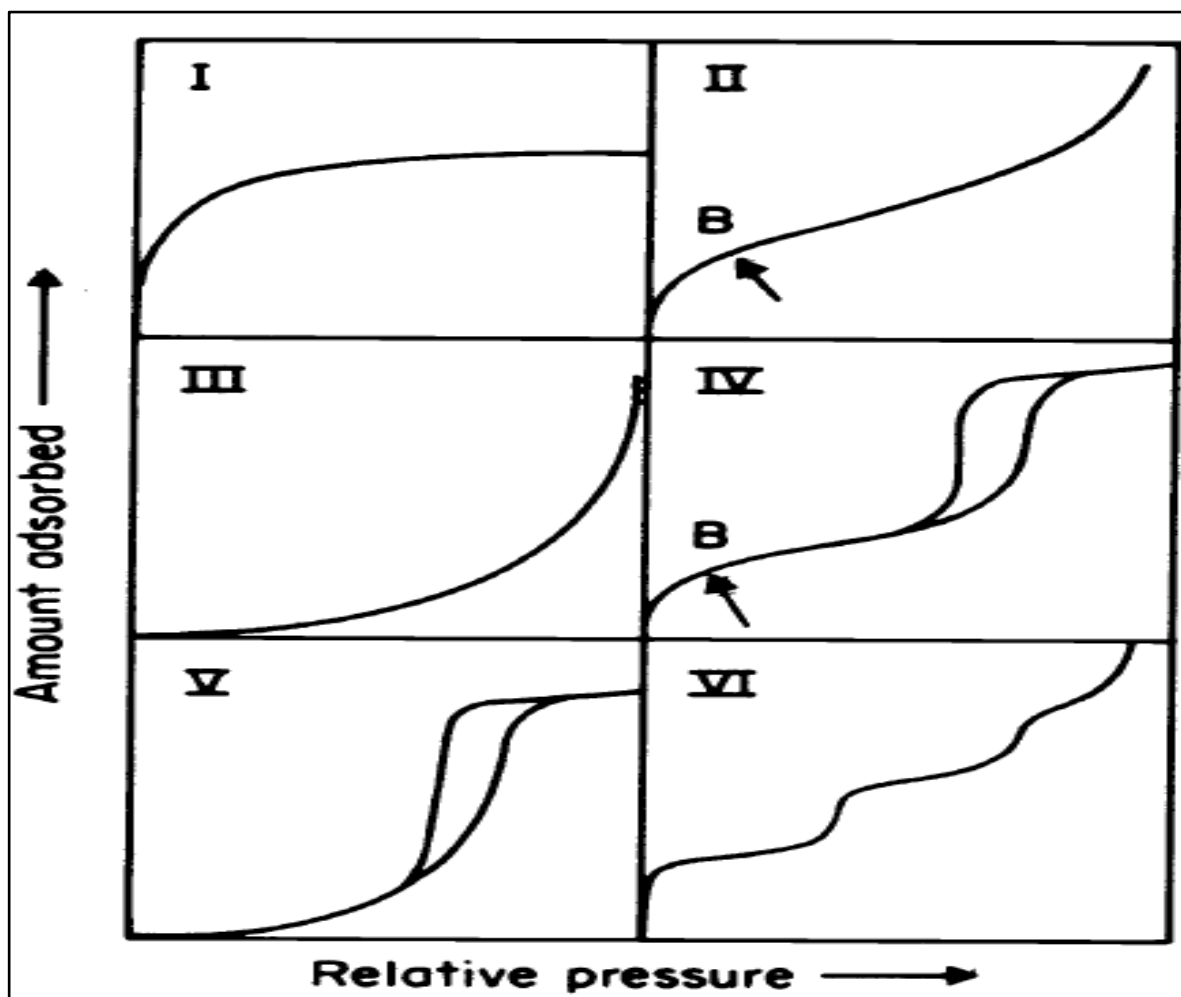
Figure 3.2 Types of Physisorption isotherms (Sing, 1982)

The development of hysteresis especially in type IV and type V materials may be due to a number of factors. One is that this effect is due to a delay in meniscus formation. According to this idea, capillary condensation equilibrium, as represented by the Kelvin equation is established over the desorption branch, while multilayer adsorption plays a more important role along the adsorption branch (Sing, 2014; Sing and Williams, 2004). It is consistent with these findings that well-defined hysteresis loops begin to appear in the multilayer/capillary condensation range when the pore size is increased to more than a few molecular diameters (Brunauer *et al.,* 1940). However, other forms of sorption hysteresis have been observed at lower P/P_0 values (in the normal monolayer range of the isotherm). The interpretation of physisorption hysteresis is important in the context of pore structure characterization. Thus, nitrogen sorption measurements at 77 K are routinely used for characterizing porous materials. According to Sing *et al*., (1985) hysteresis appearing in the multilayer range of physisorption isotherms is usually associated with capillary condensation in mesopore structures. Such hysteresis loops may exhibit a wide variety of

shapes. Two extreme types are shown as H1 and H4 in Figure 3.3. In the former the two branches are almost vertical and nearly parallel over an appreciable range of gas uptake, whereas in the latter they remain nearly horizontal and parallel over a wide range of P/P_0. In certain respects Types H2 and H3 may be regarded as intermediate between these two extremes. A feature common to many hysteresis loops is that the steep region of the desorption branch leading to the lower closure point occurs (for a given adsorbate at a given temperature) at a relative pressure which is almost independent of the nature of the porous adsorbent but depends mainly on the nature of the adsorbate (e.g. for nitrogen at its boiling point at P/P_0 0.42 and for benzene at 25°C P/P_0 0.28) (Sing, 1982; Sing *et al.,* 1985).
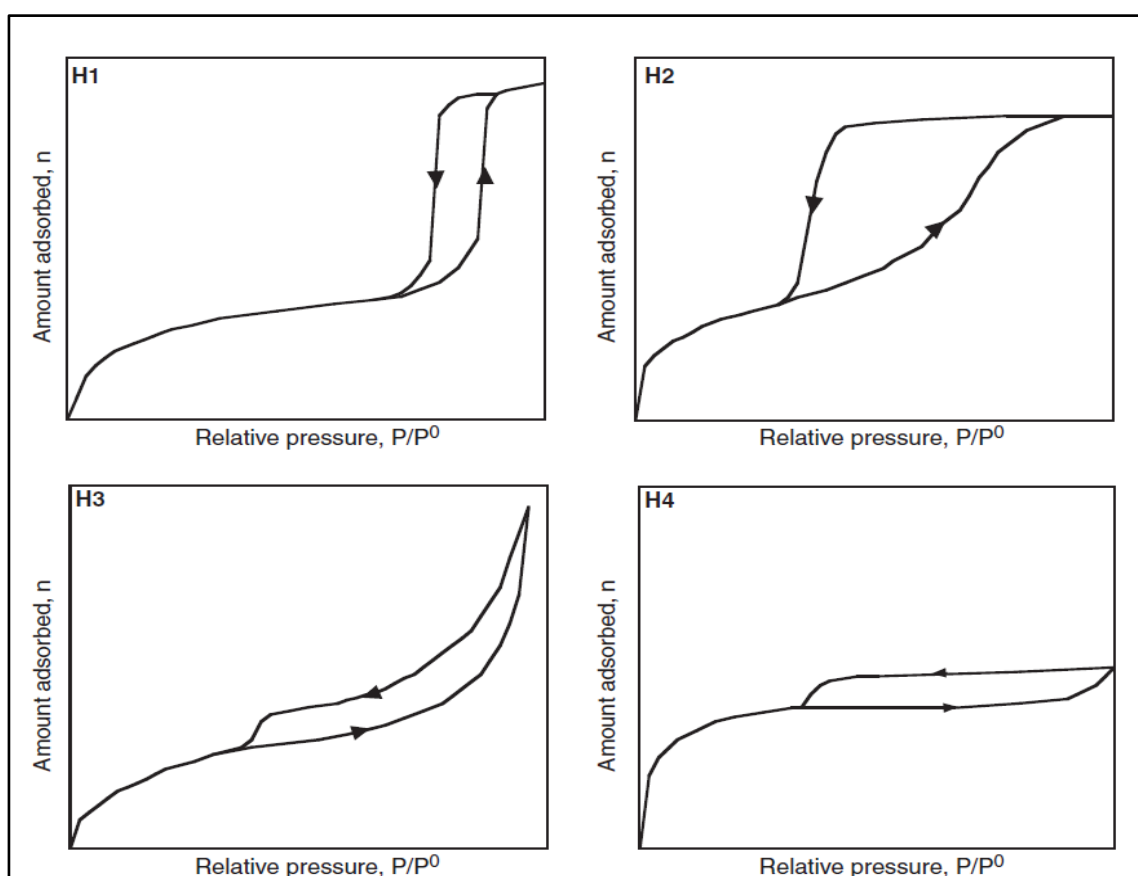
Figure 3.3 Types of hysteresis loops identified by IUPAC isotherms (Sing, 1982; Sing *et al.,* 1985; Sing and Williams, 2004)

In the review of physisorption presented by Sing *et al.,* (1985), the authors observed that although the effect of various factors on adsorption hysteresis is not fully understood, the shapes of hysteresis loops can be associated with the specific pore structures of materials.

The Type H1 can be associated with porous materials and consist of agglomerates or compacts of approximately uniform spheres in fairly regular array, which implies that these materials have narrow distributions of pore size. Many porous adsorbents tend to give Type H2 loops, but in such systems the distribution of pore size and shape is not well-defined. Based on their observation, the H2 loop is a difficult one to interpret as it was previously attributed to a difference in mechanism between condensation and evaporation processes occurring in pores with narrow necks and wide bodies (often referred to as 'ink bottle' pores), but recently this explanation has been seen as providing an over-simplified picture and the role of network effects must be taken into account (Sing *et al.,* 1985). The Type H3 loop, which does not exhibit any limiting adsorption at high P/P0, is observed with aggregates of plate-like particles giving rise to slit-shaped pores. Similarly, the Type H4 loop is often associated with narrow slit-like pores (Sing, 1982).

In the BET surface area determination, four or more data points of the adsorption isotherm must be measured and the BET (after Brunauer, Emmett and Teller) equation is used to give the specific surface area of the material from this data. The BET equation is used to give the volume of gas needed to form a monolayer on the surface of the sample. The actual surface area can be calculated from knowledge of the size and number of the adsorbed gas molecules. Nitrogen is used most often to measure BET surface but if the surface area is very low, argon or krypton may be used as both give a more sensitive measurement, because of their lower saturation vapour pressures at liquid nitrogen temperature. The total surface area of the material can be determined using the BET Eqn. for multilayer adsorption (Brunauer *et al.,* 1938) and is given as:

$$\frac{P}{V(P_0 - P)} = \frac{1}{V_m\,C} + \frac{C-1}{V_m C}\,\frac{P}{P_0}$$
(3.1)

The plot of P/V (Po-P) versus P/Po gives a straight line with the slope $(C - 1)/V_m C$ and the intercept $1/V_m C$. Therefore, V_m can be determined by measuring the adsorbed gas volume as a function of P.

The monolayer volume (V_m) of the adsorbate and the surface area (S) of the solid can be determined from the BET equation. Here P is the equilibrium pressure, P_o is the saturated vapour pressure at the test temperature (77 K), V is the adsorbed gas volume and C is the constant depending on the solid. Knowing the area occupied by one adsorbate molecule, σ (σ = 16.2 Å^2 for nitrogen), and using the Eqn 3.2.:

$$As = \sigma V_m N_A / V_0 \qquad\qquad\qquad (3.2)$$

Where; N_A is the Avogadro number (6.023×10^{23} mol^{-1})

V_o is the molar volume of nitrogen (22.414 dm^{3}mol^{-1} at STP)

The BET surface area is thus calculated from the BET plot using the relative pressure range where a monolayer of nitrogen molecule is formed on the surface. The BET method was used to determine the surface area of the adsorbents used in this study as described in section 4.3.4 of this work and is discussed in chapters 5-9.

3.3 Thermogravimetric analysis (TGA)

In this study the thermogravimetric analysis (TGA) technique was used to determine the thermal degradation profile of materials and the results of this degradation profile provide information on the proximate composition of the agricultural residues. This degradation profile can provide information on the approximate amount of ash, moisture, fixed carbon and volatile components of lignocellulosic materials due to the nature of their degradation with increasing temperature. Thermogravimetric analysis (TGA) is one of the basic methods in thermal analysis and it is based on an instrument built around a furnace where a sample is mechanically connected to an analytical balance. It is an instrumental technique whereby a controlled heating programme is used to examine the weight changes in a sample as a function of temperature or time (Kellner *et al.,* 2004). This analysis method has been reliably used over many decades in studying the thermal behaviour and properties of various types of materials. Its application includes characterisation of materials used in pharmaceutical, food, environmental and petrochemical industries (Stodghill, 2010).

Thermogravimetric analysis is also an important tool in material science research because of the possibility of monitoring weight changes in solid samples as a result of increasing temperature thereby yielding information on the different components of a material. The technique is used to characterize materials that exhibit weight loss or gain due to thermal decomposition, oxidation, or dehydration. It can also give information of the chemical properties of the degradation products if coupled with other instruments such as the FT-IR spectrometer or the mass spectrometer - a process called evolved gas analysis (EGA) (Barontini *et al.,* 2013; PerkinElmer, 2010). This analysis technique involves heating a sample in an inert or oxidizing atmosphere and measuring the weight. The weight change over specific temperature ranges provides indications of the composition of the sample and

thermal stability. The applications of this technique include determination of composition, thermal stability, oxidative stability and the decomposition kinetics of a sample. The thermogravimetric analyser (TGA) records the mass of the sample as a function of temperature or time, thereby giving information on the weight loss (%) using a single TG (thermogravimetric) curve recorded at a certain heating rate and atmospheres (under nitrogen or air flow) (Al-Maydama *et al*., 2006). The thermogravimetric curve can also be illustrated as a derivative often called derivative thermogravimetry (DTG) and this process expresses the TG results as a first derivative curve as a function of temperature or time (Dodd and Tonge, 1987).

Thermogravimetric analysis is also used to give information on the thermal stability and proximate composition of materials. This information is obtained from the different weight loss regimes that relate to different components of the material such as moisture, volatile carbon, fixed carbon and ash. The TGA instrument consists of a sample pan that is supported by a precision balance as shown in Figure 3.4, the pan is designed in such a way that it resides in a furnace and is heated or cooled during the experiment.
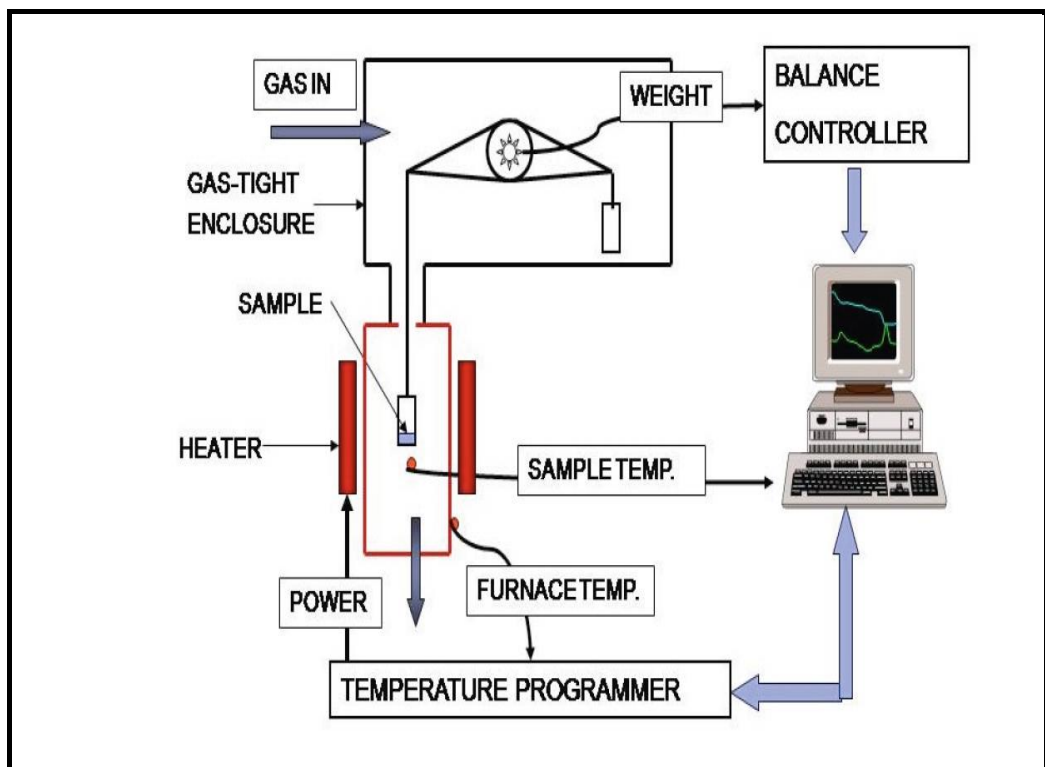
Figure 3.4: Schematic diagram of TGA instrument (Anandhan, 2008)

From Figure 3.4 the instrumentation for the TGA is observed to consist of the following;

- A thermo balance/microbalance- this balance sensitivity is usually around one milligram, with a total capacity of a few hundred milligrams

- Furnace, which has a temperature programmer-with a typical operating range from $20^\circ C$ to $1500^\circ C$, with heating rates up to $200^\circ C$ /min.

- A temperature sensor-the thermocouple is placed closed to the sample

- Sample holder/pan and an enclosure for establishing the required atmosphere- this will be an inert (N_2) or reactive (air)

A computer interface that has instrument control and data acquisition and display is the last component of the system (Anandhan, 2008).

When a sample is placed in the pan for analysis, the initial mass of the sample is recorded and this mass of the sample is subsequently monitored during the experiment as it changes due to application of heat. A sample purge gas controls the sample environment to maintain it as programmed during the analysis. This gas may be an inert or a reactive gas that flows over the sample and exits through an exhaust. At the end of the combustion process a temperature degradation profile of the sample of interest is displaced by the interfaced computer to indicate the rate of weight loss with temperature. The TGA characterisation was used to evaluate the thermal degradation profile of the residue adsorbents as described in section 4.3.7 and discussed in section 5.4 of this study.

3.4 Scanning electron microscopy/Energy Dispersive X-ray Analysis (SEM/EDAX)

The surface of an adsorbent is a complex structure that has diverse arrays of micro, meso and macropores and these surface structures play an important role during adsorption. Since adsorption is a surface phenomenon, it is important that insight into the morphology of these materials be determined. This is also important considering the different types of modification processes that will be used on the residue adsorbents. The use of the scanning electron microscopy (SEM) will provide information on the changes that occur on surface of these different adsorbents as well as those subjected to adsorption. Scanning electron microscopy (SEM) is a versatile and well-established technique used in the generation and analysis of topographical and elemental information of solid materials. It generates images of samples with a virtually large depth of field allowing different aspects of a sample to

stay in focus at a time. SEM has a high resolution, ensuring higher magnification of samples (Arief *et al*, 2008). By using a beam of electrons instead of photons, samples can be imaged at far higher magnifications. For most of the cases, electrons are emitted from a heated tungsten filament. The accelerated beam travels through a series of condenser and objective lenses that, by creating a symmetric electromagnetic field, focus and shape the electron flow, so that when it reaches the specimen, it has a diameter of only a few nanometres. It then scans the sample, which is kept in a vacuum chamber (Flegler, *et al.,* 1993; Goodhew *et al.,* 2001). The reflected/emitted electrons are received by a detector, the resulting signal amplified and then interpreted.

Energy Dispersive X-ray Analysis (EDAX) is also employed in scanning electron microscopy (SEM) and transmission electron microscopy (TEM) for chemical identification. In this technique, the incident electron beam introduces X-rays in the sample which is energy-analysed using a cooled semiconductor detector. The element-specific spectral lines are then identified to give the local elemental composition**.** EDAX is used in many different application areas such as in the chemical, environmental and food industries.

3.4.1 Principle of SEM

SEM can use different signals to generate contrast mechanisms. The back-scattered electron and secondary electron signals can be used to form images that can give information about the structure, topography and compositional features of a sample. The secondary images can be easily interpreted since they contain light and shades that resemble optical imagery. Secondary electrons are rather abundant and the most commonly used signal is SEM. Scanning electron microscopy is thus a method of image analysis that generates an image of the sample of interest using electrons generated from an electron gun instead of light as indicated in Figure 3.5.

This method of image analysis has many advantages over use the traditional microscopes in generating sample images. It has a large depth of field, which allows more parts of a specimen to be in focus at one time. It also has much higher resolution, and this can make closely spaced specimens to be magnified at much higher levels. The use of electromagnets in the generation of SEM images rather than lenses makes this technique a versatile one as there is more control in the degree of magnification. In addition, the instrument is seen as one with versatility of various modes of imaging. It also has excellent spatial resolution and a very modest requirement on sample preparation and conditioning. Its wide

application is also based on the relatively straightforward interpretation of the acquired images and the accessibility of associated spectroscopy and diffraction techniques (Bindell, 2000).
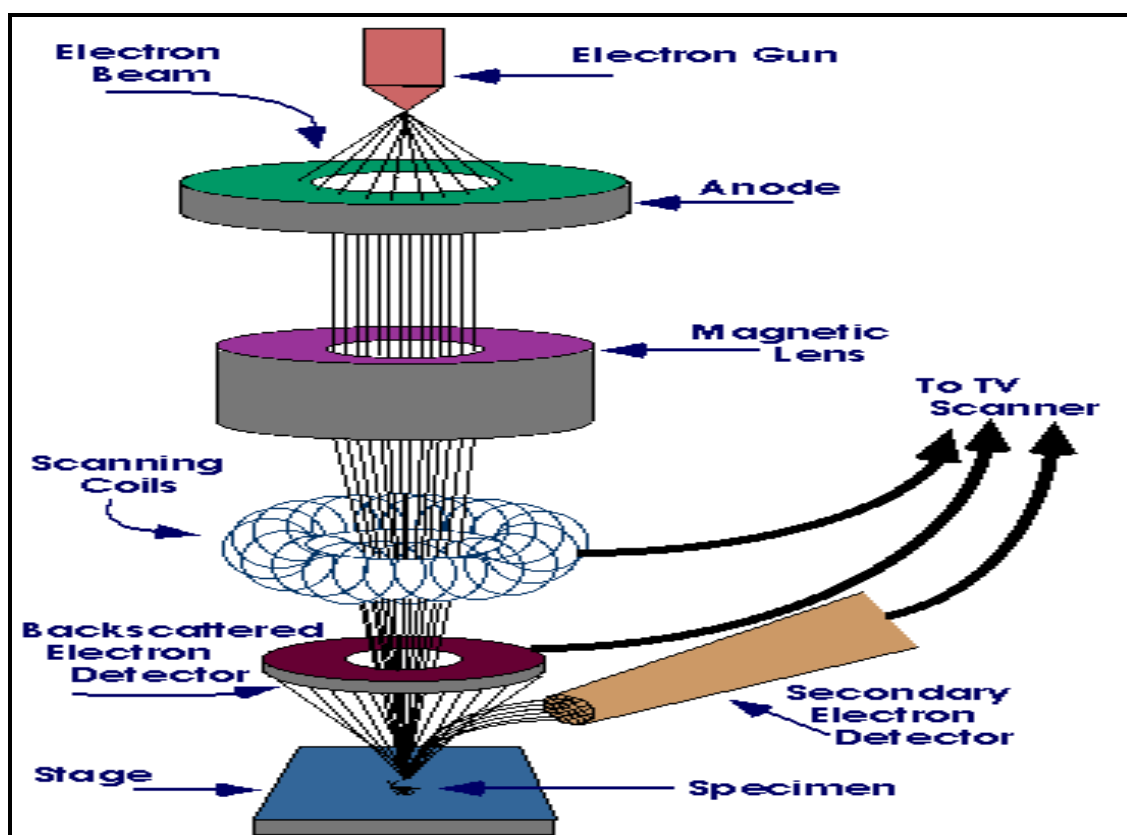
Figure: 3:5. Schematic of Scanning Electron Microscope (Purdue, 2010)

There are two main components of the scanning electron microscope and these are the electron column and the electron detector. In the electron column, an electron cathode generates an electron beam which is then collimated by electromagnetic condenser lenses, focused by an objective lens and finally backscattered across the sample surface by the scanning coils. Secondary electrons and backscattered electrons are emitted from the specimen at the irradiated spot of the primary electron beam. They are collected by the detector which forms the specimen image in the microscope (Bindell, 2000). The scanning electron microscope (SEM) was used to obtain images of the morphology of the adsorbents used in this study as described in Section 4.3.2 and discussed in chapters 5-9 of this study.

3.4.2 Energy Dispersive X-ray Analysis (EDAX)

Adsorption process involves both physical and chemical interactions that are associated with different materials. Information regarding the type and nature of chemical species of adsorbents can be obtained using the EDAX technique that is associated with the scanning electron microscope. The capabilities of spot and line analysis of materials using this technique provide chemical composition information that is representative of the local material environment. However, this technique gives a semi-quantitative analysis of the elemental composition of the adsorbents. The EDAX technique thus measures the energy of X-rays that are generated by the atoms of the sample during interactions with the electron beam as shown in Figure 3.6.
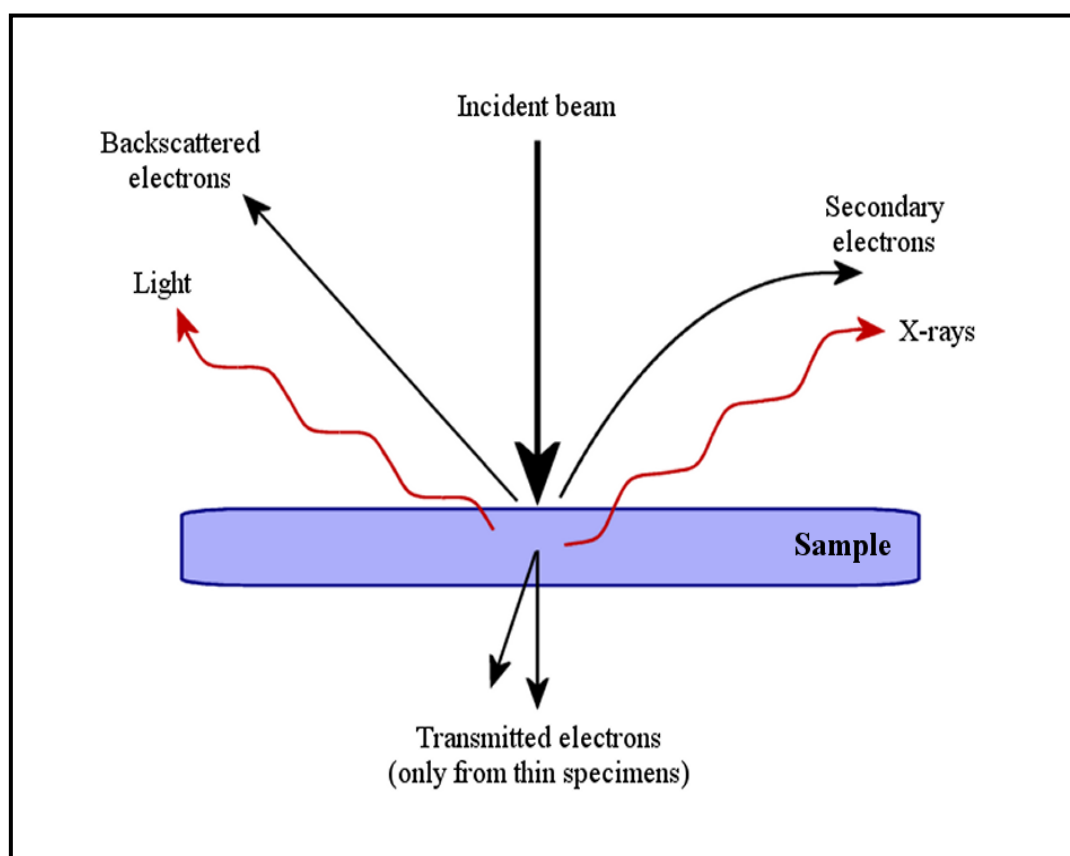
Figure 3.6: Electron signals from specimen interaction with incident beam (Hernandez-Ramirez, 2009)

Hence, the energy dispersive X-ray analysis (EDAX) is a useful technique for elemental analysis or chemical characterisation of adsorbents. In adsorbent characterisation, this technique is routinely coupled with SEM analysis to achieve a more complete profile of the material under investigation (Arief, *et al*., 2008). The X-ray spectra formed are

characteristic of the atoms generated, thus allowing the chemical composition of the sample to be determined. The chemical composition of the adsorbents before and after adsorption were determined using the EDAX technique as described in Section 4.3.2 and discussed in chapters 5-9 of this study.

3.5 X-ray fluorescence spectrometry & elemental micro-analysis

The determination of the composition of materials is an important aspect of adsorbent and catalyst characterisation. For adsorbents, their composition may vary with different elements and their identification is of priority as the composition of materials contributes to the nature and extent of their application. For the elemental characterisation of the agricultural residues used to develop adsorbents in this research; two important techniques were used and these were X-ray fluorescence spectrometry and elemental analysis of carbon, hydrogen, nitrogen, sulphur and oxygen (CHNS/O).

3.5.1 X-Ray fluorescence spectrometry

X-ray fluorescence spectrometry (XRF) is used to obtain characteristic inorganic compositions of materials. It is an important and versatile physical characterisation technique for elemental analysis of solids and liquids with minimal sample preparation and treatment. The atoms in a sample of interest emit fluorescence characteristic X-ray radiations (with discrete energies equivalent to colours in the optical light) when subjected to appropriate excitation (photoelectric effect) (Tertian and Claisse, 1982; Kellner *et al.,* 2004). The emission of characteristic line spectra can be induced by either the impact of accelerated particles such as electrons, protons and ions or by the impact of high energy radiations from an x-ray tube. The energy (or wavelength) of these characteristic X-rays is different for each element and forms the basis for qualitative analysis, while the number of characteristic X-rays of a certain element is proportional to its concentration which gives the basis for quantitative analysis. Quantitative X-ray fluorescence analysis technique uses a combination of classical high power sealed-ray tube and wavelength dispersion by selected crystals to ensure high sensitivity and versatility (Tertian and Claisse, 1982; Kellner *et al.,* 2004).

In principle, the XRF is based on the process of electrons being ejected from an inner shell of an atom and being replaced immediately by electron from a higher shell with the resulting emission of X-ray photon which is equivalent to the difference in energy between the two shells. All the elements from boron to uranium in the periodic table can be determined using XRF wherein trace elements analysis in parts per million (ppm) ranges and the determination of minor and major elemental concentrations (% range) can be carried out on the same sample (Kellner *et al.,* 2004).

In practice, depending on how the characteristic X-rays are measured, two techniques are used in X-ray fluorescence spectrometry namely wavelength-dispersive (WD-XRF) and energy-dispersive X-ray fluorescence spectrometry (ED-XRF). The application of XRF in multi-element analysis is used in many applications such as industrial process control (metallurgy, cement, glass and ceramic industry) as well as mining, environmental and materials research (Kellner *et al.,* 2004). The precision and reproducibility of the XRF analysis is very high and measurement time depends on the number of elements to be determined.

3.5.1.1 XRF Principle

X-rays are part of the electromagnetic spectrum situated between ultra-violet radiation and gamma rays. The diffraction of X-rays by matter is described by considering X-rays as electromagnetic waves characterised by wavelength (λ). The interaction of materials with X-rays are classified into 3 groups namely Compton scatter, fluorescence and Rayleigh scatter. X-ray fluorescence analysis uses to X-rays between 100 and 0.5 Angstrom (0.100 and 25 KeV) and the energy is usually expressed in kiloelectronvolts (KeV); where 1 eV is the energy that an electron acquires when it is accelerated by a potential of 1 volt and relating this with 1 joule of energy gives the intensity of the X-ray as:

$$E(KeV) = \frac{12.4}{\lambda(\text{Å})} \tag{3.3}$$

Where; λ is the wavelength of radiation in meters (10^{-10} m).

X-rays with wavelength longer than 1 Angstrom is termed "soft" X-rays and those with shorter wavelength are called "hard" X-rays. When these X-rays are beamed towards a material, a fraction will be transmitted through, another fraction absorbed (which produces fluorescent radiation) and another fraction scattered back. The fluorescence and the scatter radiation depend on the thickness (d), density (ρ) and composition of the material as well as the energy of the material as shown in Figure 3.7.
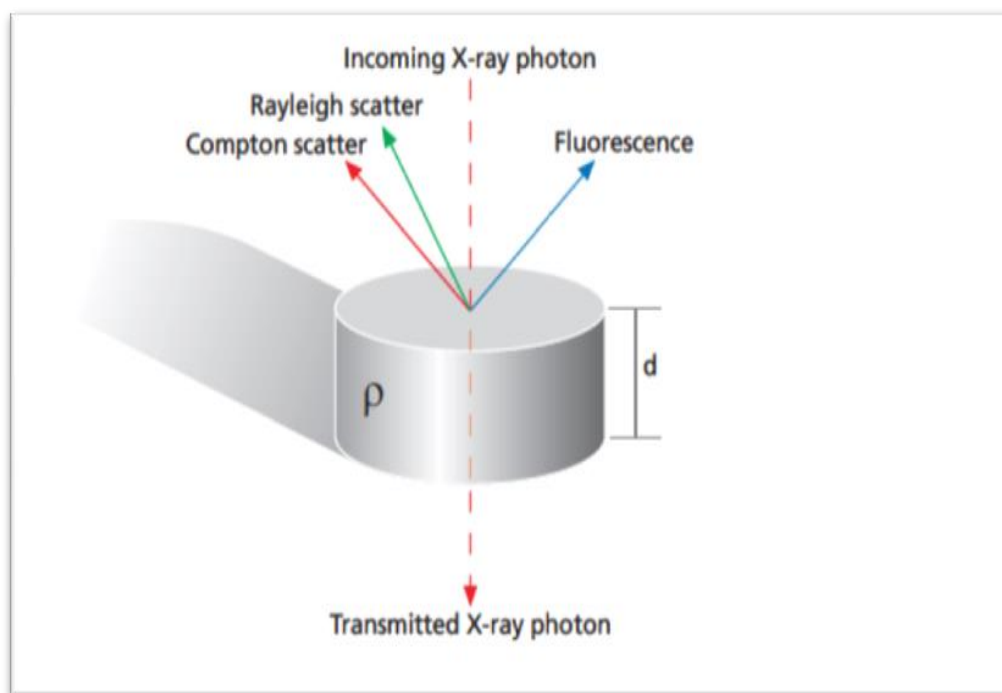
Figure 3.7: Three main interactions of X-rays with Matter (Brouwer, 2010)

The fluorescence and scattering of the X-rays is responsible for most of the continuum observed in XRF spectra because part of the exciting radiation is scattered by the sample and enters the detector system (Kellner *et al.,* 2004; Brouwer, 2010). The XRF spectrometer is the instrument used for XRF analysis and it is composed of a source of X-ray (usually high energy electrons fired at anode-usually made from Ag or Rh). This source can have varying excitation energies from $15 - 50$ kV and current from$10 - 200$ μA. The instrument also has a sample holder where the sample is placed as well as a detection system. XRF spectrometers are generally divided into two main groups: wavelength-dispersive XRF systems (WDXRF) which uses a high-vacuum x-ray tube and an analysing crystal (Si (Li)) which diffracts the radiation to disperse it. The energy-dispersive XRF system (EDXRF) uses a detector to directly measure the different energies of the characteristic radiation coming from the sample (Brouwer, 2010). Figure 3.8 shows the basic designs of the energy dispersive X-ray fluorescence (EDXRF) or wave length dispersive X-ray fluorescence (WDXRF) spectrometer while Figure 3.9 schematic diagram of the XRF system.
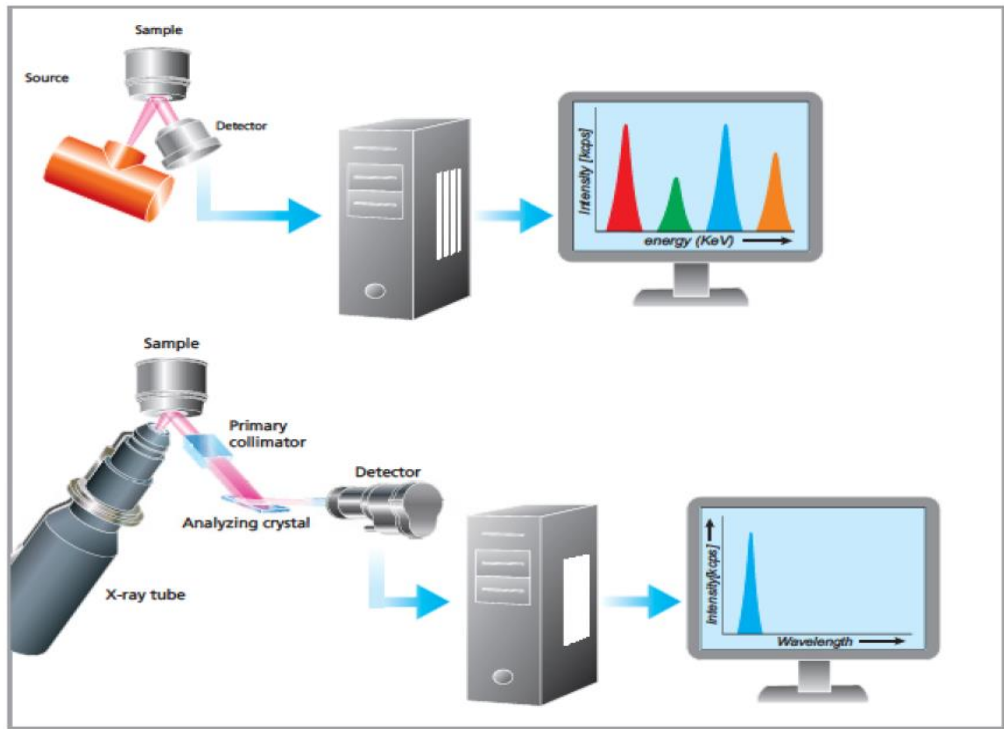
Figure 3.8: Basic designs of EDXRF and WDXRF Spectrometers (Brouwer, 2010)
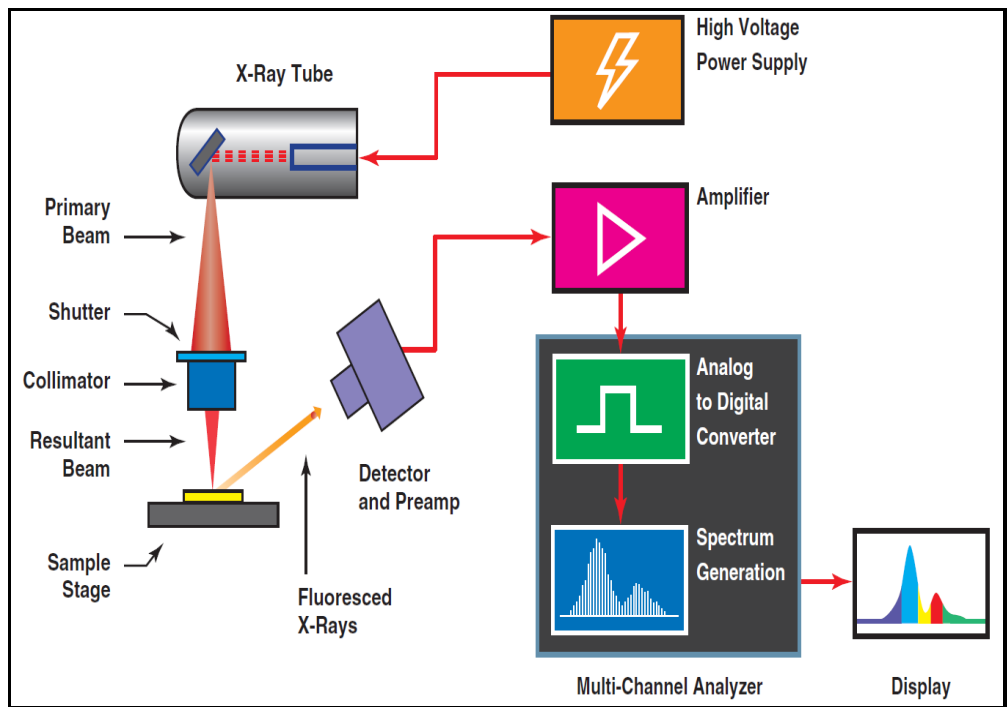
Figure 3.9: Schematic of XRF System (Matrix Metrologies, 2012)

From both figures, it can be seen that the source of the X-ray (x-ray tube) produces a primary beam which goes through a collimator and the resultant beam of specified wavelength irradiates the sample. The emitted fluorescence radiation enters the detection system where it travels through a set of collimators and is focused on to a set of crystal

planes which are kept in an orientation to reflect the X-ray wavelength radiation at a given angle based on Bragg's law which is given as:

$$n.\lambda = 2d.\sin\theta \qquad\qquad (3.4)$$

Where: n is a positive integer that gives the order of reflection; d is the inter-planar spacing of the atoms and λ is the wavelength of the incident X-ray.

The detector measures the radiation emitted from the sample as a result of atomic excitations of the elements present in the sample. In the detector system, the signal is detected and amplified and the amplified signal goes into a multi-channel analyser where a digital pulse processor transforms the signal into an XRF spectrum display using a plot of counts per second (cps) vs. kilo-electron volts (KeV) axis. From the spectrum, the XRF software converts the spectrum information into elemental concentrations (% or ppm). From the analysis using this instrumental technique, the elemental composition of a material and the concentration therein can be obtained. The XRF spectrometer was used to obtain the elemental composition of the residue adsorbents as described in section 4.3.5 and discussed in section 5.2.1 of this study.

3.5.2 Elemental micro-analysis

The analysis of the carbon, hydrogen, nitrogen, sulphur and oxygen (by difference) components of organic materials and other matrices of materials can be carried out using a carbon, hydrogen, nitrogen and sulphur (CHNS) elemental analyser. The oxygen component is obtained by difference; taking into account the composition of the other elements. This instrument provides rapid analysis of the material of interest and its versatility arises from its ability to analyse samples of liquid, solid or gaseous phases thereby making it a very powerful tool used for materials characterisation in the food, chemicals, environment, energy and pharmaceutical fields (Thompson, 2008). Depending on the configuration of the instrument, it can be designed with a double reactor to simultaneously carry out CHN or CHNS and oxygen analysis or with a single reactor for CHN or CHNS analysis (Thermo Scientific, 2008). The CHN and CHNS modes of the elemental analyser are based on the classical Pregl-Dumas method wherein the samples of interest are combusted in a pure oxygen rich environment and the combustion product gases are measured in an automated process. The combustion process can be carried out using static conditions or dynamic conditions. In the static condition process, a given amount of oxygen is introduced while the dynamic condition has a constant flow of oxygen

for a defined period of time. In most processes, catalysts are added to the combustion tube to aid conversion (Thompson, 2008; PerkinElmer, 2011).

The elemental analyser can be divided into four component units namely combustion, gas control, separation and the detection units. A schematic representation of the analyser process is shown in Figure 3.10. In the combustion unit, samples are encapsulated in tin or aluminium vials and inserted either automatically into the auto-sampler or manually using a single-sample auto injector. The samples are combusted in oxygen and the process has a temperature of 1000°C. At this temperature, carbon is converted to carbon dioxide, hydrogen to water, nitrogen to nitrogen gas/oxides of nitrogen and sulphur to sulphur dioxide. If other elements such as chlorine are present, they will also be converted to combustion products such as hydrogen chloride and can be removed using adsorbents in the gas control unit.
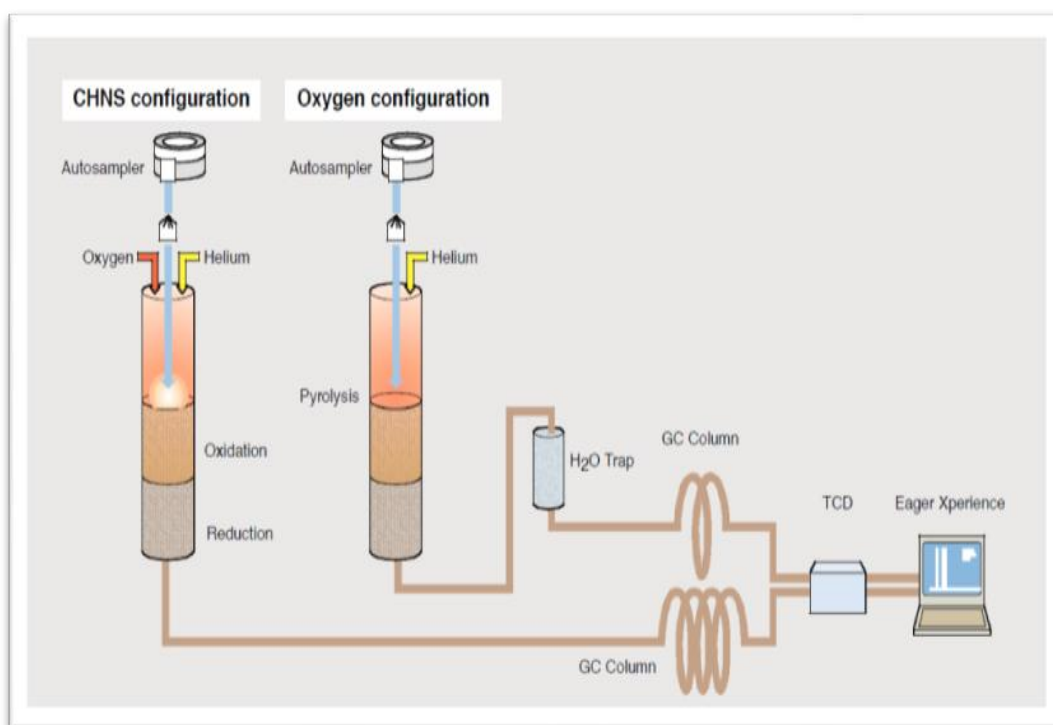
Figure 3.10: Schematic diagram of the CHNS Elemental Analyzer
(Krotz and Giazzi, 2012; PerkinElmer, 2011)

The combustion products are swept out of the combustion chamber by inert carrier gas such as helium into the mixing chamber of the gas control and passed over a heated (about 600°C) high purity copper. This copper can be situated at the base of the combustion chamber or in a separate furnace. The function of this copper is to remove any oxygen not

consumed in the initial combustion and to convert any oxides of nitrogen to nitrogen gas (reduction process). The gases are then passed through the absorbent traps in order to leave only carbon dioxide, water, nitrogen and sulphur dioxide (Thompson, 2008). The resulting gaseous products are thereafter mixed rapidly and precisely maintained at controlled conditions of pressure, temperature and volume. This mixing process is aimed at ensuring that the product gases from combustion/pyrolysis are maintained at the same exact conditions (pressure, volume and temperature) for every run thereby eliminating external influences such as barometric pressure changes and altitude from the system (Krotz and Giazzi, 2012; PerkinElmer, 2011)

After homogenization of product gases, the mixing chamber is depressurized through a column in the separation of the instrument. Detection of the gases can be carried out in a variety of ways depending on the instrument configuration. These separation and detection units may include:

(1) A gas chromatographic separation of the products followed by quantification using thermal conductivity detection.

(2) A partial separation by gas chromatography also known as ('frontal chromatography') followed by thermal conductivity detection for carbon, hydrogen and nitrogen but not for sulphur constituents.

(3) A series of separate infra-red and thermal conductivity cells for detection of individual compounds.

Quantification of the elements in this manner will require calibration for each element by using high purity 'micro-analytical standard 'compounds such as acetanilide and benzoic acid (Thompson, 2008; PerkinElmer, 2011). The carbon, hydrogen, nitrogen and oxygen (CHON) content of the residue adsorbents were determined using the CHNS elemental analyser as described in section 4.3.11 and discussed in section 5.2 of this study.

3.6 Photon correlation spectroscopy for zeta potential

Photon correlation spectroscopy (PCS) is a dynamic light scattering (DLS) method that measures particles in a solution and the diffusion of these particles within a solution. The technique measures the Brownian motion through the detection of the time-dependent fluctuations in the intensity of scattered light on a timescale of 10^{-3} to 10^{-9} seconds from a suspension of particles to produce a correlation curve from which the particle diffusion coefficient (and subsequently particle size) is obtained. The Brownian motion arises from collisions between the particles and the solvent molecules and the light scattering is a

consequence of the interaction of the light with the electric field of a particle or small molecule. This electrostatic interaction influences the particle stability (Mattison *et al.,* 2003). One property of interest of this system is the zeta potential of the solution.

Zeta potential is a measure of the magnitude of the electrostatic repulsion or attraction between particles and it is an important parameter that affects stability of the species in solution. The development of a net charge on a particle surface affects the ion distribution in the surrounding interfacial region. This leads to an increase in the concentration of the counter ions (those with different charge to the particle) which are close to the surface (Kaszuba *et al.,* 2010). This generates an electrical double layer around each particle as shown in Figure 3.11. The electrical double layer consists of charged surface and neutralizing surplus of opposite and equal charged ions diffusely spreading through a liquid medium. The liquid layer that surrounds the particle has two distinct parts. The first being an inner region where the ions are bound strongly called the Stern layer and the other region, an outer or diffuse region where the ions are less bound (Malvern Instrument 2004; 2014; Kaszuba *et al.,* 2010).
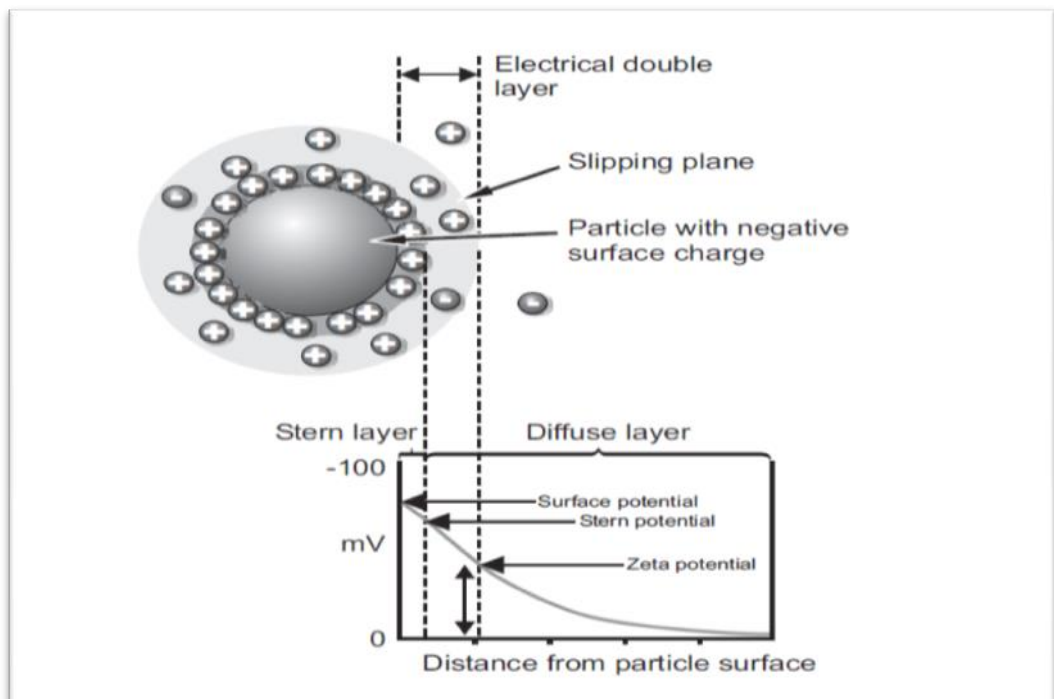
Figure 3.11: Particle Surface and Electrical Double layer (Malvern instrument, 2004; Kaszuba *et al.,* 2010).

There also exist within the diffuse layer a notional boundary which the ions and particles forms a stable system. When there is the movement of the particles, the ions that exist within the boundary also move but this movement is not observed with any ions beyond the boundary. This boundary is described as the surface of hydrodynamic shear or the slipping plane and the electrostatic potential that exists at this boundary is known as the zeta potential (Malvern instrument, 2004; Kaszuba *et al.,* 2010).

The zeta potential value is affected with changes in a solution/suspension and the measurement of the zeta potential gives an indication of the nature of these changes. Thus monitoring the zeta potential in a solution is an important parameter that will influence solution properties and thereby affect many processes (Salopek *et al.,* 1992). The most important factor that affects the zeta potential is the pH and this describes the zeta potential value. This description is seen in the curve of zeta potential of a suspension versus pH and the curve will be positive at low pH and negative at high pH. Hence, the zeta potential value is either positive or negative depending on the H^+ or OH^- ion concentration in a suspension or solution (Malvern instrument, 2004). The curve of zeta potential versus pH has a point where the plot goes through a zero potential called the iso-electric point as shown in Figure 3.12.
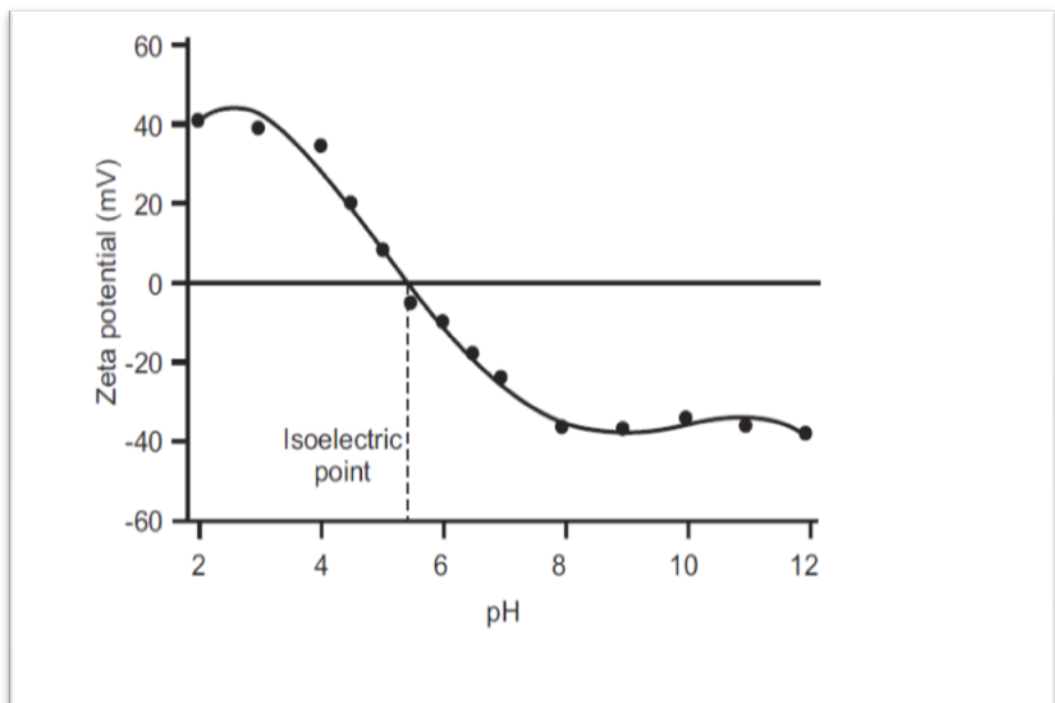
Figure 3.12: Plot of Zeta potential vs pH indicating the iso-electric point (pHpzc) (Malvern Instrument, 2004).

This point has important applications as it is the point where the system is least stable as there are fewer tendencies for repulsion to occur. This is because the particles with positive and negative potential are balanced and there is no dominating potential that can cause repulsion of the particles, hence they tend to come together and flocculate. The pH at the point of zero charge (pHpzc) is measured using the dynamic light scattering using a Zetasizer (Malvern instrument, 2014; Saleh *et al.,* 2008). The value of the zeta potential for each adsorbent system is determined automatically by the Zetasizer software based on the modified Helmholtz-Smoluchowski mobility equation (Askarieh *et al.,* 2010) given as :

$$\zeta = 4\pi \frac{\eta\mu}{D} \qquad\qquad (3.5)$$

Where the symbols

ζ represents the value of the zeta potential of the suspension/solution,

η is the absolute zero-shear viscosity of the suspension and

μ is the electrophoretic mobility of the particles in the suspension/solution

D is known as dielectric constant of the medium.

The zeta potential of the adsorbents used in this study was determined using the Malvern Zetasizer as described in section 4.3.3 and discussed in chapters 5-9 of this study.

3.7 X-ray Diffractometry (XRD)

X-ray diffraction (XRD) studies have been used to indicate that the nature of arrangement of the cellulose molecules in the structure is what results in the existence of crystalline and amorphous regions in cellulose. Thus in the aggregates of cellulose macromolecules, the molecules in crystalline region arrange regularly and display a clear X-ray pattern, so the density of cellulose in the crystalline region is high (1.588 g.cm^{-3})(Chen, 2014). On the other hand the molecular chains in the amorphous region are arranged irregularly and loosely. Hence the distance between molecules is large resulting in a low density of cellulose in the amorphous region, (1.500g.cm^{-3}). This ordering in the cellulose regions results in varying cellulose crystallinity, which is generally between 30 and 80% and this refers to the percentage of all the cellulose occupied in the crystalline region (Yang, 2008). Lignocellulosic materials are also composed of crystalline and amorphous regions, wherein the crystalline region is made up of crystalline cellulose and amorphous region is composed of amorphous cellulose, hemicellulose and lignin and the degree of ordering of

these structures in residue materials can be determined using X-ray diffraction (Poletto *et al.,* 2014). X-ray diffractometry is thus a technique that is used to determine the degree of crystallinity in cellulosic and lignocellulosic materials as these characteristic may be used to give insight into the processes that occur during the use of these lignocellulosic materials as adsorbents.

XRD is based on the generation of X-rays using a metal ion source and the sudden deceleration of high-energy electrons when it strikes a metal target leads to the generation of X-rays which is used to analyse the characteristics of materials. Using this technique, the structural analysis of materials is evaluated and their level of crystallinity or otherwise is known. At the basic level, the goal of such structural analysis is restricted to the determination of atom connectivity in molecular or solid-state compounds. X-rays are an important means of molecular analysis of materials because the wavelengths of X-rays are within or close to the distances between chemically bonded atoms which is typically about 0.9 to 3 Å (1 Å = 1.0 x 10^{-10} m) thereby giving capacity to view molecular structures. This gives a fingerprint characterisation of crystalline or polycrystalline materials (Kellner *et al.,* 2004).

3.8.1 Principle of XRD

The interaction of X-rays with atoms leads to a scattering, which can be both elastic (Rayleigh Effect) or inelastic (Compton Effect) as shown in Figure 3.7. When a crystal is bombarded with X-rays of a fixed wavelength (similar to spacing of the atomic-scale crystal lattice planes) and at certain incident angles, intense reflected X-rays are produced when the wavelengths of the scattered X-rays interfere constructively. For amorphous materials or liquid samples with a restricted degree of internal order (which is in a range of only a few atoms or molecules), the atoms are arranged in a disorderly manner similar to liquid molecules and the interference effects between the wave fronts from neighbouring atoms lead to a continuous scattering pattern of limited use. However, crystalline materials with their long range ordered structure provide an excellent diffraction grating for X-rays, which results in a discontinuous scattering pattern that is dependent on the relative positions of the individual atoms (Kellner *et al.,* 2004).

In order for the waves to interfere constructively, the differences in the travel path must be equal to integer multiples of the wavelength. When this constructive interference occurs, a diffracted beam of X-rays will leave the crystal at an angle equal to that of the incident beam. The general relationship between the wavelengths of incidence X-rays, angle of

incidence and spacing between the crystal lattice planes of atoms as shown in Figures 3.13 and 3.14 is known as Bragg's law (Clearfield *et al.*, 2008):

$$n.\lambda = 2d.\sin\theta \qquad\qquad (3.6)$$

Where:

n = order of reflection

λ = wavelength of the incident X-rays

d = inter-planar spacing of the crystal and

θ = angle of incidence
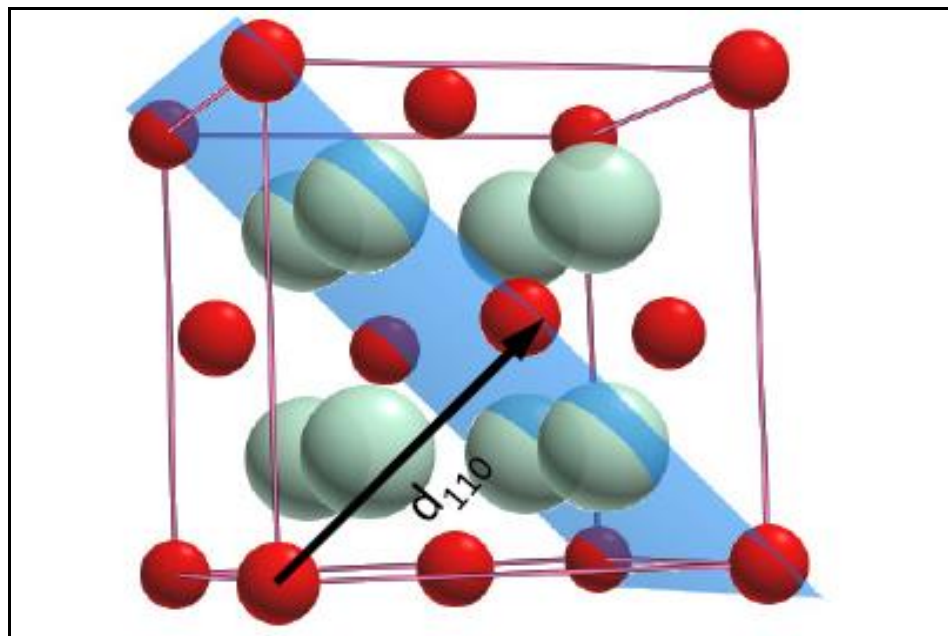
Figure 3.13: Representation of interplanar spacing in crystalline materials (Speakman, 2012)

The position of the diffraction peaks are determined by the distance between the parallel planes of the atoms and Braggs law provides a simplistic model using the vector d_{hkl} to understand the conditions under which diffraction is allowed to occur. Each plane in a crystal is defined by Miller's indices represented as "hkl". The "d" term in the Bragg's law is a geometric function of the size and shape of the unit cell and is often defined as d_{hkl}, where d_{hkl} is a vector extending from the origin to the plane (hkl) and is normal to hkl (Speakman, 2012). The diffracted X-rays detected by the diffractometer produces a series of peaks that build a characteristic "fingerprint" of the material or crystal under

investigation. Such peaks are generated according to Bragg's law of diffraction and a schematic representation is shown in Figure 3.13. When the incoming X-rays collide with several planes of atoms, the structure of the materials is such that the deeper the plane, the longer the distance travelled by the beam. The implication of this is that it will result in the reflected beams being *out of phase* (meaning that the crests and troughs of the waves will not be in alignment) (Kellner *et al.*, 2004; Hammond, 1992).
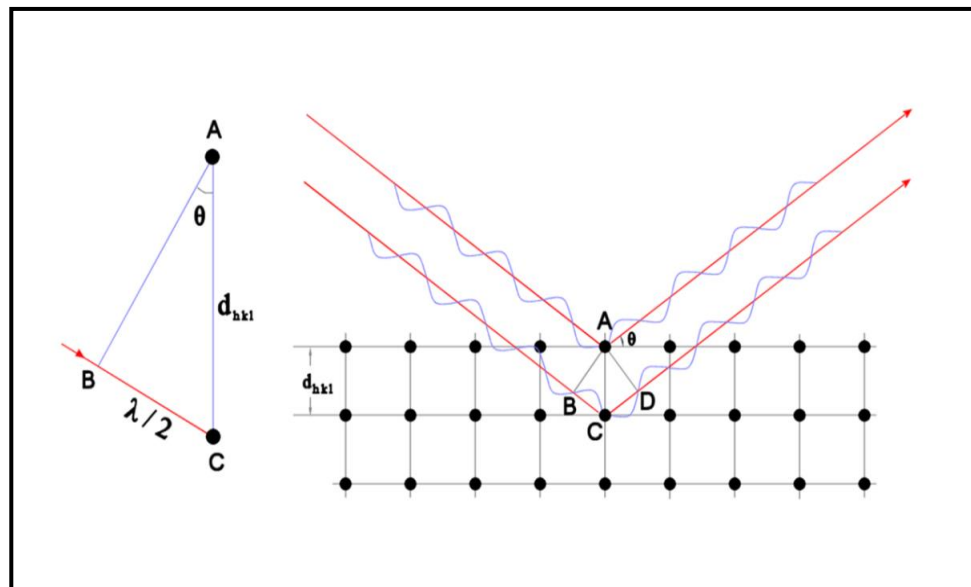
Figure 3.14: Schematic representation of Bragg's law
(Clearfield *et al.*, 2008; Cullity and Stock, 2001; Hammond, 1992)

The XRD diffractometer has three main components; the goniometer, detector and monitor. The goniometer consist of a high voltage transformer X-ray control, the X-ray tube, sample holder and a goniometer control detector high voltage PHA as shown in Figure 3.14. X-ray diffraction patterns may be obtained from both single crystals or from a powder sample depending on the type of analysis that is desired. Single crystals are used when a detailed analysis of the molecular structure is required and has been the basis for determining the atomic arrangement within crystalline materials. Powder X-ray diffraction has a more limited reach and is used mainly to identify materials given their fingerprint pattern. Commonly used diffractometers have X-ray wavelength (λ) fixed such as CuKα (1.5418Å) or MoKα (0.7107 Å); hence a family of planes produces a diffraction peak only at a specific angle 2θ (Kellner *et al.,* 2004; Clearfield *et al*., 2008). X-ray powder diffractometers are typical designed to use the Bragg-Bretano geometry, wherein the

diffraction vectors is always normal to the surface of the sample having the following characteristics:

➢ The incident angle, ώ is defined between the X-ray source and the sample

➢ The diffraction angle, 2θ is defined between the incident beam and the detector

➢ The incident angle ώ is always ½ of the detector angle 2 θ as shown in Figure 3.15.
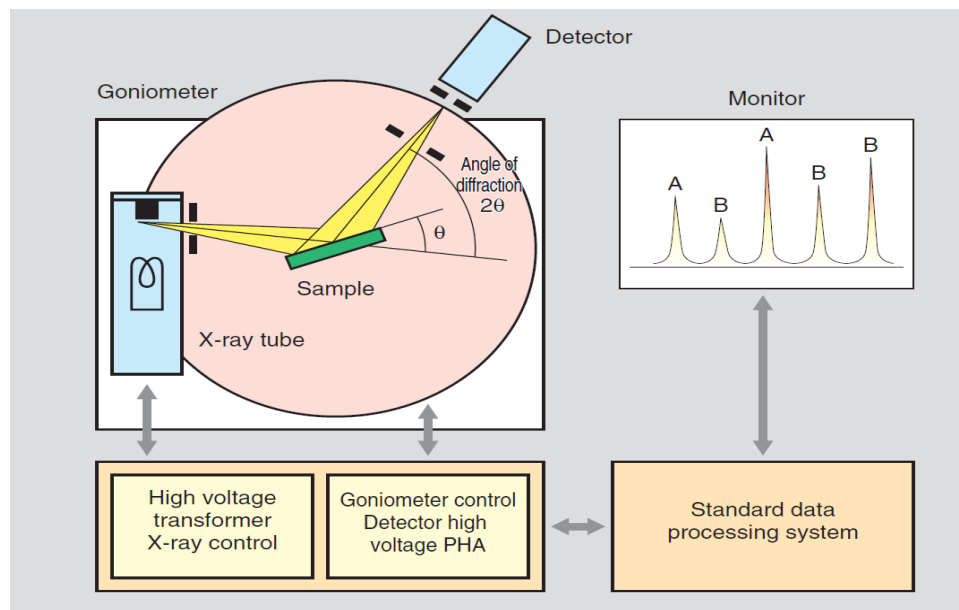
Figure 3.15: Schematic Representation of X-ray diffractometer (Shimadzu, 2010)
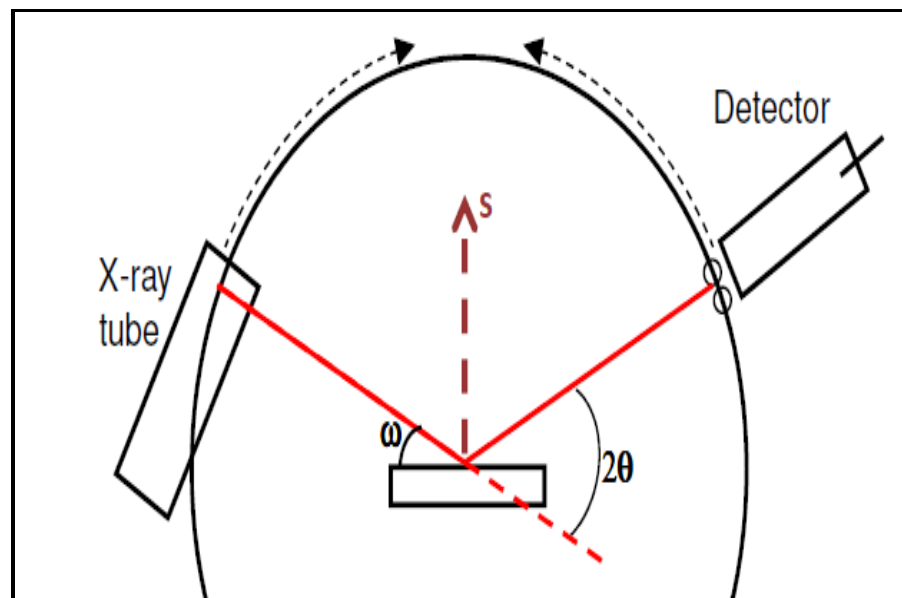
Figure 3.16: Schematic of Bragg-Bretano geometry for the X-ray diffractometer (Speakman, 2012)

Diffraction patterns can offer a lot of other information such as arrangement of atoms, nature of chemical bonds and orientation of molecules. Qualitative analysis of XRD patterns involves the identification of a phase or phases in a sample of interest with standard XRD patterns existing in the XRD database. The relative estimation of proportions of different phases in multiple phase specimens are carried out by comparing peak intensities attributed to the identified phase. Quantitative XRD analysis is used to determine the amounts of different phases in multi-phase samples and may involve the characteristic determination of single phase crystal structure, shape and size (Connolly, 2010). Here the determination of the structural characteristics and phase proportions with quantifiable numerical precision can be carried out using the experimental data. This may involve the use of standard patterns and structural data to initiate the modelling of the diffraction pattern in a way that the calculated pattern(s) is similar to the experimental patterns (Clearfield *et al*., 2008; Connolly, 2010).

In this study powdered XRD was used to analyse the residue adsorbents and the cellulose crystallinity (CrI) was calculated based on formula in Eqn. (3.7) (Xiao *et al*., 2011 and Segal *et al*., 1959) as follows:

$$CrI(\%) = \left[\frac{I_{002} - I_{am}}{I_{002}}\right] X\ 100 \qquad\qquad (3.7)$$

Where, I_{002} is the intensity of the crystalline region in the residue at 2θ about $22.5°$

I_{am} is the intensity of the amorphous region (cellulose, hemicellulose and lignin) at a baseline at 2θ about $18.7°$. Certain literatures have also observed this peak at $16.4°$ (Xiao *et al*., 2011). The X-ray diffractometer was used to determine the degree of crystallinity of the residue adsorbents used in this study as described in section 4.3.6 and discussed in chapters 5.6 of this study.

3.8 Inductively coupled plasma-optical emission spectrometry (ICP-OES)

The inductively coupled plasma-optical emission spectrometer (ICP-OES) is used to determine concentrations of a wide range of elements in solution. ICP-OES is a fast multi-element technique used for a wide range of elements in the periodic table with a linear range and moderate-low detection limits (~ 0.2 – 100 ppb). The ICP-OES consist of three

general steps: ionisation, excitation and emission. The instrument uses an ICP source-plasma (ionised gas) to dissociate the sample into its constituent atoms or ions, exciting them to a level where they emit light of a characteristic wavelength (Manning and Grow, 1997).

Inductively Coupled Plasma Optical Emission Spectrometry is a technique ideally suited for the analysis of naturally occurring materials, including water, sediments, soils, rocks, minerals and biological matter. One of the most important advantages of ICP-OES results from the excitation properties of the high temperature sources used in OES. These thermal excitation sources can populate a large number of different energy levels for several different elements at the same time. All of the excited atoms and ions can then emit their characteristic radiation at nearly the same time. This results in the flexibility to choose from several different emission wavelengths for an element and in the ability to measure emission from several different elements concurrently. However, a disadvantage associated with this feature is that as the number of emission wavelengths increases, the probability also increases for interferences that may arise from emission lines that are too close in wavelength to be measured separately) (Thomas, 2008; Boss and Fredeen, 1997).

3.8.1 Principles of ICP

The technique is based upon the spontaneous emission of photons from atoms and ions that have been excited in a RF discharge. Liquid and gas samples may be injected directly into the instrument, while solid samples require extraction or acid digestion so that the analytes will be present in a solution. The sample solution is converted to an aerosol and directed into the central channel of the plasma as indicated in Figure 3.16. At its core the inductively coupled plasma (ICP) sustains a temperature of approximately 10,000 K, so the aerosol is quickly vaporized. Analyte elements are liberated as free atoms in the gaseous state as shown in Figure 3.16. Further collisional excitation within the plasma imparts additional energy to the atoms, promoting them to excited states (Hou and James, 2000). Sufficient energy is often available to convert the atoms to ions and subsequently promote the ions to excited states. Both the atomic and ionic excited state species may then relax to the ground state via the emission of a photon as shown in Figure 3.17. These photons have characteristic energies that are determined by the quantized energy level structure for the atoms or ions. Thus the wavelength of the photons can be used to identify the elements from which they originated. The total number of photons is directly proportional to the concentration of the originating element in the sample (Hou and James, 2000).
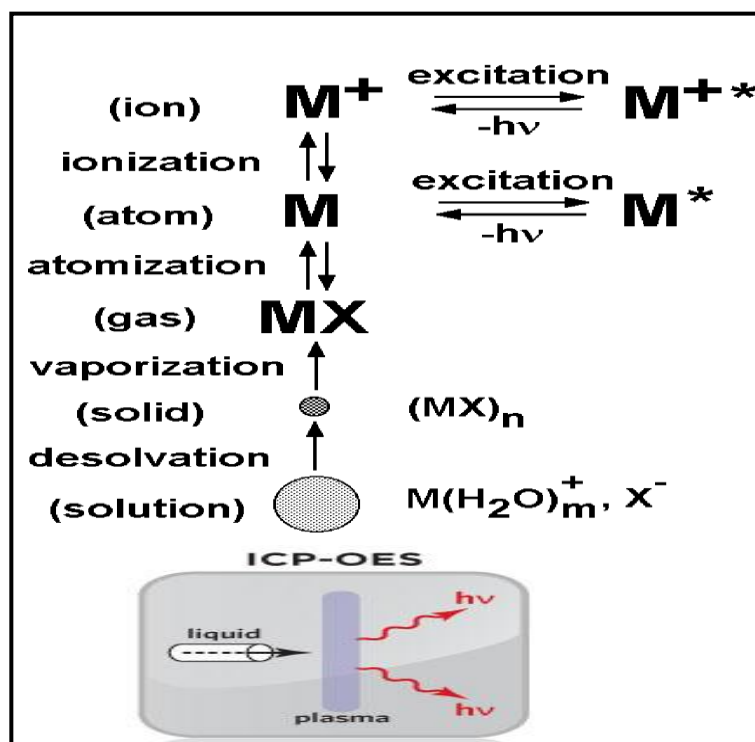
Figure 3.17: Operating Principle of ICP-OES with on sample droplet introduction
(Boss and Fredeen, 1997; EAG, 2013)
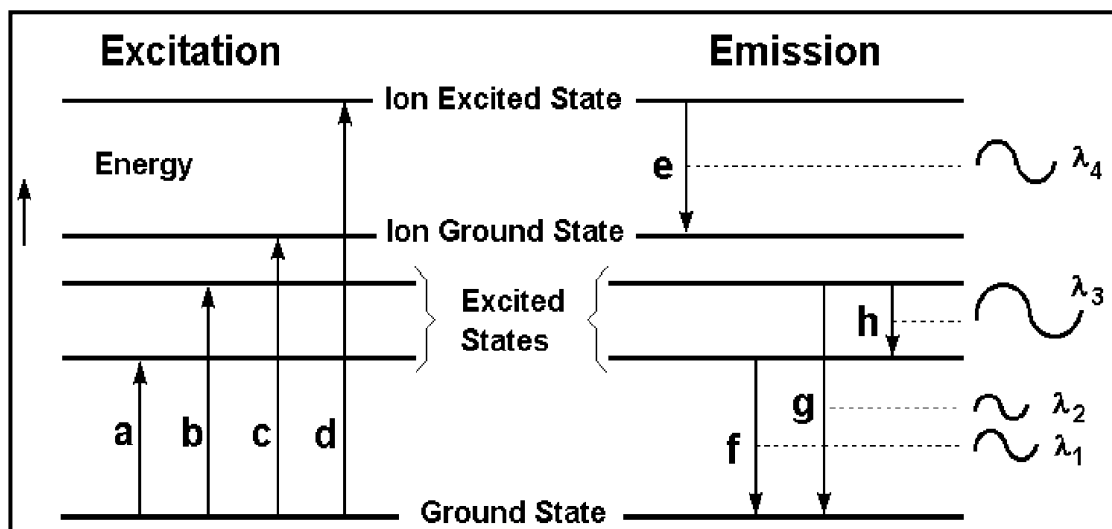
Figure 3.18: Energy transition diagram where **a** & **b** -excitation, **c**-ionisation,
d-ionisation/excitation, **e**-ion emission, **f, g** & **h**-atom emission (Boss and Fredeen, 1997)

The instrumental technique is thus based on the principle of measurement of light emitted at element-specific characteristic wavelength from these thermally excited analyte ions. Thus the resulting atomic emission emanating from the plasma is consequently separated

and measured in an optical emission spectrometer (OES) using either a radial or axial configuration, here the signals are collected with a lens or mirror, and imaged onto the entrance slit of a wavelength selection device. The intensity of the emitted light is then measured and converted into an elemental concentration by comparison with a calibrated standard (EAG, 2013; Hou and James, 2000). Single element measurements can be performed cost effectively with a simple monochromator/photomultiplier tube (PMT) combination, and simultaneous multi-element determinations are performed for up to 70 elements with the combination of a polychromator and an array detector.

The main features of the ICP-OES are the nebuliser, spray chamber, ring torch, and detector as shown in Figure 3.17. When plasma energy from the ionised argon gas is applied to a sample, the component elements (atoms) are ionised excited. When the excited atoms return to low energy position, emission rays (spectrum rays) are released and the emission rays that correspond to the photon wavelength are measured. The element type is determined based on the position of the photon rays, and the content of each element is determined based on the rays' intensity (Boss and Fredeen, 1997).
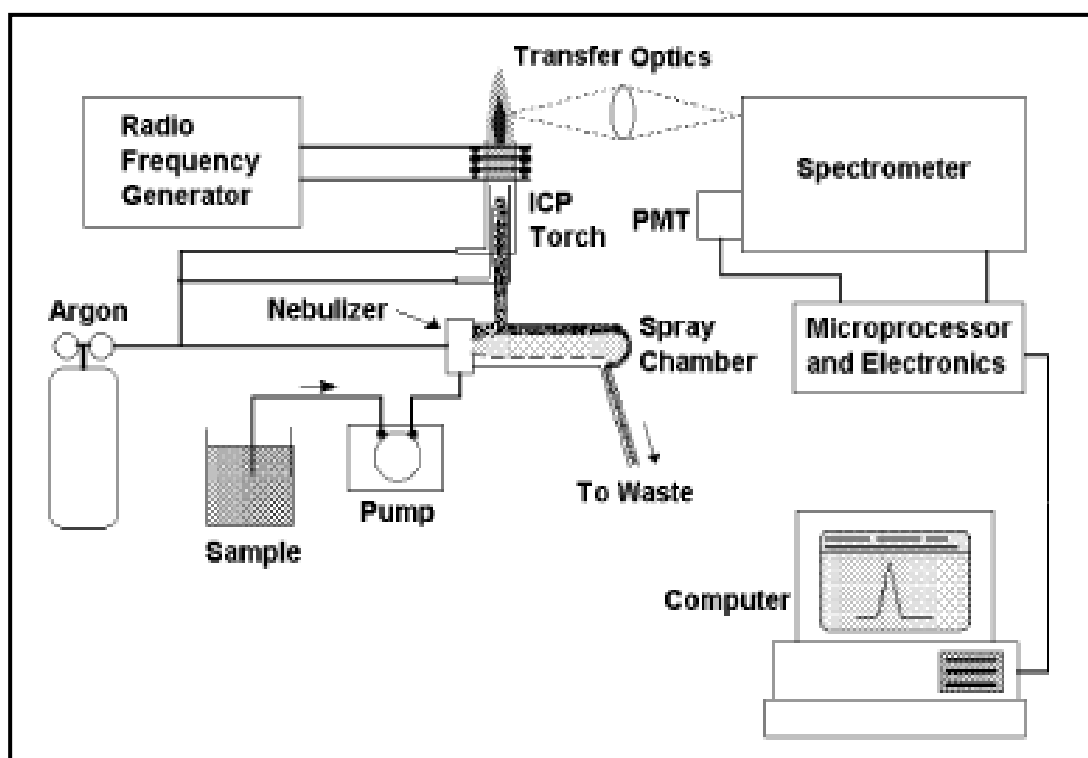
Figure 3.19: Major components of ICP-OES equipment (Boss and Fredeen, 1997)

Before this can be achieved, the sample which is usually in liquid form is pumped via a pump (1 mlmin^{-1}) into the nebulizer where it is converted into a fine aerosol by its contact

with argon gas. The fine droplets of the aerosol, which represent only $1 - 2\%$ of the sample, are separated from larger droplets by means of a spray chamber. The fine aerosol then exits the spray chamber and passes through the ring torch. The plasma is used to generate photons of light by the excitation of electrons from a ground-state atom to a higher energy level. When the electrons "fall" back to ground state, wavelength-specific photons are emitted that are characteristic of the element of interest (Boss and Fredeen, 1997; Thomas, 2008).

The light emitted by the excited atoms and ions in the plasma is measured to obtain information about the sample. Since the excited species in the plasma emit light at several different wavelengths, the emission from the plasma is polychromatic. This polychromatic radiation must be separated into individual wavelengths so the emission from each excited species can be identified and its intensity can be measured without interference from emission at other wavelengths. The separation of light according to wavelength is generally done using a monochromator, which is used to measure light at one wavelength at a time, or a polychromator, which can be used to measure light at several different wavelengths at once. The actual detection of the light, once it has been separated from other wavelengths, is done using a photosensitive detector such as a photo-multiplier tube (PMT) or other advanced detector techniques such as a charge-injection device (CID) or a charge-coupled device (CCD) (Boss and Fredeen, 1997).

The concentration of an element in a sample is determined using plots of emission intensity versus concentration (calibration curves). Solutions with known concentrations of the elements of interest, *standard solutions,* are introduced into the ICP and the intensity of the characteristic emission for each element or analyte is measured. These intensities can then be plotted against the concentrations of the standards to form a calibration curve for each element. When the emission intensity from an analyte is measured, the intensity is checked against that element's calibration curve to determine the concentration corresponding to that intensity (Boss and Fredeen, 1997).

The main analytical advantages of the ICP over other excitation sources originate from its capability for efficient and reproducible vaporization, atomization, excitation, and ionization for a wide range of elements in various sample matrices. This is mainly due to the high temperature which can reach temperatures up to $6000 - 7000$ K, in the observation zones of the ICP. This temperature is much higher than the maximum temperature of flames or furnaces (3300 K). The high temperature of the ICP also makes it capable of

exciting refractory elements, and renders it less prone to matrix interferences. Other electrical-discharge-based sources, such as alternating current and direct current arcs and sparks, and the MIP, also have high temperatures for excitation and ionization, but the ICP is typically less noisy and better able to handle liquid samples. In addition, the ICP is an electrodeless source, so there is no contamination from the impurities present in an electrode material (Hou and James, 2000). The ICP-OES technique was used to determine the initial and final concentration of the two metal ions in solution before and after adsorption as described in section 4.3.8 and discussed in chapters 5-9 of this study.

3.9 Summary

The major adsorbents and sorption characterisation techniques used in this study have been reviewed and the operating principles of these instrumental techniques and their application have also been examined. The characterisation techniques considered include attenuated total reflectance Fourier transform infra-red spectroscopy (ATR-FTIR) employed for functional group analysis; nitrogen-BET adsorption for determining the surface area and porosity of the adsorbent materials; thermogravimetric analysis used to evaluate the thermal degradation profile and proximate composition of the residues; scanning electron microscopy (SEM) used for the determination of surface morphology of the adsorbents; energy dispersive X-ray (EDAX) used to analyse the relative elemental composition of materials; X-ray fluorescence used to ascertain the inorganic elemental composition of the agricultural residues; the carbon, hydrogen, nitrogen, sulphur and oxygen (CHON) elemental analysis of the residues gave insight into the organic composition of the residue; while photon correlation spectroscopy (PCS) was used for zeta potential measurement. X-ray diffractometry was also reviewed and it was used to determine the crystallinity of the residues. The concentration of Pb(II) and Cd(II) ions the aqueous solutions before and after adsorption were determined using inductively coupled plasma-optical emission spectroscopy (ICP-OES). These characterisation techniques were used to elucidate the physical and chemical properties of the different residues and adsorbents developed and used in this study. In addition, characterisation studies were carried out to give insight into the specific nature of these materials with the aim of understanding their structure-property relationship which can be exploited to optimise their metal ion adsorption potential.

CHAPTER FOUR

MATERIALS AND EXPERIMENTAL METHODS

CHAPTER FOUR

4.0 Materials and experimental methods

4.1 Agricultural residue identification and collection

The different agricultural residues namely: oil palm fruit fibre (OPF), coconut shell fibre (CNF), cocoa pod (CCP), plantain peel (PTH), sweet potato peel (PTP), cocoyam peels (CCYB) and white yam tuber peels (YTB) were obtained from two different sampling locations in Uyo, Akwa Ibom in Nigeria as indicated in the map below Figure 4.1. The samples were washed with hot deionised water, dried at 100°C, kept in sealed polypropylene bottles and transported to Manchester for the development of adsorbents for metal ion removal.

Figure 4.1: Map of Residue Collection Site – Akwa Ibom State in Nigeria.

The experimental protocols used in this research from the collection of raw residues to the utilisation of these residues as adsorbents in the removal of Cd(II) and Pb(II) from aqueous solutions are summarised in Figure 4.2 .
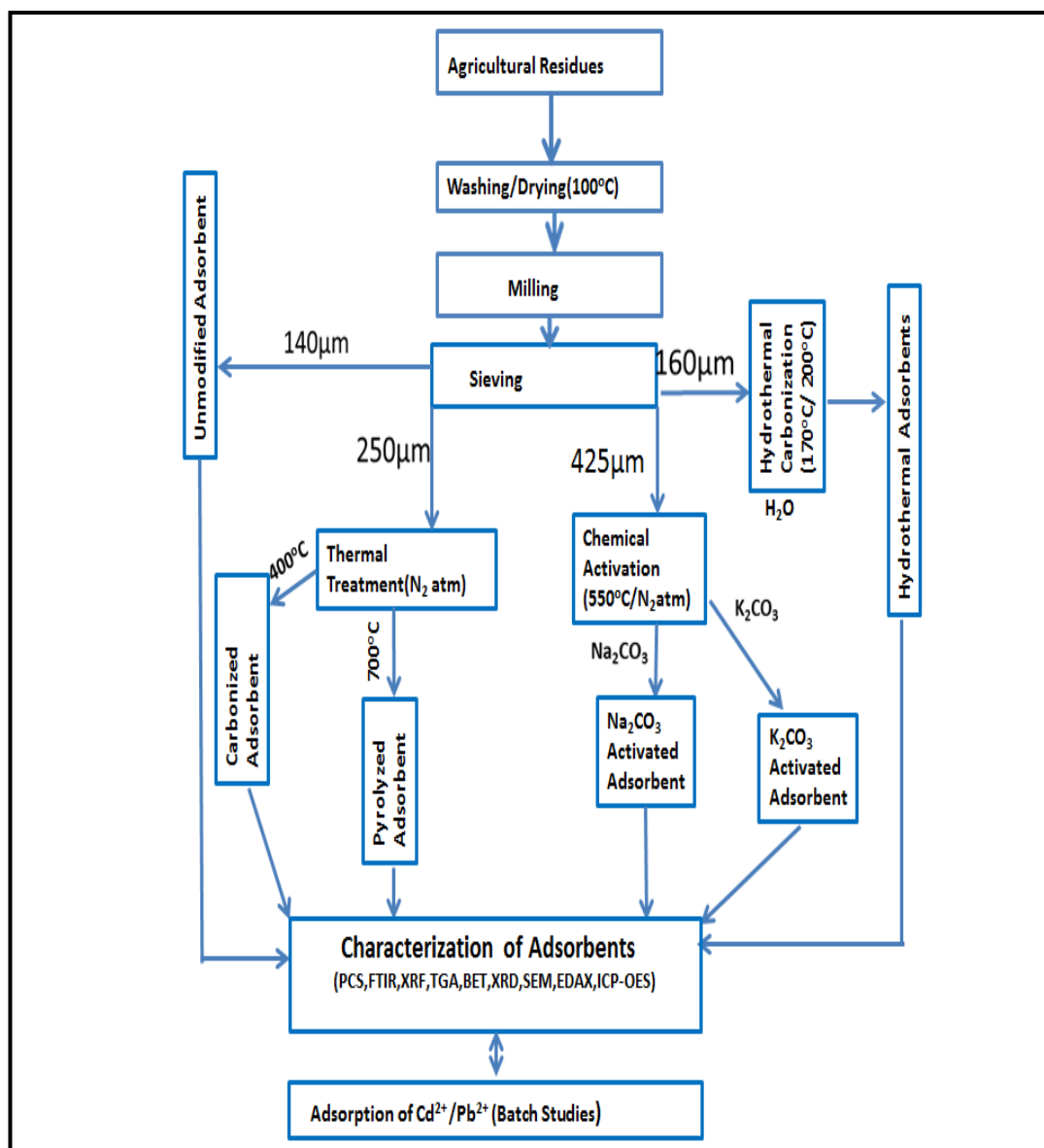
Figure 4.2: Protocols for Residue Conversion & Utilisation as adsorbents

4.2 Adsorbent preparation and particle size separation

On collection, residues were washed with hot deionized water to remove dirt and colour and oven dried at $100°C$ for 24 hours. The dried residues were pulverized using a Coors porcelain mortar and pestle. Thereafter, residues were separated according to their particle sizes carried out by sequential sieving through a 7-tray laboratory test sieve shaker (E.V.L.1. by Endecott's Limited London). Sieves with aperture sizes of 26 μm, 32 μm, 45

µm, 140 µm, 160 µm, 250 µm and 425 µm were used in this study, as shown in Figure 4.3. The shaker was operated for 60 minutes.

Figure 4.3: A 7 Tray-Laboratory Test Sieve Shaker

4.2.1 Unmodified adsorbents

After the sieving, residues in the 140 µm sieve tray were stored in clean polypropylene bottles and labelled as unmodified residues and stored at room temperature for further use in adsorption studies. This sample set was labelled as the unmodified adsorbent with the following nomenclature: OPFS- unmodified oil palm fruit fibre residue. (CCPS) unmodified cocoa pod residue. (CNFS) unmodified coconut shell fibre residue. (PTHS) unmodified plantain peel residue. (CCYBS) unmodified cocoyam peel residue. (PTPS) unmodified sweet potato peel residue. (YTBS) unmodified white yam peel residue. Samples with sizes of 425, 250 and 160 µm in each residue group were stored for the modification and activation processes in order to produce the carbonized, pyrolysed, hydrothermally carbonized and chemically activated carbon adsorbents as indicated in Figure 4.2.

4.2.2 Pyrolysed adsorbents

Samples with 250 μm diameter were weighed and then pyrolysed in a stainless steel tubular reactor converting them into pyrolysed adsorbents. The temperature ramps used in the pyrolysis was illustrated below in Figure 4.4. The two isothermal steps at 250°C and 400°C were designed to ensure an efficient removal of volatile compounds in the residue. The maximum pyrolysis temperature of 700°C was chosen.
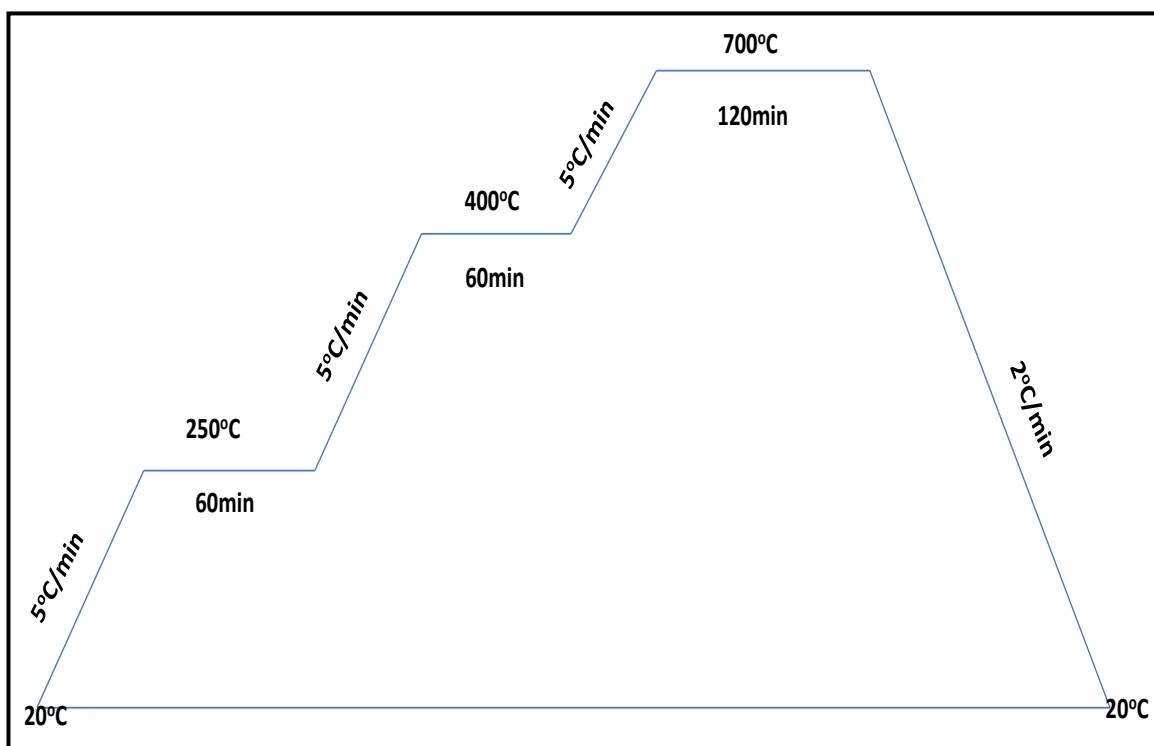
Figure 4.4: Temperature programme of pyrolysis under Nitrogen Atmosphere in a Tubular Furnace.

4.2.2.1 Operating conditions for tubular furnace

In the pyrolysis sequence, a known mass of each residue was placed in a stainless steel sample holder and inserted into a horizontal steel tubular reactor with length of 75 cm and internal diameter of 6.5 cm as shown in Figure 4.5.

Figure 4.5: Stainless Steel Sample Holder and Horizontal Steel Tubular Reactor used for pyrolysis.

The steel tubular reactor was inserted into a ceramic horizontal tubular furnace (Severn Furnace Ltd-Bristol) of length and internal diameter of 46 cm and 8 cm respectively. The horizontal tubular furnace was controlled via a Eurotherm temperature controller and a thermocouple was used to monitor the temperature in the furnace. The nitrogen flow was introduced into the furnace via a rotameter. The pyrolysis was carried out in a fume cupboard to extract the exhaust gases and the schematic diagram is indicated in Figure 4.6. In a routine operation, the steel tube was firstly purged with N_2 at a flow rate of 100 mlmin^{-1} for 20 minutes to ensure an inert atmosphere. Then a dry sample was carefully inserted into the central region of the steel tube reactor ensuring the uniform heating of materials. Subsequently, the nitrogen flow rate was adjusted to 200mlmin^{-1} for the pyrolysis process according to the heating programme shown in Figure 4.4.
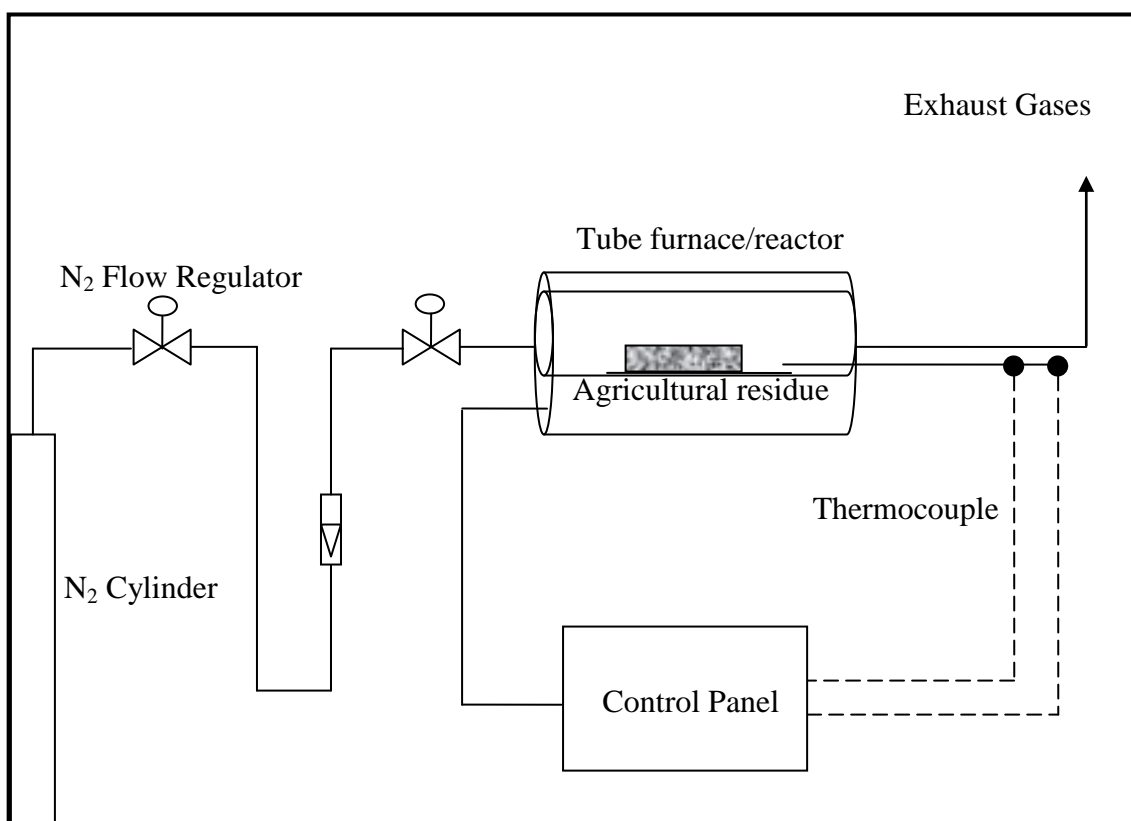
Figure 4.6: Schematic Representation of Pyrolysis of agricultural residue using a Tubular Steel Reactor and tube-type ceramic furnace.

Thereafter, the furnace was cooled at the rate of 2°Cmin^{-1} until it reached 20°C after cooling the furnace to room temperature, materials in the furnace was kept under N$_2$ atmosphere for 4 hours and then removed from the furnace. The resulting residues were then washed with hot deionized water and dried in an oven under air at 110°C. Dried pyrolysed adsorbents were initially weighed and thereafter pulverized to reduce the particle size. The pulverized adsorbents were then sieved through the 140 μm sieve tray and the adsorbents retained were preserved in polypropylene bottles for subsequent adsorption and characterisation studies. Materials from the pyrolysis sequence were labelled as follows: (OPFPCA) pyrolysed oil palm fruit fibre carbon adsorbent, (CCPPCA) pyrolysed cocoa pod carbon adsorbent, (CNFPCA) pyrolysed coconut shell fibre carbon adsorbent, (PTHPCA) pyrolysed plantain peel carbon adsorbent, (CCYBPCA) pyrolysed cocoyam peel carbon adsorbent, (PTPPCA) pyrolysed sweet potato peel carbon adsorbent and (YTBPCA) pyrolysed white yam peel carbon adsorbent. The yield of materials from the pyrolysis treatment was determined by using eqn. (4.1):

$$Yield \ (\%) = \frac{Dry \ Weight \ of \ final \ carbon \ after \ carbonisation (g)}{Dry \ Weight \ of \ precusor \ before \ carbonisation (g)} \times 100 \qquad (4.1)$$

4.2.3 Carbonized adsorbents

The 250 μm portions of each residue were also weighed into a stainless steel sample holder and inserted into the tubular stainless steel tube and converted into carbonised adsorbent using the heating sequence outlined below in Figure 4.7. One isothermal condition at 250°C was used to aid the removal of volatile compounds in the residue matrix.
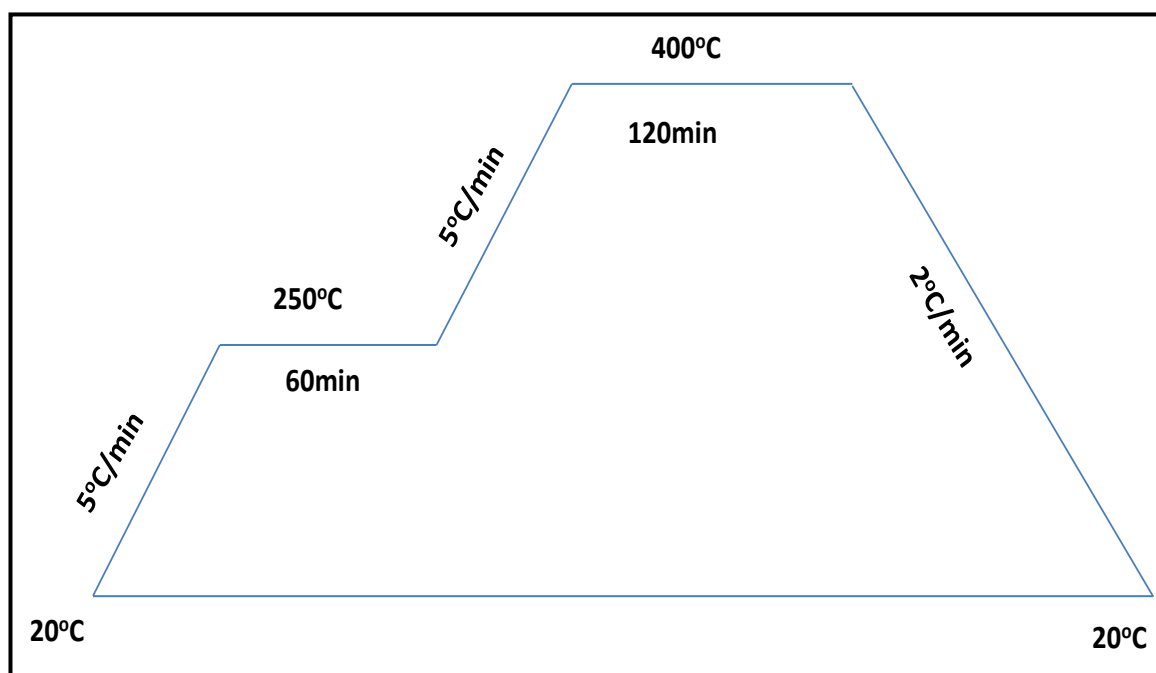
Figure 4.7: Schematic heating sequence for carbonized adsorbent preparation in limited air atmosphere in a tubular furnace.

The furnace operating conditions is same as reported in Section 4.2.2.1 with the system heated from 20°C at the rate of 5°Cmin^{-1} leading up to a maximum of 400°C maintained for 120 minutes with one isothermal step at 250°C in limited air environment. Thereafter, the furnace was cooled at the rate of 2°Cmin^{-1} until it reached 20°C. The furnace was then allowed under nitrogen flow for 4 hours, thereafter the carbonized samples were removed and washed with deionized water and dried at 110°C. Dried carbonised adsorbents were initially weighed and thereafter pulverized to reduce the particle size. The pulverized carbonised adsorbents were then sieved through the 140 μm sieve tray and the adsorbents retained were stored in clean polypropylene bottles for used in adsorption and characterisation studies.

This adsorbent set was labelled as follows: (OPFCA) carbonised oil palm fruit fibre carbon adsorbent, (CCPCA) carbonised cocoa pod carbon adsorbent, (CNFCA) carbonised coconut shell fibre carbon adsorbent, (PTHCA) carbonised plantain peel carbon adsorbent,

(CCYBCA) carbonised cocoyam peel carbon adsorbent, (PTPCA) carbonised sweet potato peel carbon adsorbent and (YTBCA) carbonised white yam peel carbon adsorbent. The yield of product from the carbonisation treatment is described as a percentage using the weight of the carbon obtained after carbonization, washing and drying to that of the dry residue prior to chemical activation as shown in eqn. (4.1).

4.2.4 Chemically activated adsorbents

Chemical activation of the agricultural residues was carried out using two salts; sodium carbonate (Na_2CO_3) and potassium carbonate (K_2CO_3) and the heating sequence is illustrated in Figure 4.8.
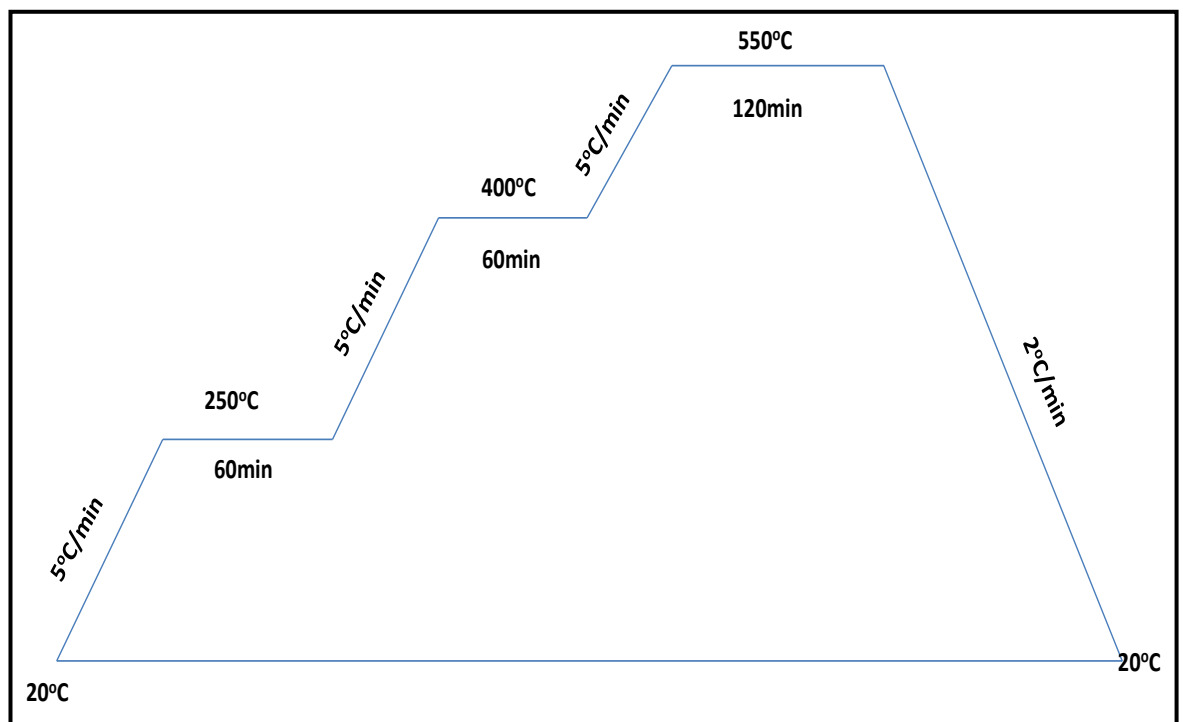
Figure 4.8: Schematic heating sequence for chemically activated carbon adsorbent preparation using Na_2CO_3 and K_2CO_3 activating agent in nitrogen atmosphere.

In the chemical activation of raw materials for the production of activated carbon, the precursors are usually impregnated with chemical agents in a three step process of carbonisation at temperatures between 300 and 700°C, impregnation with chemical agents and activation at temperatures between 700 and 1000°C (Ioannidou and Zabaniotou, 2007; Zhang *et al*., 2014). However, in this study the chemical activation of the agricultural residues involved the carbonization and activation of each residue in two step process of impregnation followed by chemical activation. This approach is taken in order to reduce the time and energy consumed in the activated carbon production sequence. A range of

chemical agents are often used in the chemical activation process but the most commonly used reagents include: phosphoric acid (H_3PO_4), zinc chloride ($ZnCl_2$), sulphuric acid (H_2SO_4), potassium hydroxide (KOH) and sodium hydroxide (NaOH). These reagents act as dehydrating agents and as oxidants so that carbonization and activation can take place simultaneously (Hsi *et al.,* 2011). The focus of this study however was on the utilisation of sodium carbonate (Na_2CO_3) and potassium carbonate (K_2CO_3) as precursors because of two reasons:

- Their reduced polluting effect
- The less deleterious effect they have on the activated carbon matrix.

For the chemical activation procedure, the 425 µm portions of each of the different residues were utilized for the production of activated carbon in a two-step process. One important parameter to be considered in the utilization of chemical agents in the production of activated carbon is the ratio of the mass of chemical activating agent to the mass of residue to be activated called the impregnation ratio and the relationship is given as:

$$Impregnation\ ratio\ (IR) = \frac{weight\ of\ chemical\ activating\ agent\ (g)}{weight\ of\ precursor\ residue\ (g)} \times\ 100\quad (4.2)$$

The chemical activation process involved the weighing out of a known mass (200 g) of each 425 µm portion into an Erlenmeyer beaker of 2 L. 10 g of the activating agents Na_2CO_3 and K_2CO_3 were weighed into the beaker and 500 ml of deionized water was added and the contents were mixed and kept in contact for 24 h. The mixtures were subsequently oven dried at 110°C for 24 h and thereafter pyrolysed in the tubular furnace described in Figure 4.5 using the heating scheme illustrated in Figure 4.8 under nitrogen atmosphere. The furnace operating conditions is as described in Section 4.2.2.1 with the system heated from 20°C at the rate of 5°Cmin[-1] leading up to a maximum of 550°C maintained for 120 minutes with two isothermal steps at 250 and 400°C. Thereafter, the furnace was cooled at the rate of 2°Cmin[-1] until it reached 20°C. The furnace was then allowed under nitrogen flow for 4 hours to cool.

After the cooling of the furnace, the obtained char was washed with hot deionized water to eliminate residual matter until the pH of the washing water was neutral. The wet char was dried in an oven at 110°C for 24 h. The dried activated carbon products obtained were initially weighed and thereafter pulverized in a mortar using a ceramic pestle to reduce the particle size. The pulverized activated carbon adsorbents were sieved through the 140 µm

sieve tray and the adsorbents retained were stored in polypropylene bottles for subsequent use in characterisation and adsorption studies. The Na_2CO_3 chemically activated adsorbent set was labelled as follows: (OPFNCA) Na_2CO_3 activated oil palm fruit fibre carbon adsorbent, (CCPNCA) Na_2CO_3 activated cocoa pod carbon adsorbent, (CNFNCA) Na_2CO_3 activated coconut shell fibre carbon adsorbent, (PTHNCA) Na_2CO_3 activated plantain peel carbon adsorbent, (CCYBNCA) Na_2CO_3 activated cocoyam peel carbon adsorbent, (PTPNCA) Na_2CO_3 activated sweet potato peel carbon adsorbent and (YTBNCA) Na_2CO_3 activated white yam peel carbon adsorbent. The K_2CO_3 chemically activated adsorbent set was labelled as follows: (OPFKCA) K_2CO_3 activated oil palm fruit fibre carbon adsorbent, (CCPKCA) K_2CO_3 activated cocoa pod carbon adsorbent, (CNFKCA) K_2CO_3 activated coconut shell fibre carbon adsorbent, (PTHKCA) K_2CO_3 activated plantain peel carbon adsorbent, (CCYBKCA) K_2CO_3 activated cocoyam peel carbon adsorbent, (PTPCA) K_2CO_3 activated sweet potato peel carbon adsorbent and (YTBKCA) K_2CO_3 activated white yam peel carbon adsorbent. The activated carbon yield is described as a percentage using the weight of the carbon obtained after carbonization, washing and drying to that of the dry residue prior to chemical activation as shown in eqn.4.1.

4.2.5 Hydrothermally carbonized adsorbents

The hydrothermally carbonized adsorbents were produced using a weighed amount of each of the agricultural residues with the particle size of 160 μm. 50 g of each residue was weighed into a 150 ml volume Teflon lined autoclave shown in Figure 4.9 below and 80 ml of deionized H_2O was added and the mixture stirred for 3 minutes. An amount of water was added to ensure that the residues were completely submerged in the Teflon autoclave.

Figure 4.9: Teflon lined autoclave

Thereafter, the autoclave was closed securely and inserted into a Thermostat Vacuum oven. The sequence of the hydrothermal carbonisation of each residue is illustrated in Figure 4.10 below.
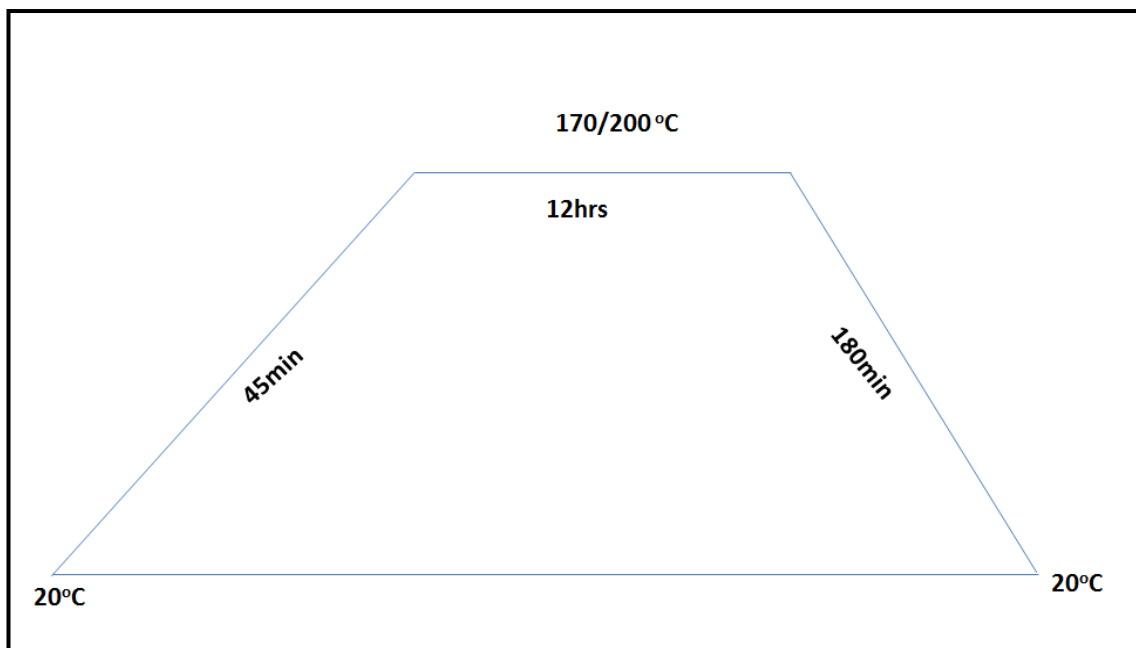
Figure 4.10: Schematic heating sequence for hydrothermally carbonized adsorbent preparation

Two different temperatures were chosen for the hydrothermal carbonisation treatment (170°C and 200°C). The oven was heated to 170°C/200°C and that temperature was maintained for 12 hrs. At the end of the heating sequence, the oven was switched off and allowed to cool for 180 minutes. The hydrothermally carbonised products were subsequently filtered off, washed in hot deionized water and dried at 110°C in an air oven. The oven dried hydrothermal adsorbents were weighed and thereafter pulverized in a mortar using a ceramic pestle to reduce the particle size. The pulverized hydrothermal adsorbents were then sieved through the140 µm sieve tray and the adsorbents retained were stored in polypropylene bottles and preserved for utilisation for adsorption and characterisation studies.

The adsorbents produced therein were labelled using the following nomenclature: (OPFS-HTC170 & 200) hydrothermally carbonised oil palm fruit fibre adsorbent, (CCPS-HTC170& 200) hydrothermally carbonised cocoa pod adsorbent, (CNFS-HTC170 & HTC200) hydrothermally carbonised coconut shell fibre adsorbent, (PTHS-HTC170 & HTC200) hydrothermally carbonised plantain peel residue, (CCYBS-HTC170 & HTC200) hydrothermally carbonised cocoyam peel adsorbent, (PTPS-HTC170 & HTC200)

hydrothermally carbonised sweet potato peel adsorbent and (YTBS-HTC170 & HTC200) hydrothermally carbonised white yam peel adsorbent.

4.2.6 Commercial activated carbon

Commercial activated carbon (granular, diameter > 425µm, Chemviron Carbon sample F-400) was also utilised in this study as the benchmark and it was used as received without any further pre-treatment The commercial activated carbon was used as the benchmark material in adsorption experiments. The performances of developed adsorbents were compared with that of commercial activated carbon during the course of this study.

4.3 Adsorbent characterisation

The equipment and experimental conditions for characterising adsorbents are described in the following sections of this chapter.

4.3.1 Ash composition analysis of adsorbents

The ash content of all adsorbents was determined using the procedure described by the association of analytical communities AOAC (2000) and reported by Jun *et al.,* (2010). Crucibles with lids were initially dried in a furnace at 600 °C for 10 minutes. Then a dried adsorbent (1g) was added into the crucible. The crucible was thereafter inserted into a muffle furnace and heated at 600°C for 6 h, after which the furnace was allowed to cool naturally for 24 h. The ash content of materials was determined by eq. 4.3:

$$\text{Ash content (\%)} = \frac{(\text{ Weight of ash(g))}}{\text{weight of dried adsorbent(g)}} \times 100 \qquad (4.3)$$

4.3.2 Scanning electron microscopy (SEM) and Energy Dispersive X-ray (EDAX) Analysis

SEM/EDAX analysis was performed using FEI Quanta 200 Environmental SEM. 0.1 g of each sample was placed and pressed onto a carbon tab (9mm) (Agar Scientific) and mounted on a 0.5" SEM pin stubs (Agar Scientific) of length 6mm. All samples were coated with gold using an EMITECH K550X sputter gold coater prior to SEM analysis. Coating was carried out for 15 minutes. 7 samples mounted on the SEM pin stubs as shown in Figure 4.11 were placed inside the SEM instrument using tweezers for each analysis.

Figure 4.11: SEM samples for analysis mounted on SEM pin stubs.

The chamber was vacuumed for 10 minutes until a chamber pressure of 8.2×10^{-1} Torr was achieved. High voltage of 20.0 kV and filament current of 2.49 A were used in a routine analysis. The Y, Z and R coordinates of the microscope were adjusted to ensure maximum resolution and focus and thereafter the images of the samples in the chamber were recorded at different magnifications using a spot size of 4.0. The chemical composition of each sample was thereafter determined using the Energy Dispersive analysis system (EDAX) in the standard-less mode (manufacture's calibration) attached to the ESEM system. For this analysis, spot analysis was carried out on the adsorbent surface at a voltage 30 kV, a take-off angle of 35.49, spot size of 3.0, tilt 0.0 and the chemical composition was recorded using the EDAX Genesis software using the EDAX ZAF quantification (standard-less) method.

4.3.3 Zeta potential using photo correlation spectroscopy (PCS)

The zeta potential of the different adsorbents was measured using a Zetasizer 3000(Malvern Instruments). The samples were prepared by weighing 0.1 g of sample into 20 ml of 0.01 M NaCl solution at pH range of 2 – 12 for each adsorbent and agitating it in a shaker for 24 h. After which it was filtered and 10ml of each filtrate was taken out and put in a polypropylene bottle for analysis. The Zetasizer syringe was first of all cleaned and the analysis cell purged with deionized water using the syringe. The samples of each of the adsorbents at different pH values were inserted into the Zetasizer electrophoresis cell (3ml polystyrene curvette) with a light path of 10 mm. The zeta potential at each pH value was

measured and recorded. Three measurements were carried out and an average zeta potential for each adsorbent suspension at the different pH values were recorded.

4.3.4 BET surface area and pore volume/size analysis

The equipment employed was the Tristar 3000 Surface Area and Porosity analyzer, manufactured by *Micromeritics,* a schematic of the instrument is presented in Figure 4.12. Each sample was pre-conditioned by drying in an oven for 24 h at 150°C after which the samples were weighed into the BET sample tube and conditioned (degassed) for 2 hr at 200°C under nitrogen flow in order to eliminate moisture and other gases on the adsorbent using the *Micromeritics Flow prep 060 sample degas system*. Thereafter it was cooled under nitrogen flow for 5mins in the cooling section of the Flow prep system and thereafter weighed again to determine the actual weight of sample to be analysed. The sample (inside) the BET tube was exposed to nitrogen at 77 K, whereby the gas pressure in the tube with the sample was allowed to reach equilibrium before subsequent dosing and then a series of 55 successive incremental pressures of nitrogen doses were carried out to obtain an adsorption isotherm.
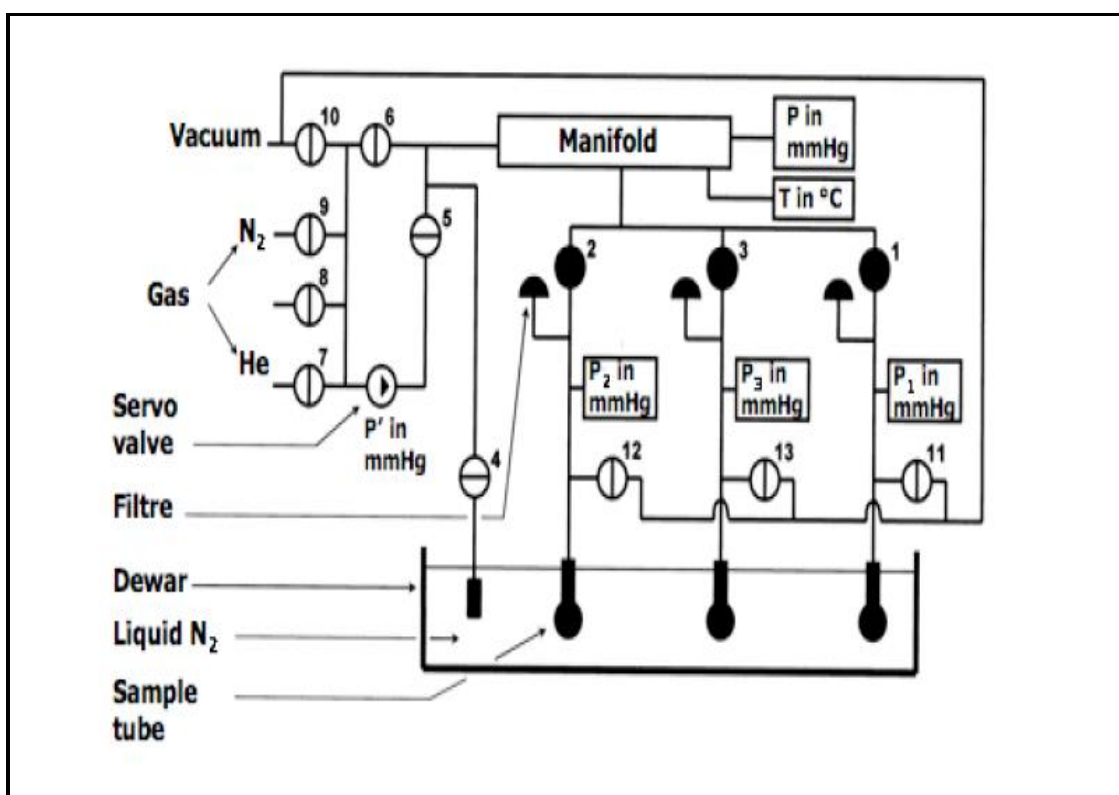
Figure 4.12: A schematic of the Tristar 3000 (Micromeritics, 2001)

The nitrogen isotherms were measured at 77 K with the adsorption and desorption sequences to determine the amount of N_2 adsorbed or desorbed from the surface of the adsorbent. The relationship between the partial pressure of nitrogen during the adsorption and desorption cycles were measured and recorded. P is the pressure at the level of the gas collector; P_1, P_2, and P_3 are the pressures at the level of the analysis port 1, 2 and 3; P' is the pressure requested by the servo-valve in a direction or in the other; T is the temperature inside the instrument. The software in the instrument Tristar 3000 v 6.06 provided the average total pore volume and pores size distribution of the material using the BJH theory. The BET surface area, the average pore volume and average pore size of each adsorbent was measured by the instrument.

4.3.5 X-ray fluorescence spectrometry

The XRF instrument used was a wave-length dispersive XRF (WDXRF) model AXIOS, manufactured by Panalytical. Samples were pelletized to 6mm masks, using wax as binder with a powder to wax ratio of 10g to 3g and analysed to determine the chemical composition of the residues.

4.3.6 X-ray diffractometry

X-ray powdered diffraction (XRPD) patterns were obtained using a Rigaku Miniflex X-ray powder diffractometer utilizing Cu Kα radiation (λ =1.5406 Å), operating over 5-60° 2θ at $1.5°$ min^{-1} with a 0.03° step, 30 kV voltage, and 15 mA current. Typically, 5 mg of sample was placed on a small aluminium sample attachment and smoothed to achieve a well packed level surface and analysed. After the analysis, the POWDLL converter software was used to retrieve the data into a format accessible via excel for pattern identification and interpretation using the JCPDS database.

4.3.7 Thermogravimetric analysis

The Thermogravimetric analyzer (TGA) used in the analysis of the agricultural residues was the TGA Q5000 manufactured by TA instrument. A known mass of the sample was weighed onto a ceramic pan and subjected to temperature profile analysis from 20°C to 500°C under nitrogen atmosphere to monitor the thermal degradation at a heating rate of $10^{o}C$ min^{-1}. The nitrogen flow rate was at kept at 50 $mlmin^{-1}$ and the temperature was equilibrated at 25°C and maintained for 5 minutes. Thereafter it was increased to 100°C at a rate of $10°Cmin^{-1}$ and maintained for 60 minutes. After this time interval it was ramped at

10°C min^{-1} up to 500 °C and maintained for 60 minutes. Subsequently, air was selected as to burn off the residue at a flow rate of 50mlmin^{-1} and the temperature ramped up to 600°C and maintained for 30 minutes. The thermal degradation profile of the sample gives information on the weight loss (%) with temperature and time using a single thermogravimetric curve. From the TG profile, information of the different components of the sample like the moisture content, volatile content, fixed carbon and ash composition were obtained using the TA Instruments Universal Analysis 2000 software.

4.3.8 Inductively coupled plasma-optical emission spectrometry

The instrument used was an ICP-OES model Vista-MPX, by Varian. The two elements measured were Cd(II) and Pb(II) ions. Calibration curves were prepared for two elements with 1, 10 20 and 50 mgL^{-1} standard solutions prepared from the 1000 mgL^{-1} ICP-standards of Pb(II) and Cd(II) ions. Blanks prepared using deionized H$_2$O were also used in each analysis step after the standards were analysed. A calibration using the standards was carried out after every 20 samples analysed. The concentration of the two metal ions in the prepared stock solutions and the aqueous solution before adsorption were determined using ICP-OES. The analysis of the concentration of samples for each metal ion concentration was carried out at specific wavelengths of 214.439, 226.502, 219.463 and 231.275 nm for Cd(II) ion and 220.353, 283.326 and 261.418 nm for Pb(II) ion.

4.3.9 Acidic/Basic Nature of Adsorbent

The acidic/basic character of each adsorbent in an aqueous system was estimated by pH measurement of the suspensions according to the following methods using deionized water, 18.2 MΩ cm^{-1} (Millipore).

- Calibration of the pH meter with buffer solutions of pH 4, 7 and 9.
- Preparation of CO$_2$-free deionized water by boiling 200 ml of deionized water for 60 minutes and allowing the water to cool.
- Placing 0.5 g of each adsorbent and 25 ml of the degassed water in a sealed conical flask and shaking for 24 h. Subsequently, the pH of each adsorbent suspension after 24 h of stirring was determined using an accumet$^{(R)}$ pH-meter (Fisher-Scientific).

4.3.10 Fourier transform infrared spectroscopy

Fourier transform infra-red spectroscopy was used to evaluate the functional groups in the unmodified adsorbents (residues). Prior to the analysis, the residue samples were dried in an air oven for 24 h at 110°C to remove the moisture contents of the sample. This was to eliminate any interference in the spectrum arising from H_2O content in the samples. The infra-red spectrums of the residues were then collected using attenuated total reflectance FT-IR spectroscopy (ATR-FT-IR). The instrument used was the Smart Golden Gate Thermo Nicolet Avatar 360 FT-IR with ATR probe. The spectra range was from 4000 – 400 cm^{-1} and the spectra were collected using a total average of 32 scans and a spectral resolution of 4 cm^{-1} with background subtraction. All the measurements were performed at room temperature. Infrared spectra were recorded using percentage transmittance mode where (A = log 1/T).

4.3.11 CHNS elemental analysis using elemental analyser

The carbon, hydrogen, nitrogen and oxygen content of the residues were determined using a Flash 2000 CHNS/O automatic elemental analyser manufactured by Thermo Fisher Scientific. The samples were weighed and the samples were then put into tin capsules and placed inside the Thermo-Fisher MAS 200R auto-sampler. It was thereafter dropped into an oxidation/reduction reactor kept at temperature of 1000°C. The exact amount of oxygen for the combustion was delivered into the combustion reactor and the reaction of the oxygen with the tin capsule was exothermic. This enabled the temperature to rise to 1800°C for a few seconds. At this high temperature both organic and inorganic substances in the residue were converted to their elemental gases. After combustion, the resulting gases were carried by a helium flow to a layer filled with copper where further reduction occurred. Thereafter, the gases were swept through a GC column and were separated in the chromatographic column. Finally, the component gases and their proportions were detected by a highly sensitive thermal conductivity detector (TCD) (Thermo Scientific, 2008). The C, H, S and N were thus calculated by the instrument and the oxygen content was determined by difference (Krotz and Giazzi, 2012).

4.3.12 Wet attrition resistance test

The attrition resistance of the adsorbents was determined using a modification of the wet attrition test procedure (Lima and Marshall, 2005). Two grams (2 g) of each adsorbent was weighed into a 20 mesh screen and 1 g of the amount retained on the mesh was weighed into a 250 ml Erlenmeyer flask. 100 ml deionized water was thereafter added to the flask and the suspension stirred for 24 h at 25°C on a magnetic stirrer at 200 rpm using ½ inch magnetic stir bars. After 24 h the suspension was poured into a 20 mesh screen and the retained adsorbent dried in an oven of 100°C for 24 h. Thereafter, the dried adsorbent was weighed using a Mettler Sauter RL 200 electric weighing balance (August Sauter GmbH, Switzerland). Three replicates of each measurement was carried out and the average taken. The percentage attrition was calculated for each adsorbent as follows:

$$Loss\ on\ Attr.(\%) = \frac{\text{Initial } wt.of\ adsorbent - Wt.of\ adsorbent\ retained\ (g)}{Initial\ adsorbent\ weight(g)} \times 100 \qquad (4.4)$$

4.4 Batch sorption

Standard stock solutions of 1000 mgL^{-1} of the two metal ions were prepared by dissolving appropriated amounts of analytical grade reagents in deionised water using a 1000 ml volumetric flask (±0.8 ml MBL Boro England). The stock solutions were acidified to prevent hydrolysis by adding 5ml HNO_3 and the volume was made up to the 1000 ml mark. The content of each volumetric flask was agitated in a Heidolph Unimax instrument 1010 shaker at 300 rpm for 3 h to ensure complete dissolution at room temperature (23°C). For Cd(II) ion, the reagent was cadmium nitrate tetra hydrate-Cd $(NO_3)_2.4H_2O$ (Sigma-Aldrich) (99% assay) and for Pb(II) ion, the reagent source was Pb(II) nitrate-Pb $(NO_3)_2$ (Sigma-Aldrich) (99% assay).

The working solutions for individual sorption experiments were prepared by serial dilution of aliquots of each stock solution. Batch kinetic sorption experiments for the adsorption of cadmium and lead for the equilibrium studies modelling was carried out using the unmodified, hydrothermally carbonized, pyrolysed, carbonised and chemically activated carbon forms of each of the agricultural residue as well as the commercial activated carbon adsorbent (CGAC). Equilibrium adsorption experiments were carried out by agitating known weights of each adsorbent with 100 ml of adsorbate solutions of desired

concentration and pH 6.5 was used for the residue adsorbents, while pH 7 was used for sorption studies involving the chemically activated, carbonised and pyrolysed adsorbents. The conditions for each experimental parameter are stated in Table 4.1 and the pH for each experiment was modified using NaOH and HCl. The reaction vessel for each adsorption experiment was a 250 ml conical flask and the sorption was carried out at a laboratory temperature of 25°C ± 0.5. Each conical flask with the adsorbate and adsorbent was agitated for a specified contact time in a Heidolph MR 3001 magnetic stirrer with speed and temperature controls at a speed of 200 rpm. The temperature measurement carried out in this study was determined using an Immersion Zeal 76 mm Thermometer (England). Temperature studies were carried out in a Lauda A100 hot bath mounted on a Stuart Hot Plate Stirrer (SB302). At the end of each experiment, the resulting solution was separated from the adsorbent using Whatman (541) filter paper (Whatman International, England) and the filtrate analysed by taking out 5ml of each filtrate using a Volac high precision micropipette (Poulten & Graf GmbH, Germany) and diluting it to 50ml with deionized H_2O. Thereafter, 10 ml of the resulting metal ion solution was taken out using a micropipette into a sample analysis tube for metal ion determination. The metal ion concentrations of the adsorbate solution were determined spectrophotometrically using ICP-OES. The effect contact time, pH and dose were also studied and the conditions for each type of parameter analysis are presented in Table 4.1.

Table 4.1: Conditions for batch adsorption of Cd(II) and Pb(II) ions

Initial Concentration	Contact Time			Dose	pH
mgL^{-1}	min	Min	Hr	(g)	
50	5	105	6	0.5	2
100	10	120	9	1	3
150	15	135	12	1.5	4
200	20	150	15	2	5
250	25	165	18	3	6
300	30	180	24		7
350	45		48		8
400	60		72		9
450	75				10
500	90				

4.4.1 Adsorbent disposal studies

Adsorbent disposal studies were carried out by carbonisation of the used adsorbents at 600°C in air environment in a furnace. The used adsorbents were initially dried in an air oven at 110°C after adsorption studies. The crucibles with lids for the carbonization of the used adsorbents were initially dried in a furnace at 600°C for 10 minutes. Thereafter known amounts of each dried used adsorbent with either Cd(II) or Pb(II) ions were weighed into pre-dried and weighed crucibles. Each crucible was thereafter inserted into a muffle furnace and the temperature of the furnace was raised to 350°C for 6 h for the combustion of the organic component of the adsorbents. The temperature of combustion of the adsorbents was based on the temperature of decomposition of the metal ion precusors- 401°C for $Cd(NO_3)_2.4H_2O$ (Wojciechowski and Malecki, 1999) and 470°C for $Pb(NO_3)_2$ (Fisher Scientific, 2014). After the combustion of the adsorbents, the furnace was allowed to cool for 24 h after which the resulting ashes in the crucibles were obtained. Each set of used adsorbent ash after carbonisation was thereafter divided to three equal groups for different treatments/analysis and for each treatment 0.2g of the ash obtained after carbonisation was used. These treatments were:

- Ash digestion and direct analysis to determine metal ion concentration- Wet digestion of ash was carried out using a 3:1 (HNO_3: HCl) mixture followed by metal ion determination of the concentration of the metal ions {Cd(II) and Pb(II)}in the used adsorbents using ICP- OES. This group of samples were labelled used ash (UA).

- Ash leaching in deionized water- Leaching of the dried ash in 50ml of deionzed water 18.2 MΩ cm^{-1} (Millipore) at pH 6 for 60 days at 25°C was carried out for this sample set to analyse the amount of metal ions leached into water. This group of samples were labelled deionized water leached ash (DWA).

- Ash encapsulation and leaching in deionized water- The ash sample was encapsulated in a polydimethylsiloxane (PDMS) matrix. PDMS pre-polymer and curing agents were weighed in a 10: 1 ratio into a 250ml cup. Thereafter the mixture was vortex 5 minutes to eliminate gas bubbles. The vortex sample was subsequently degassed for 25 minutes. The degassed sample was poured into a mould (Fig.4.13) at two intervals with the ash samples sandwiched between and samples were cured at 120°C for 24h. Thereafter, the encapsulated samples were subjected to leaching in 50ml of deionzed water (18.2 MΩ cm^{-1} Millipore) at pH 6

for 60 days at 25°C. This was carried out to determine the amount of metal ions that can be leached into water from the encapsulated polymer matrix. This group of samples were labelled encapsulated deionized water leached ash (EWA).

Fig: 4.13: Mould used to prepare PDMS encapsulated samples

4.5 Data quality assurance

All adsorption experiments were carried out in triplicates to ensure reproducibility and accuracy of results. The relative standard deviation was used as the error parameter for all analysis and the value for each set of measurements was $< 5\%$. Each experimental set was carried out using blanks in to ensure the elimination of errors associated with experimental conditions. For each experimental analysis procedure, blanks were prepared using deionized H_2O and the blank samples were subjected to the same treatment process using the same type of experimental vessel. In the analysis of each metal ion in solution, the blank samples were also analysed first in the ICP-OES instrument prior to analysis of the standards and the samples. A calibration curve for each set of measurements was prepared by the ICP-OES software using the standards prepared for each metal ion and the metal ion concentration in the stock solution and prepared aqueous solution before adsorption were also analysed to ensure the correct concentration was prepared and used for adsorption. The instrument was programmed to take into account any blank concentration and the actual metal ion concentration of Cd(II) ion or Pb(II) ion in the solution remaining after each adsorption experiment was calculated using eqn. (4.5) follows:

$$M_C = X_a\text{-} X_{blk} \tag{4.5}$$

Where M_c represents the final concentration of the metal ion

       X_a represents the measured concentration of metal ion and

       X_{blk} represents the blank concentration value

In the experimental analysis results from the ICP-OES, all analysis was carried in triplicates with a correlation coefficient limit of 0.9995 using 3 standards.

4.6 Summary

In this chapter, the experimental methods used in the different stages of this research have been presented. Residue sample collection and adsorbent preparation were carried out via physical and chemical pre-treatment processes such as washing, drying, milling sieving, hydrothermal carbonization, thermal treatment and chemical activation. These processes were used to produce unmodified adsorbents, hydrothermal adsorbents, carbonised adsorbents, pyrolysed adsorbents and Na_2CO_3/K_2CO_3 chemically activated adsorbents depending on the treatment process used. These adsorbents were subjected to various characterization processes such as PCS, FTIR, XRF, TGA, BET, XRD, SEM, EDAX and ICP-OES to evaluate the chemical and physical characteristics of the adsorbents and give an insight into the various properties of these adsorbents that could facilitate the adsorption process. Batch sorption studies in aqueous solutions were also carried out on the characterised adsorbents based on Cd(II) and Pb(II), the two metal ions investigated taking into consideration different parameters such as contact time, pH, sorbent dose and adsorbate concentration and these results are discussed in the next chapters. Adsorption disposal studies were also carried out to determine a method of safe disposal of the used adsorbents.

CHAPTER FIVE

AGRICULTURAL RESIDUE ADSORBENTS

CHAPTER FIVE

5.0 Agricultural residue adsorbents

Agricultural residues have been used as adsorbents for the removal of heavy metal ions, organic and pharmaceutical compounds as well as radioactive elements from wastewater systems and aqueous solutions in a number of laboratory studies (Ajimal *et al.,* 2003; Amir *et al.,* 2005). These residues have become one of the major sources of materials for research in water purification as they are in many instances of low value, are sources of waste disposal issues and are readily available in local environments. Based on these considerations, they can be used for water and air treatment applications in place of the commercial activated carbon adsorbents that are not economically sustainable in these local situations. The agricultural residues considered in this study were chosen based on the agricultural residues available in a developing country (Nigeria) but their utilisation transcends this country as these materials are also available in other countries and continents. The implication of the choice of these resides in the assumption that if these materials can be used successfully as adsorbents for the target pollutants of choice in this study $\{Cd(II)$ and $Pb(II)\}$; then the prospect of investigating these materials for pilot and large scale applications in Nigeria can be explored as substitute adsorbent materials instead of the expensive commercial activated carbon adsorbent presently being imported into the country at a huge economic cost. In addition, since these materials presently pose waste disposal problems in their local environments, their utilisation as adsorbents will contribute to providing a sustainable approach to a waste management problem.

Prior to the utilisation of these residues for the removal of the target heavy metal ions from aqueous solutions, characterisation of their physical and chemical properties was carried out as described in Chapter 4 of this study. The evaluation of adsorbent properties of these materials provides relevant information that is fundamental in determining their suitability for any particular application. It can also provide information that can be used to determine the conditions the adsorbent can be utilised to maximize its adsorption properties. The used (spent) adsorbents were also subjected to some characterisation analysis to confirm the presence or absence of species of the ions on each adsorbent after adsorption, thus providing information on the adsorption process and mechanism.

5.1 Adsorbent nomenclature

The nomenclature of the natural agricultural residues are indicated in Table 5.1 and these residues were subjected to different physical and chemical characterisation procedures to provide insight into their physical and chemical properties.

Table 5.1: Nomenclature of unmodified agricultural residue adsorbents

Sample Treatment Natural Residues	Nomenclature
Unmodified oil palm fruit fibre residue	OPFS
Unmodified cocoa pod residue	CCPS
Unmodified coconut shell fibre residue	CNFS
Unmodified plantain peel residue	PTHS
Unmodified cocoyam peel residue	CCYBS
Unmodified sweet potato peel residue	PTPS
Unmodified white yam peel residue	YTBS

5.2 Proximate and ultimate analysis of residue adsorbents

The proximate and ultimate analysis of the residues adsorbents (raw residues) was carried out to quantify the various components of the adsorbents and the results are shown in Table 5.2. The results indicate that the adsorbents have variations in composition which may be due to the intrinsic nature of each residue. The CCPS adsorbent had the highest moisture content of 9.03% while OPFS had the least with 1.73% and these values were similar to what has been reported in a study by Oladayo (2010) on the proximate composition of some agricultural waste in Nigeria. From table 5.2 it can be observed from the ultimate analysis that the carbon content in the residues are within the range of 38.2% to 48.4% with OPFS having the highest and CCPS with the least. From this composition, the proportion of fixed carbon from the proximate analysis indicates that CNFS has the highest value and OPFS with the least. The organic content (carbon, nitrogen hydrogen and oxygen) of the 7 residue adsorbents are consistent with what has been reported in literature

for other types of dried biomass (Chang *et al.,* 2015). The carbon content of these residues is an important parameter in the carbonisation, pyrolysis and activation procedures for the synthesis of carbon-rich adsorbents as it determines the final composition of the carbon which relates to the yield of the transformation process. A similar observation of high carbon content for agricultural residues has been reported by Soleimani and Kaghazchi (2014b) in their evaluation of six different agricultural by-products; bagasse, apricot stones, almond, hazelnut, pistachio and walnut hard shells which were used as the raw materials of the synthesis of activated carbon adsorbents. In their study, the percentage carbon content of the residues reported were; bagasse (46%), apricot stones (50%), almond (50%), hazelnut (51%), pistachio (47%) and walnut (49%),thus, it is presumed that high carbon residues will result in high yield from the activation or carbonisation process.

Table 5.2: Proximate and ultimate analysis of residue adsorbents (Ashless)

Property	Adsorbent						
	OPFS	CNFS	CCPS	CCYBS	PTHS	PTPS	YTBS
Ultimate Analysis (wt%)[a]							
Carbon	48.49	44.45	38.21	41.79	42.13	40.12	41.47
Hydrogen	7.13	4.92	4.75	5.89	5.94	5.87	6.26
Nitrogen	1.91	0.91	2.12	1.95	1.19	1.66	0.82
Oxygen	40.42	42.34	44.74	42.34	44.31	46.35	48.30
Sulphur	0.83	0.32	0.70	0.36	0.18	0.30	0.15
Proximate Analysis(wt%)[b]							
Fixed carbon	11.97	28.85	22.93	21.95	20.31	20.55	21.75
Volatile matter	65.42	55.76	46.83	61.50	62.59	62.49	66.14
Moisture content	1.73	5.19	9.03	6.86	5.00	4.98	5.34

[a] Elemental analysis using CHNS elemental analyser

[b]Proximate analysis using thermogravimetric analyser

These materials have low sulphur and nitrogen content with the YTBS residue having the least amount of both elements. All the seven residues had high volatile matter content that is characteristic of the organic nature of the precursors which as lignocellulosic materials contain cellulose, lignin and hemicellulose (Khor *et al.,* 2009). The hydrogen content of the different adsorbents discussed in this study is similar to what has been reported for olive stones (6.33%) and sugar cane bagasse (5.41%) by Moubarik and Grimi, (2015) but their nitrogen content are all higher than those of olive stones (0.04%) and sugar cane bagasse (0.36%).

5.2.1 Inorganic composition of residue adsorbents

The inorganic composition of the unmodified residue adsorbents was determined using X-ray fluorescence (XRF) spectrometry as described in section 4.3.5 of this work. The results obtained from this characterisation are presented in Table 5.3. The elements identified on the residue adsorbents have characteristic X-ray peaks of different wavelengths and the fluorescence intensity of each spectral line is related to the elemental concentration (Zhang *et al.,* 2014). This characterisation was used to determine the percentage composition of the different elements and the composition of the elements in the residues is presented as oxides. The organic content of each residue was also determined and is presented in Table 5.3 in which the respective organic composition of the residue adsorbents are given as 94% (PTPS), 96% (YTBS), 92% (CCYBS), 93% (PTHS), 89% (CCPS), 90% (OPFS) and 92% (CNFS). The high values obtained for organic composition of the 7 residue adsorbents is expected as these are lignocellulosic materials. A similar observation of high organic content for a biomass based adsorbent obtained using XRF spectrometry has been reported by Mafra *et al.,* (2013) in their study on the characterisation of an agricultural waste material-orange peel for use as adsorbent in the removal of Remazol Brilliant Blue from artificial textile-dye effluent.

From Table 5.3 it is observed that the ash content of CCPS and OPFS are the highest with values of 18.9 and 18.3% respectively. The results also indicate that the CCPS residue has the highest elemental content for potassium-K_2O (6.38%) amongst the residues. The other elements in the CCPS of significant concentrations are CaO (0.82%), MgO (0.63%), silica-SiO_2 (0.56%), phosphate-P_2O_5 (0.66%) and sulphate-SO_3 (0.70%). The OPFS residue is observed to have the highest amount of silica, alumina, sulphate (SO_3) and calcium oxide (CaO) content when compared to the other residues with values for silica (3.99%) alumina (1.03%), sulphate (0.87%) and CaO (1.23%). The PTPS residue also has a high inorganic content with its two highest constituents being K_2O (2.65%) and SiO_2 (1.32%). K_2O is also the main component of PTHS with a value of 4.51(%). The PTHS residue also contains trace amounts of silica (0.32%), phosphate (0.44%) and chloride (0.52%). For the YTBS residue, K_2O is the highest constituent with a percentage value of 1.51 and silica is the next abundant element with a value of 0.75%. The CNFS residue has the highest concentration of Na_2O (0.26%) and chloride (0.98%) amongst the residues. It also has a significant amount of K_2O (3.69%) and silica (0.63%). The PTPS residue has major elemental components as follows; MgO (0.22%), alumina (0.32%), silica (1.32%), phosphate (0.40%), chloride (0.39%) and K_2O (2.65%). CCYBS residue has a larger number of

constituent elements with significant concentrations with K_2O still the highest component with a value of 3.81%, its alumina content has a value of 0.731% while the silica and phosphate content were 0.82% and 0.921% respectively. The CCYBS residue also has considerable amounts of CaO and MgO with values of 0.470% and 0.386% respectively.

The sum of the elemental compositions of the residues in Table 5.3 is observed to be lower than the ash content and this can be interpreted as a factor of the form of the element analysed in the XRF instrument. The analysis technique quantifies the elemental component as oxides of the metals, while the ash content was obtained using the thermogravimetric analyser at which carbonization in occurred at 600°C under nitrogen and oxygen atmosphere with the resulting inorganic components existing as carbonates. The results of the inorganic composition of these unmodified residues are similar to what has been reported in literature for some agricultural residues used as adsorbents. The inorganic constituents of the seven residue adsorbents contributed to their respective ash composition and may also play an important role in improving the ability of these residues to remove Cd(II) and Pb(II) ions from aqueous systems via ion-exchange mechanism for the processes under investigation (Sardella *et al.,* 2015). The percentage composition of calcium oxide (CaO) in the OPFS residue adsorbent is similar to what has been reported by Mafra *et al.,* (2013) for an orange peel adsorbent used for the adsorption of Remazol brilliant blue dye even though the percentage compositions of all the other elements in the residues in this study are higher than what they obtained in their study. The inorganic content of the 7 residues examined in this work were also similar to that of orange peel adsorbent (OPA) reported by Mafra *et al.,* (2013). From their study it was observed that the SiO_2 and Al_2O_3 content of the residue adsorbents with exception of the Al_2O_3 content of the CCPS were higher than that of the OPA {008%(SiO_2) and 0.01(Al_2O_3), however the CaO content of the OPA (1.4%) was higher than those obtained for the residue adsorbents in this study.

Table 5.3: Mineral Residue Composition of Unmodified Adsorbents

Adsorbent	Ash Content [d]	Elemental Composition [c]												Organic Matter
		Na_2O	MgO	Al_2O_3	SiO_2	P_2O_5	SO_3	Cl	K_2O	CaO	Ti	Mn	Fe_2O_3	
	(%)	(%)	(%)	(%)	(%)	(%)	(%)	(%)	(%)	(%)	(%)	(%)	(%)	(%)
PTPS	11.26	0.051	0.221	0.321	1.323	0.403	0.302	0.393	2.654	0.168	0.032	0.002	0.128	93.992
		±0.007	±0.014	±0.017	±0.035	±0.019	±0.016	±0.019	±0.049	±0.012	±0.005	±0.001	±0.011	
YTBS	5.50	0.009	0.08	0.151	0.752	0.361	0.157	0.011	1.515	0.05	0.011	0.002	0.052	96.841
		±0.003	±0.008	±0.012	±0.026	±0.018	±0.012	±0.003	±0.037	±0.007	±0.003	±0.001	±0.007	
OPFS	18.31	0.027	0.627	1.038	3.996	0.753	0.877	0.181	0.75	1.233	0.043	0.005	0.468	89.943
		±0.005	±0.024	±0.031	±0.06	±0.026	±0.028	±0.013	±0.026	±0.033	±0.006	±0.002	±0.021	
CCYBS	9.02	0.015	0.386	0.731	0.823	0.921	0.383	0.192	3.818	0.47	0.016	0.012	0.174	92.039
		±0.004	±0.019	±0.026	±0.027	±0.029	±0.019	±0.013	±0.059	±0.021	±0.004	±0.003	±0.013	
CNFS	7.83	0.268	0.391	0.159	0.632	0.424	0.382	0.981	3.695	0.35	0.01	0.005	0.079	92.578
		±0.016	±0.019	±0.012	±0.024	±0.02	±0.019	±0.03	±0.058	±0.018	±0.003	±0.002	±0.008	
PTHS	11.36	0.022	0.196	0.045	0.324	0.447	0.18	0.526	4.518	0.142	0.018	0.003	0.006	93.583
		±0.004	±0.013	±0.006	±0.017	±0.02	±0.013	±0.022	±0.064	±0.011	±0.001	±0.002	±0.002	
CCPS	18.99	0.061	0.637	0.19	0.562	0.665	0.706	0.073	6.388	0.828	0.006	0.005	0.051	89.769
		±0.007	±0.024	±0.013	±0.022	±0.024	±0.025	±0.008	±0.076	±0.027	±0.002	±0.002	±0.007	

[c] Analysis using X-ray fluorescence spectrometry
[d] Ash analysis using thermogravimetric analyser

The sodium and magnesium content in the PTPS residue was higher than that of the rice husk adsorbent reported by Zhang *et al.,* (2014) for Cu (II) adsorption. Similarities and differences have also been observed in the inorganic composition of the residue adsorbents in this study and that reported by Zhang *et al.,* (2014). The percentage aluminium content of the PTHS residue adsorbent was similar to that of the rice husk adsorbent used by Zhang *et al.,* 2014 for Cu (II) adsorption, while that of the CCPS was lower than the rice husk. The percentage silica content of the rice husk (15) was higher than the results obtained for all the residue adsorbents in this study, while the sodium and magnesium content in the residues were higher than those of the rice husk adsorbent. The inorganic constituents of the residue adsorbents reported in this work are presumed to play a significant role in the ability of the adsorbents to remove metal ions such as Cd(II) and Pb(II) from aqueous solutions as they can contribute to cation removal via ion-exchange and surface complexation processes which will depend on the type of inorganic constituents on the residues (Sardella *et al.,* 2015).

5.2.2 Yield, loss on attrition and ash content

The unmodified residues used in this study were subjected to washing and drying at 110$^{\text{o}}$C. The characteristic properties of the residue adsorbents such as yield, loss on attrition and ash content are shown in Table 5.4. The yield of the residue was taken as 100% since it was not subjected to any thermal or chemical treatment. The ash content of each residue is also an important parameter for consideration in the analysis of lignocellulosic materials as it gives information of the inorganic (mineral) components in the residue. The ash content of the residues presented in Table 5.3 was obtained using the thermogravimetric analyser (TGA) which gave information on the proximate composition of the residues previously discussed in section 5.2 and Table 5.2.

The inorganic elements such as silica, alumina, phosphates, calcium and potassium are the major components of the ash content of agricultural residues based on the XRF analysis previously discussed. These components in the adsorbent matrix will have significant effect on the transformation process for the adsorbents especially the chemically activated and pyrolysed adsorbents. This is because the temperature and chemical agents used in the transformation processes for these residues may initiate chemical reactions on the residue structure that may affect the final structure and composition of the resulting adsorbent. This is due to the series of reactions that are presumed to take place during the interaction

of the chemically activating agent and the adsorbent surface structure. The effects of these reactions are presumed to influence the carbonisation and pyrolysis process and affect the development of pore structure in the adsorbents. The values of ash content of the residues in Table 5.4 obtained using the methodology reported by AOAC(2000) are similar to the results shown in Table 5.3 obtained from TGA measurements and confirm that these materials are primarily organic (Djilani *et al.,* 2012). Sardella *et al.,* (2015) reports that the ash content of residues is an important parameter that has to be considered for materials that can be converted into carbon adsorbents using thermal treatment. This is because residues that have high quantities of ash in their composition have the probability of having higher metal ion retention in adsorption applications due to the effect of the ash in ion-exchange processes that is present in addition to any other chemisorption or physisorption mechanism of metal ion removal.

Table 5.4: Ash content, Loss on Attrition and Yield of Adsorbents

Adsorbent	Ash[e] (%)	Loss on Attrition (%)	Yield (%)
OPFS	16.8 ±0.013	24.3 ±1.28	100
CNFS	7.4 ±0.219	21.75 ±0.099	100
CCPS	12.9 ±0.045	18.1 ±2.73	100
CCYBS	8.9 ±0.051	11.95 ±1.23	100
PTHS	10.1 ±0.031	22.65 ±1.03	100
PTPS	10.6 ±0.031	19.2 ±2.01	100
YTBS	8.3 ±0.044	16.4 ±1.63	100

[e] Ash content using AOAC(2000)

One important mechanical characteristic of adsorbents that gives a measure of the material mechanical strength is the attrition resistance of the adsorbent. The movement of adsorbent particles in a reactor or vessel makes them susceptible to the attrition phenomena leading to the undesirable formation of smaller particle size materials (fines). All the residue adsorbents had high attrition losses (11- 24%) that would severely impact on their utilisation in agitated adsorbent systems where mixing is involved. Sugumaran *et al.,*

(2012) has also reported a similar high attrition of (10.3%) for *Delonix regia* fruit pod in their study on the production and characterization of activated carbon from banana empty fruit bunch and *Delonix regia* fruit pod. The characteristic of attrition resistance of adsorbents is important in the utilisation of adsorbents as it gives information on what type of reactor system can be most suited for an adsorbent. Adsorbents that have high resistance to attrition (low losses) such as some commercial activated carbon (the commercial activated carbon used in this study had losses of 4.1% due to attrition) can be used in agitated reactor systems where there is mixing. On the other hand the adsorbents that have high losses due to attrition -such as the residue adsorbents discussed here can be used in batch systems by pressing them into pellet forms to increase their resistance to attrition or used in column based reactor systems where there is no agitation and mixing. In addition transforming these materials into other forms of carbon adsorbents may improve this property. According to Sugumaran *et al.,* (2012) the conversion of agricultural residues into activated carbon type adsorbents can also improve their attrition resistance when used in adsorption systems.

5.3 Surface area and porosity of residue adsorbents

The nitrogen adsorption and desorption isotherms of each adsorbent was obtained at a liquid nitrogen temperature of 77 K (-196.15^{0}C) using a Micromeritics TriStar 3000 surface area analyser as described in section 4.3.4. The Nitrogen adsorption-desorption plot obtained was used to determine the adsorbent surface properties (surface area, total pore volume and pore size). The specific surface area of each adsorbent was determined using the BET theory plot designed by Brunauer, Emmet and Teller (BET) (Brunauer *et al.,* 1938). A multi-point BET plot with eight points of the adsorption isotherm between relative pressure values was used in the determination of each specific surface area. The total pore volume of each adsorbent was determined using the desorption branch of the Nitrogen adsorption-desorption isotherm based on the Barrett-Joyner-Halenda (BJH) method while the average pore diameter were calculated using the BJH adsorption and desorption pore distribution plot (Storck *et al.,* 1988; Iza *et al.,*2000).

The N$_2$ adsorption-desorption curve for OPFS and CNFS residues are shown in Figures 5.1 and 5.2 and those of the CCPS, CCYBS, PTHS, PTPS and YTBS residues are presented in Appendix 1. From these analysis the surface area, pore size and pore volume of the residue adsorbents obtained are presented in Table 5.5. The results show that the residue

adsorbents had low or no surface area with CNFS having the highest BET surface area of 12.42 m^2 g^{-1}, while that of the OPFS was 1.44 m^2 g^{-1}. The average pore diameters of the residues were within the range for mesoporous materials (10 to 32) nm indicating that these residues are mesoporous according to the IUPAC classification of porous materials (Sing, 1982; Sing, 2001).

Table 5.5: Surface area and porosity agricultural residue adsorbents

Adsorbent	Surface Area (m^{2}g^{-1})	Total Pore Volume (cm^{3}g^{-1})	Pore Diameter (nm)
OPFS	1.44	4.56E-03	13.2
CNFS	12.4	3.82E-02	10.4
CCPS	0.71	9.18E-03	26.2
CCYBS	0.45	4.03E-03	32.4
PTHS	3.98	1.69E-02	13.0
PTPS	1.91	4.87E-03	22.3
YTBS	0.50	2.70E-03	21.1
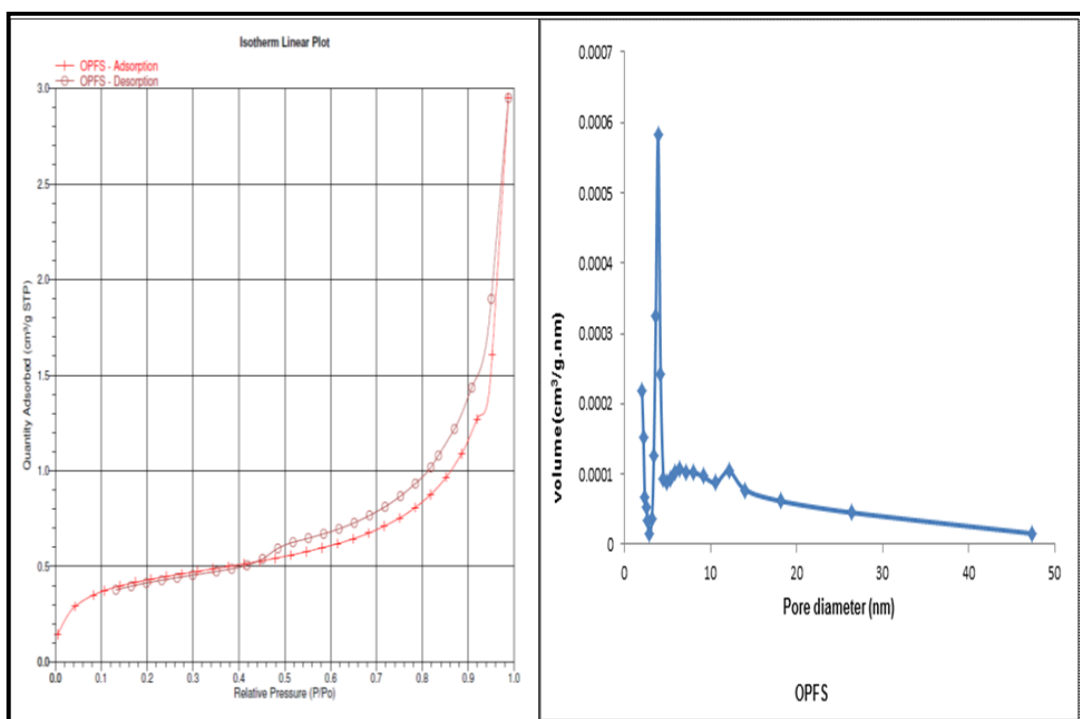
Figure 5.1: N$_2$ adsorption-desorption isotherm and pore size distribution of OPFS residue adsorbent
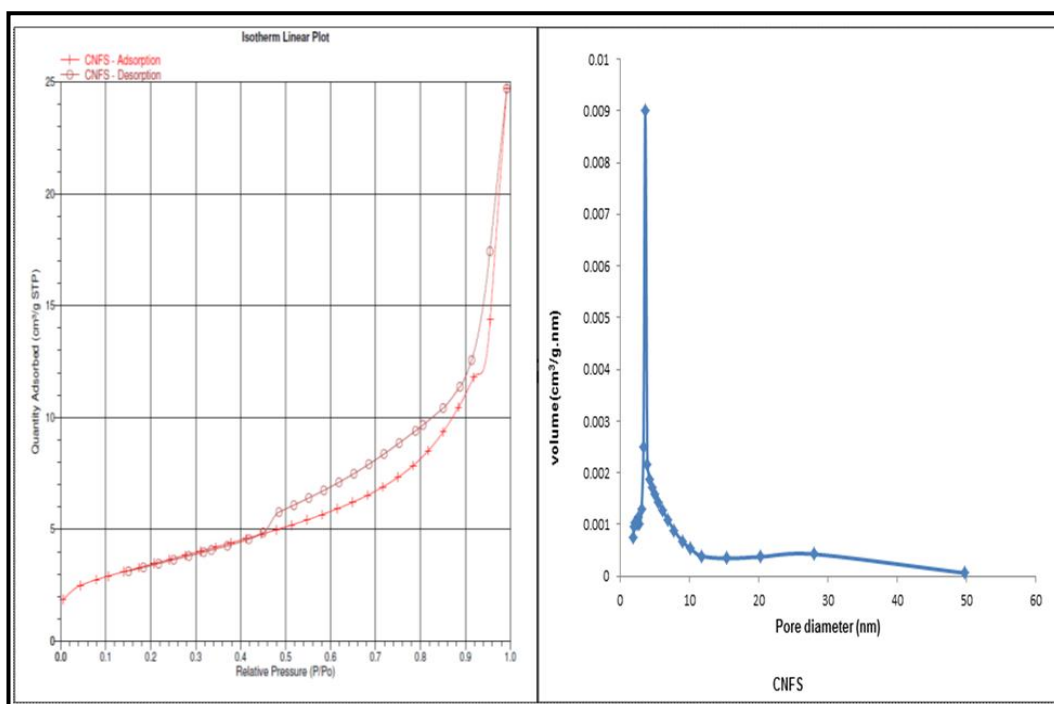
Figure 5.2: N_2 adsorption-desorption isotherm and pore size distribution of CNFS residue adsorbent

The size of pores and volume of adsorbent pores plays an important role in the adsorption process and the mesopores found in these 7 residues indicates that these adsorbents would have pores that permit access for the transport of the Cd(II) and Pb(II) onto the active sites (Ali *et al.*, 2016). The total pore volumes of the residue adsorbents are also presented in Tables 5.5 and it can be observed that the CNFS residue adsorbent had the highest pore volume of 3.82×10^{-2} cm^{3}g^{-1}, while the least was 2.70×10^{-3} cm^{3}g^{-1} obtained for the YTBS residue. Thus, the trend in surface area for the residue adsorbents was CNFS > PTHS > CCPS > PTPS > OPFS > CCYBS > YTBS. The total pore volumes obtained for the residue adsorbents are within the range reported for lignocellulosic residues in literature. Lacerda *et al.,* (2015) has also reported on the total pore volume of some lignocellulosic biomass and in their study the total pore volumes obtained for the residues were; 3.59×10^{-4} cm^{3}g^{-1} (carnauba palm leaves); 2.01×10^{-3} cm^{3}g^{-1} (macauba seed endocarp) and 3.16×10^{-3} cm^{3}g^{-1} (pine nut shell).

However, it can be observed that the pore volumes for these residue adsorbents used in this study are low and this can be assumed to limit the uptake ability for the two cations considered in this study as the pores may not have enough capacity to contain the adsorbate molecules. However, it has to be noted that the determination of the volume of pores in an adsorbent is based on the adsorption of liquid N_2 onto the adsorbent pores during the adsorption-desorption process and the differences in physical and chemical

characteristics between liquid N_2 and cations in solution in an adsorbate with respect to its ability to be contained in the pores of an adsorbent implies that these low pores may still be able to contain more Cd(II) and Pb(II) ions than N_2.

The low values of BET surface area obtained for these agricultural residues are similar to what has been reported in literature for some biomass residues. Ibrahim *et al.,*(2010) reported a low BET surface area (0.26 m^2 g^{-1}) for modified soda lignin (MSL) obtained from oil palm empty fruit bunches (EFB) in their study on the use of a novel agricultural waste adsorbent for the removal of lead(II) ions from aqueous solution. Miralles *et al.,*(2010) has reported on the observation of a BET surface area of 0.42m^2g^{-1} for grape stalk waste. Lacerda *et al.,* (2015) have also reported on the BET surface areas of some lignocellulosic biomass, in their study the surface area obtained for the residues were; 0.85 m^2 g^{-1} (carnauba palm leaves); 0.60 m^2 g^{-1} (macauba seed endocarp) and 0.86 m^2 g^{-1} (pine nut shell). The low surface area of agricultural residues has been suggested as a limitation in their application as adsorbents, hence the need to improve their surface area using different treatment methods. Thus, these residues were subjected to a number of thermal and chemical treatment protocols to improve their surface properties and these are discussed in the subsequent chapters of this study.

The size of pores on an adsorbent has an effect on the nitrogen adsorption-desorption isotherm as it influences the relative pressure used to fill the pores. The increasing size of pores of an adsorbent from microporous (< 2nm) to mesoporous (between 2 -50nm) results in a corresponding increase in the relative pressure required to fill the pores. This result in different shapes of the nitrogen adsorption-desorption curve that is associated with the presence of hysteresis (Sing, 1982; Sing and Williams, 2004). An examination of the nitrogen adsorption-desorption of plot the residue adsorbents in Figures 5.1 and 5.2 as well as Appendix 1 indicates that the shape of the isotherm of the agricultural residue adsorbents can be described based on the type H3 hysteresis loop (see Figure 3.3). This characteristic hysteresis loop of the residue adsorbents is associated with the development of multilayer fillings on the adsorbent when the monolayer coverage of nitrogen is complete thereby resulting in capillary condensation (Sing and Williams, 1982; Xu *et al*., 2013). This type of hysteresis in these residues may also indicate the presence of slit shaped pores as this type of loop has been associated with slit shaped mesoporous materials (Zhao *et al.,* 2014).

5.4. Thermogravimetric analysis

The chemistry of biomass is a complex one but the major components of biomass are most often given as cellulose, hemicellulose and lignin. Thermal degradation is often used to provide information on the different components of biomass or lignocellulosic materials and the main reactions that occur during thermal degradation process include depolymerisation, decarbonisation and cracking (Hooi *et al.*, 2009). Thermogravimetric analysis (TGA) was used to obtain information on the thermal decomposition behaviour of the residues and information from the thermal degradation profile was used to generate the proximate composition of these residues. The thermogravimetric (TG) and derivative thermogravimetric (DTG) plot of the seven residue adsorbents are shown in Figures 5.3 to 5.7, while the raw TGA analysis profile from the instrument are presented in Appendix 2. TGA pyrolysis in nitrogen atmosphere was set to operate from 20 – 500°C while combustion in oxygen atmosphere took place from 500 – 600°C as described in section 4.3.7 yielding the thermal degradation profiles.

From Figures 5.3 to 5.7, it can be seen that the thermal decomposition of the residues occurred in three main weight loss regions; namely moisture removal (drying) which took place in the range 25 – 100°C accompanied with a small exothermic effect. The weight loss here is associated with the evolution of water molecules in the residues and this was as the result of keeping all the residues at this stage (20-100°C) for 60 minutes to eliminate all moisture. The second weight loss regime is associated with the evolution of volatile matter (devolatilisation) in the range of 110 – 500°C which is due to the decomposition of the major components of the residue (cellulose, hemicellulose and lignin). The cellulose and hemicellulose components are the major component of the volatile matter, while the lignin is a main component in the formation of chars (Sanchez-Silva *et al.,* 2012). These components have been observed to have different initial decomposition temperatures. Studies carried out by Stefany *et al.,* (2005) observed that the sequence of degradation begins with hemicellulose between the temperature ranges (150 – 350°C).
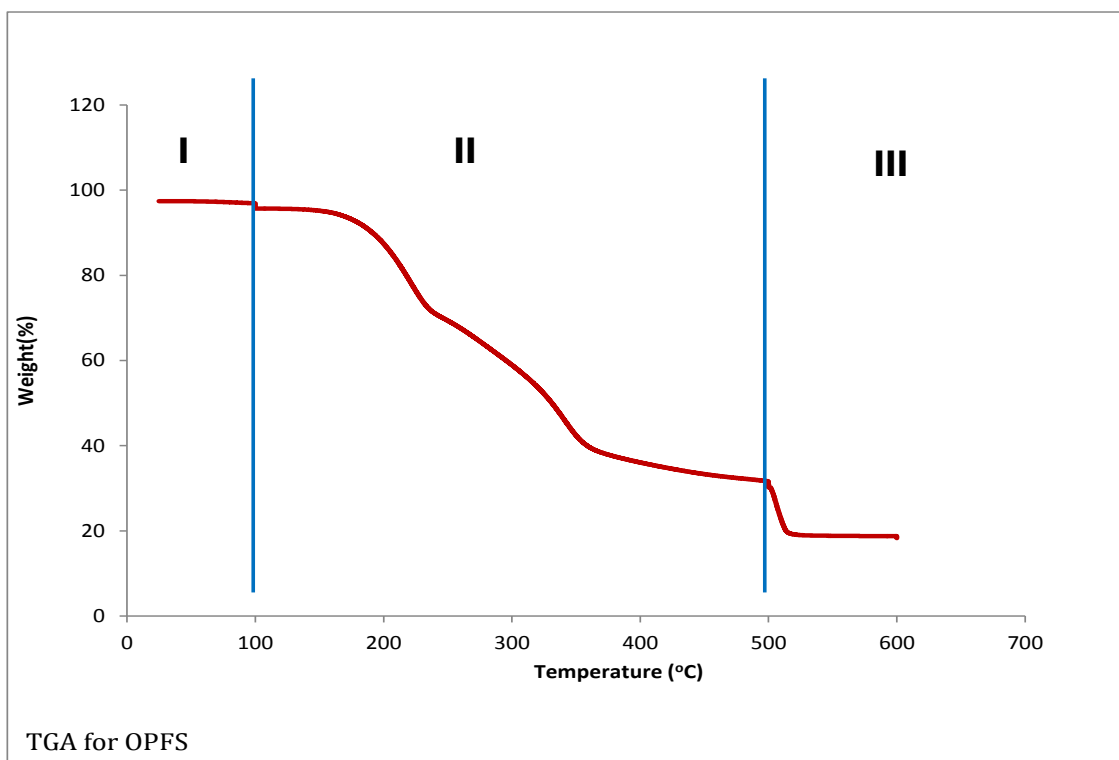
Figure 5.3: Thermogravimetric analysis of OPFS in N_2 (I-II) & air (III) environments

The cellulosic material is the second component that degrades between the range 275 – 380°C and lignin degrades between 300 – 500 °C. The third stage of weight loss is the oxidation of the fixed carbon occurring from 500°C to 600°C with the resulting ash residue.

For the OPFS residue (Fig 5.3 & 5.4), the weight loss in the first stage-I (moisture evolution) was 1.73%, the second stage of the weight loss regime-II (volatile component) was 65% with two peaks in the derivative TG plot (Fig 5.4) that can be associated with hemicellulose and cellulose decomposition between 180 and 380°C. The final region for the OPFS adsorbent decomposition (III) is associated with the oxidation of the carbon between 500 – 600°C. The onset of degradation for the CNFS residue shown in Figure 5.5a & b commences from 24°C to 100°C associated with water loss of approximately 5.19 % (I). The second stage (II) that is associated with loss of volatile content has a single maximum with a little shoulder between 180°C and 350°C that is associated with hemicellulose and cellulose weight loss accounting for about 55% of the residue. The onset of lignin degradation occurred at about 350°C and this continued up to the highest temperature (500°C) for pyrolysis (Stage II). Also this stage of the weight loss also contains the final stage of the cellulose and the residual lignin decomposition (Titiloye *et al*., 2013). The last stage (III) which is in air environment is the oxidation of the fixed

carbon component of the residue to give the final ash content with a DTG peak (Fig 5.5b) between 500-520 °C. The ash content for this adsorbent was 7.8% (Table 5.3).

For the YTBS adsorbent the TG curve (Fig. 5.5a) shows 3 regions (I, II & III) which can be used to describe the major stages in the decomposition of the residue adsorbent. The DTG curve (Fig. 5.5b) shows three exothermic peaks at a maximum of 71 °C, 281 °C and 509 °C. The first region (I) (20-100 °C) corresponds to the elimination non-dissociative physically absorbed and hydrogen bonded water molecules on the residue surface (Li *et al.,* 2016; Ali *et al.,* 2016) with a weight loss of 5% and the temperature in this region was held at 100 °C for 60 minutes to ensure complete moisture removal. The second stage (II) with a weight loss of 66% indicates the elimination of the volatile components in the lignocellulosic adsorbent and this can be associated to the removal of the 3 major constituents which are; cellulose, hemicellulose and lignin (Ali *et al.,* 2016).
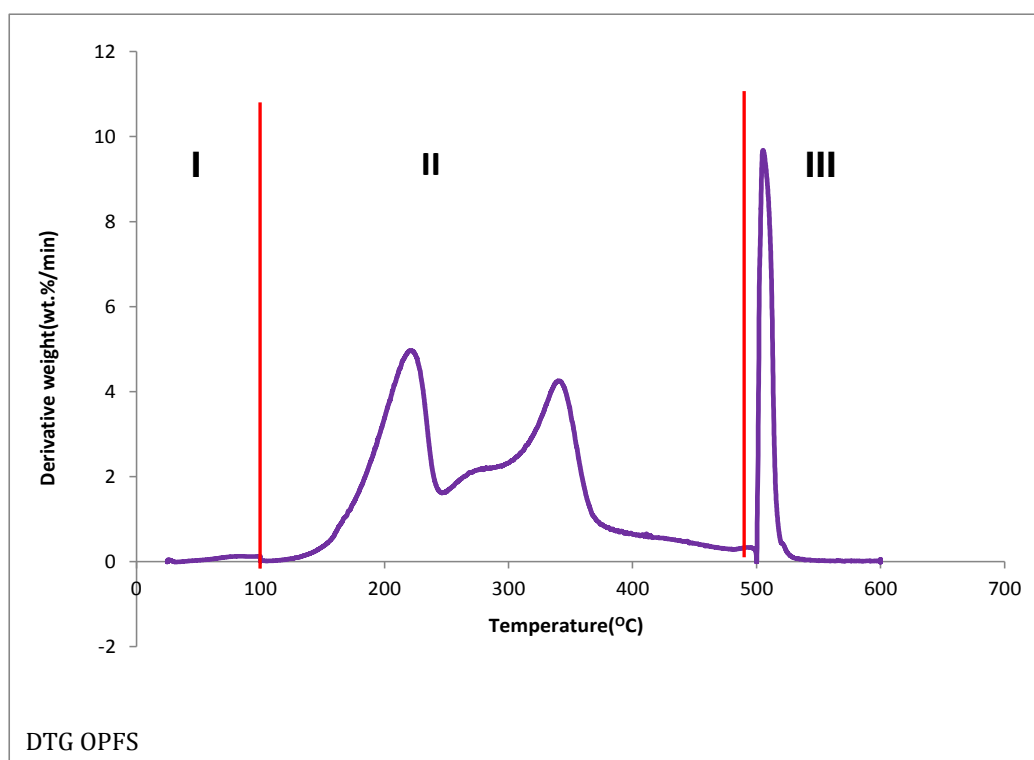
Figure 5.4: Derivative thermogravimetric analysis of OPFS in N_2 (I-II) & air (III) environments.
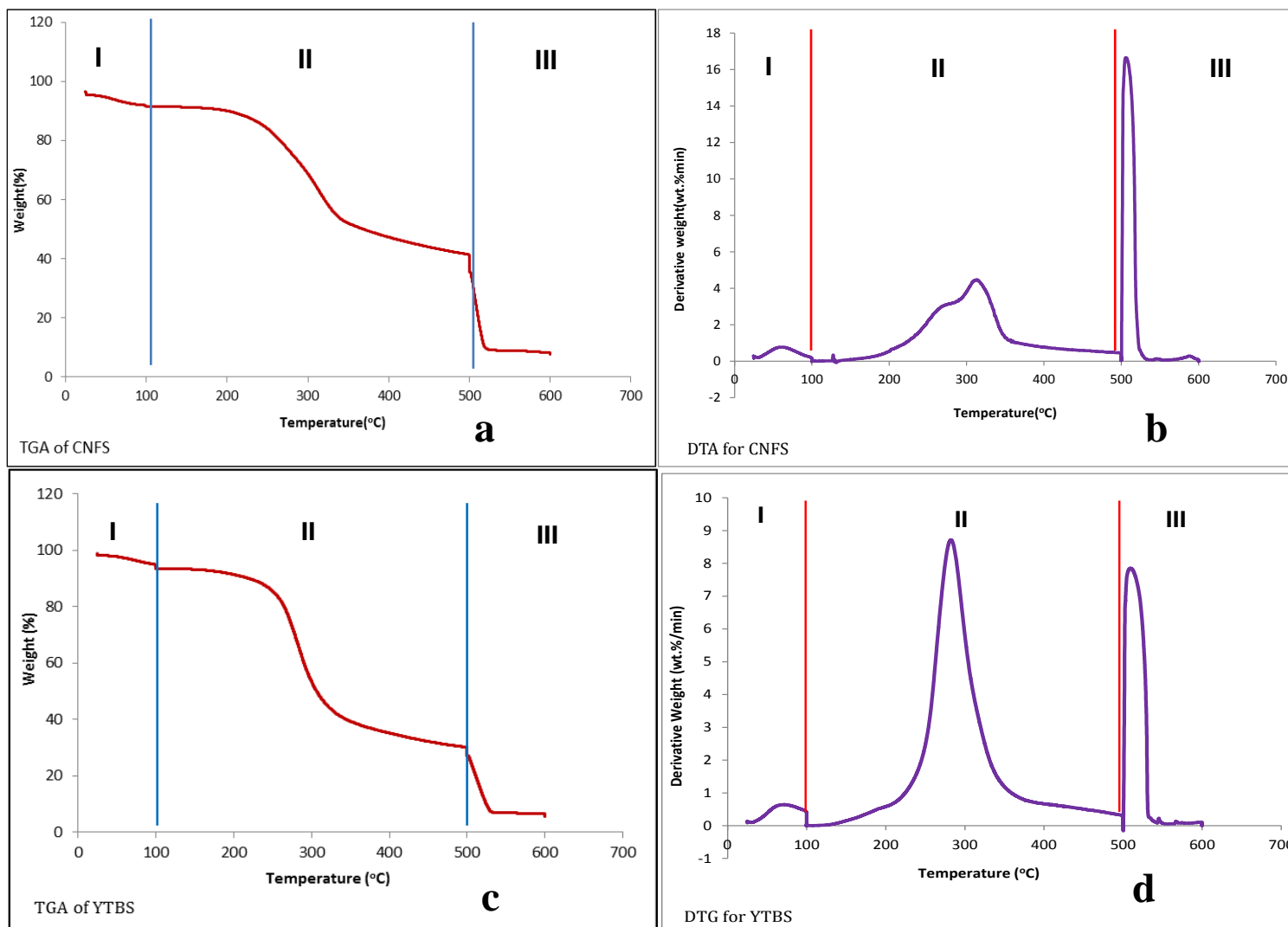
Fig 5.5 Thermogravimetric (TGA) and derivative thermogravimetric (DTG) analysis of CNFS & YTBS in N_2 (I-II) & air (III) environments
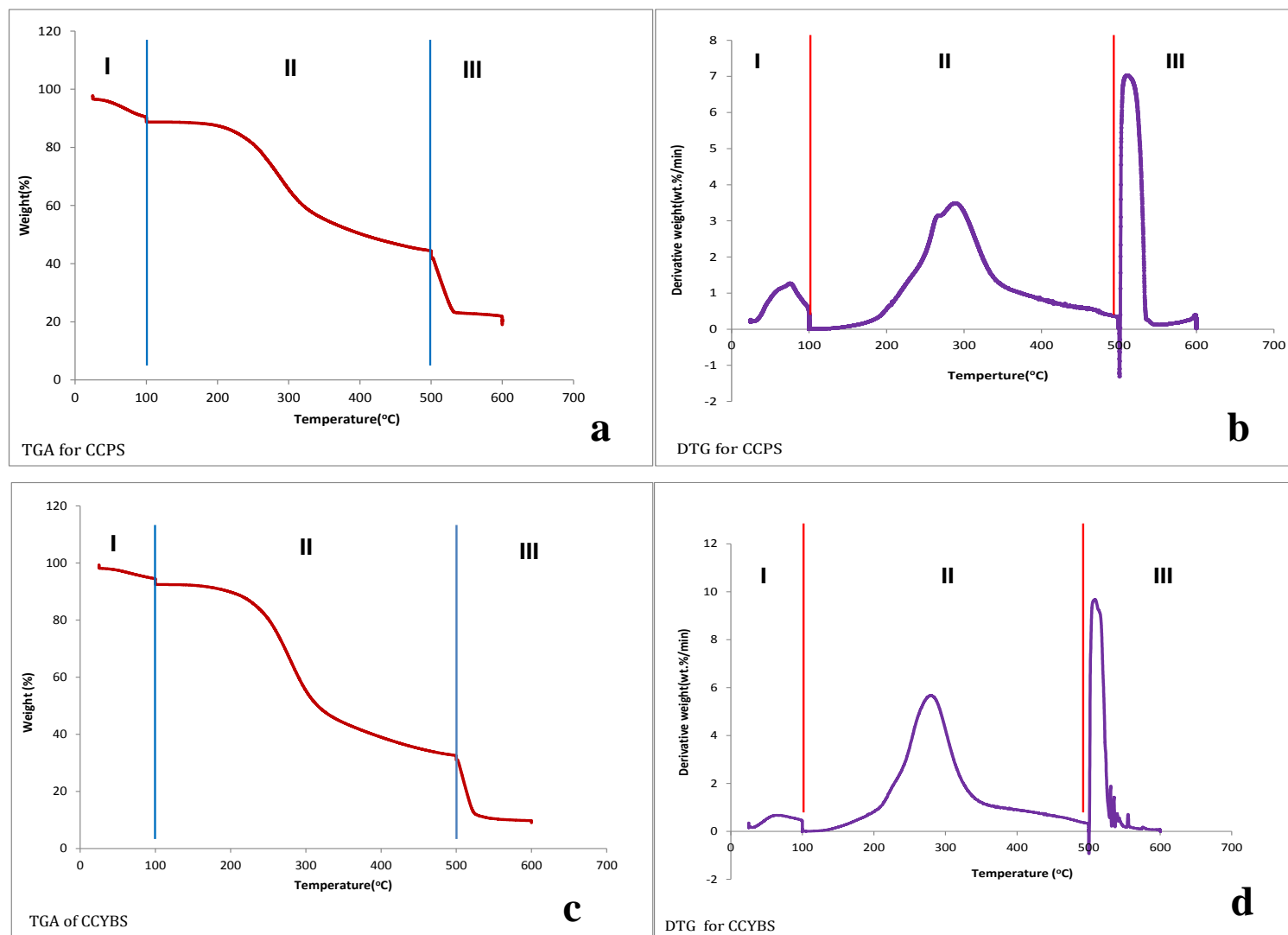
Fig 5.6 Thermogravimetric (TGA) and derivative thermogravimetric (DTG) analysis of CCPS & CCYBS in N_2 (I-II) & air (III) environments
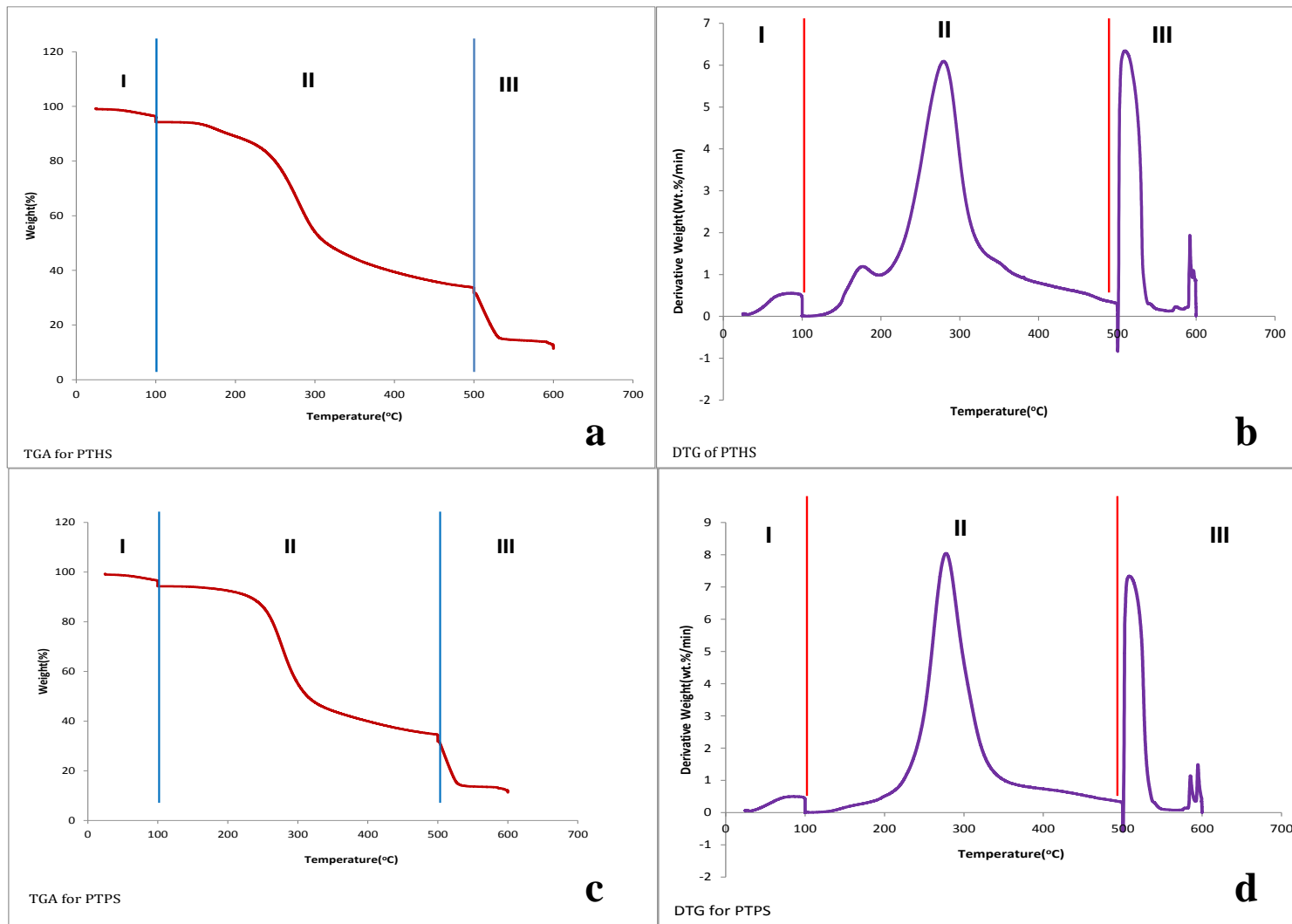
Fig 5.7: Thermogravimetric (TGA) and derivative thermogravimetric (DTG) analysis of PTHS & PTPS in N_2 (I-II) & air (III) environment

This stage is characteristic of the thermal decomposition of lignocellulosic biomass with a high rate of weight losses and has maxima in the DTG curve (Fig.5.5b) between 270-310°C which indicates the simultaneous thermal depolymerisation of residual hemicellulose and cellulose components (Li *et al.,* 2016; Unuabonah *et al.,* 2013; Liu *et al.,* 2006). Lignin is the most stable component of the lignocellulosic biomass due to its aromatic content and its thermal decomposition proceeds slowly and gradually to the end of the pyrolysis section of the TG curve at 500°C making it an important contributor to the fixed carbon content of the residue (Chang *et al.,* 2015). At the end of this regime (II), the fixed carbon content of the YTBS adsorbent was 21% which shows its carbon content that is intrinsic in the chars. The third region (III) in the TG curve (Fig. 5.5a) shows the carbonisation of the resulting chars from the pyrolysis regime (20- 500 °C) to obtain the residual ash composition of the YTBS adsorbent. This region is characterised by a peak in the DTG curve (Fig.5.5b) between 503-530°C which corresponds to the decomposition of the chars in air. The resulting residue from the char carbonisation gives the ash content of the YTBS adsorbent (5%) which was comparable to the ash content obtained via the AOAC (2000) method (8%) as shown in Table 5.4.

The thermograms of CCPS, CCYBS and PTHS in Figs 5.6 & 5.7 all presented similar degradation profiles as that of the CNFS adsorbent and YTBS however there were certain distinguishing characteristics for each of these residues. The CCPS and CCYBS had higher weight loss percentage in both region (I) and (II) corresponding to moisture and volatile content elimination. For the CCPS residue, weight loss due to moisture and volatile fractions are 9 and 46% respectively. While CCYBS residue has a 6.8 and 61.50% weight loss for the same fractions. The PTHS residue has a moisture loss of 5%, while its corresponding volatile component loss was 62.5%. In the degradation profile of the PTHS adsorbent (Fig 5.7b), there is a small peak that can be identified between 180 – 200°C which may be associated to a faster rate of decomposition of the hemicelluloses in the residue structure (Ramos *et al.,* 2008).

The degradation profile of the PTPS residue presented in Figs 5.7c & d indicates that the weight loss in the first stage (I) (moisture evolution) was 4.9%, the second stage (II) of the weight loss regime (evolution volatile component) was 62.4% with a peak in the DTG plot (Fig. 5.7d) that can be associated with hemicellulose, cellulose and lignin decomposition between 180 and 380°C. Lignin decomposition is the last component of the volatile matter

that is eliminated at temperatures up to 500°C. The third stage (III) is the oxidation of fixed carbon on the residue (20.5%) and occurs between 500 and 600°C with the ash component as the final residue which is composed of the inorganic elements (11.2%).

From the thermal degradation profiles of the residues, it is observed that the amount of the residue that had decomposed below 500°C varied between 55% and 70% with most of it occurring between 150°C and 450°C. The derivative thermogram (DTG) of all the residues indicated a single peak for the volatile component elimination (stage II) (with the exception of OPFS and PTHS) corresponding to the hemicellulose, cellulose and lignin degradations. The two peaks in the DTG curve for the PTHS and OPFS adsorbents indicates that there may be two competing devolatilisation reactions corresponding to the degradation of the three components (hemicellulose, cellulose and lignin degradations) occurring simultaneously with a little time lag (Padmavathy *et al*., 2003).

An examination of all the residue adsorbents indicates that the CCPS residue had the highest percentage moisture loss (9%), while the OPFS had the least (1.73%) thereby implying that the OPFS residue will have the least energy requirement prior to its use as an adsorbent. The CCPS residue also had the least volatile content (46.8%), while the YTBS residue had the highest. For ash content, the YTBS residue had the least (5.50%), while the CCPS residue had the highest (18.9%) indicating that the CCPS residue had the highest inorganic elemental composition amongst the all the reside adsorbents. The percentage fixed carbon content of the residue is an indication of the carbon content and its useful when evaluating biomass that may be used for the production of activated carbon based adsorbents. The fixed carbon content of the 7 residues shows that the OPFS adsorbent had the least (11.9%), while the CNFS residue had the highest (27.8%) and the other six residues had fixed carbon content between 20.3% and 21.9%. This result showed that these residues can be used for the production of activated carbon based adsorbents.

The thermal degradation profile of the residue adsorbents are similar to the profile of orange and almond peels reported by Boumediene *et al.,* (2015) in their study on the characterisation of two cellulosic waste materials for use in removal of methylene blue from aqueous solutions. A three stage thermogravimetric analysis (TGA) and differential thermal analysis (DTA) profile for ryegrass leaves (*Lolium the perenne*) showing the different stages of weight loss associated with the different components of a lignocellulosic polysaccharide has also been reported by Liu *et al.,* (2006). Furthermore, the degradation profile of all the 7 residues adsorbents evaluated here have similar profiles to that reported

in selected literature as noted by Titiloye *et al*., (2013) based on the evaluation of the thermo-chemical characteristic of some agricultural waste from West Africa. Comparing the results in their study with the residue adsorbents produced in this work, it is observed that the percentage moisture content of the OPFS adsorbent (1.73) was lower than those reported for the various agricultural wastes such as corn straw (9.15), corn cob (8.72), rice straw (7.23), rice husk (8.59), cocoa pod (10.2), Jatropha cakes (10.0), moringa cakes (10.38), sugar cane bagasse (8.52) and *Parinari* fruit shell (2.65). Also the percentage volatile matter component of the CCPS residue (46.8) was lower than those of the corn straw (75.0), corn cob (80.72), cocoa pod (68.4), Jatropha cakes (72.5), rice husk (58.2), moringa cakes (75.0) *Parinari* fruit shell (78.1) and sugar cane bagasse (79.4).

However, the volatile content of the CCPS residue was higher that of rice straw (45.6) (Titiloye *et al*., 2013). The percentage fixed carbon of the CNFS residue (27.8) was higher than those of all the agricultural residues - corn straw (9.70), corn cob (7.60), cocoa pod (10.4), rice straw (1.33), rice husk (8.48), Jatropha cakes (10.97), moringa cakes (8.26), *Parinari* fruit shell (14.51) and sugar cane bagasse (8.12) reported by Titiloye *et al*., (2013). Finally it was also observed that the percentage ash content of the CCPS residue (18.9) was higher than those of corn straw (6.13), corn cob (2.93), cocoa pod (10.81), Jatropha cakes (6.47), moringa cakes (6.28), *Parinari* fruit shell (4.67) and sugar cane bagasse (3.91) with exception of those of rice straw and rice husk which were 45.76 and 24.7 respectively. Hence, the thermograms shown in Figures 5.3 to 5.9 are thus representative for lignocellulosic materials and are similar to what has been reported in literature for lignocellulosic materials (Abdullah *et al.,* 2010; Stefany *et al.,* 2005).

5.5 Adsorbent zeta potential, pH and pHpzc

The adsorbate pH is a very important variable in the adsorption of metals as it determines the speciation and degree of ionization of both adsorbate species and functional groups on the adsorbent in solution (Sardella *et al.,* 2015). The pH of the residues was determined as described in Section 4.3.9 and the results are presented in Table 5.6. The pH value of the adsorbate-adsorbent suspension gives an indication of the types of surface groups on the adsorbent. From Table 5.6, the value of pH of the different residues was observed to be from 6.3 to 6.9 indicating that these adsorbents are acidic.

Another property of the residues that has an effect on the pH of adsorption is the zeta potential and this zeta potential describes the charge on the hydrated surface of each

adsorbent particle when it is dispersed in water. The zeta potential of the adsorbents was determined according to the description given in Section 4.3.3. This charge is determined by the adsorbent particle reaction with the ions in solution which is either the hydronium ion (H_3O^+) or the hydroxyl ion (OH^-). When there is an addition of H_3O^+ ion into the aqueous system, there is a reduction in pH which results in the uncharged particle surface being protonated leading to a positive charge. When there is addition of OH^- ions, this ion will remove the hydrogen from the surface (neutralizing) all the protons until all the positive charge is eliminated thereby producing a negative surface charge. This drive to the negative surface charge zone passes through a point at which sum of H_3O^+ and OH^- ions are equal resulting in a zero net surface charge (Gonzalez-Navarro *et al.*, 2014).

Table 5:6: pHpzc and pH of unmodified residue adsorbents

Adsorbent	pHpzc	Adsorbent pH
OPFS	6.5	6.90
CNFS	5.5	6.77
CCPS	6.3	6.67
CCYBS	5.5	6.86
PTHS	6.1	6.56
PTPS	5.7	6.32
YTBS	5.9	6.43

Hence, the zeta potential of an adsorbent in solution is an important tool used to characterise the electrokinetic behaviour of the solid-liquid interface. It is influenced not only by the surface charge on the particle but also by the environmental conditions in which the particles are suspended thus giving the characteristic property of the adsorbent in solution. The pH point of zero charge (pHpzc) is defined as the pH of the suspension at which the surface acidic (or basic) functional groups of an adsorbent no longer contributes to the pH of the solution. The pH at which this point of zero charge occurs is called the pH point of zero charge (pHpzc) and this is the point of interest as this pH indicates the two regions on which an adsorbent can be used for the adsorption of positive or negative species (Nomanbhay and Palanisamy, 2005).

Thus for the adsorption of positive species such as metal ions as is the case in this study, the pH at which the adsorption will be carried out must be above the pHpzc as the adsorbent surface charge has to be negative to attract and adsorb positive ions like the two ions of interest in this research. The pH of the adsorbent also plays an important role in the determination of the working pH for the sorption system for Cd (II) and Pb (II) ion removal hence the determination of the zeta potential must be based on the solution pH. The plot of the adsorbent suspension zeta potential vs. the pH is used to determine the pH point of zero charge (pHpzc) of each adsorbent. The pHpzc of the unmodified residues determined from the procedure in Section 4.3.2 are presented in Table 5.6 and the zeta potential vs pH plot for each residue adsorbent is presented in Appendix 3. From the results it can be seen that all the residues had pHpzc between 6.5 and 5.53 and their corresponding solution pH are from 6.43 to 6.9, so to have an optimum metal ion sorption the pH of the adsorbate should lie between 6.5 and 7 for both ions taking into consideration the metal ion tendency to form hydroxides and precipitate at higher pH values (Ibrahim *et al.,* 2010).

Hence the pH of 6.5 was chosen for metal ion sorption studies as the target ions of were cations, this is because a pH that is above the pHpzc has to be chosen to facilitate the adsorption of the positive Cd(II) and Pb(II) ions by the different residue adsorbents. Similar results for the pHpzc of lignocellulosic adsorbents have been reported in literature. A pHpzc of 6.6 was also obtained for African white star apple (*chrysophyllum albidium*) shell by Onwu and Ogah (2010) in their studies on the effect of pH on the sorption of Cd(II), nickel(II) and chromium(VI) from aqueous solution. Prola *et al.,* (2013) has also reported a pHpzc of 5.85 for *Jatropha curcas* shell used as a biosorbent for the removal of Reactive Red 120 textile dye from aqueous solution.

5.6 Powdered X-ray diffraction analysis of residue adsorbents

The crystalline or amorphous nature of the residue adsorbents was determined using X-ray powder diffractometry and the nature of the phases was characterised based on the diffraction pattern exhibited. The X-ray diffraction patterns which show the phase composition and microstructure of the residues were determined according to the description in section 4.3.6 and are shown in Figures 5.8 to 5.12. The XRD data and patterns of the residues were analysed using the Joint Committee on Powder Diffraction Standards (JCPDS) files (Park *et al*., 2008) and related literature. The peaks on the residue adsorbents were also compared with of that of cellulose diffraction peaks in Wang *et al.,*

(2009) as shown in Fig. 5.11. The peak height method for dermination of cellulose crystalinity in cellulose I as presented in Fig 5.11 was used to evaluate the cellulose crystalinity of the different residues (Terinte *et al.,* 2011). The main peaks on the XRD belong to cellulose (amorphous and crystalline) and silica. The XRD pattern of crystalline cellulose I is also inserted in Figure 5.11 as a basis for comparison. The XRD of the 7 residue adsorbents and those obtained after Cd(II) ion sorption of the 7 adsorbent were used for the characterisation study.

The crystalline cellulose phases are between $2\theta = 21.60^\circ$ to 21.75° for cellulose II and $2\theta = 22.56^\circ$ to 22.65° for cellulose I, whereas the amorphous cellulose peaks are between $2\theta = 18.96^\circ$ to 19.05° for amorphous cellulose I and $2\theta = 15.96^\circ$ for amorphous cellulose II (Tserki *et al.*, 2005). The peaks at $2\theta = 26.75^\circ$ to 26.82° in the different residue adsorbents are assigned to crystalline silica as observed by (Ghorbani *et al.,* 2013). These peaks assignments are in agreement with those of native cellulose - that is at $2\theta = 22.60^\circ$ (Deraman *et al.,* 1999). The analysis of these peaks in all the residues indicates that the same type of cellulose is present within the structure of the seven different residues and this was also observed by Deraman *et al.*, (1999).

Figure 5.8 shows the diffractograms for the fresh OPFS adsorbent and the adsorbent after Cd(II) sorption(OPFS-Cd). The pattern of the fresh adsorbent (OPFS) shows the presence of few well-defined diffraction peaks. The well-defined diffraction peaks in the XRD pattern is due to highly ordered areas in the structure and indicates the presence of crystalline cellulose I phases and silica (SiO_2). The three main peaks in the OPFS are at $2\theta = 21.52^\circ$, 14.95° and 26.67° which can be indexed to the diffraction planes associated to cellulose (002), (101) and (SiO_2). For the OPFS-Cd adsorbent, two diffraction planes can be identified and these are at $2\theta = 21.74^\circ$ and $2\theta = 26.91^\circ$ that can be associated to the cellulose (002) and SiO_2 reflections.
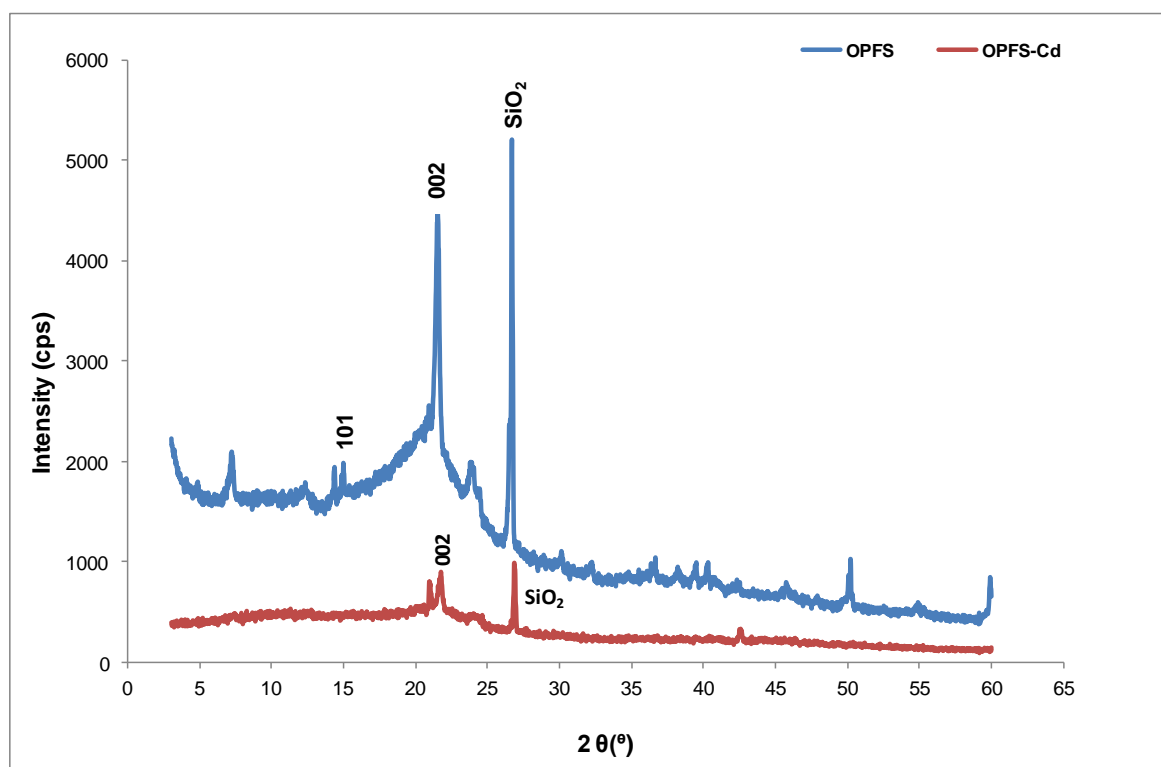
Figure 5.8: X-ray diffractogram of OPFS and OPFS-Cd

The diffractograms of the PTHS and CNFS adsorbents are presented in Figure 5.9. The XRD of the raw PTHS adsorbent and the adsorbent after Cd(II) ion sorption (Fig 5.9a) all show 3 similar peaks. The diffraction planes at $2\theta = 21.53°$, $17.22°$ and $14.94°$ for the PTHS adsorbent and at $2\theta = 21.58°$, $17.22°$ and $14.92°$ for the PTHS-Cd adsorbents indicate the diffraction planes of cellulose (002), (10Ī) and (101) respectively. There was no peak associated with SiO_2 in the XRD of the PTHS adsorbents. For the CNFS adsorbent shown in Fig. 5.9b the diffraction peaks were less pronounced indicating the amorphous nature of the adsorbent. The diffraction planes at $2\theta = 21.67°$, $15.65°$ and $26.62°$ were diffraction planes of cellulose (002), (101) and (SiO_2). There was no diffraction peaks associated with the CNFS-Cd adsorbent thus implying that the adsorbent obtained after sorption was very amorphous.

Figure 5.10 displays the diffractograms of the CCYBS and CCPS adsorbents. The XRD of the CCYBS adsorbent (Fig.5.10a) shows the presence of four diffraction planes at $2\theta = 15.02°$, $18.00°$, $22.72°$ and $26.75°$ which are associated to the diffraction planes of cellulose (101), (10Ī), (002) and (SiO_2). The XRD pattern of the adsorbent after Cd(II) ion sorption (CCYBS-Cd) confirmed only the presence of the SiO_2 peak at $2\theta = 21.74°$ which meant that the sorption process decreased the crystalline phases in the adsorbent thereby making it more amorphous.
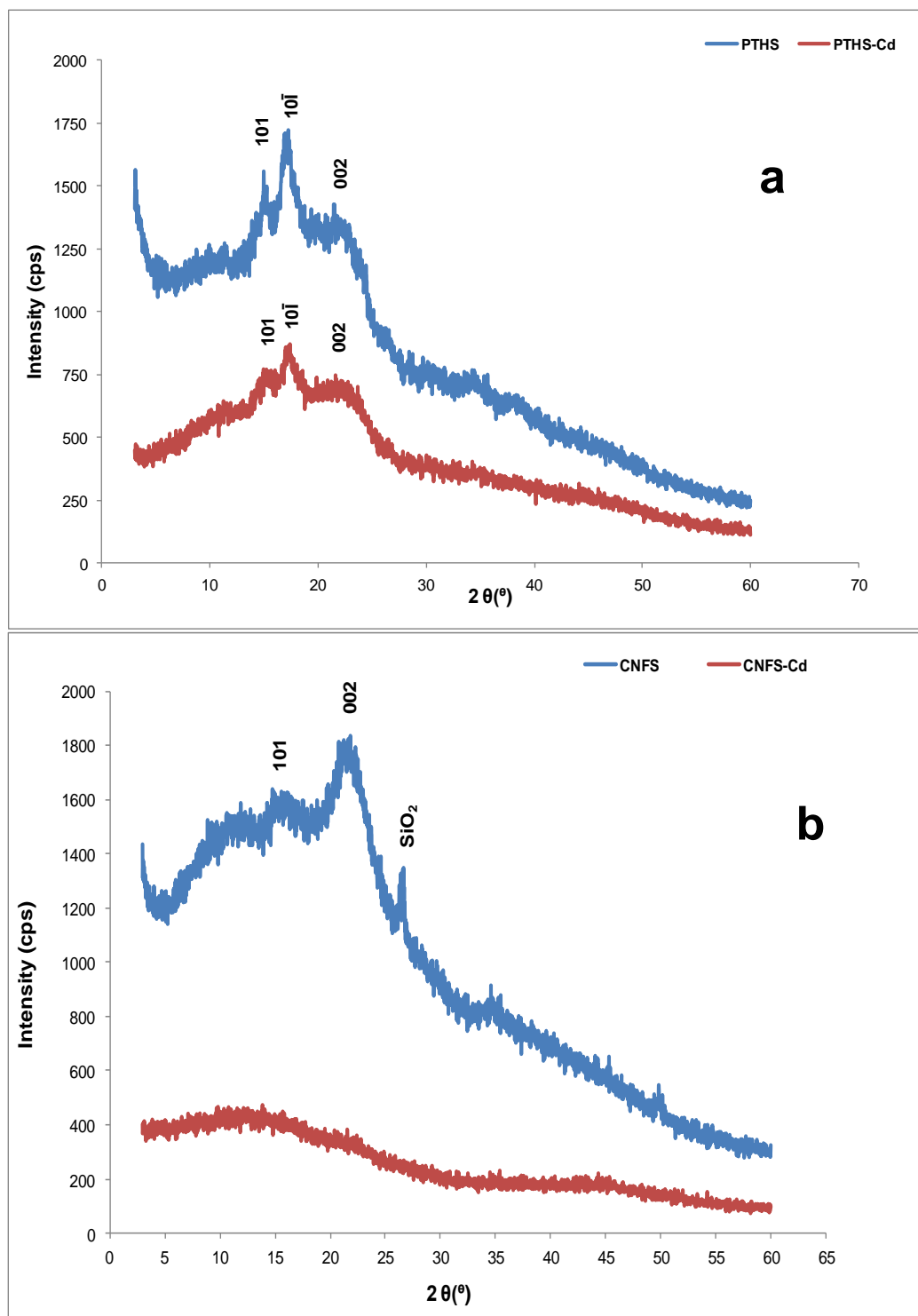
Figure 5.9: X-ray diffractograms of (a)PTHS and PTHS-Cd and (b) CNFS and CNFS-Cd.
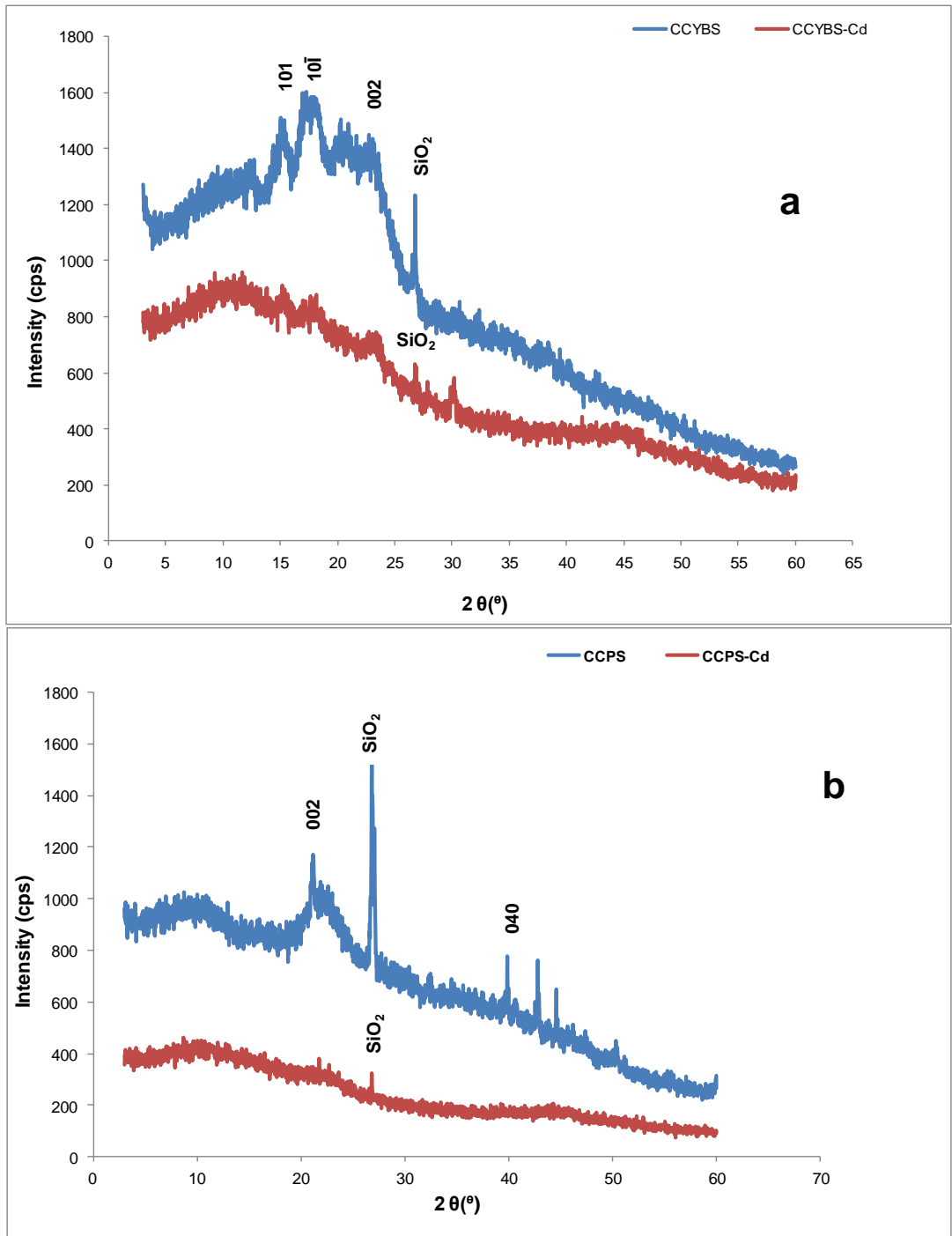
Figure 5.10: X-ray diffractograms of (a)CCYBS and CCYBS-Cd and (b) CCPS and CCPS-Cd.
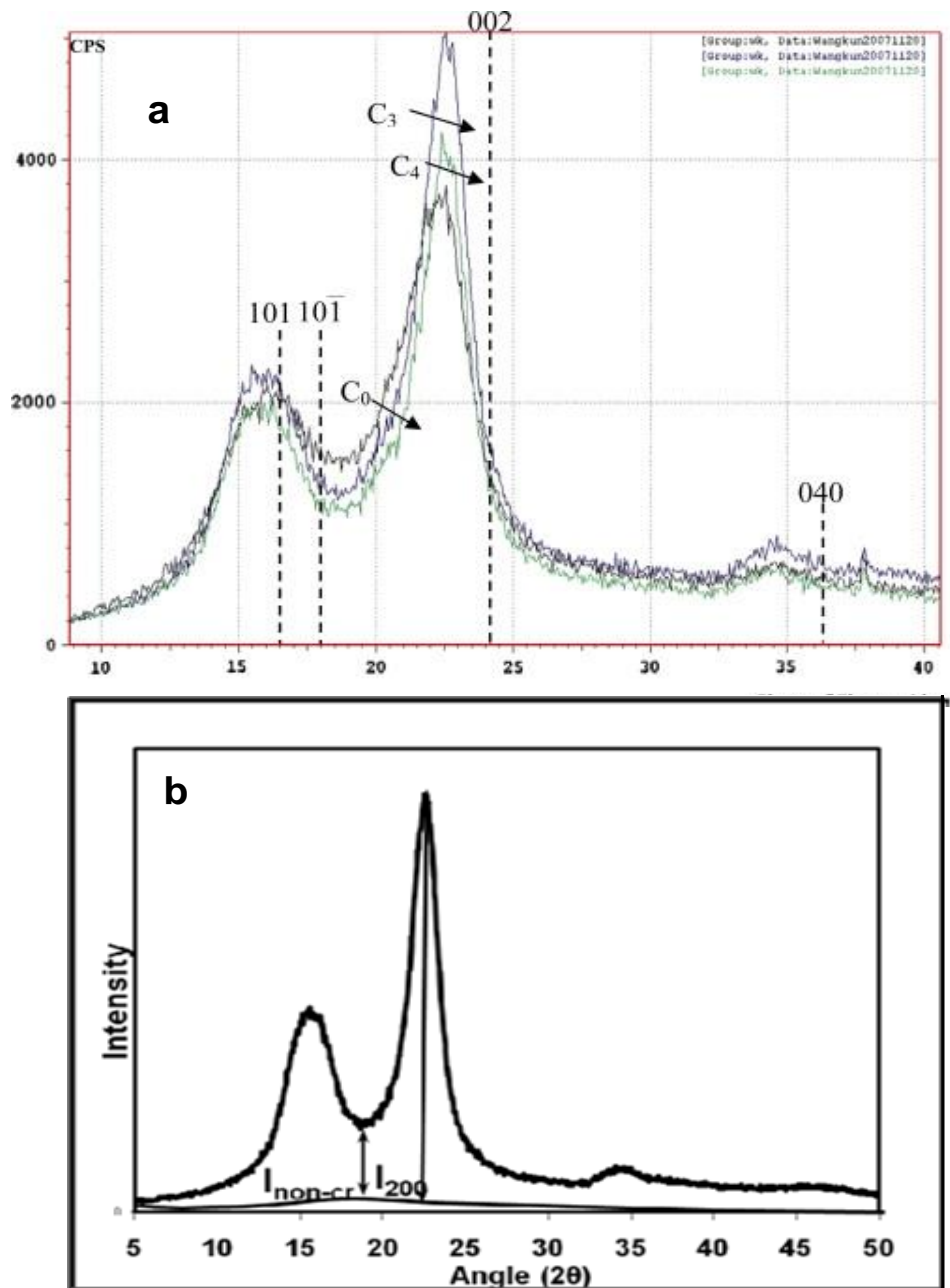
Fig 5.11: (a) XRD of diffractogram of cellulose diffraction peaks (Wang *et al.*, 2009) and peak height method for dermination of cellulose crystalinity in cellulose I (Terinte *et al.*, 2011)

The XRD of the CCPS adsorbents shown in Fig. 5.10b indicates the presence of three peaks for the residue before sorption (CCPS) and a single peak for the adsorbent after Cd(II) ion sorption (CCPS-Cd). For the CCPS adsorbent the diffraction planes at $2\theta = 21.64°$, $39.86°$ and $26.82°$ can be associated with the diffraction planes of cellulose (002), (040) and (SiO$_2$). For the CCPS-Cd there was a single peak at $2\theta = 26.80°$ which confirms the presence of SiO$_2$ in the adsorbent after sorption. The diffractograms of the PTPS and YTBS adsorbents are presented in Fig. 5.12. For the PTPS adsorbent shown in Fig. 5.12a,

197

three diffraction planes are present at $2\theta = 17.05^{°}$, $21.06°$ and $26.65°$ which are associated to the diffraction planes of cellulose ($(10\bar{1})$, (002) and (SiO_2)). The XRD of the PTPS adsorption after Cd(II) ion sorption was amorphous as it did not possess any diffraction peaks. The XRD of the YTBS and YTBS-Cd adsorbents are shown in Fig. 5.12b. The pattern of the fresh adsorbent (YTBS) shows the presence of few well-defined diffraction peaks and a broad peak which indicates that the YTBS adsorbent is mainly amorphous. The well-defined diffraction peaks in the XRD pattern is due to highly ordered areas in the structure and indicates the presence of crystalline cellulose I phases and silica (SiO_2). The broad peak which is due to less ordering in the lignocellulosic structure confirms the presence of amorphous lignocellulosic material such as amorphous cellulose, hemicellulose and lignin (Nascimento *et al.,* 2012). For the YTBS adsorbent, the main diffraction signals at 2θ values of $15.5°$, $17.2°$, $21.0°$ and $36.7°$ can be indexed to the (101), ($10\bar{1}$), (002) and (040) diffraction planes of cellulose I respectively (Wang *et al*., 2009; Nascimento *et al.,* 2012). The diffractogram peak at $2\theta = 26.7$ $°$ which indicates the presence of silica (SiO_2) on the adsorbent matrix confirms the results of the chemical analysis of the residues reported previously using XRF. For the YTBS-Cd adsorbent the diffraction signals observed were at $2\theta = 16.9°$ and $26.8°$ which were assigned to the ($10\bar{1}$) diffraction plane of cellulose I and silica respectively. The peaks for cellulose I ($10\bar{1}$) and silica (SiO_2) were observed to decrease after Cd(II) sorption in the YTBS-Cd diffractogram which reveals that there was a change in the crystallinity of the YTBS adsorbent after sorption (Sarada *et al.,* 2014).

The crystalline cellulose peak at $2\theta = 21.60$ to 22.65 is well defined in the PTPS and OPFS residues but that of the CNFS, CCYBS, YTBS, CCPS and PTHS residue show broader peaks. These broad peaks are presumed to arise from the interference of the adjacent peaks due to the amorphous signals (linked to the presence of the amorphous cellulose, lignin and hemicellulose within this region) with the crystalline cellulose peak. The diffractograms of all the residues indicates that most of the structures in each residue are amorphous therefore it can be inferred that these lignocellulosic residues used in this study had low crystallinity due to the absence of ordered periodicity in their diffraction patterns.
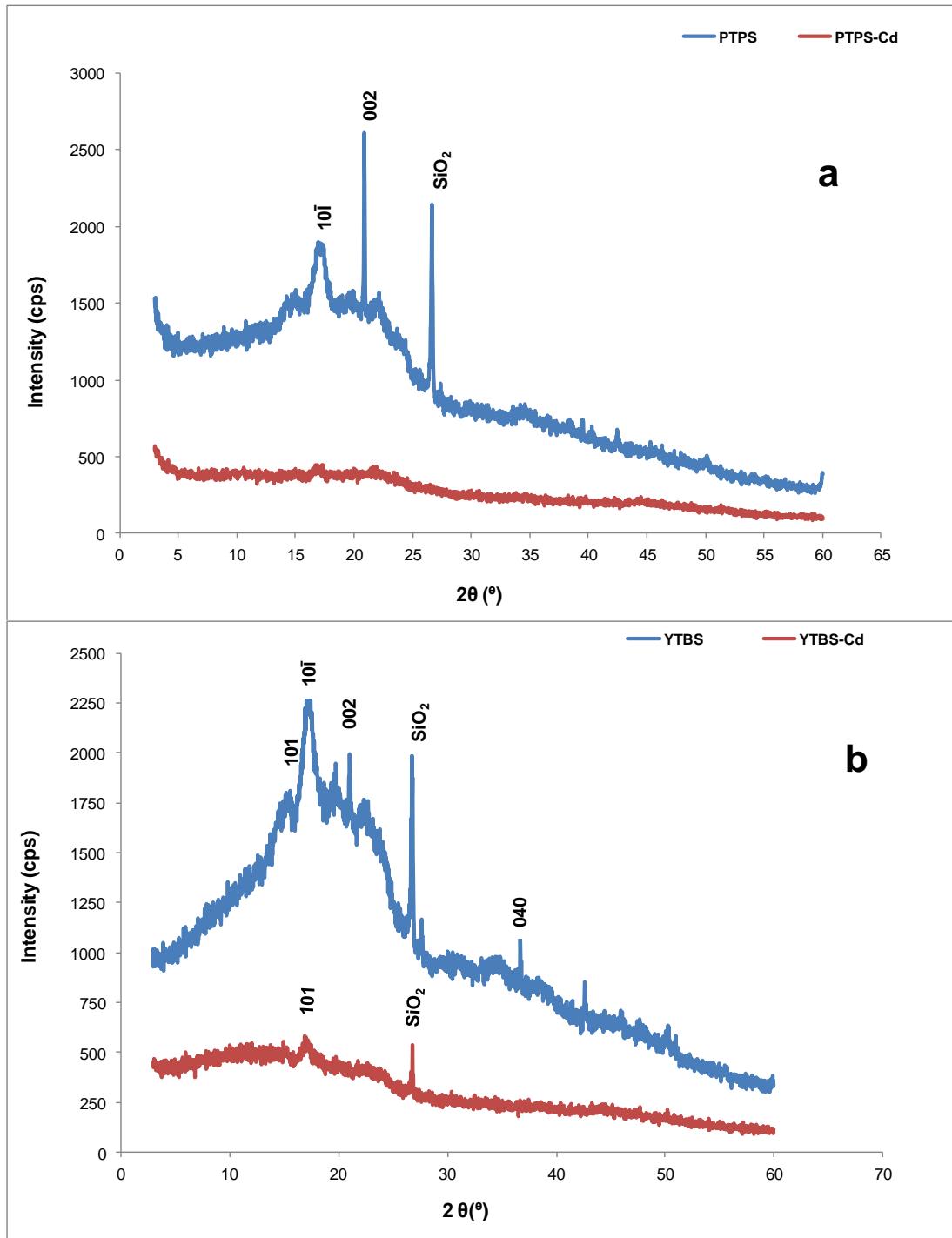
Figure 5.12: X-ray diffractograms of (a)PTPS and PTPS-Cd and (b) YTBS and YTBS-Cd.

The cellulose crystallinity index (CrI) of the 7 residue adsorbents were calculated using the peak height method based on eqn. 5.1 (Terinte *et al.,* 2011; Xiao *et al.*, 2011 and Segal *et al.*, 1959) as follows:

$$CrI(\%) = \left[\frac{I_{002} - I_{am}}{I_{002}}\right] X\ 100 \qquad (5.1)$$

Where, I_{002} is the intensity of the crystalline region in the residue at 2θ about 21.0°.

I_{am} is the intensity of the amorphous region (cellulose, hemicellulose and lignin) at a baseline at 2θ about 16.0° as shown in Fig. 5.11b.

Eqn. 5.1 was used to determine the cellulose crystallinity index (CrI) of the 7 residue adsorbents and these were 58% (OPFS), 7.3% (PTHS), 45% (PTPS), 29.4% (CCPS), 7.87% (CCYBS), 20.6% (CNFS) and 19.2% (YTBS). This implies that the OPFS was the most crystalline and the PTHS adsorbent was the least. It was not possible to determine CrI of the residue adsorbents after Cd(II) ion sorption as the peak for the (002) phase was not well defined due to the amorphous nature of the different adsorbents. The crystallinity indexes of most of residue adsorbents (except OPFS) are lower than that reported for Teff straw adsorbent (52.0%) by Wassie and Srivastava (2016) in their study on chromium removal from wastewater using Teff straw. The presence of different diffraction peaks for Cellulose I and the cellulose crystallinity index of *Lespedeza crytobotrya* stalks has also been reported by Wang *et al.,* (2009) in their study on the Influence of streaming pressure on steam explosion pre-treatment of Lespedeza stalks (*Lespedeza crytobotrya*). The contribution of lignin to the structure of the cellulose may also be a factor that contributes to the absence of ordered periodicity in the structure of the residues as lignin is mainly amorphous and high lignin content in the residues will affect the diffraction pattern of the residues (Cheng *et al.*, 2011).

The main aim of the carrying out the XRD analysis of these residue adsorbents was to investigate the effect of metal sorption on the degree of crystallinity of the residue adsorbents. This was not possible due to the broadening of the peaks associated with amorphous cellulosic phases on the matrix of these residue adsorbents and the disappearance of some of the characteristic peaks for cellulose (002) after Cd(II) ion sorption. It may however be inferred from the diffractograms after Cd(II) ion that the interaction of residues with the adsorbate system reduced or destroyed the crystalline cellulose components on the different adsorbents. This may be due to the effect of the pH of the adsorbate system on these crystalline phases thereby making the resulting used adsorbent more amorphous. This has also been observed by Diaz-Teran *et al.,* (2003) in their study on the crystallinity of lignocellulosic materials and they report that the amorphous structure of cellulose in lignocellulosic biomasses presents different band widths that make the correct assignment of peak associated with the crystalline cellulose difficult.

5.7 Adsorbent surface morphology

The use of scanning electron microscopy for the imaging and characterisation of natural residues and adsorbents provides information on the morphology and effect of the modification of the adsorbent after sorption. SEM imaging is obtained by the scanning of the surface of the residue or adsorbent with a high energy beam of electrons and the resulting surface interactions with the atoms of the sample generate signals that contain information on the topography, morphology and chemical composition of the sample surface (Sarada *et al.,* 2014). SEM imaging of the residue adsorbents was carried out as described in section 4.3.2. The SEM analysis of the adsorbents was carried out to obtain textural and surface morphological information of each adsorbent before adsorption and to determine its surface characteristics and evaluate any change in the surface as a result of the adsorption. The morphology of the OPFS, CCPS and CNFS residues are shown in Figures 5.13, 5.14 and 5.16 while that of the other residue adsorbents are presented in Figure 5.15.

| HV | Mag | WD | Det | Spot | Pressure | 400.0μm |
| 30.0 kV | 300x | 9.8 mm | LFD | 4.0 | 0.75 Torr | OPFS |
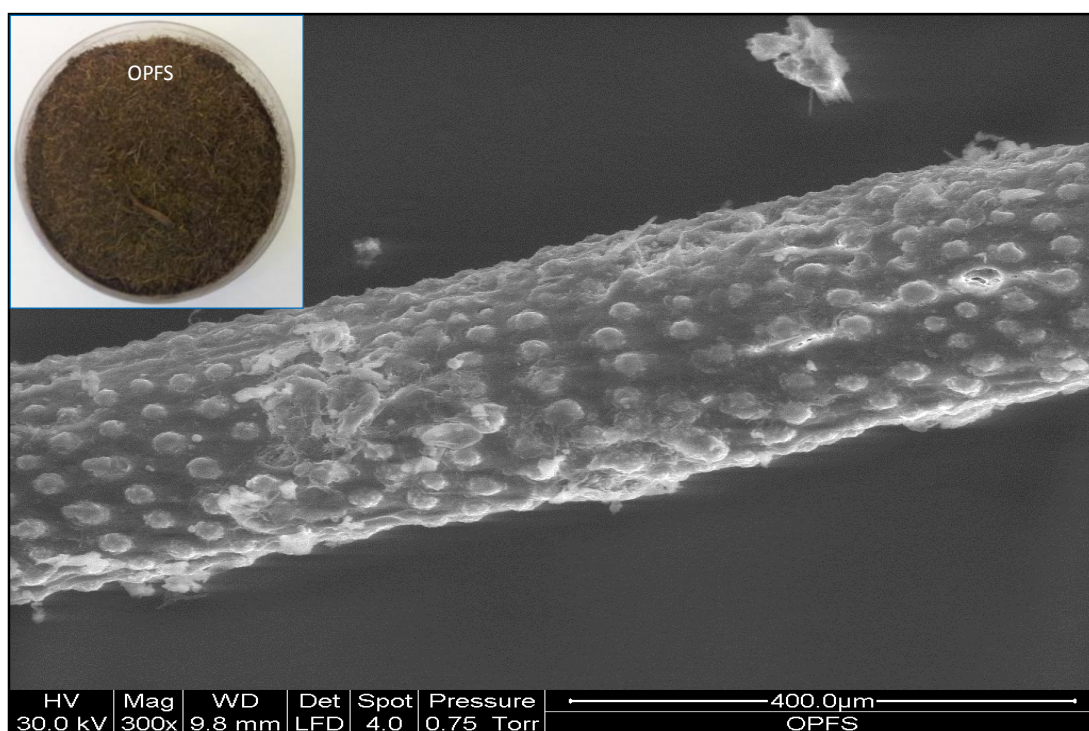
Figure 5.13: SEM micrograph for OPFS (Scale bar = 400 μm). Insert photograph of OPFS residue

The SEM micrographs of the residues indicate a rough surface on all the materials with fissures found in some of them. Some of the raw residues can be seen to have no obvious

pore structure while some had spongy structure (CCPS), the CNFS residue had pores within its structure. The microstructure, shape and size of the particles seen under the SEM show structures that can be associated with plant based materials. The SEM of some of the residues also reveals a surface texture with fine particle size indicating the presence of pore with varying sizes with the particle (Srivastava *et al.,* 2006). Photographs of the OPFS, CCPS and CNFS residues are also shown in Figure 5.13, 5.14 and 5.16, while those of the CCYBS, PTHS, PTPS and YTBS residues are presented in Appendix 4. The pictures of these residues indicate they had different surface colourations which may be attributed to their extractive (tannins) compositions. From these Figures, it can be seen that the surface of each of the residues are very rough with fissures and cavities which can be presumed to play a major role in the molecular transport of the ions during sorption (Wahab *et al*., 2012).
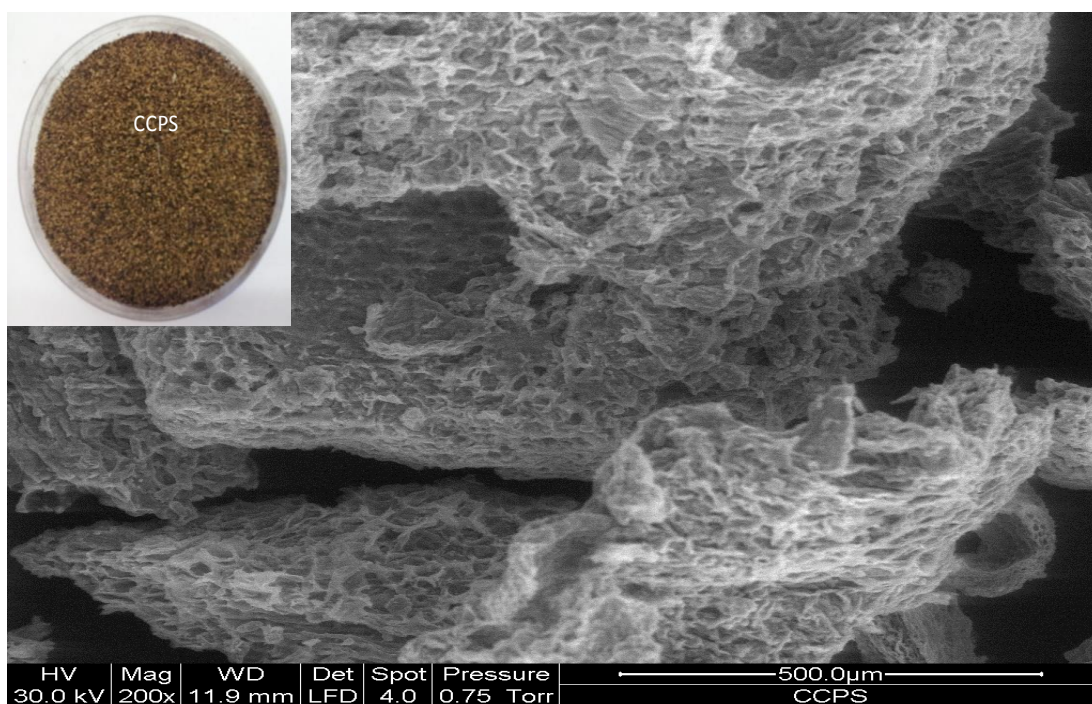
Figure 5.14: SEM micrograph for CCPS (Scale bar = 500 µm). Insert photograph of CCPS residue

These SEM images also indicate the type of botanical pores that are present in the natural residues and it is assumed that the pores can form the template for mesopores development during thermal treatment with the elimination of the volatile components on these residues (Guo *et al.,* 2005). The residues used for adsorption of Cd(II) and Pb(II) were further analysed using via SEM and the micrographs (not shown) it was observed that the structures of the residues were not altered after adsorption thereby indicating that the morphology of the residues could withstand the adsorption system. Sarada *et al.,* (2014)

reports on the imaging of algal biomass using SEM before and after adsorption and in their study the biomass surface was uneven and heterogeneous with pores on the surfaces.
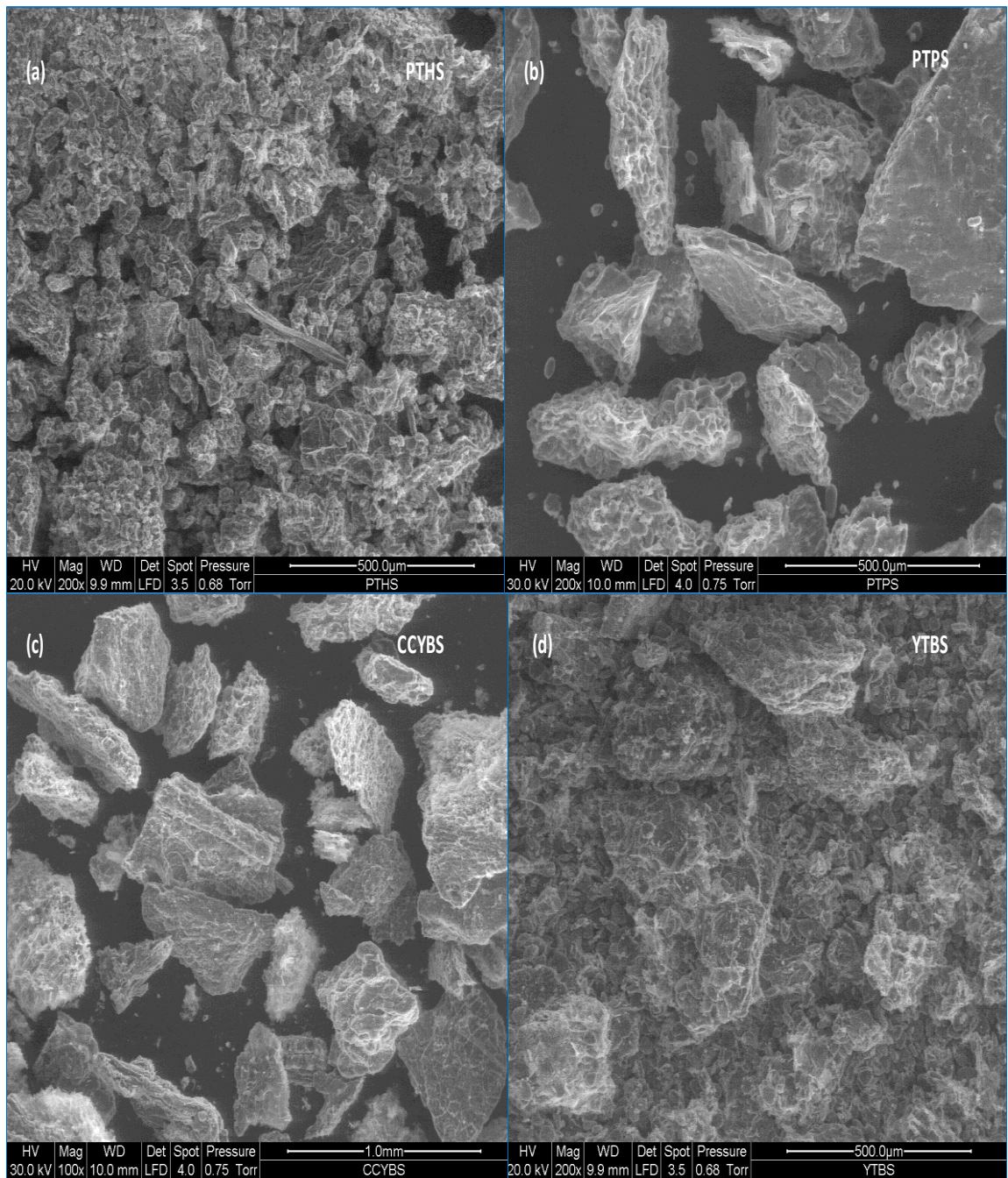
Figure 5.15: SEM micrographs for (a) -PTHS, (b) -PTPS, (c) -CCYBS & (d) -YTBS residues (Scale bars = 1.0 mm & 500 µm)
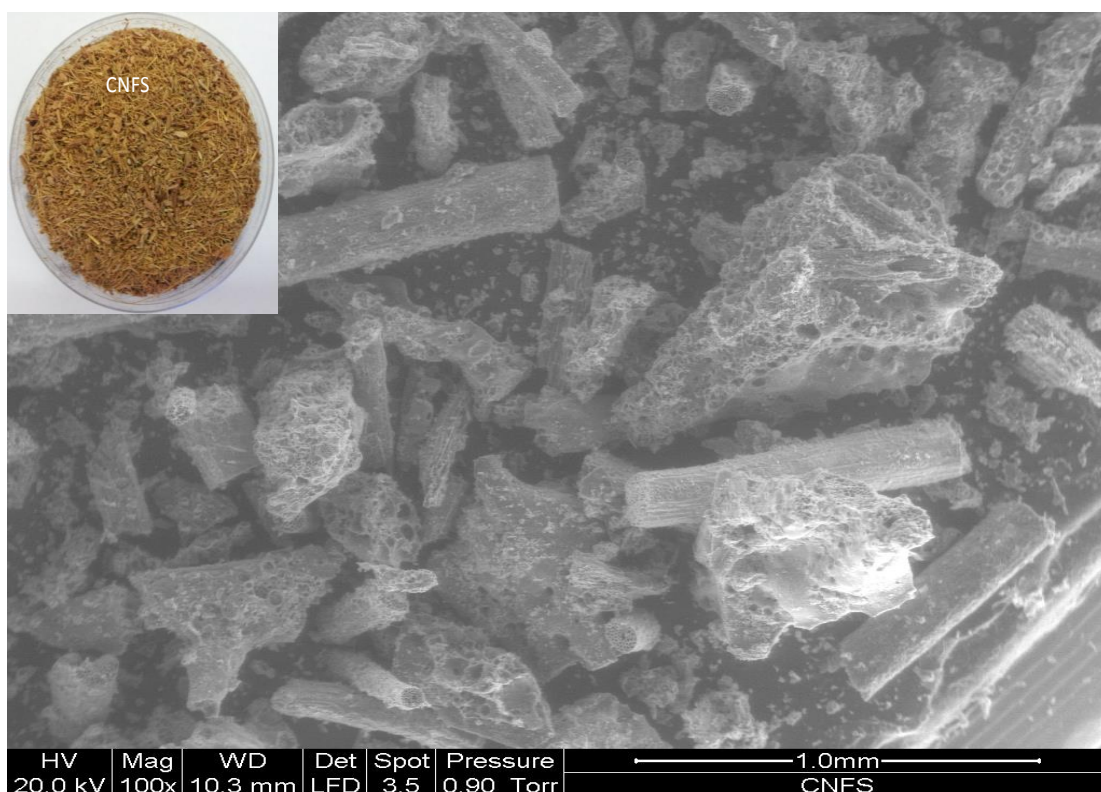
Figure 5.16: SEM micrograph for CNFS (Scale bar= 1.0mm). Insert photograph of CNFS residue

The biomass surface after adsorption had a change in morphology and this was attributed to the effect of liquid accumulation on the biomass surface. Gautam *et al.,* (2014) used SEM images in their study of mustard husk and showed that the husk had a number of pores and fissures on its surface; the information obtained from this image analysis was used to compare the residue morphology with that of the activated mustard husk.

5.8 Adsorbents chemical composition

The presence of chemical elements in an adsorbent and their relative compositions can also be determined using the energy dispersive X-ray coupled on the SEM instrument. The EDAX analysis of some of the residue adsorbents were carried out as a spot size analysis wherein the spot of interest was examined for chemical information as described in section 4.3.2. The EDAX spectrum and the relative elemental composition of the unmodified OPFS, CCPS and YTBS residue adsorbents are shown in Figures 5.17, 5.19 and 5.21, while the EDAX spectra of the CNFS, PTHS, CCYBS and PTPS adsorbents are presented in Appendix 5.

OPFS	
Element	Wt %
C	71.69
O	23.14
Mg	0.44
Al	0.69
Si	1.04
P	0.25
S	0.47
Cl	0.11
K	0.54
Ca	1.3
Fe	0.33
Total	100
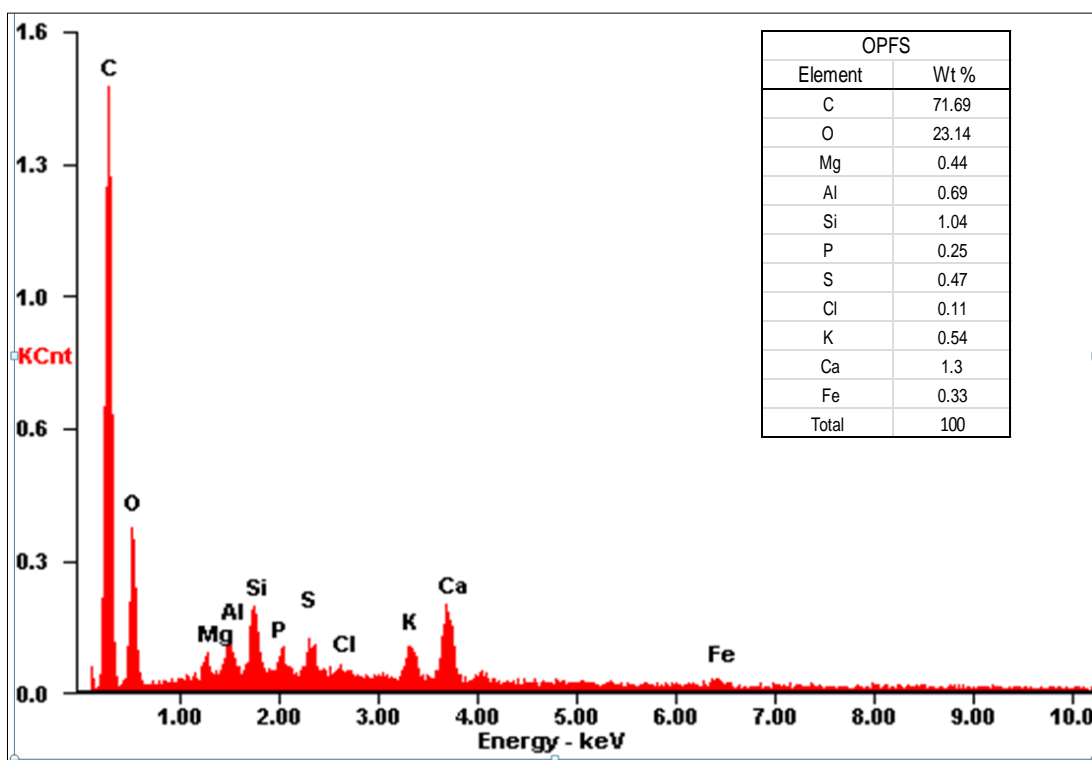
Figure 5.17: EDAX spectrum for OPFS

From Figures 5.17, 5.19, 5.21 and Appendix 5, it can be observed that the residues adsorbents are composed of carbon, oxygen and a number of inorganic elements which include magnesium, aluminium, silicon, phosphorus, sulphur, chloride, potassium, calcium and iron. The presence of these inorganic elements in the EDAX spectrum also confirms the results of the characterisation of the residue adsorbents using X-ray fluorescence and ash content analysis that has been previously reported in section 5.2 and 5.21 of this work.

The values of the elements in the EDAX spectrum is given as a percentage of elements found at a specific spot on the residues using a spot size of analysis in the SEM/EDAX system. From the EDAX spectrum of the residue adsorbents, it can be observed that all the residues namely: OPFS CNFS, CCPS, PTPS, YTBS, PTHS and CCYBS had high amount of carbon and oxygen but the percentage of calcium, iron, phosphorus, sulphur and aluminium were comparatively low. The residues used for adsorption of Cd (II) were further subjected to EDAX analysis to confirm the presence of the adsorbed metal ions. These are shown in Figures 5.18 5.20 and 5.22 for the OPFS-Cd, CCPS-Cd and YTBS-Cd residues.
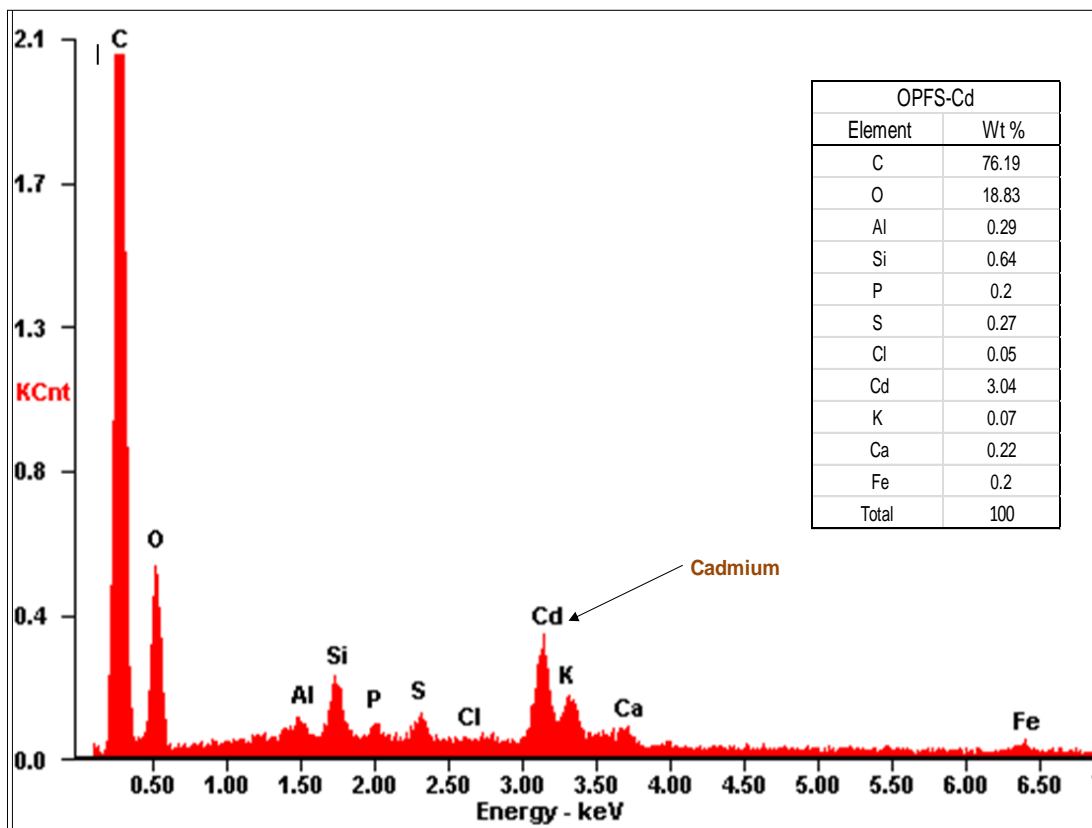
Figure 5.18: EDAX spectrum for OPFS after Cadmium adsorption

OPFS-Cd	
Element	Wt %
C	76.19
O	18.83
Al	0.29
Si	0.64
P	0.2
S	0.27
Cl	0.05
Cd	3.04
K	0.07
Ca	0.22
Fe	0.2
Total	100

Fig 5.19: EDAX spectrum for CCPS

CCPS	
Element	Wt %
C	68.89
O	26.04
Mg	0.25
Al	0.08
Si	0.12
P	0.2
S	0.43
Cl	0.09
K	3.35
Ca	0.42
Fe	0.13
Total	100
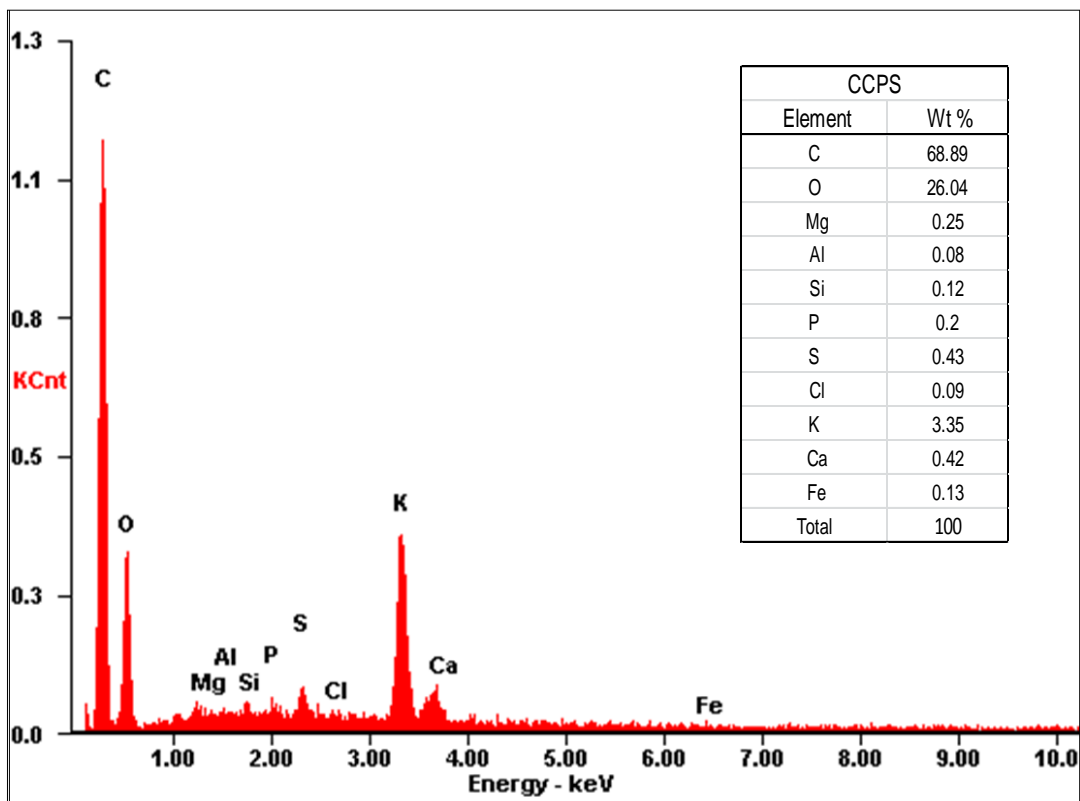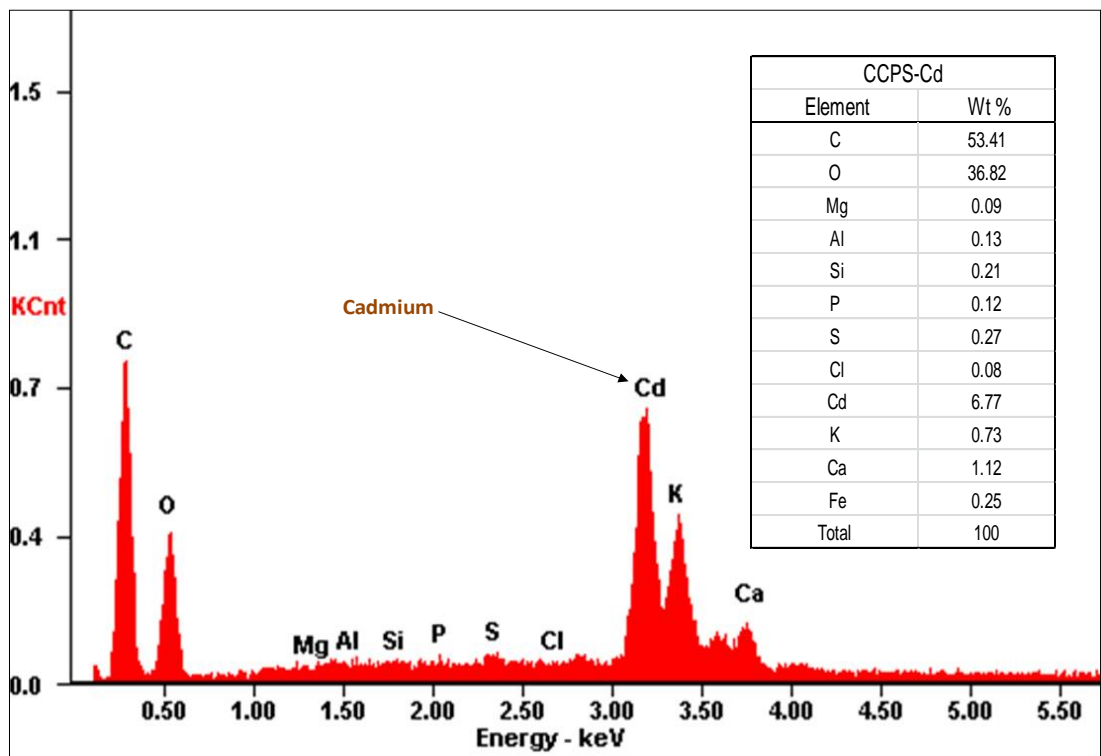
Figure 5.20: EDAX spectrum for CCPS after Cadmium adsorption

CCPS-Cd	
Element	Wt %
C	53.41
O	36.82
Mg	0.09
Al	0.13
Si	0.21
P	0.12
S	0.27
Cl	0.08
Cd	6.77
K	0.73
Ca	1.12
Fe	0.25
Total	100

Fig 5.21: EDAX spectrum for YTBS

YTBS	
Element	Wt %
C	65.45
O	31.52
Mg	0.07
Al	0.19
Si	0.2
P	0.17
S	0.32
Cl	0.12
K	1.42
Ca	0.4
Fe	0.14
Total	100

YTBS-Cd	
Element	Wt %
C	57.26
O	33.2
Mg	0.18
Al	0.13
Si	0.12
P	0.17
S	0.15
Cl	0.09
Cd	7.81
K	0.57
Ca	0.11
Fe	0.21
Total	100
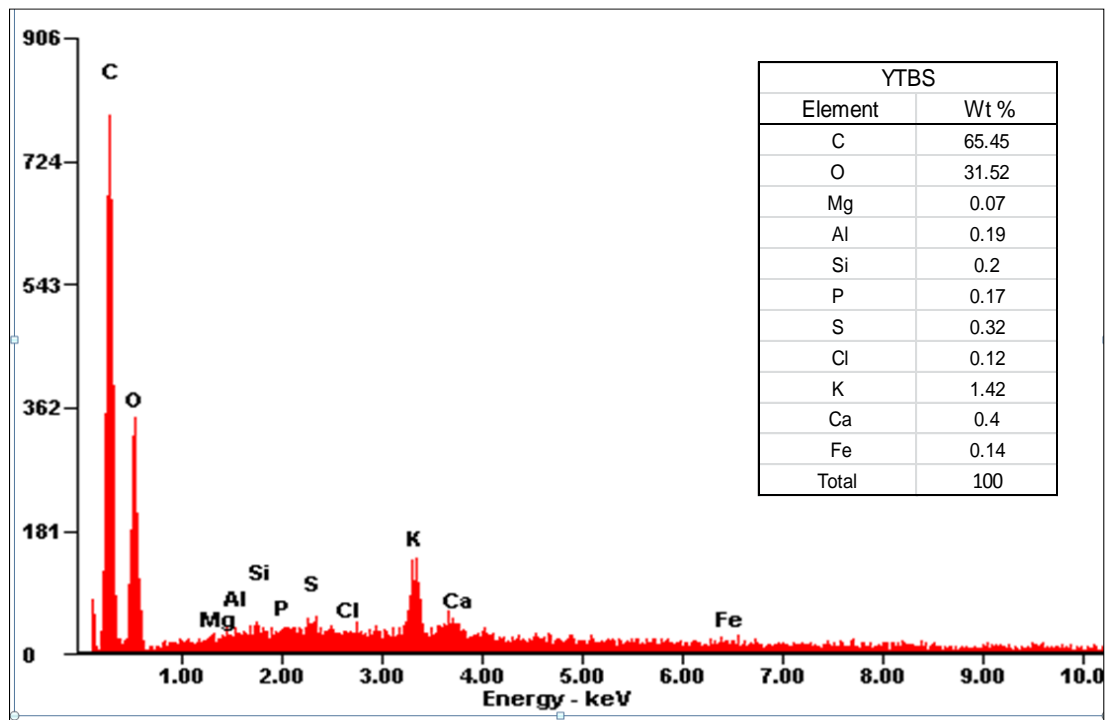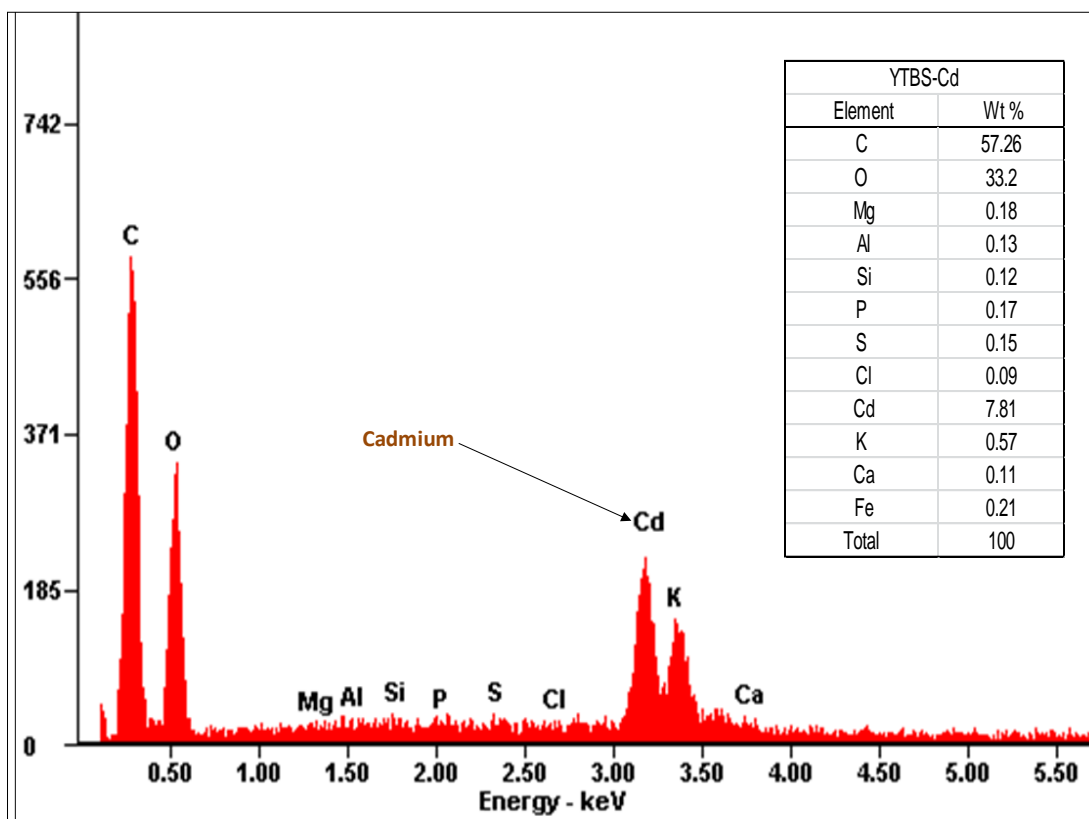
Fig 5.22: EDAX spectrum for YTBS after cadmium adsorption

An examination of these spectra after metal ion sorption indicates they all had the characteristic peak associated with Cd (II) ions thus confirming the possibility that Cd (II) metal ion sorption had occurred on the surface of these residue adsorbents. This approach has also been reported by Iqbal *et al.,* (2009b) on the use of the EDAX analysis of grapefruit peel to confirm the mechanism of ion-exchange for the removal of Zn (II) from aqueous solutions. The study also observed that the calcium and potassium ions identified in the EDAX spectrum of the fresh grapefruit peel were absent in the peel used for Zn(II) ion adsorption, thus suggesting that these ions may be involved in the ion-exchange with the Zn(II) ions. From the EDAX spectra in Figures 5.17-5.22, it can be observed that the percentage composition of some of the inorganic elements on the residue adsorbents were lower after adsorption especially those of calcium and potassium. This can be used to infer that there may be some contributions to the mechanism of metal ion removal via ion-exchange in these residue adsorbents for Cd (II) ions.

5.9 Functional group analysis of residue adsorbents using infrared spectroscopy

The agricultural adsorbents evaluated in this study are composed of a number of functional groups that can act as active sites during adsorption with cations or anions. Lignocellulosic biomass is composed of polysaccharides (~70% dry weight) and lignins (~25% dry weight) as well as trace quantities of proteins and minerals. The polysaccharides include; cellulose, hemicellulose and pectins, while the lignins are composed of groups of highly branched phenylpropanoid polymers found in lignified cell walls (Ding, 2014). The major and minor components of lignocellulosic biomass have been reported to contain a number of hydroxyl, carbonyl, carboxylic, phenolic and amine functional groups (Azargohar *et al.,* 2014; Pandey *et al.,* 2015; Ali *et al.,* 2016). The main functional groups in cellulose and hemicellulose chains in lignocellulosic structures are the aliphatic hydroxyl (-OH) and ether (C-O-C) groups, while there are a number of functional groups in the lignin structures such as; aliphatic and aromatic hydroxyl groups, double bonds, oxygenated and methoxy groups and phenyl groups (Sadeek *et al.,* 2015). These groups have been identified in a number of studies using infra-red (IR) spectroscopy and their interaction has been used to elucidate the mechanism of metal ion uptake. This technique uses the vibrations associated with the functional groups present in these materials to indicate shifts when interactions exist with metal ions either as covalent, hydrogen bonding or other electrostatic interactions (Roman *et al.,* 2013; Ibrahim *et al.,* 2010).

5.9.1 FT-IR characterisation of residue before adsorption

In this study, the infra-red spectra of the residue adsorbents before and after adsorption of Cd(II) and Pb(II) were determined using a Fourier transform infrared spectroscopy as described in Section 4.3.9. The FTIR spectra of the residue adsorbents were used to determine the functional groups present based on their characteristic vibrations. The FTIR spectra obtained for the unmodified residues are shown in Figures 5.23 − 5.29 and those obtained after metal ion sorption are shown in Figures 5.30 − 5.36. The peaks were assigned to various functional groups and bonds based on their respective wavenumbers (cm^{-1}) as reported in literature (Iqbal *et al.,* 2009a). From the FT-IR of the residues, it is observed that comparable vibrational peaks were seen across the residues indicating the presence of similar chemical functional groups and moieties in the residues.
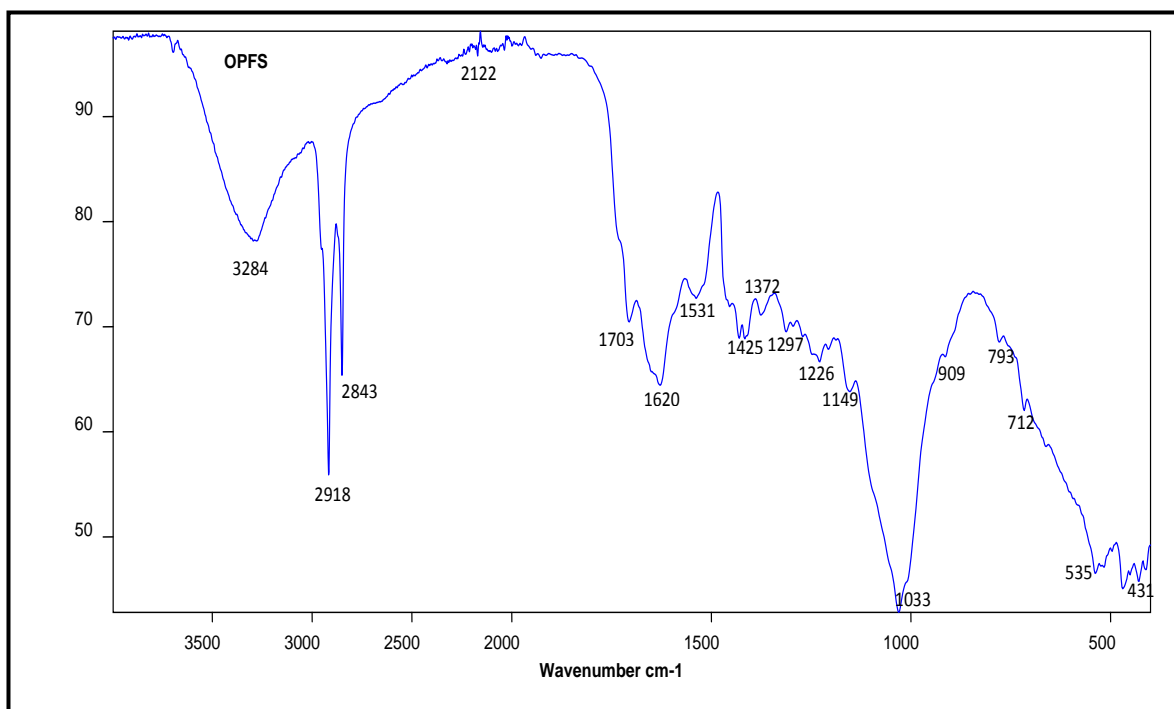
Figure 5.23: FTIR spectrum of unmodified oil palm fibre residue (OPFS)

The spectra of all the residue adsorbents indicates a broad peak between 3100 and 3600 cm^{-1} for all the adsorbents indicating the presence of free and associated (O-H) ν(O-H) stretching vibrations in hydroxyl groups (commonly appearing between $3550cm^{-1}$ and $3200cm^{-1}$) (Gurses *et al.,* 2014). For the different residue adsorbents this group appears at $3284cm^{-1}$(OPFS),$3355cm^{-1}$(CNFS),$3315cm^{-1}$(CCPS),$3315cm^{-1}$(CCYBS),$3268cm^{-1}$(PTHS), $3286cm^{-1}$(PTPS) and $3280cm^{-1}$ (YTBS). The groups with this functionality found in the different lignocellulosic adsorbents are as follows; absorbed water, aliphatic primary and secondary alcohols found in cellulose, hemicellulose, lignin, extractives, pectin, phenols with intermolecular hydrogen bonds and carboxylic acid groups in the extractives (Ahmadzedeh and Zakaria, 2009; Paduraru *et al.,* 2015). This peak is observed to be broad in all the residue adsorbents due to the complex vibrational modes arising from a mixture of stretching vibrational bands of −OH groups in hydrogen bonded and chemisorbed water as well as the inter and intramolecular hydrogen bonding vibrations (Ali *et al.,* 2016; Lim *et al.,* 2014).
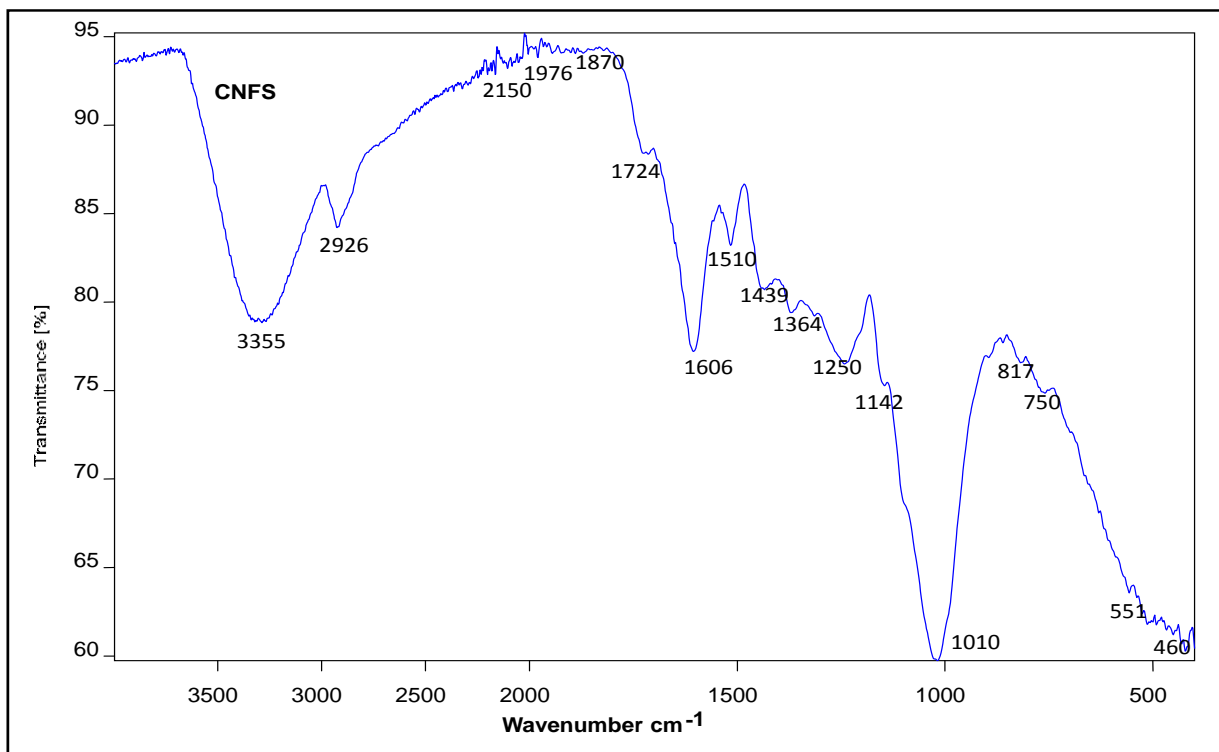
Figure 5.24: FTIR spectrum of unmodified coconut shell fibre residue (CNFS)
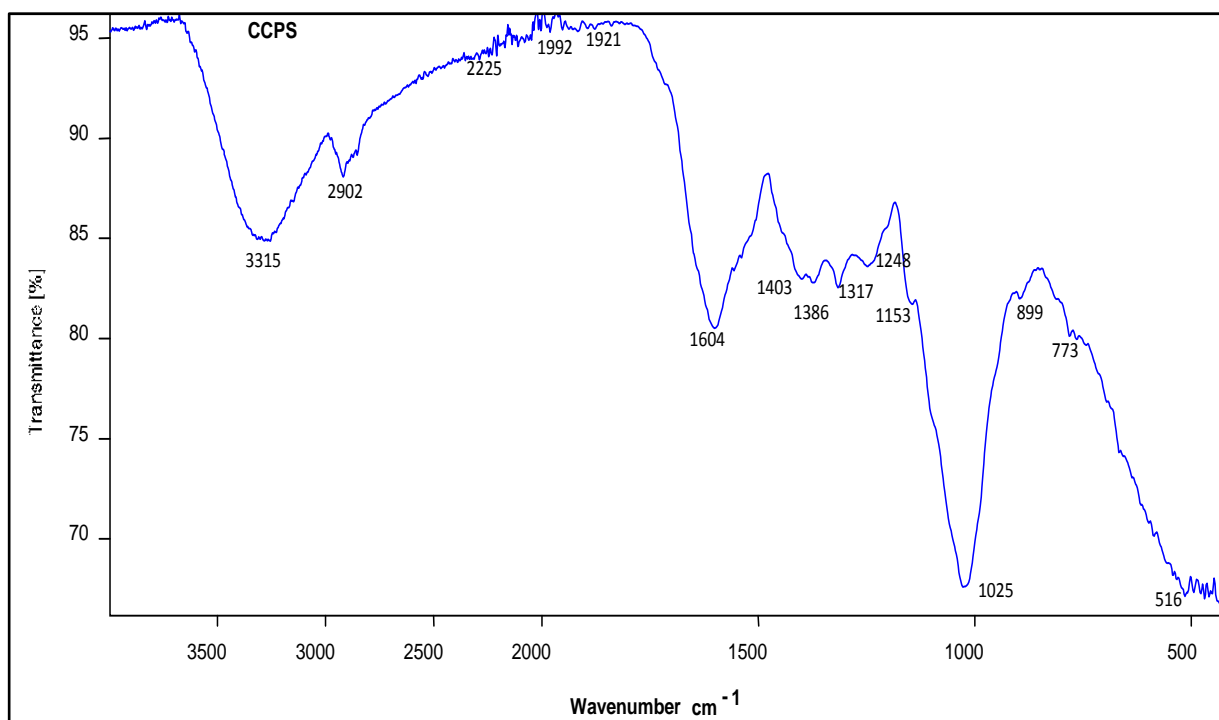
Figure 5.25: FTIR spectrum of unmodified cocoa pod residue (CCPS)
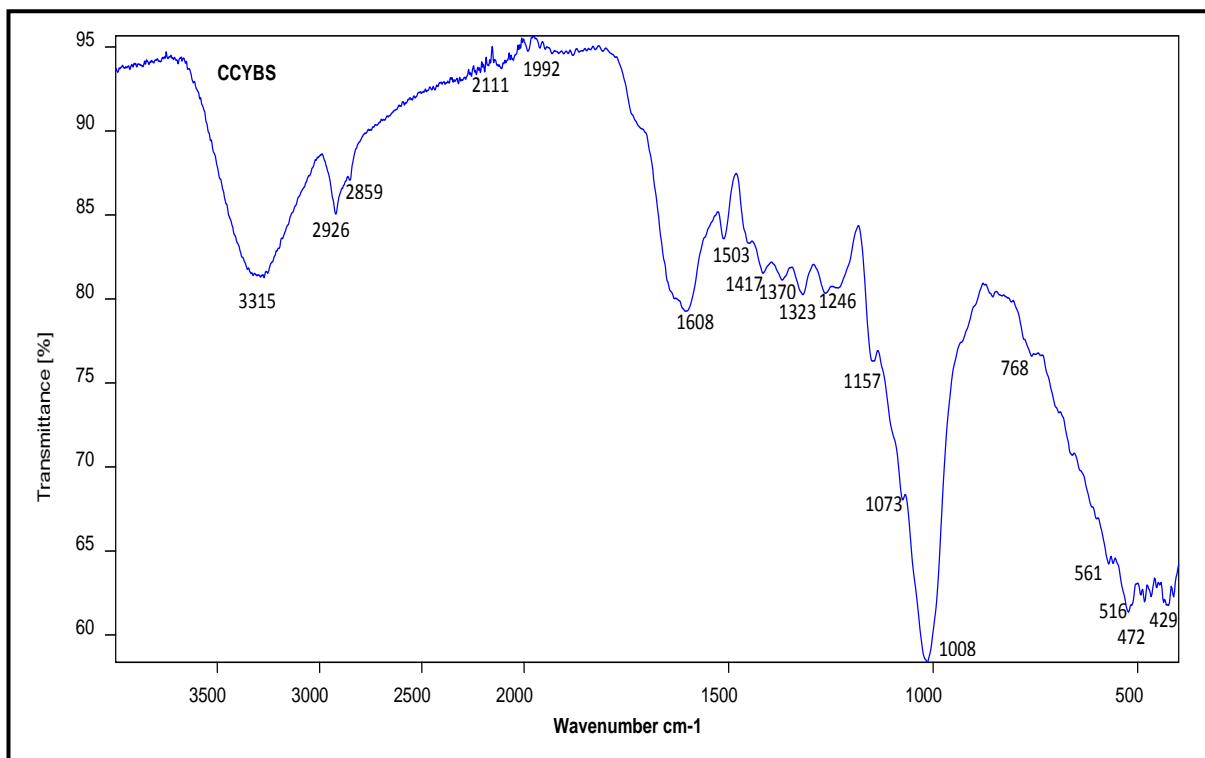
Figure 5.26: FTIR spectrum of unmodified cocoyam peel residue (CCYBS)
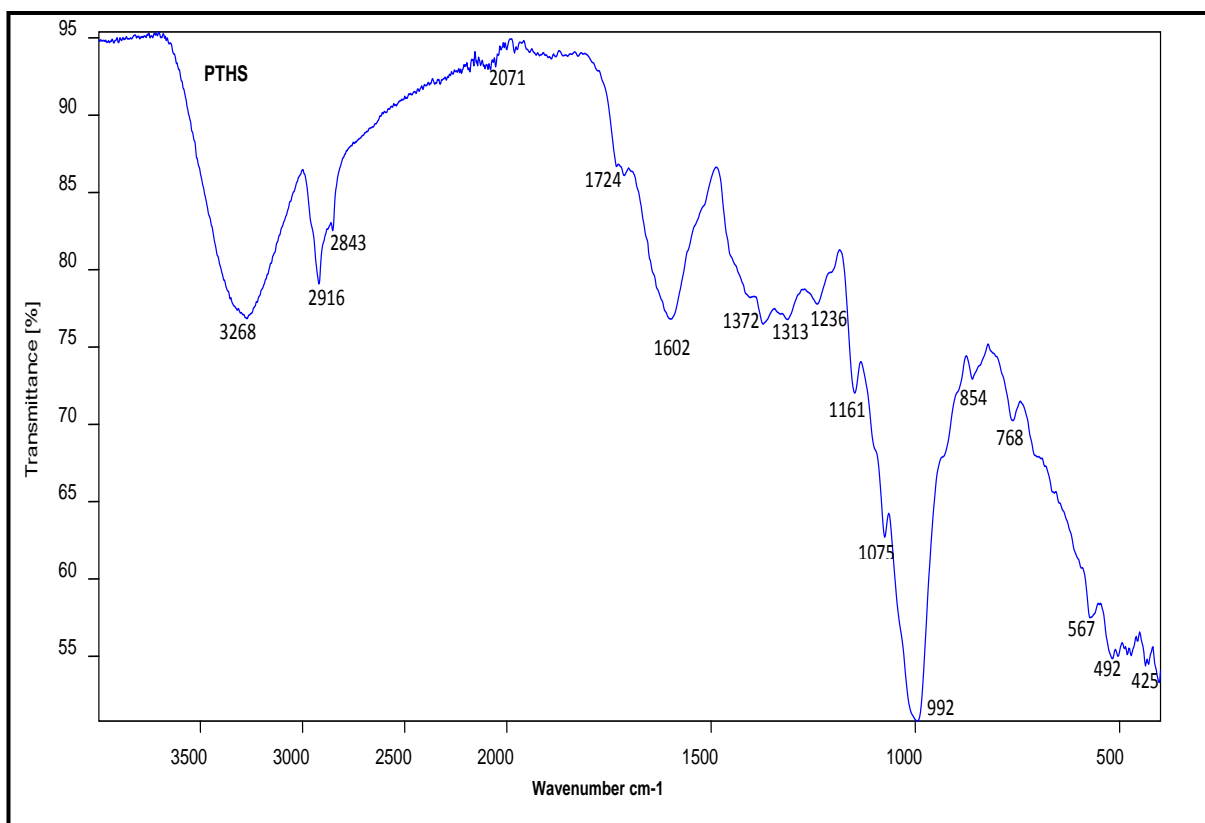
Figure 5.27: FTIR spectrum of unmodified plantain peel residue (PTHS)
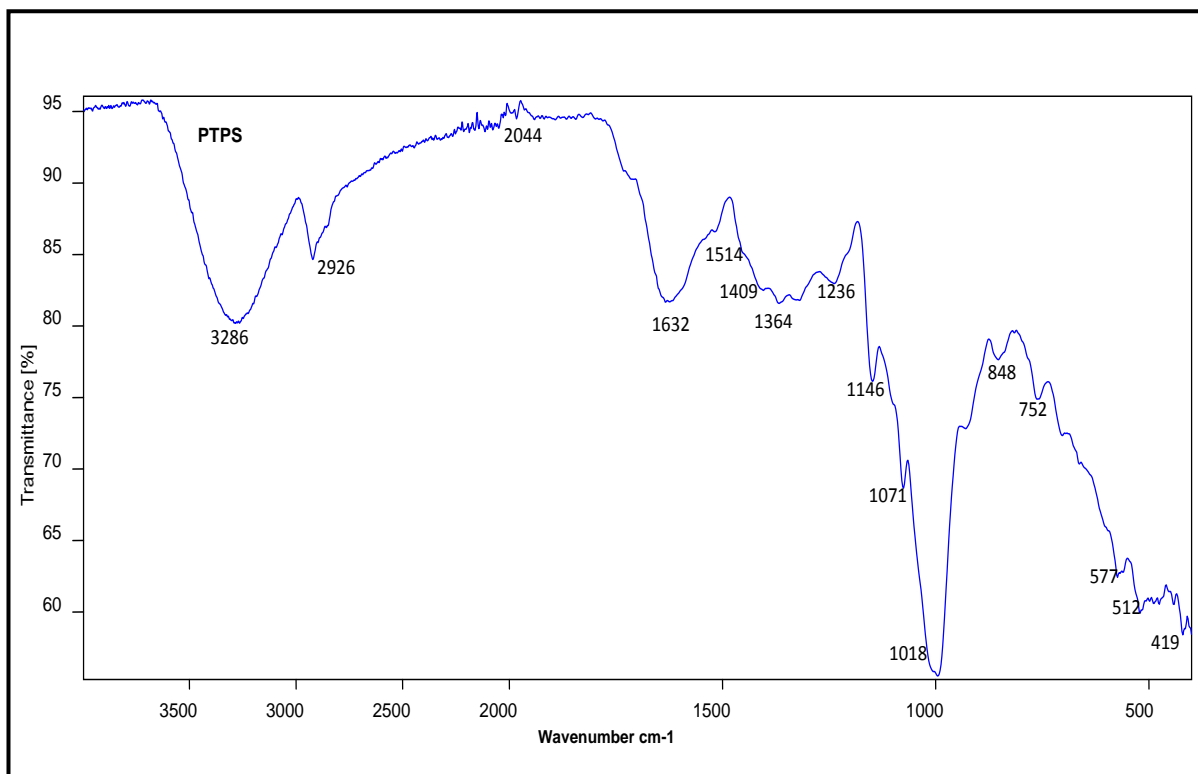
Figure 5.28: FTIR spectrum of unmodified sweet potato residue (PTPS)
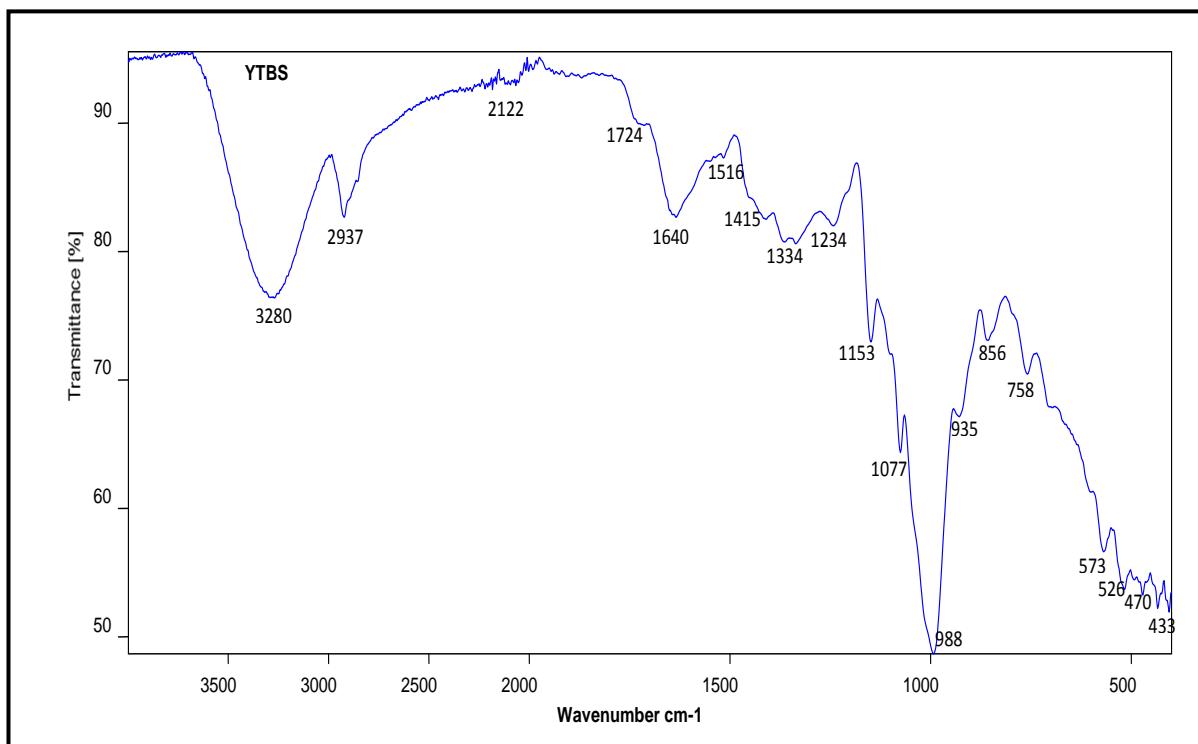
Figure 5.29: FTIR spectrum of unmodified white yam residue (YTBS)

The peaks observed at 2902 cm^{-1} (CCPS), 2916 cm^{-1} (PTHS), 2918 cm^{-1} (OPFS), 2926 cm^{-1} (CNFS, CCYBS & PTPS) and 2937 cm^{-1} (YTBS) can be attributed to the C-H symmetric or asymmetric stretching vibrations of the CH$_2$ and CH$_3$ groups of side chains and aromatic methoxy groups in the different lignocellulosic structures in the different residue adsorbents (Zhou *et al.,* 2013; Ahmadzedeh and Zakaria, 2009). These vibrations confirm the presence of aliphatic and aldehyde groups that can be associated with cellulose and hemicellulose and aromatic methoxy groups associated with lignin in the adsorbent structures (Feng *et al.,* 2009; Rao *et al.,* 2006).

The small peaks observed at 1724 cm^{-1}(CNFS, PTHS, YTBS), 1703 cm^{-1}(OPFS) in the spectra of the OPFS, CNFS, PTHS and YTBS residues and at 1602cm^{-1}(PTHS), 1606cm^{-1}(CNFS),1604 cm^{-1}(CCPS),1608 cm^{-1}(CCYBS), 1620 cm^{-1}(OPFS), 1632 cm^{-1}(PTPS) and 1640 cm^{-1}(YTBS) can be attributed to the presence of oxygen functional groups such as the highly conjugated carbonyl (C=O) stretching which are characteristics of aldehydes, ketones, esters, amides and carboxylic acid in the lignin and extractives components of the adsorbent (Simonescu, 2012). These groups could exist on these residues as non-conjugated (1724, 1703 cm^{-1}) in lignin/carboxylic acid ester groups (Markovic *et al.,* 2009) or conjugated (1620,1632,1640 cm^{-1}) moieties such as amides linked to other aromatic rings, carboxylic groups and carboxylate moieties of pectin, hemicellulose and lignin within the lignocellulosic structure of the different residue adsorbents (Run *et al.,* 2000; Ahmadzedeh and Zakaria, 2009; Lewin, 1991; Tarley and Arruda, 2000; Zhou *et al.,* 2013; Rao *et al.,* 2006; Feng *et al.,* 2009). The peaks at 1620 cm^{-1}, 1632 cm^{-1} and 1640 cm^{-1} can also be associated with the bending vibrations in amide (N-H) groups in the lignocellulosic structure of the different residue adsorbents (Moyo *et al.,* 2016).

The small peaks on the residues observed at 1531 cm^{-1}(OPFS), 1510 cm^{-1}(CNFS), 1503 cm^{-1}(CCYBS), 1514 cm^{-1} (PTPS) and 1516 cm^{-1}(YTBS) corresponds to the skeletal mode stretching of the aromatic ring for the symmetrical C=C vibration of the phenylpropane skeleton in the lignin component of the different residue adsorbents (Moyo *et al.,* 2016; Ahmadzedeh and Zakaria, 2009; Ibrahim *et al.,* 2010), while the those at 1425 cm^{-1}(OPFS), 1439 cm^{-1} (CNFS), 1403cm^{-1}(CCPS), 1417cm^{-1}(CCYBS), 1409cm^{-1}(PTPS) and 1415cm^{-1}(YTBS) corresponds to the C-H stretching deformation and aromatic ring vibrations in lignin structures in the lignocellulosic different adsorbent (Paduraru *et al.,* 2015; Ibrahim *et al.,* 2010; Markovic *et al.,* 2009). It can also be associated to the symmetric stretching vibrations of the carboxylate ion (COO$^-$) in the pectin component of the lignocellulosic adsorbent (Sahu *et al.,* 2010; Kakalanga *et al.,* 2012).

The small peaks found at 1372 cm^{-1} (OPFS),1364 cm^{-1} (CNFS, PTPS), 1386 cm^{-1} (CCPS), 1370 cm^{-1} (CCYBS),1372 cm^{-1} (PTHS) and 1334cm^{-1} (YTBS) indicates the presence of C-H vibration associated with cellulose and the axial deformation of the C-O bond of the carboxylic groups in pectin (Gurses *et al.,* 2014, Iqbal *et al.,* 2009a), as well as the C$_1$–O vibration in syringyl derivatives rings in lignin (Yang *et al.,* 2007; Markovic *et al.,* 2009). The peaks observed at 1226 cm^{-1} (OPFS), 1250 cm^{-1} (CNFS),1248 cm^{-1} (CCPS),1246 cm^{-1}(CCYBS), 1236 cm^{-1} (PTHS, PTPS) and 1234cm^{-1} (YTBS) corresponds to the syringyl ring and C–O stretching in lignin and xylan (hemicellulose) components of the different adsorbents (Markovic *et al.,* 2009; Paduraru *et al.,* 2015; Simonescu, 2012; Ahmadzedeh and Zakaria, 2009).

The sharp shoulder at the different residue adsorbents at 1142cm^{-1}(CNFS), 1149cm^{-1}(OPFS), 1146cm^{-1}(PTPS), 1153cm^{-1}(CCPS,YTBS), 1157cm^{-1}(CCYBS) and 1161cm^{-1}(PTHS) is representative of the aromatic C–H in plane deformation of the guaiacyl-lignin (Markovic *et al.,* 2009), while the peaks at 1071cm^{-1}(PTPS), 1073cm^{-1}(CCYBS) , 1075cm^{-1}(PTHS) and 1077 cm^{-1} (YTBS) are attributed to the anti-symmetric bridge stretching of the ether bonds on the C-O-C groups (pyranose ring skeletal vibration) in cellulose and hemicelluloses (Moyo *et al*., 2016; Markovic *et al.,* 2009; Zhou *et al.,* 2013; Yang, 2007).
The peaks at 1033 cm^{-1} (OPFS), 1010 cm^{-1} (CNFS), 1025 cm^{-1} (CCPS), 1008 cm^{-1} (CCYBS), 992 cm^{-1} (PTHS), 1018 cm^{-1} (PTPS) and 988 cm^{-1} (YTBS) are due to the vibrations of the out-of-plane C=C aromatic functional groups in the lignin (Liang and Ibrahim, 2013), while the peaks at 909cm^{-1} (OPFS) and 935cm^{-1} (YTBS) arises from the vibration associated with the C-O-C stretching at the *β*-(1→4)glycosidic linkages that is a characteristic peak associated with cellulosic polymers (Yu *et al.,* 2013; Liu *et al.,* 2006; Oh *et al.,* 2005). The bands at 793 cm^{-1} and 712 cm^{-1} (OPFS) , 817 cm^{-1} and 750 cm^{-1} (CNFS) , 899 cm^{-1} and 773 cm^{-1} (CCPS) , 768 cm^{-1} (CCYBS) , 854 cm^{-1} and 768 cm^{-1} (PTHS) , 848 cm^{-1} and 752 cm^{-1} (PTPS) and 856 cm^{-1} and 758 cm^{-1} (YTBS) can be attributed to the aromatic C-H out of plane deformations of the para and meta benzene groups of the phenolic structures of lignin in the different lignocellulosic adsorbents (Ahmadzedeh and Zakaria, 2009; Yang *et al.,* 2007).

Finally, it can be stated that the FT-IR spectra of the 7 residue adsorbents shows that these lignocellulosic materials were composed of a number of chemical species such as; esters, aromatics, carboxylic acid, aldehydes, amines, ethers, ketones and alcohol with different oxygen-containing groups that can be associated with the presence of cellulose,

hemicellulose, lignin, extractives and pectins on their structure. The carboxylate and hydroxyl groups also present on these lignocellulosic materials have been reported to have the potential to interact with metal ions during adsorption (Naiya *et al.,* 2011), thus these functional groups and others are likely active sites for metal ion sorption during the application of these residues in aqueous metal ion systems. The role of these groups on the sorption of the two metal ions-{Cd(II) and Pb(II)} was investigated by characterising the different residue adsorbents using FT-IR after adsorption and this is discussed in the next section.

5.9.2 FT-IR characterisation of residue after adsorption

The spectra of the residues after Cd (II) and Pb (II) metal ion sorption are illustrated in Figures 5.30 – 5.36. Peak shifts on the vibrations associated with the residues after metal ion sorption can be seen in all the Figures. The broad O-H peak at 3284 cm^{-1} for the OPFS residue was observed at different wavenumbers after Cd (II) and Pb (II) adsorption, this peak showed a shift to 3307 cm^{-1} and 3280 cm^{-1} for Cd (II) and Pb (II) ions respectively. These indicated a blue shift (to higher wavenumbers) for the O-H peak for the OPFS adsorbent for OPFS-Cd but a red shift (lower wavenumber) for OPFS-Pb. For the CCPS adsorbent this broad O-H peak observed at 3315 cm^{-1}, were observed also as broad peaks at 3335 cm^{-1} (CCPS-Cd) and 3355 cm^{-1} (CCPS-Pb) indicating a blue shift (to higher wavenumbers) for this residue adsorbent. For the CNFS adsorbent, the broad O-H peak shift was observed to have shifted from 3355 cm^{-1} (CNFS) to 3347 cm^{-1} (CNFS-Cd) which was observed to have more peak broadening and 3304 cm^{-1} (CNFS-Pb), thereby indicating a red shift due to the adsorption process. The broad hydroxyl group shift in wavenumber for the CCYBS adsorbent was from 3315 cm^{-1}(CCYBS) to 3331 cm^{-1} (CCYBS-Cd) and 3272 cm^{-1}(CCYBS-Pb), while that of the PTHS adsorbent was from 3268 cm^{-1} (PTHS) to 3311 cm^{-1} (PTHS-Cd) and 3276 cm^{-1} (PTHS-Pb). The PTPS shift for the hydroxyl group was from 3286 cm^{-1} (PTPS) to 3260 cm^{-1} (PTPS-Cd) and 3311 cm^{-1} (PTPS-Pb). The YTBS adsorbent shift was observed to occur from 3280 cm^{-1} (YTBS) to 3276 cm^{-1} (YTBS-Cd) and 3284 cm^{-1}(YTBS-Pb). These observed shifts red and blue shifts in the hydroxyl group peak for the different residue adsorbents after Cd(II) and Pb(II) sorption may indicate that the hydroxyl group is involved in the biosorption process. The blue shift indicates that the bond length decreased after adsorbent, while the red shift signifies that the bond length increased after sorption.
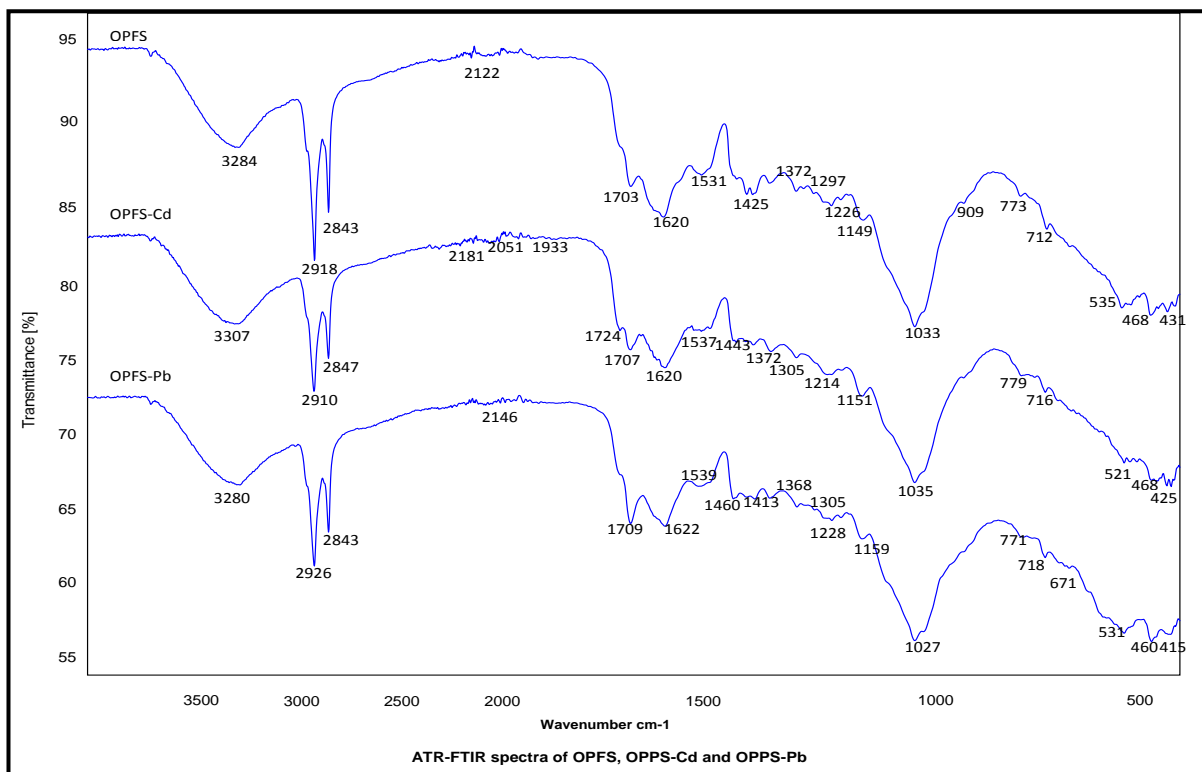
Figure 5.30: FTIR spectrum OPFS before and after metal ion sorption
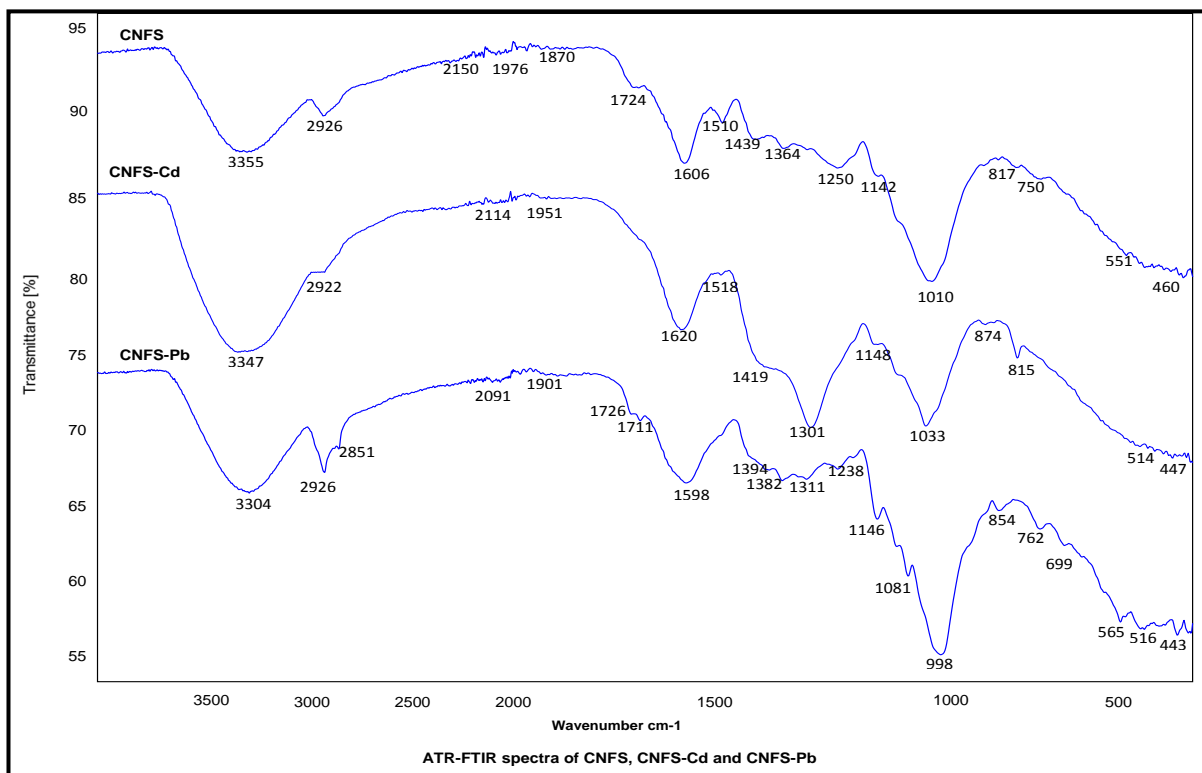
Figure 5.31: FTIR spectrum CNFS before and after metal ion sorption
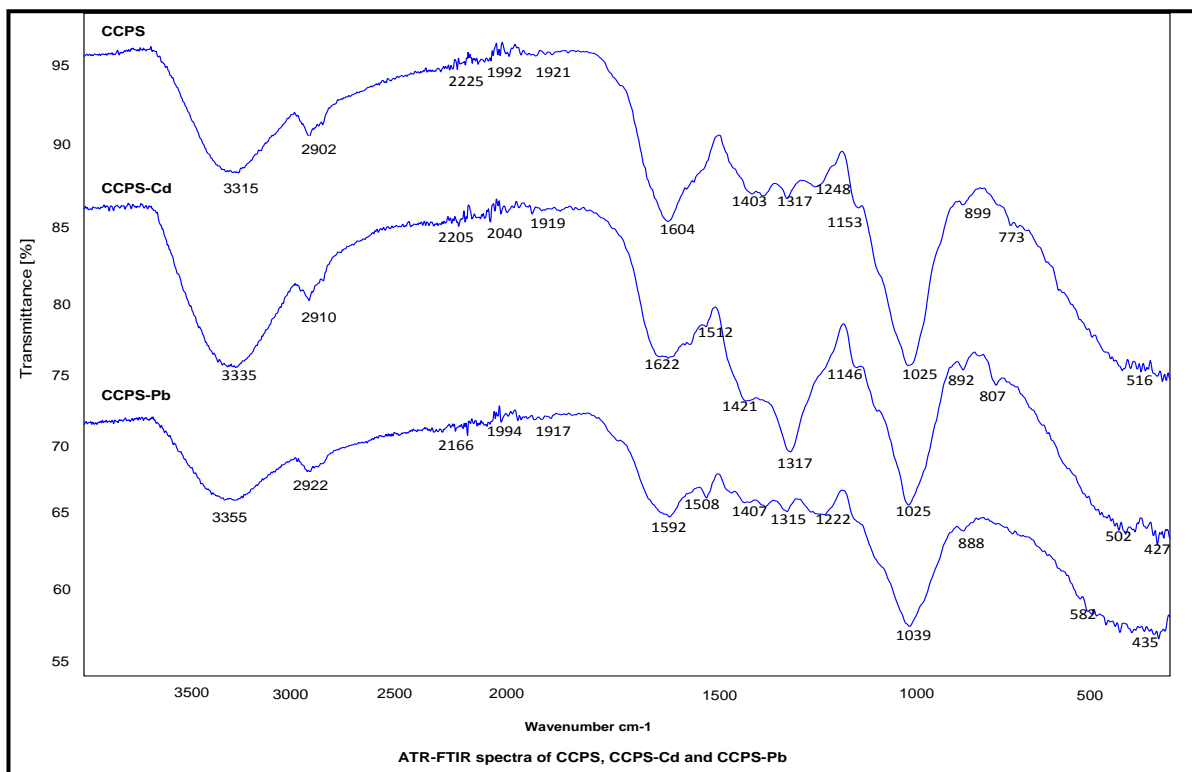
Figure 5.32: FTIR spectrum CCPS before and after metal ion sorption
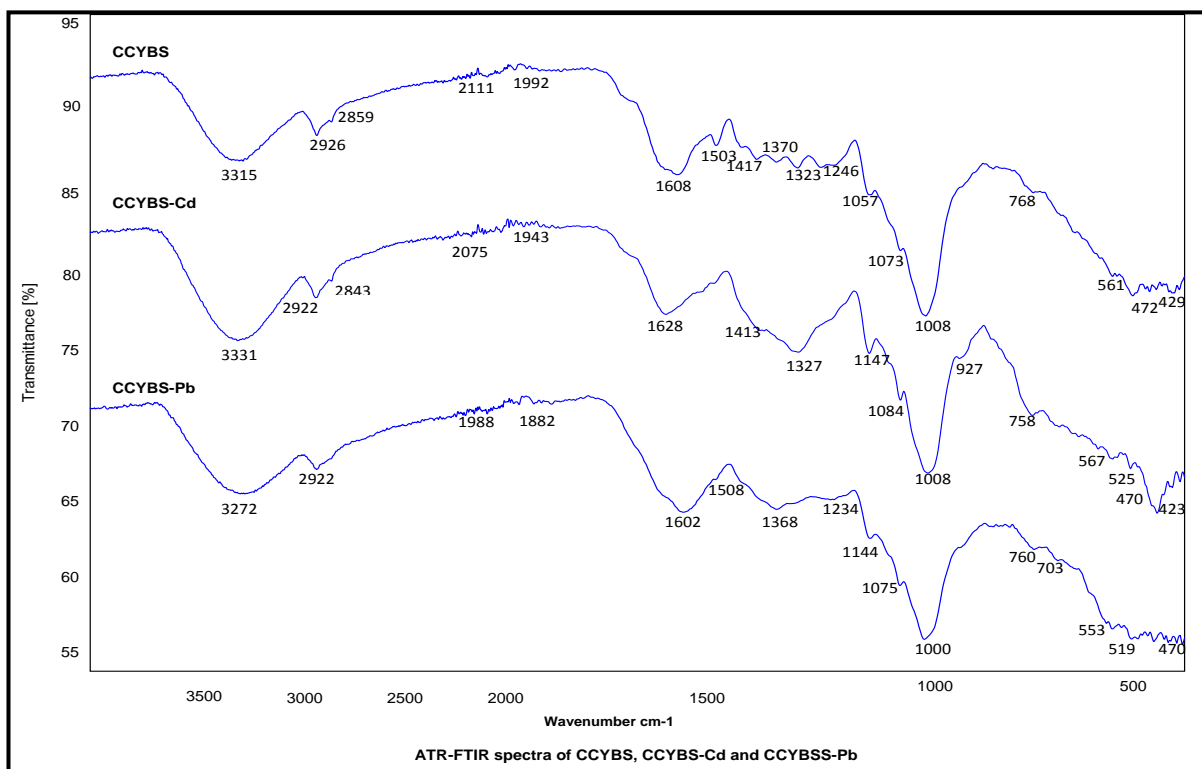
Figure 5.33: FTIR spectrum CCYBS before and after metal ion sorption
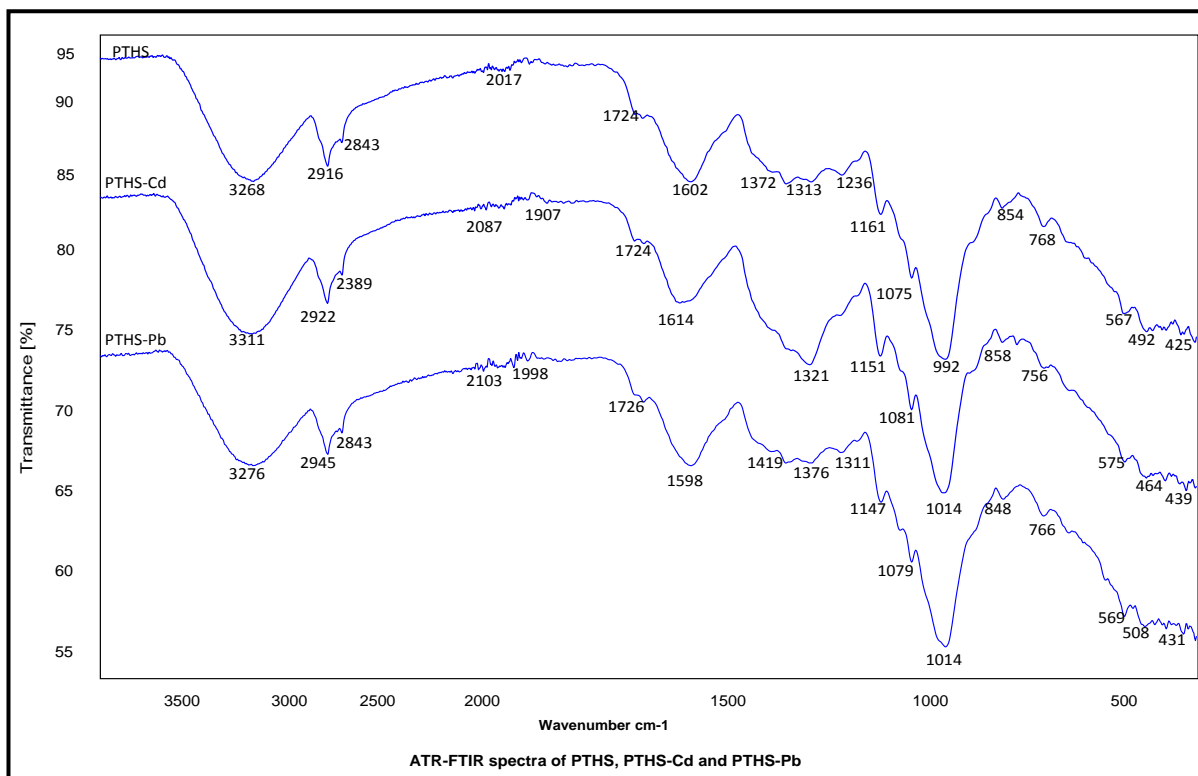
Figure 5.34: FTIR spectrum PTHS before and after metal ion sorption
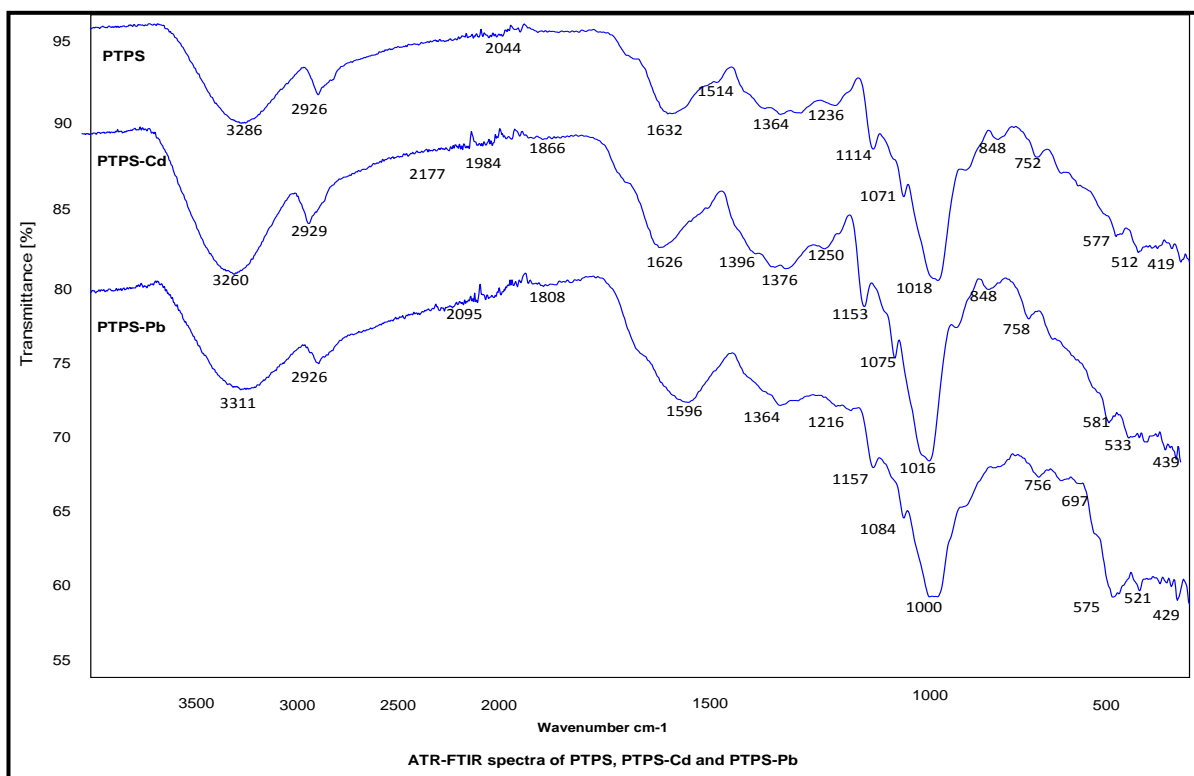
Figure 5.35: FTIR spectrum PTPS before and after metal ion sorption
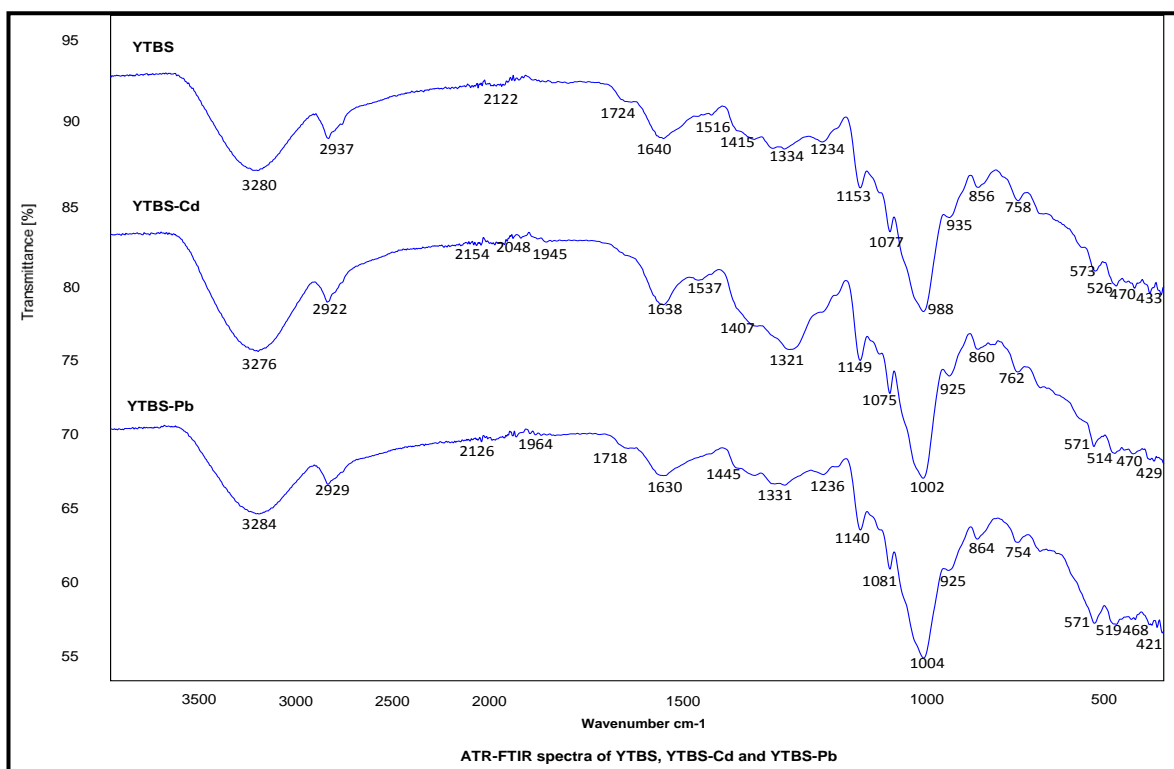
Figure 5.36: FTIR spectrum YTBS before and after metal ion sorption

These changes in bond length may be associated with the type of chemical interactions that exist between the functional groups on the adsorbent surface and the Cd(II) and Pb(II) ions. These bonding interactions may be via co-ordination interaction or hydrogen bonding with metal aquo complexes as it may function as a proton donor than can become deprotonated hydroxyl groups prior to co-ordination with the metal ions (Moyo *et al.,* 2016; Wang *et al.,* 2015a; Iqbal *et al.,* 2009a). Peak shift after Cd(II) and Pb(II) metal ion sorption was also observed for the both the non-conjugated and conjugated carboxyl group vibrations for the different residue adsorbents. For non-conjugated carbonyl groups, for the OPFS adsorbent the shifts in wavenumber of the sharp C=O peak was from 1703 cm^{-1} (OPFS) to 1707 cm^{-1} (OPFS-Cd) and 1709 cm^{-1} (OPFS-Pb) and the OPFS-Pb peak was observed to be sharper than the other two peaks. For the CNFS adsorbent the shift was from 1724 cm^{-1} (CNFS) to 1726 cm^{-1} (CNFS-Pb) and there was no peak within this wavenumber obtained for the CNFS-Cd adsorbent. For the PTHS adsorbent, the peak was observed to be small and the shift was from 1724 cm^{-1} (PTHS) to 1726 cm^{-1} (PTHS-Pb), the PTHS-Cd spectrum did not indicate any shift as the vibration was at 1724 cm^{-1}. For the YTBS the shift pattern was similar to what was obtained for the CNFS as the change was from 1724 cm^{-1} (YTBS) to 1718 cm^{-1} (YTBS-Pb) with no recorded peak for the YTBS-Cd adsorbent. Also, for the conjugated carbonyl groups, the sharp peak observed at 1620 cm^{-1}

(OPFS) did shift to 1622 cm^{-1} for the OPFS-Pb adsorbent, while that of the OPFS-Cd adsorbent remained at 1620 cm^{-1} but both peaks were smaller than that of the OPFS adsorbent. For the CNFS adsorbent the sharp carbonyl peak at 1606 cm^{-1} (CNFS) did shift to 1620 cm^{-1} (CNFS-Cd) and 1598 cm^{-1} (CNFS-Pb) with considerable peak broadening observed for CNFS-Cd and CNFS-Pb, while for the CCPS adsorbent this shift was from 1604 cm^{-1} (CCPS) to 1622 cm^{-1} (CCPS-Cd) and 1592 cm^{-1} (CCPS-Pb) and there also broadening of these two peaks. For the CCYBS adsorbent the shift observed for the broad carbonyl functional group was from 1608 cm^{-1} (CCYBS) to 1628 cm^{-1} (CCYBS-Cd) and 1602 cm^{-1} (CCYBS-Pb) with considerable peak broadening observed for the CCYBS-Pb adsorbent. For the PTHS adsorbent the shift in the broad peak was from 1602 (PTHS) to 1614 cm^{-1} (PTHS-Cd) and 1598 cm^{-1} (PTHS-Pb). For the PTPS adsorbent the peak shift for the carbonyl group was from 1632 cm^{-1} (PTPS) to 1626 cm^{-1} (PTPS-Cd) and 1596 cm^{-1} (PTPS-Pb) and there was broadening of these peaks after sorption, while for the YTBS adsorbent the carbonyl peak was smaller than those observed for the other residues and the shift in peak was from 1640 cm^{-1} (YTBS) to 1638 cm^{-1} (YTBS-Cd) and 1630 cm^{-1} (YTBS-Pb) indicating a red shift for the YTBS adsorbent.

The shift in peaks for both the conjugated and non-conjugated carbonyl groups at in the different residue adsorbents can associated with the interaction of a number of carbonyl functional groups within the different adsorbents such as the carboxylic acid/ester(-COO) groups with the Cd(II) and Pb(II) ions from the adsorbate and the influence of these interactions on the bond lengths of these functional groups. This decrease in wavenumbers of these peak that is characteristic for the C=O group from the carboxylic acid, aldehydes and ketone moieties on the adsorbent and the disappearance of the peak at 1724cm^{-1} for some adsorbents after sorption indicates that there may be interactions between the Cd(II) and Pb(II) ions and these functional groups during adsorption (Paduraru *et al.,* 2015;Chand *et al.,* 2014; Simonescu, 2012; Iqbal *et al.,* 2009a). Furthermore, the overall spectra of the 7 residue adsorbents after Pb(II) and Cd(II) ion sorption when compared to that of the fresh adsorbents as shown in Figs.5.30 – 5.36 suggests that the different functional groups that are present in cellulose, hemicellulose, lignin and extractives had shift in peaks at which suggests that cellulose, lignin and hemicellulose polysaccharides in the different chemical environments in the lignocellulosic structure had interactions with the Cd(II) and Pb(II) ions during sorption which resulted in the variations in the wavenumbers of the functional groups present in them (Wang *et al.,* 2015a).

Based on the shifts in the peaks observed in the IR spectra obtained, it can be inferred that some of the functional groups on the residues such as carboxylic groups (pectin and lignin), phenolic groups (lignin and extractives) and hydroxyl and ether groups associated with cellulose, lignin, hemicellulose, extractives and pectin were the active sites for the Cd (II) and Pb (II) ion sorption from the adsorbate. The shift in vibrations of some of the functional groups after metal ion sorption as observed in this study can be explained based on the change in coordination sites of the functional groups due to the interactions with the Cd (II) and Pb (II) ions. This observation has also been reported by Thirumavalavan *et al.,* (2011) in their study on the Fourier Transform spectroscopic analysis of fruit peels before and after adsorption of heavy metal ions from aqueous solution. The study observed that the C-H peak intensity was reduced on the fruit peels after adsorption, while on some peels the peaks were absent thereby indicating that the functional groups which exhibit these peaks can be associated with metal ion adsorption. These shift in peaks in the functional groups after Cd(II) ion sorption has also been reported in a number of studies in literature. Wang *et al.,* (2015a) observed that the vibrations for the carbonyl, amine and hydroxyl groups in *Phylolacca americana* L. biomass did shift due to their participation in the biosorption of Pb(II) ion. Peak shifts have also been reported for the sorption of Cu(II) ion from aqueous solution using a lignocellulosic based adsorbent- chemically treated potato (*Solanum tuberosum*) leaf powder. In the study, the peaks for hydroxyl and amino groups were observed to have shifted from both hydroxyl (3428 cm^{-1} to 3416 cm^{-1}) and amino groups (1612 cm^{-1} to 1614 cm^{-1}) thus indicating that both amino and hydroxyl groups on the adsorbent might be involved in Cu(II) sorption (Moyo *et al.,* 2016). Iqbal *et al.,* (2009a) has also reported on the shift in wavenumbers of functional groups in a lignocellulosic adsorbent after Cd(II) and Pb(II) ion sorption in their study on mango peel waste (MPW) sorption of Cd(II) and Pb(II) ions. In their study, they attributed these shift to the changes in the counter ions associated with the carboxylate and hydroxylate anions thereby suggesting that the carboxyl and hydroxyl groups were the main contributors to metal ion uptake. A similar observation was also made in the study on the sorption of Pb(II) on alkali treated tea residue for the shift in wavenumbers associated with some functional groups after Pb(II) sorption reported by Yang and Cui, (2013). The authors in this study associated these shift to ion-exchange mediated interactions between the Pb(II) ion with the carboxylate and hydroxylate anions (Yang and Cui, 2013; Aksu, 2002).

5.10 Adsorption studies on effect of parameters on metal ion sorption

From the characterisation of the residue adsorbents a number of parameters were chosen to evaluate their impact on the removal of Cd (II) and Pb (II) using the agricultural adsorbents. From the zeta potential and pHpzc characterization of the residues, the pH of 6.5 was chosen for the sorption studies for both metal ions. The parameters studied were contact time, pH, and adsorbent dose, in addition equilibrium sorption studies was also carried out to evaluate the metal ion loading for the each residue adsorbent. For the determination of metal ion loading after sorption the amount of metal ion adsorbed at time (t) was calculated using eqn. (5.2).

$$qt = \frac{(C_i - C_t)V}{m} \qquad\qquad (5.2)$$

Where C_t (mgL^{-1}) is the metal ion concentration at time t, q_t (mgg^{-1}) is the loading of the metal ion at time t, C_i is the initial metal ion concentration, m is the mass of the adsorbent and V is the volume of the aqueous system. This was used to calculate all values of metal ion loading in this work.

5.11 Effect of contact time on sorption using residue adsorbents

The effect of contact time on the removal of a metal ion from an aqueous solution using an adsorbent is an important characteristic of an adsorption system as it gives insight into the nature of adsorbent − adsorbate interactions as well as the transport profiles during metal ion uptake. The kinetics of the adsorption process also gives an indication on the time required for sorption equilibrium to be attained or presumed to be attained. This parameter is also used to estimate design parameters for scale up adsorbers and cost of the adsorption system. The effect of contact time on Cd (II) and Pb (II) ions uptake using the unmodified residues (OPFS, CNFS, CCPS, CCYBS, PTHS, PTPS and YTBS) were studied at pH 6.5 with initial metal ion concentration of 500 mgL^{-1}, temperature of 25°C and a volume of 0.1 L. The amount of each adsorbent used was mass of 2.0 g and the duration of kinetic studies was from 5 to 1440 minutes (72 h). The kinetic profile for Cd (II) is shown in Figure 5.37 while that of Pb (II) is presented in Figure 5.38.
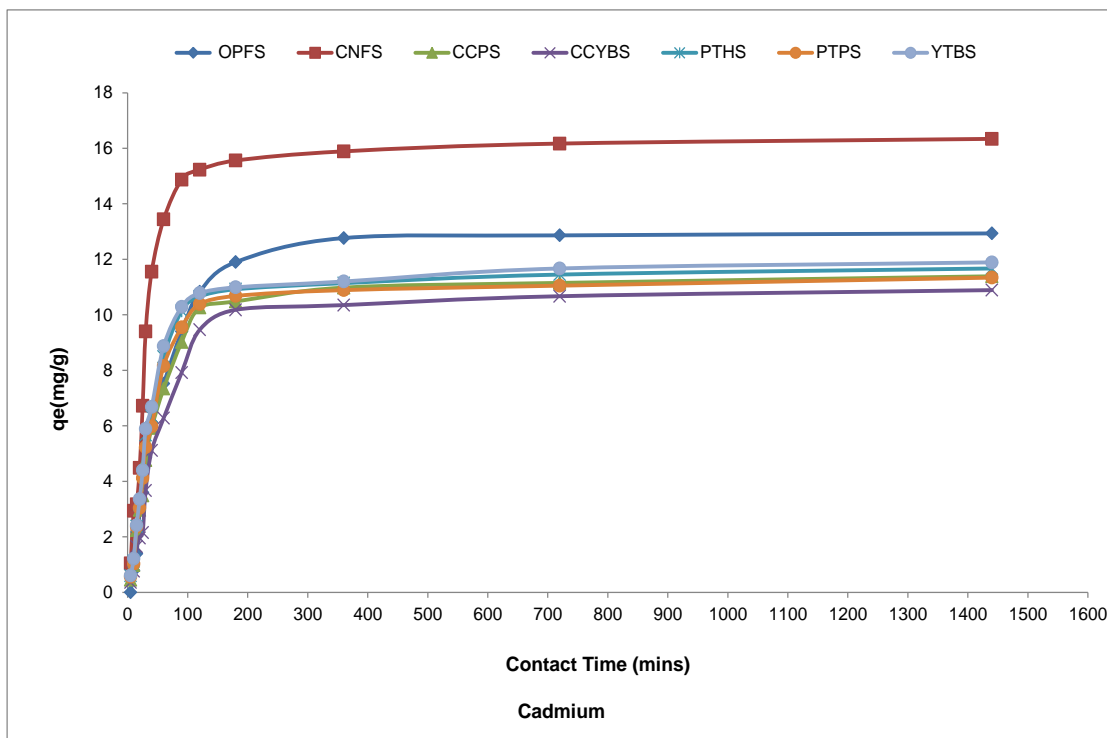
Figure 5.37: Effect of contact time on Cd(II) ion sorption using residue adsorbents
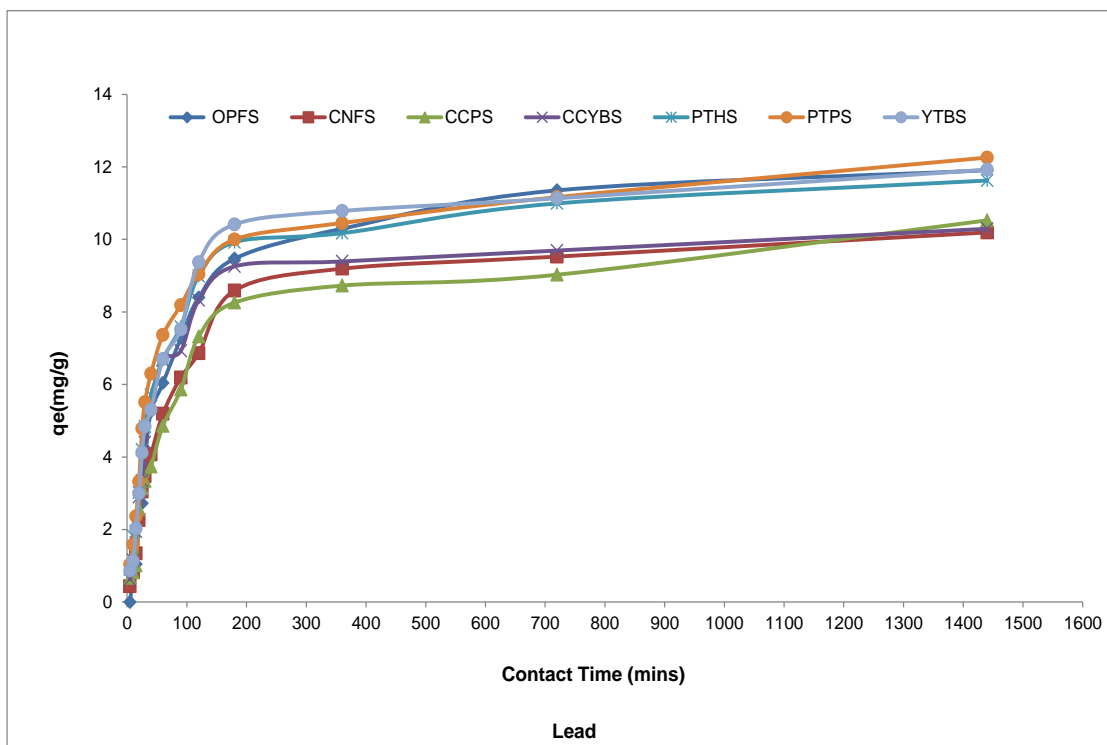
Figure 5.38: Effect of contact time on Pb(II) ion sorption using residue adsorbents

From both figures, it is observed that there was a rapid uptake of metal ions by the adsorbents up to 180 minutes and subsequently a gradual loading up to 1440 minutes. For Cd(II), the maximum loading at attainment of equilibrium time were 13.48mgg^{-1} (OPFS), 16.34mgg^{-1} (CNFS), 11.38mgg^{-1} (CCPS), 10.89mgg^{-1} (CCYBS), 11.67mgg^{-1} (PTHS),

11.34mgg^{-1} (PTPS), and 11.89 mgg^{-1} (YTBS). For the Pb(II) ion, the maximum uptake at equilibrium were: 12.46 mgg^{-1} (OPFS), 10.19mgg^{-1} (CNFS), 10.53 mgg^{-1} (CCPS), 10.29 mgg^{-1} (CCYBS), 11.61 mgg^{-1} (PTHS), 12.26 mgg^{-1} (PTPS) and 11.92 mgg^{-1} (YTBS). These values show that for Cd(II) ion, the CNFS adsorbent had the highest loading while the least was obtained by the CCYBS adsorbent. For the Pb(II) ions, OPFS adsorbent had the highest loading while the CNFS adsorbent was the least.

An examination of Figures 5.37 and 5.38 indicates that the metal ion loading on the different residues occurred in two stages over the duration of contact with the different residues. The first stage was characterised by a fast uptake lasting up to 180 minutes for all the residues and the second stage proceeded slowly from 180 minutes up till 1440 minutes where equilibrium was attained. This two stage process can be explained based on the availability of active sites on the residues for Cd(II) and Pb(II) ion loading. At the inception of the metal ion-adsorbent contact, there are a number of readily accessible active sites on the adsorbents making the uptake of Pb(II) and Cd(II) ions onto these sites rapid. According to Sarada *et al.,* (2014) during metal ion uptake as a function of time, as contact time increases the vacant sites on the adsorbent surface become occupied and the number of sites available for uptake by incoming metal ions decreases thereby making the process slow. In addition, as more metal ions adsorb onto the surface of the adsorbents, there is a repulsive interaction between the metal ions in solution and those on the surface of the adsorbent due charge similarity thereby hindering the rapid uptake of metal ions since surface of the residues are now predominantly positive (Sarada *et al.,*2014). These effects contribute to the gradual metal ions uptake noticed until equilibrium is attained.

It is pertinent to note that the maximum loading for each metal ion for the different adsorbent after 1440 minutes was not dissimilar to the values after 180 minutes. So the time 180 minutes was taken as the basis for further adsorption experiments with respect to the other adsorbents developed in this study and discussed in subsequent chapters of this work.. Furthermore, the two state profile of the metal ion loading as a function of time has been attributed in literature to the availability of vacant active sites for metal ion loading. According to Iqbal *et al*., (2009a), the initial rapid uptake can be attributed to the availability of active sites on the adsorbent which decreases with time, with more occupancy by the metal ions thus reducing the rate of the sorption. Krishnani *et al.,* (2008) also reports a two stage metal ion sorption for rice husk for the removal of a number of heavy metal ions in which the first stage was within 90 − 120 minutes after which

equilibrium was reached at 150 minutes contact time. Hence, the trend of the metal ion kinetics reported in this study is similar to those reported in literature.

5.11.1 Kinetic modelling

The nature of the kinetics of metal ion sorption has also been evaluated using a number of adsorption reaction and adsorption diffusion models. For the purpose of this work two models were used to analyse the kinetics of Cd(II) and Pb(II) ions as previously described in section 2.6.2 of this work. These are the pseudo first order (PFO) and pseudo second order (PSO) kinetic models. These two models have different fundamental asssuptions that premise their existence and this is used to interpret the significance of the rate constants. For the PFO model, the rate constant K_1 is based on the relationship between the sorption rate and equilibrium, whereby the assumption is that the kinetic rate is dependent on the concentration of ions in solution (Miyake *et al.,* 2013; De Haro-Del Rio *et al.,* 2015; Qiu *et al.,* 2009). On the other hand for the PSO model, the rate constant K_2 is based on the assumption that the chemisorption based interactions between the ions and the sorbent are the rate limiting step, whereby sorption is dependent on the adsorptive solid capacity in the form of available fraction of active sites on adsorbent (Ho and McKay, 1999; Ho and McKay, 2004; De Haro-Del Rio *et al.,* 2015; Qiu *et al.,* 2009; Ho and McKay, 1998).

The assumption of the pseudo-second order model is that one cadmium ion is adsorbed onto two sorption sites on the surface of the adsorbent which can be represented as equation 5.3 according to Boparai *et al*., (2011).

$$2A + Cd^{2+}_{sol} \xrightarrow{k2} A_2Cd_{solid\ phase} \tag{5.3}$$

Where A is an unoccupied sorption site on the adsorbent and K_2 is the pseudo second order rate constant($gmg^{-1}h^{-1}$).

The co-efficient of determination (r^2) and two non-linear error parameters the chi-square test (χ^2) and the root mean square error (RMSE) were used to analyse the two kinetic models (Basha *et al*., 2009; Hossain *et al*., 2013). The coefficient of determination (r^2) formula is given in eqn. 5.4:

$$r^2 = \frac{\sum(qe,model-qe,av.)\ 2}{\sum(qe,model-qe,av.)2+\sum(qe,model-qe,exp.)2} \tag{5.4}$$

The non-linear error functions of Chi-square test (χ^2) and the root mean square error (RMSE) were used to evaluate the model and these are given in eqns. 5.5 and 5.6 as follows:

$$\chi 2 = \sum_{n=1}^{n}(\frac{(qe,exp.n - qe,model.n.)2}{(qe,exp.n)}$$ (5.5)

$$RMSE = \sqrt{\frac{1}{m-p}}\sum_{i=1}^{m}(qm - qe)^2$$ (5.6)

Where: $qe,_{model}$ is the sorption capacity obtained from the model

$qe,_{exp.}$ is the sorption capacity obtained from experiment

$qe,_{av}$ is the average $q_{e,\ exp}$.

qe and qm are the measured and model amount of Cd(II) and Pb(II) ions adsorbed at time t respectively

m is the number of data points evaluated

p is the number of parameters in the regression model

Whereby low values of RMSE and χ^2 implies a good fitting of the model to experimental data, conversely high r^2 values indicate good fitting of model with the experimental data (Basha *et al*., 2009).

5.11.1.1 Cadmium (II) ion kinetic modelling

Kinetic modelling of Cd(II) ion sorption for the 7 residue adsorbents were carried out for the pseudo first order (PFO) and pseudo first order (PSO) equations using the solver add-in optimization procedure in Microsoft excel 2010 software. The plots of the PFO and PSO models for Cd(II) are presented in Figures 5.39 and 5.40. From these models, the kinetic parameters and their respective error functions obtained are presented in Table 5.7. The results presented in figure 5.39-5.40 and Table 5.7 indicates that the two models (PFO & PSO) could be used to characterise the kinetics of Cd(II) ion sorption and their prediction of the parameter ($qe,_{model}$) is close to the result obtained from the experimental analysis of Cd(II) ion sorption.

For the PFO model the $q_{e,cal}$ obtained for the 7 residue adsorbents for Cd(II) ion sorption were in the range 11.2 mgg^{-1} (PTPS) to 16.3 mgg^{-1}(CNFS) with the order being CNFS > OPFS > YTBS > PTHS > CCPS > PTPS > CCYBS. The rate constant of the pseudo first order reaction (K_1) for the adsorbents were in the range 1.38 $\times10^{-2}$ min^{-1}(CCYBS) to 2.40 $\times$ 10^{-2} min^{-1}(YTBS). The value of the coefficient of determination and the two error parameters – the root mean square (RMSE) and Chi square (χ^2) can be used to determine

the Cd(II) ion uptake kinetics is best described by the PFO model. From Table 5.7, it is observed that all the residue adsorbents had the same r^2 value of 0.99 with the exception of CNFS, which depicts a close agreement of the PFO model with the adsorbents. To further discriminate amongst the six adsorbents, the χ^2 and the RMSE values are used with the lowest values being an indication of best fitting. Based on this assumption, the sorption of Cd(II) ion onto the CCPS adsorbent is best described by the PFO model with the lowest χ^2 (0.02) and RMSE (6.88×10^{-2}) values, the PFO rate constant (K_1) obtained was 1.71×10^{-2} min^{-1} and the PFO model metal ion loading ($q_{e,cal}$) was 11.3 mgg^{-1}.

The PSO model was also used to evaluate the kinetics of Cd(II) ion sorption onto the 7 residue adsorbents and the results are presented in Table 5.7. The data obtained for the PSO rate constant (K_2) for the 7 adsorbents were in the range 1.30×10^{-3} gmg^{-1}min^{-1}(CCYBS) to 1.90×10^{-3} gmg^{-1}min^{-1}(YTBS), which is similar to what was observed for the PFO with respect to the lowest and highest values of the rate constant. The initial sorption rate (h) obtained from the PSO model as $q_t/t \rightarrow 0$ which gives an indication of the intial kinetic rate of sorption were in the order of CNFS > OPFS > YTBS > PTHS > PTPS > CCPS > CCYBS with the CNFS adsorbent having the highest value of 0.53mgg^{-1}min^{-1}. This rate also follows the trend in the amount of metal ion loading as fastest the initial sorption rate (h) gives rise to the highest loading($q_{e,cal}$). The $q_{e,cal}$ obtained for the for Cd(II) ion sorption were in the range 12.3mgg^{-1} (CCYBS) to 18.0 mgg^{-1}(CNFS) with the order being CNFS > OPFS > YTBS > PTHS > CCPS > PTPS > CCYBS. The value of the coefficient of determination and the two error parameters – the root mean square (RMSE) and Chi square (χ^2) can be used to determine the adsorbent the kinetics of Cd(II) sorption that is best described by the PSO model.

The value of these error parameters in Table 5.7 shows a trend of three bands of r^2. The first group has a single adsorbent (CNFS) with the least r^2 value of 0.94.The second group is made up of CCYBS, PTHS, PTPS and YTBS adsorbents and all have values of 0.96. The third group is composed of CCPS and OPFS and these have the highest r^2 value of 0.97. To further discriminate the adsorbent that is best described by the PSO model, consideration was given to the values of the two error parameters- the χ^2 and the RMSE. The adsorbent with the lowest values for these two parameters was thereafter chosen as the best described by the PSO model. Based on this assumption, the CCPS adsorbent uptake of Cd(II) ion is best described by the PSO model with the lowest χ^2 (0.08) and RMSE (2.89 $\times 10^{-1}$) values. The PSO rate constant (K_2) obtained for this adsorbent was 1.62×10^{-3} gmg^{-1}min^{-1} and the PSO model metal ion loading ($q_{e,cal}$) was 12.6 mgg^{-1}.
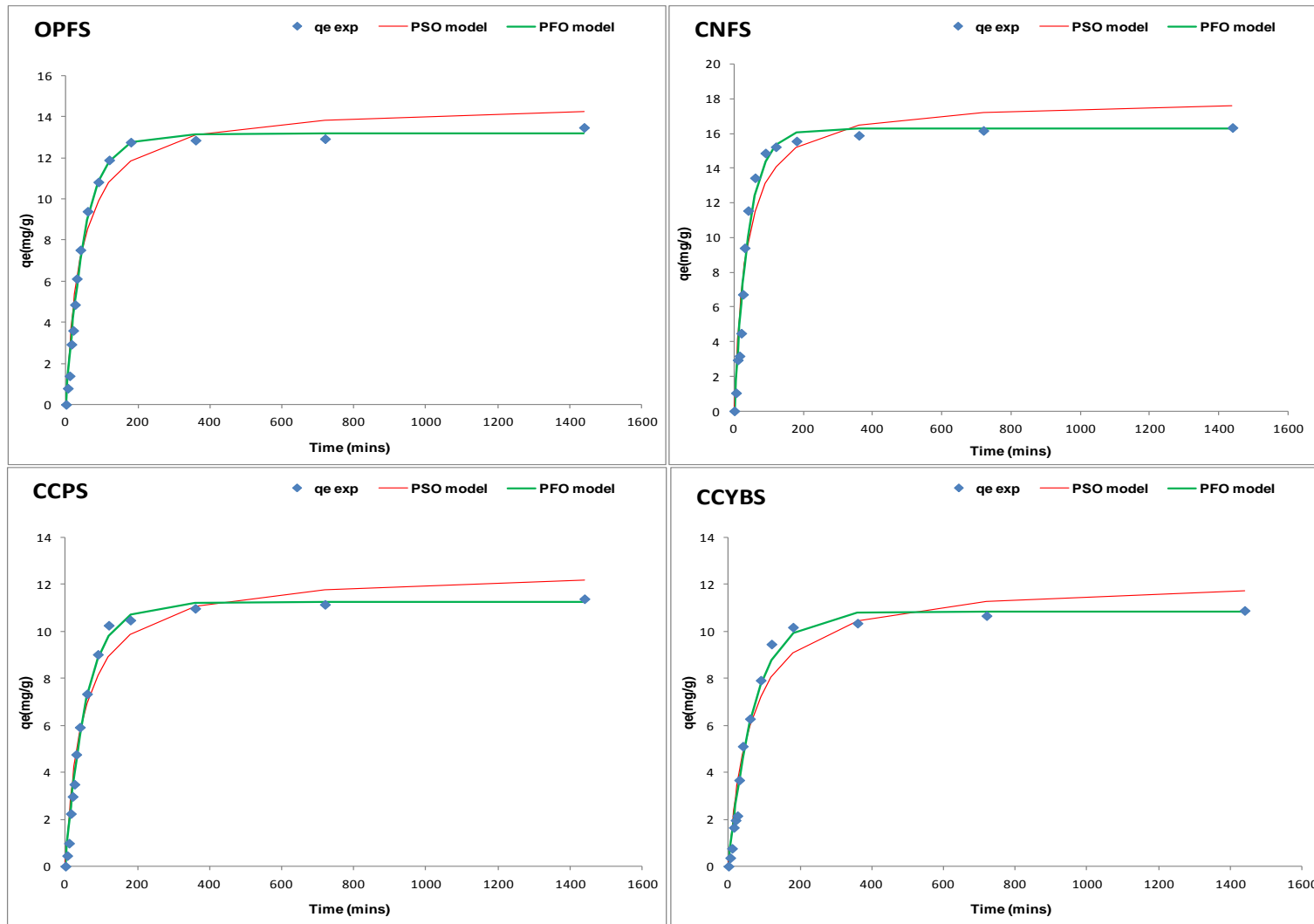
Fig 5.39: PFO & PSO kinetic models for Cd(II) ion sorption onto OPFS, CNFS, and CCPS & CCYBS residue adsorbents
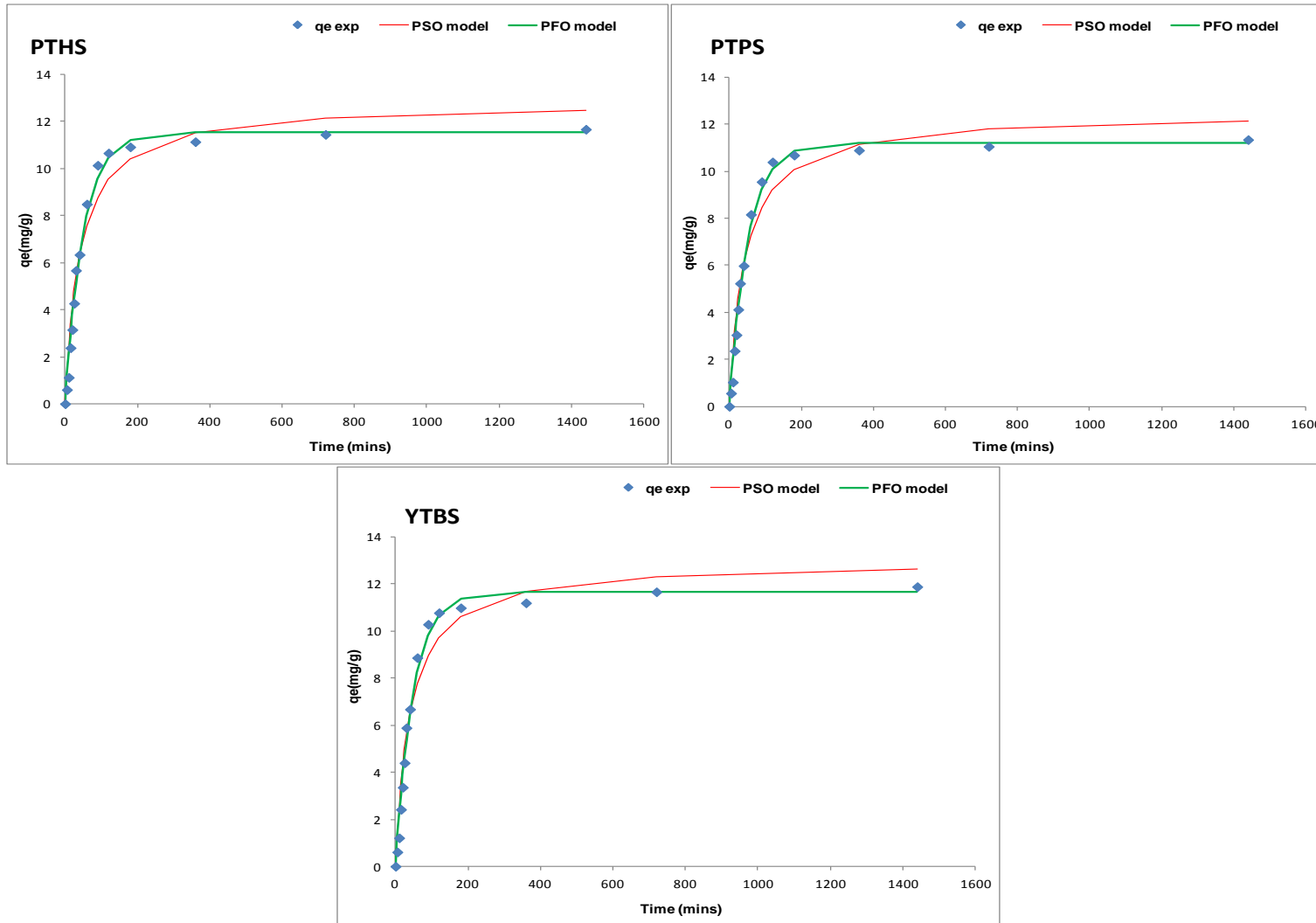
Fig 5.40: PFO & PSO kinetic models for Cd(II) ion sorption onto PTHS, PTPS & YTBS residue adsorbents

Table 5.7: PFO & PSO modelling parameters for Cd(II) sorption on unmodified adsorbents

	Pseudo First Order Model					Pseudo Second Order					
Adsorbent	$q_{e,cal}(mgg^{-1})$	$K_1(min^{-1})$	r^2	$\chi 2$	RMSE	$q_{e,cal}(mgg^{-1})$	$K_2(gmg^{-1}min^{-1})$	$h(mgg^{-1}min^{-1})$	r^2	$\chi 2$	RMSE
OPFS	13.2	1.91E-02	0.99	0.02	8.68E-02	14.7	1.59E-03	0.34	0.97	0.09	3.80E-01
CNFS	16.3	2.40E-02	0.97	0.08	4.77E-01	18.0	1.64E-03	0.53	0.94	0.20	1.15E+00
CCPS	11.3	1.71E-02	0.99	0.02	6.88E-02	12.6	1.62E-03	0.26	0.97	0.08	2.89E-01
CCYBS	10.9	1.38E-02	0.99	0.04	1.23E-01	12.3	1.30E-03	0.19	0.96	0.11	3.66E-01
PTHS	11.5	1.97E-02	0.99	0.03	1.15E-01	12.8	1.86E-03	0.31	0.96	0.10	4.00E-01
PTPS	11.2	1.91E-02	0.99	0.02	8.84E-02	12.5	1.85E-03	0.29	0.96	0.09	3.52E-01
YTBS	11.7	2.04E-02	0.99	0.03	1.29E-01	13.0	1.90E-03	0.32	0.96	0.10	4.06E-01

A comparison of the values obtained for the PFO and PSO models can be used to determine which of the two kinetic models best gives the description of metal ion sorption kinetics. Table 5.8 presents the value of metal ion loading at the end of sorption (q_e) for both experimental and models for Cd(II) ion uptake kinetics onto the different residue adsorbents. From Table 5.8, it is observed that the values for qe_{model} of the PFO for all the 7 residue adsorbents are closer to the experimental (q_e) than that of the PSO model. Thus, it can be stated that the PFO model gave a better approximation of the kinetics of Cd(II) sorption than the PSO order model and this can also be seen in the lower values for error parameters and correlation coefficient in Table 5.7.

Table 5.8: Comparison of q_e values for experimental and model sorption for Cd(II) ion

Adsorbent	q_e (mgg^{-1})		
	Experiment	PFO model	PSO model
OPFS	13.5	13.2	14.7
CNFS	16.3	16.3	18.0
CCPS	11.4	11.3	12.6
CCYBS	10.9	10.9	12.3
PTHS	11.7	11.5	12.8
PTPS	11.3	11.2	12.5
YTBS	11.9	11.7	13.0

This suggest that the kinetics supports the assumption that the rate limiting step of Cd(II) ion sorption onto the 7 different residue adsorbents is dependent on the concentration of the Cd(II) ions in solution (Azizian, 2004; Liu and Liu, 2008). However, the closeness of the parameters obtained from the PSO indicate that chemical interactions between the ions in the adsorbate solution and the adsorbent may still influence sorption kinetics but this may depend on the rate of diffusion.This implies that pore diffusivity of the ions onto the active sites may also influence the kinetics as previously discussed in the analysis of the two stage metal uptake (fast and slow) kinetics of Cd(II) ion sorption.

A number of studies have carried out for the sorption of Cd(II) ions from aqueous solution in which the PFO and PSO models have been used to characterised metal ion uptake. Nouri *et al.,* (2007) reports on the sorption of Cd(II) ions using wheat bran. In their study the

PSO gave a better description of metal sorption than the PFO order model with q_e(10.51 mgg^{-1}), K_2(31.83 10^{-3} gmg^{-1}min^{-1}) and h(3.52 mgg^{-1}min^{-1}). Sarada *et al.,* (2014) also reports on the better fitting the PSO model for the description of the kinetics of Cd (II) ion removal by macro algae *Caulerpa fastigiata* than the PFO model. However, Hameed and El-Khaiary, (2008a) have also reported on the better fitting of the PFO model than the PSO for the description of the kinetics of sorption of a cationtic dye onto an agricultural waste; broad bean peels. In their study they also observe that it is not know what are the properties of an adsorption system that makes it to be better represented by one model rather than the other. Irrespective of this, the pseudo kinetic models are still important as simple equations that are used to predict the kinetics of an adsorption system and in the design of adsorption units (Hameed and El-Khaiary,2008a).

5.11.1.2 Lead (II) ion kinetic modelling

The sorption of Pb(II) ions onto the 7 residue adsorbents were also modelled using the pseudo first order (PFO) and pseudo first order (PSO) equations using the solver add-in optimization procedure in Microsoft excel 2010 software. The plots of the PFO are PSO models for Pb(II) sorption are presented in Figures 5.41 and 5.42 while the kinetic parameters and their respective error functions obtained from the modelling are presented in Table 5.9. The Figures for the PFO and PSO modelling of Pb(II) sorption by the 7 adsorbents indicates that the adsorption rate decreases with time until it gradually approaches the equilibrium state due to the continuous decrease in the driving force (q_e-q_t)(Hameed and El-Khaiary, 2008b). From the plots of the experimental data with the PFO and PSO models, it can also be observed that both model lines were quite close to the experimental data at onset of Pb(II) ion sorption until t=60 min. After 60 min the model lines for both PFO and PSO deviated from the experimental data points. This may be attributed to the decrease in the adsorbate concentration gradient after the initial rapid uptake due to the initial availability of a large amount of vacant active sites (Ofomaja and Unuabonah, 2011). It has also been suggested that the point of deviation of the two models from the experimental data may also be the regions of change in the kinetic mechanism from mass transfer to pore diffusion as the number of vacant sites begins to diminish due to increase in metal ion uptake as sorption increases with time (Ofomaja, 2008; Ofomaja and Unuabonah, 2011).

It can be seen from Table 5.9 that for the PFO model the $q_{e,cal}$ obtained for the 7 residue adsorbents for Pb(II) ion sorption were in the range 9.41 mgg^{-1} (CCPS) to 11.7 mgg^{-1}(OPFS) with the order being OPFS > YTBS > PTPS > PTHS > CCYBS > CNFS > CCPS.

The rate constant of the pseudo first order reaction (K_1) for the adsorbents were in the range 1.24×10^{-2} min^{-1}(CCPS) to 1.89×10^{-2} min^{-1}(PTPS). The two error parameters – the root mean square (RMSE) and Chi square (χ^2) and the coefficient of determination can be used to determine the adsorbent uptake of Pb(II) ion that is best described by the PFO model. From Table 5.9, it can be observed that all the residue adsorbents had the same r^2 value of 0.99 with the exception of CCPS and PTPS, which depicts a close agreement of the PFO model with the adsorbents. To further discriminate amongst the five adsorbents, the χ^2 and the RMSE values were used with the lowest values being an indication of best fitting. Based on this assumption, the sorption of Pb(II) ion onto the CNFS adsorbent is best described by the PFO model with the lowest χ^2 (0.02) and RMSE (6.38×10^{-2}) values, the PFO rate constant (K_1) obtained was 1.25×10^{-2} min^{-1} and the PFO model metal ion loading ($q_{e,cal}$) was 9.59 mgg^{-1}.

The second model used to characterise the kinetics of Pb(II) onto the 7 residue adsorbents was the PSO equation and the results of the modelling are presented in Table 5.9. From the table, it can be observed that the data obtained for the PSO rate constant (K_2) for the 7 adsorbents were in the range 1.35×10^{-3} gmg^{-1}min^{-1}(CCPS) to 1.95×10^{-3} gmg^{-1}min^{-1}(CCYBS. The initial sorption rate (h) obtained from the PSO model as $q_t/t \rightarrow 0$ which gives an indication of the intial kinetic rate of sorption were in the order of PTPS > PTHS > OPFS > CCYBS =YTBS> CNFS> CCPS with the PTPS adsorbent having the highest value of 0.28mgg^{-1}min^{-1}. The loading of the Pb(II) ions onto the surface of the 7 different adsorbents based on the PSO model ($q_{e,cal}$) were in the range 10.7 mgg^{-1} (CCPS) to 13.1 mgg^{-1}(OPFS) with the order being OPFS > YTBS > PTPS > PTHS > CCYBS > CNFS > CCPS. The value of the coefficient of determination and the two error parameters – the root mean square (RMSE) and Chi square (χ^2) can be used to determine the adsorbent the kinetics of Pb(II) sorption that is best described by the PSO model. The value of these error parameters in Table 5.9 shows a trend of two bands of r^2. The first group is made up of CCPS and CCYBS adsorbents with the r^2 value of 0.98.The second group is made up of OPFS, CNFS, PTHS, PTPS and YTBS adsorbents and all have values of 0.99 indicating the close proximity of the PSO model to the experimental data for the sorption onto these adsorbents. To further discriminate the adsorbent that is best described by the PSO model, consideration was given to the values of the two error parameters- the χ^2 and the RMSE.

Table 5.9: PFO & PSO modelling parameters for Pb(II) sorption on unmodified adsorbents

Adsorbent	Pseudo First Order Model					Pseudo Second Order					
	$q_{e,cal}$(mgg^{-1})	K_1(min^{-1})	r^2	χ^2	RMSE	$q_{e,cal}$(mgg^{-1})	K_2(gmg^{-1}min^{-1})	h(mgg^{-1}min^{-1})	r^2	χ^2	RMSE
OPFS	11.7	1.55E-02	0.99	0.04	1.30E-01	13.1	1.40E-03	0.24	0.99	0.03	1.26E-01
CNFS	9.59	1.25E-02	0.99	0.02	6.38E-02	10.8	1.36E-03	0.16	0.99	0.02	6.14E-02
CCPS	9.41	1.24E-02	0.98	0.05	1.24E-01	10.7	1.35E-03	0.15	0.98	0.04	9.87E-02
CCYBS	9.70	1.75E-02	0.99	0.02	7.47E-02	10.9	1.95E-03	0.23	0.98	0.04	1.19E-01
PTHS	10.7	1.69E-02	0.99	0.03	1.08E-01	12.0	1.72E-03	0.25	0.99	0.02	5.83E-02
PTPS	10.9	1.89E-02	0.98	0.05	1.93E-01	12.2	1.86E-03	0.28	0.99	0.03	1.00E-01
YTBS	11.2	1.52E-02	0.99	0.03	9.83E-02	12.5	1.47E-03	0.23	0.99	0.03	1.19E-01
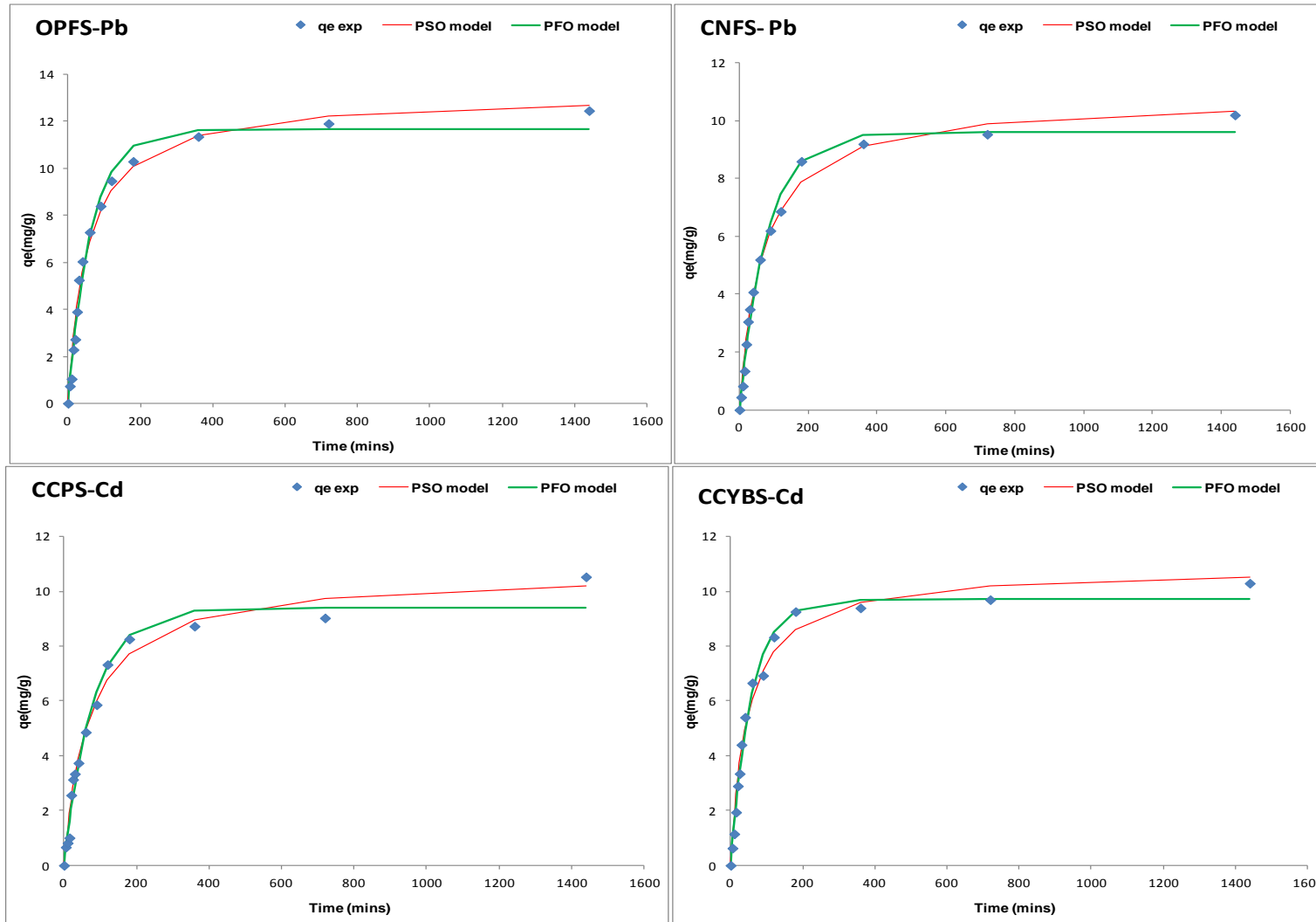
Fig 5.41: Lead (II) ion PFO & PSO sorption kinetic models for OPFS,CNFS, CCPS & CCYBS residue adsorbents
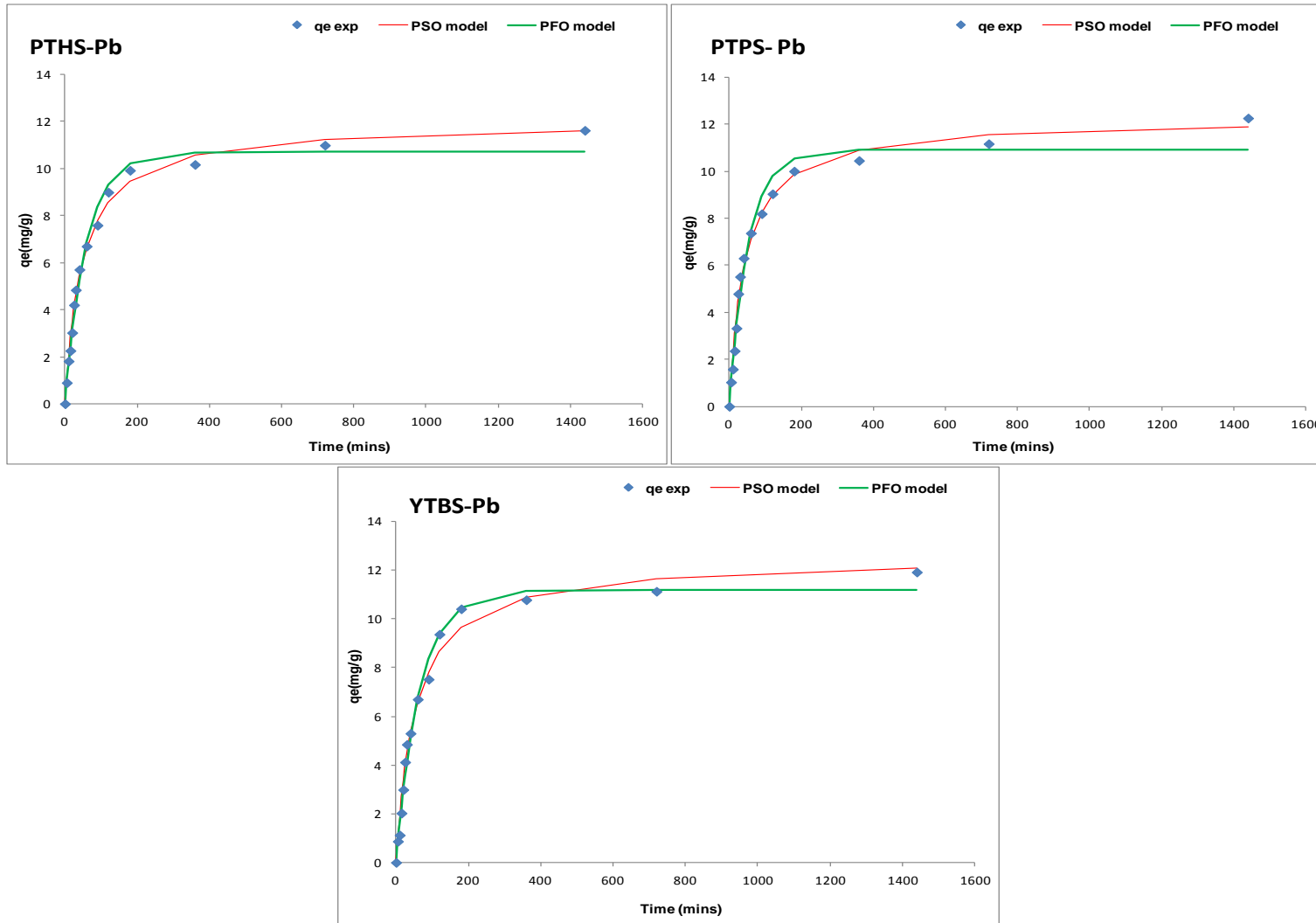
Fig 5.42: Lead (II) PFO & PSO sorption kinetic models for PTHS, PTPS & YTBS residue adsorbent

The adsorbent with the lowest values for these two parameters was thereafter chosen as the best described by the PSO model. Based on this assumption, the PTHS adsorbent uptake of Pb(II) ion is best described by the PSO model with the lowest χ^2 (0.02) and RMSE (5.83 $\times10^{-2}$) values. The PSO rate constant (K_2) obtained for this adsorbent was 1.72×10^{-3} gmg^{-1}min^{-1} and the PSO model metal ion loading ($q_{e,cal}$) was 12.0 mgg^{-1}.

Table 5.10: Comparison of q_e values for experimental and model sorption for Pb(II) ion

Adsorbent	q_e (mgg^{-1})		
	Experiment	PFO model	PSO model
OPFS	12.5	11.7	13.1
CNFS	10.2	9.6	10.8
CCPS	10.5	9.4	10.7
CCYBS	10.3	9.7	10.9
PTHS	11.6	10.7	12.0
PTPS	12.3	10.9	12.2
YTBS	11.9	11.2	12.5

The PSO and PFO models used to described the sorption of Pb(II) onto the surface of the 7 residue adsorbents can be compared to determine which model best describes the kinetics of metal ion uptake based on the value of q_e as presented in Table 5.10. The results presented in figures 5.41,5.42 and Table 5.9 indicates that the two models can be used to describe the kinetics of Pb(II) ion uptake from aqueous solutions onto the 7 different residue adsorbents and the determination of the loading parameter for each model ($q_{e,model}$) is close to the experimental q_e. A comparison of the experimental and model q_e values for Pb(II) for the two models is presented in Table 5.10. From Table 5.10, it is observed that both PFO and PSO models have q_e values that are close to the experimnetal q_e. However, a discernible model that was closer to the experimental data could not be readily determined as the PFO gave q_e values that underestimated the experimental q_e, while that of the PSO model overestimated the q_e. A comparison of the error parameters and coefficient of determination values for both models showed that both models did fit the experimental data with similar precision. Thus, it can be suggest that based on the kinetic

modelling of Pb(II) ion sorption both models could be used to describe the sorption process. The PFO and PSO kinetic models have been used to describe the sorption of Pb(II) from aqueous solution using a number of natural biomasses. Boudrahem *et al.,* (2011) has described the kinetics of Pb(II) ion from aqueous solution using date tree leaves as an adsorbent. In their study, the PSO did describe the metal sorption kinetics better than the PFO model as the error parameter -r^2 was close to unity and the calculated $q_{e,cal}$ values did agree well with experimental data. A similar observation has been made by Wang *et al.,* (2015a) in their study on the removal of Pb(II) from aqueous solution using *Phytolacca americana L.*biomass.

5.12 Effect of pH on sorption

The pH of an aqueous solution is a fundamental parameter that influences the sorption of metal ions due to its effect on the speciation of ions in solution and hence the types of ions that are available at particular hydrogen or hydroxyl ion concentrations to facilitate their removal by the adsorbents. Since the surface chemistry of the adsorbent is influenced by the pH of the solution, the characterisation of the zeta potential of each adsorbent as discussed in Section 5.5 of this work was important. Based on the zeta potential determination of the pHpzc of the residue adsorbents, the pH of 6.5 was chosen as the pH for adsorption study using the unmodified residue adsorbents. However, it was important to understand the effect of pH on the sorption behaviour of the adsorbents for the two metal ions. This would give insight into the effect the adsorbate pH has on the overall loading of these metal ions on the adsorbents. In addition this pH evaluation would also contribute to the elucidation of the mechanism of the adsorption process involving these residue adsorbents.

The effect of pH was thus studied for the two metal ions based on the procedure described in Section 4.4 of this work. pH 2-10 was taken as the window for analysis for all adsorbents. This was taken to give information on the acidic and basic ranges of metal ion in aqueous adsorbates which lie between the pH range for discharged effluents based on WHO standard guidelines (6.5 – 9.5 (Ipeaiyeda and Onianwa, 2011). In addition, metal ion precipitation has been reported for both Cd (II) and Pb (II) ions as the pH increases from 7.5 to 12 according to Ho., *et al* (2002). Also Mohan *et al.,* (2007) in their study on the sorption of arsenic, cadmium and lead by chars produced from fast pyrolysis of wood and bark during bio-oil production reports that in metal ion sorption studies, the onset of metal hydrolysis and precipitation is estimated to occur at pH 8.2 for $Cd(OH)_2$ and 7.7 for

Pb(OH)$_2$ and this was also observed during the evaluation of these two heavy metal ions in this study. Hence for the evaluation of the effect of adsorbate pH on the removal of Cd(II) and Pb(II) ions using the residues (OPFS, CNFS, CCPS, CCYBS, PTHS, PTPS and YTBS) the experimental conditions were; pH was 2-10, with an initial metal ion concentration of 500 mgL^{-1}, temperature of 25 ºC and a reaction volume of 0.1 L. The amount of adsorbent used was 2.0 g and HCl and NaOH were used to vary the different adsorbate pH. The effect of pH on Cd (II) ion sorption is shown in Figure 5.43 while that of Pb (II) ion is seen in Figure 5.44. From the two figures, it is observed that the optimum pH for Cd (II) ion removal using the residue adsorbents was 7, while that of Pb (II) ion was at pH 6. An evaluation of pH of the adsorbate after sorption of Cd (II) ion was carried out and the results are presented in Table 5.11.
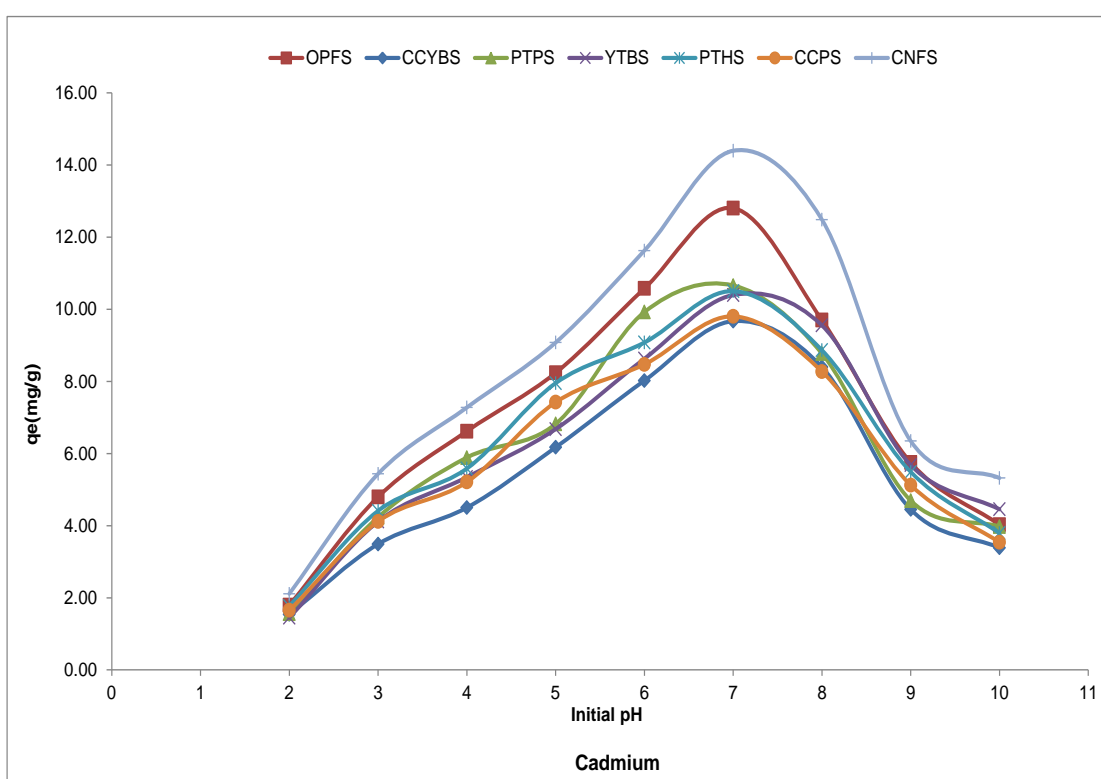
Figure 5.43.: Influence of pH on Cd(II) ion sorption using residue adsorbents
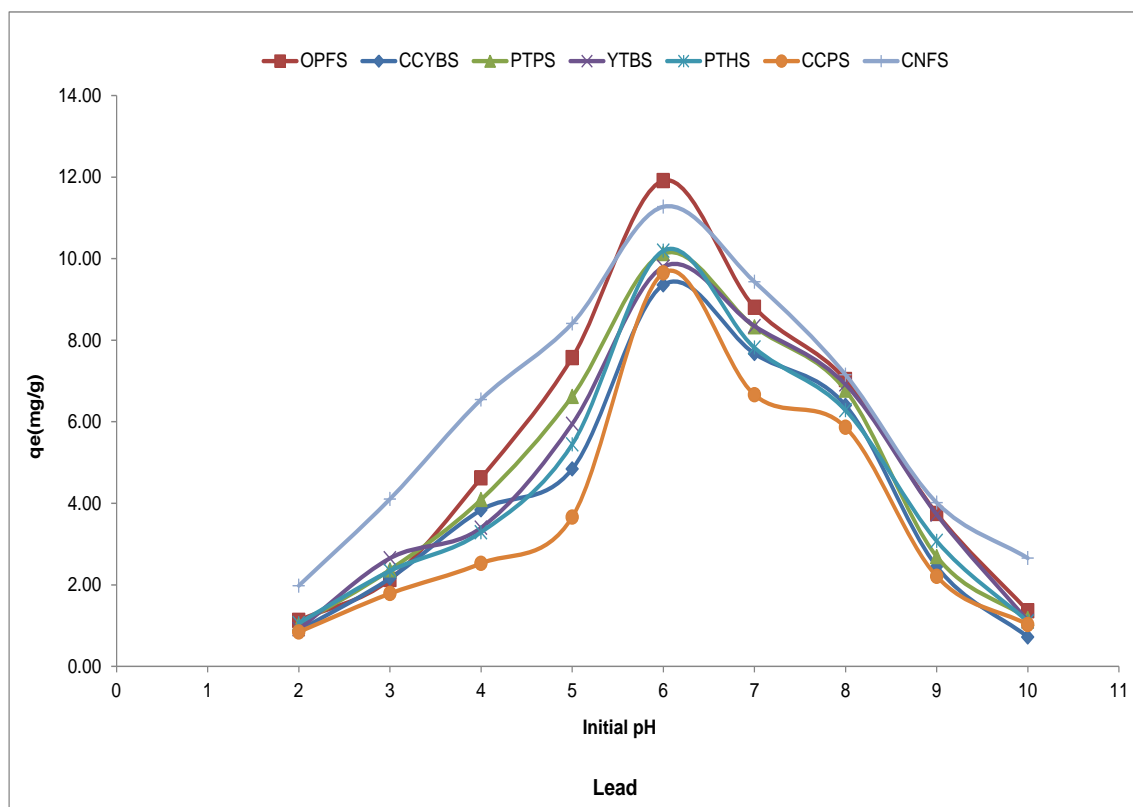
Figure 5.44.: Influence of pH on Pb(II) ion sorption using residue adsorbents

The pH of the adsorbate solution has been reported to affect the surface charge of the adsorbent, level of dissociation of functional groups on the adsorbent surface, degree of ionization and speciation of adsorbate, solubility of metal ions as well as concentration of the counter ions in solution and these parameters may affect the uptake of metal ions from an adsorbate (Teker *et al.,* 1999; Antunes *et al.,* 2003). Furthermore, the affinity of the Cd(II) and Pb(II) ions for the surface of the different residue adsorbents may be influenced by the degree of hydration of the metal ion precursors {(Pb(NO$_3$)$_2$ and Cd(NO$_3$)$_2$.4H$_2$O}, whereby higher degrees of metal hydration may result in less adsorption probability due to the difficulty in accessing the adsorbent surface (Bartczak *et al.,*2015).

From Figures 5.43 and 5.44 it can be observed that the amount of metal adsorbed increased slowly at first with increase in initial pH from 2 to 4, reached a maximum value at pH 7.0 for Cd(II) and 6 for Pb(II) and thereafter gradually decreased as the pH increased up till pH 10. At pH 2, the amount adsorbed of both Cd (II) and Pb (II) ions was least for all the adsorbents. It is presumed that the amount adsorbed at pH 2 was low probably due to the influence of the competing protons (H$^+$) in solution leading to competition for the adsorbent surface between H$^+$ and positive metal ions Cd(II) and Pb(II). These protons will also hinder the uptake of the two metal ions by the different residue adsorbents as the

induced positive surface on the adsorbents at low pH will lead to a repulsive effect for the metal ions ultimately leading to a reduction in the binding ability of the adsorbent (Wang *et al.,* 2015a). This explanation is based on the surface complexation theory which states that the increase in metal removal as pH increases can be explained on the basis of a decrease in competition between protons and metal species for the surface of active sites and by a decrease in positive charge (Krishnani *et al*., 2008).

Hence low pH values would favour protonation of the groups at the binding sites (hydroxyl, carboxyl, phenolic) and high pH values on the other hand would lead to the precipitation of metals especially at alkaline medium (pH 9 to 10) thereby reducing the amount of metal ions adsorbed by the different residue adsorbents as can be observed in both figures. At pH 5-7 the H^+ concentration in the adsorbate decreases and the functional groups on the surface of the different residue adsorbents become deprotonated thereby facilitating the uptake of Cd(II) and Pb(II) ions from the adsorbate via a number of interactions such as electrostatic interactions, complexation, ion-exchange and surface adsorption (Athar *et al.,*2013;Wang *et al.,*2015b). These different mechanisms for metal uptake may account for the optimum metal ion sorption for the different residue adsorbents within this pH window (5-7).

Sari *et al.*, (2008) reports that metal ion removal by sorbents often involves complex mechanism such as ion exchange, chelation, adsorption by physical forces, ion entrapment in the intrafibrillar capillaries and spaces of the adsorbents and since the adsorbent surface is composed of functional groups such as carbonyl, hydroxyl and amines. These groups will be most probably be involved in the different metal ion binding mechanism which will be influenced by the pH of the adsorbate. The high uptake of the Cd(II) and Pb(II) ions in the pH window of 5-7 for all the different residue adsorbents can also be explained based on the influence of the pHpzc of the adsorbents as these range from 5.5 for CNFS to 6.5 for OPFS and positive metal ion uptake is preferential at adsorbate pH that is higher than the adsorbent pHpzc. This is what is presumed to occur between pH 5-7, since the adsorbent surface is negatively charged at pH above the adsorbent pHpzc. This scenario has also been observed by Wang *et al.,* (2015a) in their study on the removal of Pb(II) from aqueous solution using *Phytolacca americana* L. biomass which had a pHpzc of 3.30 and the sorption of Pb(II) was reported to increase to a maximum at pH 6.

Table 5.11: Initial and final pH of adsorbate solution for Cd(II) sorption

pH	Adsorbent						
	OPFS	CCPS	CNFS	CCYBS	PTHS	YTBS	PTPS
Initial	2.00	2.00	2.00	2.00	2.00	2.00	2.00
Final	2.11	2.10	2.09	2.06	2.58	2.56	2.46
Initial	3.00	3.00	3.00	3.00	3.00	3.00	3.00
Final	2.94	3.15	2.83	3.43	3.57	3.84	3.34
Initial	4.00	4.00	4.00	4.00	4.00	4.00	4.00
Final	4.58	4.25	4.45	4.94	5.09	5.37	5.28
Initial	5.00	5.00	5.00	5.00	5.00	5.00	5.00
Final	4.52	5.24	4.44	5.08	5.39	5.42	5.26
Initial	6.00	6.00	6.00	6.00	6.00	6.00	6.00
Final	4.51	5.57	4.64	5.23	5.45	5.54	5.36
Initial	7.00	7.00	7.00	7.00	7.00	7.00	7.00
Final	4.73	6.06	5.52	5.46	5.57	5.87	5.48
Initial	8.00	8.00	8.00	8.00	8.00	8.00	8.00
Final	6.53	7.68	7.30	7.50	6.80	7.37	7.02
Initial	9.00	9.00	9.00	9.00	9.00	9.00	9.00
Final	7.32	8.79	8.09	8.06	7.86	7.40	7.80
Initial	10.0	10.0	10.0	10.0	10.0	10.0	10.0
Final	9.78	9.88	9.74	9.82	9.52	9.84	9.86

The low amount of Cd (II) and Pb (II) ions removed from the aqueous solution at pH 2 to 4 as seen in both Figures may also be due in part to the interaction of H_3O^+ ions on the adsorbent surface. Low *et al.,* (1995) and Ho *et al* (2002) report that at low pH values, the surface of the adsorbents could be closely associated with hydronium ions (H_3O^+) which hinder the access of metal ions to the functional groups on adsorbent surface due the repulsive force, hence the amount of metal ions removed at this pH will be low. An increase in pH however results in a gradual dissociation of the hydronium and the positively charged metal ions are then associated with free binding at the active sites on the adsorbent surface (Kim *et al.,* 2013).

Table 5.11 indicates that the final pH of the adsorbate decreases after Cd (II) ion sorption and this can be related to the complex nature of the adsorption process especially at various pH values as is the case in the present study; which involves the occurrence of a number of mechanisms such as ion-exchange, complexation and adsorption. The deprotonation of the different functional groups on the adsorbent surface has been suggested as the initial step in the uptake of metal ions and this process releases protons (H^+) into solution (Vaghetti *et al.,* 2009). The Cd(II) ions which compete for the adsorbent binding sites may then interact

with the negatively charged functional groups on the adsorbent (hydroxyl, phenolic, carboxylic). Thus as more metal ions are sorbed onto the adsorbents surface; more H^+ are probably released from the adsorbent surface into solution, thereby decreasing the final pH of the adsorbate solution. The magnitude of the difference between the values of the initial and final pH from Table 5.11 is also observed to indicate the trend in Cd (II) ion removal by the different adsorbents.

The above results show that the final pH of sorption solutions decreases as the amount of metal adsorbed increases, confirming that ion-exchange mechanism (cation displacement of protons) may be one of the processes of metal ion removal. The hydrogen ion sources are most likely to be the carboxyl, phenolic and hydroxyl groups on the adsorbents. However, the extent of hydrogen ion exchange could depend on the relative concentration of the exchangeable protons and the hydrogen ion concentration of the medium (Okieimen *et al.,* 1988). This is in line with observations from an examination of the sorption of Pb (II) and Ni (II) on chrysosporium biomass by Ceribasi and Yetsi (2001) which indicated that the most probable reason for the rapid decrease of protons by the adsorbent during the sorption of metal ions was ion-exchange. The work of Low *et al* (1993) is also in agreement with this observation based on findings of a low copper sorption obtained at pH of 2.0 from a study on the sorption of copper by dye-treated oil-palm fibres which was also attributed to the hydrogen ions competing with the copper ions for sorption sites.

5.13 Effect of adsorbent dose on metal ion sorption

The effect of absorbent dose on the removal of Cd(II) and Pb(II) ions from aqueous solutions using the different residues (OPFS, CNFS, CCPS, CCYBS, PTHS, PTPS and YTBS) was studied at pH 6.5, with initial metal ion concentration of 500 mgL^{-1}, a temperature of 25 $^{\circ}$C and a reaction volume of 0.1 L. The amounts of adsorbent used were 0.5, 1.0, 1.5, 2.0, 2.5 and 3.0 g. The effect of adsorbent quantity on the loading of Cd (II) and Pb (II) ions are shown in Figures 5.45 and 5.46 respectively. Figures 5.45 and 5.46 show that for Cd (II) and Pb (II) ion sorption, the percentage of metal ion removed from the aqueous solution by the different residues increases as the amount of adsorbent increases from 0.5 to 3.0g. The nature of the metal ion removal with increase in adsorbent dose can be attributed to the presence of active sites or surface area at higher amount as an increase in the quantity of adsorbent will result in a higher number of sites for metal ion binding until the saturation of the active sites within the adsorbent structure. Sarada *et al.*, (2014) makes a similar observation during an examination of the removal of Cd(II) ion by

C. *fastigiata* biomass with the increase in biomass attributed to the increase in the number of binding sites available to remove the metal ions at a specified initial metal ion concentration.
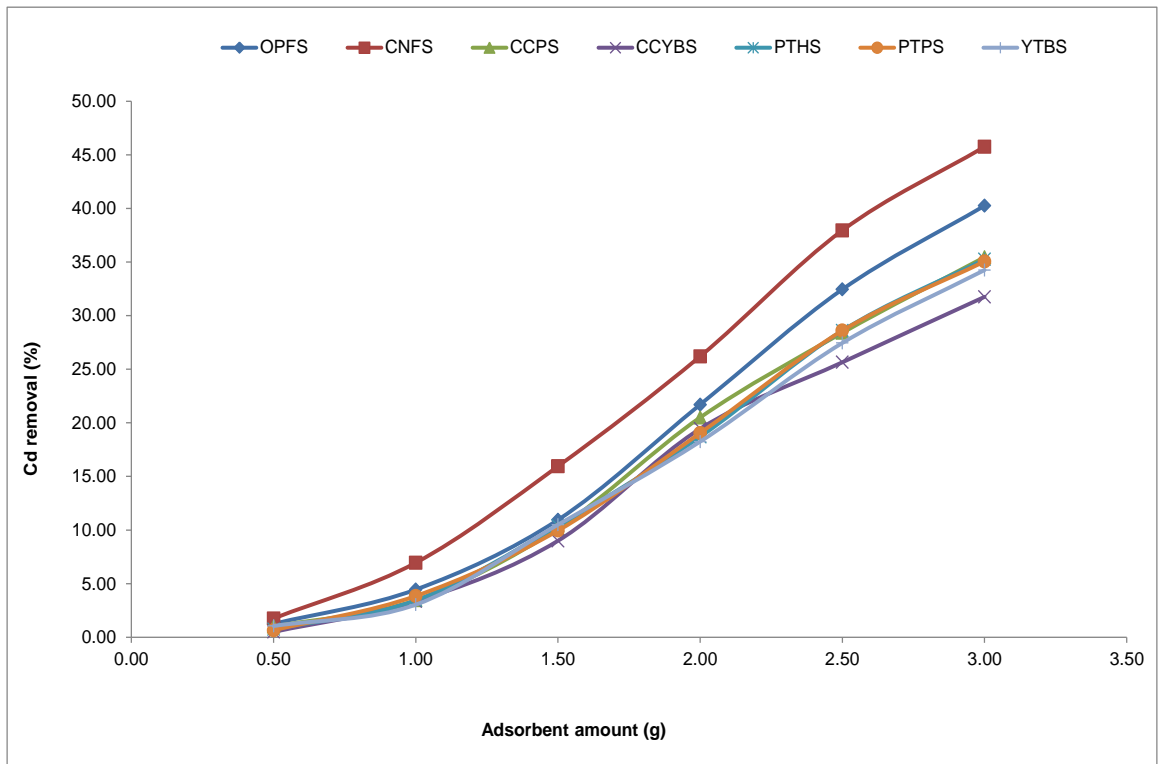

Figure 5.45: Influence of adsorbent amount on Cd(II) ion sorption using residue adsorbents
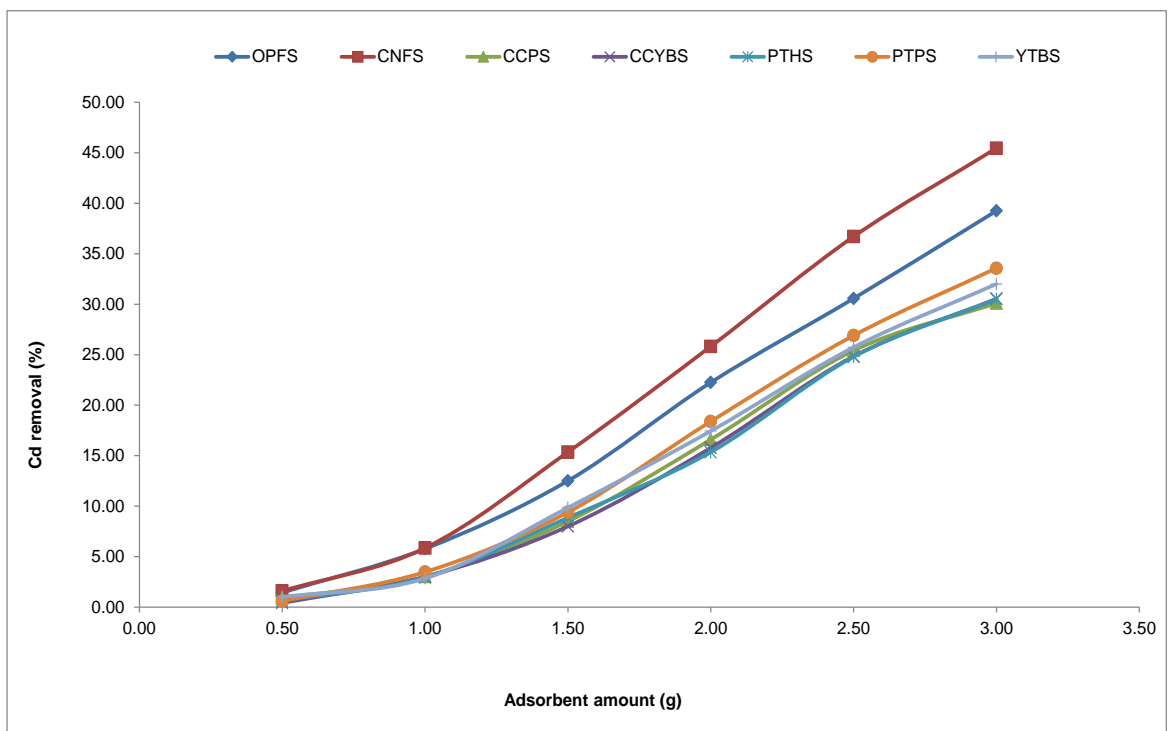

Figure 5.46: Influence of adsorbent amount on Pb(II) ion sorption using residue adsorbents

This trend has also been reported by Barkar *et al.*, (2013) in their study of Cd(II) and Pb(II) ion sorption onto dried cactus (*opuntia ficus indica*) cladodes. In the study, there was an enhancement of metal ion loading from 10% to 36% when the biosorbent dosage was increased from (0.5 to 4.0) gL^{-1}. It can also be observed that for all the residues, the Cd (II) ion percentage removal at 2.5 g was not different from those at 3.0 g implying that further increase of the adsorbent doses from 2.5 to 3.0 g did not provide a significant increase in loading. Barkar *et al.,* (2013) also reports this trend of no significant increase in biosorption yield when the adsorbent was increased from 4.0 gL^{-1} for Cd(II) and 10 gL^{-1} for Pb(II) ions and it was explained based on the effect of partial aggregation of the biomass at higher loading which leads to a decrease in the effective surface area available for metal ion sorption (Hanif *et al.,* 2007). Boudrahem *et al.,* (2011) in their study on the sorption of Pb(II) from aqueous solution using date tree leaves have also observed an increase in percent removal of Pb(II) ions from aqueous solution with increase in adsorbent dose from (0.3 to 1.5)$g.L^{-1}$. In their study the percent removal increased up to $1gL^{-1}$ after which the increase in Pb(II) loading as the adsorbent dose increased to $1.5gL^{-1}$ was less and this was attributed to adsorbent-adsorbate system attaining equilibrium thereby limiting the amount of the metal ion that is further removed from the system.

5.14 Adsorption equilibrium studies

The interaction in an adsorption system between the adsorbent and the adsorbate is a dynamic process and the quantification of the impact of the adsorbent on the adsorbate is described by the amount of adsorbate that is removed by the adsorbent. This also depends on the loading of the adsorbent. The loading of an adsorbent can be described by an equilibrium isotherm which is characterised by certain constants whose values express the surface properties and affinity of the adsorbent to the adsorbate (Sari *et al.,* 2008). Hence, equilibrium modelling or adsorption isotherms are studied to characterize the equilibrium. In order to represent the equilibrium adsorptive behaviour of the adsorbent-adsorbate interaction, it is important to have a satisfactory description of the equilibrium relationship between the two phases comprising the adsorption system. These equations represent the relationship between the amount of substance adsorbed on the adsorbent and the amount of adsorbate remaining in solution (Athar *et al*., 2013; El-Ashtoukhy *et al*., 2008). The adsorption equilibrium data indicates the relationship between the mass of the adsorbate sorbed per unit mass of adsorbent (q_e) and the adsorbate concentration for the solution at

equilibrium C_e (Sarada *et al*., 2014). Sorption equilibria can thus be used to provide fundamental physicochemical data for evaluating the applicability of the sorption process as a unit operation and the analysis of experimental equilibrium data by fitting them to isotherm models is an important step to determine suitable models than can be applied in the design of the adsorption system (Nouri *et al.,* 2007).

Two equilibrium isotherm models were used to characterize the removal of Cd(II) and Pb(II) ions from aqueous solutions using the 7 residue adsorbents as described in Section 4.4. These were the Langmuir and Freundlich isotherms. The Langmuir isotherm model is based on the assumption that the highest adsorption corresponds to a saturated monolayer of adsorbate molecules on the solid surface and that sorption takes place at specific sites, which are uniformly distributed across the surface of the adsorbent (Langmuir, 1918; Basha *et al.,* 2009). The Langmuir equation in its non-linear format was used for the modelling of equibrium sorption and is given as:

$$q_e = \frac{q_m K_L C_e}{1 + K_L C_e} \qquad\qquad (5.7)$$

Where q_e is the equilibrium metal ion concentration on the adsorbent (mgg^{-1}),
C_e is the equilibrium metal ion concentration in the solution (mgL^{-1}),
q_m is the monolayer adsorption capacity of the adsorbent (mgg^{-1}) also known as q_{max}
K_L is the Langmuir adsorption constant (Lmg^{-1}) related with the free energy of adsorption (Sari *et al*., 2008).

The Langmuir isotherm modelling of the sorption of Cd(II) and Pb(II) from aqueous solution using the 7 unmodified residue adsorbents was carried out using the Excel solver add-in optimization procedure in Microsoft Excel 2010. This process uses the co-efficient of determination as the normalization parameter to optimize the model and correlate it with the experimental isotherm data. This is done by the software by minimizing the distance between the experimental data points and the theoretical isotherm model predictions with the solver add-in function of the Microsoft Excel (Wong *et al*., 2004).

The second isotherm model considered in this study was the Freundlich isotherm. The Freundlich isotherm assumes a heterogeneous adsorption surface and active sites with different energy based on multilayer adsorption. The model estimates the adsorption intensity of the adsorbate on an adsorbent (Freundlich, 1906; Athar *et al*., 2013). The model in its non-linear form is given as:

$$q_e = K_F(C_e)^{1/n} \qquad\qquad\qquad (5.8)$$

Where K_F is a constant relating to the adsorption capacity $(mg\ g^{-1})(Lmg^{-1})^{1/n}$

C_e is the concentration of metal ions at equilibrium (mgL^{-1})

1/n is an empirical parameter relating to the adsorption intensity which varies with the heterogeneity of the material (Sari *et al*., 2008).

The Freundlich isotherm modelling of the sorption of Cd(II) and Pb(II) from aqueous solution using the 7 unmodified residue adsorbents was carried out using the non-linear optimization approach based on the solver add-in function in Microsoft Excel as previously described. The Langmuir and Freundlich isotherm plots for Cd(II) and Pb(II) ions using the unmodified adsorbents are shown in Figures 5.47 – 5.53 and these figures indicate that the adsorption of the two metal ions were concentration dependent increasing with increase in initial metal ion concentration (C_e). From these experimental values, equilibrium isotherm models (Langmuir and Freundlich) were used to further characterize the sorption process. To determine the goodness of fit of the isotherm models to the experimental data using non-linear regression, the optimization procedure requires that error functions be defined to enable the fitting of the model parameters with the experimental values. In this study, the coefficient of determination (r^2), the root mean square error (RMSE) and the Chi square test (χ^2) were used as error parameters for each model and these were determined based on eqns. 5.4, 5.5 and 5.6 which have been previously described in section 5.11 of this chapter.

5.14.1 Cadmium isotherm modelling

Adsorption isotherm studies were carried out for Cd(II) ion removal from aqueous solutions using the OPFS, CNFS, CCPS, CCYBS, PTHS, PTPS and YTBS adsorbents for initial metal ion concentrations, 50 –500 mgL^{-1} with step size of 50. The non-linear isotherm plots obtained for the Langmuir and Freundlich isotherms are shown in Figures 5.47 – 5.53 for Cd(II) ion sorption. From these plots, the Langmuir and Freundlich constants and the value of the coefficient of determination (r^2) for each adsorbent are given in Table 5.12. From the Figures, it can be seen that Cd(II) metal ion removal for all the adsorbents is concentration dependent as the loading for Cd (II) ion increases as the concentration increases. For the OPFS adsorbent, it is observed that the Cd(II) metal ion loading increased from 1.75 mgg^{-1} for initial concentration 50 mgL^{-1} to 11.49 mgg^{-1} for 500 mgL^{-1} and the trend is also observed for all the other residue adsorbents.

5.14.1.1 Langmuir Isotherm

The plot of the Langmuir isotherm for the 7 residue adsorbents are shown in Figures 5.47 – 5.53 for Cd(II) ion sorption. From these plots, the isotherm constants, the error parameters of root mean square error (RMSE), Chi square (χ^2) and the coefficient of determination (r^2) of each adsorbent for Cd(II) sorption were obtained and presented in Table 5.12. From this model, the value of Langmuir constant K_2 which gives an indication of the affinity between the adsorbate-Cd(II) and the different residue adsorbents ranged from 1.01×10^{-2} Lmg^{-1} for PTHS to 8.00×10^{-3} Lmg^{-1} for the OPFS adsorbent as presented in Table 5.12. The value of the Langmuir isotherm constant q_{max} (q_m) from each of the isotherm plots for the adsorbents is also shown in Table 5.12. These values indicate the maximum monolayer capacity of the different adsorbents based on the Langmuir isotherm assumption of a saturated monolayer (Athar *et al.,* 2013). It should be noted that the value of the q_{max} for each adsorbent is higher than the loading of each adsorbent at the initial metal ion concentration (500 mgL^{-1}) which was the maximum initial concentration used in this study. Hence, the isotherm constant q_{max} models the maximum adsorption loading (capacity) of the surface of the adsorbent assuming the Langmuir monolayer coverage. This q_{max} value is an important parameter that is used to aid the design of adsorption systems when scaling up an adsorption process as it provides information on the maximum saturation capacity of the adsorbent (Rao *et al*., 2006). From Table 5.12, it is observed that PTHS had the least q_{max} value of 16.0 mgg^{-1}, while CCPS has the highest value of 24.5 mgg^{-1} and the trend can be seen as CCPS > YTBS > CNFS > CCYBS > PTPS > OPFS > PTHS.

The values of the co-efficient of determination (r^2) and the two error parameters {the root mean square error (RMSE) and Chi square (χ^2)} obtained based on the non-linear isotherm modelling of the Langmuir equation were also used to give an indication of how the modelled data agreed with the experimental obtained data as shown in Table 5.12.

Figure 5.47: Isotherm plot for Cd(II) ion sorption for OPFS adsorbent

Figure 5.48: Isotherm plot for Cd(II) ion sorption for CNFS adsorbent

Figure 5.49: Isotherm plot for Cd(II) ion sorption for CCPS adsorbent

Figure 5.50: Isotherm plot for Cd(II) ion sorption for CCYBS adsorbent

Table 5.12: Isotherm Parameters for Cd(II) ion adsorption on unmodified residues

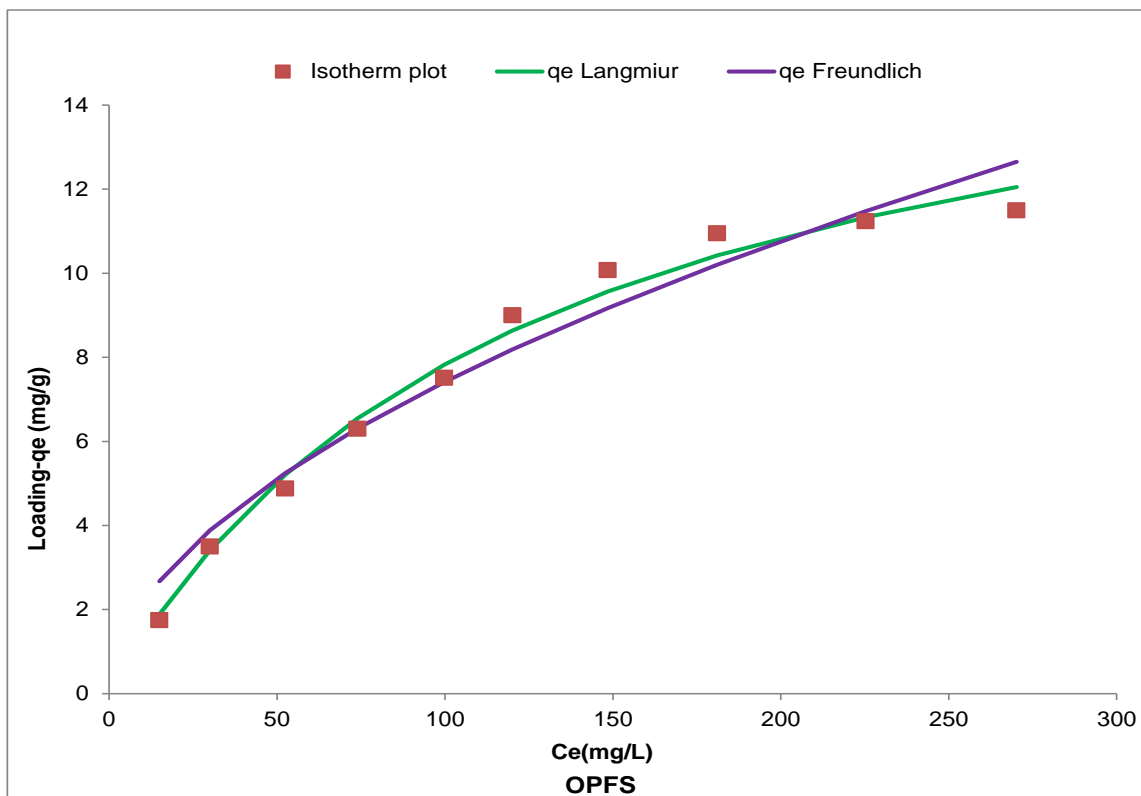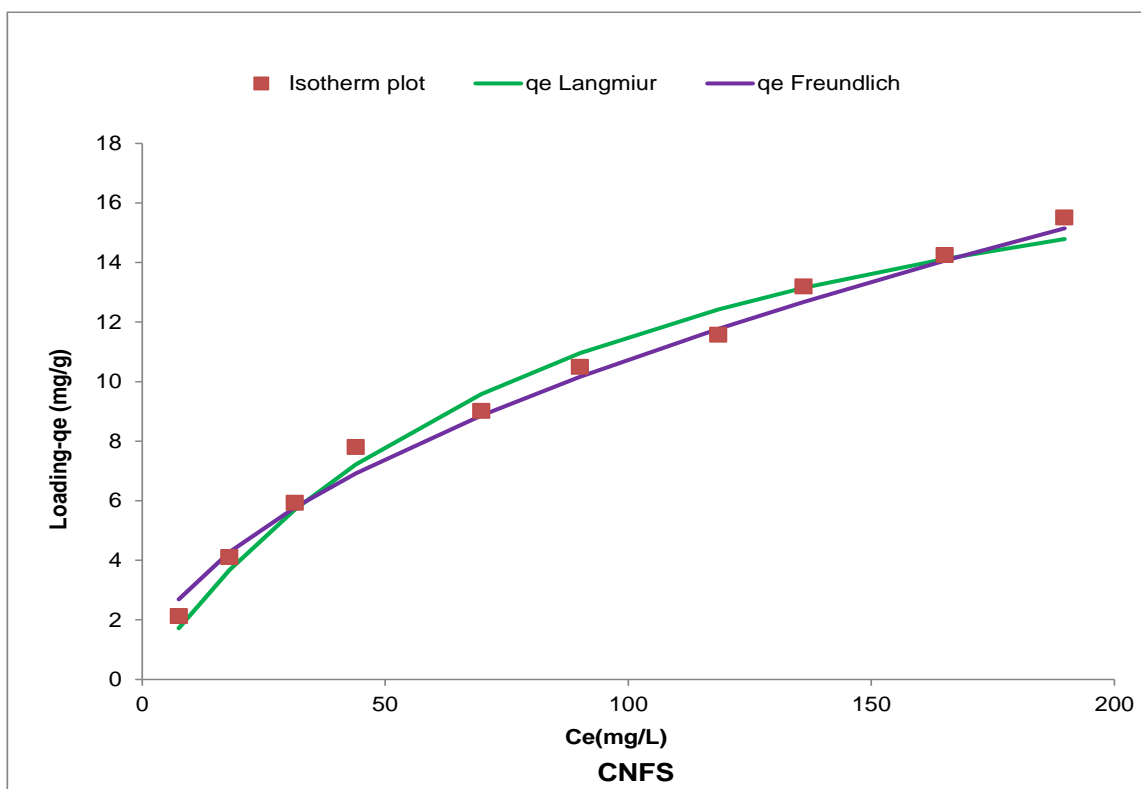| Adsorbent | Langmuir Model | | | | | Freundlich Model | | | | |
	$q_{max}(mgg^{-1})$	$K_L(Lmg^{-1})$	r^2	χ^2	RMSE	$K_F(mgg^{-1})(Lmg^{-1})^{1/n}$	n	r^2	χ^2	RMSE
OPFS	17.6	8.00E-03	0.99	1.66E-02	7.95E-02	0.63	1.86	0.95	5.93E-02	2.86E-01
CNFS	21.6	1.14E-02	0.99	2.72E-02	1.59E-01	0.91	1.86	0.99	1.92E-02	1.10E-01
CCPS	24.5	5.33E-03	0.99	2.34E-02	1.20E-01	0.41	1.54	0.96	6.37E-02	3.29E-01
CCYBS	21.4	3.63E-03	0.98	2.72E-02	1.13E-01	0.25	1.48	0.95	5.90E-02	2.47E-01
PTHS	16.0	1.01E-02	0.97	3.81E-02	1.84E-01	0.75	2.00	0.91	1.08E-01	5.20E-01
PTPS	18.9	5.21E-03	0.98	2.66E-02	1.17E-01	0.36	1.61	0.96	5.64E-02	2.49E-01
YTBS	22.4	3.47E-03	0.99	1.80E-02	7.57E-02	0.24	1.46	0.99	1.55E-02	6.56E-02
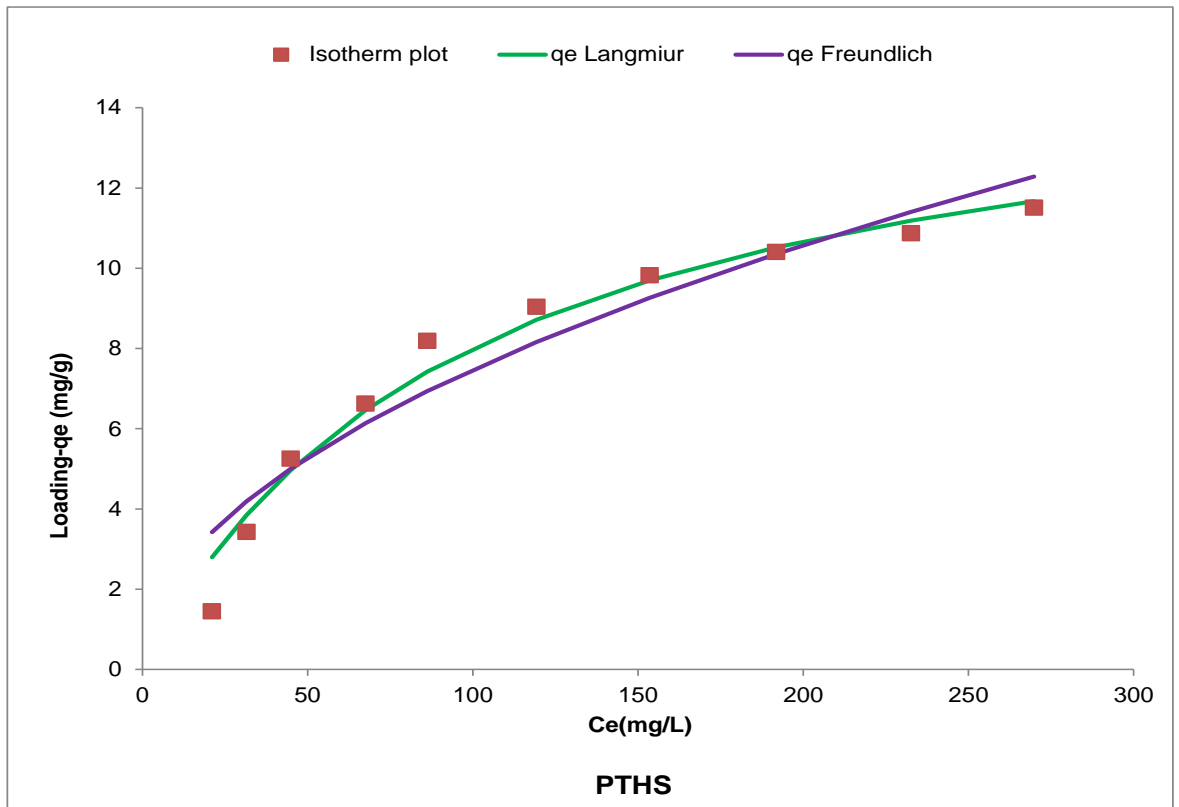
Figure 5.51: Isotherm plot for Cd(II) ion sorption for PTHS adsorbent
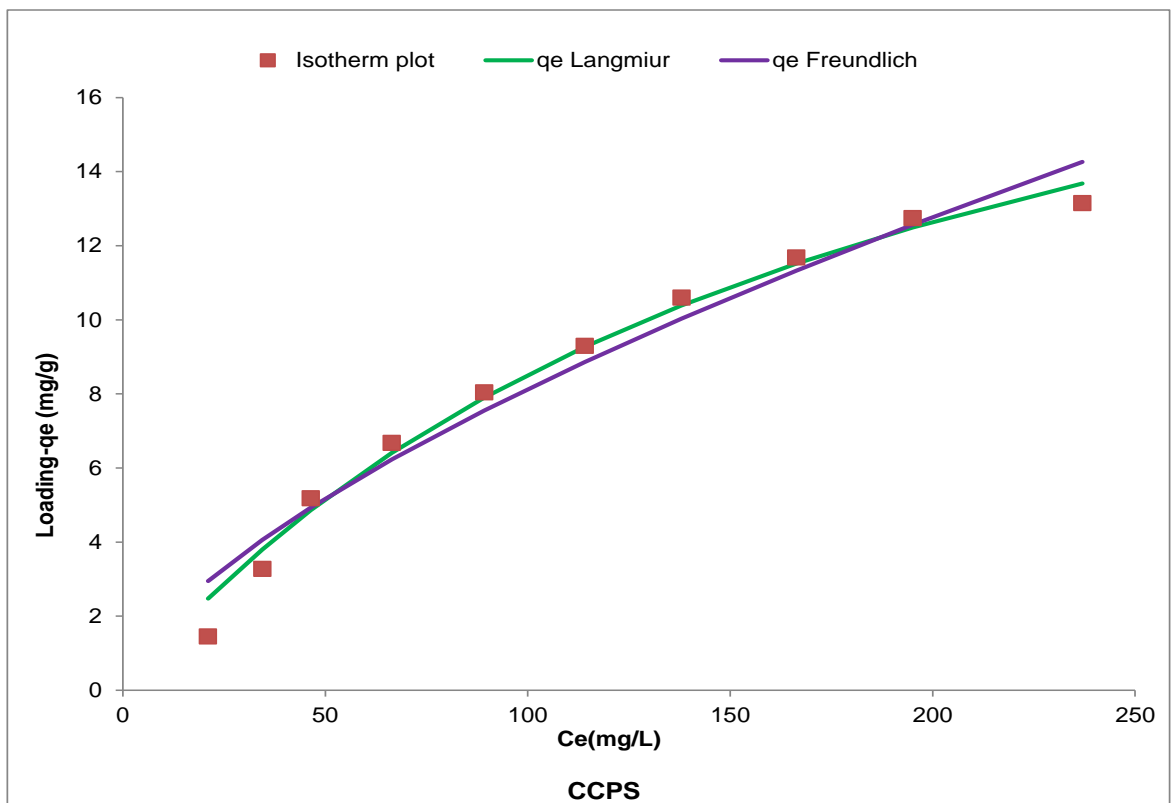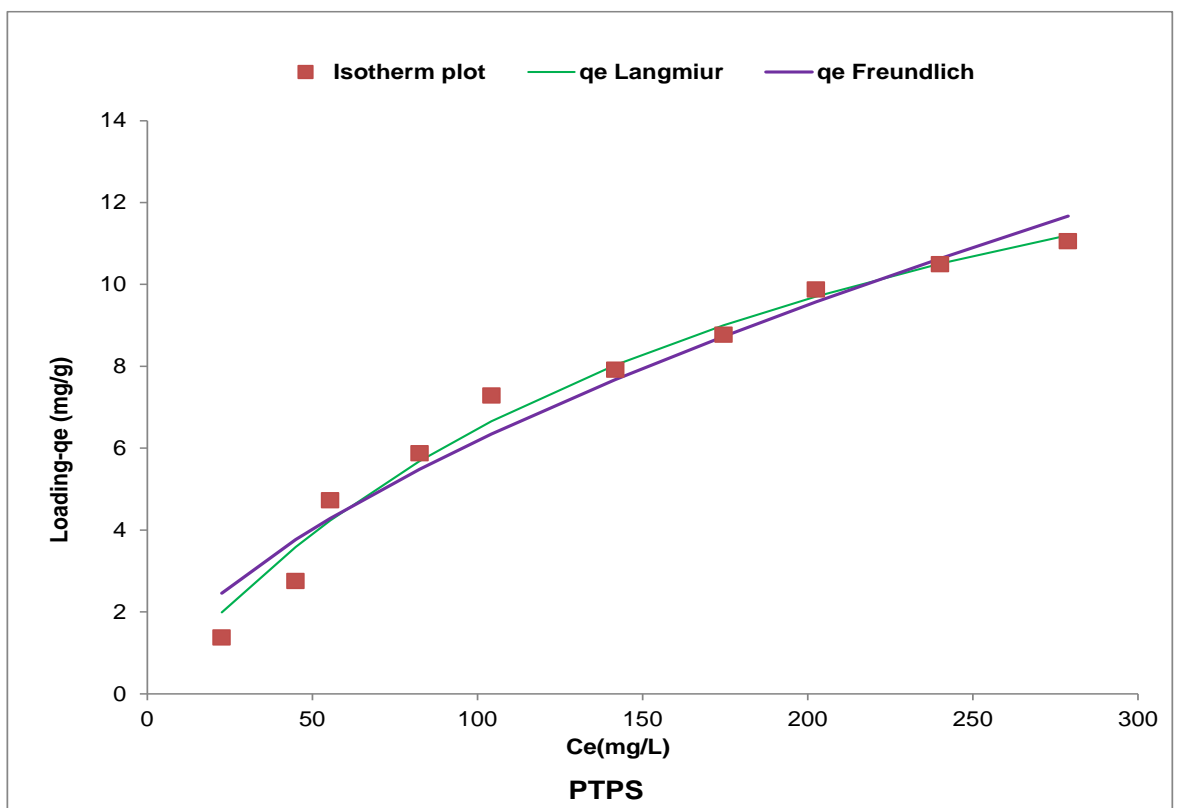

Figure 5.52: Isotherm plot for Cd(II) ion sorption for PTPS adsorbent

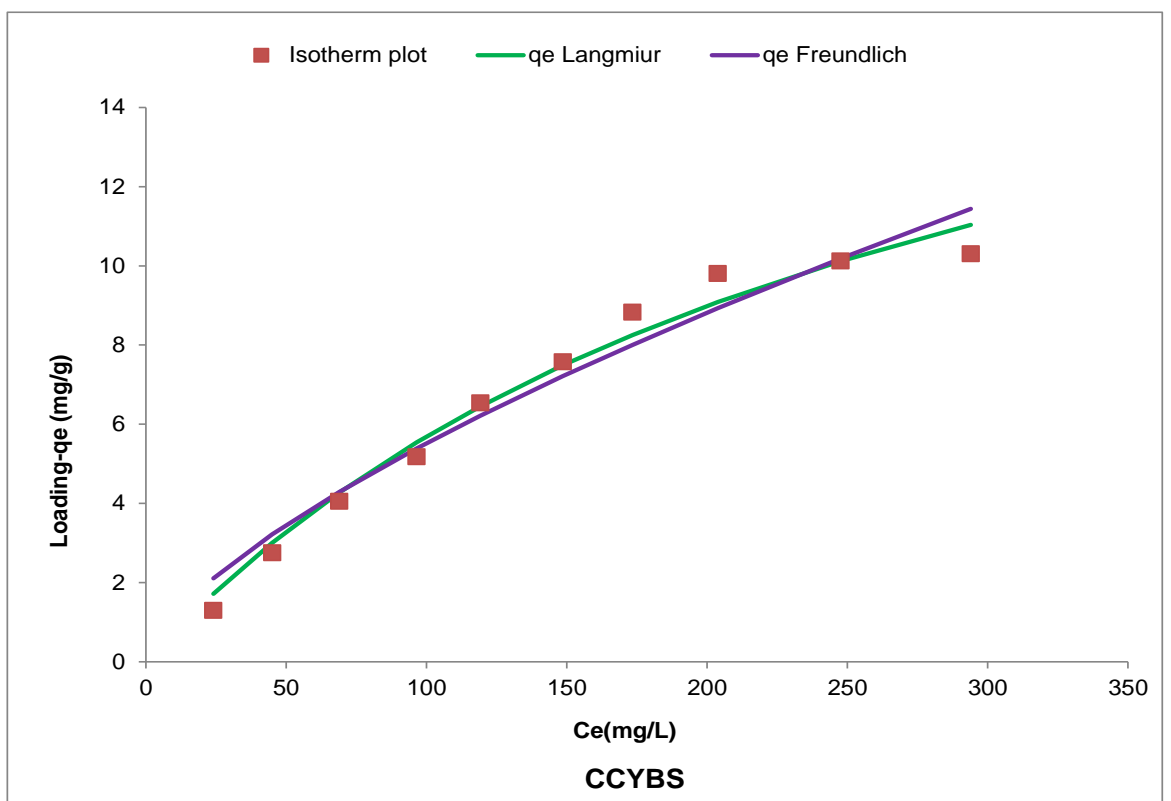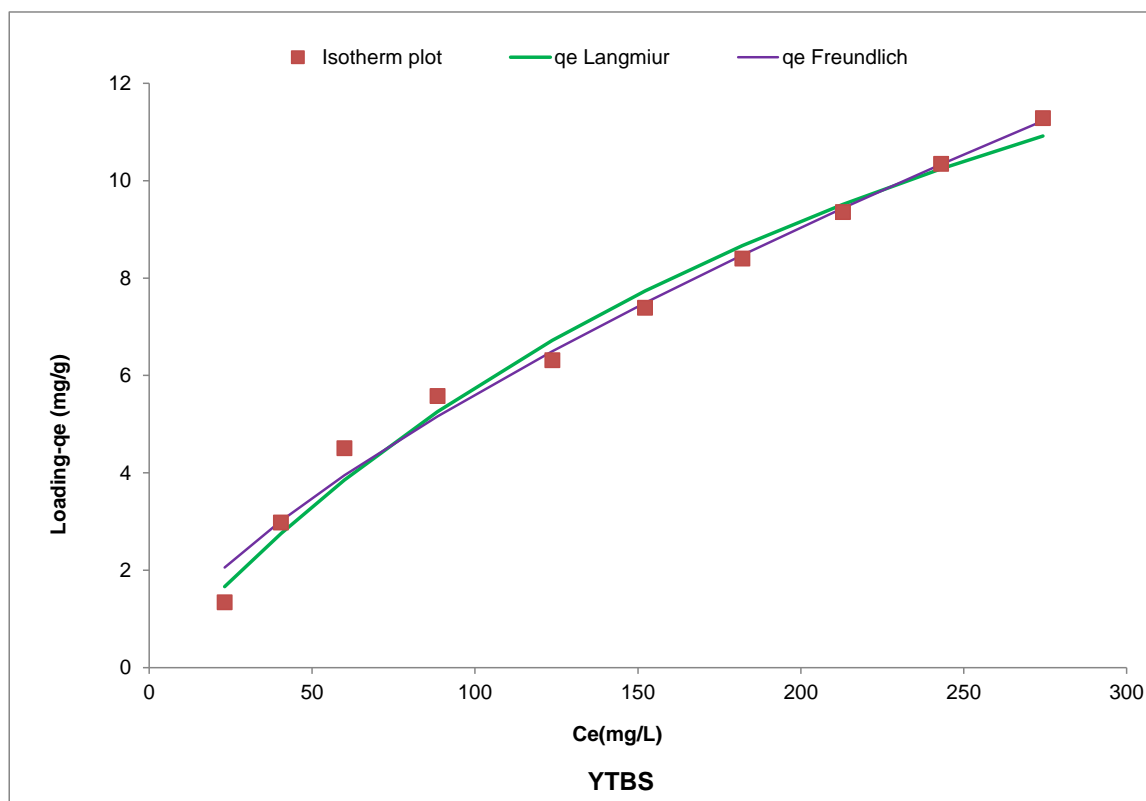Figure 5.53.: Isotherm plot for Cd(II) ion sorption for YTBS adsorbent

From an examination of the r^2 values for the Langmuir model of Cd(II) for the 7 residue adsorbents it can be inferred that the experimental data were quite in close agreement with the Langmuir isotherm model. The values of the coefficient of determination (r^2) ranged from 0.97 for PTHS to 0.99 for YTBS, CNFS, CCPS and OPFS adsorbents. The values obtained for the two error parameters {the root mean square error (RMSE) and Chi square ($\chi2$)} were in the range of $3.81.56 \times 10^{-2}$ (PTHS) to 1.66×10^{-2} (OPFS) for $\chi2$ and 1.84×10^{-1} (PTHS) to 7.57×10^{-2} (YTBS) for RMSE. An evaluation of the error parameters and r^2 values for the adsorbents indicates that the experimental data for Cd(II) sorption using the OPFS and YTBS adsorbents were better described by the Langmuir model as both had high r^2 values and low χ^2 and RMSE. Further comparison of the Langmuir isotherm parameters shows that the sorption of Cd(II) ions onto the surface of the YTBS adsorbent was best described by the Langmuir isotherm.

A number of natural biomasses have been evaluated as potential candidates for the removal of Cd(II) ions from aqueous systems using the Langmuir model. Sarada *et al.,* (2014) studied the uptake of Cd(II) from aqueous solution by a macro algae-*Caulerpa fastigiata* and the Langmuir constant parameter q_{max} reported in the study was 16.5 mgg[-1]. In a similar study Kumar *et al.,* 2012 investigated the removal of Cd(II) ions from aqueous solution using an agricultural waste (cashew nut shell). In their study the value of the

Langmuir constant (q_{max}) was 22.1mgg^{-1}. Research into the use of Prunus Avium leaves for the biosorption of Cd(II) from aqueous solution has also been reported and in the study the q_{max} value obtained from the Langmuir isotherm modelling was 45.5mgg^{-1}(Salem *et al.,* 2012). Furthermore, in the equilibrium studies on the sorption of Cd(II) by Rape Straw, the obtained Langmuir constant was 17.5mgg^{-1}(Gong, 2013). The Cd (II) ion values of the maximum monolayer loading capacity q_{max} for the adsorbents in this study were further compared to those of some adsorbents in literature as seen in Table 5.13. From the Table 5.13, it is observed that the adsorbents in this study had q_{max} values that were higher and comparable to those reported in literature, thereby indicating that the agricultural residue adsorbents were similar to those used in previous studies and can be used as representative biomass for Cd(II) ion sorption.

Table 5.13: Langmuir constant (q_{max}) with those reported in literature for Cd(II) ion sorption

Adsorbent	q_{max}(mgg^{-1})	Reference
Rice husk	16.7	Krishnani *et al.*, 2008
Rape straw	17.5	Gong, 2013
Moss (*Hylocomium Splendens*)	32.5	Sari *et al.*, 2008
Spirodela polyrhiza (L) biomass	36.0	Meitei and Prasad, 2013
Cactus(*Opundiaficus indica*) cladodes	30.4	Barka *et al.*, 2013
Rice husk	21.3	Kumar *et al.*, 2010
Caulerapa fastigiata	16.5	Sarada *et a*l., 2014
Teak leaf powder	29.9	Rao *et al.,* 2010
Cashew nut shell	22.1	Kumar *et al.*, 2012
Tea waste	15.0	Wan *et al.*, 2014
Prunus Avium leaves	45.5	Salem *et al.*, 2012
Olive stone waste	6.9	Fiol *et al.*, 2006
Cashew nut shell	11.2	Coelho *et al.*, 2014
Eucalyptus bark	20.7	Ghodbane *et al*, 2008
Wheat bran	15.9	Nouri *et al.*, 2007
CCPS	24.5	This study
YTBS	22.4	This study
CNFS	21.6	This study
CCYBS	21.4	This study
PTPS	18.9	This study
OPFS	17.6	This study
PTHS	16.0	This study

5.14.1.2 Freundlich Isotherm

The Freundlich isotherm model differs from the Langmuir model because it assumes a heterogeneous adsorption surface with active sites with different energy thereby implying a multilayer surface coverage whereas the Langmuir model assumes a homogenous surface with monolayer coverage. The Freundlich isotherm plots for the 7 residue adsorbents are shown in Figures 5.47 − 5.53. From these plots, the isotherm constants, the error parameters of root mean square error (RMSE), Chi square (χ^2) and the of determination (r^2) of each adsorbent for Cd(II) sorption were obtained and presented in Table 5.12. The values obtained for the r^2 indicate a close proximity of the model with the experimental data even though the data obtained for the Langmuir model were better. However, the r^2 values were still an indication of a good fit with experimental values ranging from 0.91 for PTHS to 0.99 for CNFS and YTBS adsorbents implying that the Freundlich model described the sorption of Cd(II) for these two residue adsorbents better than the other five. To further discriminate the adsorbent that the Freundlich best fitted, the data obtained for the two error parameters {the root mean square error (RMSE) and Chi square (χ^2)} shown in Table 5.12 were used. From the results in Table 5.12, it is observed that the values of 6.56×10^{-2} (RMSE) and 1.55×10^{-2} (χ^2) obtained for these two error parameters for the YTBS adsorbent were lower than those for the CNFS adsorbent, thus implying that the Freundlich model best described the sorption of the Cd(II) ion onto the YTBS adsorbent. The value of the Freundlich isotherm constant "n" which describes the adsorption intensity of the adsorbents also shown in Table 5.12 indicates that the adsorption of Cd(II) ions by the 7 adsorbents were favourable. The "n" values were 1.86 (OPFS), 1.86 (CNFS), 1.54 (CCPS), 1.48 (CCYBS), 2.00 (PTHS), 1.61 (PTPS) and 1.46 (YTBS) and according to Sarada *et al*., (2014), Freundlich isotherm constant "n" values between 1 and 10 indicates that the adsorption intensity is favourable and this parameter is presumed to give an indication of the heterogeneity of the adsorbent and it has been reported to vary with the heterogeneity of the adsorbent material (Sari *et al*., 2008).

Furthermore, the value of the Freundlich constant "K_F" which relates to the adsorption capacity for a multilayer system is also presented in Table 5.12 for the 7 adsorbents. This parameter also gives indication on the degree of Cd(II) ion affinity and mobility to adsorbents (Ammari *et al.,* 2015), hence can be used to compare the adsorption performance of the 7 different residue adsorbents. The values of K_F range from 0.24 (mgg^{-1})(Lmg^{-1})$^{1/n}$ for YTBS which was the least to 0.91(mgg^{-1})(Lmg^{-1})$^{1/n}$ ^{1} for CNFS which was the highest. The trend in K_F value for the residue adsorbents was CNFS > PTHS > OPFS >

CCPS > PTPS > CCYBS > YTBS. A number studies have also been carried out for some sorption of Cd(II) onto some lignocellulosic adsorbents and the values for the Freundlich constant (K_F) reported. These include: $1.07(mgg^{-1})(Lmg^{-1})^{1/n}$ obtained for Cd (II) sorption using teak leaf powder (Rao *et al.,* 2010a), $0.93mgg^{-1}$ for Cd(II) sorption onto sugar cane bagasse adsorbent (Garg *et al.,*2008); $(mgg^{-1})(Lmg^{-1})^{1/n}$ for Cd(II) removal from aqueous solution using cashew nut shell adsorbent (Kumar *et al.,*2012) and $0.24(mgg^{-1})(Lmg^{-1})^{1/n}$ obtained for the sorption Cd(II) onto coconut (*Cocos nucifera L.*) shell adsorbent (Okafor *et al.,*2012). Further comparisons of the Freundlich constant (K_F) values obtained in this study with those reported in literature for some lignocellulosic adsorbents are shown in Table 5.14.

Table 5.14: Comparison of Freundlich constant (K_F) with reported literature for Cd(II) ion sorption.

Adsorbent	$K_F((mgg^{-1})(Lmg^{-1})^{1/n})$	Reference
Teak leaf powder	1.07	Rao *et al.*, 2010a
Sugar cane bagasse	0.93	Garg *et al*, 2008
Cashew nut shell	1.74	Kumar *et al.*, 2012
Unmodified sugarcane bagasse	0.37	Isa *et al.*, 2010
Unmodified coconut coir	0.80	Isa *et al.*, 2010
Corncob	0.14	Ali *et al.*, 2013
Palm karab	0.20	Ali *et al.*, 2013
Caulerpa *fastigiata*	1.08	Sarada *et al.*, 2014
Hylocomium splendens biomass	1.20	Sari *et al.*, 2008
Coconut (*Cocos nucifera L.*) shell	0.24	Okafor *et al.*, 2012
Zea maize leaves	0.28	Nadeem, 2013
CNFS	0.91	This study
PTHS	0.75	This study
OPFS	0.63	This study
CCPS	0.41	This study
PTPS	0.36	This study
CCYBS	0.25	This study
YTBS	0.24	This study

From Table 5.14 it can be observed that the value of K_F obtained in this study for the 7 residue adsorbents are comparable with results obtained in literature for metal ion sorption using biomass adsorbents. This implies that the lignocellulosic materials used for metal ion

adsorption studies in this work can be representative of the characteristic biomass applied for adsorption based on its location and availability. It also indicates that these results are also similar to other lignocellulosic materials that have been previously studied.

Furthermore, from Table 5.12 a comparison of the two models can be made based on the value of their respective error parameters. It is observed that the high r^2 values and low root mean square error (RMSE) and Chi square (χ^2) values for the two isotherm models implies that both can be used to described the sorption of Cd(II)ions onto all the residue adsorbents. However, the Langmuir model was a better fit as the r^2 values for the different residue adsorbents were higher than those of the Freundlich, while the RMSE and Chi square (χ^2) values were lower than those of the Freundlich model.

5.14.2 Lead isotherm modelling

Equilibrium sorption studies for Pb(II) ion removal from aqueous solutions using the OPFS, CNFS, CCPS, CCYBS, PTHS, PTPS and YTBS adsorbents was also carried out using initial metal ion concentrations of 50 – 500 mgL^{-1} with step size of 50. The non-linear isotherm plots obtained for the Langmuir and Freundlich isotherms are shown in Figures 5.54 – 5.60 for Pb(II) ion sorption. From these plots, the isotherm constants, the error parameters of root mean square error (RMSE), Chi square (χ^2) and the coefficient of determination (r^2) of each adsorbent for Cd(II) sorption were obtained and presented in Table 5.15. The figures indicate a concentration dependent relationship for the removal of Pb(II) ion for all the adsorbents as the loading of the metal ion increases as the initial Pb(II) ion concentration increases from 50 to 500mgL^{-1}.

5.14.2.1 Langmuir isotherm

The equilibrium metal ion sorption data obtained for the different initial Pb(II) ion concentrations was evaluated with the Langmuir isotherm model for the 7 agricultural residue adsorptions as shown in Figures 5.54 – 5.60 using the non-linear optimization method previously described. From these plots, the Langmuir isotherm constants q_{max} and K_L were obtained. The error parameters of root mean square error (RMSE), Chi square (χ^2) and the coefficient of determination (r^2) values obtained from the isotherm modelling are also presented in Table 5.15. Figures 5.54 – 5.60 and the results presented in Table 5.15 indicates that the Langmuir model gave a good approximation and fit to the experimental equilibrium sorption data based on the values of RMSE, Chi square (χ^2) and r^2 for each of the seven adsorbents and it can thus be inferred that the monolayer approach to the surface

loading of the Pb(II) ions onto the adsorbents based on the Langmuir isotherm is applied in this instance (Athar *et al.,* 2013).

The Langmuir constant K_L values obtained for the adsorbents is also presented in Table 5.15 and the values of K_L ranged from 1.859×10^{-3} (Lmg^{-1}) for CCYBS to 8.961×10^{-3} (Lmg^{-1}) for OPFS adsorbents. The Langmuir constant K_L is related to the free energy of adsorption (Sari *et al.,* 2008) and these K_L values indicate the affinity of the Pb(II) metal ion to the adsorbent surface. Since the Langmuir model is based on the assumption that the binding of the adsorbate onto the surface of the adsorbent occurs primarily through a interactions where all the sites have equal affinity for the metal ion (Cechinel *et al.*, 2014), the affinity of Pb(II) ion to the adsorbents can be expressed based on the K_L values.

The fundamental constant of the Langmuir model is the q_{max} which indicates an equilibrium saturation point of an adsorbent beyond which the adsorbent surface cannot adsorb any further adsorbate (Foo and Hameed, 2010). From the Langmuir isotherm plots in Figures 5.54 − 5.60, the non-linear optimization procedure using the solver add-in protocol in Microsoft Excel was used to obtain the value of q_{max} for each of the resident adsorbents. These values are also presented in Table 5.15. From this table, it is observed that the value of q_{max} for Pb(II) sorption using the residue adsorbents follows the trend CCYBS > CCPS > PTPS > YTBS > CNFS > PTHS > OPFS. The maximum q_{max} value, 33.3mgg^{-1} was obtained for CCYBS while the least value, 15.1mgg^{-1} was obtained for the OPFS adsorbent.
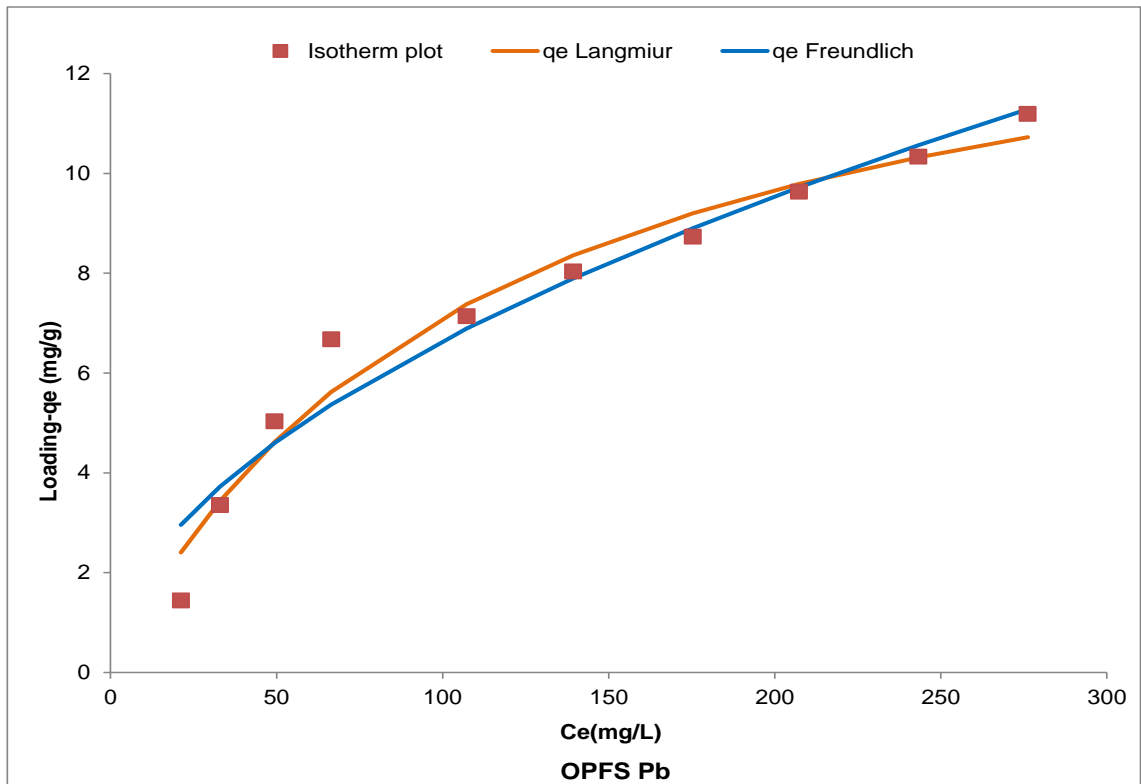
Figure 5.54: Isotherm plot for Pb(II) ion sorption for OPFS adsorbent
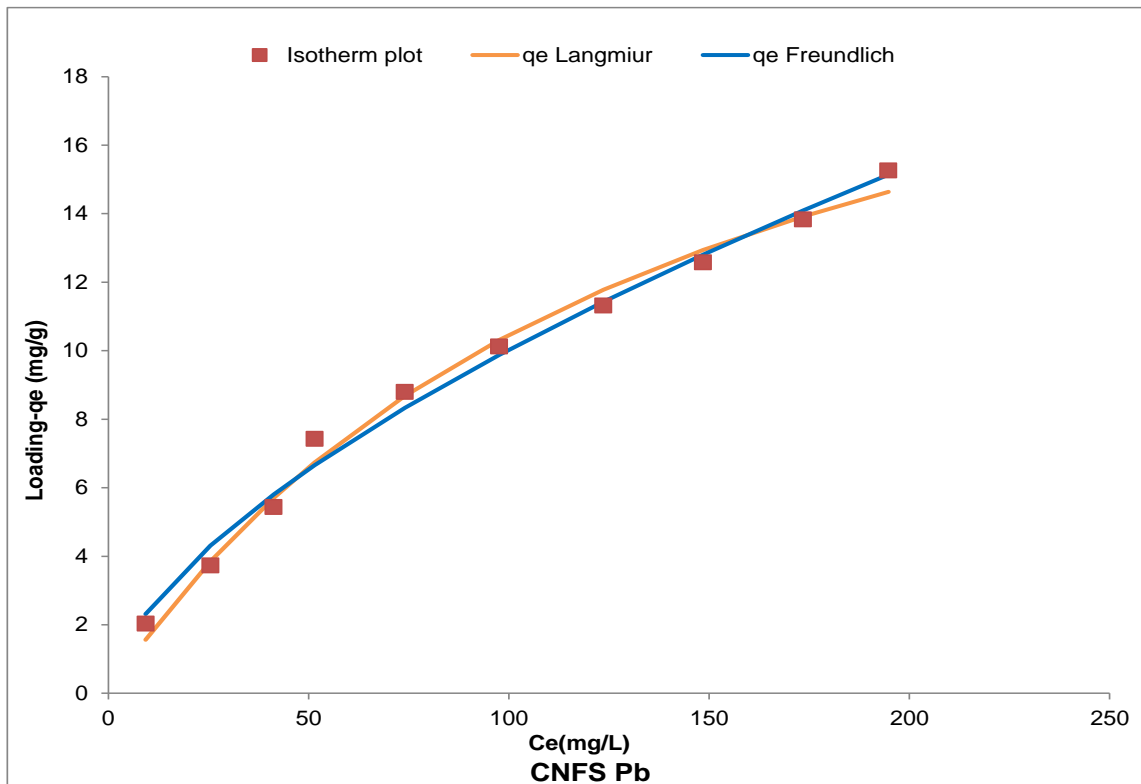
Figure 5.55: Isotherm plot for Pb(II) ion sorption for CNFS adsorbent
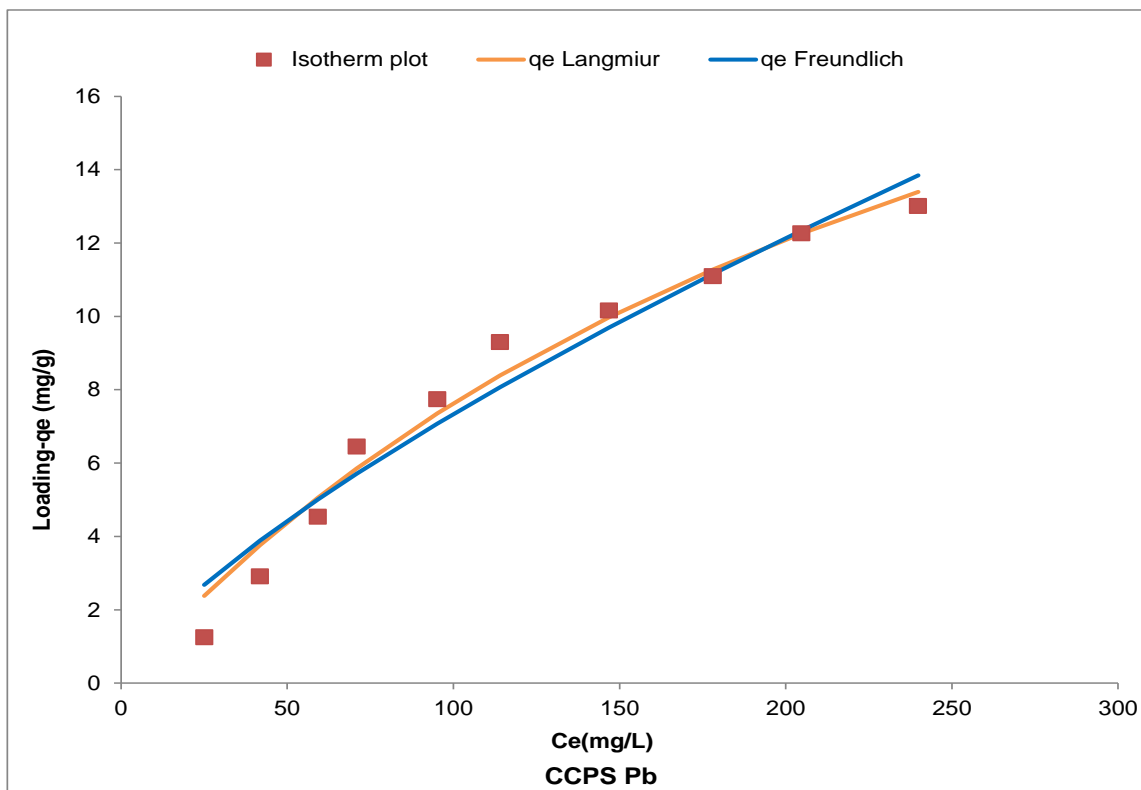
Figure 5.56: Isotherm plot for Pb(II) ion sorption for CCPS adsorbent
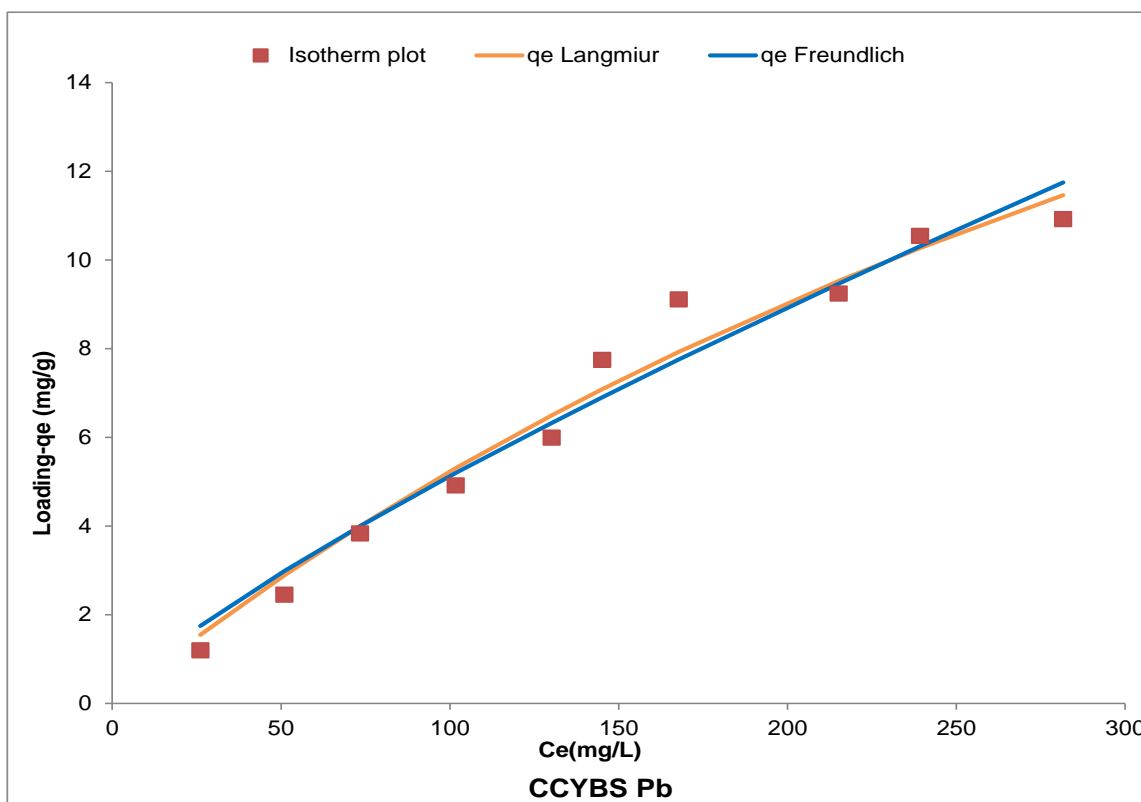
Figure 5.57: Isotherm plot for Pb(II) ion sorption for CCYBS adsorbent
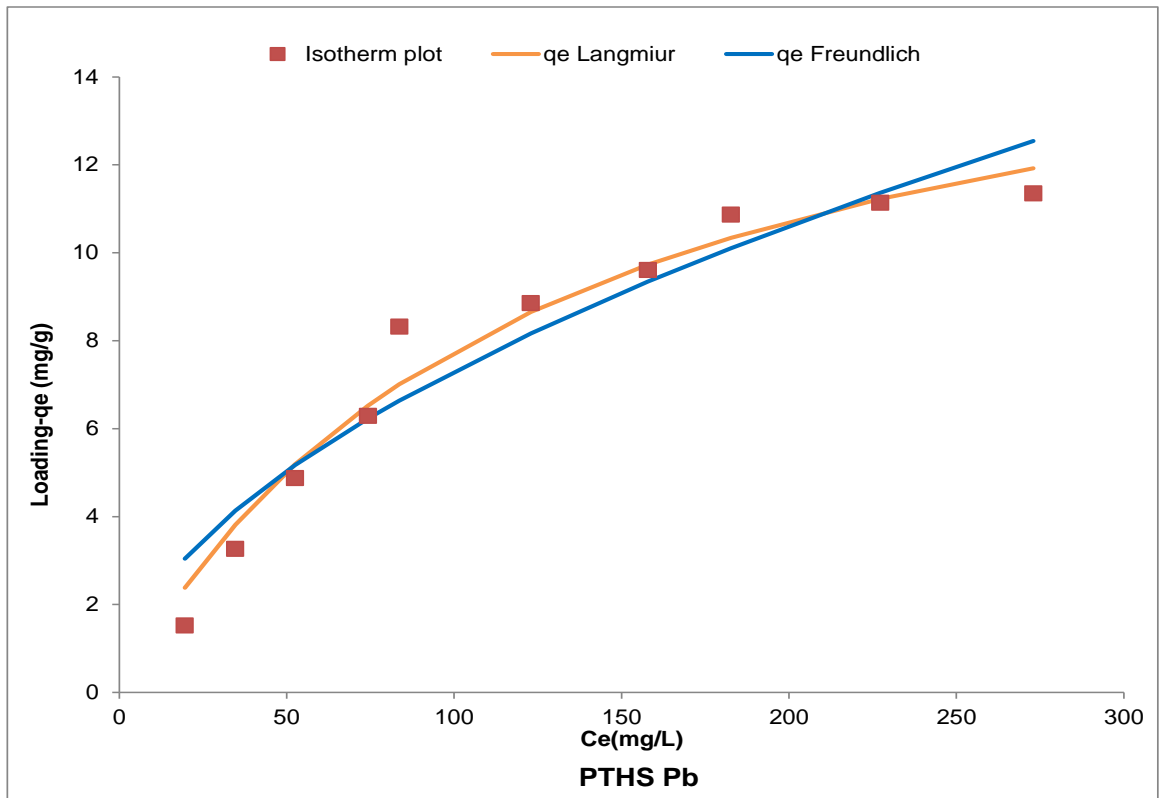
Figure 5.58: Isotherm plot for Pb(II) ion sorption for PTHS adsorbent
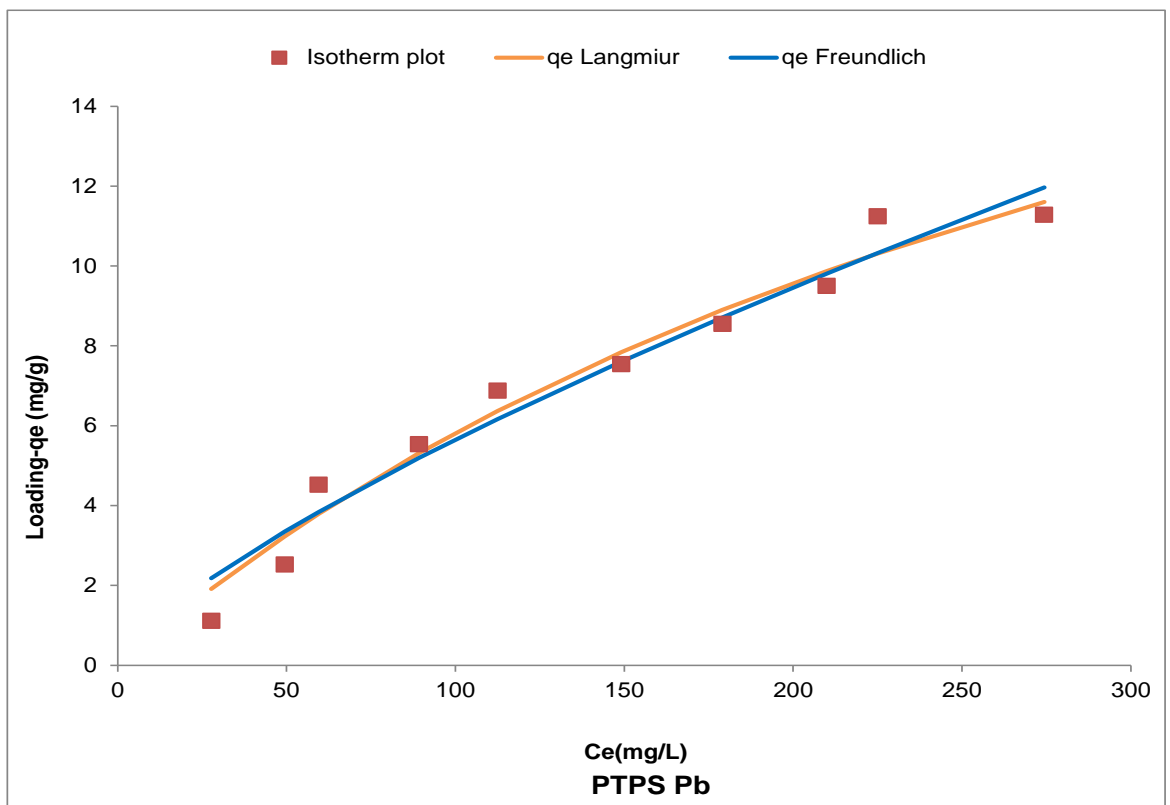
Figure 5.59: Isotherm plot for Pb(II) ion sorption for PTPS adsorbent

Table 5.15: Isotherm Parameters for Pb(II) ion adsorption on unmodified residues

Langmuir Model						Freundlich Model				
Adsorbent	$q_{max}(mgg^{-1})$	$K_L(Lmg^{-1})$	r^2	x^2	RMSE	$K_F(mgg^{-1})(Lmg^{-1})^{1/n}$	n	r^2	x^2	RMSE
OPFS	15.1	8.96E-03	0.97	3.96E-02	1.78E-01	0.60	1.92	0.95	6.28E-02	2.82E-01
CNFS	25.3	7.06E-03	0.99	1.75E-02	9.85E-02	0.58	1.62	0.99	1.73E-02	9.82E-02
CCPS	29.2	3.54E-03	0.97	4.79E-02	2.39E-01	0.26	1.38	0.95	8.40E-02	4.17E-01
CCYBS	33.3	1.86E-03	0.97	4.54E-02	1.89E-01	0.13	1.25	0.96	6.21E-02	2.58E-01
PTHS	17.3	8.19E-03	0.96	4.63E-02	2.22E-01	0.62	1.86	0.91	1.11E-01	5.35E-01
PTPS	27.0	2.74E-03	0.97	4.77E-02	2.06E-01	0.19	1.34	0.96	6.25E-02	2.71E-01
YTBS	25.7	2.49E-03	0.96	5.99E-02	2.39E-01	0.18	1.38	0.96	5.01E-02	2.02E-01
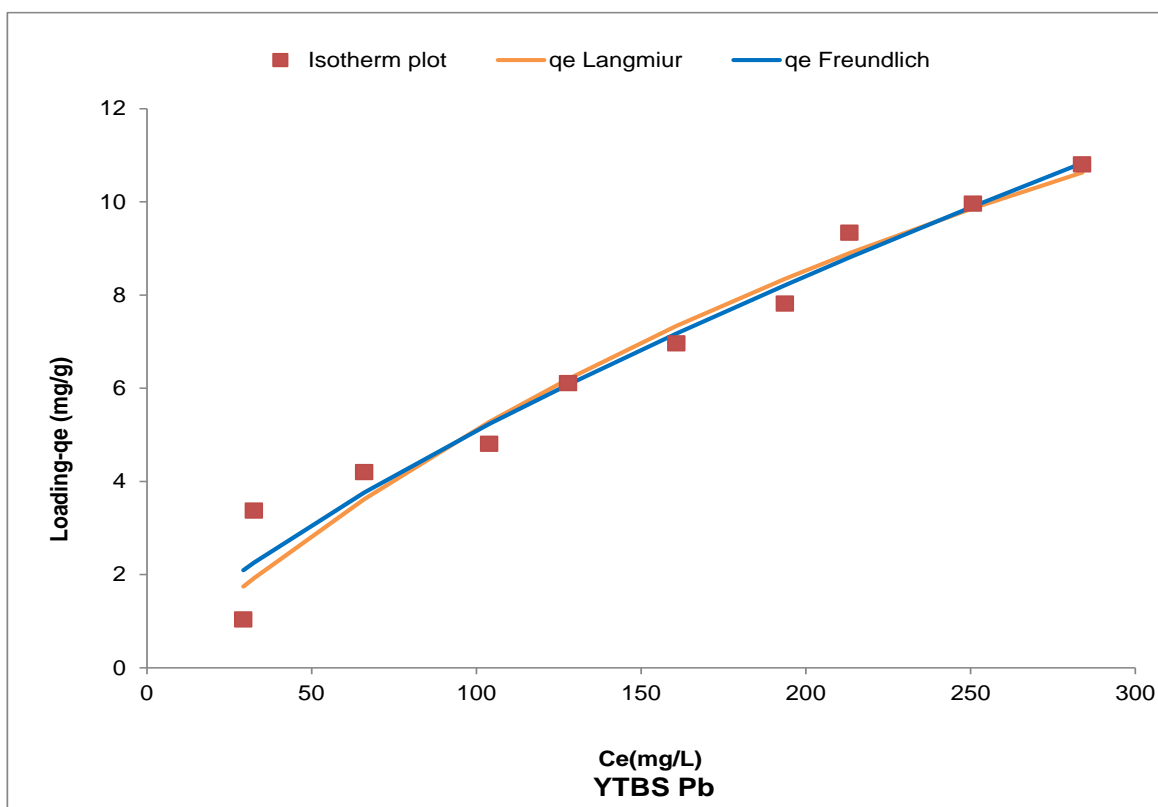
Figure 5.60: Isotherm plot for Pb(II) ion sorption for YTBS adsorbent

The values of RMSE, Chi square (χ^2) and r^2 for each of the seven adsorbents can also be used to characterise the fitting of the Langmuir isotherm to the experimental equilibrium sorption data for the different adsorbents. Examination of the values for these error parameters in Table 5.13 indicates that the Langmuir model gives the best description for Pb(II) ion sorption for the CNFS adsorbent. This is because this adsorbent has the highest r^2 value of 0.99 and the least values for the two error parameters RMSE (9.85×10^{-2}) and Chi square (1.75×10^{-2}).

The maximum monolayer loading capacity based on the Langmuir isotherm model for the 7 residue adsorbents obtained in this study were compared with q_{max} values reported in literature for some biomass residues as shown in Table 5.16. From this table, it can be observed that the residue adsorbents prepared in this study had q_{max} values that were comparable and in some instances better than those reported in literature. This therefore indicates that these adsorbents would be useful for Pb(II) ion removal from aqueous solutions.

Table 5.16: Comparison of Langmuir constant (q_{max}) with reported literature for Pb(II) ion

Adsorbent	$q_{max}(mgg^{-1})$	Reference
Modified lignin from oil palm	20.0	Ibrahim *et al.*, 2010
Trifolium resupinatum	10.4	Athar *et al.*, 2013
Pomegranate peel	13.9	El-Ashtoukhy *et al.*, 2008
Meranti sawdust	32.1	Rafatullah *et al.*, 2009
Rice husk	6.39	Kafia and Surchi, 2011
Sunflower husk	6.29	Kafia and Surchi, 2011
Sesame husk	6.93	Kafia and Surchi, 2011
Chalf	6.85	Kafia and Surchi, 2011
Saraca indica leaf	3.23	Goyal *et al.*, 2008
Olive stone waste	4.47	Fiol *et al.*, 2006
Olive tree pruning waste	22.8	Blazquez *et al.*, 2011
Cashew nut waste	26.7	Coelho *et al.*, 2014
Heartwood of Areca Catechu powder	11.7	Chakravarty *et al.,* 2010
CCYBS	33.3	This study
CCPS	27.2	This study
PTPS	27.0	This study
YTBS	25.7	This study
CNFS	25.3	This study
PTHS	17.3	This study
OPFS	15.1	This study

5.14.2.2 Freundlich isotherm

The Freundlich isotherm model was also used to characterize the equilibrium metal ion sorption data for Pb(II) removal using the OPFS, CNFS, CCPS, CCYBS, PTHS, PTHS, PTPS and YTBS adsorbents. The Freundlich model applies to adsorption on heterogeneous surfaces with the interaction between adsorbates and adsorbent described based on multilayer surface interaction and active sites of different energies (Sari *et al.,* 2008). The Freundlich plot for the 7 adsorbents for Pb(II) sorption is shown in Figures 5.54 – 5.60 and the isotherm constant "K_F" and empirical parameter "n" as well as the error parameters of root mean square error (RMSE), Chi square (χ^2) and the coefficient of determination (r^2) values obtained from these plots using the non-linear optimization procedure are presented in Table 5.15. From the Table, it can be observed that the value of the coefficient of determination (r^2) for the 7 adsorbents for Pb(II) sorption were within the range 0.91 (PTHS) – 0.99 (CNFS) indicating a close association of the isotherm model with the

Freundlich model for Pb(II) ion even though the Langmuir isotherm gave a better fit and association with the experimental data than the Freundlich model. The RMSE and Chi square values of the Freundlich isotherm can be used to further characterise the degree of closeness of the model to the experimental data obtained for the different adsorbents. Therefore, a closer examination of the values of the error parameters in Table 5.15 indicates a similar trend observed for the fitting of the Langmuir isotherm, that is the Freundlich model best describes the sorption of Pb(II) ion onto the CNFS residue adsorbent. Thus, it can be observed from Table 5.15 that the CNFS adsorbent has the highest r^2 value of 0.99 and the least values for the two other error parameters RMSE (9.82 $\times 10^{-2}$) and Chi square (1.73×10^{-2}).

The Freundlich empirical parameter "n" relating to the adsorption intensity of the Pb (II) ion to the adsorbents obtained in Table 5.15 have values within the range 1.25 − 1.92 representing a favourable adsorption process as the "n" values lie between 1 and 10; which has been reported as the range for favourable adsorption as described by the Freundlich model (Naiya *et al*., 2009; Cruz-Olivares *et al*., 2011). The trend in the "n" values for the 7 adsorbents are OPFS > PTHS > CNFS > YTBS > CCPS > PTPS > CCYBS. In addition, the constants obtained in Table 5.15 also include the Freundlich constant "K_F" which relates to the adsorption capacity of the adsorbents for Pb (II) ion. The K_F values obtained from the non-linear approximation of the Freundlich model for the residue adsorbents are within the range 0.13 to 0.60 $(mgg^{-1})(Lmg^{-1})^{1/n}$ and the trend in these values for the adsorbent are OPFS > PTHS > CNFS > CCPS >PTPS > YTBS > CCYBS with the highest being 0.60 $(mgg^{-1})(Lmg^{-1})^{1/n}$ (OPFS) and the least was 0.13 $(mgg^{-1})(Lmg^{-1})^{1/n}$ (CCYBS).

A number of studies have been carried out on Pb(II) ion sorption using some biological materials and the value of the Freundlich constant (K_F) is similar to the present study. Pb(II) ion sorption from aqueous solution onto *Pimenta dioica* L. has been reported by Cruz-Olivares *et al.,* (2011). In their study the value obtained for K_F from the Freundlich isotherm modelling was $0.25(mgg^{-1})(Lmg^{-1})^{1/n}$. Modified lignin obtained from oil palm fruit bunches (EFB) has also been reported as an adsorbent for Pb(II) ion removal from aqueous solution and the Freundlich isotherm constant K_F value obtained was $1.80mgg^{-1}$ (Ibrahim *et al.,* 2010). The "K_F" values obtained in this study been further compared with data obtained from previous literature as presented in Table 5.17.

Table 5.17: Comparison of Freundlich Constant (K_F) with literature for Pb(II) ion sorption

Adsorbent	$K_F(mgg^{-1})(Lmg^{-1})^{1/n}$	Reference
Trifolium resupinatum	0.79	Athar *et al.,* 2013
Pimenta dioica L.	0.25	Cruz-Olivares *et al.,* 2011
Pomegranate peel	2.93	El-Ashtoukhy *et al.,* 2008
Olive stone waste	2.77	Fiol *et al.,* 2006
Modified lignin from oil palm fruit bunches	1.80	Ibrahim *et al.,* 2010
Meranti saw dust	1.50	Rafatullah *et al.,* 2010
Rice husk	1.20	Kafia and Surchi, 2011
Sesame husk	1.79	Kafia and Surchi, 2011
Sunflower husk	1.14	Kafia and Surchi, 2011
Chalf	1.12	Kafia and Surchi, 2011
Coconut (*cocos nucifera* L.) Shell	1.51	Okafor *et al.,* 2012
Saraca indica leaf	0.42	Goyal *et al.,* 2008
OPFS	0.60	This study
PTHS	0.62	This study
CNFS	0.58	This study
CCPS	0.26	This study
PTPS	0.18	This study
YTBS	0.18	This study
CCYBS	0.13	This study

The results indicates that the "K_F" values obtained from this study for the 7 adsorbents were lower than those reported in literature in Table 5.17 with only two of those values (0.252 and 0.42) $(mgg^{-1})(Lmg^{-1})^{1/n}$ comparable with the data in this study. These low values for the Freundlich isotherm constant for the residues used in this study necessitates the consideration of alternatives for improving the loading of these materials for Cd(II) and Pb(II) ions. These alternative processes are considered in the subsequent chapters of this study

5.15 Summary

Seven agricultural residues were characterised in this study to determine their physical and chemical properties to provide the basis of understanding their role in adsorption of two heavy metal ions – Cd(II) and Pb(II) from aqueous solutions. The residues had high ash content indicating a high amount of inorganic compounds but their sulphur and nitrogen content were low. Proximate and ultimate analysis carried out using TGA and CHNS analyser indicated that their carbon content was in the range of 38 – 48% with the OPFS residue having the highest and the CCPS residue with the least. The results from the fixed carbon content from the TGA also showed that the residues can be used for production of activated type adsorbents. Chemical analysis of the residues using XRF indicated that these residues were composed of elements such sodium, potassium, silicon, calcium and phosphorus with the potassium content as the highest in the CCPS and PTHS residues. These residues had poor mechanical strength when subjected to the attrition test with losses of 11-24%. The residues had low BET surface areas with the highest being $12.42 m^2 g^{-1}$ for the CNFS residue and the lowest was $0.50 m^2 g^{-1}$ obtained for the YTBS residue. The total pore volumes of the residues were low and their average pore dimensions were in the range of 10-32 nm indicating that they were mesoporous materials. The thermal degradation profiles of these residues were similar and depict the trend in lignocellulosic materials.

All residues had acidic pH and their pHpzc values were from 5.7 to 6.6, hence the pH of 6.5 was chosen for both metal ion sorption studies. The XRD diffraction studies of the residues showed that all residues were mainly amorphous with few crystalline cellulose and silica phases. The SEM imaging of the morphology of the residues showed rough and spongy microstructures with no obvious pore arrangement except for the CNFS residue. The chemical analysis using EDAX and elemental analysis indicated that these residues were mainly composed of carbon, oxygen with some inorganic content and this reflects on the high ash content observed previously. EDAX analysis of the residues after Cd(II) ion sorption confirmed the presence of the metal ion in the adsorbent matrix and this could be used to infer the participation of ion-exchange as one of the mechanisms of metal ion removal. Infrared spectroscopy of the residues confirmed the presence of functional groups such as hydroxyl, carboxyl and amine and phenolic which are the main active sites for adsorption using lignocellulosic residues. The effect of contact time, adsorbent dose and

adsorbate pH on the sorption of Cd(II) and Pb(II) were also studied using these residues and the results showed that the optimum time for sorption was 180 minutes and this was taken as the time for the subsequent adsorption studies. The results of the kinetics of Cd(II) and Pb(II) ion sorption indicated that for the unmodified residues, the highest uptake was observed for the OPFS adsorbent for Pb(II) ion ($12.5 mgg^{-1}$) and CNFS for Cd(II) ion ($16.3 mgg^{-1}$). Kinetic modelling of the sorption of Cd(II) and Pb(II) ions was also studied using the pseudo-first order (PFO) and pseudo-second order (PSO) equations. For Cd(II) ion sorption the PFO model was fitted the uptake using the residue adsorbents better than the PSO model, while for Pb(II) ion sorption both models did fit metal ion uptake for the residue adsorbents.

The characterization of the adsorption of Cd(II) and Pb(II) was also carried out using Langmuir and Freundlich isotherms for the seven adsorbents and the results of the modelling indicates that the values of the constants q_{max} and K_F for the adsorbents were comparable to values obtained in reported literature. The Langmuir isotherm constant q_{max} values for Cd(II) ion sorption indicated that the CCPS adsorbent had the highest value ($24.5 mgg^{-1}$), while the PTHS adsorbent had the least ($16.0 mgg^{-1}$). For the Pb(II) ion sorption the OPFS adsorbent had the least maximum loading capacity ($15.1 mgg^{-1}$) while the CCYBS adsorbent had the highest loading capacity ($41.9 mgg^{-1}$). However, while these residue adsorbents showed considerable levels of metal ion loading, the time required for adsorption was considerable -1440minutes (72h). Hence, it was necessary to undertake some modification of these materials using chemical and thermal procedures to ascertain whether these modifications would improve the kinetics and loading of the metal ions as well as the physicals and chemical properties of the resulting adsorbents. These approaches are the subject of the next chapters in this work.

CHAPTER SIX

HYDROTHERMAL CARBONISED ADSORBENTS

CHAPTER SIX

6.0 Hydrothermal carbonised adsorbents

Hydrothermal carbonization (HTC) involves the heating of an aqueous dispersion of raw material in an autoclave at temperatures of $190 - 300^{\circ}C$ for about $2 - 24$ hours at saturated pressures to yield water soluble organics and a carbon rich, hydrophilic solid called "hydrochar" or "biochar" (Sevilla *et al*, 2011; Unur, 2013). The use of an aqueous media in the hydrothermal reaction set up provides a practical advantage in which it eliminates the costly and complicated drying steps normally used in pyrolysis and carbonization as well as expands the choice of raw materials that can be used. The mechanism of the hydrothermal process is dominated by dehydration and decarboxylation reactions which inherently are exothermic thereby making the process self-sufficient (Funke and Ziegler, 2010).

The final product of the hydrothermal carbonization reaction is often composed of a carbon rich material that contains oxygen functional groups such as hydroxyl, phenolic, carbonyl or carboxylic groups (Sun and Li, 2004; Hu *et al.*, 2010; Sevilla and Fuertes, 2009; Unur, 2013). The attractiveness of the ease of application and nature of resulting products has made hydrothermal carbonization an interesting route in the synthesis of carbon based materials for applications such as energy storage, catalyst, soil enrichment materials and catalyst supports (Titirici *et al*., 2007a; Titirici *et al*., 2007b). The hydrothermal carbonization of the agricultural residue adsorbents described in Chapter 5 of this study was carried out to produce adsorbents for removal of Cd(II) and Pb(II) ions from aqueous solutions. The methodology of the hydrothermal carbonization is described in Section 4.2.5 of this work. Two temperature regimes were chosen for the hydrothermal carbonization process: $170^{\circ}C$ and $200^{\circ}C$. The former was chosen as the lower temperature to examine the possibility of preparing effective carbon based adsorbents as reported by Busch *et al.,* (2013) and Parshetti *et al.,*(2013), while the latter was chosen as the upper temperature because it has been reported in literature for a number of hydrothermal carbonization treatments of biomass materials with substantial degradation of cellulose (Xu *et al*., 2013). According to Funke and Ziegler (2010), substantial hydrolysis for hydrothermal treatment of biomass starts at $180^{\circ}C$ and the hydrothermal carbonization process is reported as most

"severe" at temperatures between 180 – 250°C. Titirici *et al.*, (2015b) also reports on the hydrothermal carbonization of biomass with the maximum yield for the biomass obtained at 200°C. The two sets of hydrothermally carbonized adsorbents (HTC200 and HTC170) obtained from the process described above using the seven different agricultural residues were characterized as described in Section 4.3 of this work and their nomenclature is presented in Table 6.1.

Table 6.1: Nomenclature of hydrothermal carbonised adsorbents

Sample and Treatment	Nomenclature
Hydrothermally carbonised residue-170 °C (HTC-170)	
Hydrothermally carbonised oil palm fruit fibre residue	OPFS-HTC 170
Hydrothermally carbonised cocoa pod residue	CCPS-HTC 170
Hydrothermally carbonised coconut shell fibre residue	CNFS-HTC 170
Hydrothermally carbonised plantain peel residue	PTHS-HTC 170
Hydrothermally carbonised cocoyam peel residue	CCYBS-HTC 170
Hydrothermally carbonised sweet potato peel residue	PTPS-HTC 170
Hydrothermally carbonised white yam peel residue	YTBS-HTC 170
Hydrothermally carbonised residue- 200 °C (HTC 200)	
Hydrothermally carbonised oil palm fruit fibre residue	OPFS-HTC 200
Hydrothermally carbonised cocoa pod residue	CCPS-HTC 200
Hydrothermally carbonised coconut shell fibre residue	CNFS-HTC 200
Hydrothermally carbonised plantain peel residue	PTHS-HTC 200
Hydrothermally carbonised cocoyam peel residue	CCYBS-HTC 200
Hydrothermally carbonised sweet potato peel residue	PTPS-HTC 200
Hydrothermally carbonised white yam peel residue	YTBS-HTC 200

This characterization included the determination of the ash content, loss on attrition, adsorbent yield, surface morphology of adsorbents, chemical composition, surface area and porosity. Adsorption studies were also carried out using these two sets of hydrothermal carbonized adsorbents to determine the effect of contact time on the removal of Cd(II) and Pb(II) ions from aqueous solutions. This was aimed at comparing the effect of the hydrothermal treatment on the effectiveness of the adsorbents compared to the raw residue adsorbents.

6.1 Characterisation – ash content, loss on attrition and yield

The hydrothermal carbonization treatment was used to convert the agricultural residue adsorbent into carbon rich hydrothermal adsorbents. The effectiveness of this transformative process can be measured based on the residual product obtained. One characteristic of this process is the yield of hydrothermal carbonization which gives a means of comparing the amount of carbon and inorganic components that is converted into the adsorbent. The yield of the hydrothermal carbonised adsorbents for each agricultural residue adsorbent was computed based on eqn. (4.1) and the results for HTC170 adsorbents (adsorbents from hydrothermal carbonization at 170°C) and HTC200 (adsorbents from hydrothermal carbonization at 200°C) are presented in Tables 6.2 and 6.3 respectively.

Table 6.2: Ash content, loss on attrition and yield of hydrothermal carbonised (HTC170) adsorbents

Adsorbent	Ash [e] (%)	Loss on Attrition (%)	Yield (%)
OPFS-HTC 170	9.7	37.5	69.4
	±0.053	±1.97	±5.43
CNFS-HTC 170	7.4	29.25	63.8
	±0.280	±0.166	±1.41
CCPS-HTC 170	8.6	21.75	67.7
	±0.034	±2.18	±2.65
CCYBS-HTC 170	7.2	19.95	59.78
	±0.091	±1.48	±2.13
PTHS-HTC 170	8.8	29.7	68.6
	±0.038	±1.41	±3.63
PTPS-HTC 170	8.3	25.4	60.2
	±0.056	±2.17	±3.76
YTBS-HTC 170	7.9	26.2	66.1
	±0.049	±1.23	±2.49

[e] Ash content using AOAC(2000)

From the two Tables, it can be observed that the yields of the hydrothermal adsorbents were in the range of PS-HTC 50 – 70% with the highest yield of 70% obtained for the PTHS-HTC200 adsorbents while the least was for the PTPS-HTC200 adsorbent. The trend in yield for the HTC170 adsorbents was OPFS-HTC170 > PTHS-HTC170 > CCPS-

HTC170 > YTBS-HTC170 > CNFS-HTC170 > PTPS-HTC170 > CCYBS-HTC170 while that of the HTC200 adsorbents was PTHS-HTC200 > CCPS-HTC200 > OPFS-HTC200 > YTBS-HTC200 > CNFS-HTC270 > CCYBS-HTC200 > PTPS-HTC200. It can be deduced from these results that the temperature of hydrothermal carbonization did not affect the yield of the two sets of adsorbents significantly as the values obtained for both sets of adsorbents were similar.

Table 6.3: Ash content, loss on attrition and yield of hydrothermal carbonised (HTC-200) adsorbents

Adsorbent	Ash [e] (%)	Loss on Attrition (%)	Yield (%)
OPFS-HTC 200	8.3.	27.5	64.8
	±0.0533	±2.67	±5.93
CNFS-HTC 200	7.2	25.25	61.4
	±0.280	±0.77	±1.81
CCPS-HTC 200	8.2	20.75	69.2
	±0.034	±2.23	±2.65
CCYBS-HTC 200	7.00	20.795	60.78
	±0.0291	±1.67	±2.03
PTHS-HTC 200	8..6	34.87	70.876
	±0.0038	±1.56	±3.23
PTPS-HTC 200	8.33	26.94	56.82
	±0.065	±2.79	±3.56
YTBS-HTC 200	7.59	26.4	63.61
	±0.0149	±1.53	±2.29

[e] Ash content using AOAC(2000)

The high yields of this process can be associated with the absence of any chemical reagent in the process as these are known to result in more decomposition processes. Also, the temperature window in which the hydrothermal treatment was carried out was at the lower end of the scale for hydrothermal carbonization and this may have affected the extent of reactions such as hydrolysis, polymerization and condensation which are known to occur during hydrothermal carbonization. It has also been observed that HTC when carried out under mild conditions, maintain the functional groups present on the surface of the raw material in an effective way (Unur, 2013). This implies that during mild HTC, as those under which this experiment was carried out, the severity of the decomposition and dehydration reactions are reduced resulting in a higher carbon adsorbent yield. There are reports also, of a rapid decline in the yield of the biochar from hydrothermal carbonization

observed at temperature of $400^{\circ}C$ due to the loss of organic matter and non-condensable gases (CO_2, CO, H_2 and CH_4), with a steady yield at temperatures $> 400^{\circ}C$ (Ahmad *et al.*, 2014a). The high yield from hydrothermal carbonized adsorbents has also been reported by Uchimiya *et al.*, (2011) and this was from the hydrothermal carbonization of cottonseed hull at $200^{\circ}C$ with a resulting char yield of 83.4%. Parshetti *et al.*, (2013) reports on the chemical, structural and combustion characteristics of carbonaceous products obtained by hydrothermal carbonization of empty palm fruit bunches. In the study, higher yields of hydrochar was observed at lower temperatures with a 75% yield obtained for HTC at $150^{\circ}C$ while the yields of biochar at temperature of $250^{\circ}C$ and $350^{\circ}C$ were 62% and 49% respectively. Equally, the hydrothermal carbonization of the biomass *Spartina alterniflora* at $240^{\circ}C$ has been reported with a hydrochar yield of 32.48% (Xu *et al.*, 2014). Fernandez *et al.*, (2015) also reports a yield of 37% for HTC orange peels at $200^{\circ}C$. This implies that the nature of the precursor used for hydrothermal carbonization influences the yield of the resulting hydrochar or biochar in addition to the temperature of treatment (Falco *et al.*, 2013). This assumption holds true for the hydrothermal carbonized adsorbent synthesized in this study as their yields were varied even though hydrothermal carbonization was carried out at isothermal conditions for all residues.

Another characteristic of the hydrothermal carbonised adsorbents determined in this study was the ash content. This property gives an indication of the amount of inorganic species in the residue and hence the resulting hydrochar. The ash content for the sets of hydrothermal carbonized adsorbents (HTC170) and HTC200 are presented in Tables 6.2 and 6.3 respectively. The ash content of the HTC200 adsorbents were in the range of $7 - 8.7\%$ while that obtained for the HTC170 adsorbents was between $7.2 - 9.7\%$. The high ash content of the two sets of adsorbents can be associated with the nature of the residue used for the hydrothermal carbonization. The results of the ash content for the residue adsorbents discussed in Chapter 5 of this study indicates that the residues had high ash content within the range of $8.3 - 16.8\%$. These results obtained are also within the range of values obtained for the ash content of some crop residue reported in literature. Yuan *et al.*, (2011) reports that on conversion of some crop residues into biochar, the ash content of the crop residue subjected to thermal treatment at $300^{\circ}C$ were: Canola straw (10.7%), corn straw (30.1%), soybean straw (11.15%) and peanuts straw (20.1%). Meszaros *et al.*, (2007) also reports that the ash content of a char depends on that of the feedstock with different feedstock have varying inorganic composition that determine their ash content.

The resistance of an adsorbent material to the wear and attrition processes that occur when the particles come into contact was also measured for the HTC170 and HTC200 adsorbents based on the procedure described in Section 4.3.11. From the measurement, the percentage loss on attrition of the adsorbents was calculated based on Eqn. 4.4. The results obtained are presented in Table 6.2 and 6.3 for HTC170 and HTC200 respectively. The attrition process that exists on adsorbent interaction during agitation can either be due to particle fragmentation or surface abrasion (Wu *et al*., 2015) and the type seen in this study is due to abrasion as the generation of fines was observed during the filtration process. The results show that the HTC170 adsorbents had attrition losses within the range of 20 − 34% while that of the HTC200 adsorbent ranged from 19.9 − 37.5%. The attrition losses reported by Cordero *et al*., (2013) from granular chars obtained from grape seed are lower at 7.5% compared to that of both set of adsorbents used in this study. Nonetheless, the range of percentage loss on attrition obtained in this study are better than what is reported for some activated carbon adsorbents such as granular activated carbon from broiler manure at 83.9 − 97.1% and 76.2 − 96.3% (Lima and Marshall, 2005). The nature of attrition losses for the HTC adsorbents indicates that these materials had low mechanical strength and are not well suited for batch agitated vessels where mixing would result in abrasion. They would rather be well suited for column based application where mixing does not occur.

6.2 pH and zeta potential of hydrothermal adsorbents

Hydrothermal conversion processes for agricultural residue absorbents has been reported to have an influence on the degree of functional groups on an adsorbents surface. Hence, it is important that the pH of the adsorbent in solution be determined so that information on the characteristic of the surface can be obtained. The pH of the adsorbents in solution is also an important parameter that determines the solubility of metal ions in solution and the nature of the functional group species that exists on the surface of the adsorbent, in the aqueous phase as well as the degree of ionization of the ions in the solution (Nomanbhay and Palanisamy, 2005). The effect of pH of the adsorbent and the solution on the adsorption process can be studied using a plot of the zeta potential against the pH to determine the pH at which the charge on the surface is zero (pHpzc) (Gautam *et al*., 2014). This is an important parameter as it gives information on the pH that can be used for adsorption of cations and anions; due to the understanding of the regions within the pH window that is dominated with basic or acidic functional groups (Fernandez *et al*., 2015).

The pH and zeta potential of the different hydrothermal carbonized adsorbents (HTC170 and HTC200) were determined based on the protocol described in Section 4.3.9 and 4.3.3 respectively. The results obtained are presented in Table 6.4 and they indicate that for the HTC170 adsorbents, the distribution of acidic and basic adsorbent was in the ratio 4:3 with the OPFS-HTC170, CCYBS-HTC170, PTHS-HTC170 and YTBS-HTC170 adsorbents having an acidic nature with pH in the range of 6.2 – 6.78. The CNFS-HTC170, CCPS-HTC170 and PTPS-HTC170 were basic in nature with pH in the range 7.1 –7.15. However, for the HTC200 adsorbents, all the adsorbents were acidic with pH in the range of 6.45 – 6.79. Fernandez *et al*., (2015) in their study on the hydrothermal carbonization of orange peel biomass at 200°C describes the HTC adsorbents surface as acidic. This could be linked to the decomposition of hemicelluloses and pectins during hydrothermal carbonization at 200°C (Lynam *et al*., 2011; White *et al*., 2010). Fang *et al*., (2015) also reports a similar trend from the synthesis of hydrochars from plant derived biomass (peanut hull, hickory and sugar bagasse) at hydrothermal temperatures of 200, 250, and 300°C. The development of acidic hydrothermal adsorbents at 200°C occurred with pH of 4.0, 4.9 and 6.2 for sugar bagasse, hickory and peanut hull respectively. These trends reported in literature are similar with what has been observed in this study.

Table 6.4: pHpzc and pH of hydrothermal carbonised adsorbents

Adsorbent	pHpzc	Adsorbent pH	Adsorbent	pHpzc	Adsorbent pH
OPFS-HTC 200	7.7	6.78	OPFS-HTC 170	7.9	6.2
CNFS-HTC 200	7.35	6.78	CNFS-HTC 170	7.5	7.1
CCPS-HTC 200	7.3	6.79	CCPS-HTC 170	7.9	7.1
CCYBS-HTC 200	7.6	6.6	CCYBS-HTC 170	7.1	6.5
PTHS-HTC 200	7.67	6.45	PTHS-HTC 170	7.8	6.78
PTPS-HTC 200	7.3	6.5	PTPS-HTC 170	7.7	7.15
YTBS-HTC 200	7.4	6.7	YTBS-HTC 170	7.5	6.51

The zeta potential which is a function of the pH of each adsorbent was also determined in this study as described in Section 4.3.3. The zeta potential-pH plots for the hydrothermal carbonized adsorbents are shown in Appendix 3. From these Figures, the point of

inflection on the zeta potential plot was recorded as the point of zero charge of each adsorbent and presented in Table 6.4. From the Table, it is observed that both HTC170 and HTC200 adsorbents had pHpzc values that were higher than 7 indicating that the adsorbents had moderately more negative surface functional groups. The pHpzc of an adsorbent is a very important parameter that determines the pH at which the adsorbents surface has a net electrical neutrality thus when the solution pH is below the pHpzc, the surface of the adsorbent is positively charged and can be used to adsorb anions. When the solution pH is above the pHpzc, the surface of the adsorbents is negatively charged and can be used to absorb cations (Sardella *et al*., 2015). Furthermore, Table 6.3 shows that the value of the pHpzc for the HTC170 and HTC200 adsorbents decreased as temperature increased with exception of the CCYBS-HTC adsorbents where the reverse occurred. This decrease in the value of pHpzc with increase in the temperature of the thermal treatment for biochar obtained from crop residues has also been observed by Yuan *et al*., (2011). Based on the pHpzc values obtained, the pH at which adsorption was carried out for evaluation of the kinetics of Cd(II) and a Pb(II) metal ions was 7.

6.3 Surface area and porosity of hydrothermal adsorbents

The surface area and porosity of the adsorbents was determined using the procedure described in Section 4.3.4. For adsorption applications of material in areas such as wastewater treatment, the performance of the desired material is found to be dependent on its pore volume, pore size and surface area (Unur, 2013). These textual properties were also investigated for the adsorbents used in this Chapter. The hydrothermal carbonisation process (HTC170 and HTC200) was used to modify the residue adsorbents described in Chapter 5 of this study. The N_2 adsorption-desorption plot of the two sets of adsorbents are presented in Figures 6.1-6.2 and Figures 6.3-6.4 for the HTC170 and the HTC200 adsorbents respectively, The BET surface area, pore volume and pore size are presented in Tables 6.5 for HTC170 and 6.6 for the HTC200 adsorbents.

From tables 6.5 and 6.6, it is observed that for HTC170 adsorbents, the CNFS-HTC had the highest BET surface area of 75.54 $m^2\,g^{-1}$ and pore volume, while the CCYBS-HTC170 adsorbents had the lowest BET surface area of 13.0 $m^2\,g^{-1}$ and pore volume with the trend in surface area for the adsorbents being CNFS-HTC170 > OPFS-HTC170 > CCPS-HTC170 > YTBS-HTC170 > PTPS-HTC170 > PTHS-HTC170 > CCYBS-HTC170. The HTC200 adsorbents showed a significant increase in adsorbent surface area compared to

the HTC170 adsorbents and this may be due to the effect of increase in temperature on the residues. The trend was similar to the first three HTC170 adsorbents with BET surface areas of 260 m^2 g^{-1},64 m^{2}g^{-1} and 39 m^2 g^{-1} for CNFS-HTC200, OPFS-HTC 200 and CCPS-HTC200 respectively. The trends for the remaining four adsorbents were as follows: PTPS-HTC200 > CCYBS-HTC200 > PTHS-HTC200 > YTBS-HTC200 with the least BET of 26.83 m^2 g^{-1} obtained for the YTBS-HTC200 adsorbent.

Table 6.5: Surface area and porosity of hydrothermal carbonised adsorbents (HTC170)

Adsorbent	BET Surface Area (m^{2}g^{-1})	Total Pore Volume (cm^{3}g^{-1})	BJH Desorption Average Pore Diameter (nm)
OPFS-HTC 170	49	3.13E-02	5.49
CNFS-HTC 170	75	1.21E-01	7.7
CCPS-HTC 170	31	2.05E-02	6.71
CCYBS-HTC 170	13	9.40E-03	6.79
PTHS-HTC 170	16	5.05E-02	10.97
PTPS-HTC 170	18	2.85E-02	7.66
YTBS-HTC 170	20	1.39E-02	6.8

Table 6.6: Surface area and porosity of hydrothermal carbonised adsorbents (HTC200)

Adsorbent	BET Surface Area (m^{2}g^{-1})	Total Pore Volume (cm^{3}g^{-1})	BJH Desorption Average Pore Diameter (nm)
OPFS-HTC 200	64	7.70E-02	8.80
CNFS-HTC 200	260	1.75E-01	5.58
CCPS-HTC 200	39	2.94E-02	7.37
CCYBS-HTC 200	27	3.51E-02	12.09
PTHS-HTC 200	30	5.50E-02	8.27
PTPS-HTC 200	35	2.71E-02	7.67
YTBS-HTC 200	26	2.35E-02	9.61

The trend in the variation of BET surface area between the HTC170 and HTC200 adsorbents can be attributed to the increase in the removal of volatile organic compounds

from the residues as the temperature increases from 170 to 200°C (Gonzalez-Navarro *et al.*, 2014). On the other hand, the variation in the BETs surface area of the different hydrothermally carbonised adsorbents within each thermal modification regime (HTC170 and HTC200) may be associated to the nature of the different residues. The OPFS-HTC 170/200 and CNFS-HTC170/200 adsorbents are obtained from fibrous residues {oil palm fibre (OPFS) and coconut fibre (CNFS), while the CCPS-HTC170/200 adsorbents are from cocoa pod (CCPS) which has a stronger texture than the fibres. The remaining adsorbents- PTHS-HTC170/200; CCYBS-HTC170/200; PTPS-HTC170/200 and YTBS-HTC 170/200 are all based on precusors than are peels which have softer texture than the fibres and pod residues. These characteristics of the precursors of the hydrothermally carbonised adsorbents are presumed to influence the development of porosity and surface area during the thermal modification process thereby leading to the differences in BET surface area and adsorbent pore characteristics.

A comparison of the surface area and porosity of the HTC adsorbents with that of the precusors (unmodified residues) described in Table 5.5 (Chapter 5) indicates that the HTC adsorbents had significantly higher BET surface area and porosity due in part to the hydrothermal carbonization process, hence the effect of the hydrothermal carbonization process on the textual characteristics of the resulting adsorbents can be seen using the BET surface area. The agricultural residue adsorbents had little or no porosity with BET surface area in the range of 0.45 – 12.42 m^2 g^{-1}. A comparison of these BET values with those obtained for the HTC170 adsorbents in Table 6.5 and 6.6 for the HTC200 adsorbents shows significant increases which can be associated with the transformation of the residue into hydrochars. A similar effect of hydrothermal treatment on the BET surface area of a biomass (hazelnut) has been observed by Unur, (2013). In this study, the surface area of the hazelnut residue was 30$m^2 g^{-1}$, however upon hydrothermal treatment at 250°C, the surface area of the resulting hydrochar increased to 60 m^2 g^{-1}. The BET surface area of the HTC adsorbents reported in this work was higher for some adsorbents and for others similar to what is reported in literature. Titrici *et al* (2007b) obtained BET surface values of 15.5, 12 and 34 m^2 g^{-1} for hydrothermally carbonized chars from oak leaf, pine needle and pine cone respectively. Xu *et al*, (2013) also describes the optimization of the BET surface area of hydrothermally carbonized *Sargassum Horneri* biomass using a Taguchi method for temperatures in the range 180 – 210°C. The BET surface area of the *Sargassum Horneri* biomass was non-existent but after hydrothermal carbonization, the surface areas of l6.3, 16.6, 15.5, 21.0, 27.7, 27.4, 21.9 and 20.0 m^2 g^{-1} were obtained for the hydrochars

with the highest being 31.8 $m^2 g^{-1}$. In a similar investigation by Roman *et al*., (2013), the BET surface area obtained for three residues (walnut shell, sunflower stem and olive stone) subjected to hydrothermal treatment at 220$^°$C were 22, 27 and 31 $m^2 g^{-1}$ for the hydrochars of olive stone, sunflower steam and walnut shell respectively.

The nature of the pores on the HTC adsorbents can be described using the N_2-adsorption-desorption isotherm. From the shape of the nitrogen adsorption-desorption isotherm previously mentioned, the type of isotherm can be deduced as well as the type of porous structure existing on the adsorbent. Thus it can be inferred that each N_2 adsorption-desorption isotherm of the HTC adsorbents had three characteristic regions and these are:

> The initial curve with a sharp knee related to nitrogen uptake at $P/P_0 < 0.2$.

> The second part which in some adsorbents is the plateau section of the curve, while in others it still indicates increasing nitrogen uptake between $0.2 < P/P_0 < 0.9$.

> The third section of the curve is an upward curve with increasing nitrogen uptake up to the point where $P/P_0 = 1.0$ (Chowdhury *et al*., 2012).

This is observed for the OPFS-HTC170, CCPSHTC170, CCYBS-HTC170, YTBS-HTC170, CNFS-HTC200, PTPS-HTC200 and YTBS-HTC200 adsorbents and these regions are also characterised by small hysteresis loops. However for the remaining HTC adsorbents, this third region is marked by a steep rise in the nitrogen uptake as P/P_0 increases and this is associated with a mixture of hysteresis loops. These hysteresis are well defined in the CNFS-HTC170, PTHS-HTC170, PTPS-HTC170, CCPS-HTC200 and PTHS-HTC200 adsorbents and the presence of hysteresis loops in the nitrogen adsorption-desorption plot of the hydrothermal carbonized adsorbents is common with all the adsorbents. The hysteresis seen on figures 6.1 – 6.4 can be used to classify these adsorbents as type IV based on the IUPAC and Brunauer-Deming-Deming-Teller (BDDT) method which indicates the presence of mesopores (Brunauer *et al*., 1940; Ip *et al*., 2008 and Wickramaratne *et al*., 2014). The presence of this hysteresis has been associated with a number of processes and properties of mesoporous materials. For instance, Wickramaratne *et al*., (2014) associates the hysteresis loops in mesoporous materials to the effects of voids created within the adsorbent particles which influence the nature of the nitrogen adsorption and desorption processes and others like Banerjee *et al*., (2015) and Li *et al*., (2014) link it to capillary condensation and non-uniform or disordered packing of layers.
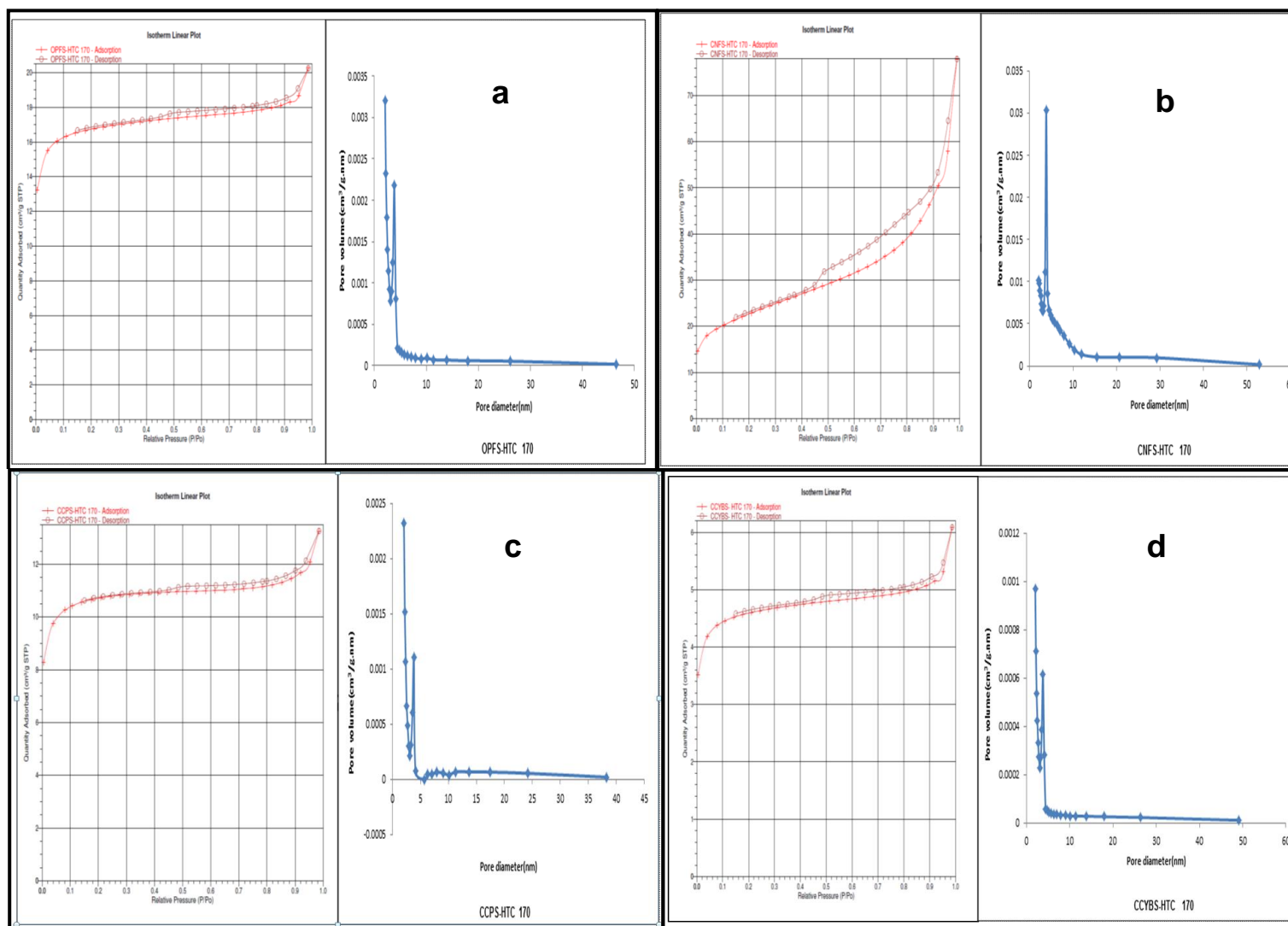
Figure 6.1: N$_2$ adsorption-desorption isotherm and pore size distribution of OPFS, CNFS, CCPS and CCYBS-HTC170 adsorbents
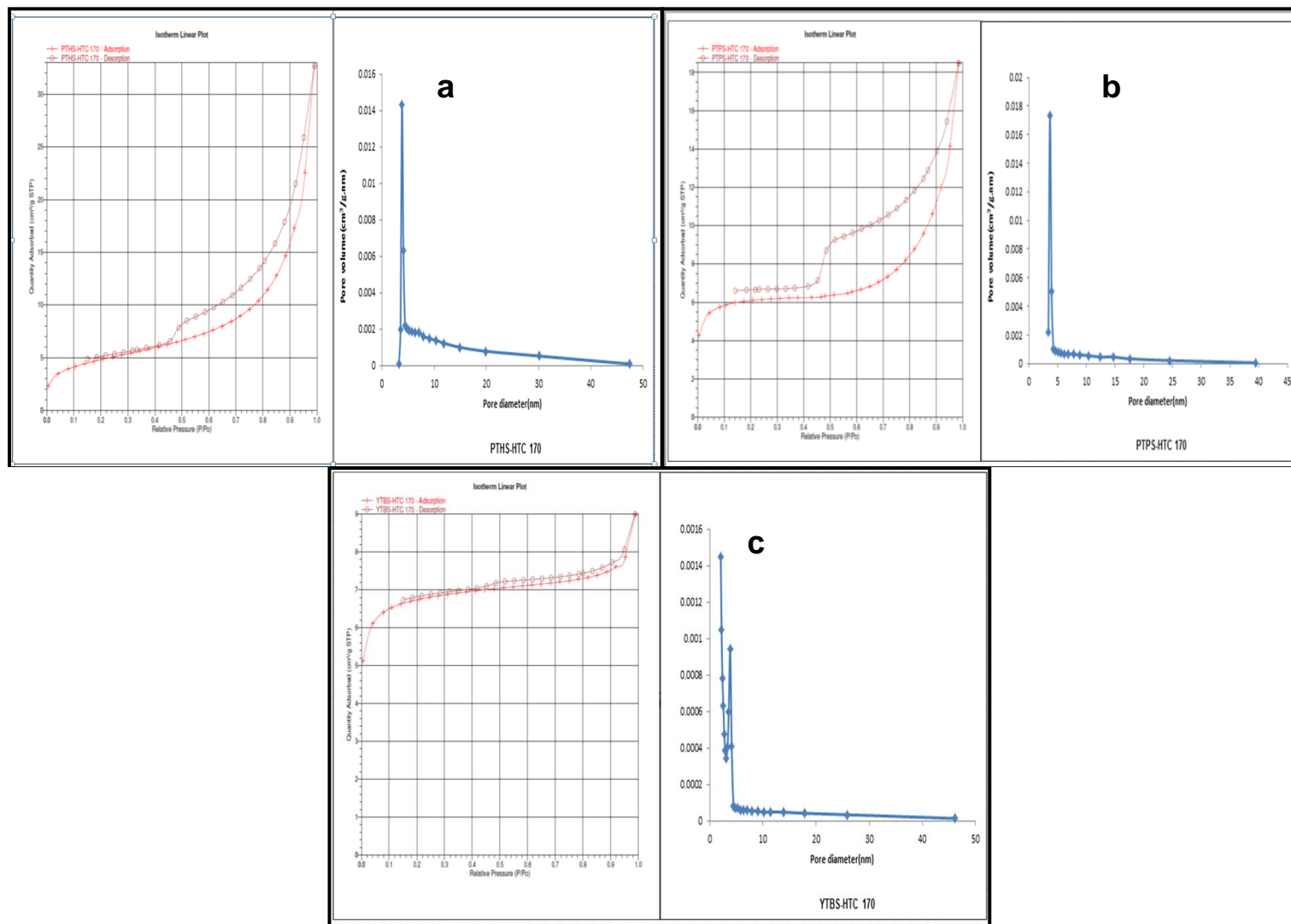
Figure 6.2: N$_2$ adsorption-desorption isotherm and pore size distribution of PTHS, PTPS and YTBS-HTC170 adsorbents
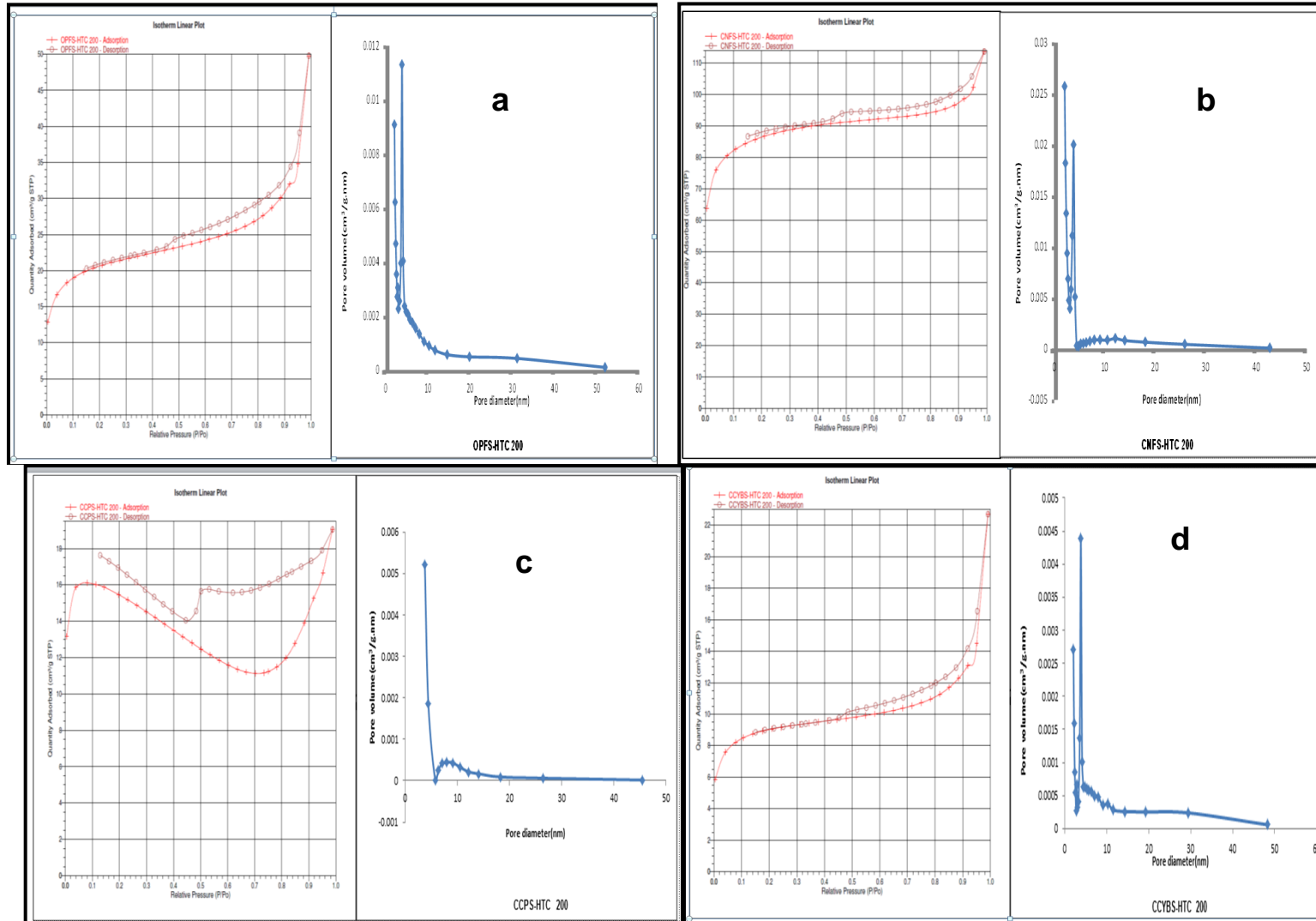
Figure 6.3: N$_2$ adsorption-desorption isotherm and pore size distribution of OPFS, CNFS, CCPS and CCYBS-HTC 200 adsorbent
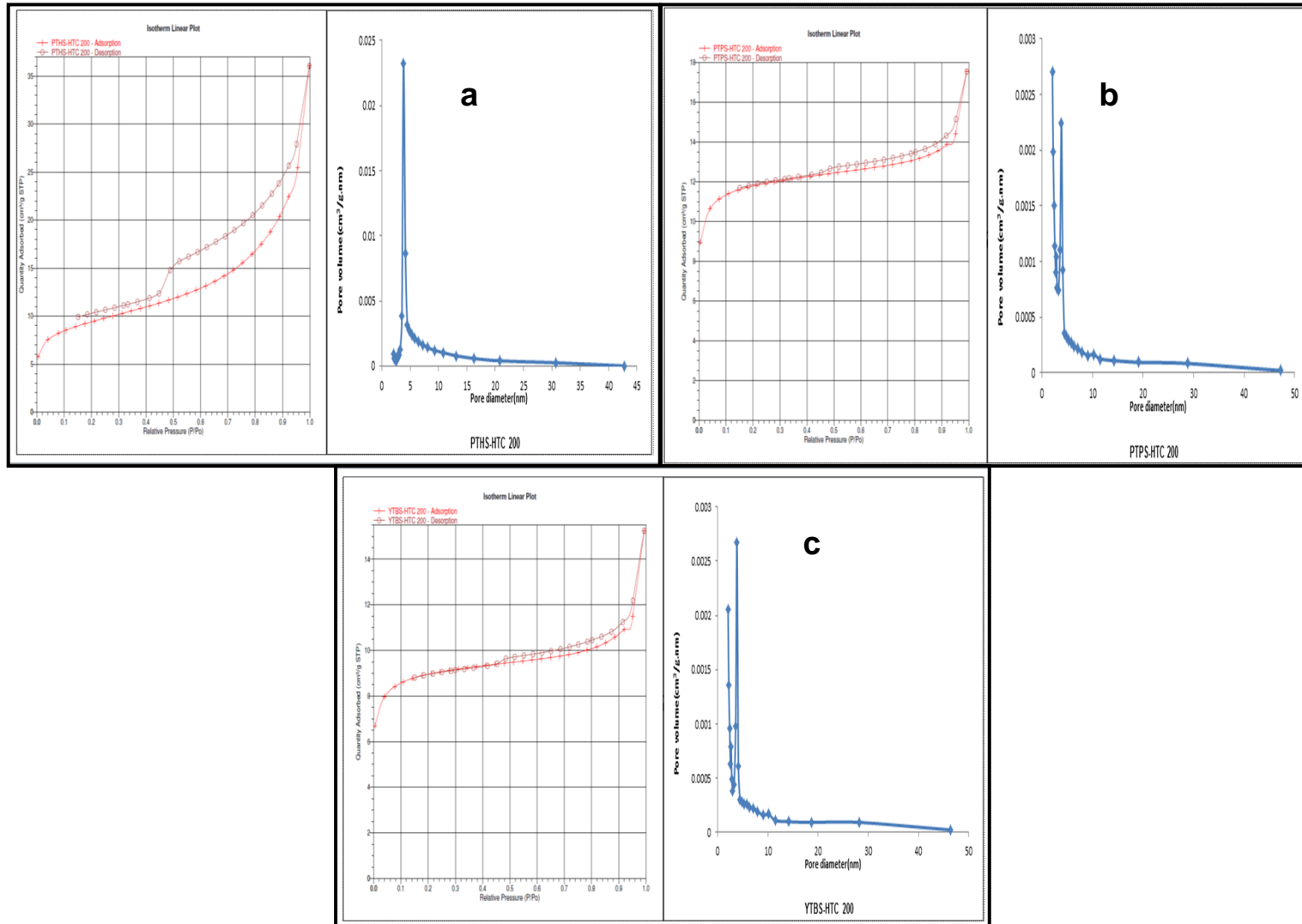
Figure 6.4: N$_2$ adsorption-desorption isotherm and pore size distribution of PTHS, PTPS and YTBS-HTC 200 adsorbents

Examination of the nitrogen plots for the hydrothermal carbonized adsorbents in Figures 6.1 – 6.4 shows different configurations of the hysteresis loop. The H_1 loop is a relatively narrow loop according to Banerjee et al., (2015) and it indicates the presence of a narrow distribution of pore sizes in adsorbents. This loop was observed for the CNFS-HTC170, PTHS-HTC170, OPFS-HTC200, CNFS-HTC200, CCYBS-HTC200 and PTHS-HTC200 adsorbents. The H_2 loop arises due to the interconnectivity of pore sizes as described by Mason (1982) and is observed for the CCPS-HTC200 adsorbent as shown in Figure 6.3c. This N_2 adsorption-desorption sequence in the CCPS-HTC200 adsorbent is affected by the heterogeneity of the pore distribution thereby leading to network effects which results in disordered N_2 adsorption-desorption. These disordered effects in the pores results in an asymmetry of the hysteresis loop which become associated with the nature of the filling effects of the nitrogen molecules (Mason, 1982).

The H_3 hysteresis loop was observed for the PTPS-HTC170 adsorbent as seen in Figure 6.2b and the loop is characterised with no plateaus at high relative pressure in the nitrogen adsorption-desorption curve. It has been suggested by Zhao et al., (2014), that this type of hysteresis loop relates to slit-shaped mesoporous materials. Sing (1982) and Giraldo and Moreno-Pirajan (2012) also describe this hysteresis loop in association with solid adsorbents consisting of aggregates. Other studies involving hydrothermal adsorbents have also reported the presence of this loop in the nitrogen-adsorption-desorption curve. For instance, Liu and Zhang (2011) report a slit shaped and porous hydrochar obtained at $300°C$ while investigating the removal of copper(II) and phenol from an aqueous solution using porous carbon derived from hydrothermal chars. The study relates this property to the presence of the type H_3 isotherm hysteresis loop on the N_2 adsorption-desorption curve of the hydrochars adding that although the adsorbent used for the study was largely microporous, the presence of some mesopores in the hydrochar matrix resulted in this hysteresis shape of the curve. In the same way, Xu et al., (2013) describes the presence of H_3 hysteresis loop on hydrochar obtained after the hydrothermal treatment of S. horneri biomass at $180 – 210°C$ which used to indicate the presence of aggregates of slit-shaped plate-like particles on the hydrochar.

The size of pores on an adsorbent and their distribution within an adsorbent surface is also an important parameter that affects adsorbent performance. According to Ioannidou et al., (2010), the significance of the pore size distribution of an adsorbent is due to the fact that it influences migration and transport of adsorbents within the pore structure. For the

hydrothermal carbonized adsorbents (HTC170 and HTC200), the pore size distribution was calculated based on the desorption branch of the nitrogen adsorption isotherm using the Barrett-Joyner-Halenda (BJH) method (Iza *et al*., 2000; Strock *et al*., 1998). From this calculation, the pore size distribution plots were obtained as shown in Figures 6.1 - 6.4; the BJH average pore diameter and total pore volume of the adsorbents were also obtained as presented in Tables 6.5 and 6.6 for the HTC170 and HTC200 adsorbents respectively. The results obtained show that for the HTC170 adsorbents, the CNFS-HTC170 adsorbents had the largest pore volume of 1.2×10^{-1} cm^3 g^{-1} while the CCYBS-HTC adsorbents had the least (9.0×10^{-3} cm^3 g^{-1}). The range in the BJH average pore diameter for the HTC170 adsorbents reveals that the adsorbents were mesoporous with pore diameters between 5.49 nm (OPFS-HTC170) and 10.97 nm (PTHS-HTC170). For the HTC200 adsorbents, the range in total pore volume is form 1.75×10^{-1} cm^3 g^{-1} (CNFS-HTC200) to 2.35×10^{-2} cm^3 g^{-1} (YTBS-HTC200); indicating the CNFS-HTC200 had the highest total pore volume as previously observed for the HTC170 adsorbents. The BJH average pore diameter for the HTC200 adsorbents ranged from 5.58 nm (CNFS-HTC200) to 12.09 nm (CCYBS-HTC200) indicating that these adsorbents are mesoporous (Sing, 1982). The pore size distribution of the hydrothermal carbonized adsorbents in Tables 6.5 and 6.6 also indicates that the hydrochars (HTC170/HTC-200) have wide pore size distributions with bimodal pore size peaks appearing in the range of 3 – 10 nm.

The pore size and volume characteristics of the hydrothermal carbonised adsorbents (HTC170 and HTC200) indicates that the temperature difference for these two types of adsorbents did not significantly alter the pore characteristics between them with the exception of the OPFS-HTC and CCYBS-HTC adsorbents. For the OPFS-HTC adsorbents, the pore volume increased from 3.13×10^{-2} cm^3 g^{-1}(OPFS-HTC 170) to 7.70×10^{-2} cm^3 g^{-1}(OPFS-HTC 200) indicating that the increase in temperature of hydrothermal treatment resulted in a twofold increase in the adsorbent pore volume. For the CCYBS-HTC adsorbents the temperature increase resulted in a three-fold increase in pore volume from the HTC-170 to the HTC-200 adsorbent. From these observations, it can be presumed that the temperature difference between the two hydrothermally carbonised adsorbents did have an effect on the porosity of the adsorbents. A comparison of the pore volume and pore size of the hydrochars (HTC-170/HTC-200) with those of the residues (precursors) in Chapter five indicates that the hydrochars have larger pore volumes and smaller average pore sizes than the residues. This shows that a significant improvement of porosity in residues can be achieved using the hydrothermal carbonisation process.

6.4 Surface morphology and chemical composition of hydrothermal adsorbents

Scanning electron microscopy (SEM) was used to characterise the morphology of the hydrochars obtained from the hydrothermal carbonisation process. This was necessary to give insight into how the hydrothermal carbonisation treatment affects the structural morphology of the resulting hydrochars when compared to the residues. The chemical composition of an adsorbent after hydrothermal treatment was also evaluated using the EDAX coupled to the scanning electron microscope as described in Section 4.3.2. This was carried out to assess the effect of the hydrothermal treatment on the chemical species on the residues, hence determine whether the treatment had any significant effect on the elemental composition of the resulting hydrochars. The presence or absence of chemical elements on the adsorbent surface is used to confirm the adsorption process and this information was also obtained for some adsorbents using the EDAX analysis.

6.4.1 Adsorbent surface morphology

SEM is a primary tool used for characterising the surface, shape and size properties of an adsorbent (Li *et al.,* 2014). It is used to obtain information on the morphology of surfaces and was used to examine the surface structure of the hydrothermal carbonised adsorbents described in this study. The SEM micrographs of the HTC170 adsorbents are shown in Figures 6.5 to 6.8, while that of the HTC200 adsorbents are shown in Figures 6.9 to 6.12. In addition, insert on the SEM micrographs of the OPFS-HTC, CNFS-HTC, CCPS-HTC adsorbents are photographs of the respective adsorbents, while those of the CCYBS-HTC, PTHS-HTC, PTPS-HTC and YTBS-HTC adsorbents are shown in Appendix 4. These images were taken to give information on the characteristic nature of the obtained hydrothermal adsorbents at the different temperatures- 170° C and 200 °C.
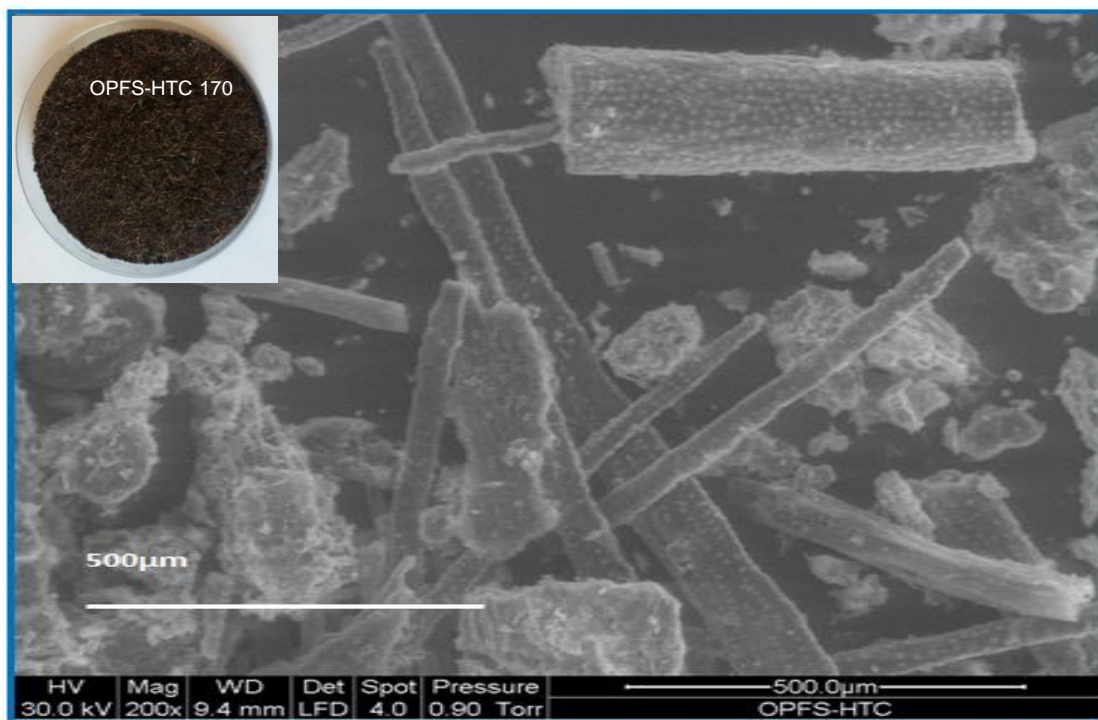
Figure 6.5: SEM micrograph for OPFS-HTC 170 (Scale bar = 500 µm), Insert photograph of OPFS-HTC170 adsorbent
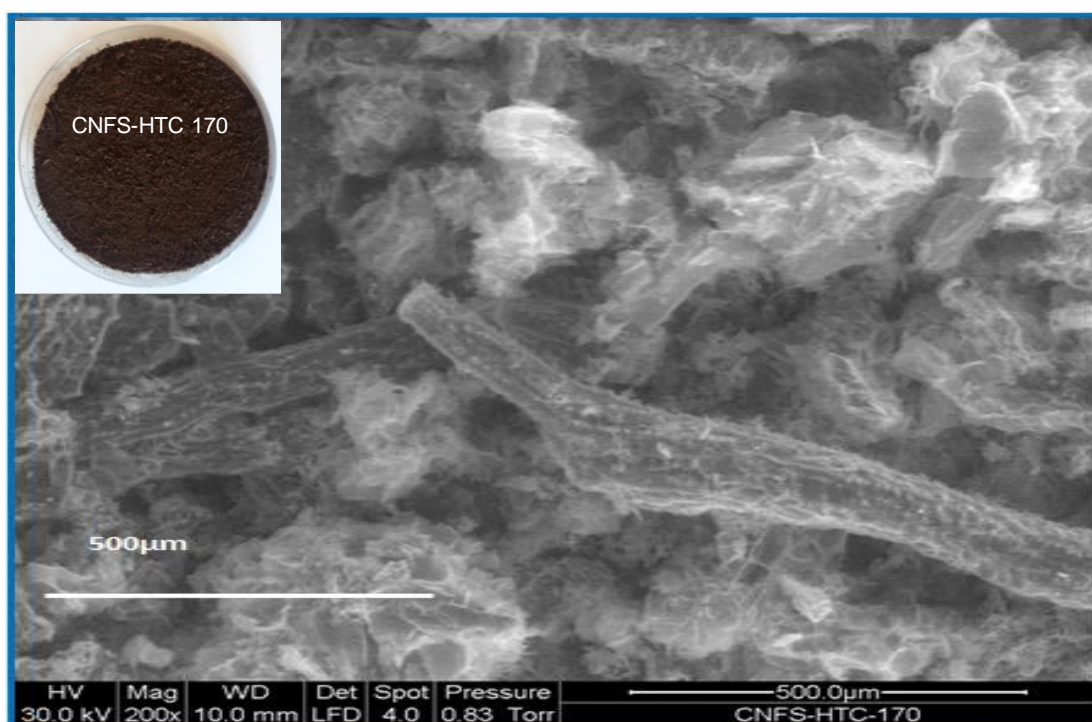
Figure 6.6: SEM micrograph for CNFS-HTC 170 (Scale bar = 500 µm), Insert photograph of CNFS-HTC170 adsorbent
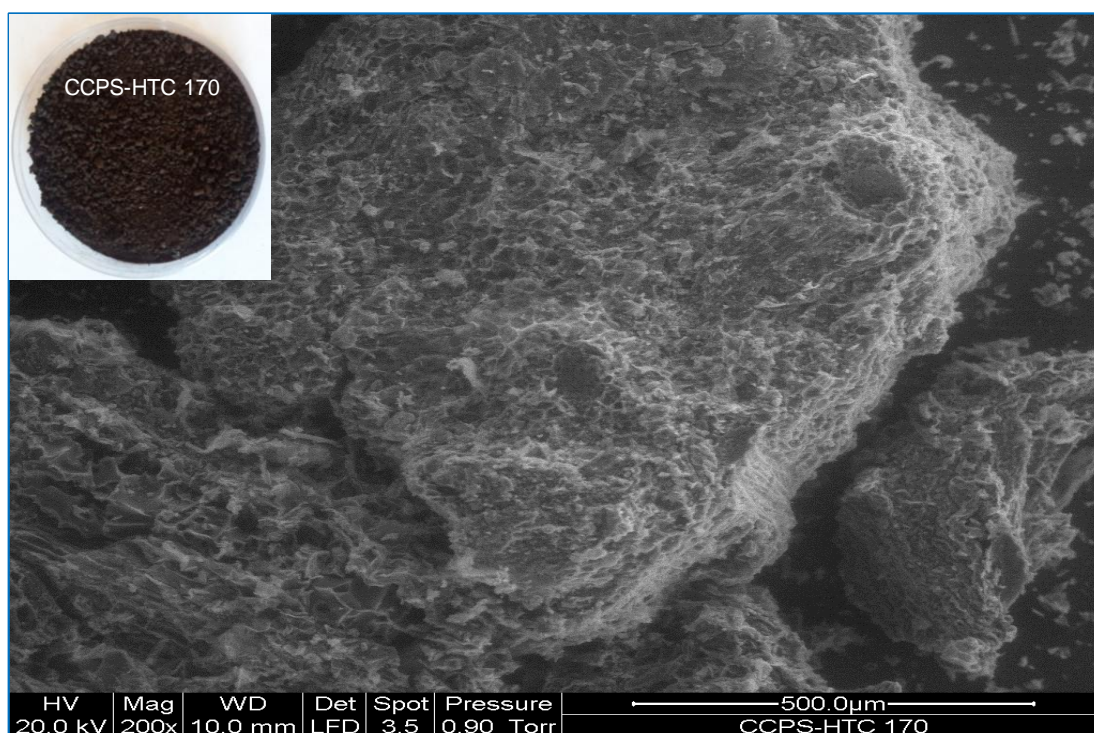
Figure 6.7: SEM micrograph for CCPS-HTC 170 (Scale bar = 500 µm), Insert photograph of CCPS-HTC170 adsorbent.

From these hydrochar photographs, it was observed that there was distinct difference in colouration between the HTC170 and HTC200 adsorbents. The HTC170 adsorbents were brown in colour, which is consistent with pictures of partially carbonised products while the pictures of the HTC200 adsorbents showed black colouration which can be associated with fully carbonised hydrochars (Parshetti *et al.*, 2013). The hydrolysis initiated chemical breakdown of lignin and extractives has been reported as associated with the colouration of the hydrothermal adsorbents according to Wang *et al.,* (2009). In their study, it was proposed those condensation reactions such as the activation of tannins and flavonoids and their reaction with furfural and hydroxymethyl furfural may be responsible for the development of the brown colouration in hydrothermal carbon materials.
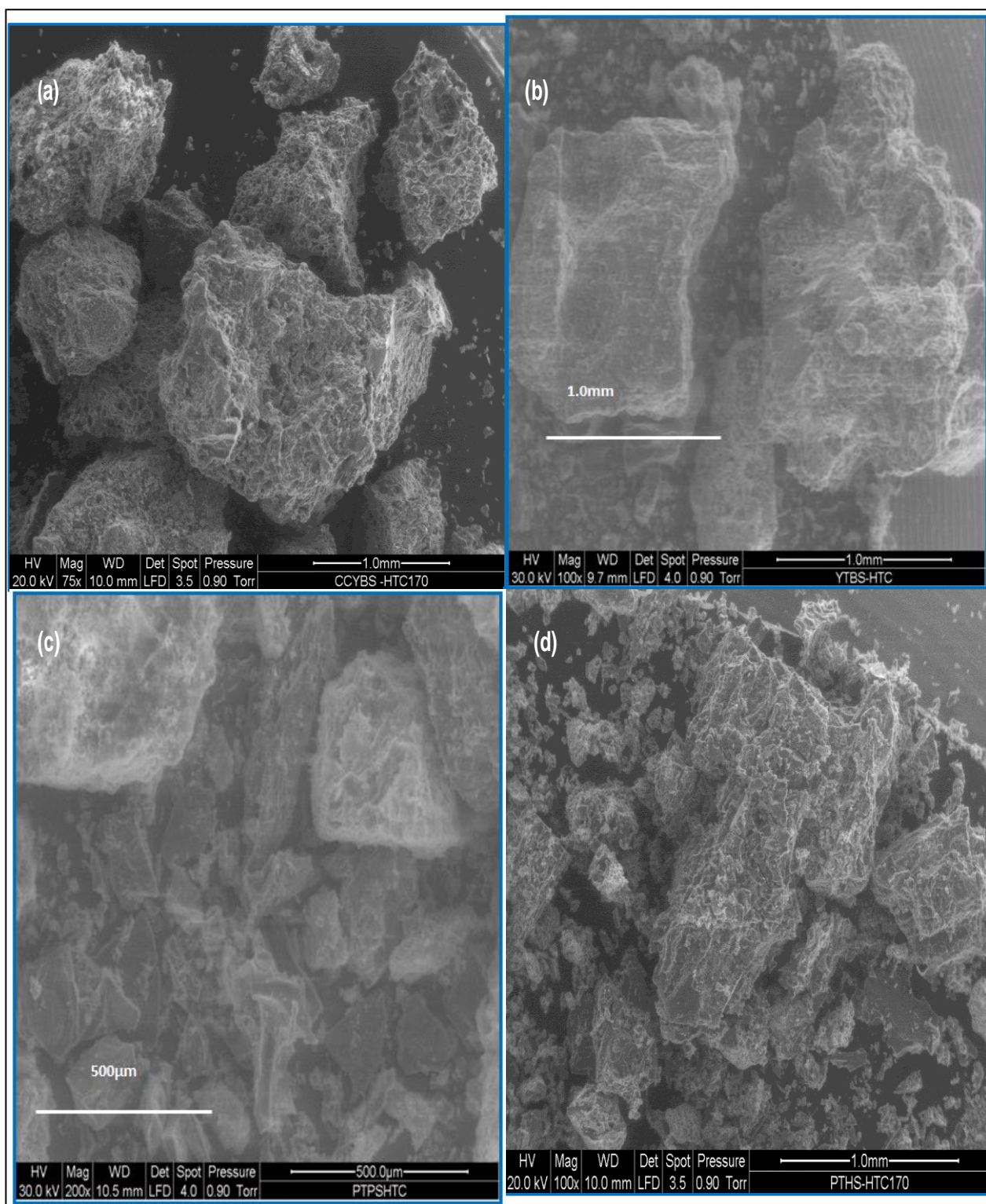
Figure 6.8 SEM micrographs for (a) CCYBS-HTC170, (b) YTBS-HTC170, (c) PTHS-HTC170 & (d) PTPS-HTC170 adsorbents (Scale bars = 1.0 mm & 500 μm)
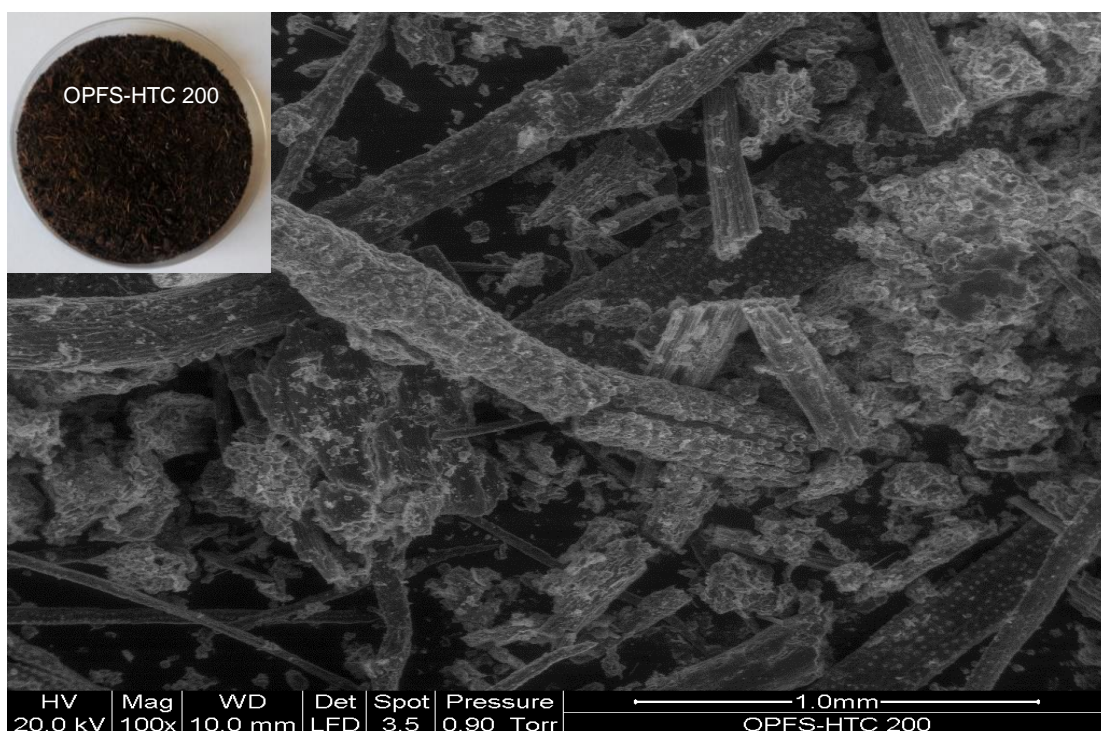
Figure 6.9: SEM micrograph for OPFS-HTC200 (Scale bar = 1 mm), Insert photograph of OPFS-HTC200 adsorbent
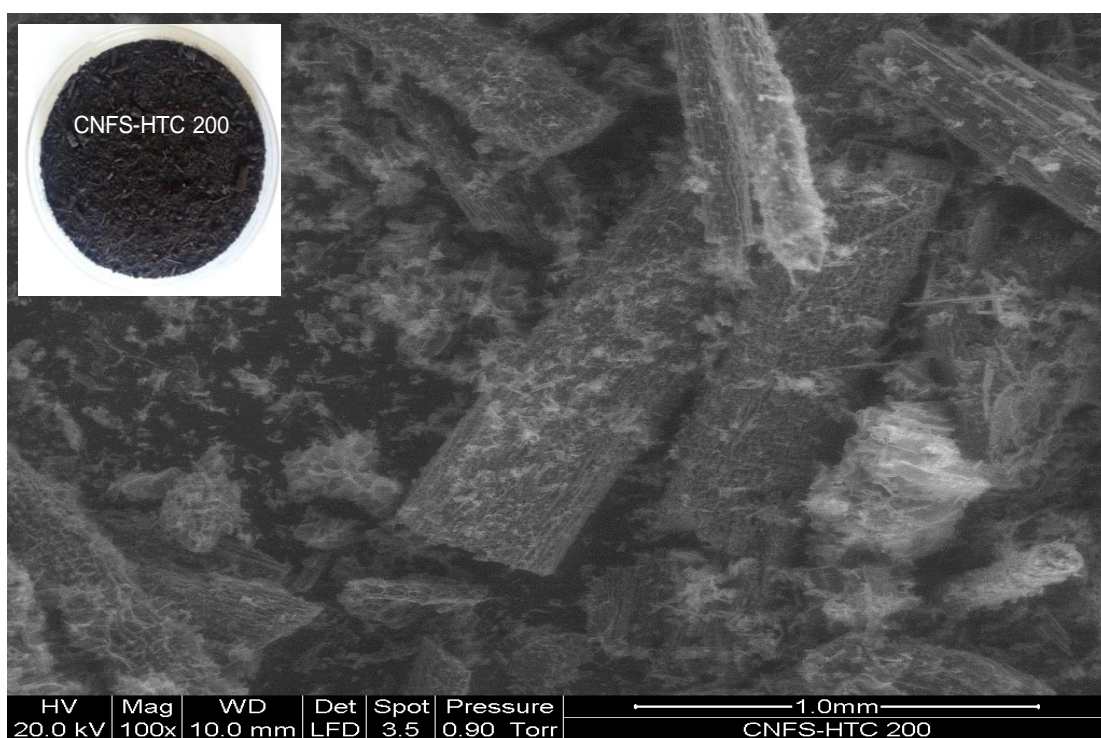
Figure 6.10: SEM micrograph for CNFS-HTC200 (Scale bar = 1 mm), Insert photograph of CNFS-HTC200 adsorbent

HV	Mag	WD	Det	Spot	Pressure	500.0μm
20.0 kV	200x	10.0 mm	LFD	3.5	0.90 Torr	CCPS-HTC 200
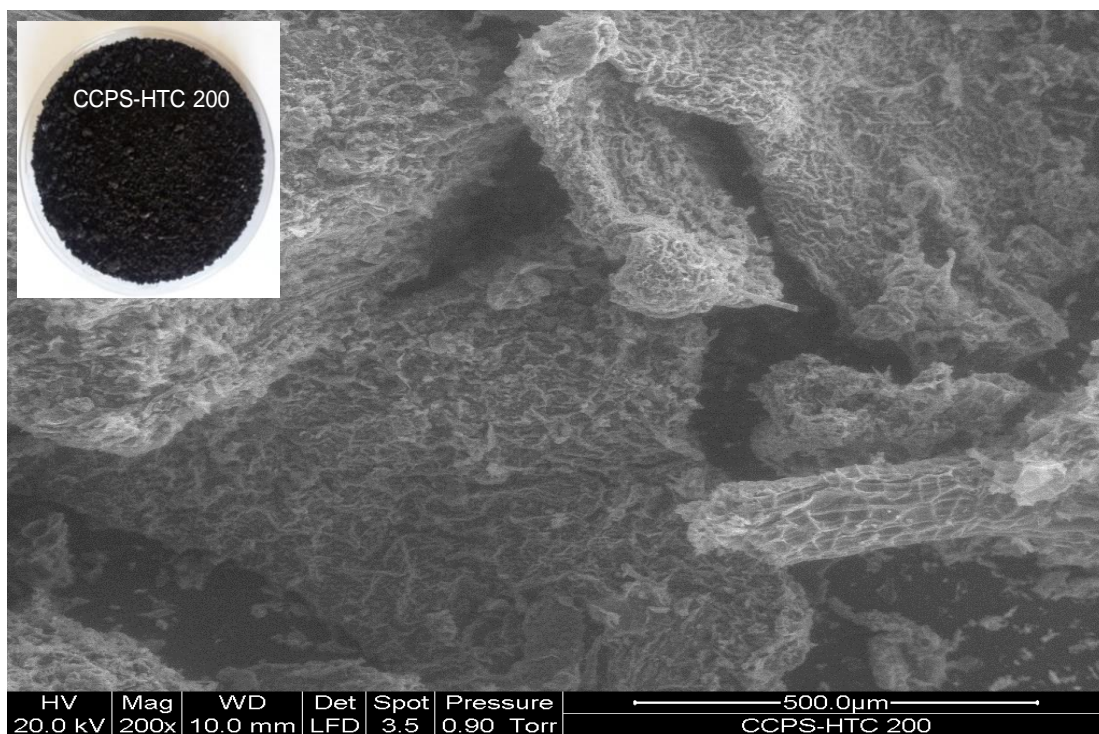
Figure 6.11: SEM micrograph for CCPS-HTC 200 (Scale bar = 500 µm), Insert photograph of CCPS-HTC200 adsorbent

The SEM micrographs of the HTC adsorbents indicates that the fibre like structures observed in the residues were still present in the OPFS-HTC and CNFS-HTC adsorbents indicating that degradation of the residues was only partial at the temperatures of hydrothermal treatment. In addition it can be observed that the even though the images of the HTC adsorbents are not very different from those of the residues, the surface of the HTC adsorbents especially the HTC200 adsorbents appeared very rough and irregular indicating the effect of thermal degradation of hemicellulose and cellulose components of the residues.
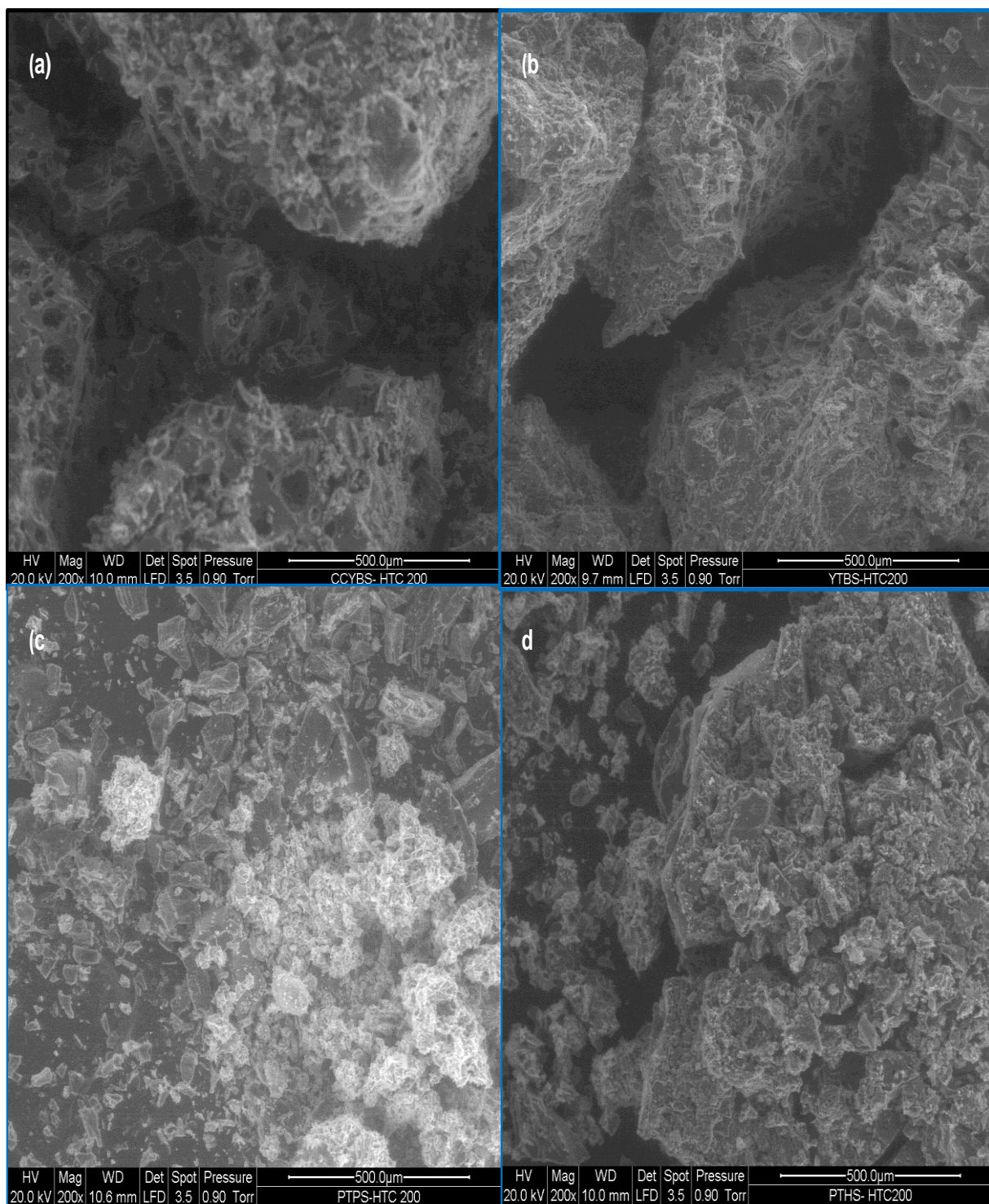
Figure 6.12: SEM micrographs for (a) CCYBS-HTC200, (b) YTBS-HTC200, (c) PTPS-HTC200 & (d) PTHS-HTC200 adsorbents (Scale bar = 500 µm)

It was also observed that the HTC adsorbents had some rudimentary pores within their structure especially the OPFS-HTC, CNFS-HTC and CCPS-HTC adsorbents and these can be related to the onset of pore development due to decomposition of the volatile constituents of the residue matrix (Zhu *et al.,* 2014; Liu *et al.,*2010). The uneven surfaces

of these hydrothermal adsorbents and the presence of cavities of different sizes and with irregular shapes in their structure suggest that the HTC process conditions had exerted influence on the various mechanism associated with hydrothermal decomposition of lignin, cellulose and hemicellulose which affects the extent of development of porosity on these materials as confirmed by the BET surface area results previously discussed.

6.4.2 Chemical composition of hydrothermal adsorbents

The chemical composition of the hydrothermal carbonised adsorbents was also carried out as previously discussed. The EDAX spectrum of the PTPS- HTC170 and that of the OPFS-HTC200 were used to evaluate the chemical composition of the hydrothermal carbonised adsorbents. The spectrum of the PTPS-HTC170 adsorbent is shown in Figure 6.13, while that of the OPFS-HTC200 adsorbent is seen in Figure 6.16. It is observed from Figure 6.13 that the PTPS-HTC170 adsorbent had carbon, oxygen and potassium and chloride contents of 66%, 19% and 11 and 1.2% respectively. For the OPFS-HTC200 adsorbent, the main elements in the adsorbent matrix were carbon, oxygen, aluminium and silicon with contents of 78%, 14%, 3.5% and 1.4% respectively. A comparison of the EDAX spectrum of the HTC adsorbents with those of the relevant residue adsorbents in Figure 5.21 (OPFS) and Appendix 5 (PTPS) shows their variability in chemical composition. The PTPS-HTC170 had carbon and oxygen content of 66% and 19% respectively, while for the PTPS residue the composition of these elements were 58 and 32%. For the OPFS-HTC adsorbent, its carbon and oxygen content were 78 and 14% respectively, while those of the OPFS residue were 71% and 23% respectively. This indicates that the HTC adsorbents had higher carbon content than their respective residues and their oxygen content was lower than those of the residues. This is due to the process of carbon enrichment that is usually associated with hydrothermal carbonisation of lignocellulosic materials (Titirici *et al.,* 2015a).
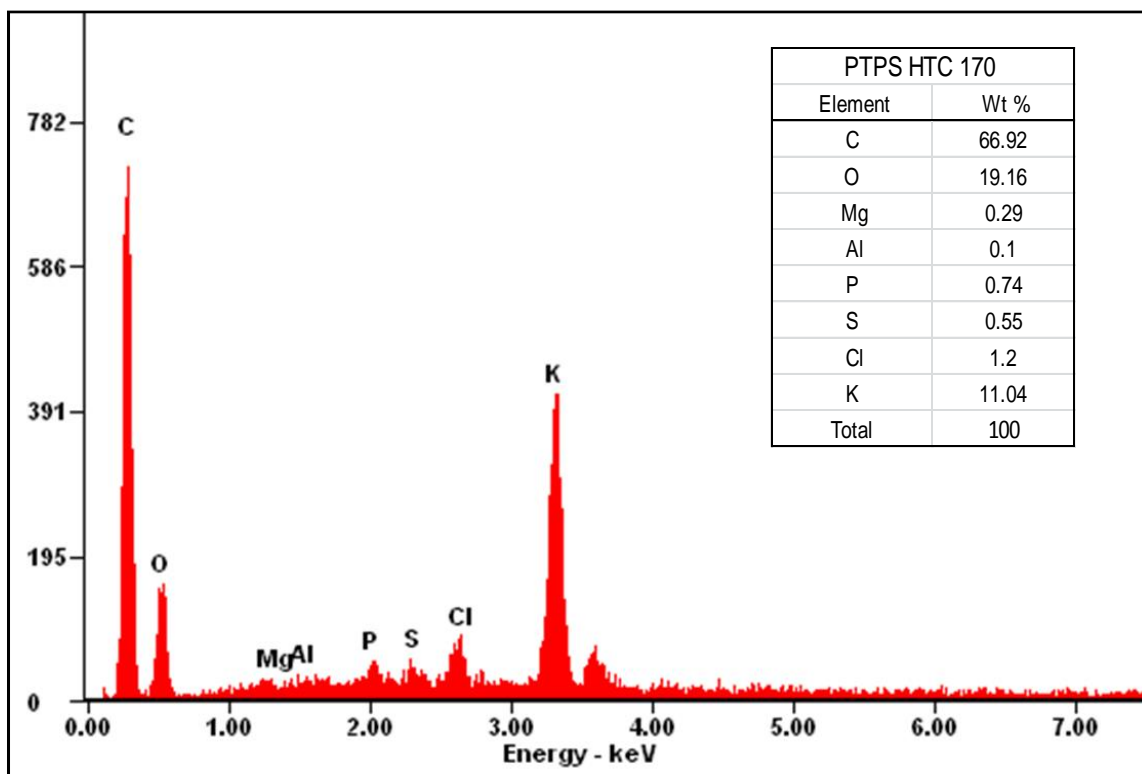
Figure 6.13: EDAX spectrum for PTPS-HTC 170

PTPS HTC 170	
Element	Wt %
C	66.92
O	19.16
Mg	0.29
Al	0.1
P	0.74
S	0.55
Cl	1.2
K	11.04
Total	100
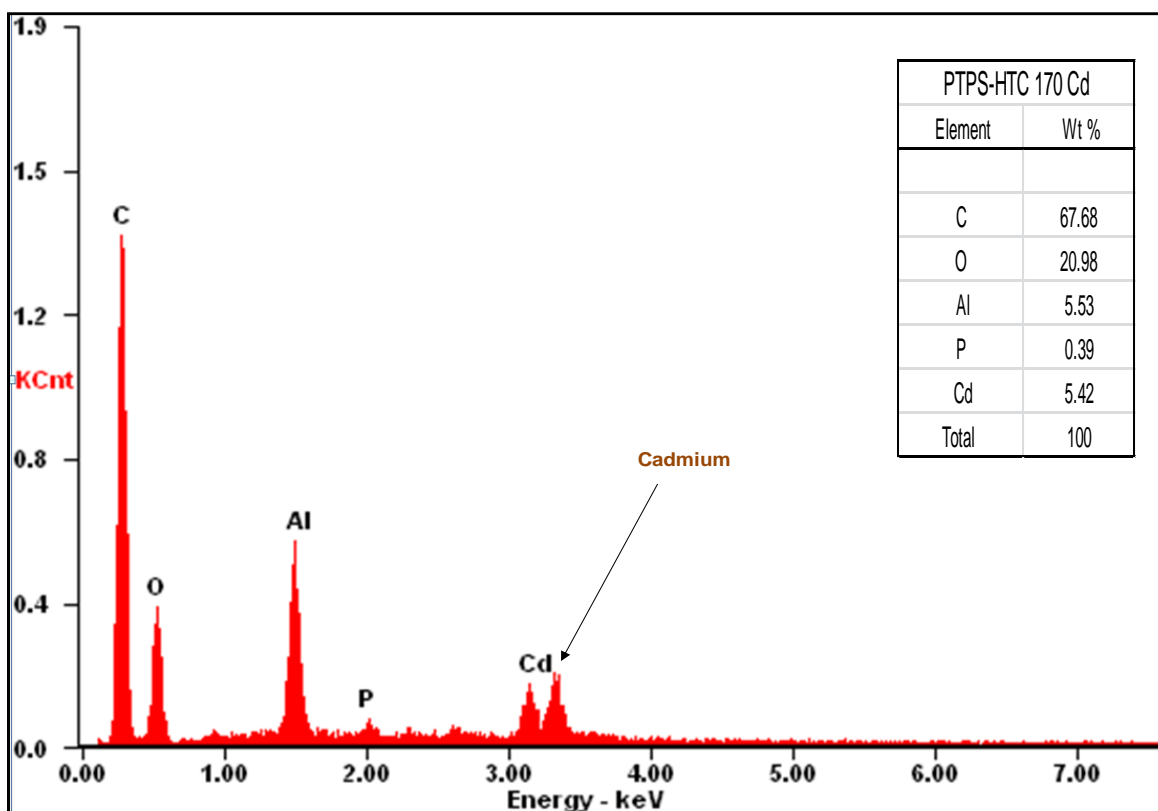
Figure 6.14: EDAX spectrum for PTPS-HTC 170 after Cd(II) ion adsorption

PTPS-HTC 170 Cd	
Element	Wt %
C	67.68
O	20.98
Al	5.53
P	0.39
Cd	5.42
Total	100

296

PTPS HTC 170-Pb	
Element	Wt %
C	64.69
O	24.2
Al	0.47
Si	0.23
P	0.23
Pb	0.65
K	9.53
Total	100
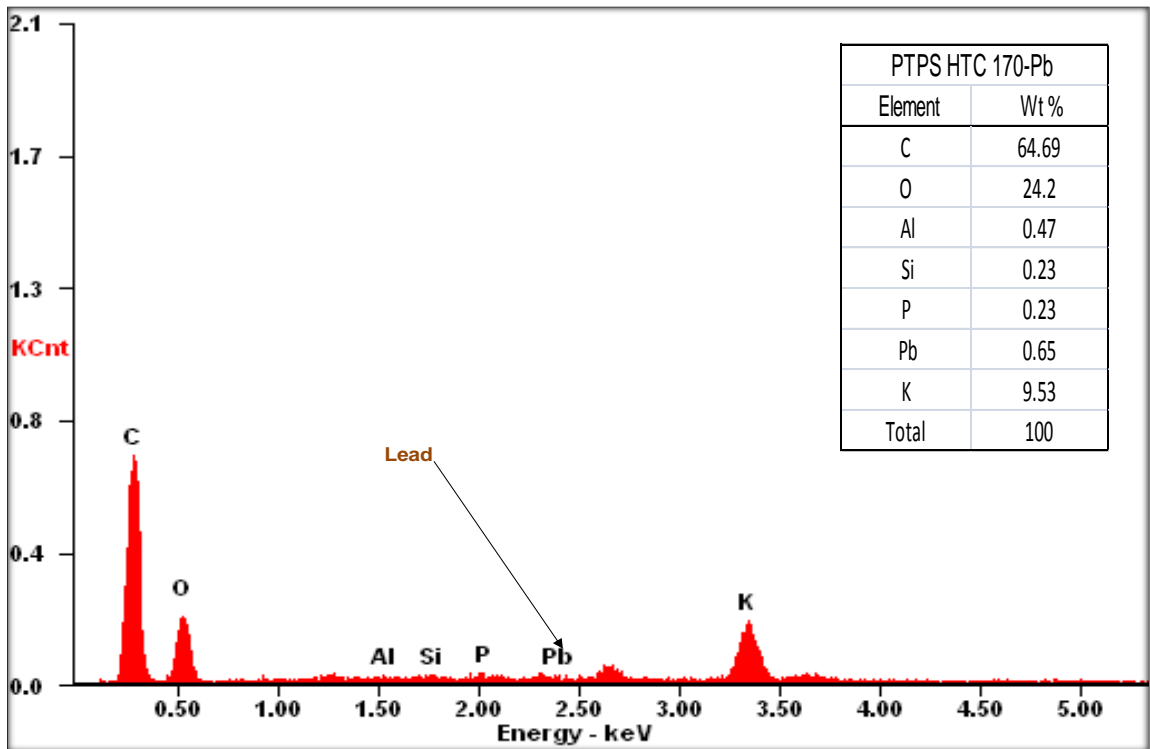
Figure 6.15: EDAX spectrum for PTPS-HTC 170 after lead adsorption

OFPS-HTC 200	
Element	Wt %
C	78.51
O	14.4
Al	3.51
Si	1.4
S	0.53
K	0.86
Ca	0.79
Total	100
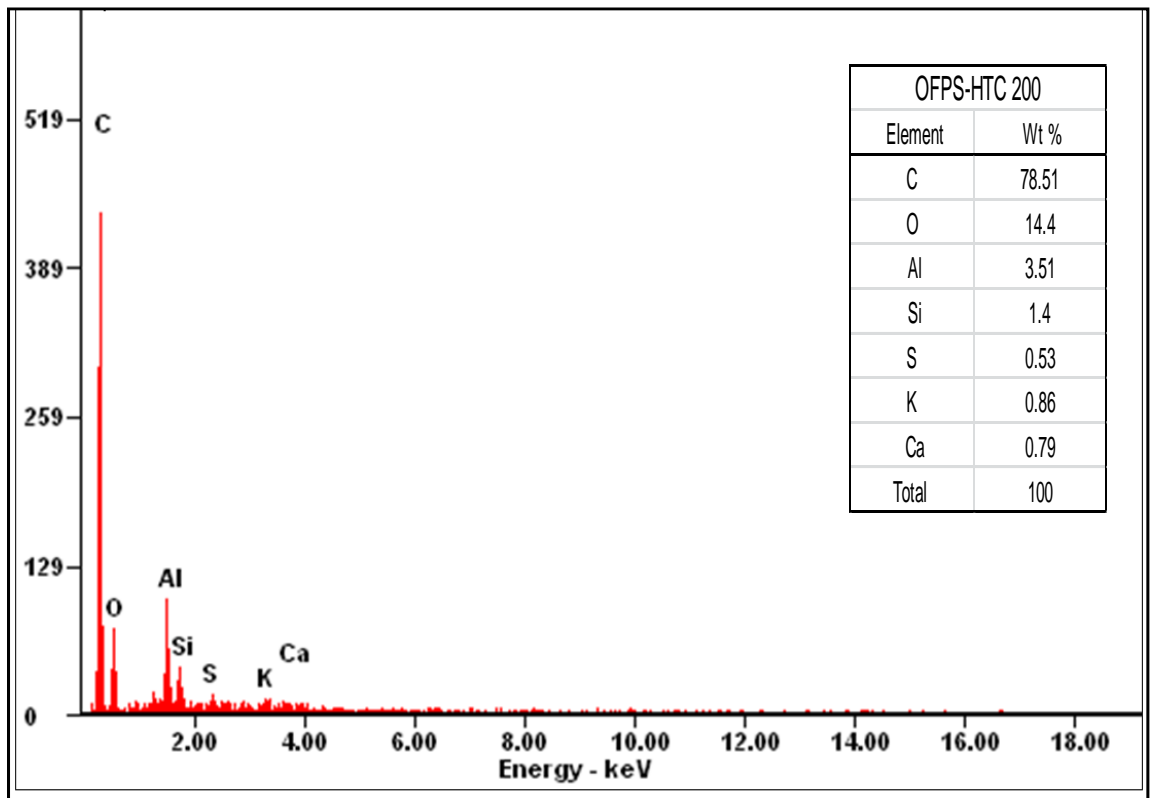
Figure 6.16: EDAX spectrum for OPFS-HTC 200
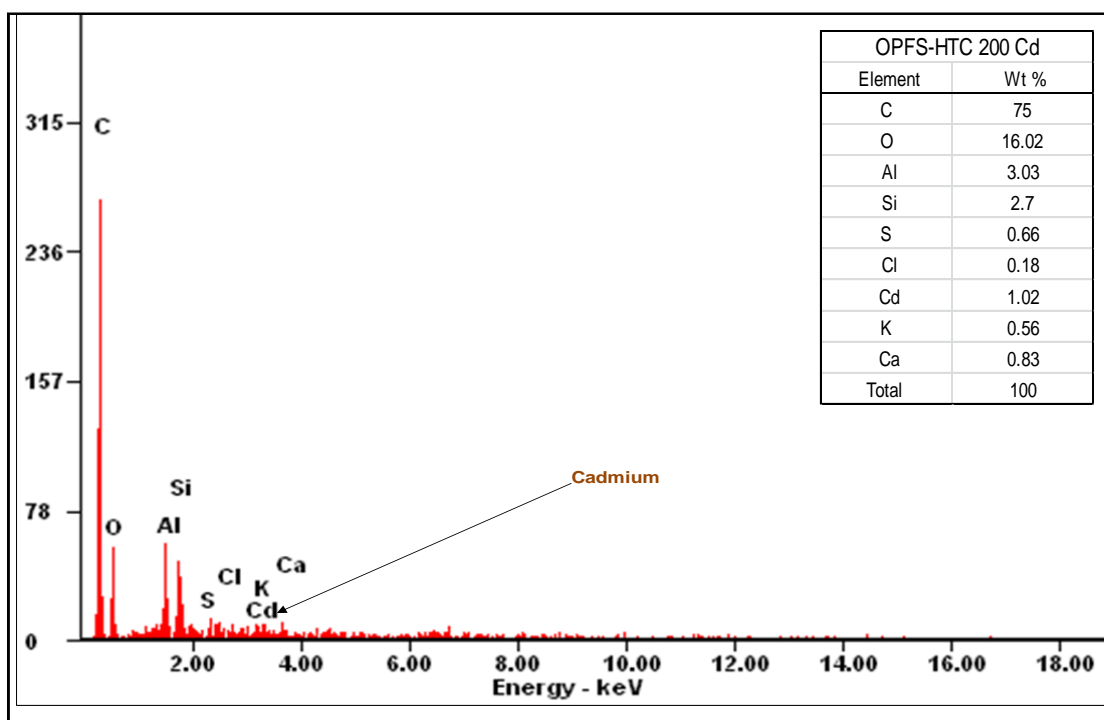
Fig 6.17: EDAX spectrum for OPFS-HTC200 after Cd(II) ion adsorption.
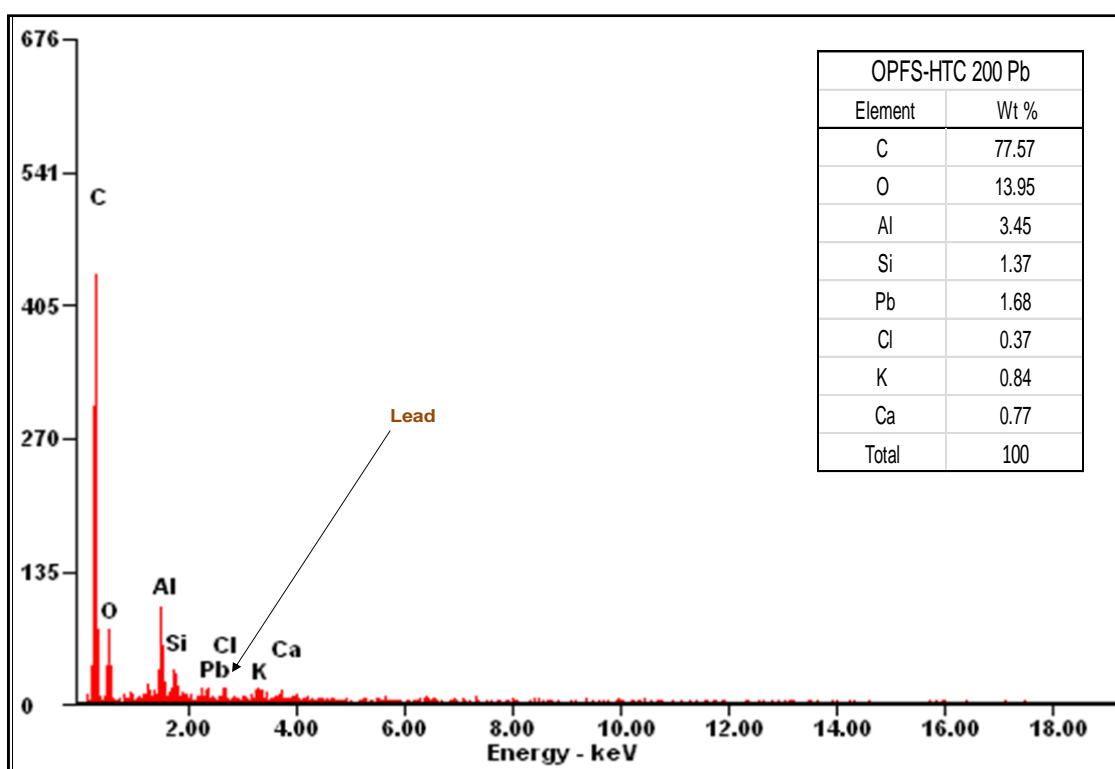
Fig 6.18: EDAX spectrum for OPFS-HTC200 after Pb(II) ion adsorption

A similar observation in the carbon, oxygen difference between hydrochars and residues has been reported by Kumar *et al.,* (2011). In their study, a comparison was made between the content between switchgrass from hydrochars produced at a temperature of 300°C and

the raw residue. The carbon content of the hydrochar was 70.5, while that of the residue was 44%, in the same approach the oxygen content of the hydrochar was observed to be lower than that of the raw residue.

The chemical composition of the two HTC adsorbents after Cd(II) and Pb(II) ions sorption were also determined using the EDAX analysis and the results are shown in Figures 6.14 and 6.15 for PTPS-HTC 170 adsorbent and Figure 6.17 and 6.18 for the OPFS-HTC200 adsorbent. The analysis of the EDAX spectrum in Figures 6.13 – 6.18 for the two adsorbents shows that of these HTC adsorbents were able to absorb both Cd(II) and Pb(II) ions onto their matrix on contact with the aqueous solution of the metal ions. It is pertinent to observe that the percentage of chemical elements on the adsorbents such as calcium, aluminium, potassium and silicon were observed to decrease in the EDAX spectra of the adsorbents after metal ion sorption. This may indicate the existence of ion-exchange mechanism playing a role in the removal of the Cd(II) and Pb(II) ions from the aqueous solution on the adsorbent surface. This observation has also been reported by Iqbal *et al.,* (2009b) in their study wherein the EDAX spectrum of the grapefruit peel adsorbent after Zn(II) ion adsorption did not indicate any signal for calcium or potassium ions that were previously present in the spectrum of the fresh grapefruit peel adsorbent.

6.5 Kinetic sorption studies

Adsorption kinetic studies is an important component for the effective design of models for batch, fixed and fluidized adsorption systems as it provides information on residence time interactions between the adsorbent and adsorbate which is used in reactor configurations (Chen *et al.,* 2001). In this study, the kinetics of the uptake of Cd(II) and Pb(II) ions using the hydrothermal carbonized adsorbents was carried out at pH 7, temperature 25°C with initial metal ion concentration of 500 mgL^{-1} using 0.1 L of aqueous solution. The adsorbent mass for each study was 1 g while contact time intervals were 5, 10, 15, 20, 25, 30, 40, 60, 90, 120 and 180 minutes at 200 rpm. The determination of the metal ion loading after sorption at time "t" was calculated using eqn. 5.1. The study of the kinetics of metal sorption in this work gives information on the rate of removal of adsorbate species {Cd(II) and Pb(II)} from aqueous solutions   using the different hydrothermally carbonised adsorbents prepared in at the two temperatures-170°C and 200°C.

6.5.1 Cadmium (II) ion sorption

The results of the contact time studies for the removal of Cd(II) ions for both HTC170 and HTC200 adsorbents are shown in Figures 6.19 and 6.20. From the figures, it can be seen that metal ion loading occurred in two phases: the first was a rapid loading up to 90 minutes for Cd(II) by HTC170 adsorbents and then a slow and gradual loading up to 180 minutes. From the Cd(II) ion loading for both sets of adsorbents shown in Figures 6.19 and 6.20, the maximum loading of Cd(II) on the HTC170 adsorbents were 19.6 mgg^{-1} (OFFS-HTC170), 25.9 mgg^{-1} (CNFS-HTC170), 17.15 mgg^{-1} (CCPS-HTC170), 13.3 mgg^{-1} (CCYBS-HTC-170), 16.3 mgg^{-1} (PTHS-HTC170), 15.6 mgg^{-1} (PTPS-HTC170) and 18.29 mgg^{-1} (YTBS-HTC170). However, the HTC200 adsorbents had higher maximum loading for the Cd (II) ions compared to the HTC170 adsorbents which had loadings of 29.6mgg^{-1} for OPFS-HTC200, 31.1 mgg^{-1} for CNFS-HTC200, 25.1 mgg^{-1} for CCPS-HTC200, 17.4 mgg^{-1} for CCYBS-HTC200, 24.1 mgg^{-1} for PTHS-HTC200, 24.2 mgg^{-1} for PTPS-HTC200 and 24.6 mgg^{-1} for YTBS-HTC200. This higher loading is attributed to the higher surface area available on these adsorbents compared to the HTC170 adsorbents; it can also be observed that the CCYBS-HTC 170/200 had the lowest loadings which can be attributed to their low surface area compared to the other adsorbents.
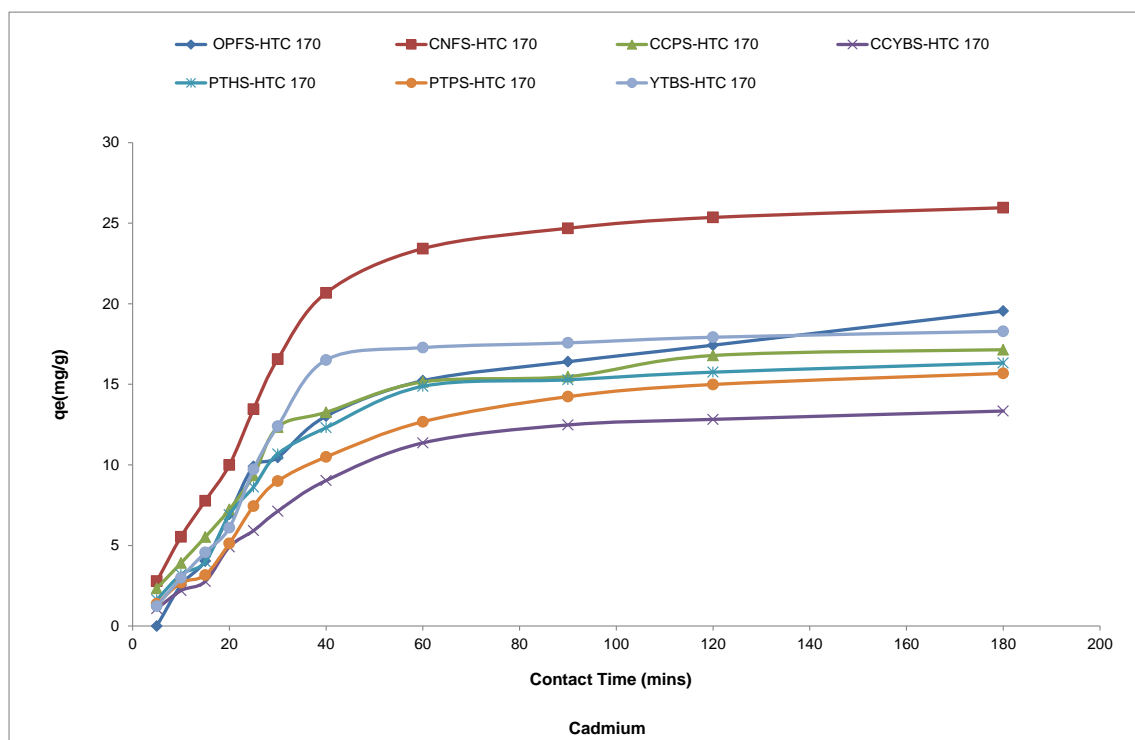
Figure 6.19: Kinetic profile for Cd(II) hydrothermal carbonised HTC170 adsorbents
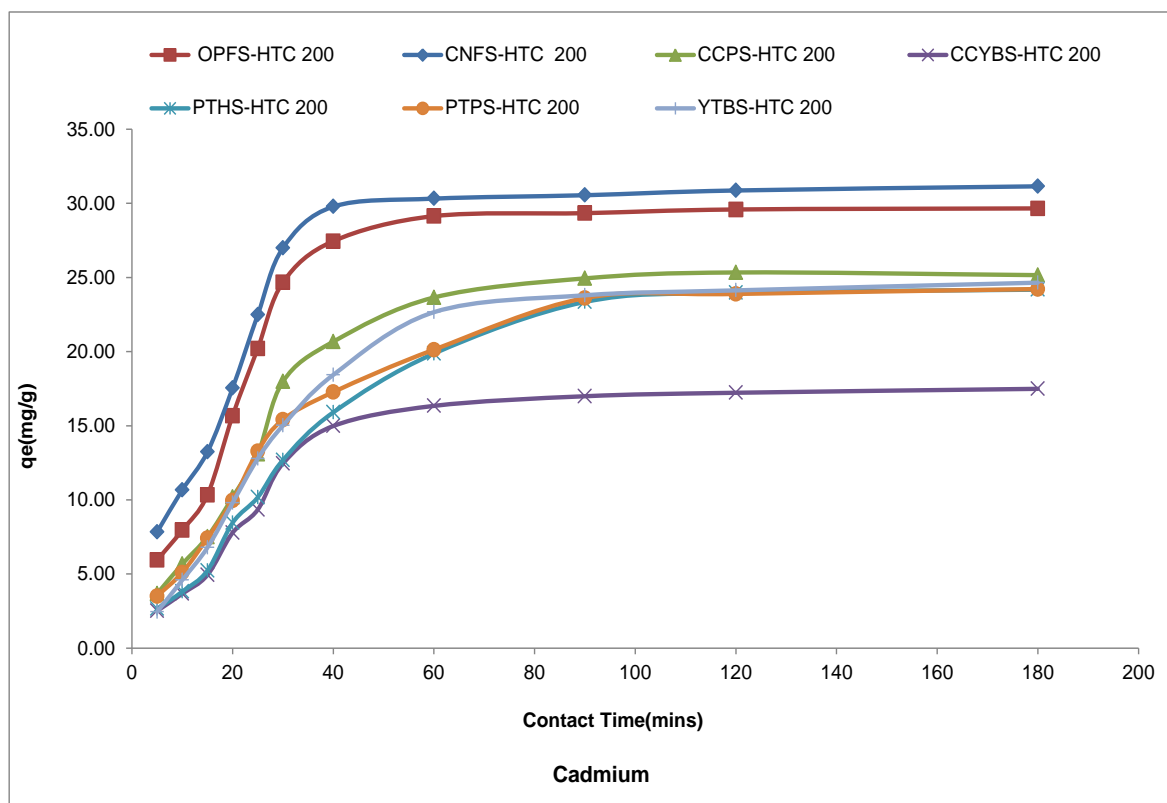
Figure 6.20: Kinetic profile for Cd (II) hydrothermal carbonised HTC200 adsorbents

The kinetic profile for Cd (II) using the two sets of HTC adsorbents shows a two stage metal ion uptake as seen in Figures 6.19 and 6.20. In the HTC170 adsorbents the first stage is rapid lasting up to 90 minutes and for the HTC200 adsorbents, the rapid loading stage ends at 60 minutes, thereafter there is a gradual loading of the Cd (II) ion till 180 minutes. This two-stage loading of metal ions have been attributed to the presence of vacant active sites on the surfaces of the adsorbents. This is because when sorption commences, the vacant sites are rapidly filled with the Cd (II) metal ion, thereafter the number of occupied sites increase while the number of vacant sites reduces. This limited site availability as sorption progresses results in a slower uptake of the incoming metal ions (Liu and Zhang 2011). In addition to this there exist inherent metal ion-metal ion repulsion between the loaded metal ion on the adsorbent surface and those in the aqueous solution further restricting the access to these sites thereby reducing the rate of uptake of these ions. A similar two stage adsorption reaction was reported by Liu and Zhang (2011) on the sorption of copper (II) ion by hydrochars produced from pinewood sawdust and rice husk at 300°C. Iqbal *et al*., (2009b) also reports this trend in a study involving metal ion loading using mango peel waste as an adsorbent. According to the report, a rapid uptake was observed up till 30 minutes after which the uptake was gradual till equilibrium was reached at 120 minutes. The kinetic profile of the two HTC adsorbents for Cd(II) ion sorption

indicates that optimum contact time for metal ion sorption can be taken as 60 and 90 minutes for the HCT200 and HTC170 adsorbents respectively.

6.5.1.1 Cadmium (II) ion kinetic modelling

Kinetic modelling has been used to examine the controlling mechanisms of adsorption process such as chemical reaction, diffusion control and mass transfer using a number of kinetic equations to test experimental data (Ozacar and Sengil, 2006). For the sorption of Cd(II) and Pb(II) ions onto the hydrothermally carbonised adsorbents, two kinetic models were evaluated and these are the pseudo-first order (PFO) and pseudo second order (PSO). To determine the goodness of fit of the kinetic models to the experimental data using non-linear regression, the optimization procedure requires that error functions be defined to enable the fitting of the model parameters with the experimental values. In this study, the coefficient of determination (r^2), the root mean square error (RMSE) and the Chi square test (χ^2) were used as error parameters for each model and these were determined based on eqns. 5.4, 5.5 and 5.6 which have been previously described in section 5.11 of chapter 5 in this study.

Kinetic modelling of Cd(II) ion sorption onto the HTC170 and HTC200 adsorbents were carried out based on the pseudo first order (PFO) and pseudo first order (PSO) equations using the solver add-in optimization procedure in Microsoft excel 2010 software. The plots of the PFO are PSO models for Cd(II) are presented in Figures 6.21 and 6.22 for HTC170 and Figures 6.23 and 6.24 for HTC200 adsorbents. From these models, the kinetic parameters and their respective error functions obtained are presented in Table 6.7 and 6.8 for the HTC170 and HTC200 adsorbents respectively. Figures 6.21-6.24 and Tables 6.7-6.8 confirms that the two models (PFO & PSO) could be used to characterise the kinetics of Cd(II) ion sorption and the prediction of each model for the kinetic parameter $(qe,_{model})$ is close to the result obtained from the experimental sorption of Cd(II) ion onto the different hydrothermally carbonised adsorbents.

For the PFO model the $q_{e,cal}$ obtained for the HTC170 adsorbents for Cd(II) ion sorption were in the range 14.0mgg^{-1} (CCYBS-HTC 170) to 26.8 mgg^{-1}(CNFS-HTC 170) with the order being CNFS-HTC 170 > OPFS-HTC 170 > YTBS-HTC 170 > CCPS-HTC 170 > PTHS-HTC 170 > PTPS-HTC 170 > CCYBS-HTC 170, thus implying that the CNFS-HTC 170 adsorbent had the highest loading with the least being the CCYBS-HTC 170 adsorbent. For the HTC200 adsorbents, the PFO model $q_{e,cal}$ obtained Cd(II) ion sorption were in the range 18.1mgg^{-1} (CCYBS-HTC 200) to 31.8 mgg^{-1}(CNFS-HTC 200) with the

order being CNFS-HTC 200 > OPFS-HTC 200 > CCPS-HTC 200 > PTHS-HTC 200 > YTBS-HTC 200 > PTPS-HTC 200 > CCYBS-HTC 200. From these two different types of hydrothermally carbonised adsorbents, it can be observed that the CCYBS-HTC 200 had the highest value for $q_{e,cal}$ from the PFO model, while the CCYBS-HTC 170 adsorbent had the least. The rate constant of the pseudo first order (PFO) reaction (K_1) for the HTC 170 adsorbents were in the range 2.29×10^{-2} min^{-1}(CCYBS-HTC 170) to 3.23×10^{-2} min^{-1}(OPFS-HTC 170), while that of the HTC 200 adsorbents were in the range 2.16×10^{-2} min^{-1}(PTHS-HTC 200) to 4.74×10^{-3} min^{-1}(CNFS-HTC 200).

The value of the coefficient of determination (r^2) and the two error parameters – the root mean square (RMSE) and Chi square (χ^2) were used to determine the Cd(II) ion uptake kinetics is best described by the PFO model. From Table 6.7 and 6.8, it is observed that for the HTC 170 adsorbents, the OPFS-HTC 170 adsorbent had an r^2 value of 0.99, while the CNFS-HTC 170, CCPS-HTC 170, CCYBS-HTC 170, PTHS-HTC 170 and PTPS-HTC 170 adsorbents had r^2 value of 0.98. The lowest r^2 value was 0.94 and obtained for the YTBS-HTC 170 adsorbent. These r^2 values indicates that the experimental data for the kinetics of Cd(II) ion sorption onto the OPFS-HTC 170 adsorbent is in close agreement what that of the PFO model. To further discriminate the best adsorbent that the PFO best fits, two error parameters- χ^2 and the RMSE values were used with the lowest values being an indication of best fitting. Based on this assumption, the sorption of Cd(II) ion onto the OPFS-HTC 170 adsorbent is best described by the PFO model with the lowest χ^2 (0.04) and RMSE (2.78×10^{-1}) values. For this adsorbent, the PFO rate constant (K_1) obtained was 3.23×10^{-2} min^{-1} and the PFO model Cd(II) ion loading ($q_{e,cal}$) was 19.6 mgg^{-1}.

For the HTC 200 adsorbents, r^2 value of 0.99 was obtained for the PTHS-HTC 200 and PTPS-HTC200 adsorbents while an r^2 value of 0.98 was obtained for the YTBS-HTC 200 adsorbent. The least r^2 value of 0.97 was obtained for the OPFS-HTC 200, CNFS-HTC 200,CCPS-HTC 200 and CCYBS-HTC 200 adsorbents. These r^2 values suggest that the sorption of Cd(II) ion onto these adsorbents were better represented by the PFO model for the PTHS-HTC 200 and PTPS-HTC 200 adsorbents. Further evaluation of the values of the error parameters (χ^2 and the RMSE) for these two adsorbents were used to determine which one was better described by the PFO model. From Table 6.8, it is observed that the PTPS-HTC200 adsorbent is best described by the PFO model with the lowest χ^2 (0.04) and RMSE (2.70×10^{-1}) values. For this adsorbent, the PFO rate constant (K_1) obtained was 2.84×10^{-2} min^{-1} and the Cd(II) ion loading ($q_{e,cal}$) for the PFO model was 24.9 mgg^{-1}. Comparing between the HTC170 and HTC200 adsorbents for Cd(II) ion sorption, it is

observed that the PTPS-HTC200 adsorbent was best described by the PFO model as it had the lowest values for the error parameters (χ^2 and the RMSE) and the highest r^2 value.

The PSO model was also used to evaluate the kinetics of Cd(II) ion sorption onto the HTC 170 and HTC 200 adsorbents and the results are also presented in Tables 6.7 and 6.8. From these table it can be observed that the PSO rate constant (K_2) for the HTC 170 adsorbents were in the range 1.08×10^{-3} $gmg^{-1}min^{-1}$(YTBS-HTC 170/CCYBS-HTC170) to 8.14×10^{-4} $gmg^{-1}min^{-1}$(CNFS-HTC170), while that of the HTC200 adsorbents were in the range 1.20×10^{-3} $gmg^{-1}min^{-1}$(OPFS-HTC200) to 8.96×10^{-4} $gmg^{-1}min^{-1}$(CCPS-HTC 200). The initial sorption rate (h) obtained from the PSO model as $q_t/t \rightarrow 0$ which gives an indication of the intial kinetic rate of sorption. For the HTC 170 te value of the initial sorption rate were in the order of CNFS-HTC170 > OPFS-HTC170 > CCPS-HTC170 > YTBS-HTC170 > PTHS-HTC170 > PTPS-HTC170 > CCYBS-HTC170 with the CNFS-HTC170 adsorbent having the highest value of $0.93mgg^{-1}min^{-1}$. For the HTC 200 adsorbents, the order for the initial sorption rate (h) was CNFS-HTC200 > OPFS-HTC200 > CCPS-HTC200 > PTPS-HTC200 > YTBS-HTC200 > CCYBS-HTC200 > PTHS-HTC200 with the CNFS-HTC200 having the highest value of $2.05mgg^{-1}min^{-1}$. Comparing the initial adsorption rate for the HTC170 and HTC 200 adsorbents shows that the HTC 200 adsorbents had higher values for the initial adsorption rate than the HTC170 adsorbents.

The maximum loading $q_{e,cal}$ obtained from the PSO model for Cd(II) ion sorption onto the HTC 170 adsorbents were in the range 18.4 mgg^{-1} (CCYBs-HTC170) to 33.8 mgg^{-1}(CNFS-HTC170) with the order being CNFS-HTC170 > YTBS-HTC170 > OPFS-HTC170 > CCPS-HTC170 = PTPS-HTC170 > PTHS-HTC170 > CCYBS-HTC170, while that of the HT200 adsorbents were in the range 22.5 mgg^{-1} (CCYBS-HTC200) to 37.1 mgg^{-1}(CNFS-HTC200) with the order being CNFS-HTC200 > OPFS-HTC200 > PTHS-HTC200 > CCPS-HTC200 > YTBS-HTC200 > PTPS-HTC200 > CCYBS-HTC200 implying that the CNFS-HTC200 adsorbent had the highest Cd(II) ion loading.

Table 6.7: PFO & PSO modelling parameters for Cd(II) sorption on HTC-170 adsorbents

Adsorbent	Pseudo First Order Model					Pseudo Second Order					
	$q_{e,cal}$(mgg^{-1})	K_1(min^{-1})	r^2	χ^2	RMSE	$q_{e,cal}$(mgg^{-1})	K_2(gmg^{-1}min^{-1})	h(mgg^{-1}min^{-1})	r^2	χ^2	RMSE
OPFS-HTC 170	19.6	3.23E-02	0.99	0.04	2.78E-01	24.2	1.33E-03	0.78	0.98	0.08	4.86E-01
CNFS-HTC 170	26.8	2.89E-02	0.98	0.10	7.81E-01	33.8	8.14E-04	0.93	0.96	0.19	1.58E+00
CCPS-HTC 170	17.2	3.21E-02	0.98	0.06	3.21E-01	21.3	1.49E-03	0.68	0.97	0.11	5.83E-01
CCYBS-HTC 170	14.0	2.29E-02	0.98	0.05	1.82E-01	18.4	1.08E-03	0.37	0.97	0.09	3.44E-01
PTHS-HTC 170	16.7	2.87E-02	0.98	0.08	3.81E-02	21.2	1.27E-03	0.57	0.96	0.14	6.98E-01
PTPS-HTC 170	16.2	2.31E-02	0.98	0.06	2.57E-01	21.3	9.53E-04	0.43	0.97	0.10	4.36E-01
YTBS-HTC 170	19.2	2.88E-02	0.94	0.25	1.43E+00	24.5	1.08E-03	0.65	0.91	0.36	2.08E+00

Table 6.8: PFO & PSO modelling parameters for Cd(II) sorption on HTC-200 adsorbents

Adsorbent	Pseudo First Order Model					Pseudo Second Order					
	$q_{e,cal}(mgg^{-1})$	$K_1(min^{-1})$	r^2	χ^2	RMSE	$q_{e,cal}(mgg^{-1})$	$K_2(gmg^{-1}min^{-1})$	$h(mgg^{-1}min^{-1})$	r^2	χ^2	RMSE
OPFS-HTC 200	30.7	4.06E-03	0.97	0.18	1.90E+00	36.7	1.20E-03	1.61	0.93	0.34	3.62E+00
CNFS-HTC 200	31.8	4.74E-03	0.97	0.13	1.51E+00	37.1	1.48E-03	2.05	0.94	0.27	3.12E+00
CCPS-HTC 200	26.4	3.04E-02	0.97	0.13	1.07E+00	33.0	8.96E-04	0.98	0.95	0.25	2.01E+00
CCYBS-HTC 200	18.1	3.18E-02	0.97	0.11	6.00E-01	22.5	1.38E-03	0.70	0.94	0.19	1.07E+00
PTHS-HTC 200	25.9	2.16E-02	0.99	0.07	4.94E-01	34.4	5.39E-04	0.64	0.97	0.15	1.02E+00
PTPS-HTC 200	24.9	2.84E-02	0.99	0.04	2.70E-01	31.2	8.78E-04	0.86	0.98	0.09	6.90E-01
YTBS-HTC 200	25.7	2.74E-02	0.98	0.09	6.73E-01	32.7	7.77E-04	0.83	0.96	0.19	1.42E+00
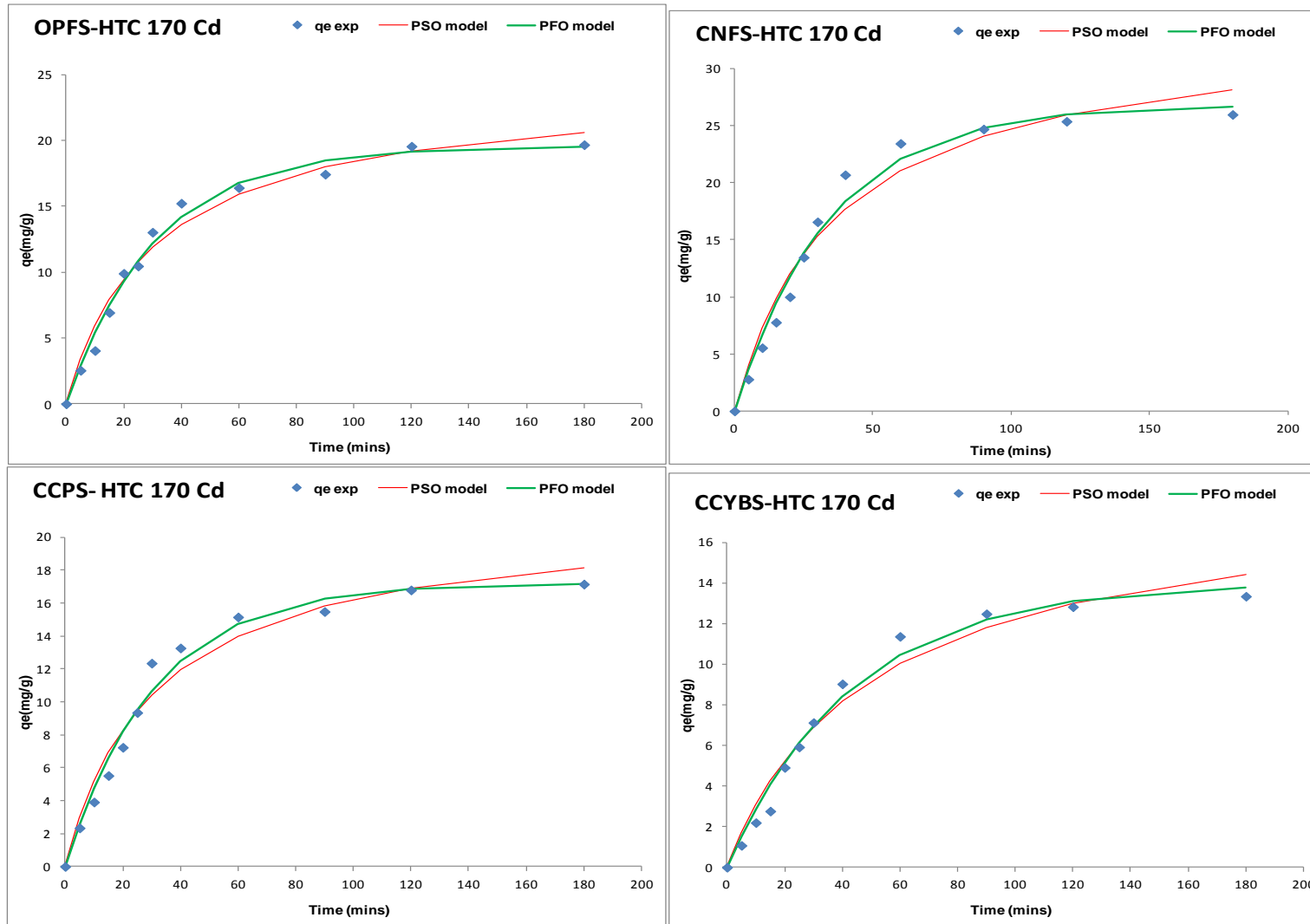
Fig 6.21: Cd(II) ion PFO & PSO sorption kinetic models for OPFS,CNFS, CCPS & CCYBS-HTC 170 adsorbents
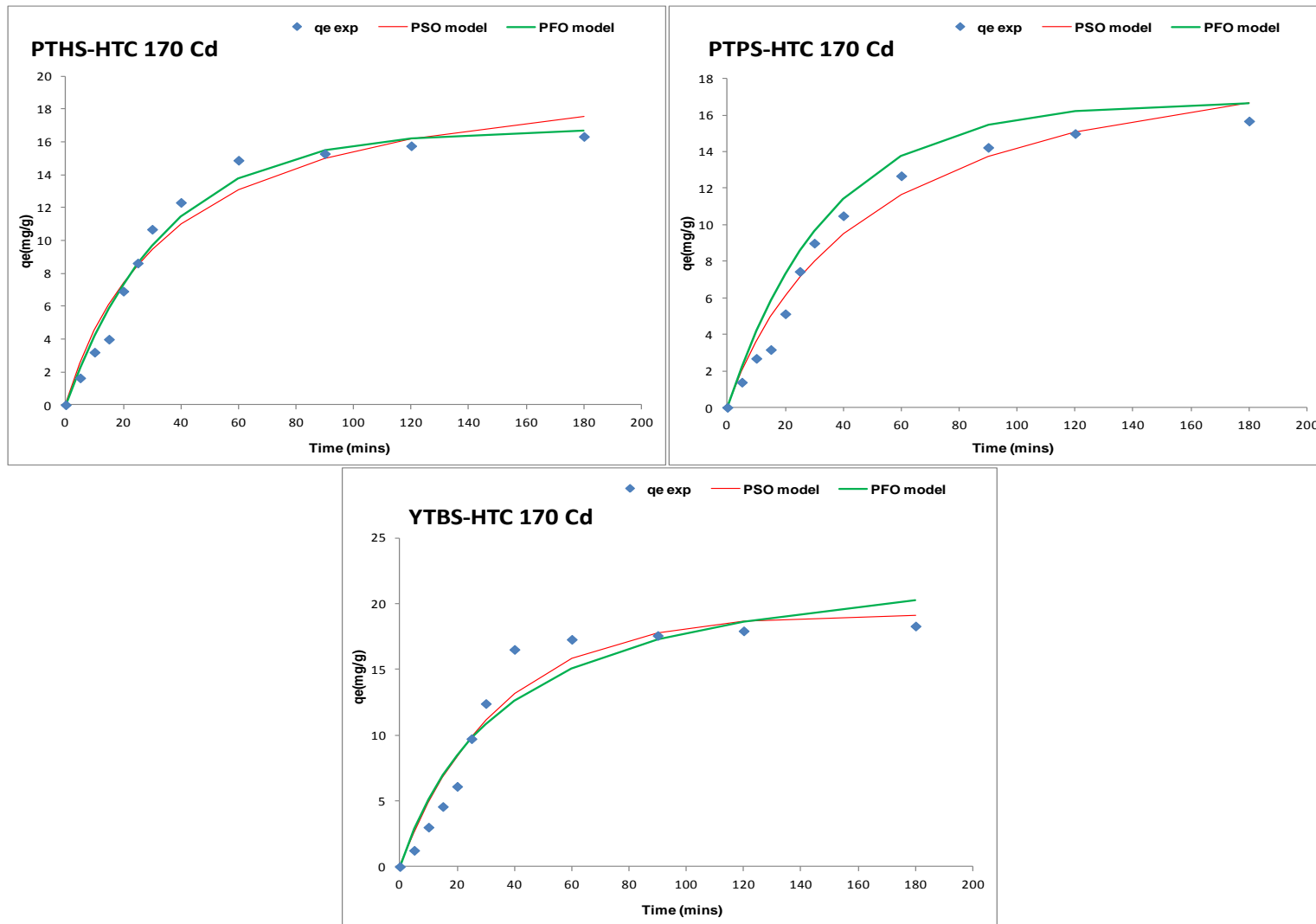
Fig 6.22: Cd(II) ion PFO & PSO sorption kinetic models for PTHS, PTPS & YTBS-HTC 170 adsorbents
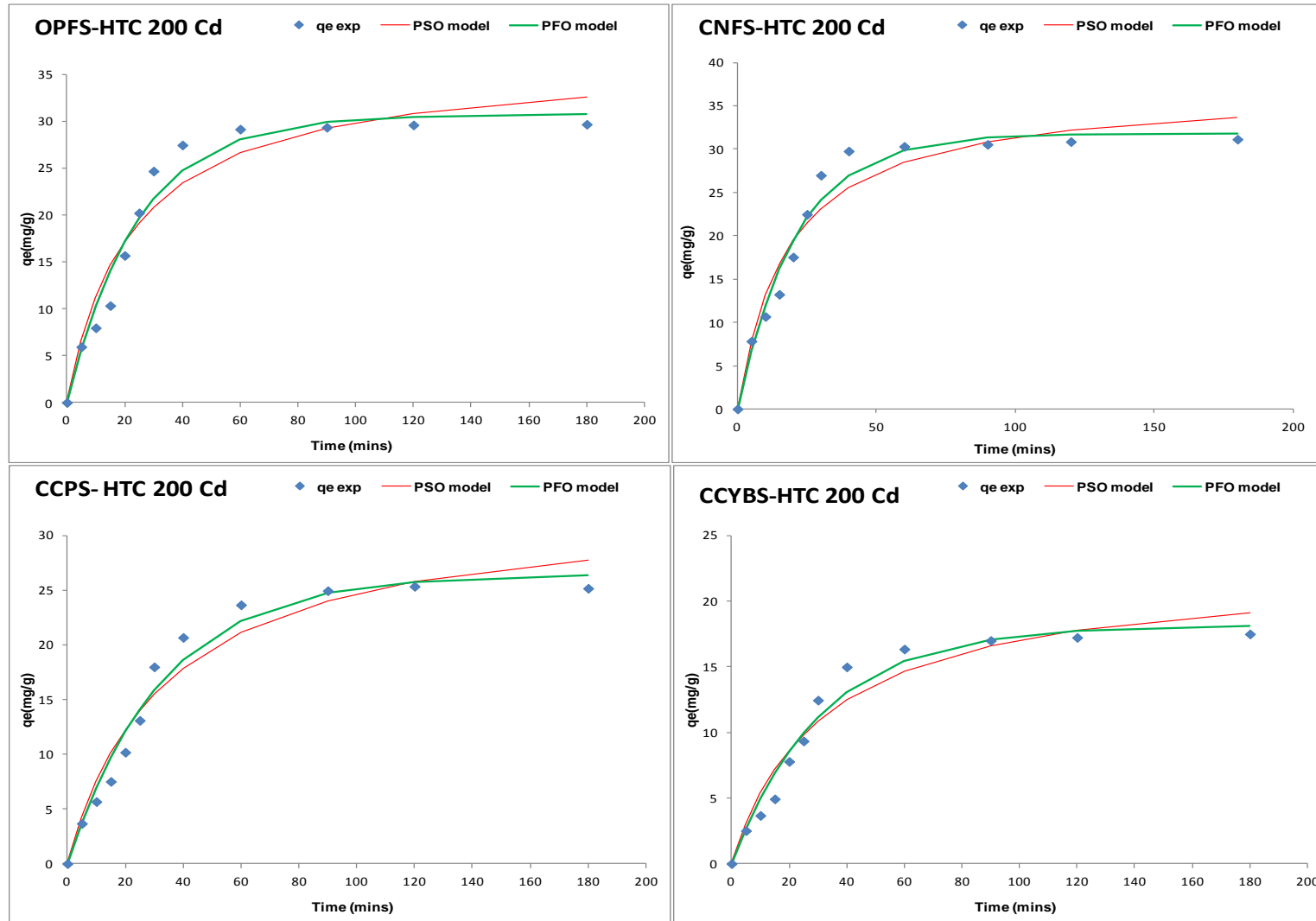
Fig 6.23: Cd(II) ion PFO & PSO sorption kinetic models for OPFS,CNFS, CCPS & CCYBS-HTC 200 adsorbents
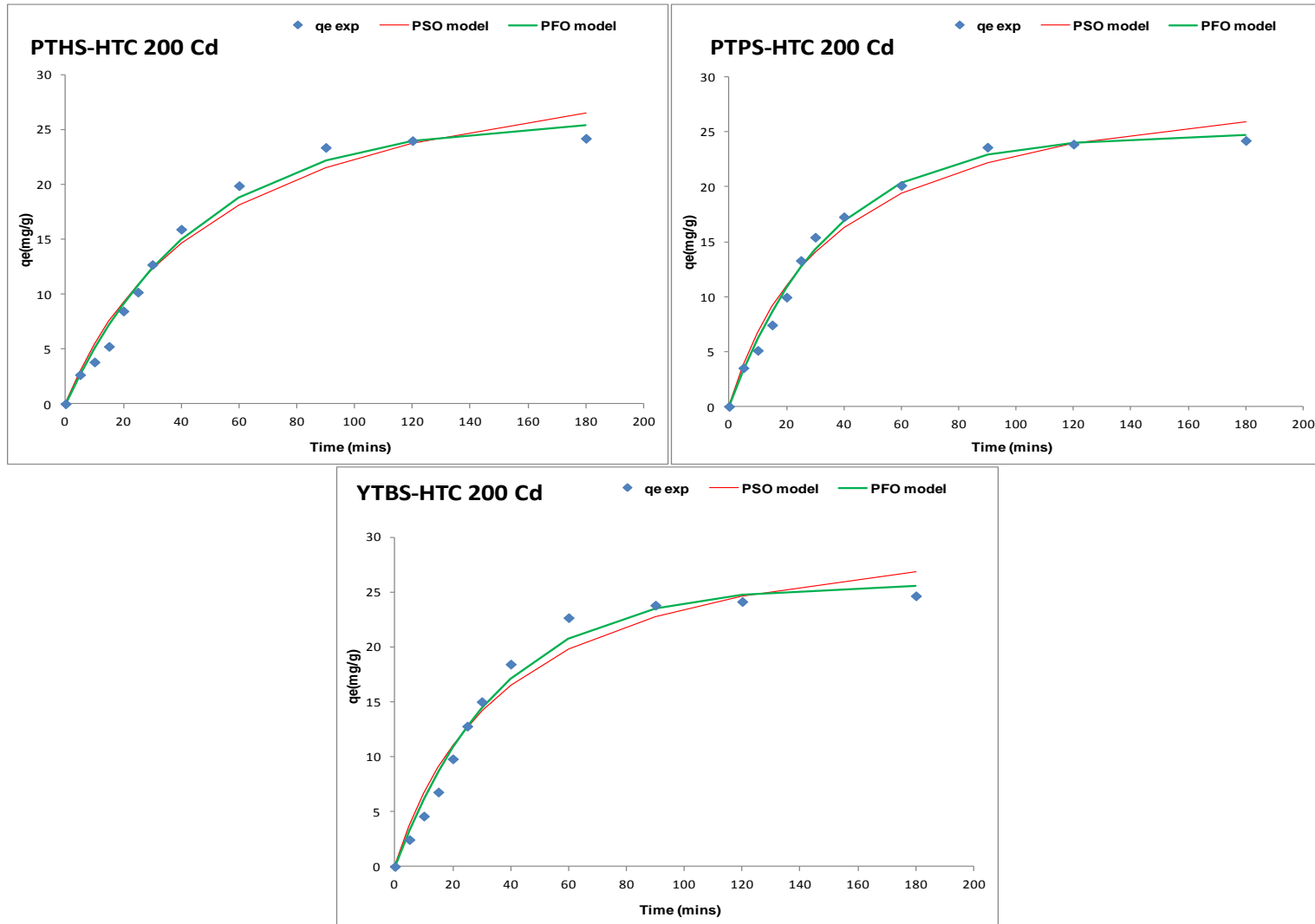
Fig 6.24: Cd(II) ion PFO & PSO sorption kinetic models for PTHS, PTPS & YTBS-HTC 200 adsorbents

The value of the coefficient of determination and the two error parameters – the root mean square (RMSE) and Chi square (χ^2) were used to determine the adsorbent whose kinetics of Cd(II) sorption is best described by the PSO model. The value of these error parameters in Table 6.7 and 6.8 shows that there variations in the r^2 values for the HTC170 and HTC200 adsorbents. For the HTC170 adsorbents, four sets of r^2 values were obtained, the first was the highest value of 0.99 obtained for the OPFS-HTC170 adsorbent. The second was 0.97 for CCPS-HTC170, CCYBS-HTC170 and PTPS-HTC170 adsorbents; the third was 0.96 for the CNFS-HTC170 and PTHS-HTC 170 adsorbents while the final value of 0.91 was for the YTBS-HTC170 adsorbent. For the HTC200 adsorbents, the r^2 values obtained were 0.98(PTPS-HTC200), 0.97(PTHS-HTC200), 0.96(YTBS-HTC200), 0.95(CCPS-HTC200), 0.94(CNFS-HTC 200 and CCYBS-HTC 200) and 0.93(OPFS-HTC200). To further discriminate the adsorbent that is best described by the PSO model, consideration was given to the values of the two error parameters- the χ^2 and the RMSE. The adsorbent with the lowest values for these two parameters was thereafter chosen as the best described by the PSO model. For the HTC170 adsorbents, based on the values for these two error parameters in Table 6.7, the OPFS-HTC170 adsorbent uptake of Cd(II) ion is best described by the PSO model with the lowest χ^2 (0.08) and RMSE (4.86 $\times10^{-1}$) values. The PSO rate constant (K_2) obtained for this adsorbent was 1.33 $\times10^{-3}$ gmg^{-1}min^{-1} and the PSO model metal ion loading ($q_{e,cal}$) was 24.2 mgg^{-1}. For the HTC200 adsorbents, based on the error parameter comparison from the results in Table 6.8, the PTPS-HTC200 adsorbent uptake of Cd(II) ion is best described by the PSO model with the lowest χ^2 (0.09) and RMSE (6.90 $\times10^{-1}$) values. The PSO rate constant (K_2) obtained for this adsorbent was 8.78 $\times10^{-4}$ gmg^{-1}min^{-1} and the PSO model metal ion loading ($q_{e,cal}$) was 31.2 mgg^{-1}. A comparison of the PSO values for r^2 and the two error parameters between the HTC170 and HTC200 adsorbents for Cd(II) ion sorption, indicates that the OPFS-HTC170 adsorbent was best described by the PSO model as it had the lowest values for the error parameters (χ^2 and the RMSE) and the highest r^2 value.

Futhermore, to determine which of the two kinetic models (PFO or PSO) gives the best description of Cd(II) sorption kinetics onto the HTC170 and HTC200 adsorbents an examination of the $q_{e,cal}$ values obtained for the PFO and PSO models is used to compare with the experimental q_e value obtained at the end of sorption (after 180 mins) also called q_t. The assumption is that the model with $q_{e,cal}$ values that are closer to the experimental obtained q_e is the model that describes the Cd(II) ion sorption better. Table 6.9 presents the

q_e for both experimental sorption and kinetic models for Cd(II) ion uptake by the HTC170 and HTC200 adsorbents.

Table 6.9: Comparison of q_e values for experiment and model sorption for Cd(II) onto hydrothermally carbonised adsorbents

Adsorbent	q_e (mgg^{-1})		
	Experiment	PFO model	PSO model
OPFS-HTC 200	29.7	30.7	36.7
CNFS-HTC 200	31.2	31.8	37.1
CCPS-HTC 200	25.2	26.4	33.0
CCYBS-HTC 200	17.5	18.1	22.5
PTHS-HTC 200	24.2	25.9	34.4
PTPS-HTC 200	24.2	24.9	31.2
YTBS-HTC 200	24.7	25.7	32.7
OPFS-HTC 170	19.7	19.6	24.2
CNFS-HTC 170	26.0	26.8	33.8
CCPS-HTC 170	17.2	17.2	21.3
CCYBS-HTC 170	13.3	14.0	18.4
PTHS-HTC 170	16.3	16.7	21.2
PTPS-HTC 170	15.7	16.2	21.3
YTBS-HTC 170	18.3	19.2	24.5

From Table 6.9, it is observed that the values for $q_{e\,model}$ for both PFO and PSO models were close to the experimental (q_e) for both HTC170 and HTC200 adsorbents. However, the PFO model for some of the adsorbents gave a closer q_e value to the experimental sorption q_e than the PSO. The PSO mainly gave values that were an overestimate of the experimental qe while that of the PFO was for some adsorbents an underestimation of the experimental q_e. Further evaluation of the values for error parameters (χ^2 and the RMSE) and correlation coefficient (r^2) in Table 6.7 and 6.8 for the two sets of adsorbents indicates that the PFO model had lower values for both error parameters and higher r^2. Thus, it can be said that the PFO model gave a better approximation of the kinetics of Cd(II) sorption by the HTC170 and HTC200 adsorbents than the PSO order model.This implies that the kinetics supports the assumption that the rate limiting step of Cd(II) ion sorption onto the Na_2CO_3 and K_2CO_3 chemically activated adsorbents is dependent on the concentration of the Cd(II) ions in the adsorbate (Azizian, 2004; Liu and Liu, 2008). However, the closeness of the parameters obtained from the PSO model may also indicate that chemical interactions between the ions in the adsorbate solution and the adsorbent may still

influence sorption kinetics but this may depend on the rate of diffusion.This implies that pore diffusivity of the ions onto the active sites may also influence the kinetics as previously discussed in the analysis of the two stage metal uptake (fast and slow) kinetics of Cd(II) ion sorption.

Studies have been reported on the application of the PFO and PSO models for the characterisation of the kinetics of Cd(II) ion sorption using hydrothermally carbonised adsorbents. Elaigwu *et al.,* (2014) has reported on the removal of Cd(II) ions from aqueous solutions using microwave-assisted hydrothermal carbonised *Prosopis africana* shell. In their study, the PSO model gave a better fitting for the sorption of Cd(II) than the PFO model based on higher values of the correlation coefficient(r^2). The kinetics of sorption of Cd(II) ions onto hydrochars produced from different feedstocks (sawdust, wheatstraw and corn stalk) has also been reported by Sun *et al.,* (2015). In their study the pseudo-second order (PSO) equation was used to model the kinetics of Cd(II) sorption uisng the r^2 value as fitting parameter and the results indicated that the PSO model was able to represent metal ion sorption with r^2 value in the range 0.89-0.99.

6.5.2 Lead (II) ion sorption

The removal of Pb (II) ions from aqueous solution using both hydrothermal carbonized adsorbents HTC170 and HTC200 was also carried out as shown in Section 6.5 and the kinetic studies obtained for Pb (II) sorption are shown in Figure 6.25 for HTC170 adsorbents and Figure 6.26 for the HTC200 adsorbents. For the HTC170 adsorbents, the maximum loadings obtained were; 15.7 mgg^{-1} (OFFS-HTC170), 19.0 mgg^{-1} (CNFS-HTC170), 16.6 mgg^{-1} (CCPS-HTC170), 12.2 mgg^{-1} (CCYBS-HTC170), 14.8 mgg^{-1} (PTHS-HTC170), 14.5 mgg^{-1}(PTPS-HTC170) and 16.7 mgg^{-1} (YTBS-HTC170). The loading for the HTC200 adsorbents were observed to be higher than those of the HTC170 adsorbents with values of 23.41 mgg^{-1} (OPFS-HTC200), 26.75 mgg^{-1} (CNFS-HTC200), 23.41 mgg^{-1} (CCPS-HTC200), 16.67 mgg^{-1} (CCYBS-HTC200), 23.34 mgg^{-1} (PTHS-HTC200), 22.17 mgg^{-1} (PTPS-HTC200) and 21.35 mgg^{-1} for YTBS-HTC200 adsorbent. The trend in the loading for these two groups of adsorbent may be associated with their surface area and pore characteristics as the HTC200 adsorbents have higher surface area than the HTC170 adsorbents. Figure 6.25 and Figure 6.26 shows that the kinetic profile for Pb (II) ion loading on both sets of adsorbents occurred via two steps: the first was a rapid loading from initial contact up till 90 minutes for HTC170 and HTC200 adsorbents and the

second stage which continued slowly up till 180 minutes when equilibrium was attained. This two-stage kinetic profile may also be linked to the amount of active sites present on the adsorbent at any time interval as previously mentioned in the case of Cd (II).
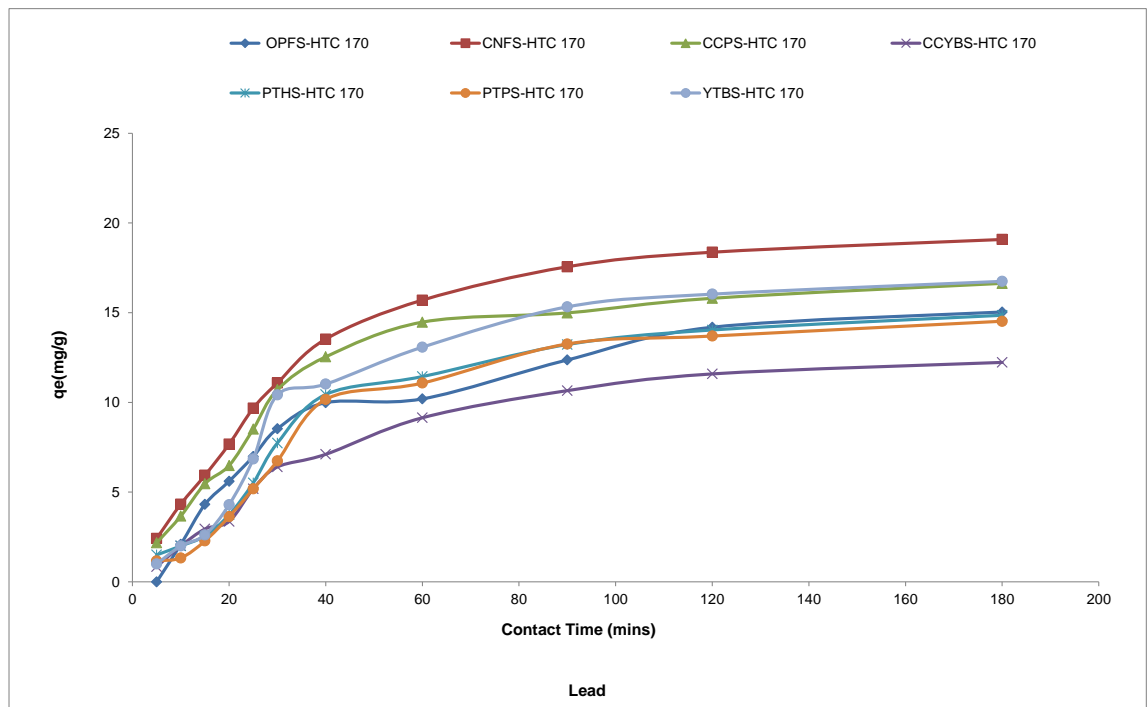
Figure 6.25: Kinetic profile for Pb(II) hydrothermal carbonised HTC170 adsorbents
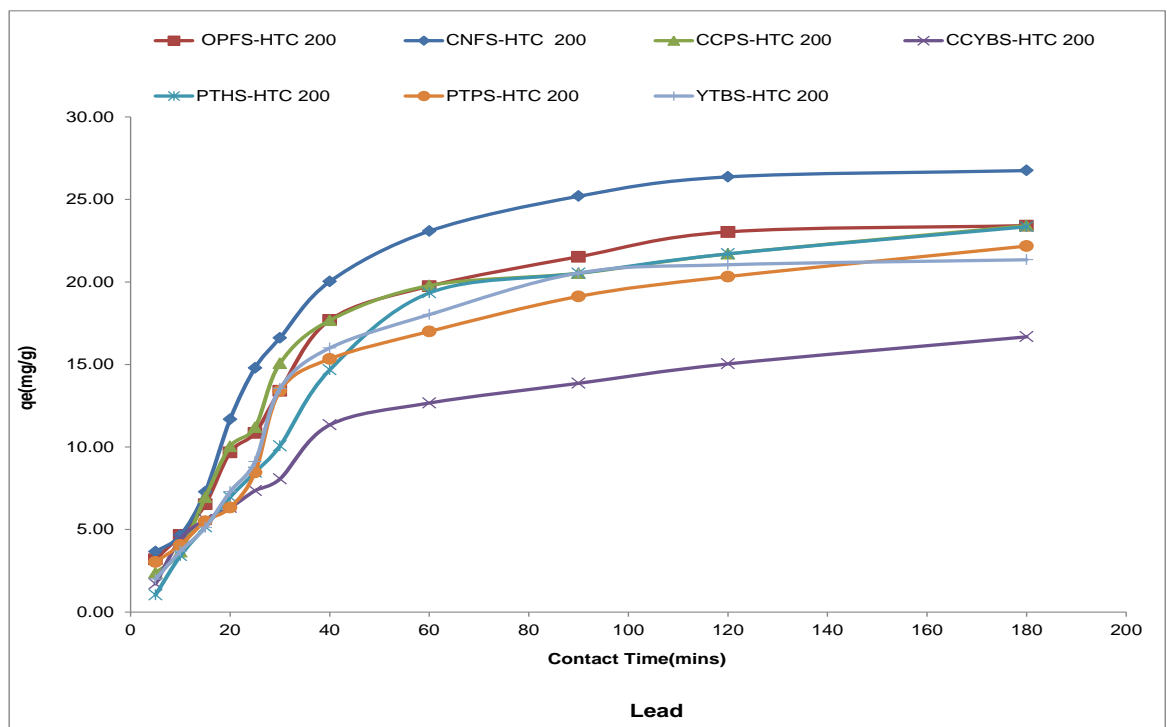
Figure 6.26: Kinetic profile for Pb (II) ion hydrothermal carbonised HTC200 adsorbents

The findings by Ibrahim *et al*., (2010) while investigating the use of novel agricultural waste adsorbents for the removal of Pb (II) ions from aqueous solution suggest a similar trend as the rapid stage in the study lasted for 60 minutes while the slow stage proceeded to 360 minutes when equilibrium was attained. Hence 90 minutes can be taken as the optimum sorption time for Pb (II) ion removal using these two hydrothermal carbonised adsorbents.

6.5.2.1 Lead (II) ion kinetic modelling

To gain better insight into the adsorption process, kinetic modelling of Pb(II) sorption by the hydrothermally carbonised adsorbents (HTC170 & HTC200) was also evaluated to determine which mechanism may determine the metal ion uptake process. This was carried out using the pseudo first order (PFO) and pseudo first order (PSO) equations based on the solver add-in optimization procedure in Microsoft excel 2010 software. The plots of the PFO are PSO models for Pb(II) are presented in Figures 6.27 and 6.28 for HTC170 and Figures 6.28 and 6.29 for the HTC200 adsorbents. From these models, the kinetic parameters and their respective error functions obtained are presented in Table 6.10 and 6.11 for the HTC170 and HTC200 adsorbents respectively. These results presented in Figures 6.27-6.29 and Tables 6.10-6.11 confirms that the two models (PFO & PSO) could be used to characterise the kinetics of Pb(II) ion sorption and the prediction of each model for the kinetic parameter ($q_{e,model}$) is close to the result obtained from the experimental analysis of Pb(II) ion sorption.

For the PFO model the $q_{e,cal}$ obtained for the HTC170 adsorbents for Pb(II) ion sorption were in the range 12.7mgg^{-1} (CCYBS-HTC170) to 19.3 mgg^{-1}(CNFS-HTC170) with the order being CNFS-HTC170 > YTBS-HTC170 > CCPS-HTC170 > PTHS-HTC170 > PTPS-HTC170 > OPFS-HTC170 > CCYBS-HTC170 thus implying that the CNFS-HTC 170 adsorbent had the highest loading with the least being the CCYBS-HTC 170. For the HTC200 adsorbents, the PFO model $q_{e,cal}$ obtained Pb(II) ion sorption were in the range 16.1mgg^{-1} (CCYBS-HTC200) to 27.4 mgg^{-1}(CNFS-HTC200) with the order being CNFS-HTC200 > PTHS-HTC200 > OPFS-HTC200 > CCPS-HTC200 > YTBS-HTC200 > PTPS-HTC200 > CCYBS-HTC200. From these two hydrothermally carbonised adsorbents, it can be observed that the CNFS-HTC200 had the highest value for $q_{e,cal}$ from the PFO model, while the CCYBS-HTC170 adsorbent had the least. The rate constant of the pseudo first order (PFO) reaction (K_1) for the HTC170 adsorbents were in the range

1.84×10^{-2} min^{-1}(PTPS-HTC170) to 3.04× 10^{-2} min^{-1}(OPFS-HTC170), while that of the HTC200 adsorbents were in the range 1.93 ×10^{-2} min^{-1}(PTHS-HTC200) to 2.89 × 10^{-2} min^{-1}(CCPS-HTC200).

The value of the coefficient of determination (r^2) and the two error parameters – the root mean square (RMSE) and Chi square (χ^2) were used to determine the Pb(II) ion uptake kinetics is best described by the PFO model. From Table 6.10, it is observed that for the HTC170 adsorbents, the OPFS-HTC170, CNFS-HTC170, CCPS-HTC170 and CCYBS-HTC 170 had the same r^2 value of 0.99. The PTHS-HTC170 adsorbent had an r^2 value of 0.97, while the PTPS-HTC 170 and YTBS-HTC 170 adsorbents had r^2 value of 0.96. These r^2 values indicates that the experimental data for the kinetics of Pb(II) ion sorption onto the OPFS-HTC170,CNFS-HTC170,CCPS-HTC170 and CCYBS-HTC 170adsorbents are in close agreement what that of the PFO model. To further discriminate amongst these four adsorbents with the highest r^2 values, the error parameters- χ^2 and the RMSE were used with the lowest values being an indication of best fitting. Based on this assumption, the sorption of Pb(II) ion onto the CNFS-HTC170 adsorbent is best described by the PFO model with the lowest χ^2 (0.01) and RMSE (5.66 ×10^{-2}) values. For this adsorbent, the PFO rate constant (K$_1$) obtained was 2.75 ×10^{-2} min^{-1} and the PFO model Cd(II) ion loading (q$_{e,cal}$) was 19.3 mgg^{-1}.

For the HTC200 adsorbents, r^2 value of 0.99 was obtained for the CNFS-HTC200, CCYBS-HTC200 and OPFS-HTC200 adsorbents while the CCPS-HTC200 and PTHS-HTC200 adsorbents had an r^2 value of 0.98. The lowest r^2 value was obtained for the PTPS-HTC200 and YTBS-HTC200 adsorbents. These r^2 values suggest that the sorption of Pb(II) ion onto these adsorbents were better represented by the PFO model for the CNFS-HTC200, CCYBS-HTC200 and OPFS-HTC200 adsorbents. Further evaluation of the values of the error parameters (χ^2 and the RMSE) for these three adsorbents were used to determine which one was best described by the PFO model. From Table 6.11, it is observed that the CCYBS-HTC200 adsorbent is best described by the PFO model with the lowest χ^2 (0.03) and RMSE (1.28×10^{-1}) values. For this adsorbent, the PFO rate constant (K$_1$) obtained was 2.58 ×10^{-2} min^{-1} and the Pb(II) ion loading (q$_{e,cal}$) for the PFO model was 16.1 mgg^{-1}. Comparing between the HTC170 and HTC200 adsorbents for Pb(II) ion sorption, it is observed that the CNFS-HTC170 adsorbent was best described by the PFO model as it had the lowest values for the error parameters (χ^2 and the RMSE) and the highest r^2 value.

Table 6.10: PFO & PSO modelling parameters for Pb(II) sorption on HTC-170 adsorbents

Adsorbent	Pseudo First Order Model					Pseudo Second Order					
	$q_{e,cal}(mgg^{-1})$	$K_1(min^{-1})$	r^2	χ^2	RMSE	$q_{e,cal}(mgg^{-1})$	$K_2(gmg^{-1}min^{-1})$	$h(mgg^{-1}min^{-1})$	r^2	χ^2	RMSE
OPFS-HTC 170	15.4	3.04E-02	0.99	0.02	7.80E-02	19.0	1.62E-03	0.59	0.99	0.01	6.93E-02
CNFS-HTC 170	19.3	2.75E-02	0.99	0.01	5.66E-02	24.3	1.08E-03	0.64	0.99	0.04	2.37E-01
CCPS-HTC 170	16.6	2.90E-02	0.99	0.04	1.89E-01	20.8	1.39E-02	0.60	0.97	0.08	3.93E-01
CCYBS-HTC 170	12.7	2.00E-02	0.99	0.02	6.20E-02	17.1	9.90E-04	0.28	0.98	0.04	1.13E-01
PTHS-HTC 170	15.7	1.99E-02	0.97	0.11	4.36E-01	21.2	7.73E-04	0.35	0.95	0.15	5.99E-01
PTPS-HTC 170	15.6	1.84E-02	0.96	0.13	4.94E-01	21.6	6.77E-04	0.32	0.95	0.17	6.68E-01
YTBS-HTC 170	17.7	2.06E-02	0.96	0.16	7.49E-01	23.9	7.15E-04	0.41	0.94	0.21	9.92E-01

Table 6.11: PFO & PSO modelling parameters for Pb(II) sorption on HTC-200 adsorbents

	Pseudo First Order Model					Pseudo Second Order					
Adsorbent	$q_{e,cal}$(mgg^{-1})	K_1(min^{-1})	r^2	χ^2	RMSE	$q_{e,cal}$(mgg^{-1})	K_2(gmg^{-1}min^{-1})	h(mgg^{-1}min^{-1})	r^2	χ^2	RMSE
OPFS-HTC 200	24.0	2.66E-02	0.99	0.05	3.64E-01	30.6	8.11E-04	0.76	0.98	0.11	7.73E-01
CNFS-HTC 200	27.4	2.85E-02	0.99	0.08	6.23E-01	34.6	7.83E-04	0.94	0.97	0.16	1.29E+00
CCPS-HTC 200	23.2	2.89E-02	0.98	0.10	6.89E-01	29.3	9.28E-04	0.80	0.96	0.16	1.11E+00
CCYBS-HTC 200	16.1	2.58E-02	0.99	0.03	1.28E-01	20.5	1.20E-03	0.50	0.99	0.03	1.13E-01
PTHS-HTC 200	24.7	1.93E-02	0.98	0.10	6.50E-01	33.6	4.67E-04	0.53	0.97	0.16	1.03E+00
PTPS-HTC 200	22.3	2.32E-02	0.97	0.12	7.43E-01	29.1	7.09E-04	0.60	0.96	0.16	9.59E-01
YTBS-HTC 200	22.5	2.46E-02	0.97	0.12	7.83E-01	29.2	7.51E-04	0.64	0.95	0.20	1.29E+00
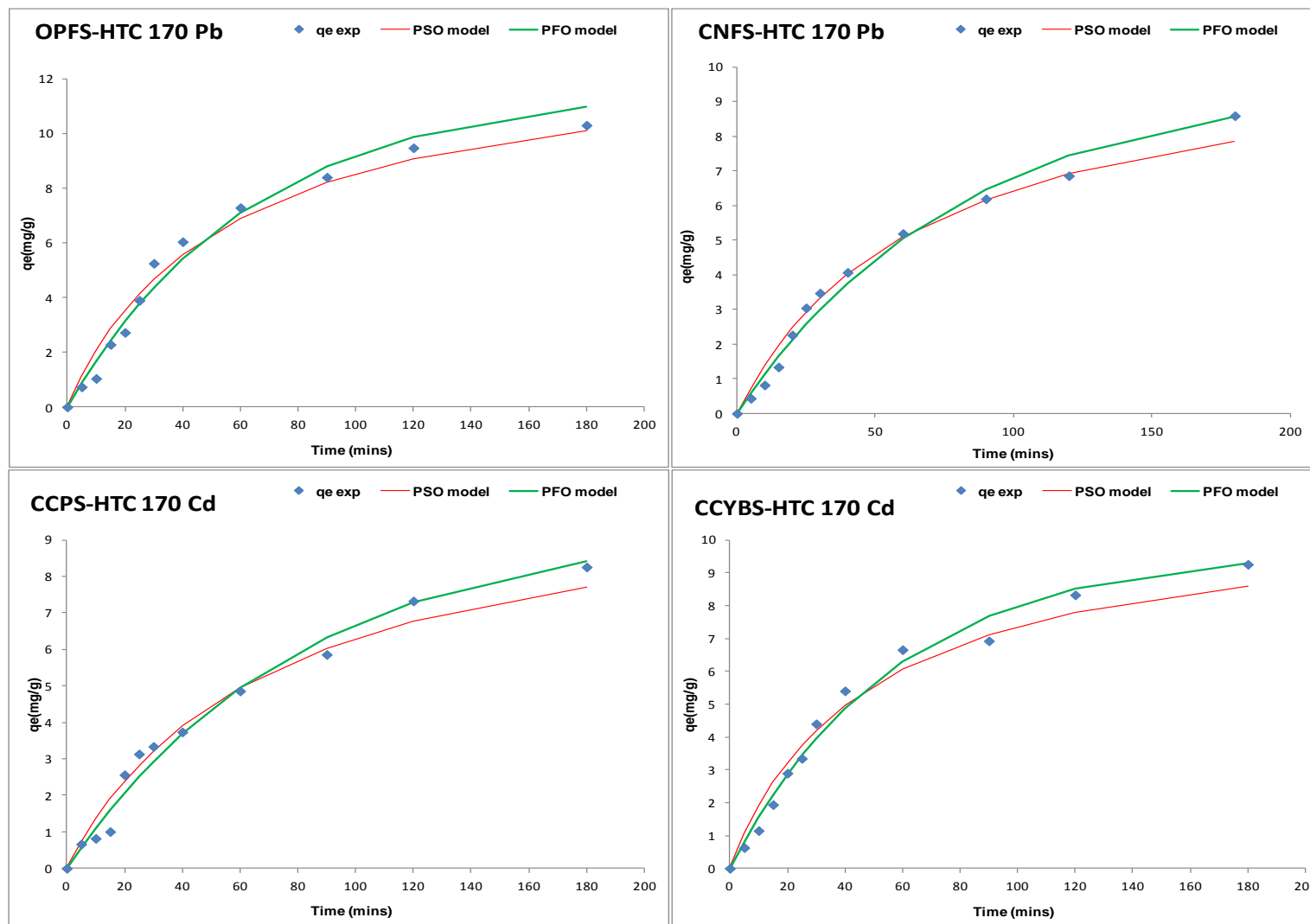
Fig 6.27: Pb(II) ion PFO & PSO sorption kinetic models for OPFS-HTC170,CNFS-HTC 170, CCPS-HTC170 & CCYBS-HTC 170 adsorbents
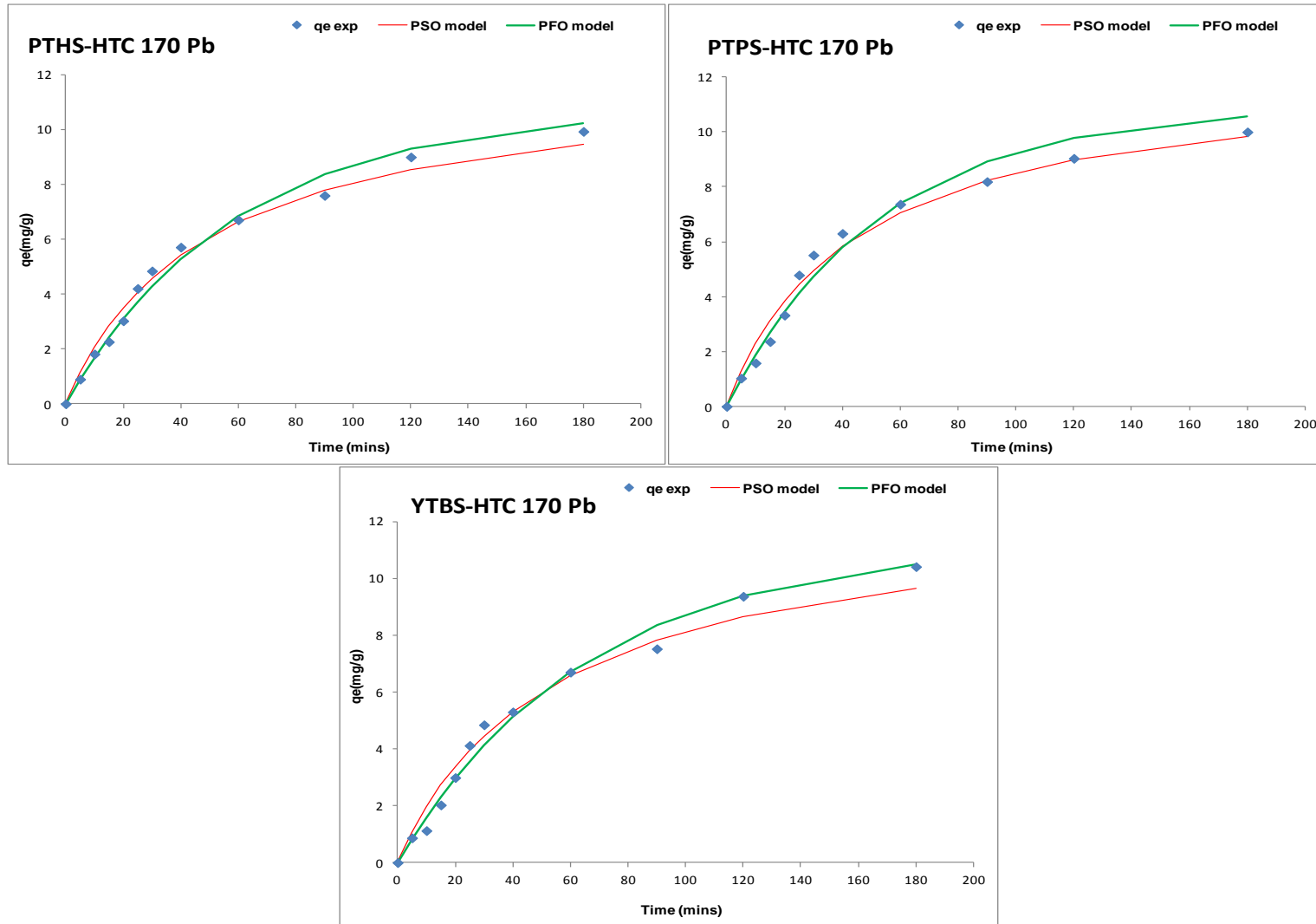
Fig 6.28: Pb(II) ion PFO & PSO sorption kinetic models for PTHS-HTC170, PTPS-HTC 170 & YTBS-HTC 170 adsorbents
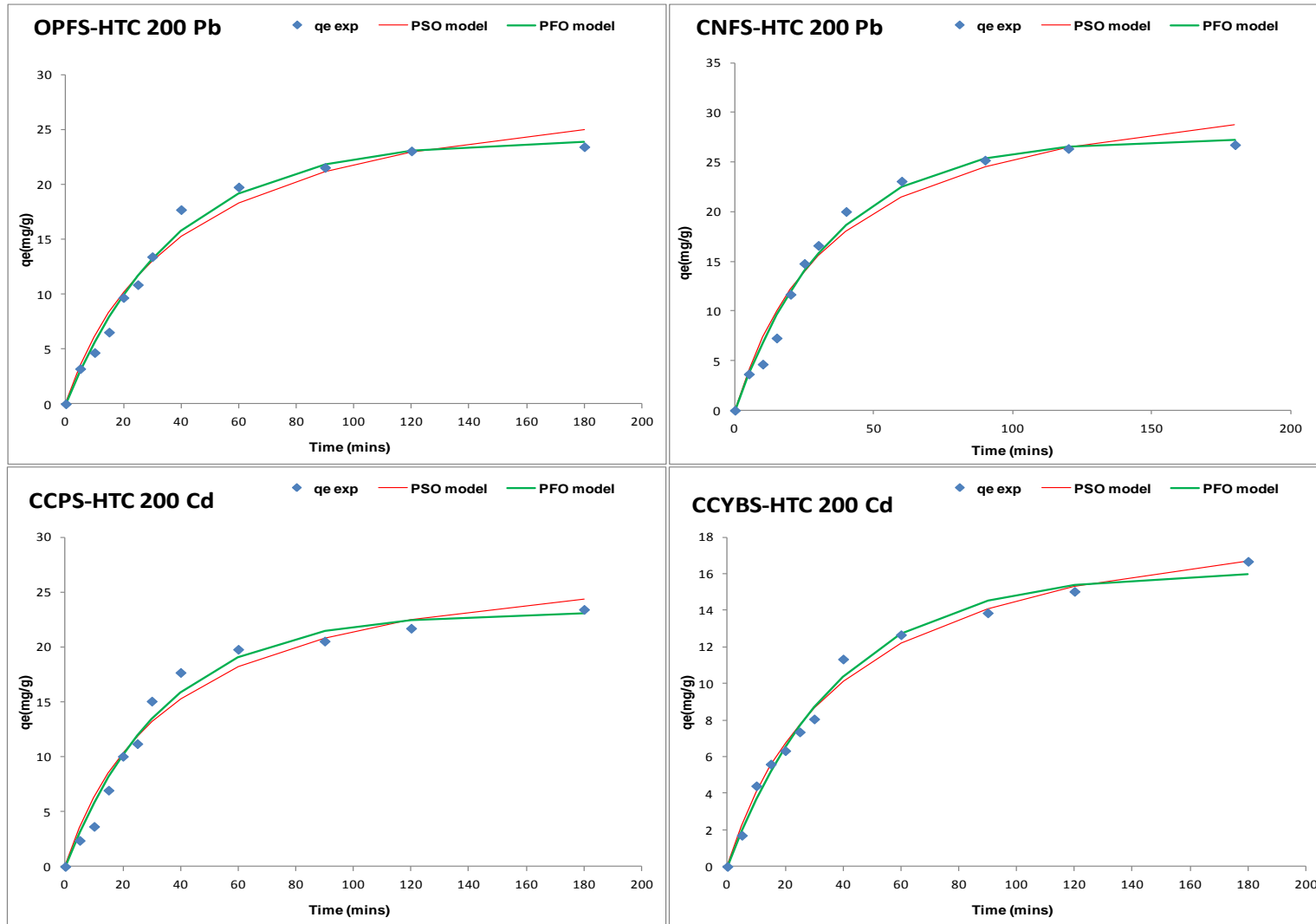
Fig 6.29: Pb(II) ion PFO & PSO sorption kinetic models for OPFS-HTC200,CNFS-HTC 200, CCPS-HTC200 & CCYBS-HTC 200 adsorbents
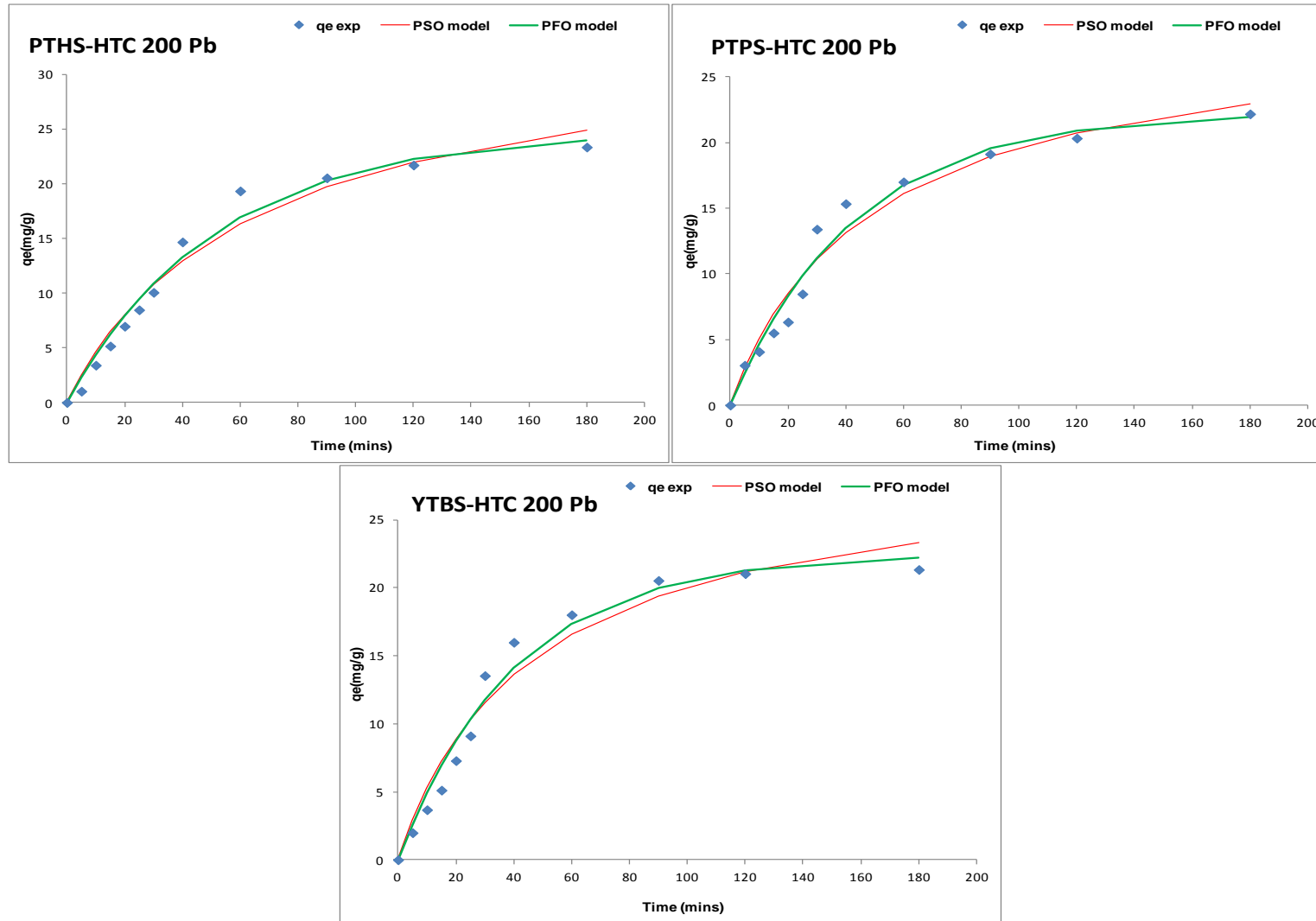
Fig 6.30: Pb(II) ion PFO & PSO sorption kinetic models for PTHS-HTC200, PTPS-HTC 200 & YTBS-HTC 200 adsorbents

The PSO model was also used to evaluate the kinetics of Pb(II) ion sorption onto the HTC170 and HTC200 adsorbents and the results are also presented in Tables 6.10 and 6.11. From these tables, it can be observed that PSO rate constant (K_2) for the HTC170 adsorbents were in the range 1.39 $\times 10^{-2}$ gmg^{-1}min^{-1}(CCPS-HTC170) to 9.90 $\times 10^{-4}$ gmg^{-1}min^{-1}(CCYBS-HTC170), while that of the HTC200 adsorbents were in the range 1.20 $\times 10^{-3}$ gmg^{-1}min^{-1}(CCYBS-HTC200) to 9.28 $\times 10^{-4}$ gmg^{-1}min^{-1}(CCPS-HYC200). The initial sorption rate (h) obtained from the PSO model as $q_t/t \rightarrow 0$ which gives an indication of the intial kinetic rate of sorption was also determined from the PSO model. For the HTC170 adsorbents, the values of the initial sorption were in the order of CNFS-HTC170 > CCPS-HTC170 > OPFS-HTC170>YTBS-HTC170 >PTHS-HTC170 > PTPS-HTC170> CCYBS-HTC170 with the CNFS-HTC170 adsorbent having the highest value of 0.64mgg^{-1}min^{-1}. For the HTC200 adsorbents, the order for (h) was CNFS-HTC200>CCPS-HTC200>OPFS-HTC200>YTBS-HTC200>YTBS-HTC200>PTPS-HTC200>CCYBS-HTC200 with the CNFS-HTC200 having the highest value of 0.94mgg^{-1}min^{-1}.Comparing the initial adsorption rate for the HTC170 and HTC200 adsorbents shows that the HTC200 adsorbents had higher values for the initial adsorption rate than the HTC170 adsorbents.

The maximum adsorbent loading $q_{e,cal}$ obtained from the PSO model for Pb(II) ion sorption onto the HTC170 adsorbents were in the range 17.1 mgg^{-1} (CCYBS-HTC170) to 24.3 mgg^{-1}(CNFS-HTC170) with the order being CNFS-HTC170>YTBS-HTC170 > PTPS-HTC170>PTHS-HTC170>CCPS-HTC170>OPFS-HTC170>CCYBS-HTC170,
while that of the HTC200 adsorbents were in the range 20.5 mgg^{-1} (CCYBS-HTC200) to 34.6 mgg^{-1}(CNFS-HTC200) with the order being CNFS-HTC200>PTHS-HTC200 > OPFS-HTC200>CCPS-HTC200 >YTPS-HTC200 > PTPS-HTC200> CCYBS-HTC200, implying that the CNFS-HTC200 adsorbent had the highest Pb(II) ion loading for the hydrothermally carbonised adsorbents.

The value of the coefficient of determination and the two error parameters − the root mean square (RMSE) and Chi square (χ^2) were used to determine the adsorbent whose kinetics of Pb(II) sorption is best described by the PSO model. The value of these error parameters in Table 6.10 and 6.11 shows that there are variations in the r^2 values for the HTC170 and HTC200 adsorbents. For the HTC170 adsorbents, the r^2 values were; 0.99 (OPFS-HTC170 and CNFS-HTC170), 0.98 (CCYBS-HTC170), 0.97(CCPS-HTC170), 0.97 (PTHS-HTC170 and PTPS-HTC170) and 0.94 for the YTBS-HTC170 adsorbents. For the

HTC200 adsorbents, the r^2 values were; 0.99 (CCYBS-HTC200), 0.98 (OPFS-HTC200), 0.97(CNFS-HTC200 and PTHS-HTC200), 0.96 (PTPS-HTC200 and CCPS-HTC200) and 0.95 for the YTBS-HTC200 adsorbents. To further discriminate the adsorbent that is best described by the PSO model, consideration was given to the values of the two error parameters- the χ^2 and the RMSE. The adsorbent with the lowest values for these two parameters was thereafter chosen as the best described by the PSO model. For the HTC170 adsorbents, the χ^2 and RMSE values were used to further compare the fitting of the PSO model to the Pb(II) ion experimental sorption data for the OPFS-HTC170 and CNFS-HTC170 adsorbents. Based on the values for these two error parameters in Table 6.10, the OPFS-HTC170 adsorbent uptake of Pb(II) ion is best described by the PSO model with the lowest χ^2 (0.01) and RMSE (6.93 $\times10^{-2}$) values.

The PSO rate constant (K_2) obtained for this adsorbent was 1.62 $\times10^{-3}$ gmg^{-1}min^{-1} and the PSO model metal ion loading ($q_{e,cal}$) was 19.0 mgg^{-1}. For the HTC200 adsorbents based on the results in Table 6.11 the CCYBS-HTC200 adsorbent uptake of Pb(II) ion is best described by the PSO model with the lowest χ^2 (0.03) and RMSE (1.13 $\times10^{-1}$) values. The PSO rate constant (K_2) obtained for this adsorbent was 1.20 $\times10^{-3}$ gmg^{-1}min^{-1} and the PSO model metal ion loading ($q_{e,cal}$) was 20.5 mgg^{-1}. A comparison of the PSO values for r^2 and the two error parameters between the HTC170 and HTC200 adsorbents for Pb(II) ion sorption, indicates that the OPFS-HTC170 adsorbent was best described by the PSO model as it had the lowest values for the error parameters (χ^2 and the RMSE) and the highest r^2 value.

Futhermore, to determine which of the two kinetic models (PFO or PSO) gives the best description of Pb(II) sorption kinetics onto the HTC170 and HTC200 adsorbents an examination of the $q_{e,cal}$ values obtained for the PFO and PSO models is used to compare with the experimental q_e value obtained at the end of sorption (after 180 mins) also called q_t. The assumption is that the model with $q_{e,cal}$ values that are closer to the experimental obtained q_e is the model that describes the Pb(II) ion sorption better. Table 6.12 presents the q_e for both experimental sorption and kinetic models for Pb(II) ion uptake by the HTC170 and HTC200 adsorbents.

Table 6.12: Comparison of q_e values for experiment and model sorption for Pb(II) onto hydrothermally carbonised adsorbents

Adsorbent	q_e (mgg^{-1})		
	Experiment	PFO model	PSO model
OPFS-HTC 200	23.4	24.0	30.6
CNFS-HTC 200	26.8	27.4	34.6
CCPS-HTC 200	23.4	23.2	29.3
CCYBS-HTC 200	16.7	16.1	20.5
PTHS-HTC 200	23.3	24.7	33.6
PTPS-HTC 200	22.2	22.3	29.1
YTBS-HTC 200	21.4	22.5	29.2
OPFS-HTC 170	15.8	15.4	19.0
CNFS-HTC 170	19.1	19.3	24.3
CCPS-HTC 170	16.6	16.6	20.8
CCYBS-HTC 170	12.2	12.7	17.1
PTHS-HTC 170	14.9	15.7	21.2
PTPS-HTC 170	14.5	15.6	21.6
YTBS-HTC 170	16.8	17.7	23.9

From Table 6.12, it is observed that the values for qe_{model} for both PFO and PSO models were close to the experimental (q_e) for both HTC170 and HTC200 adsorbents. However, the PFO model for some of the adsorbents gave a closer q_e value to the experimental sorption q_e than the PSO. The PSO mainly gave values that were an overestimate of the experimental qe while that of the PFO was for some adsorbents an underestimation of the experimental q_e. Further evaluation of the values for error parameters (χ^2 and the RMSE) and correlation coefficient (r^2) in Table 6.10 and 6.11 for the two sets of adsorbents indicates that the PFO model had lower values for both error parameters and higher r^2. Thus, it can be said that the PFO model gave a better approximation of the kinetics of Pb(II) sorption by the HTC170 and HTC200 adsorbents than the PSO order model.This implies that the kinetics supports the assumption that the rate limiting step of Pb(II) ion sorption onto the HTC170 and HTC200 adsorbents is dependent on the concentration of the Pb(II) ions in the adsorbate (Azizian, 2004; Liu and Liu, 2008). However, the closeness of the parameters obtained from the PSO model may also indicate that chemical interactions between the ions in the adsorbate solution and the adsorbent may still

influence sorption kinetics but this may depend on the rate of diffusion.This implies that pore diffusivity of the ions onto the active sites may also influence the kinetics as previously discussed in the analysis of the two stage metal uptake (fast and slow) kinetics of Pb(II) ion sorption.

A number of studies have been reported on the application of the PFO and PSO models for the characterisation of the kinetics of Pb(II) ion sorption using hydrothermally prepared adsorbents. Xue *et al.,*2012 have studied the ability of hydrochar produced from hydrothermal carbonization of peanut hull to remove Pb(II) ions from aqueous solutions in a batch process. Kinetic modelling studies were also reported and based on the r^2 value obtained for both PFO and PSO models, the PSO model gave a better fitting for metal sorption. The kinetics of removal of Pb(II) ions from water using biochars prepared from hydrothermal liquefaction of biomass (rice husk and pinewood) at 300°C has also been reported by Liu and Zhang (2009). In their study, the correlation co-efficient (r^2) of the pseudo-first order (PFO) model for the the two hydrochars were low (>0.90), while those of the pseudo-second order model were higher (<0.99) thus implying that the PSO model gave a better fitting for the sorption of Pb(II) ions onto the adsorbents.

6.6 Summary

Hydrothermal carbonization is presently viewed as a highly unconventional technique for conversion of biomass into useful products such as hydrochar. Interestingly, the full potential of this process as an important route for the development of carbon materials for useful applications has only recently been studied. Most studies involving "hydrochars" relate to investigations where their property is used to upgrade biomass feedstock quality for energy generation but this study was focused on its potential as an adsorbent. Hence, this study was to design to convert the raw lignocellulosic materials utilized in Chapter 5 into useful carbon adsorbents for the removal of Cd (II) and Pb (II) ions based on the hydrothermal process. The characterization of the resulting adsorbents from the hydrothermal carbonization (HTC) process using the two temperature regimes (200/170°C) revealed similar properties such as yield, pHpzc, surface area and ash for these materials. Thus, for this study, the two highest reaction temperatures (HRT), 170°C and 200°C chosen enabled the effect of this difference on the physicochemical properties and adsorbent

efficiency of hydrothermal carbonized adsorbents to be evaluated. The temperature of HTC did not affect the yield of carbon produced and both sets of adsorbent produced (HTC-170 and HTC-200) had high ash content that could be attributed to the intrinsic nature of the feedstock. An evaluation of the ability of the HTC adsorbents to withstand abrasion on contact using the loss on attribution test indicated high losses for the adsorbents revealing that these adsorbents had poor mechanical strength. While all the HTC200 adsorbents were acidic in nature, the HTC170 had four acidic and three basic adsorbents. In addition, a trend of decreasing value of pHpzc with increase in thermal treatment temperature was also observed in contrast to an increasing acidity of the HTC adsorbents with increase in temperature of the thermal treatment found in literature. This observation was based on the zeta potential values of the two sets of adsorbents.

The HTC200 adsorbents had higher values of BET surface area than the HTC170 adsorbents and this was associated to the effect of temperature of the degree of volatilisation of these residues resulting in improved porosity. The CNFS-HTC 200 adsorbent had the highest surface area of 260 m^2g^{-1}, while the least was the CCYBS-HTC 170 adsorbent with a surface area of 13.6m^2g^{-1}.Varying degrees of hysteresis were also detected on the hydrothermal carbonized adsorbents using the presence of hysteresis on the nitrogen – adsorption desorption plot. This suggested the presence of mesoporosity in the adsorbents and it was further confirmed from the BJH average pore diameter analysis using the desorption branch of the N_2 adsorption-isotherm.

Kinetic studies were carried on the removal of Cd(II) and Pb(II) ions from aqueous solutions using the two sets of hydrothermal carbonised adsorbents prepared. It was observed that the HTC 200 adsorbents had higher metal ion loading than the HTC170 for both Cd (II) and Pb (II) ions and this was associated with the effect of a higher surface area on the HTC200 adsorbents. The rate of uptake of both metal ions occurred via a two stage process with the first rapid stage occurring from initial contact to 90 minutes for Cd(II) loading using the HTC170 adsorbents and Pb (II) for both HTC adsorbents. For Cd(II) ion sorption using the HTC200 adsorbents, this rapid stage occurred from initial contact to 60 minutes. The second stage of Cd(II) and Pb(II) metal ion loading for both HTC adsorbents proceeded at a slow stage up till 180 minutes where equilibrium was attained. Thus, these HTC adsorbents would be effective as materials for heavy metal ion removal from wastewater systems as it has a fast kinetic profile. The results of the kinetics of Cd(II) and Pb(II) ion sorption indicated that for the hydrothermal carbonised adsorbents, optimum

uptake for Cd(II) and Pb(II) ions for the HTC-170 adsorbents was obtained for CNFS-HTC 170 adsorbent with loadings of 25.9 mgg^{-1} for Cd(II) and 19.0 mgg^{-1} for Pb(II) ions. For the HTC 200 adsorbents, the CNFS-HTC 200 adsorbent was the best with loadings of 31.2 mgg^{-1} for Cd(II) and 26.8 mgg^{-1} for Pb(II) ions. The optimum uptake obtained for these adsorbents was associated to the high BET surface area of the CNFS-HTC170 and CNFS-HTC 200 adsorbents which were 75.5 m^{2}g^{-1} and 260 m^{2}g^{-1} respectively. Kinetic modelling of the sorption of Cd(II) and Pb(II) ions onto the the HTC170 and HTC200 adsorbents were also carried out using the pseudo-first order(PFO) and pseudo-second order(PSO) equations. From the analysis, it was observed that the PFO model gave a better approximation of the kinetics of Cd(II) and Pb(II) sorption by the HTC170 and HTC200 adsorbents than the PSO order model. This study on the removal of Cd(II) and Pb(II) ions from aqueous solutions using the hydrothermal carbonised adsorbents shows that the process of hydrothermal carbonisation can be used to successfully improve the surface area and porosity of lignocellulosic residues with the associated improvements in the loadings and rate of uptake of toxic pollutants from aqueous streams.

CHAPTER SEVEN

CARBONISED AND PYROLYSED

ADSORBENTS

CHAPTER SEVEN

7.0 Carbonised and pyrolysed adsorbents

Pyrolysis is a thermo-chemical conversion process that can be used to transform biomass into gaseous, liquid and solid products. It is a process of decomposition of organic materials by heating in the absence of oxygen (White *et al.*, 2011). According to Galwey and Brown (1998), pyrolysis of biomass can be viewed as a heterogeneous reaction and the kinetics of the process can be affected by three elements; the breakage and redistribution of chemical bonds, the changing reaction geometry and the interfacial diffusion of reactants and products. These three elements are a function of various parameters such as temperature, heating rate, pressure, particle size, nature of biomass, oxygen content and gas flow rate and these affect the distribution and characteristics of the resulting solid, liquid and gaseous products of pyrolysis (Fu *et al.*, 2010; Demirbas, 2006; Wang *et al.*, 2009). Carbonisation on the other hand is the combustion of biomass into a carbonaceous residue often in the presence of air or limited oxygen environments. In this study the temperature, heating rate and flow rate for the transformation process were chosen as described in Section 4.2.2 and 4.2.3 for the thermal conversion of 7 agricultural residues into adsorbents using carbonisation and pyrolysis procedures.

The agricultural residue adsorbents reported in Chapter 5 of this work were subjected to two thermal modification procedures. Pyrolysis, at peak temperature of 700°C in nitrogen atmosphere as described in section 4.2.2 and the resulting adsorbents termed "pyrolysed adsorbents". Carbonization at a peak temperature 400°C in limited oxygen atmosphere as illustrated in section 4.2.3 was also implemented and the adsorbents obtained from the carbonization procedure were termed "carbonized adsorbents". The nomenclature of these two groups of adsorbents is presented in Table 7.1. The adsorbents obtained were thereafter characterized to determine their ash content, loss on attrition, adsorbent yield and zeta potential. The surface area and porosity, surface morphology and chemical composition of each carbon adsorbent were also determined using the procedure previously described in Chapter 4 of this study. Kinetic metal ion sorption experiments were also carried out using these carbonized and pyrolysed adsorbents to study the effect of contact time on the adsorption of Cd(II) and Pb(II) ions.

Table 7.1: Nomenclature of carbonised and pyrolysed adsorbents

Sample and Treatment	Nomenclature
Pyrolysed residue -700 °C	
Pyrolysed oil palm fruit fibre residue	OPFPCA
Pyrolysed cocoa pod residue	CCPPCA
Pyrolysed coconut shell fibre residue	CNFPCA
Pyrolysed plantain peel residue	PTHPCA
Pyrolysed cocoyam peel residue	CCYBPCA
Pyrolysed sweet potato peel residue	PTPPCA
Pyrolysed white yam peel residue	YTBPCA
Carbonised residue- 400 °C	
Carbonised oil palm fruit fibre residue	OPFCA
Carbonised cocoa pod residue	CCPCA
Carbonised coconut shell fibre residue	CNFCA
Carbonised plantain peel residue	PTHCA
Carbonised cocoyam peel residue	CCYBCA
Carbonised sweet potato peel residue	PTPCA
Carbonised white yam peel residue	YTBCA

7.1 Characterisation - ash content, loss on attrition and yield

The determination of the ash content, loss of attrition and yield of the pyrolysed and carbonised adsorbents were carried out as described in section 4.3 and the results obtained from this characterization are presented in Table 7.2 for carbonized adsorbent and 7.3 for the pyrolysed adsorbents. From the results, it can be observed that the carbonized adsorbents had ash content that were in the range of 5.3 to 7.6% with the trend being PTHCA > CNFCA >YTBCA > PTPCA > CCPCA > OPFCA > CCYBCA. This indicates that the PTHCA adsorbent had the highest ash content, while CCYBCA had the least. The ash content of an adsorbent is a function of the amount of inorganic constituents in a biomass and this value implies that the residues used here had high inorganic components as previously observed in Chapter 5 of this study.

Table 7.2: Ash content, loss on attrition and yield of carbonised adsorbents

Adsorbent	Ash [e] (%)	Loss on Attrition (%)	Yield (%)
OPFCA	7.5	10.9	54.85
	±0.043	±2.09	±3.65
CNFCA	5.4	12.15	51.95
	±0.329	±0.129	±0.236
CCPCA	7.3	13.25	56.55
	±0.078	±3.23.	±3.03
CCYBCA	5.3	10.45	48.7
	±0.071	±1.29	±2.63
PTHCA	7.6	15.25	56.55
	±0.042	±1.89	±3.63
PTPCA	6.6	12.7	57.75
	±0.042	±2.43	±4.06
YTBCA	6.5	13.55	50.6
	±0.061	±1.48	±3.47

[e] Ash content using AOAC(2000)

For the pyrolysed adsorbents, the percentage of the adsorbents that was composed of ash ranged from 4.3 to 6.5% with the lowest being CCYBPCA while the highest was the PTHPCA adsorbent. It was also observed that the adsorbents with the highest and lowest ash content for the pyrolysed and carbonized adsorbents were the same indicating that this parameter is a function of the nature of the residue (Uchimiya *et al*., 2011).

An examination of literature indicates that the ash content of agricultural residues varies. Ahmad *et al*., (2012b) has reported on the effects of pyrolysis temperature for two residues – soybean stove and peanut shell derived adsorbents subjected to pyrolysis at 300°C and 700°C. The ash content of the soybean stover adsorbents were 10.41% and 17.18% for the 300°C and 700°C adsorbents respectively, while for the peanut shell pyrolysed at 300°C, the percentage content of ash was 1.24%, and 8.91% for the one pyrolysed at 760°C. Guo and Lua (1998) have also reported on the ash content of pyrolysed oil palm stones subjected to different temperatures. These were 4.6% (400°C), 5.9% (600°C), 7.5% (700°C). 8.3% (800°C) and 9.1% (900°C). The results indicate that the values of ash content obtained in this study for the pyrolysed and carbonized residue adsorbents are similar to those obtained in previous literature.

Another parameter that was used to characterize the carbonised and pyrolysed adsorbents was the percentage loss of attrition. This property was characterized for these adsorbents using the procedure described in section 4.3.11. This characteristic describes the degree of resistance to abrasion that occurs when these adsorbent particles come into contact in an agitated adsorbent system. The percentage of attrition loss was computed based on Eqn. 4.4 and the values obtained for the carbonised adsorbents were in the range of 10.45 to 15.25% while that for the pyrolysed adsorbents were from 4.3 to 5.7%.This indicates that the pyrolysed absorbents had a resistance to losses due to attrition.

Table 7.3: Ash content, loss on attrition and yield of pyrolysed adsorbents

Adsorbent	Ash [e] (%)	Loss on Attrition (%)	Yield (%)
OPFPCA	5.7	6.95	38.35
	±0.32	±2.11	±2.13
CNFPCA	4.8	5.4	34.7
	±0.267	±0.162	±0.219
CCPPCA	5.1	7.25	36.9
	±0.067	±2.87	±3.13
CCYBPCA	4.3	5.2	39.15
	±0.056	±2.13	±3.78
PTHPCA	6.5	5.45	32.65
	±0.056	±1.563	±3.63
PTPPCA	5.5	5.9	37.6
	±0.029	±2.56	±3.69
YTBPCA	4.6	6.75	34.1
	±0.021	±1.39	±2.93

[e] Ash content using AOAC(2000)

The percentage loss on attrition for chars obtained from grape seeds has been reported as 9.5% (Cordero *et al.,* 2013). This result indicates that the carbonized adsorbents had higher losses due to attrition but the pyrolysed adsorbents had lower values indicating that they were better materials when used with fewer propensities to generate adsorbent particulate on contact and mixing and thereby cause blockage of reactor vessels. The yield for the conversion of the residues into these two carbon adsorbents was also quantified. The yield was calculated from the weight of the chars after pyrolysis while the initial weight of the residue was calculated according to eqn. 4.1. For the carbonized adsorbents, the same equation was used to determine the yield after thermal treatment as described in Chapter 4.

Pyrolysis and carbonization are important routes in the conversion of biomass into carbon enriched materials as the biomass under thermal treatment undergoes series of transformations resulting in solid, liquid and gaseous products such as prolytic oils, charcoal and CH_4. The mechanisms under which the biomass materials are transformed include: hydrolysis, dehydration, dehydrogenation, deoxygenation and decarboxylation (Demirbas, 2000) and these reactions can influence the yield. The results of the yield of the carbonized and pyrolysed adsorbents are presented in Table 7.1 and 7.2 respectively. For the carbonised adsorbents, the yields observed was in the range of (48.7 – 50) % and followed the trend PTPCA > PTHCA = CCPCA > OPFCA > YTBCA > CCYBCA. The pyrolysed adsorbents have values of yield between 39.15 – 32.65% with the following trend: CCYBPCA > OPFPCA > PTPPCA > CCPPCA > CNFPCA > PTHPCA > YTBPCA.

From an examination of the values of adsorbent yield for the pyrolysed and carbon adsorbents, it can be observed that the carbonized adsorbents had higher yields than the pyrolysed adsorbents. Thus for each adsorbent type, there was a decrease in yield from the carbonized to the pyrolysed adsorbent implying that increase in temperature led to reduction in yield. For the OPFCA and OPFPCA adsorbents, the yield was reduced by 30% while for CNFCA and CNFPCA, the reduction in yield was 33%. Similar trends in yield reduction were observed for the other set of adsorbents; CCPCA and CCPPPCA (34%); CCYBCA and CCYBPCA (19%); PTHCA and PTHPCA (42%); PTPCA and PTPPCA (34%) and YTBCA and YTBPCA (32%). The above results reveal that the highest and least reductions in yield were obtained for the PTHCA/PTHPCA and CCYBCA/CCYBPCA adsorbents respectively. This reduction in yield is due to the increase in decomposition of the biomass as the temperature increases from $400^{\circ}C$ for carbonized adsorbents to $700^{\circ}C$ for the pyrolysed adsorbents. A similar reduction in adsorbent yield with increase in temperature has been reported by Ahmad *et al.,* (2012b) for soybean stover and peanut shell stover from thermal treatment of $300^{\circ}C$ and $700^{\circ}C$. In the study, the reduction yield was 37% for soybean stover biochar while a reduction of 22% was observed for peanut shell biochar (Ahmad *et al.,* 2012b).

The yields of different thermally modified agricultural residues have also been reported, a yield of 30.2% was reported for guava seed adsorbent carbonized at $600^{\circ}C$ (Elizalde-Gonzalez and Hernandez-Montoya, 2009). Kazemipour *et al*., (2008) has also reported on

the yield of a number of crop based residue pyrolysed at 800 °C. Their yields were pistachio shell (20%); almond (38%); hazelnut (52%); walnut (57%) and apricot (63%). A comparison of these reported literature values for yields of carbon adsorbents subjected to carbonization and pyrolysis indicate that those obtained for the adsorbents prepared in this study were comparable with reported literature studies.

7.2 pH and zeta potential of carbonised and pyrolysed adsorbents

This study was aimed at converting the agricultural residues discussed in chapter 5 of this work into pyrolysed and carbonized adsorbents for the removal of Cd(II) and Pb(II) ions in an aqueous system. Since the adsorbents developed were to be deployed in aqueous system, it was therefore important to study the nature of the surface of the adsorbent in solution. When an adsorbent is immersed in an aqueous system, a number of surface and bulk interactions are suspected to occur leading to ion interactions between the aqueous system and the adsorbent. The nature of the adsorbent surface also plays a significant role in the determination of the properties of the adsorbent surface in an aqueous system. Hence it was important that the pH of an aqueous system with the adsorbents developed in this study be characterized, this is because the solution pH affects the solubility of metal ions, concentration of counter ions on the functional groups in the adsorbent and the degree of ionization of the adsorbate during reaction (Nomanbhay and Palanisamy, 2005). Thus, the pH of the adsorbate may be modified when an adsorbent is immersed into it and the resulting pH may increase or decrease depending on the types of functional groups on the adsorbent and their level of dissociation in water. A deionized water system ($18.2M\Omega cm^{-1}$) was used for the determination of the adsorbent pH as described in Section 4.3.9.

Another property of each of these adsorbent studied was their zeta potential. This parameter describes the electrophoretic and electrokinetic mobilities on the surface of an adsorbent when dispersed in an aqueous solution; characterizing the surface charge on the adsorbent surface. The zeta potential is a parameter that accounts for most surface phenomena such as agglomeration and deposition of particles as well as their stability (Alkan *et al*., 2005). When an adsorbent is immersed into an aqueous system in a powdered or granular form and subjected to agitation as is the process in batch adsorption studies, the interaction of the adsorbent surface with the species in the aqueous solution or system depends on many factors which are governed by the type and number of species,

pH of the aqueous system and the nature and type of potential or charge on the adsorbent surface. Hence, the zeta potential can be used to estimate the effects of the particle charge on adsorption and aggregation behaviour of ions with respect to the adsorbent. From the determination of the zeta potential of an adsorbent-aqueous system which is always carried out with respect to the aqueous system pH, a characteristic parameter can be obtained by plotting the zeta potentials at different pH as a function of pH.

This plot indicates that as the pH of a solution moves from acidic to basic, a point is reached where the adsorbent-aqueous system has a pH at which there is an inflection from a positive surface (associated with positive zeta potential) to a negative surface (associated with a negative zeta potential). This point of inflection on the pH has a potential of zero and is described as the pH at which the point has a zero charge (pHpzc) and here the surface acidic (or basic) functional groups no longer contribute to the pH value of the aqueous system (Nomanbhany and Palanisamy, 2005). In this study, the pH and zeta potential of the carbonized and pyrolysed carbon adsorbents were determined according to the procedures described in section 4.3.9 and 4.3.3 respectively and the results are presented in Table 7.4.

Table 7.4: pHpzc and pH of carbonised & pyrolysed adsorbents

Adsorbent	pHpzc	Adsorbent pH	Adsorbent	pHpzc	Adsorbent pH
OPFCA	6.7	6.35	OPFPCA	6.4	6.99
CNFCA	6.2	7.76	CNFPCA	6	7.36
CCPCA	6.5	7.37	CCPPCA	6.8	7.42
CCYBCA	6.3	7.17	CCYBPCA	6.5	7.45
PTHCA	6.9	7.23	PTHPCA	7	7.3
PTPCA	7.2	6.9	PTPPCA	7.6	7.2
YTBCA	7.7	7.02	YTBPCA	7.6	7.11

It can be observed from the table that the pH for the carbonized adsorbents ranged from 6.35 to 7.7; most pH occurring above 7 with the exception of PTPCA and OPFCA with pH values of 6.9 and 6.3 respectively. This is an indication that the surface of most of the

carbonized adsorbents had a higher proportion of basic functional groups, while that of PTPCA and OPFCA had higher proportion of acidic functional groups. For the pyrolysed adsorbents, the trend in pH increased as the most of them had pH above 7 except OPFPCA which had a pH of 6.99. Correlating the trend in pH between the carbonized and pyrolysed adsorbents, it can be deduced that the pH of the adsorbents increased as a function of the temperature of the thermal treatment with the exception of CNFCA and CNFPCA adsorbents. This means that the higher pyrolysis temperature result in the accumulation of more alkali salts on the surface of the adsorbent and more basic functional groups are therefore developed (Ding *et al*., 2014). This trend in higher biochar pH with increase in the temperature of pyrolysis has been also reported by Kim *et al.*, (2013). Their study involved the production of biochar from giant *miscanthus* at different pyrolytic temperatures 300, 400, 500 and 600°C and the results obtained revealed that when the adsorbent was immersed in deionized water (18.2MΩcm^{-1}) there was an increase in pH with values of 8.28 (300 $^{\circ}$C); 8.68 (400 $^{\circ}$C); 9.49 (500 $^{\circ}$C) and 10.05 (600 $^{\circ}$C) observed. Yuan *et al*., (2011) has also made a similar observation from the study of production of biochar from crop residues at different temperatures of 300, 500 and 700°C. The study reveals the occurrence of the same increase in pH as pyrolysis temperature increased for three different crop residues – canola straw biochar with pH values of 6.48 (300°C), 9.39 (500°C), 10.76 (700°C); corn straw biochar with pH values of with pH values of 9.37 (300°C), 10.77 (500°C), 11.32 (700°C); soybean biochar with pH values of 7.66 (300°C), 10.92 (500°C), 11.10 (760°C); peanut straw char with pH values of 8.60 (300°C), 10.86 (500°C) and 11.15 (700°C). These studies also corroborate the observed pH trend described in the present study for the carbonized and pyrolysed adsorbents prepared from the agricultural residues (precusors) described in Chapter 5 of this study.

The zeta potential of the carbonized and pyrolysed adsorbents at different pH values were measured as described in section 4.3.3 and the plot of the zeta potential against the pH for the different adsorbents are shown in Appendix 3. The values of the pHpzc obtained from these plots are presented in Table 7.4. The results presented in the table reveals an increasing pHpzc trend of YTBCA > PTPCA > PTHCA > OPFCA > CCPCA > CCYBCA > CNFCA ranging from 6.2 to 7.7. For the pyrolysed adsorbents, the pHpzc ranged from 6.0 to 7.6 with a trend for the carbonized adsorbents of YTBPCA = PTPPCA > PTHPCA > CCPPCA > CCYBPCA > OPFPCA > CNFPCA. Collating the pHpzc values for both the carbonized and pyrolysed adsorbents reveals a decreasing trend of the pHpzc value with

increase in temperature from 400°C to 700°C for OPFCA/OPFPCA; CNFCA/CNFPCA and YTBCA/YTBPCA adsorbents. The reverse trend is however observed for CCPCA/CCPPCA; CCYBCA/CCYBPCA; PTHCA/PTHPCA and PTPCA/PTPPCA adsorbents where an increase in the value of the pHpzc occurs as temperature increases from 400°C to 700°C.

The pHpzc of an adsorbent is related to the surface acidity or basicity hence the adsorbents with pHpzc higher than 7 have higher basic surfaces while those with pHpzc below 7 are acidic in nature. Hence, the value of the pHpzc is important for the selection of the pH for adsorption as this will influence the surface charge on the adsorbent and the degree of ionization of the different pollutants (Sardella *et al*., 2015). The pHpzc value of carbonized wastes from the viticultural industry has been reported in literature by Sardella *et al.,* (2015). The materials reported in the study were grape pomace, grape stalks and grape lex and the pHpzc values reported for the carbonization of the waste materials at 500°C were: grape pomace (11.0), grape stalk (11.2) and grape lex (12.0) (Sardella *et al*., 2015). These values were higher than what has been observed in the present study as these materials were more basic than those developed in this work.

In another study, Antonio-Cisneros and Elizalde-Gonzalez (2010) reports on the characterization of manihot residues and their conversion into carbon adsorbents at temperatures 500 – 800 °C. The results of their study indicate that the carbon adsorbents obtained from the rind, vascular system and pith of the *manihot* residues had similar pHpzc of 6.1, 6.7 and 6.6 respectively. This was similar to what was observed in the present study and it should be noted that the value of the pHpzc of adsorbents obtained from thermo-chemical processes may vary depending a number of factors such as the nature of material used, the pyrolysis temperature and the gas flow rate. These parameters will influence the degree and rate of decomposition of the precursors thereby affecting the types of acidic or basic chemical moieties that remain on the char surface (Ding *et al*., 2014). Based on the values of the pHpzc for the carbonized and pyrolysed adsorbents, the pH chosen for the sorption of Cd(II) and Pb(II) ions using these adsorbents was 7.

7.3 Surface area and porosity of carbonised and pyrolysed adsorbents

The thermal modification of the agricultural residue adsorbents discussed in Chapter 5 of this work has been observed to impart some distinct properties on the resulting carbon adsorbents. The two temperature regimes and the thermal environments {400°C (limited air) and 700°C (N$_2$ atmosphere)} used for the carbonization and pyrolysis of the residues have significant impact on the physical characteristics of the resulting chars from the different residues. One measure of this effect is in the surface area and porosity of the material. During the thermal treatment, the mechanism of de-volatilization of the organic precursors on the residue with increase in temperature and subsequent re-organisation of the adsorbent surface leads to the development of more defined pore structure on the resulting adsorbents. However, the type of pore arrangement on a lignocellulosic residue subjected to pyrolysis or carbonization is also a function of the intrinsic nature of the residue. This leads to the development of different porosity characteristics for lignocellulosic materials as the volatile materials are gradually eliminated with rudimentary pore structures on the resultant chars (Guo and Lua, 1998).

The BET surface area and porosity of the adsorbents prepared in this study were determined using the N$_2$ adsorption-desorption method at -196°C, described in Section 4.3.4 of this study. The N$_2$ adsorption-desorption isotherm plot for the carbonized adsorbents are shown in Figures 7.1 $-$ 7.2 and that of the pyrolysed adsorbents are shown in Figures 7.3 $-$ 7.4. The pore size distribution plot for each carbonized and pyrolysed adsorbent are also shown in Figures 7.1 $-$ 7.4 beside their respective N$_2$ adsorption $-$ desorption plot. From the figures, the values of the BET surface area, total pore volume an average pore diameter for each adsorbent are presented in Table 7.5 for the carbonized adsorbents and Table 7.6 for the pyrolysed adsorbents.

An examination of the surface area of the carbonized adsorbents in Table 7.5 indicates that the carbonization procedure at 400°C did have a significant effect on the texture and pore characteristics of each material when compared to the precursors (residue) and the hydrochars discussed in Chapters 5-6 of this work. However, the development of porosity and increase in surface area is also observed to be a function of the residue characteristic and this intrinsic property can be used to explain the variation in pore characteristics across the 7 carbonised adsorbents.

Table 7.5: Surface area and porosity of carbonised adsorbents

Adsorbent	BET Surface Area (m^2g^{-1})	Total Pore Volume (cm^3g^{-1})	BJH Desorption Average Pore Diameter (nm)
OPFCA	150	3.45E-01	12.3
CNFCA	252	3.12E-01	8.35
CCPCA	124	2.78E-01	8.63
CCYBCA	155	1.99E-01	10.4
PTHCA	126	2.54E-01	6.76
PTPCA	59.7	5.95E-02	3.67
YTBCA	97.8	1.87E-01	7.43

The BET surface area of 252 m^2g^{-1} obtained for the CNFCA adsorbent was the highest while that of the PTPCA adsorbent was the least (59.77 $m^2 g^{-1}$). The surface area obtained for the carbonized adsorbent was higher than those reported for the hydrothermal carbonized adsorbents (HTC170 and HTC200) in Chapter 6 of this study however, the surface area of the CNFS-HTC200 adsorbent was still higher than that obtained for the corresponding carbonized adsorbent (CNFCA). This observation may be associated with the intrinsic parameters that dominated the hydrothermal carbonization at 200°C. It is important to note that the surface area of the carbonized adsorbents were significantly higher than that of the raw residues reported in Chapter 5 of this study. The trend in BET surface area for the carbonized adsorbents was CNFCA > CCYBCA > OPFCA > PTHCA > CCPCA > YTBCA > PTPCA.

For the pyrolysed adsorbents subjected to a highest reaction temperature (HRT) of 700°C, the BET surface area obtained as shown in Table 7.6 shows a characteristic increase for all the adsorbents with the coconut based pyrolysed carbon – CNFPCA with the highest value of 439 $m^2 g^{-1}$ while the PTPPCA adsorbent was the lowest with a surface area of 177 $m^2 g^{-1}$. The trend in increasing surface area for the pyrolysed adsorbents was CNFPCA > CCYBPCA > CCPPCA>OPFPCA > YTBPCA > PTHPCA > PTPPCA. From the results in

Tables 7.5 and 7.6, it can be observed that the reaction temperature for carbonization and pyrolysis and their thermal environments played significant roles in increasing the BET surface areas of the prepared adsorbents. This can be explained based on the effect of temperature on the degree of volatilization that occurs on the adsorbent matrix. At 400°C, the organic component on the lignocellulosic residues that have been removed by decomposition is less than what is obtained at 700°C, hence, as the temperature increases from 400 to 700°C, an increasing amount of volatile compounds are evaporated thereby resulting in the development of new porosities on the adsorbent surface, which increases the BET surface area (Guo and Lua, 1998).

This effect of increased reaction temperature on the BET surface area of carbon based materials has been reported by Ahmad *et al.*, (2012b) in a study on the effects of pyrolysis temperature on soybean stover and peanut shell derived biochar using 300°C and 700°C as pyrolysis temperatures. An exponential increase in BET surface area for the biochar obtained at 700°C was observed when compared to those obtained at 300°C. The soybean stover biochar gave values of 300°C (6 $m^2\,g^{-1}$) and 700°C (420 $m^2\,g^{-1}$), while for the peanut shell biochar BET surface areas of 3 $m^2\,g^{-1}$ and 448 $m^2\,g^{-1}$ were obtained at pyrolysis temperatures of 300°C and 700°C respectively. A corresponding trend is also reported in the pyrolysis of giant *miscanthus* at varying temperatures of 300, 400, 500 and 600°C reported by Kim *et al.*, (2013). In their study, a remarkable increase in BET surface area between pyrolysis temperatures of 300°C and 600°C was observed. The surface areas obtained were 0.56 $m^2\,g^{-1}$ for 300°C, 2.41 $m^2\,g^{-1}$ for 400°C, 181 $m^2\,g^{-1}$ for 500°C and 381 $m^2\,g^{-1}$ for 600°C; indicating a rapid volatilization between 300°C and 600°C.

Figure 7.1: N$_2$ adsorption-desorption isotherm and pore size distribution of OPFCA, CNFCA, CCPCA and CCYBCA adsorbents

Figure 7.2: N$_2$ adsorption-desorption isotherm and pore size distribution of PTHCA, PTPCA and YTBCA adsorbents

Table 7.6: Surface area and porosity of pyrolysed adsorbents

Adsorbent	BET Surface Area (m^2g^{-1})	Total Pore Volume (cm^3g^{-1})	BJH Desorption Average Pore Diameter (nm)
OPFPCA	277	4.00E-01	8.47
CNFPCA	439	6.43E-01	7.75
CCPPCA	308	6.00E-01	11.8
CCYBPCA	321	1.94E-01	5.38
PTHPCA	239	4.60E-01	10.6
PTPPCA	177	3.81E-01	8.14
YTBPCA	267	4.41E-01	8.83

From the figures, it is observed that the N_2-adsorption-desorption plot for these adsorbents indicates that carbonized and pyrolysed adsorbents belong to the type IV isotherm based on the IUPAC and Brunauer-Deming-Deming-Teller (BDDT) method (Brunauer *et al*, 1940; Sing, 1992; Sing, 2014). This type IV isotherm has a distinctive hysteresis on the N_2 adsorption-desorption curve which can be associated with the nature of the mesopores which leads to capillary condensation and multilayer pore filling (Gaspard *et al*., 2014).

The existence of hysteresis in the nitrogen adsorption-desorption curve for mesoporous materials is associated with the deviation that occurs in the adsorption and desorption branches of the Nitrogen plot and the shapes of this hysteresis loop often varies from one adsorption system to another (Dabrowski, 2001). An evaluation of the N_2 adsorption-desorption plot for the carbonized and pyrolysed adsorbents indicates that most of them showed the H1 hysteresis loop with the exception of OPFCA which showed a H3 hysteresis loop. These hysteresis loops were used to understand the pore structure in the adsorbent matrix. The H1 loop is a narrow loop that indicates a narrow pore size within a characteristic property of capillary condensation and evaporation (Chi *et al*., 2012; Banerjee *et al*., 2015). On the other hand, the H3 loop which has no plateau at high relative pressure indicates that there are aggregates or agglomerates of particles and mesopores in the adsorbent matrix (Zhao *et al*., 2014).
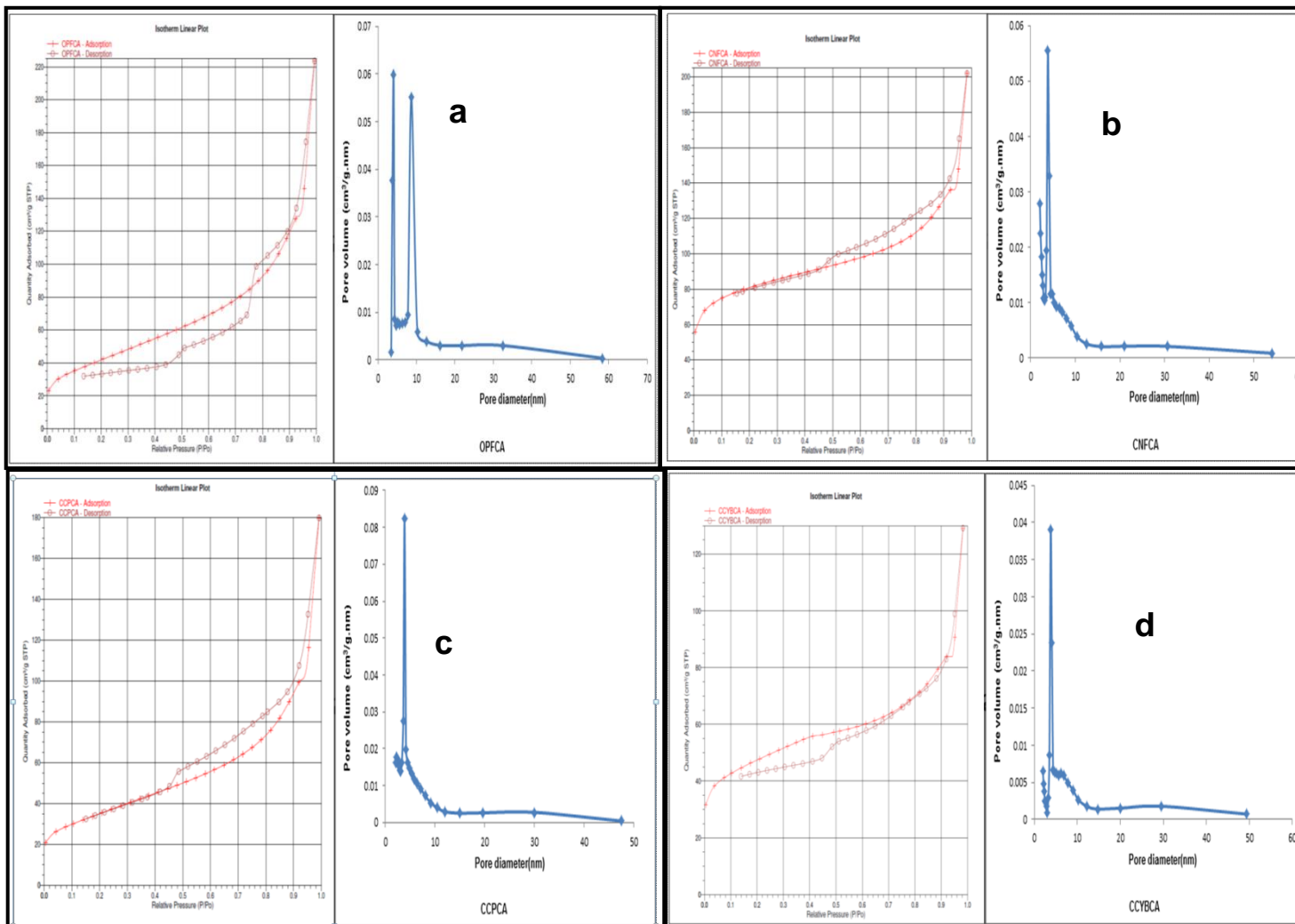
Figure 7.3: N$_2$ adsorption-desorption isotherm and pore size distribution of OPFPCA, CNFPCA, CCPPCA and CCYBPCA adsorbent

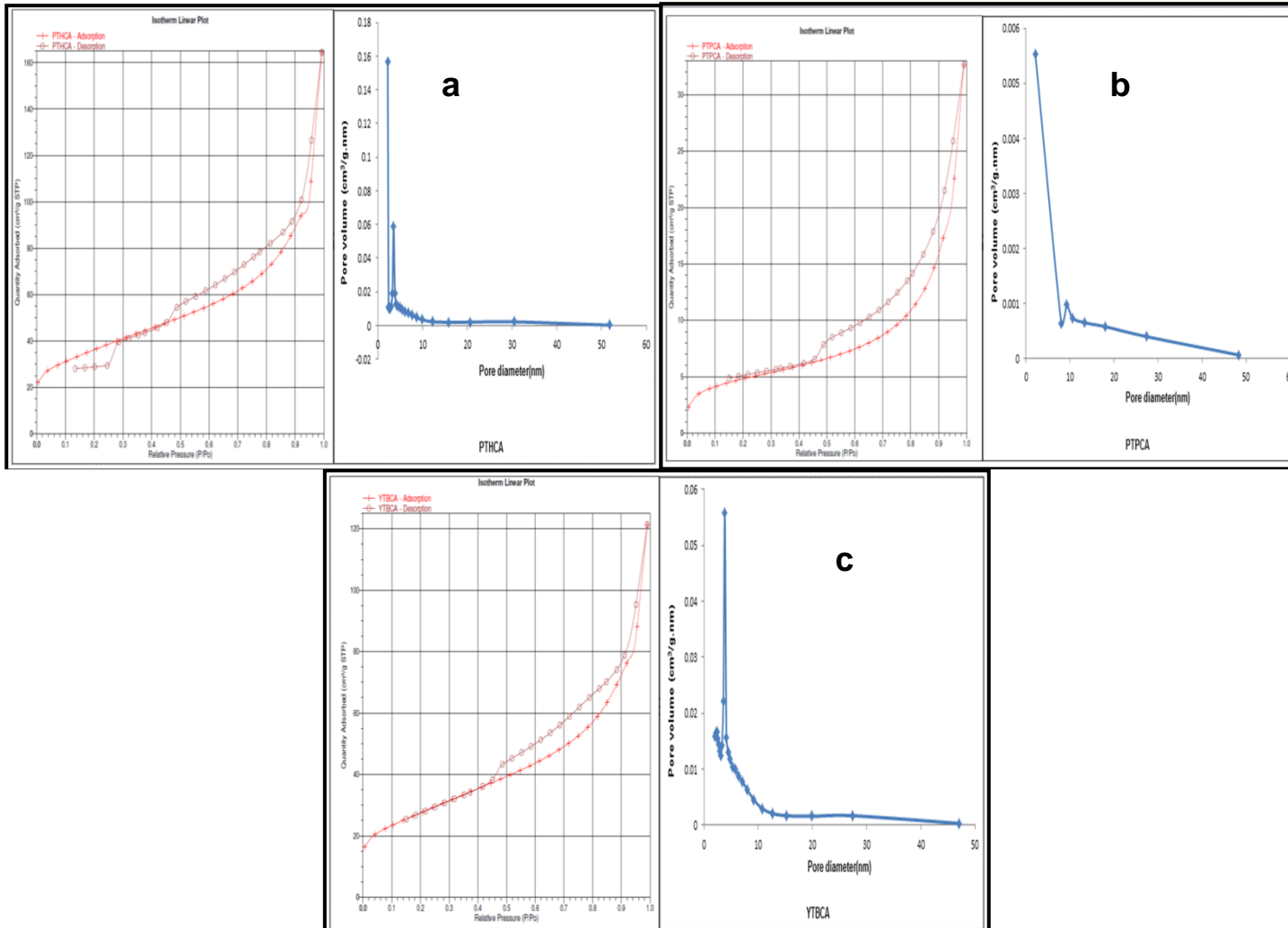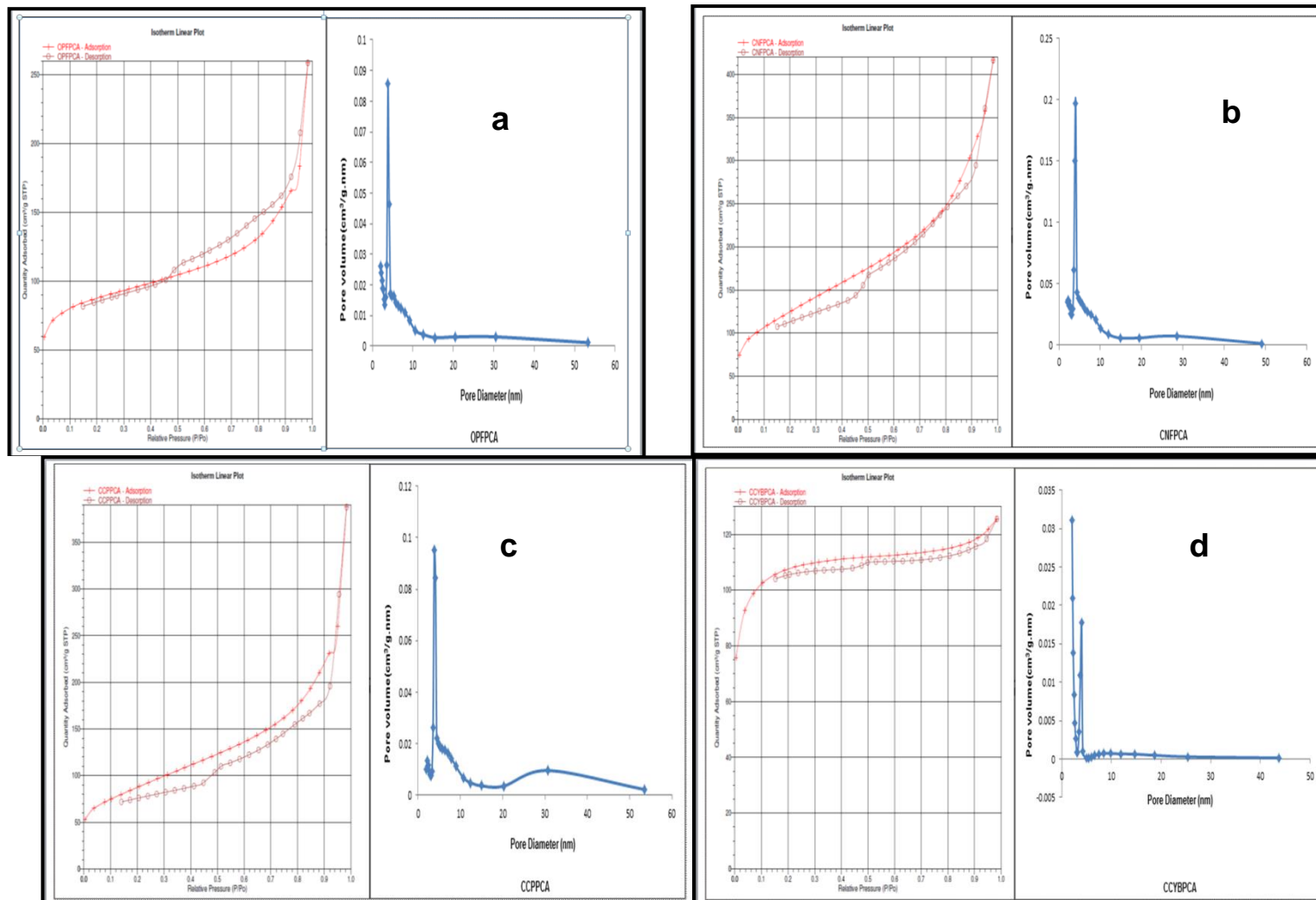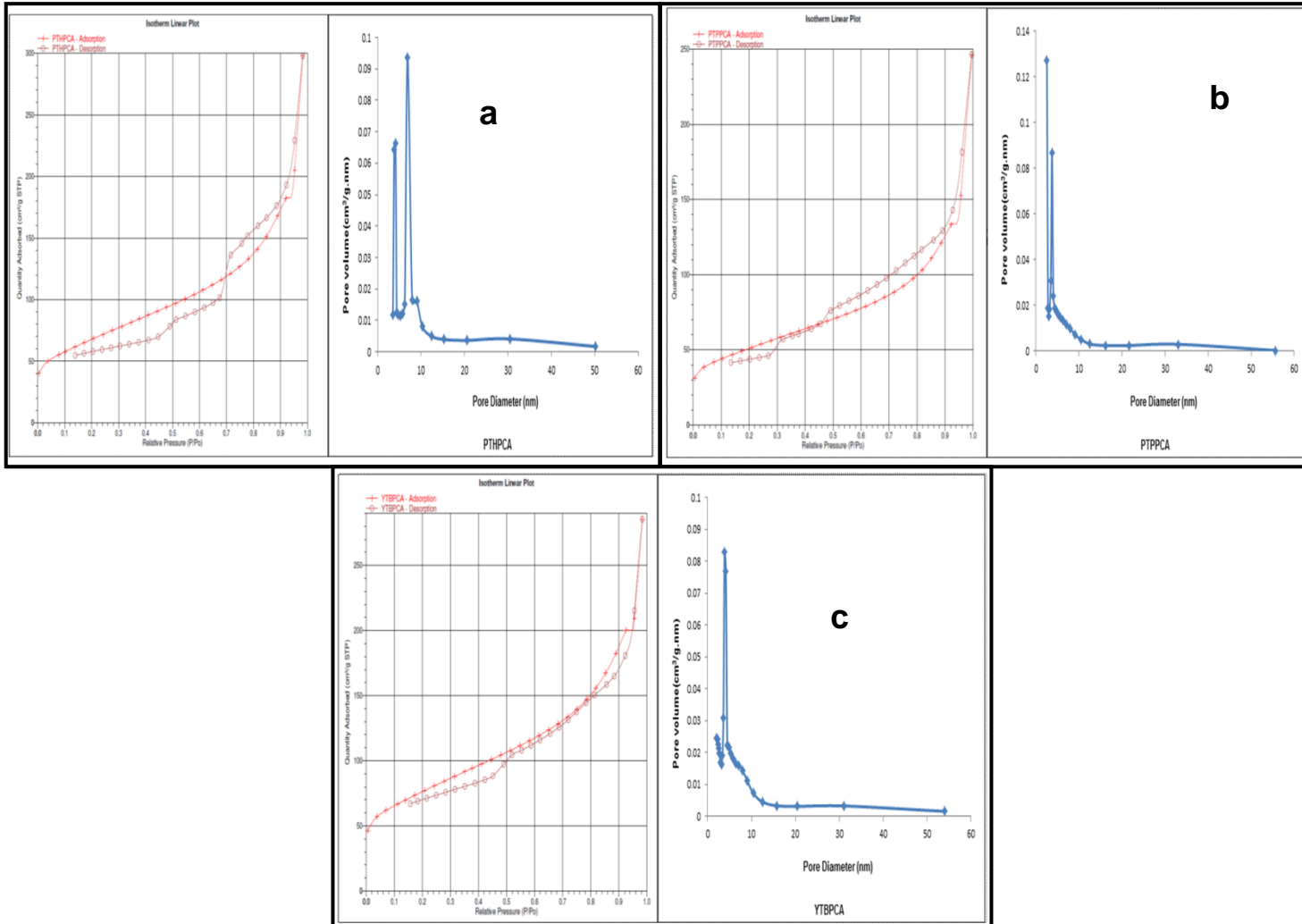Figure 7.4: N$_2$ adsorption-desorption isotherm and pore size distribution of PTHPCA, PTPPCA and YTBPCA adsorbents

These observations have also been reported for the hydrothermal carbonised adsorbents (HTC170/200) previously discussed in Chapter 6 of this work. The structures of porous carbon adsorbents has been classified as micropores (< 2 nm), mesopores (2 – 50nm) and macropores (> 50 nm) based on the pore dimensions according to IUPAC (IUPAC, 1991) and a comparison of the pore dimensions of the carbonized and pyrolysed adsorbents is presented in Table 7.5 and 7.6. From these Tables, it is observed that all the adsorbents had average pore diameter within the mesopore region thereby confirming the mesoporous characteristic of the adsorbents already observed from the shape of the N_2 isotherm. The range in average pore diameter for carbonized adsorbents was between 12.77 nm (OPFCA) and 3.67 nm (PTPCA), while that of the pyrolysed adsorbents was between 11.86 nm (CCPPCA) and 5.38 nm (CCYBPCA).

The total pore volumes on the carbonised and pyrolysed adsorbents are also presented in Tables 7.5 and 7.6. From these tables, it can be seen that the total pore volumes of the carbonised and pyrolysed adsorbents were higher than those obtained for the residue adsorbents (precusors) and the hydrothermal carbonized adsorbents previously discussed in Chapter 5 & 6 of this study. For the carbonised adsorbents, the range in total pore volume was between 0.34 cm^3 g^{-1} (OPFCA) to 0.05 cm^3 g^{-1} (PTPCA). For the pyrolysed adsorbents, the values were in the range 0.64 cm^3 g^{-1} (CNFPCA) to 0.19 cm^3 g^{-1} (CCYBPCA). This also indicates that the pyrolysed adsorbents had higher total pore volume than the carbonized adsorbents and this can be related to the increase in volatilization of the organic constituents on the residues (precursors) leading to the creation of pores as temperature increases from 400°C to 700°C as well as the different environments. The total pore volume of the carbonised and pyrolysed adsorbents developed in this study were observed to be higher than what has been reported for biochar obtained from the pyrolysis at 600°C of digested whole sugar beet char (DWSBC) under N_2 atmosphere reported by Inyang *et al.,* (2012). In their study the total pore volume of the DWSBC was 3.4×10^{-2} cm^3g^{-1}.

It was also observed that the pore volumes of some of the pyrolysed adsorbents developed in this study were similar to what is obtained for some commercial activated carbon adsorbents. In a study by Al-Lagtah *et al.,* (2016) on the chemical and physical characteristics of optimal synthesized activated carbons from grass-derived sulfonated lignin versus commercial activated carbons, the total pore volume of two commercial activated carbons are reported. These were 0.53 cm^3 g^{-1} (CAC1) commercially known as

DARCO 12X20 and 0.64 cm^3 g^{-1} (CAC2) commercially known as NORIT GAC 1240W. From this study, it can be observed that the total pore volumes of the PTHPCA, CCPPCA and the CNFPCA adsorbents are similar to those of the commercial activated carbon adsorbents reported above.

Furthermore, an evaluation of the pore size distribution plots shown in Figures 7.1 – 7.4 indicates that all the adsorbents had a narrow distribution of pores (bimodal) within the range 3 – 10 nm and the maxima of the distribution curves occurring at less than 10 nm with the exception of PTPCA where the maxima was at 10 nm. The pore size distribution of these pyrolysed adsorbents places them between the pore distribution of zeolites and carbon adsorbents (Jain *et al*., 2014). A pore size distribution for a mesoporous pyrolysed adsorbent with maxima occurring at less than 20 Å has also been reported in a study on the hydrothermal pre-treatment for mesoporous carbon synthesis by Jain *et al*., (2014). Similarly, Cordero *et al.,* (2013) in their study have reported an observation of bimodal pore size distribution for granular chars obtained from flash and conventional pyrolysis of grape seeds. Hence, the carbonised and pyrolysed adsorbents developed in this study can be said to have surface and pore characteristics that are similar to those reported in literature. These surface and pore properties are known to play important roles in sorption transport across adsorbent surfaces and thus can greatly enhance the uptake capabilities of the carbonised and pyrolysed adsorbents

7.4 Surface morphology and chemical composition of carbonised and pyrolysed adsorbents

The production of materials from carbonisation and pyrolysis of lignocellulosic feedstock depends on the transformation of residues into carbon based chars that are remarkably different in their physical and chemical characteristics. Most of these properties are influenced by the diverse reactions and processes that occur in the thermal treatment process. Some of proposed reactions that occur include; decarboxylation, dehydration, decarboxylation, demethoxylation, intermolecular rearrangement, condensation and aromatization (Funke and Ziegler, 2010). The morphology and chemical composition of the resulting biochars are two aspects that are affected by this thermal treatment and an examination of these properties can give insight that is important in understanding the complex processes that occur in these thermal environments. Scanning electron microscopy (SEM) was used to obtain information on the morphology of the carbonised

and pyrolysed adsorbents and their chemical composition was determined using the EDAX analysis coupled onto the scanning electron microscope.

7.4.1 Adsorbent surface morphology

The SEM micrographs obtained in the study for the carbonised and pyrolysed adsorbents are shown in Figures 7.5 to 7.8 for the carbonised adsorbents and Figures 7.9 to 7.12 for the pyrolysed carbon adsorbents. There is an indication of significant pore development from an examination of the images of the OPFCA and CNFCA carbonised adsorbents in Figures 7.5 and 7.6 and Figures 7.9 and 7.10 for the OPFPCA and CNFPCA pyrolysed adsorbents. This is not evident in the SEM images of the other adsorbents in Figures 7.7, 7.8, 7.11 and 7.12 and this may indicate that these residues did not have well developed pore structure that is visible from micrograph analysis. The honey-comb structures seen in the images of the CNFCA and CNFPCA adsorbents are well developed than those observed for the CNFS residue and CNFS-HTC170 and CNFS-HTC200 adsorbents previously discussed. This effect is also observed in the high BET surface area of the CNFCA and CNFPCA adsorbents and this indicates that the temperature of thermal treatment had a significant effect on the development of highly porous carbon materials from the lignocellulosic materials.
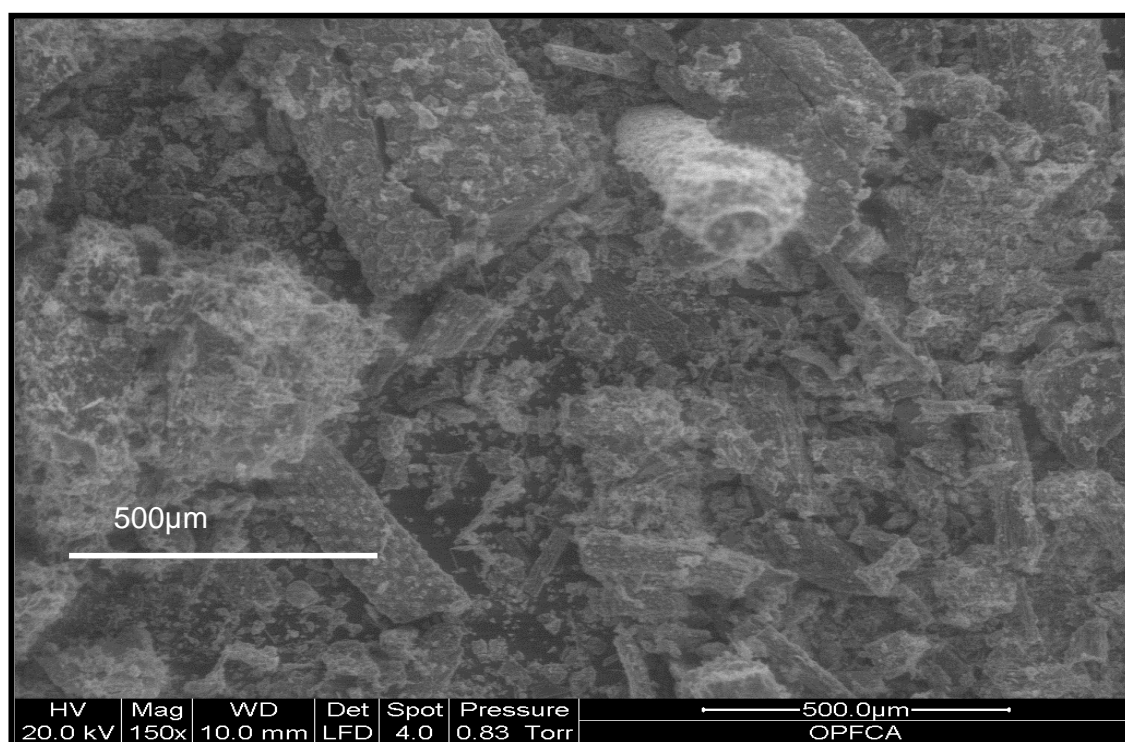
Figure 7.5: SEM micrograph for OPFCA (Scale bar = 500 µm)
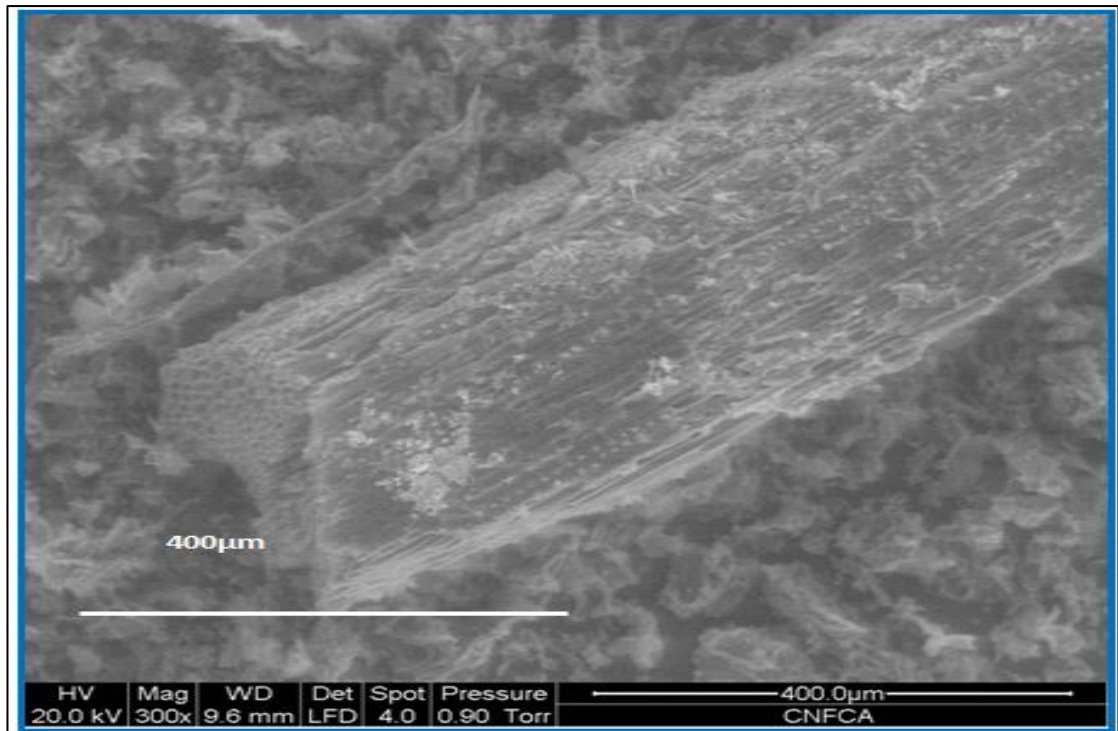
Figure 7.6: SEM micrograph for CNFCA (Scale bar = 400 µm)
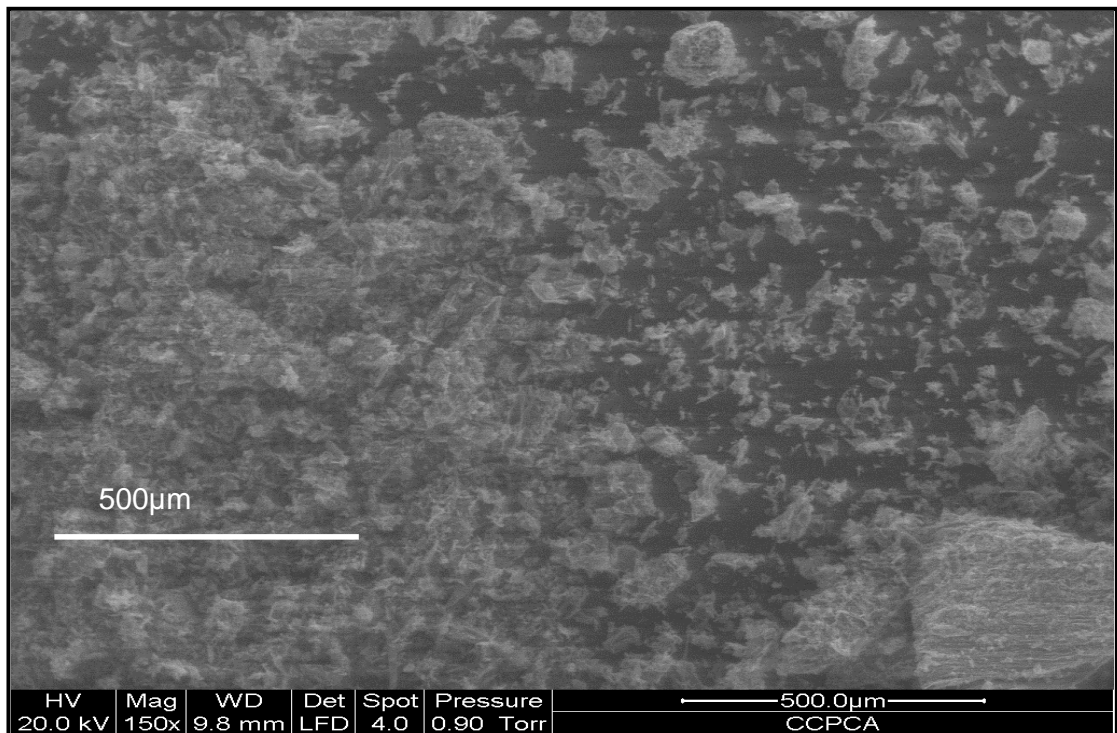
Figure 7.7: SEM micrograph for CCPCA (Scale bar = 500 µm)
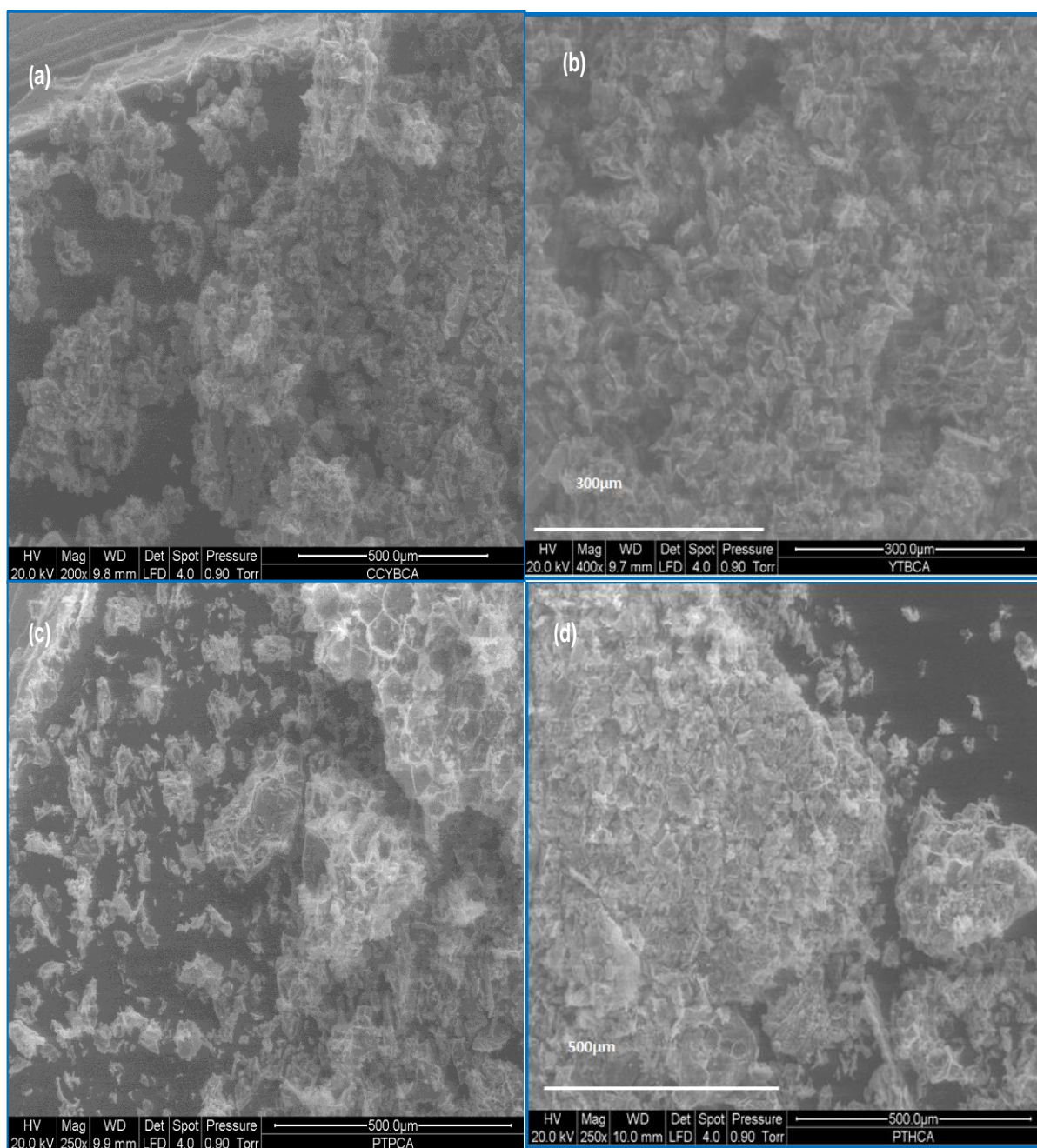
Figure 7.8: SEM micrographs for (a) CCYBCA, (b) YTBCA, (c) PTPCA & (d) PTHCA adsorbents (Scale bar = 300 and 500 µm)

The SEM images of the CCPCA, PTHCA, CCYBCA, PTPCA and YTBCA as well as those of the CCPPCA, PTHPCA, CCYBPCA, PTPCA and YTBPCA adsorbents shown in Figures 7.7, 7.8, 7.11 and 7.12 is observed to have disintegrated structures which may be due to the impact of thermal treatment with increase in the temperature of carbonisation and pyrolysis compared to those of hydrothermal carbonisation would cause the residue surface to rupture (Azargohar *et al.,* 2014).
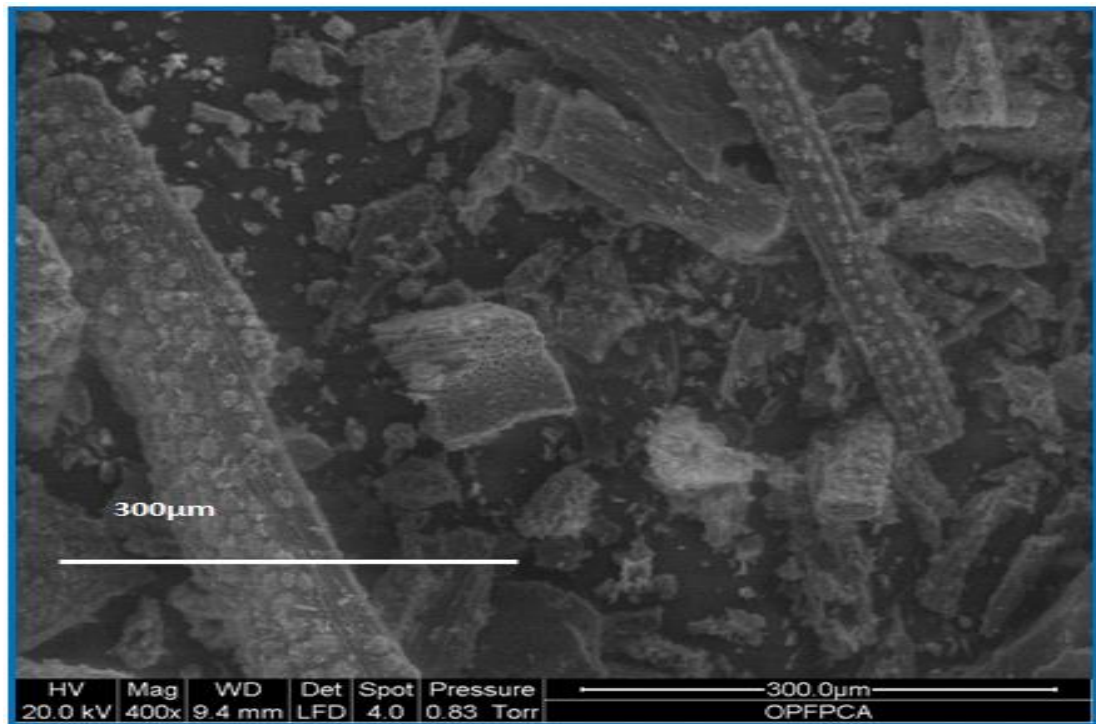
Figure 7.9: SEM micrograph for OPFPCA (Scale bar = 300 µm)
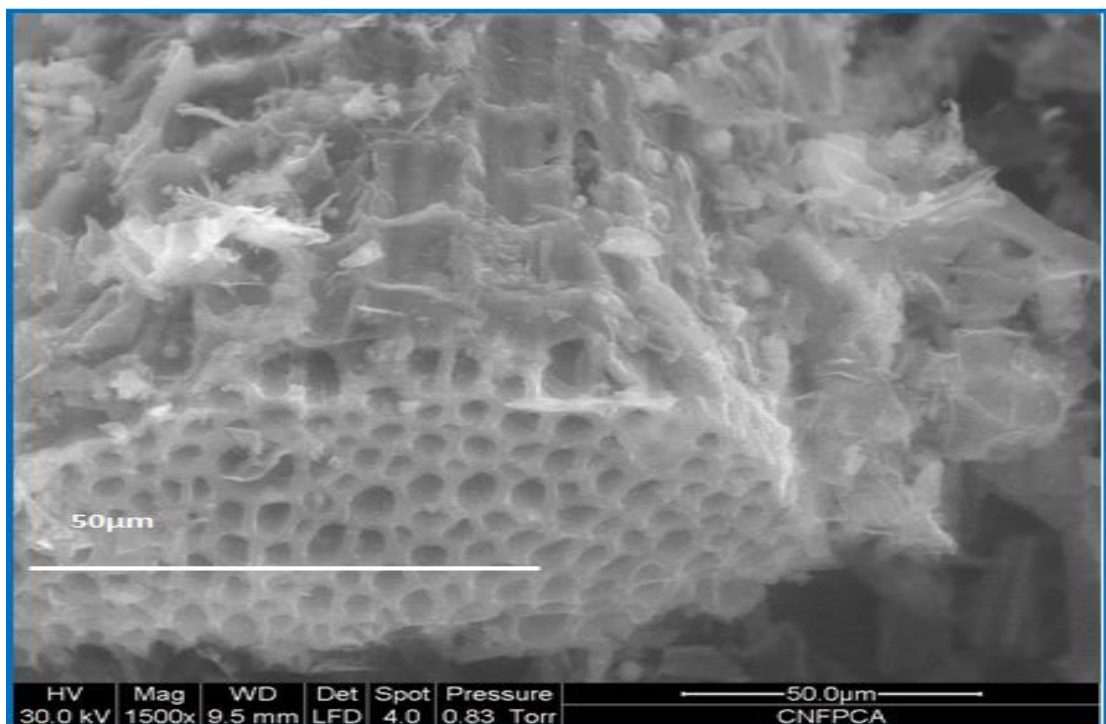
Figure 7.10: SEM micrograph for CNFPCA (Scale bar = 50 µm)
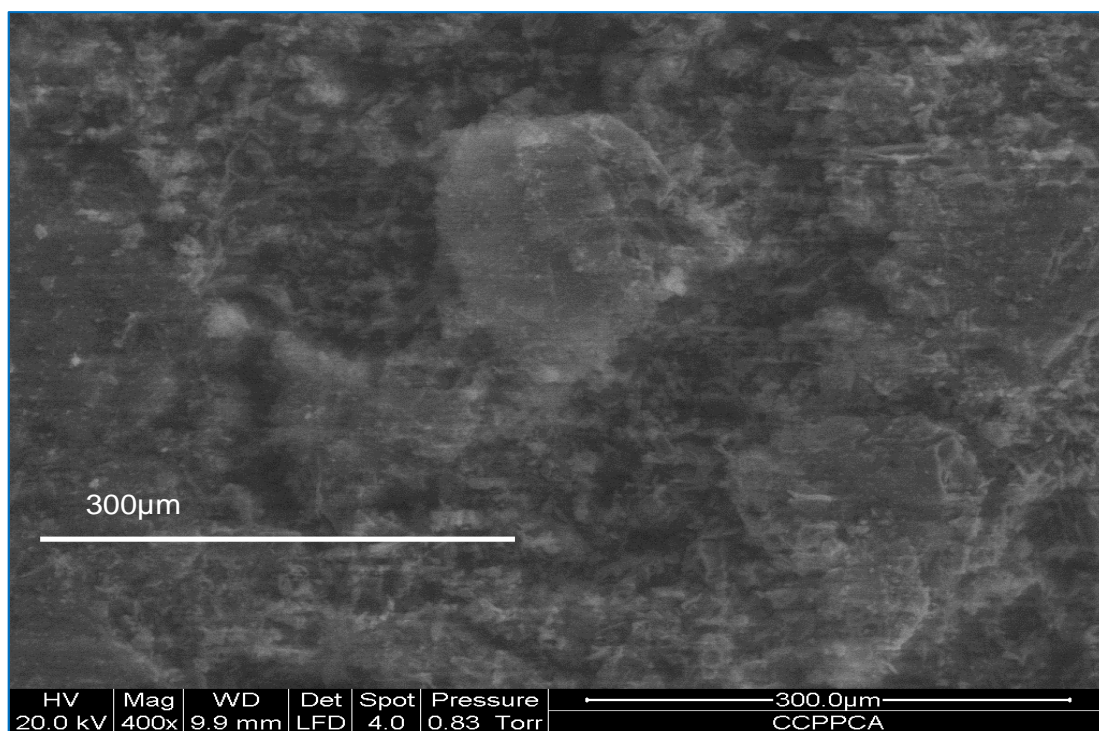
Figure 7.11: SEM micrograph for CCPPCA (Scale bar = 300 µm)

The SEM images of the carbonised and pyrolysed adsorbents were also observed to be irregular, sponge like with cavities in them thus implying that these spaces and pores were developed as a result of the thermal treatment process even though some of them like the CNFCA and CNFPCA still retained their cellular structure.
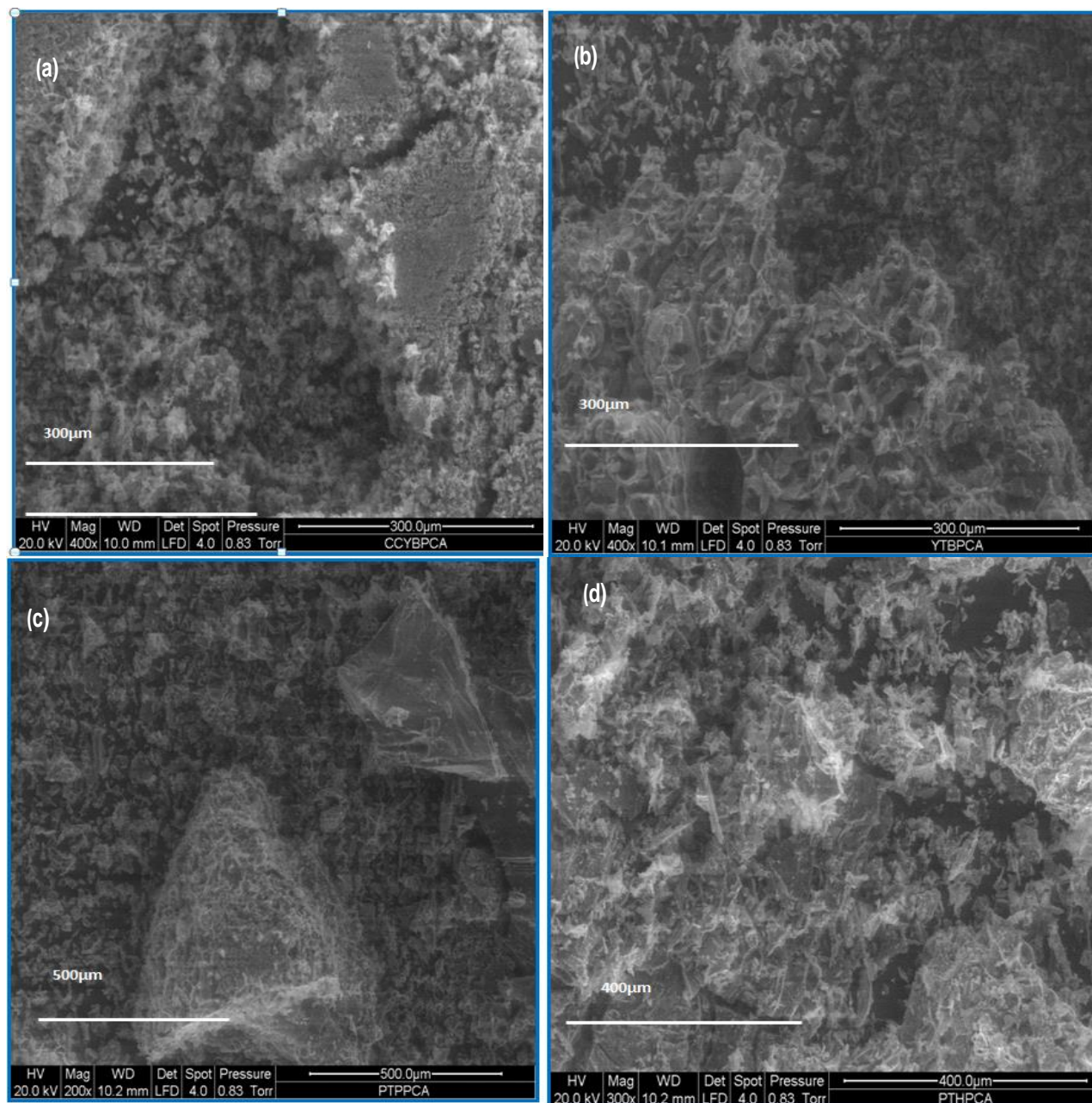
Figure 7.12: SEM micrographs for (a) CCYBPCA, (b) YTBPCA, (c) PTPPCA & (d) PTHPCA adsorbents

These irregular surfaces seen in the chars obtained from the thermal treatment of biomass has also been observed by Lopez *et al.,* (2013) in their study on the pyrolysis of wood waste. Thus it can be concluded that the morphology observed for these adsorbents are similar to what has been reported in literature.

7.4.2 Chemical composition of carbonised and pyrolysed adsorbents

The chemical compositions of the carbonised and pyrolysed adsorbents prepared in this section were also evaluated using EDAX to determine their elemental composition as

described in Section 4.3.2. Higher carbon and oxygen ratio (C: O) was expected for the thermally treated adsorbents than those of the residues due to the effect of the thermal degradation of the lignocellulosic residues in oxygen limited (carbonised) and nitrogen (pyrolysed) environments. The results of the analysis are shown in Figures 7.13 and 7.16 for the CCPCA and the CCYBPCA adsorbents. From Figure 7.13, it was observed that the carbonised adsorbent (CCPCA) had carbon, oxygen, aluminium and potassium contents of 79.7%, 9.3%, 6.81% and 2.95% respectively. The adsorbent also had trace amounts (%) of the following elements; magnesium (0.22%), silicon (0.12%), phosphorus (0.13%), sulphur (0.34%) and calcium (0.43%). The pyrolysed adsorbent (CCYBPCA) had a carbon, oxygen, aluminium and potassium content of 66.53%, 26.76%, 0.51% and 3.93% respectively. Some other chemical species on the adsorbent surface were: magnesium (0.33%), silicon (0.93%) and molybdenum (1.01%). These species may have migrated from the bulk of the adsorbent to the surface due to thermal processing. These results indicate that the carbonised adsorbent had higher carbon and aluminium content than the pyrolysed adsorbent, while the pyrolysed adsorbent had compositions of oxygen and potassium that were higher than the carbonised adsorbent. A lower carbon content with increase in the temperature of thermal treatment was observed and this might be related to the temperature of treatment and its effect on the nature and structure of the residue as the thermal degradation processes at higher temperature would result in the evolution of CO_2 and other small carbon-containing molecules, hence a reduction in the carbon content of the adsorbents.

The EDAX spectrum of the carbonised and pyrolysed adsorbents show some interesting results when compared with that of the raw residue in Figure 5.25 (CCPS) and Appendix 5. From these Figures, it is observed that for the CCPS and CCPCA adsorbents, the carbon content was higher in the carbonised adsorbent than the residue, while the CCPS residue had a higher oxygen content than the CCPCA adsorbent. The potassium content of the CCPCA adsorbent was also observed to be higher than that of the CCPS residue.
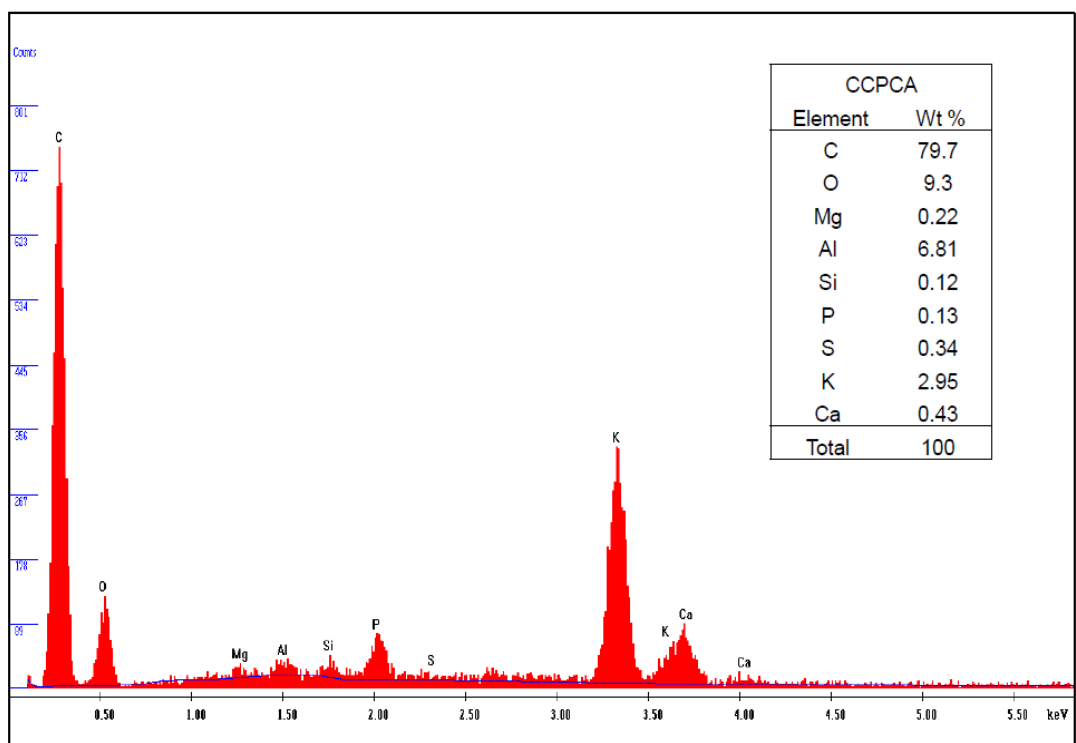
Figure 7.13: EDAX spectrum for CCPCA
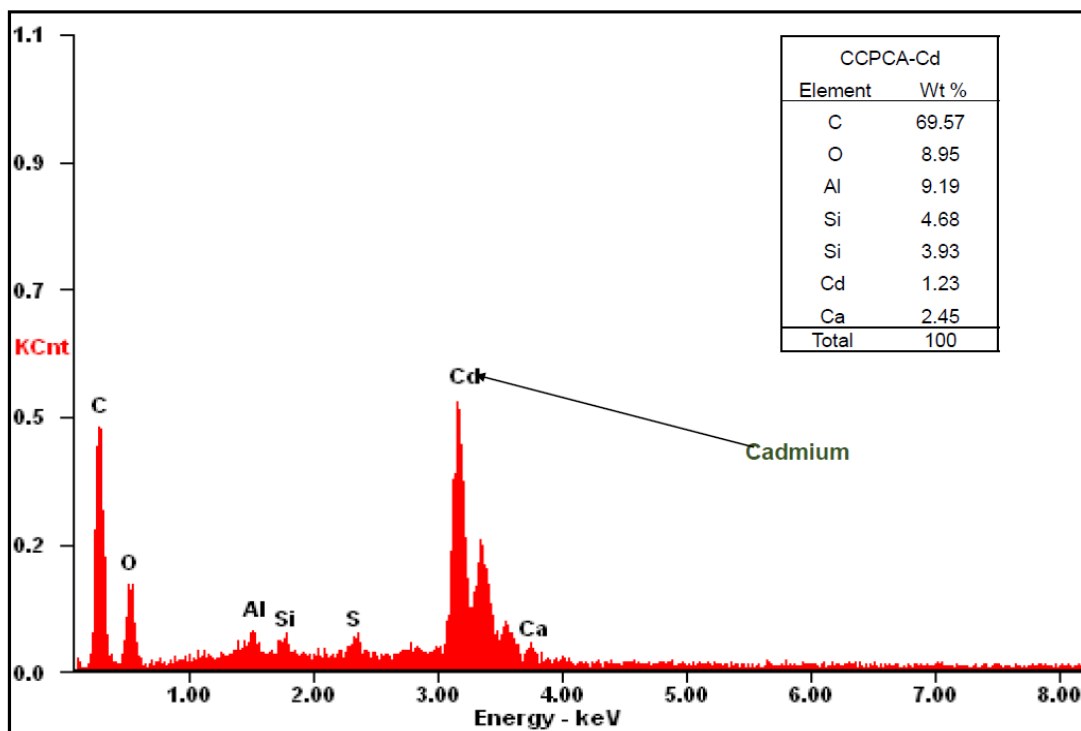
Figure 7.14: EDAX spectrum for CCPCA after cadmium adsorption
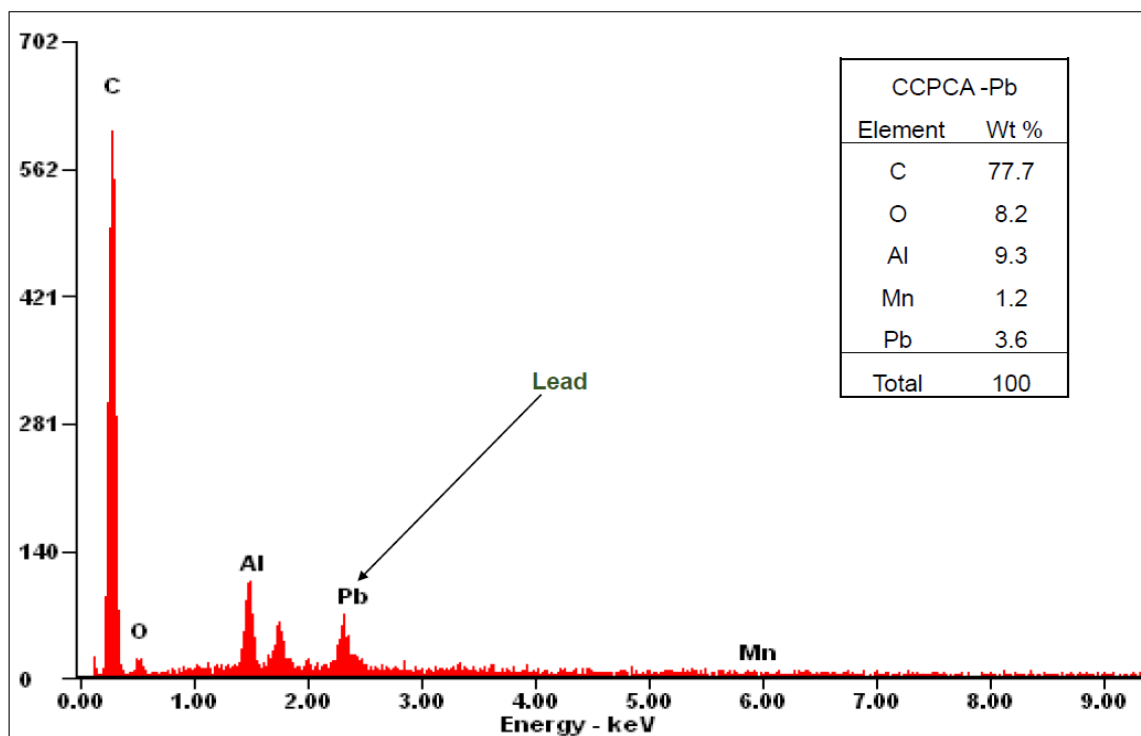
Figure 7.15: EDAX spectrum for CCPCA after lead adsorption
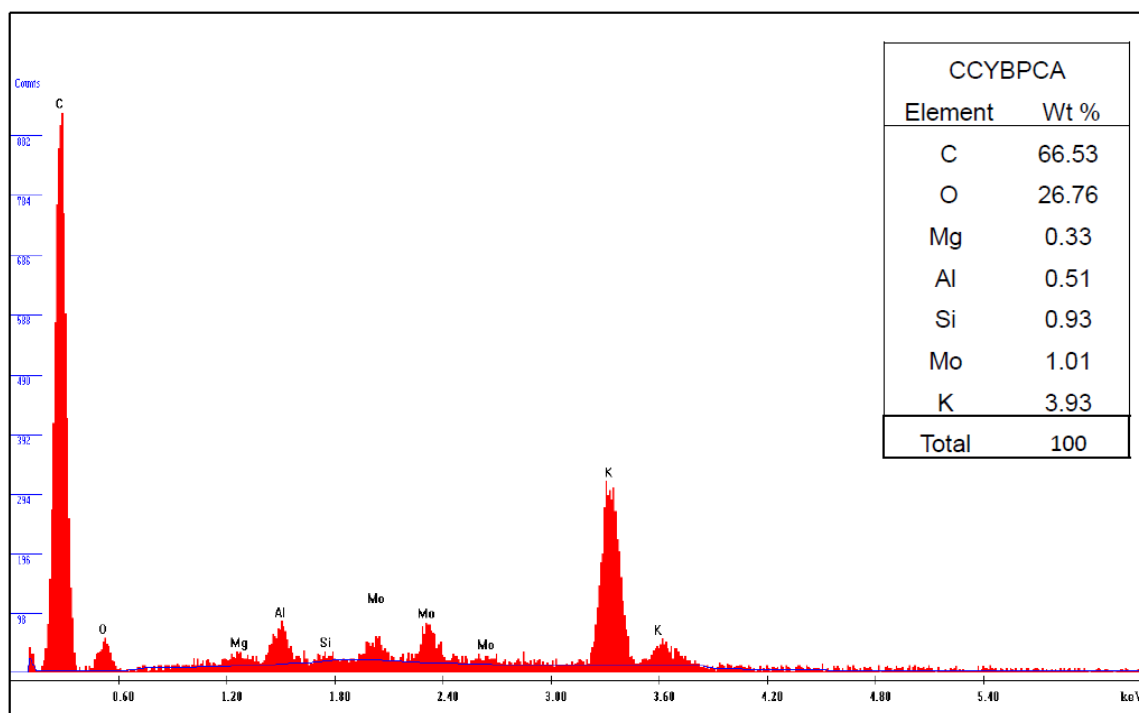
Figure 7.16: EDAX spectrum for CCYBPCA
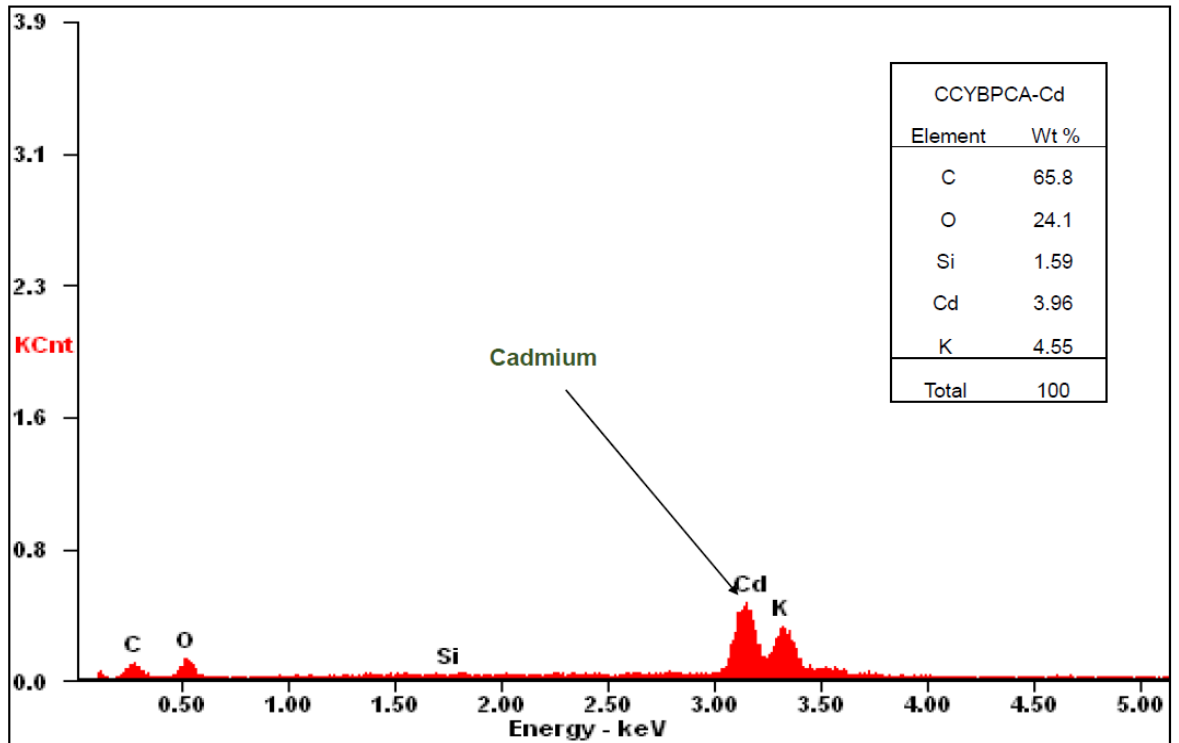
Figure 7.17: EDAX spectrum for CCYBPCA after cadmium adsorption
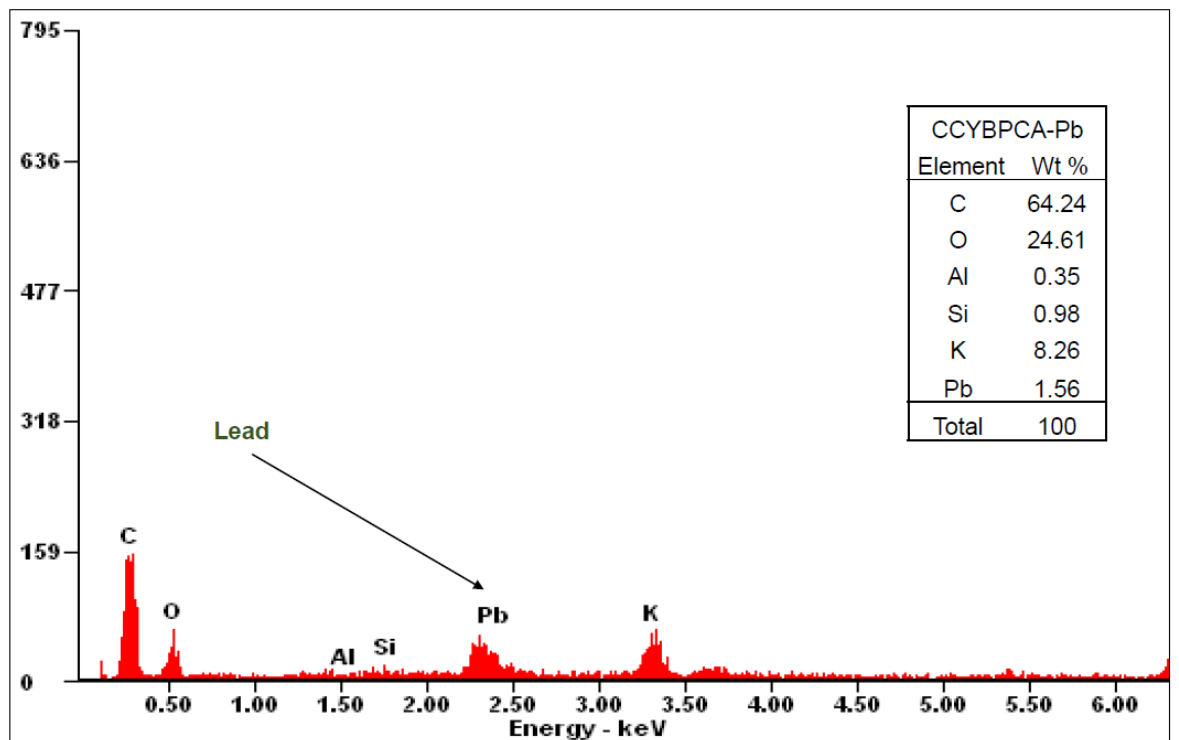
Figure 7.18: EDAX spectrum for CCYBPCA after lead (II) adsorption

The carbon and potassium content of the CCYBPCA adsorbent was observed to be higher than that of the CCYBS residue, with the CCYBPCA values being 66.5% (carbon) and 3.93% (potassium), while the carbon content of the CCYBS adsorbent was lower (62.8%),

it had a higher oxygen content (31.2%) than the pyrolysed adsorbent. According to Chen *et al*., (2011), the pyrolysis of residues at higher temperatures $300 - 800°C$ has been observed to increase the carbon content of biochar. An evaluation of the sorption capabilities of the carbonised and pyrolysed adsorbent was carried out using Cd(II) and Pb(II) ions in aqueous solution as adsorbate. An analysis and evaluation of the metal ion content of the adsorbents after sorption was carried out using EDAX. The results of this analysis are shown in Figures 7.14 and 7.15 for the CCPCA adsorbent, while that of the CCYBPCA adsorbents are shown in 7.17 and 7.18. From the Figures, it was observed that for both CCPCA and CCYBNCA adsorbents after sorption, the respective metal ions that was adsorbed on the surface of the adsorbents was seen in the EDAX spectrum thereby implying that these adsorbents were capable of adsorbing these metal ions onto their surfaces.

7.5 Kinetic Sorption Studies

The kinetic studies Cd (II) and Pb (II) ion removal for aqueous solution using the pyrolysed and carbonized adsorbents were carried out with an initial metal ion concentration of 500 mgL^{-1}. The volume of the aqueous adsorbate was 0.1 L and the sorption took place at pH 7 and a temperature of $25°C$. The adsorbent mass for each study was 1 g. The time intervals for the studies were 5, 10, 15, 15, 20, 25, 30, 40, 60, 90, 120 and 180 minutes at 200 rpm. The determination of the metal ion loading after sorption at time t was calculated using Eqn. 7.1 with amount of metal ion adsorbed (q_t) given as:

$$qt = \frac{(C_i - C_t)V}{m}$$
(7.1)

Where C_t (mg/L) is the metal ion concentration at time t,

C_i is the initial metal ion concentration

m is the mass of the adsorbent

V is the volume of the aqueous system.

7.5.1 Cadmium (II) ion sorption

The effect of contact time on the removal of Cd (II) from aqueous solution using the pyrolysed and carbonized adsorbents are shown in Figures 7.19 and 7.20. From the Figures, the maximum loading of Cd (II) for the two groups of adsorbents were as follows;

25.51 mgg^{-1} (OPFPCA), 28.8 mgg^{-1}(CNFPCA), 29.8 mgg^{-1}(CCPPCA),19.80 mgg^{-1}(CCYBPCA), 23.3 mgg^{-1}(PTHPCA), 26.6 mgg^{-1}(PTPPCA) and 28.9 mgg^{-1} (YTBPCA) for the pyrolysed adsorbents. These results show that the CCPPCA adsorbent had the highest loading capacity while CCYBPCA had the least.
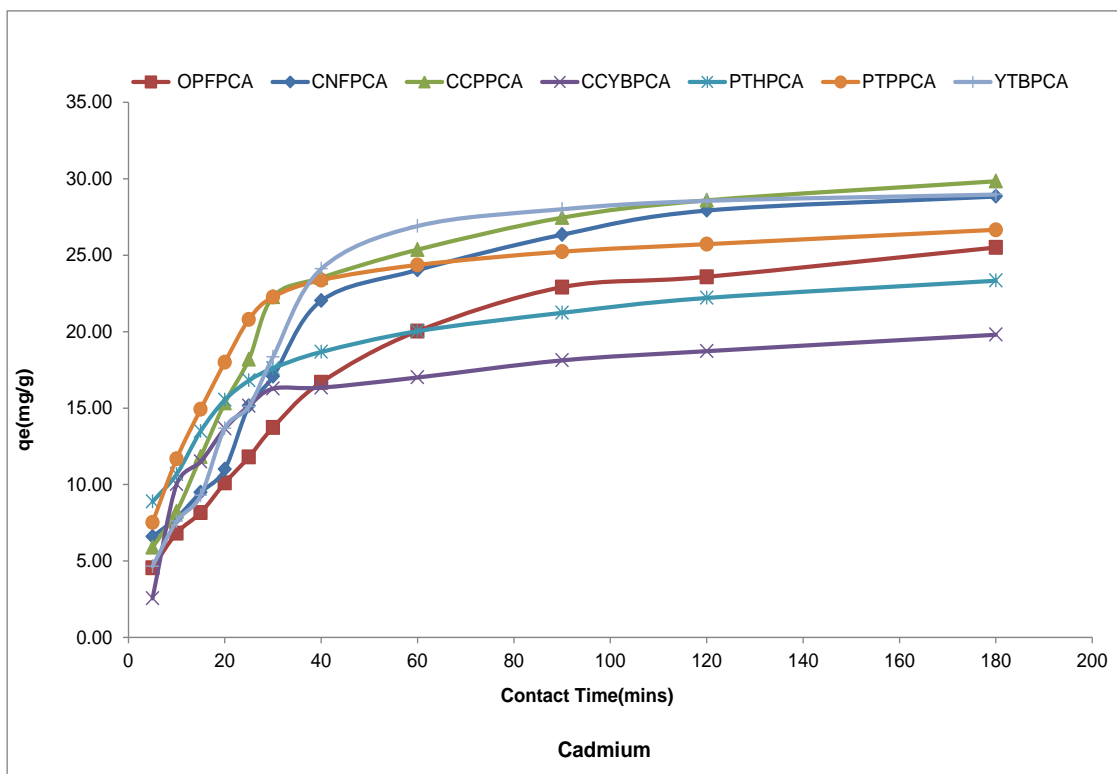
Figure 7.19: Kinetic profile for cadmium (II) ion sorption onto pyrolysed adsorbents

The carbonized adsorbents on the other hand had loadings of 26.3mgg^{-1} (OPFCA), 27.0 mgg^{-1} (CNFCA), 22.7 mgg^{-1}(CCPCA), 17.0 mgg^{-1} (CCYBCA), 23.6 mgg^{-1} (PTHCA), 20.3 mgg^{-1}(PTPCA) and 21.0 mgg^{-1}(YTBCA). For these adsorbents, the CNFPCA had the highest loading while CCYBCA had these least Cd(II) ions loading. The Cd(II) ion uptake of the pyrolysed adsorbents are higher than those of the carbonised adsorbents and this may be associated to the larger surface area and total pore volume of the pyrolysed adsorbents.
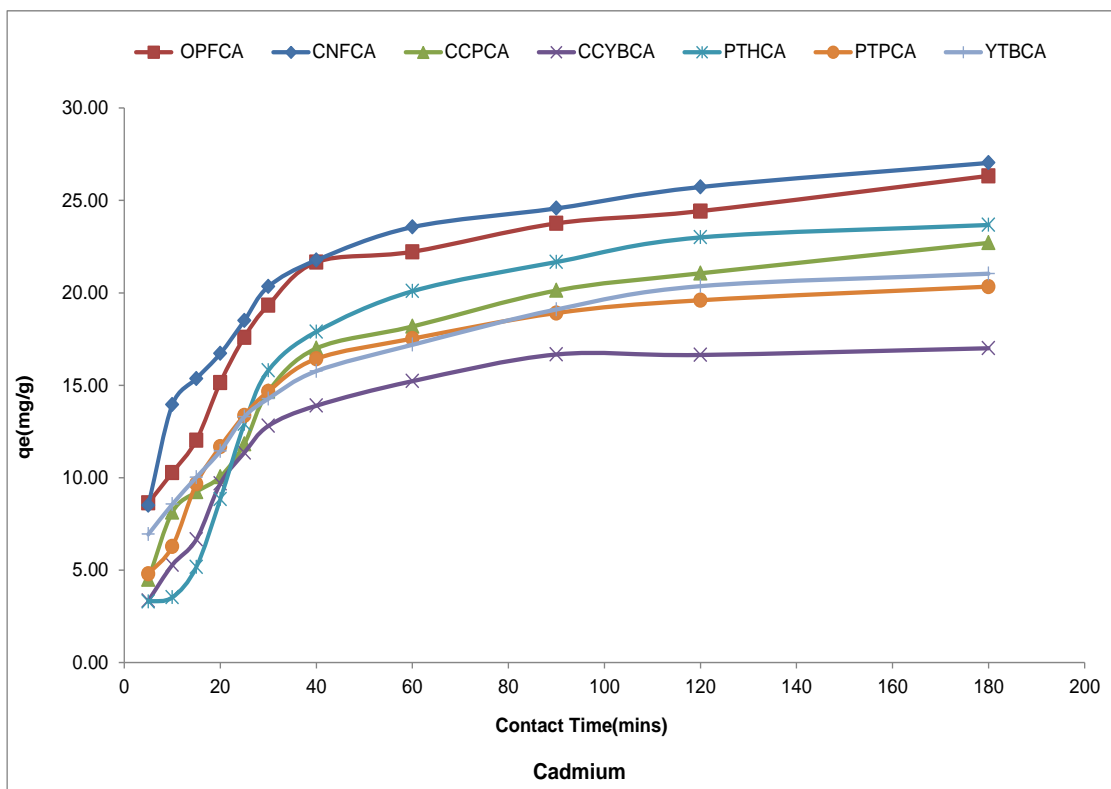
Figure 7.20: Kinetic profile for cadmium (II) ion sorption onto carbonised adsorbents

From Figures 7.19 and 7.20, it can be observed that the kinetic profile for the two groups of adsorbents follows the two stage description observed for the previous adsorbents discussed in this study. These were a rapid first stage proceeding from initial metal ion – adsorbent contact to 90 minutes for both groups of adsorbent, while the second stage proceeded via a slow step wise process of loading lasting up to 180 minutes where it is presumed that equilibrium is attained. The presence or absence of active sites on the adsorbent is linked to this two stage metal ion loading profile. The first stage is a rapid one because there are many vacant active sites for metal ion loading and the uptake is quick. However, when the vacant sites are rapidly filled, the number of available sites decreases with a decrease in the ease of uptake and this results in the slow and gradual second stage. Additionally, the repulsive interaction between the Cd(II) ions on the adsorbent active sites and the Cd(II) ions in the adsorbate reduces the speed of the second stage as the probability of uptake diminishes. This two stage metal ion uptake has been reported by Iqbal *et al.*, (2009a) in their study of the removal of Ni (II) and Zn(II) ions by grape fruits peel adsorbent. The study notes that an initial rapid stage occurring up to 60 minutes preceded a second slower stage lasting up to 180 minutes when equilibrium was attained. A similar two-stage kinetic profile was observed by Feng *et al.,* (2009) in their study on the sorption

of copper (II) using modified orange peel. In the study, it was observed that there was a sharp increase in the amount of copper (II) ion adsorbed by chemically modified orange peel within an initial duration of 30 minutes which was subsequently followed by a slow removal until 120 minutes. El-Ashtoukhy *et al.*, (2008) also reports a similar two-stage kinetic profile for the removal of metal ions using activated carbon obtained from pomegranate peel. In their study, it was observed that the removal of Pb(II) and Cu(II) ions increased rapidly during the first 10 minutes of the sorbate–sorbent contact, but it gradually decreased with time until it reached equilibrium and attained saturation in about 120 minutes. During slow phase the rate of percent removal almost insignificant due to a quick exhaustion of the adsorption sites.

7.5.1.1 Kinetic modelling of Cd(II) sorption

Adsorption kinetics also shows a large dependence of sorption on the physical characteristics of the adsorbent which also influences the adsorption mechanism. A number of models have been used to describe the rate and extent of sorption of an adsorbate onto an adsorbent and these models have assumptions for the prediction of these interactions (Chen *et al.,* 2001). The applicability of different kinetic models is often tested based on their ability to describe the experimental kinetic data. For the sorption of Cd(II) and Pb(II) ions onto the pyrolysed and carbonised adsorbents, two kinetic models were evaluated and these are the pseudo-first order (PFO) and pseudo second order (PSO). To determine the goodness of fit of the isotherm models to the experimental data using non-linear regression, the optimization procedure requires that error functions be defined to enable the fitting of the model parameters with the experimental values. In this study, the coefficient of determination (r^2), the root mean square error (RMSE) and the Chi square test (χ^2) were used as error parameters for each model and these were determined based on eqns. 5.4, 5.5 and 5.6 which have been previously described in section 5.11 of chapter 5 in this study.

Kinetic modelling of Cd(II) ion sorption onto the pyrolysed and carbonised adsorbents were carried out for the pseudo first order (PFO) and pseudo first order (PSO) equations using the solver add-in optimization procedure in Microsoft excel 2010 software. The plots of the PFO are PSO models for Cd(II) are presented in Figures 7.21 and 7.22 for the pyrolysed and Figures 7.23 and 7.24 for the carbonised adsorbents. From these models, the kinetic parameters and their respective error functions obtained are presented in Table 7.7 and 7.7 for the carbonised and pyrolysed adsorbents respectively. These results indicate

that the two models (PFO & PSO) could be used to characterise the kinetics of Cd(II) ion sorption onto the pyrolysed and carbonised adsorbents and the prediction of each model for the kinetic parameter ($q_{e,model}$) is close to the result obtained from the experimental analysis of Cd(II) ion sorption.

For the PFO model, the maximum loading parameter $q_{e,cal}$ obtained for the carbonised adsorbents for Cd(II) ion sorption were in the range 17.0 mgg^{-1} (CCYBCA) to 25.0 mgg^{-1}(CNFCA) with the order being CNFCA > OPFCA > PTHCA > CCPCA >PTPCA > YTBCA > CCYBCA, thus implying that the CNFCA adsorbent had the highest loading with the least being that of the CCYBCA adsorbent. For the pyrolysed adsorbents, the value of the PFO model $q_{e,cal}$ obtained Cd(II) ion sorption were in the range 18.6mgg^{-1} (CCYBPCA) to 29.8 mgg^{-1}(YTBPCA) with the order being YTBPCA > CCPPCA > CNFPCA > PTPPCA > OPFPCA > PTHPCA > CCYBPCA. From these two thermally modified adsorbents, it can be observed that the YTBPCA adsorbent had the highest value for $q_{e,cal}$ from the PFO model, while the CCYBCA adsorbent had the least. The rate constant of the pseudo first order (PFO) reaction (K_1) for the carbonised adsorbents were in the range 2.76×10^{-2} min^{-1}(PTHCA) to 6.20×10^{-2} min^{-1}(CNFCA), while that of the pyrolysed adsorbents were in the range 3.67×10^{-3} min^{-1}(OPFPCA) to 6.33×10^{-3} min^{-1}(CCYBPCA).

The value of the coefficient of determination (r^2) and the two error parameters – the root mean square (RMSE) and Chi square (χ^2) was used to determine the Cd(II) ion uptake kinetics is best described by the PFO model. From Table 7.7 and 7.8, it is observed that for the carbonised adsorbents, CCPCA, CCYBCA and PTPCA adsorbents all had the same r^2 value of 0.99, while the OPFCA adsorbent had an r^2 value of 0.98. The lowest r^2 value was 0.97 and was this was obtained for the CNFCA, PTHCA and YTBCA adsorbents. These r^2 values indicates that the experimental data for the kinetics of Cd(II) ion sorption onto the CCPCA, CCYBCA and PTPCA adsorbents are in close agreement what that of the PFO model. To further discriminate amongst these three adsorbents, the χ^2 and the RMSE values were used with the lowest values being an indication of best fitting. Based on this assumption, the sorption of Cd(II) ion onto the CCYBCA adsorbent is best described by the PFO model with the lowest χ^2 (0.02) and RMSE (1.17×10^{-1}) values. For this adsorbent, the PFO rate constant (K_1) obtained was 4.12×10^{-2} min^{-1} and the PFO model Cd(II) ion loading ($q_{e,cal}$) was 17.0 mgg^{-1}.

For the pyrolysed adsorbents, r^2 value of 0.99 was obtained for the OPFPCA, CCPPCA, PTPPCA and YTBPCA adsorbents. The CNFPCA adsorbent had an r^2 value of 0.98, while the CCPYBPCA and PTHPCA adsorbents both had an r^2 value of 0.98. These r^2 values suggest that the sorption of Cd(II) ion onto these adsorbents were better represented by the PFO model for the OPFPCA, CCPPCA, PTPPCA and YTBPCA adsorbents. Further evaluation of the values of the error parameters (χ^2 and the RMSE) for these 4 adsorbents were used to determine which one was best described by the PFO model. From Table 7.8, it is observed that the PTPPCA adsorbent is best described by the PFO model with the lowest χ^2 (0.01) and RMSE (1.45×10^{-1}) values. For this adsorbent, the PFO rate constant (K_1) obtained was 6.17×10^{-2} min^{-1} and the Cd(II) ion loading ($q_{e,cal}$) for the PFO model was 25.8 mgg^{-1}. Comparing between the carbonised and pyrolysed adsorbents for Cd(II) ion sorption, it is observed that the PTPPCA adsorbent was best described by the PFO model as it had the lowest values for the error parameters (χ^2 and the RMSE) and the highest r^2 value.

The PSO model was also used to evaluate the kinetics of Cd(II) ion sorption onto the carbonised and pyrolysed adsorbents and the results are also presented in Tables 7.7 and 7.8. From these Table 7.7, the PSO rate constant (K_2) for the carbonised adsorbents were in the range 1.50×10^{-3} gmg^{-1}min^{-1}(CCPCA) to 8.27×10^{-3} gmg^{-1}min^{-1}(PTHCA), while that of the pyrolysed adsorbents were in the range 1.21×10^{-3} gmg^{-1}min^{-1}(CCPPCA) to 8.67×10^{-3} gmg^{-1}min^{-1}(YTBPCA). The initial sorption rate (h) obtained from the PSO model as $q_t/t \rightarrow 0$ which gives an indication of the intial kinetic rate of sorption. For the carbonised adsorbents, the values were in the order of CNFCA > OPFCA > YTBCA > PTPCA > CCPCA > CCYBCA > PTHCA with the CNFCA adsorbent having the highest value of 2.33mgg^{-1}min^{-1}. For the pyrolysed adsorbents, the order for the initial sorption rate (h) was PTPPCA > PTHPCA > CCYBPCA > CCPPCA > YTBPCA > CNFPCA > OPFPCA with the PTPPCA having the highest value of 2.32mgg^{-1}min^{-1}.

Table 7.7: PFO & PSO modelling parameters for Cd(II) sorption on carbonised adsorbents

	Pseudo First Order Model					Pseudo Second Order					
Adsorbent	$q_{e,cal}(mgg^{-1})$	$K_1(min^{-1})$	r^2	χ^2	RMSE	$q_{e,cal}(mgg^{-1})$	$K_2(gmg^{-1}min^{-1})$	$h(mgg^{-1}min^{-1})$	r^2	χ^2	RMSE
OPFCA	24.6	5.09E-02	0.98	0.08	7.44E-01	28.3	2.23E-03	1.79	0.98	0.05	4.79E-01
CNFCA	25.0	6.20E-02	0.97	0.09	8.66E-01	28.2	2.92E-03	2.33	0.99	0.01	1.38E-01
CCPCA	21.6	3.58E-02	0.99	0.05	3.89E-01	25.9	1.50E-03	1.01	0.99	0.04	2.54E-01
CCYBCA	17.0	4.12E-02	0.99	0.02	1.17E-01	20.2	2.25E-02	0.92	0.98	0.06	3.43E-01
PTHCA	24.2	2.76E-02	0.97	0.16	1.17E+00	30.8	8.27E-04	0.79	0.95	0.24	1.74E+00
PTPCA	19.6	4.45E-02	0.99	0.02	1.22E-01	23.1	2.21E-03	1.18	0.99	0.03	1.95E-01
YTBCA	19.7	4.63E-02	0.97	0.10	6.87E-01	22.8	2.51E-03	1.30	0.99	0.03	2.21E-01

Table 7.8: PFO & PSO modelling parameters for Cd(II) sorption on pyrolysed adsorbents

| Adsorbent | Pseudo First Order Model | | | | | Pseudo Second Order | | | | | |
	$q_{e,cal}$(mgg^{-1})	K_1(min^{-1})	r^2	χ^2	RMSE	$q_{e,cal}$(mgg^{-1})	K_2(gmg^{-1}min^{-1})	h(mgg^{-1}min^{-1})	r^2	χ^2	RMSE
OPFPCA	25.2	2.67E-03	0.99	0.02	1.74E-01	31.6	8.21E-04	0.82	0.99	0.03	1.96E-01
CNFPCA	28.8	3.00E-02	0.98	0.08	7.08E-01	35.6	8.46E-04	1.07	0.98	0.11	9.82E-01
CCPPCA	29.1	3.91E-02	0.99	0.05	4.76E-01	34.9	1.21E-03	1.47	0.98	0.09	8.96E-01
CCYBPCA	18.6	6.33E-02	0.97	0.07	5.43E-01	21.3	3.64E-03	1.65	0.96	0.10	7.47E-01
PTHPCA	21.4	6.61E-02	0.97	0.09	7.28E-01	24.1	3.71E-03	2.17	0.99	0.02	1.46E-01
PTPPCA	25.8	6.17E-02	0.99	0.01	1.45E-01	29.3	2.71E-03	2.32	0.99	0.05	4.67E-01
YTBPCA	29.8	3.19E-02	0.99	0.08	7.46E-01	36.8	8.67E-03	1.17	0.97	0.18	1.68E+00
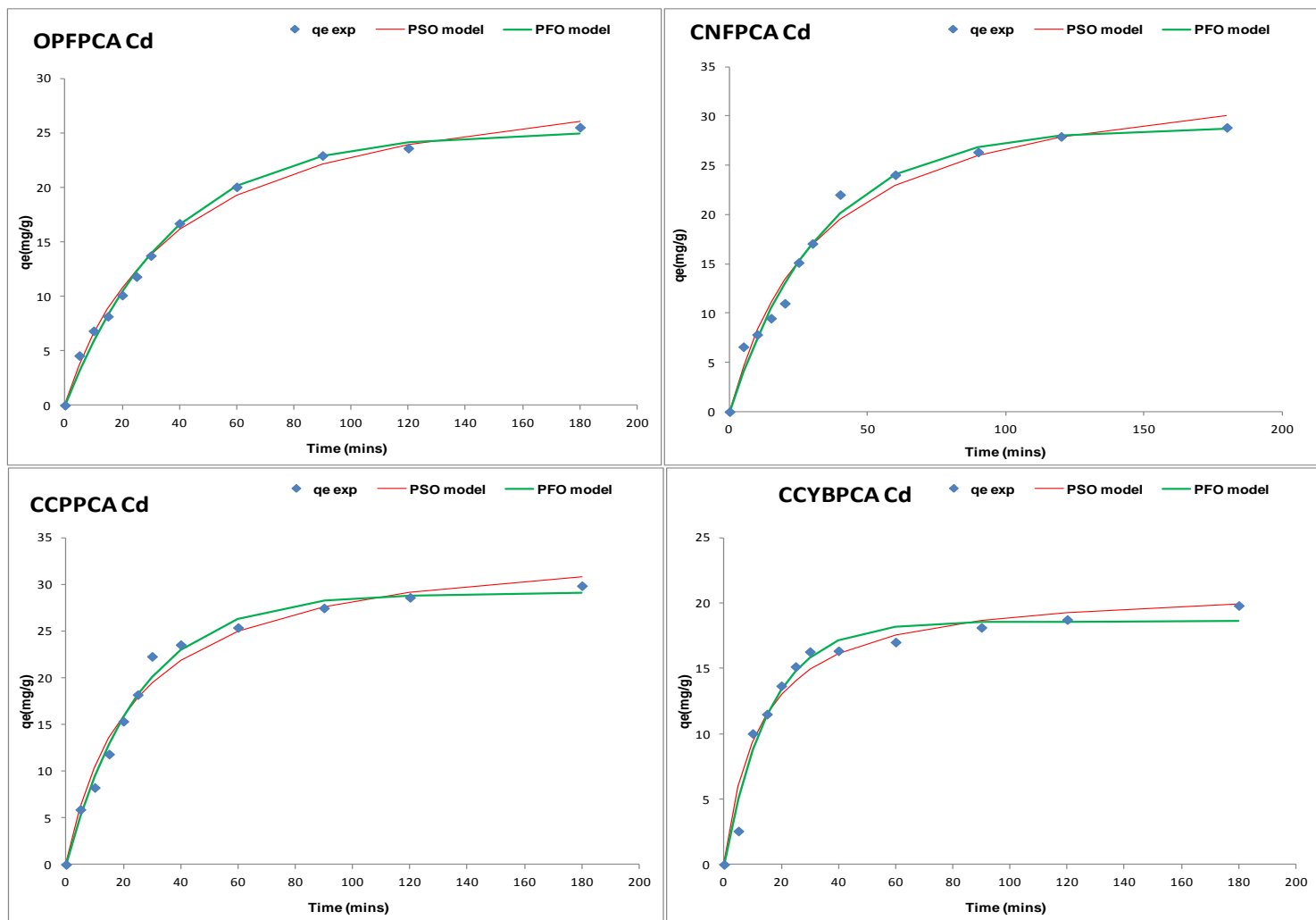
Fig 7.21: Cd(II) ion PFO & PSO sorption kinetic models for OPFPCA,CNFPCA, CCPPCA & CCYBPCA adsorbents
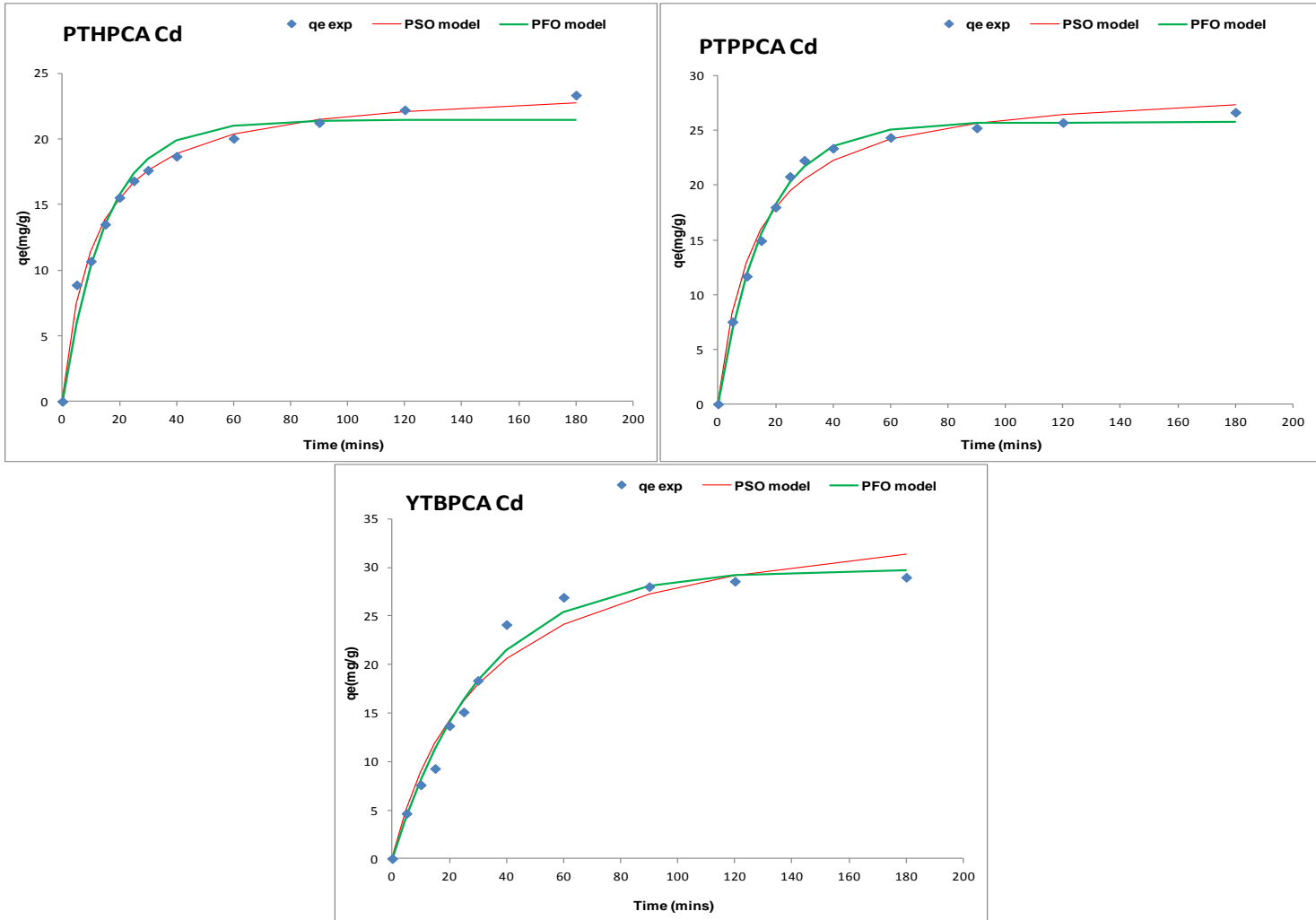
Fig 7.22: Cd(II) ion PFO & PSO sorption kinetic models for PTHPCA, PTPPCA & YTBPCA adsorbents
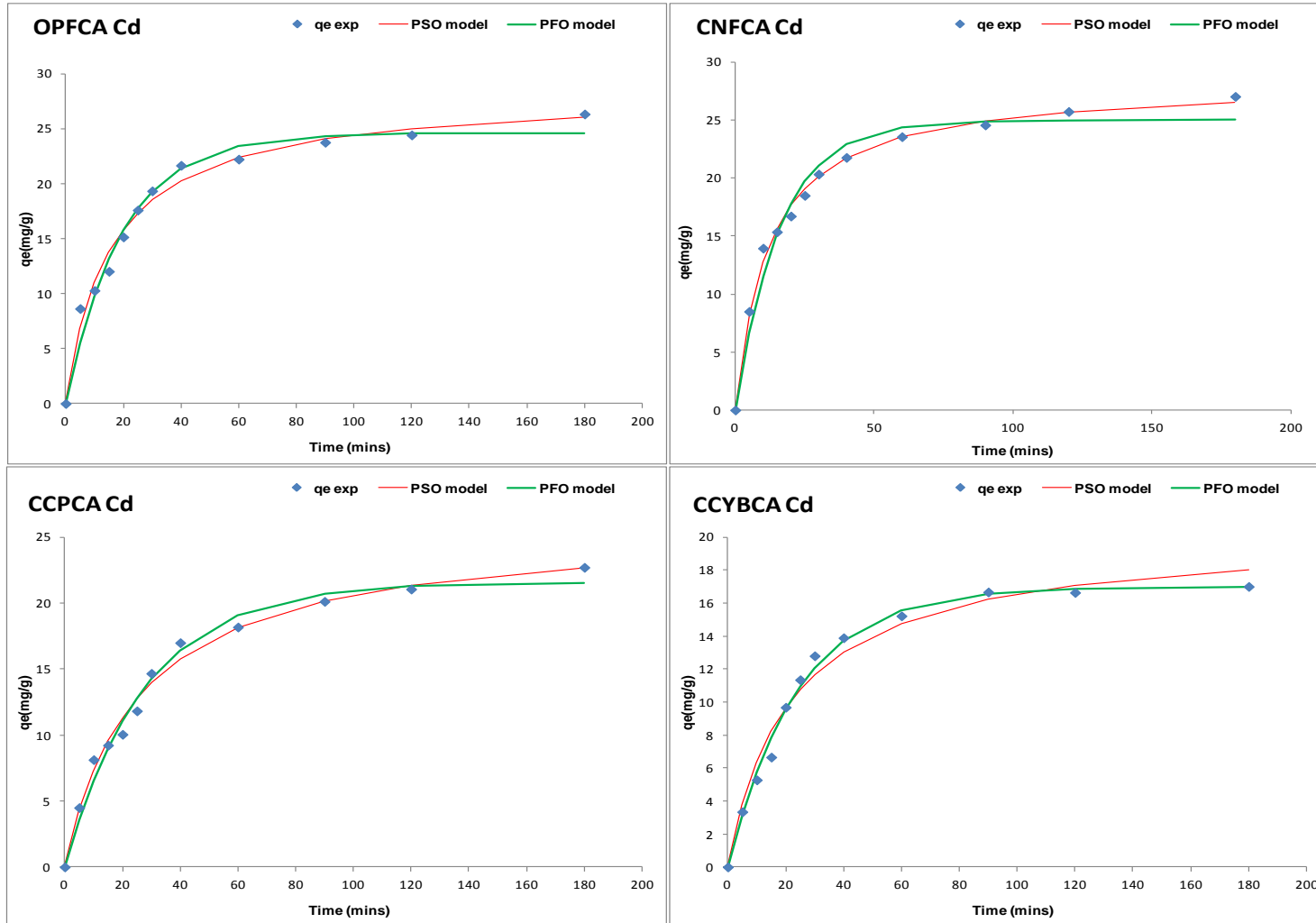
Fig 7.23: Cd(II) ion PFO & PSO sorption kinetic models for OPFCA,CNFCA, CCPCA & CCYBCA adsorbents
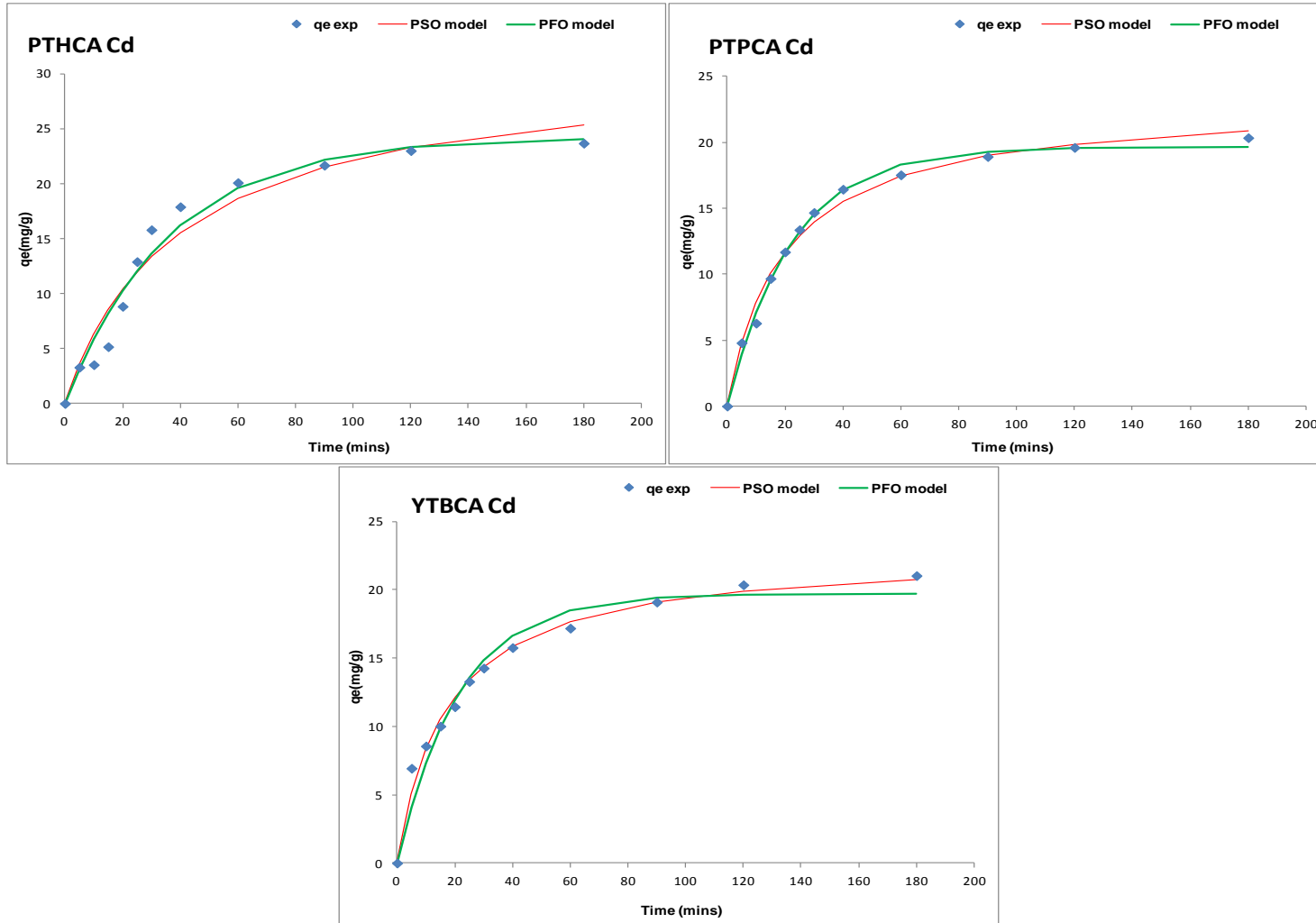
Fig 7.24: Cd(II) ion PFO & PSO sorption kinetic models for PTHCA, PTPCA & YTBCA adsorbent.

Comparing the initial adsorption rate for the carbonised and pyrolysed adsorbents shows that the pyrolysed adsorbents had higher values for the initial adsorption rate than the carbonised adsorbents. The loading at equilibrium from the PSO model, $q_{e,cal}$ for Cd(II) ion sorption onto the carbonised adsorbents were in the range 20.2 mgg^{-1} (CCYBCA) to 30.8 mgg^{-1}(PTHCA) with the order being PTPCA > OPFCA > CNFCA > CCPCA > PTPCA > YTBCA > CCYBCA, while that of the pyrolysed adsorbents were in the range 21.3 mgg^{-1} (CCYBPCA) to 36.8 mgg^{-1}(YTBPCA) with the order being YTBPCA > CNFPCA > CCPPCA > OPFPCA > PTPPCA > PTHPCA > CCYBPCA, implying that the YTBPCA adsorbent had the highest Cd(II) ion loading for all the adsorbents.

The value of the coefficient of determination and the two error parameters − the root mean square (RMSE) and Chi square (χ^2) were used to determine the adsorbent whose kinetics of Cd(II) sorption is best described by the PSO model. The value of these error parameters in Table 7.7 and 7.8 shows that there variations in the r^2 values for the carbonised and pyrolysed adsorbents. For the carbonised adsorbents, three sets of values were obtained; the first set which had highest value of 0.99 was for the CNFCA, CCPCA, PTPCA and YTBCA adsorbents. The second value of 0.98 was for the OPFCA and CCYBCA adsorbents while the lowest value of 0.95 was for the sorption onto the PTHCA adsorbent. For the pyrolysed adsorbents, four sets of values were recorded, the first set with the highest value of 0.99 was for the OPFPCA, PTHPCA and PTPPCA adsorbents. The second was 0.98 for the CNFPCA and CCPPCA adsorbents, while the third and fourth r^2 values were 0.97 and 0.96 for the YTBPCA and CCYPCA adsorbents respectively. To further discriminate the adsorbent that is best described by the PSO model, consideration was given to the values of the two error parameters- the χ^2 and the RMSE. The adsorbent with the lowest values for these two parameters was thereafter chosen as the best described by the PSO model. For the carbonised adsorbents, the χ^2 and RMSE values were used to further compare the fitting of the PSO model to the Cd(II) ion experimental sorption data for the CNFCA, CCPCA, PTPCA and YTBCA adsorbents. Based on the values for these two error parameters in Table 7.7, the CNFCA adsorbent uptake of Cd(II) ion is best described by the PSO model with the lowest χ^2 (0.01) and RMSE (1.38 $\times 10^{-1}$) values. The PSO rate constant (K_2) obtained for this adsorbent was 2.92 $\times 10^{-3}$ gmg^{-1}min^{-1} and the PSO model metal ion loading ($q_{e,cal}$) was 28.2 mgg^{-1}. For the pyrolysed adsorbents the error parameter comparison was between OPFPCA, PTHPCA and PTPPCA adsorbents from

which it was observed from the results in Table 7.8 that the PTHPCA adsorbent uptake of Cd(II) ion is best described by the PSO model with the lowest χ^2 (0.02) and RMSE (1.46 $\times 10^{-1}$) values. The PSO rate constant (K_2) obtained for this adsorbent was 3.71 $\times 10^{-3}$ gmg^{-1}min^{-1} and the PSO model metal ion loading ($q_{e,cal}$) was 24.1 mgg^{-1}. A comparison of the PSO values for r^2 and the two error parameters between the carbonised and pyrolysed adsorbents for Cd(II) ion sorption, indicates that the CNFCA adsorbent was best described by the PSO model as it had the lowest values for the error parameters (χ^2 and the RMSE) and the highest r^2 value.

Futhermore, to determine which of the two kinetic models (PFO or PSO) gives the best description of Cd(II) sorption kinetics onto the carbonised and pyrolysed adsorbents an examination of the $q_{e,cal}$ values obtained for the PFO and PSO models is used to compare with the experimental q_e value obtained at the end of sorption (after 180 mins) also called q_t. The assumption is that the model with $q_{e,cal}$ values that are closer to the experimental obtained q_e is the model that describes the Cd(II) ion sorption better. Table 7.9 presents the q_e for both experimental sorption and kinetic models for Cd(II) ion uptake by the carbonised and pyrolysed adsorbents.

Table 7.9: Comparison of q_e values for experiment and model sorption for Cd(II) onto pyrolysed and carbonised adsorbents

Adsorbent	q_e (mgg^{-1})		
	Experiment	PFO model	PSO model
OPFPCA	25.5	25.2	31.6
CNFPCA	28.8	28.8	35.6
CCPPCA	29.8	29.1	34.9
CCYBPCA	19.8	18.6	21.3
PTHPCA	23.3	21.4	24.1
PTPPCA	26.7	25.8	29.3
YTBPCA	29.0	29.8	36.8
OPFCA	26.3	24.6	28.3
CNFCA	27.0	25.0	28.2
CCPCA	22.7	21.6	25.9
CCYBCA	17.0	17.0	20.2
PTHCA	23.7	24.2	30.8
PTPCA	20.3	19.6	23.1
YTBCA	21.0	19.7	22.8

From Table 7.9, it is observed that the values for qe_{model} for both PFO and PSO models were close to the experimental (q_e) for both carbonised and pyrolysed adsorbents. However, the PFO model for some of the adsorbents gave a closer q_e value to the experimental sorption q_e than the PSO. The PSO mainly gave values that were an overestimate of the experimental q_e while that of the PFO was for some adsorbents an underestimation of the experimental q_e. Further evaluation of the values for error parameters (χ^2 and the RMSE) and correlation coefficient (r^2) in Table 7.7 and 7.8 for the two sets of adsorbents indicates that the PFO model had lower values for both error parameters and higher r^2. Thus, it can be said that the PFO model gave a better approximation of the kinetics of Cd(II) sorption by the carbonised and pyrolysed adsorbents than the PSO order model.This implies that the kinetics supports the assumption that the rate limiting step of Cd(II) ion sorption onto the carbonised and pyrolysed activated adsorbents is dependent on the concentration of the Cd(II) ions in the adsorbate (Azizian, 2004; Liu and Liu, 2008). However, as previously observed, the closeness of the parameters obtained from the PSO model may also indicate that chemical interactions between the ions in the adsorbate solution and the adsorbent may still influence sorption kinetics but this may depend on the rate of diffusion.This implies that pore diffusivity of the ions onto the active sites may also influence the kinetics as previously discussed in the analysis of the two stage metal uptake (fast and slow) kinetics of Cd(II) ion sorption.

The application application of the PFO and PSO models for the characterisation of the kinetics of Cd(II) ion sorption using pyrolysed and carbonised adsorbents has also been reported in literature. Kim *et al.,* (2013) reports on the use of PFO and PSO models to characterise the kinetics of Cd(II) ion sorption from aqueous solution by biochar produced at 300-600 °C from a giant *Miscanthus* biomass. The results from the study indicated that both PFO and PSO models did fit the experimental data well for the different biochar adsorbents except the biochar produced at 400 °C (BC400) where the PSO did fit the sorption slightly better than the PFO model. Elaigwu *et al.,* (2014) has also reported on the removal of Cd(II) ions from aqueous solutions using biochar obtained from the pyrolysis of *Prosopis africana* shell. In their study, the PSO model gave a better fitting for the sorption of Cd(II) than the PFO model based on higher values of the correlation coefficient(r^2) which were 0.88(PFO) and 0.99(PSO). These results indicate that the trend

of the results obtained for the kinetic modelling of Cd(II) ions onto the carbonised and pyrolysed adsorbents are consistent with those reported in previous studies.

7.5.2 Lead (II) ion sorption

The effects of contact time on Pb(II) ion removal using the pyrolysed and carbonized adsorbents was studied based on the description given in section 7.5. The kinetics of Pb(II) ion removal using the pyrolysed adsorbent is shown in Figure 7.25 while that of the carbonized adsorbent is shown in Figure 7.26. From the two figures it can be observed that Pb(II) ion loading increased from 5 minutes top up to 180 minutes. However, this increase proceeded via a two stage process, with the first being a fast uptake lasting up to 60 minutes for both the pyrolysed and carbonized adsorbents. The second stage proceeded slowly up to 180 minutes where equilibrium is presumed to have been attained. The maximum loading of the pyrolysed adsorbents were 24.0 mgg^{-1} (OPFPCA), 25.67 mgg^{-1} (CNFPCA), 26.0 mgg^{-1} (CCPPCA), 19.33 mgg^{-1} (CCYBPCA), 23.29 mgg^{-1} (PTHPCA), 25.93 mgg^{-1} (PTPPCA) and 26.69 mgg^{-1} (YTBPCA). The results indicate that YTBPCA had the highest loading while CCYBPCA had the least.
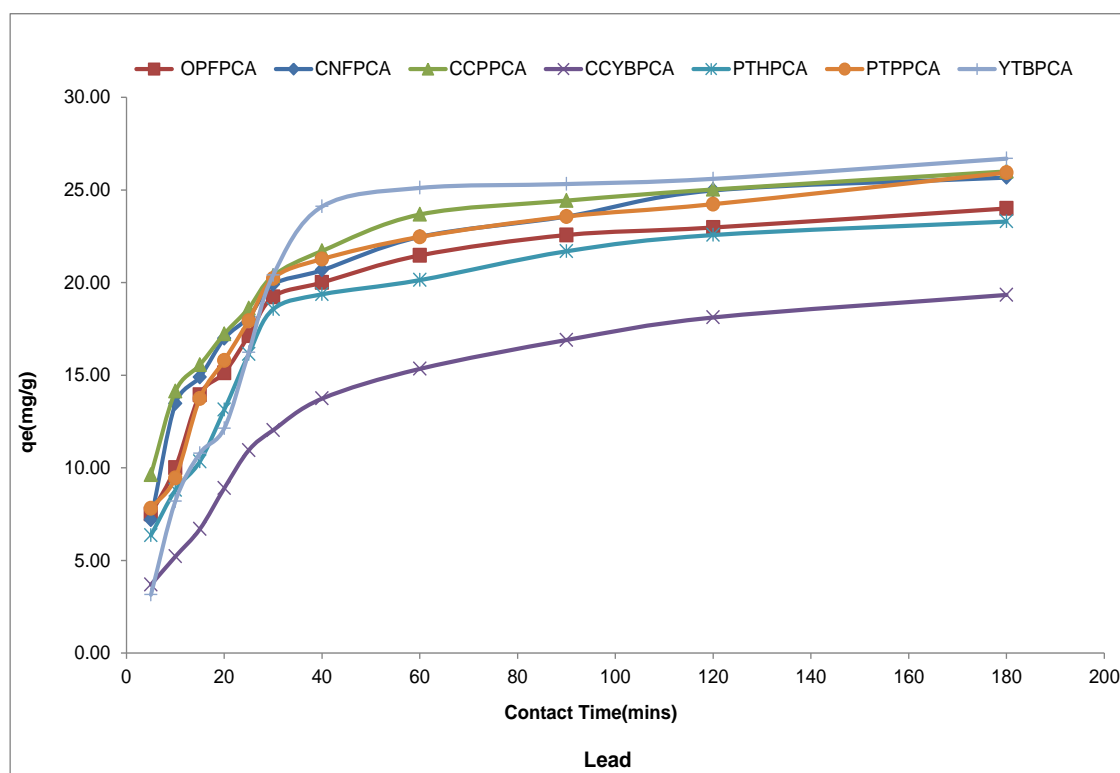
Figure 7.25: Kinetic profile for Lead(II) ion sorption on pyrolysed adsorbent
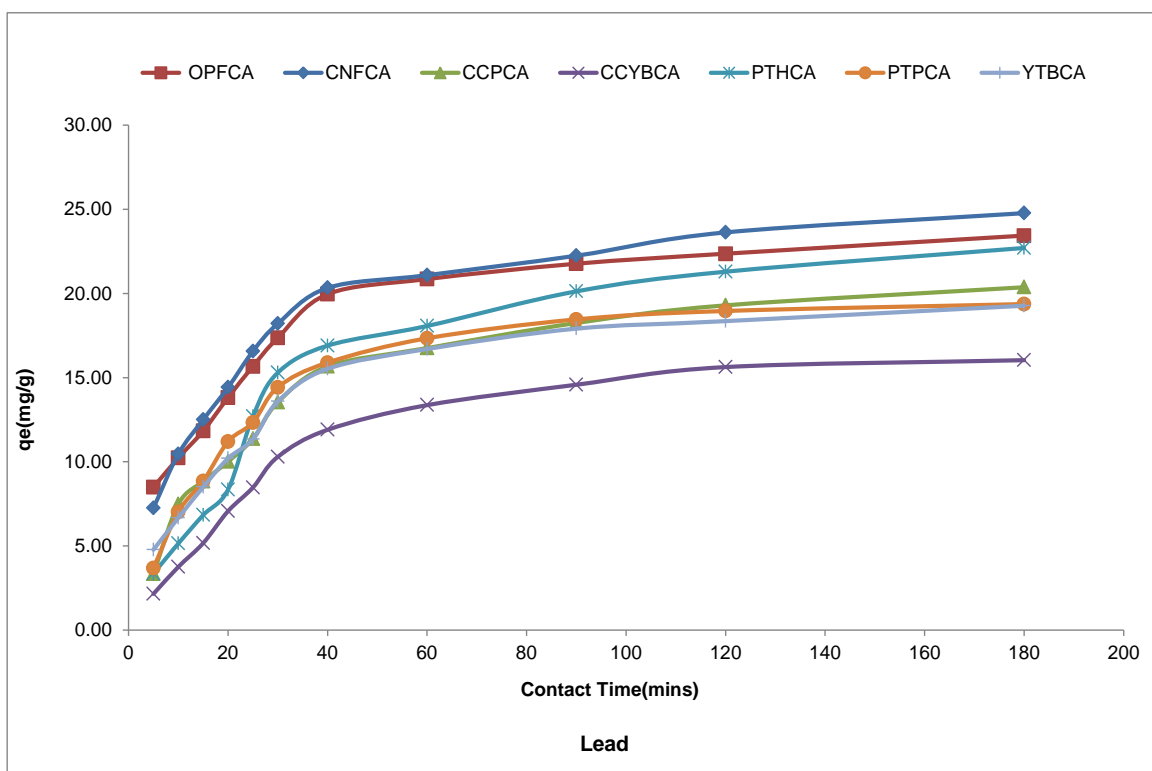
Figure 7.26: Kinetic profile for Lead (II) ion sorption on carbonised adsorbents

For the carbonized adsorbent, the maximum loading of Pb(II) were 23.44 mgg^{-1}(OPFCA), 24.77 mgg^{-1}(CNFCA), 20.33 mgg^{-1}(CCPCA), 16.04 mgg^{-1} (CCYBCA), 22.70 mgg^{-1} (PTHCA), 19.37 mgg^{-1} (PTPCA) and 19.27 mgg^{-1} (YTBCA). From the results, it can be observed that the CNFCA adsorbent had the highest loading capacity while the CCYBCA adsorbent had the least. The Pb(II) ion uptake for the pyrolysed adsorbents are higher than those of the carbonised adsorbents and this is also observed here to be closely associated with the higher surface area and total pore volume of the pyrolysed adsorbents. This indicates a similar trend that was noticed for Cd(II) ion sorption, thereby confirming the role the surface properties of the adsorbents plays in metal ion uptake.

The kinetic profiles of the two sets of adsorbents were also observed to follow a two-stage profile. This two stage process can be explained based on the availability and numbers of the sites on the adsorbents for metal ion loading. At the beginning of the metal ion-adsorbent contact, there are numerous active sites on the adsorbents that are vacant hence the rapid uptake of Pb(II) ions onto these sites. However as these sites become occupied and less number are allocated for uptake by the Pb(II) ions, the uptake process slows gradually. In addition, a repulsive effect due to charge similarity occurs on the surface of the adsorbent hindering the rapid uptake of Pb(II) ions and this is because the surface of

the adsorbents are now predominantly positive. These combined effect reduces the amount of Pb(II) ions uptake until equilibrium is attached. This effect has been observed by Ibrahim *et al*., (2010) in their study on the removal of Pb((II) ions from aqueous solution using a novel agricultural waste. The report notes that the rapid stage lasted from initial contact to 60 minutes while the slow down stage proceeded up to 360 minutes when equilibrium was attained. The observed sorption profile of these carbonised and pyrolysed adsorbents imply that they can be effectively used for the removal of heavy metal ions from wastes streams within a short interval of adsorbate-adsorbent contact.

7.5.2.1 Lead (II) ion kinetic modelling

The use of sorption kinetics to investigate the mechanism of metal ion transport and the potential rate controlling steps such as mass transport and chemical reaction processes have been explored in a number of studies using kinetic models such as the pseudo-first order (PFO) and pseudo-second order (PSO) equations (Ho and McKay, 1998). Hence, kinetic modelling of Pb(II) ion sorption onto the carbonised and pyrolysed adsorbents were carried out using the pseudo first order (PFO) and pseudo first order (PSO) equations based on the solver add-in optimization procedure in Microsoft excel 2010 software. The plots of the PFO are PSO models for Pb(II) are presented in Figures 7.27 and 7.28 for the pyrolysed adsorbents and Figures 7.29 and 7.30 for the carbonised adsorbents. From these models, the kinetic parameters and their respective error functions obtained are presented in Table 7.10 and 7.11 for the pyrolysed and carbonised adsorbents respectively. Based on the results presented in Figures 7.27-7.30 and Tables 7.10 and 7.11, it can be observed that the two models (PFO & PSO) could be used to characterise the kinetics of Pb(II) ion sorption and the prediction of each model for the kinetic parameter ($q_{e,model}$) is close to the result obtained from the experimental analysis of Pb(II) ion sorption.

The PFO model was used to determine the loading of Pb(II) as the system approaches equilibrium denoted as $q_{e,cal}$. The value for this parameter for the pyrolysed adsorbents were in the range 18.5mgg^{-1} (CCYBPCA) to 26.9 mgg^{-1}(YTBPCA) with the order being YTBPCA > PTPPCA > CCPPCA > CNFPCA > OPFPCA > PTHPCA > CCYBPCA. For the carbonizsed adsorbents, the PFO model $q_{e,cal}$ obtained Pb(II) ion sorption were in the range 16.0 mgg^{-1} (CCYBCA) to 23.2 mgg^{-1}(CNFCA) with the order being CNFCA > OPFCA > PTHCA > CCPCA > PTPCA > YTBCA > CCYBCA. From the value of $q_{e,cal}$ for these two thermally modified adsorbents, it is observed that the YTBPCA adsorbent had the highest loading with the least being the CCYBCA adsorbent. The rate constant of

the pseudo first order (PFO) reaction (K_1) for the pyrolysed adsorbents were in the range 3.31×10^{-2} min^{-1}(CCYBPCA) to 6.91×10^{-2} min^{-1}(CCPPCA), while that of the carbonised adsorbents were in the range 3.03×10^{-2} min^{-1}(CCYBCA) to 5.39×10^{-2} min^{-1}(OPFCA). The value of the coefficient of determination (r^2) and the two error parameters − the root mean square (RMSE) and Chi square (χ^2) were used to determine the Pb(II) ion uptake kinetics that is best described by the PFO model. From Table 7.10 it can be observed that for the pyrolysed adsorbents, OPFPCA, CCYBPCA, PTHPCA and PTPPCA had the same r^2 value of 0.99, while the CNFPCA adsorbent had an r^2 value of 0.98. The lowest r^2 value of 0.97 was obtained for the CCPPCA and YTBPCA adsorbents. These r^2 values indicates that the experimental data for the kinetics of Pb(II) ion sorption onto the OPFPCA, CCYBPCA, PTHPCA and PTPPCA adsorbents are in close agreement what that of the PFO model. To further discriminate amongst these four adsorbents, the χ^2 and the RMSE values were used with the lowest values being an indication of best fitting. Based on this assumption, the sorption of Pb(II) ion onto the CCYBPCA adsorbent is best described by the PFO model with the lowest χ^2 (0.02) and RMSE (1.41×10^{-1}) values. For this adsorbent, the PFO rate constant (K_1) obtained was 3.31×10^{-2} min^{-1} and the PFO model Pb(II) ion loading ($q_{e,cal}$) was 18.5 mgg^{-1}.

For the carbonised adsorbents, r^2 value of 0.99 was obtained for the CNFCA, CCPCA, CCYBCA, YTBCA and PTPCA adsorbents while the PTHCA and OPFCA adsorbents had r^2 values of 0.98 and 0.97 respectively. These r^2 values suggest that the sorption of Pb(II) ion onto these adsorbents were better represented by the PFO model for the CNFCA, CCPCA, CCYBCA, YTBCA and PTPCA adsorbents. Further evaluation of the values of the error parameters (χ^2 and the RMSE) for these 5 adsorbents were used to determine which one was best described by the PFO model. From Table 7.11, it can be observed that the PTPCA adsorbent is best described by the PFO model with the lowest χ^2 (0.01) and RMSE (3.78×10^{-2}) values. For this adsorbent, the PFO rate constant (K_1) obtained was 4.37×10^{-2} min^{-1} and the Pb(II) ion loading ($q_{e,cal}$) for the PFO model was 19.1 mgg^{-1}. Comparing between the pyrolysed and carbonised adsorbents for Pb(II) ion sorption, it can be observed that the PTPCA adsorbent was best described by the PFO model as it had the lowest values for the error parameters (χ^2 and the RMSE) and the highest r^2 value.

Table 7.10: PFO & PSO modelling parameters for Pb(II) sorption on pyrolysed adsorbents

	Pseudo First Order Model					Pseudo Second Order					
Adsorbent	$q_{e,cal}(mgg^{-1})$	$K_1(min^{-1})$	r^2	χ^2	RMSE	$q_{e,cal}(mgg^{-1})$	$K_2(gmg^{-1}min^{-1})$	$h(mgg^{-1}min^{-1})$	r^2	χ^2	RMSE
OPFPCA	22.8	5.88E-02	0.99	0.03	2.85E-01	26.0	2.92E-03	1.97	0.99	0.02	1.70E-01
CNFPCA	24.0	6.38E-02	0.98	0.06	6.09E-01	27.1	3.08E-03	2.27	0.99	0.01	1.17E-01
CCPPCA	24.3	6.91E-02	0.97	0.09	8.46E-01	27.2	3.55E-03	2.64	0.99	0.01	1.21E-01
CCYBPCA	18.5	3.31E-02	0.99	0.02	1.41E-01	22.7	1.51E-03	0.78	0.99	0.02	1.18E-01
PTHPCA	22.5	4.84E-02	0.99	0.05	3.97E-01	26.1	2.20E-03	1.51	0.98	0.06	5.00E-01
PTPPCA	24.4	5.44E-02	0.99	0.05	4.11E-01	28.0	2.41E-03	1.89	0.99	0.04	3.56E-01
YTBPCA	26.9	3.87E-02	0.97	0.12	1.10E+00	32.4	1.26E-02	1.33	0.95	0.24	2.15E+00

Table 7.11: PFO & PSO modelling parameters for Pb(II) sorption on carbonised adsorbents

	Pseudo First Order Model					Pseudo Second Order					
Adsorbent	$q_{e,cal}(mgg^{-1})$	$K_1(min^{-1})$	r^2	χ^2	RMSE	$q_{e,cal}(mgg^{-1})$	$K_2(gmg^{-1}min^{-1})$	$h(mgg^{-1}min^{-1})$	r^2	χ^2	RMSE
OPFCA	22.3	5.39E-02	0.97	0.08	6.88E-01	25.3	2.77E-03	1.78	0.99	0.04	3.70E-01
CNFCA	23.2	5.24E-02	0.99	0.05	4.41E-01	26.7	2.44E-03	1.74	0.99	0.02	1.45E-01
CCPCA	19.5	3.84E-02	0.99	0.03	1.96E-01	23.3	1.82E-03	0.98	0.99	0.02	1.41E-01
CCYBCA	16.0	3.03E-02	0.99	0.02	8.30E-02	20.0	1.49E-03	0.60	0.98	0.04	2.19E-01
PTHCA	22.2	3.05E-02	0.98	0.09	5.87E-01	27.8	1.07E-03	0.83	0.97	0.12	8.27E-01
PTPCA	19.1	4.37E-02	0.99	0.01	3.78E-02	22.4	2.23E-03	1.12	0.99	0.03	1.95E-01
YTBCA	18.6	4.16E-02	0.99	0.02	1.50E-01	22.0	2.16E-03	1.04	0.99	0.03	1.68E-01
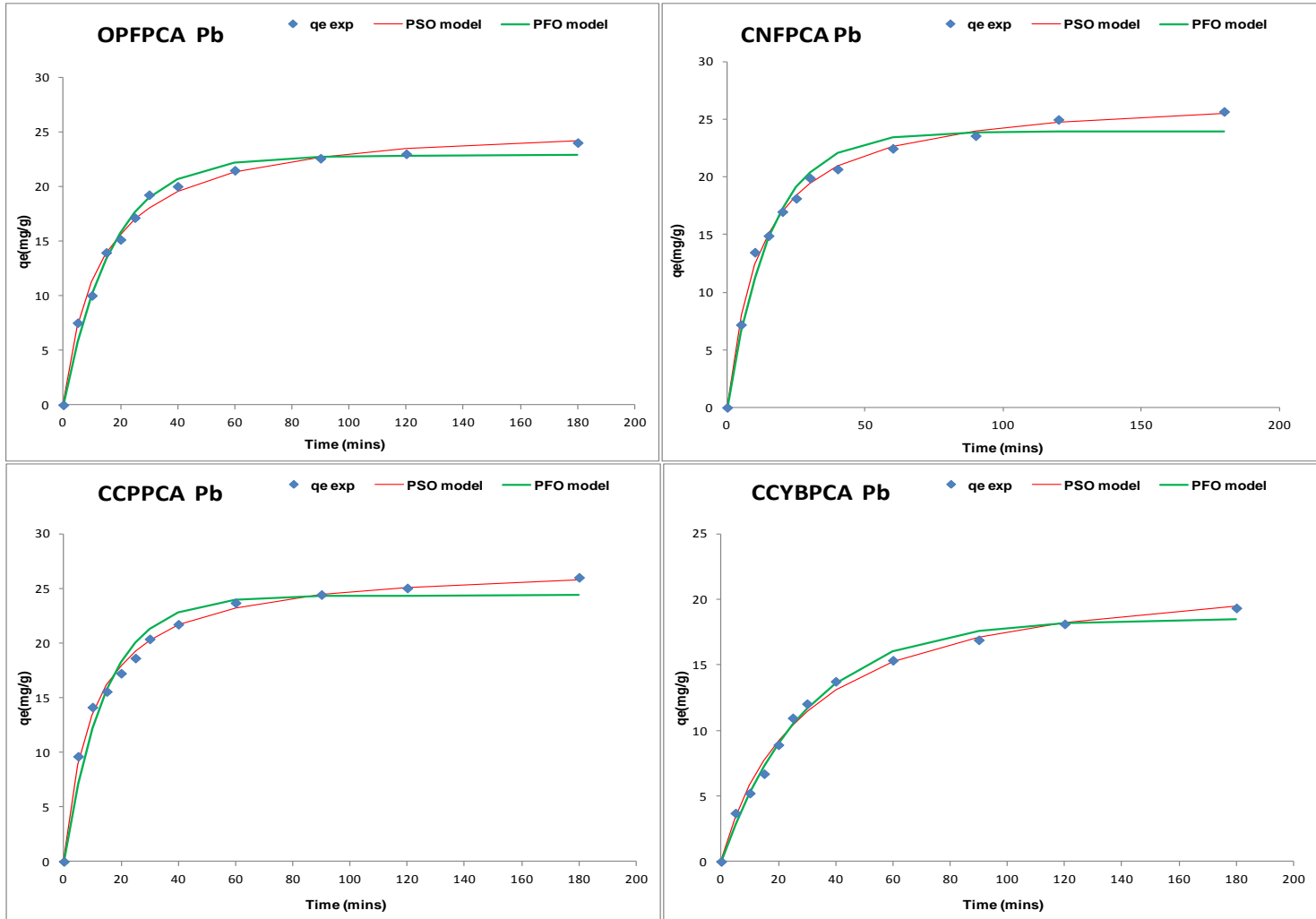
Fig 7.27: Pb(II) ion PFO & PSO sorption kinetic models for OPFPCA,CNFPCA, CCPPCA & CCYBPCA adsorbents
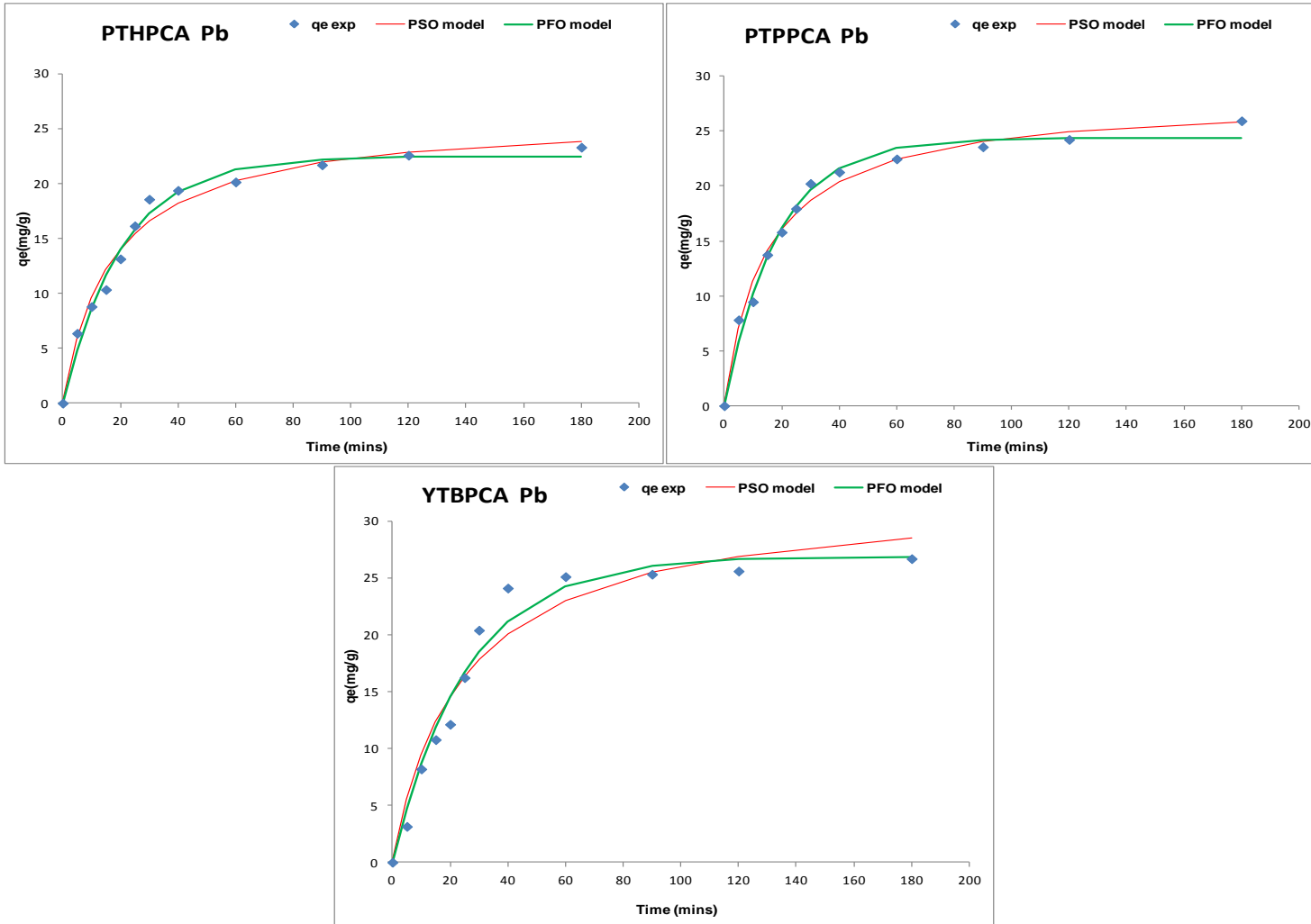
Fig 7.28: Pb(II) ion PFO & PSO sorption kinetic models for PTHPCA, PTPPCA & YTBPCA adsorbents
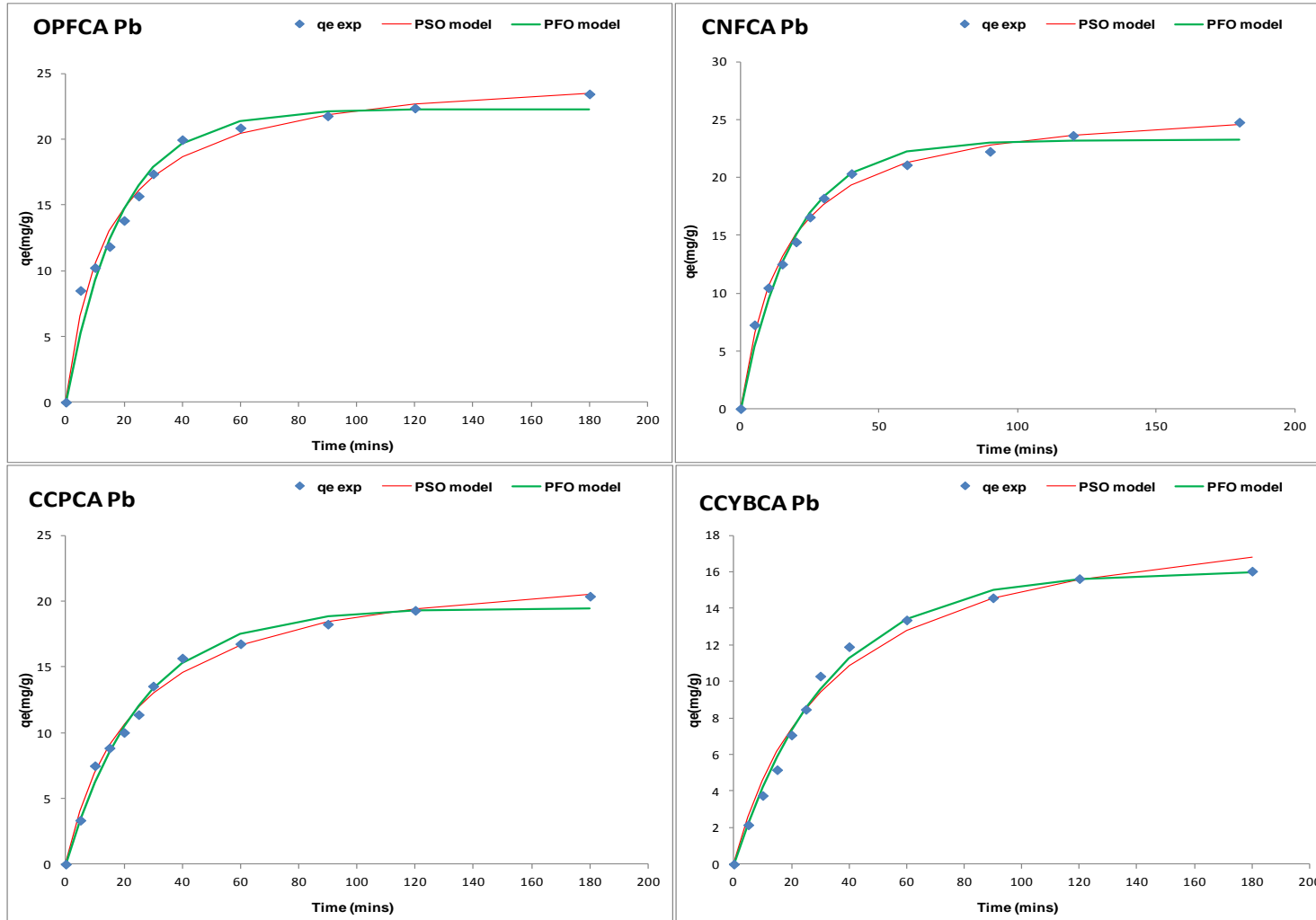
Fig 7.29: Pb(II) ion PFO & PSO sorption kinetic models for OPFCA,CNFCA, CCPCA & CCYBCA adsorbents
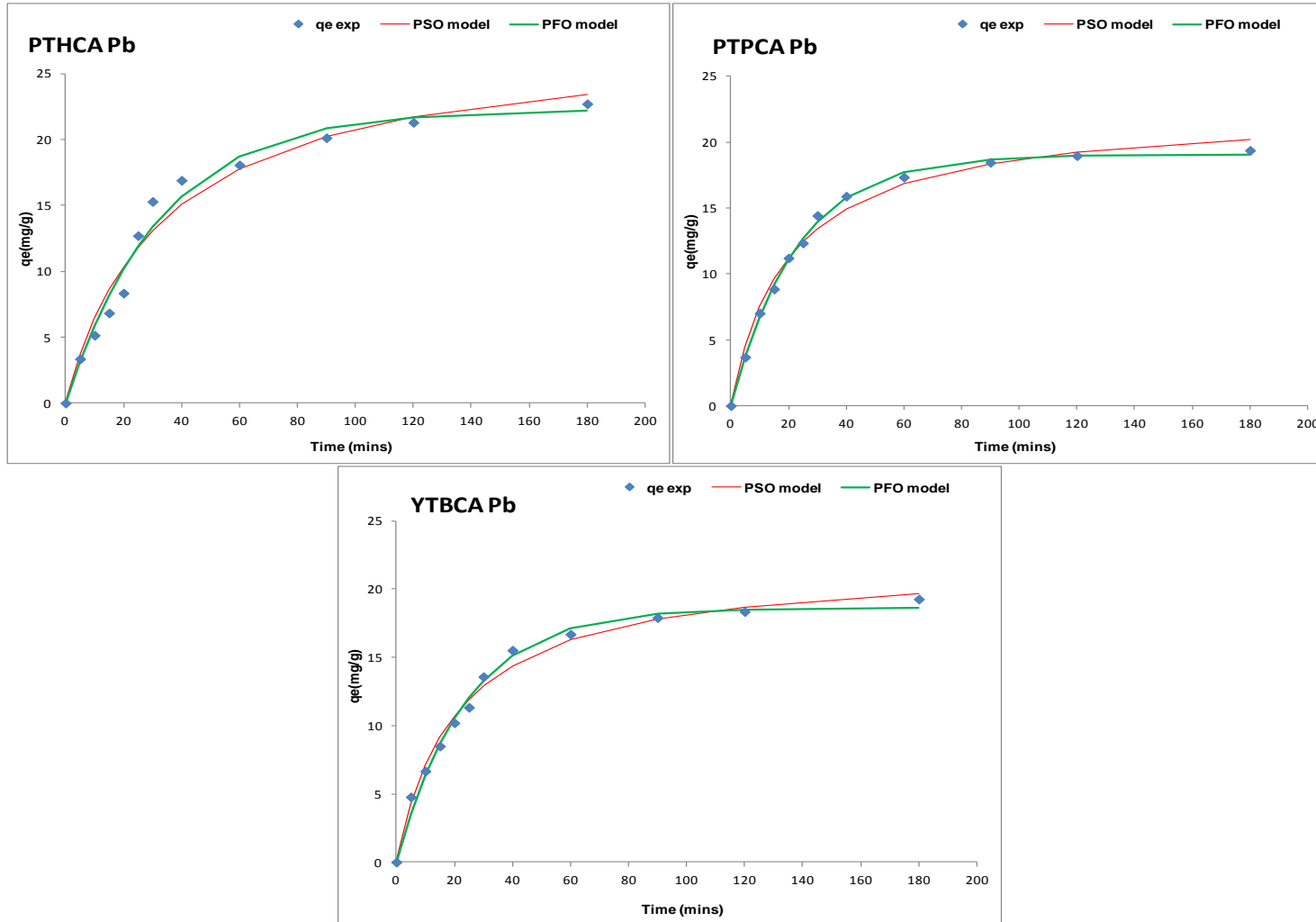
Fig 7.30: Pb(II) ion PFO & PSO sorption kinetic models for PTHCA, PTPCA & YTBCA adsorbents

The PSO model was also used to determine the loading of Pb(II) as the system approaches equilibrium denoted as $q_{e,cal}$ for the pyrolysed carbonised adsorbents and the results are also presented in Tables 7.10 and 7.11. From the tables, the PSO rate constant (K_2) for the pyrolysed adsorbents were in the range 1.26×10^{-3} gmg^{-1}min^{-1}(YTBPCA) to 3.55×10^{-3} gmg^{-1}min^{-1}(CCPPCA), while that of the carbonised adsorbents were in the range 1.07×10^{-3} gmg^{-1}min^{-1}(PTHCA) to 2.77×10^{-3} gmg^{-1}min^{-1}(OPFCA). The initial sorption rate (h) obtained from the PSO model as $q_t/t \rightarrow 0$ which gives an indication of the intial kinetic rate of sorption of Pb(II) onto the pyrolysed and carbonised adsorbent was also determined and is presented in Tables 7.10 and 7.11. For the pyrolysed adsorbents the value of the initial sorption rate was in the order of CCPPCA > CNFPCA > OPFPCA > PTPPCA > PTHPCA > YTBPCA > CCYBPCA with the CCPPCA adsorbent having the highest value of 2.64mgg^{-1}min^{-1}. For the carbonised adsorbents, the order for the initial sorption rate (h) was OPFCA > CNFCA > PTPCA > YTBCA > CCPCA > PTHCA > CCYBCA with the OPFCA adsorbent having the highest value of 1.78mgg^{-1}min^{-1}. Comparing the initial adsorption rate for the pyrolysed and carbonised adsorbents indicates that the pyrolysed adsorbents had higher values for the initial adsorption rate than the carbonised adsorbents.

The $q_{e,cal}$ obtained from the PSO model for Pb(II) ion sorption onto the pyrolysed adsorbents were in the range 22.7 mgg^{-1} (CCYBPCA) to 32.4 mgg^{-1}(YTBPCA) with the order being YTBPCA > PTPPCA > CCPPCA > CNFPCA > PTHPCA > OPFPCA > CCYBPCA, while that of the carbonised carbon adsorbents were in the range 20.0 mgg^{-1} (CCYBCA) to 27.8 mgg^{-1}(PTHCA) with the order being PTHCA > CNFCA > OPFCA > CCPCA > PTPCA > YTBCA > CCYBCA, implying that the YTBPCA adsorbent had the highest Pb(II) ion loading for the pyrolysed and carbonised adsorbents. The value of the coefficient of determination and the two error parameters – the root mean square (RMSE) and Chi square (χ^2) were used to determine the adsorbent whose kinetics of Pb(II) sorption is best described by the PSO model. The value of these error parameters in Table 7.10 and 7.11 shows that there are variations in r^2 values for the pyrolysed and carbonised adsorbents. The pyrolysed adsorbents had three sets of r^2 values. The first group which had highest value of 0.99 was composed of the OPFPCA, CNFPCA, CCPPCA, CCYBPCA and PTPPCA adsorbents. The second and third values were 0.98 and 0.95 for the PTHPCA and YTBPCA adsorbents respectively. The carbonised adsorbents also had three sets of r^2 values; the first set with the highest value of 0.99 was for the OPFCA, CNFCA, CCPCA,

PTPCA and YTBCA adsorbents. The second and third values were 0.98 and 0.97 for the CCYBCA and PTHCA adsorbents respectively. To further discriminate the adsorbent that is best described by the PSO model, consideration was given to the values of the two error parameters- the χ^2 and the RMSE. The adsorbent with the lowest values for these two parameters was thereafter chosen as the best described by the PSO model. For the pyrolysed adsorbents, the χ^2 and RMSE values were used to further compare the fitting of the PSO model to the Pb(II) ion experimental sorption data for the OPFPCA, CNFPCA, CCPPCA, CCYBPCA and PTPPCA adsorbents. Based on the values for these two error parameters in Table 7.10 the CNFPCA adsorbent uptake of Pb(II) ion is best described by the PSO model with the lowest χ^2 (0.01) and RMSE (1.17 $\times 10^{-1}$) values. The PSO rate constant (K_2) obtained for this adsorbent was 3.08 $\times 10^{-3}$ gmg^{-1}min^{-1} and the PSO model metal ion loading ($q_{e,cal}$) was 27.1 mgg^{-1}. For the carbonised adsorbents, the error parameter comparison was between the OPFCA, CNFCA, CCPCA, PTPCA and YTBCA adsorbents from which it was observed from the results in Table 7.11 that the CCPCA adsorbent uptake of Pb(II) ion is best described by the PSO model with the lowest χ^2 (0.02) and RMSE (1.41 $\times 10^{-1}$) values. The PSO rate constant (K_2) obtained for this adsorbent was 1.82 $\times 10^{-3}$ gmg^{-1}min^{-1} and the PSO model metal ion loading ($q_{e,cal}$) was 23.3 mgg^{-1}. A comparison of the PSO values for r^2 and the two error parameters between the pyrolysed and carbonised adsorbents for Pb(II) ion sorption, indicates that the CNFPCA adsorbent was best described by the PSO model as it had the lowest values for the error parameters (χ^2 and the RMSE) and the highest r^2 value.

Futhermore, to determine which of the two kinetic models (PFO or PSO) gives the best description of Pb(II) sorption kinetics onto the pyrolysed and carbonised adsorbents an examination of the $q_{e,cal}$ values obtained for the PFO and PSO models is used to compare with the experimental q_e value obtained at the end of sorption (after 180 mins) also called q_t. The assumption is that the model with $q_{e,cal}$ values that are closer to the experimental obtained q_e is the model that describes the Pb(II) ion sorption better. Table 7.12 presents the q_e for both experimental sorption and kinetic models for Pb(II) ion uptake by the pyrolysed and carbonised adsorbents. From Table 7.12, it is observed that the values for qe_{model} for both PFO and PSO models were close to the experimental (q_e) for both pyrolysed and carbonised adsorbents. However, the PFO model for some of the adsorbents gave a closer q_e value to the experimental sorption q_e than the PSO.

Table 7.12: Comparison of q_e values for experiment and model sorption for Pb(II) onto pyrolysed and carbonised adsorbents

Adsorbent	q_e (mgg^{-1})		
	Experiment	PFO model	PSO model
OPFPCA	24.0	22.8	26.0
CNFPCA	25.7	24.0	27.1
CCPPCA	26.0	24.3	27.2
CCYBPCA	19.3	18.5	22.7
PTHPCA	23.3	22.5	26.1
PTPPCA	25.9	24.4	28.0
YTBPCA	26.7	26.9	32.4
OPFCA	23.4	22.3	25.3
CNFCA	24.8	23.2	26.7
CCPCA	20.3	19.5	23.3
CCYBCA	16.0	16.0	20.0
PTHCA	22.7	22.2	27.8
PTPCA	19.4	19.1	22.4
YTBCA	19.3	18.6	22.0

The PSO mainly gave values that were an overestimate of the experimental qe while that of the PFO was for some adsorbents an underestimation of the experimental q_e. Further evaluation of the values for error parameters (χ^2 and the RMSE) and correlation coefficient (r^2) in Table 7.10 and 7.11 for the two sets of adsorbents indicates that the PFO model had lower values for both error parameters and higher r^2. Thus, it can be said that the PFO model gave a better approximation of the kinetics of Pb(II) sorption by the pyrolysed and carbonised adsorbents than the PSO order model. This implies that the kinetics supports the assumption that the rate limiting step of Pb(II) ion sorption onto the pyrolysed and carbonised adsorbents is dependent on the concentration of the Pb(II) ions in the adsorbate (Azizian, 2004; Liu and Liu, 2008). However, the closeness of the parameters obtained from the PSO model may also indicate that chemical interactions between the ions in the adsorbate solution and the adsorbent may still influence sorption kinetics but this may

depend on the rate of diffusion.This implies that pore diffusivity of the ions onto the active sites may also influence the kinetics as previously discussed in the analysis of the two stage metal uptake (fast and slow) kinetics of Pb(II) ion sorption.

A number of studies have been reported on the application of the PFO and PSO models for the characterisation of the kinetics of Pb(II) ion sorption using adsorbents obtained from pyrolysis and carbonisation of biomass. The kinetics of Pb(II) ion sorption from aqueous solution by biochar obtained from the pyrolysis of *Prosopis africana* shell has been reported by Elaigwu *et al.,* (2014). In their study, the pseudo-second order (PSO) model gave a better fitting for the sorption of Pb(II) than the pseudo-first order (PFO) model based on higher values of the correlation coefficient(r^2) which were 0.82(PFO) and 0.99(PSO). Yang *et al.,* (2014) has also reported on the kinetics of Pb(II)ion sorption from aqueous solution using biochar obtained from the pyrolysis of *Alternanthera philoxeroides* biomass at 600°C. The results from the kinetic modelling of Pb(II) ion sorption indicates that the PSO model did describe the experimental results of sorption better than the PFO based on higher r^2 values of 0.999. In addition, the sorption capacity obtained from the PSO model ($q_{e\ cal}$) was more consistent with what was obtained from the PFO model, thus indicating the sorption of Pb(II) ions onto the biochar had a chemisorption rate-controlling mechanism.

7.6 Summary

Biochar or pyrolysed carbon has relatively structured carbon matrix with high degree of porosity and extensive surface area that is similar to activated carbon and thus can be used in environmental remediation of pollutants. For such applications it is important that consideration be given to the effect of certain process parameters that may influence the nature and composition of the biochar such as yield, pH, ash content, elemental composition and heating value. Also the nature of feedstock, process temperature, thermal environment and reaction time are fundamental to the properties of the carbon based char obtained. In this study, carbonization and pyrolysis regimes were designed for the conversion of the 7 agricultural residues into adsorbents for Cd(II) and Pb(II) sorption form aqueous solutions. Carbonization was carried out up to a maximum temperature of 400°C in limited air environment, while pyrolysis was operated up to 700°C as maximum

temperature in nitrogen environment. The carbon-based adsorbents obtained from these two processes were characterized using ash content, pH, zeta potential, attrition resistance, yield, surface area and porosity. The surface morphology and chemical composition of the materials were also determined. These parameters gave significant insight into the nature of the surface and bulk properties of the materials. Temperature was observed as a crucial parameter in these two sets of adsorbents as the yield of the carbonized adsorbents was observed to be higher than that of the pyrolysed due to the pyrolysed adsorbents being subjected to higher treatment.

The pyrolysed adsorbents had higher values of BET surface area than the carbonised adsorbents and this could be associated to the effect of temperature and the different thermal environments on the decomposition of the organic components of the residues (precusors) resulting in improved the porosity of the resulting adsorbents. The CNFPCA adsorbent had the highest surface area of 439 m^2g^{-1}, while the least was the YTBCA adsorbent with a surface area of 97.8 m^2g^{-1}.The adsorbents obtained from the carbonization and pyrolysed processes were mainly basic in nature and the pyrolysed adsorbents were more basic than the carbonized indicating that temperature of thermal treatment can influence the type of surface functional groups on an adsorbent. The ash content of the two types of adsorbents was similar with carbonized adsorbent having the highest ash content of 7.6%. Both types of adsorbents were subjected to attrition test and the results obtained showed that the pyrolysed adsorbents had better resistance to attrition than the carbonised adsorbents. The zeta potential measurement for the two sets of adsorbents indicates that the value of the pHpzc decreases with increase in temperature from 400°C to 700°C, indicating the pyrolysed adsorbents had lower values of pHpzc than the carbonized. Based on this study, the pH of 7 was used for the adsorption of Cd(II) and Pb(II) in aqueous solution.

The rate of metal ion loading for Cd(II) and Pb(II) ions from aqueous solutions was also studied using the two groups of adsorbents-carbonised and pyrolysed adsorbents and the profile of loading of both metal ions followed a two-stage process. The rapid first stage duration was different for the two metal ions, for Cd(II) ion sorption this was from initial contact up to 90 minutes and for Pb(II) ion this was 60minutes. The second stage for both metal ion and adsorbents was characterised by a slow and gradual mechanism up till 180 minutes where equilibrium is assumed to have occurred. The results of the kinetics of Cd(II) and Pb(II) ion sorption indicated that for the carbonised adsorbents, optimum uptake

for Cd(II) and Pb(II) ions was obtained for CNFCA adsorbent with loadings of 27.0 mgg^{-1} for Cd(II) and 24.7 mgg^{-1} for Pb(II) ions. For the pyrolysed adsorbents, the CCPPCA adsorbent was the best for Cd(II) ion uptake with a loading of 29.8 mgg^{-1} while the YTBPCA adsorbent with a loading of 26.9 mgg^{-1} was the best for Pb(II) ion sorption. It was also observed that the optimum uptake obtained for these adsorbents could be associated to their high BET surface areas as these would improve the rate of uptake of the two cations compared to their respective residues (precursors). The BET surface areas of the optimum adsorbents were; 308 m^{2}g^{-1}(CCPPCA), 267m^{2}g^{-1}(YTBPCA) and 252 m^{2}g^{-1}(CNFCA). An examination of the kinetics of Cd(II) and Pb(II) ion sorption by the pyrolysed and carbonised adsorbents also indicates that for Cd(II) ion sorption, the CCPPCA adsorbent was the best with loading of 29.8 mgg^{-1}, while for Pb(II), the best adsorbent was YTBPCA with a loading of 26.7 mgg^{-1}. Kinetic modelling of the sorption of Cd(II) and Pb(II) ions onto the carbonised and pyrolysed adsorbents were also carried out using the pseudo-first order (PFO) and pseudo-second order (PSO) equations. From the analysis, it was observed that the PFO model gave a better approximation of the kinetics of Cd(II) and Pb(II) sorption by the pyrolysed and carbonised adsorbents than the PSO order model. Thus, the present findings in this study with respect to the kinetic profile of the carbonised and pyrolysed adsorbents are similar to what is reported in literature. It also indicates that the process of carbonisation and pyrolysis used to prepare the adsorbents developed here can be used to improve the rate of uptake of Cd(II) and Pb(II) ions and other cations from polluted effluents or wastewater systems. This offers a platform for the optimization of the sorption of toxic ions as these loadings and their kinetics are better than what was obtained using the residues (precursors).

CHAPTER EIGHT

CHEMICALLY ACTIVATED CARBON ADSORBENTS

CHAPTER EIGHT

8.0 Chemically activated carbon adsorbents

The seven different agricultural residues used in this work as previously discussed were further subjected to chemical activation to modify the residues to produce another type of carbon based adsorbent. This protocol was used to prepare activated carbon type materials that would be used for the removal of Cd(II) and Pb(II) ions from aqueous systems. This was carried out so that these chemically activated carbon adsorbents could also be tested for their ability to remove Cd(II) and Pb(II) ions from aqueous solutions using a batch system as the other adsorbents that have been discussed already in previous chapters of this thesis. This was carried out to determine if this type of modification would improve the effectiveness of the adsorbents when compared to the raw residue and the other modification regimes used in this study. In addition, the chemically activated carbon adsorbents were also prepared from the agricultural residues (precursors) so that its adsorption potential for Cd(II) and Pb(II) ions could be used to compare with that of a commercially available activated carbon adsorbent.

The chemical activated carbon adsorbents were obtained using the chemical activation procedure reported in section 4.2.4 using sodium carbonate (Na_2CO_3) and potassium carbonate (K_2CO_3) under nitrogen atmosphere. Each residue adsorbent was subjected to a heating sequence with an incremental temperature at the rate of 5 $^{\circ}$C min^{-1} up to the highest reaction temperature (HRT) of 550 $^{\circ}$C and this temperature had a hold time of 2 h. The impregnation ratio for both chemically activating agents calculated from eqn. 4.2 was 0.05 for each type of activated adsorbent produced. These chemically activated carbon adsorbents obtained using Na_2CO_3 and K_2CO_3 as impregnation agents were also characterised to determine their physical and chemical properties. Some characterisation procedures for these adsorbents were also carried out before and after metal ion adsorption to gain insight into the characteristics of these adsorbents after sorption. The nomenclatures of the different chemically activated adsorbents prepared in this study are presented in Table 8.1.

Table 8.1: Nomenclature of chemically activated adsorbents

Sample and Treatment	Nomenclature
Na_2CO_3 chemically activated residue -550 $^\circ$C	
Na_2CO_3 chemically activated oil palm fruit fibre residue	OPFNCA
Na_2CO_3 chemically activated cocoa pod residue	CCPNCA
Na_2CO_3 chemically activated coconut shell fibre residue	CNFNCA
Na_2CO_3 chemically activated plantain peel residue	PTHNCA
Na_2CO_3 chemically activated cocoyam peel residue	CCYBNCA
Na_2CO_3 chemically activated sweet potato peel residue	PTPNCA
Na_2CO_3 chemically activated white yam peel residue	YTBNCA
K_2CO_3 chemically activated residue - 550 $^\circ$C	
K_2CO_3 chemically activated oil palm fruit fibre residue	OPFKCA
K_2CO_3 chemically activated cocoa pod residue	CCPKCA
K_2CO_3 chemically activated coconut shell fibre residue	CNFKCA
K_2CO_3 chemically activated plantain peel residue	PTHKCA
K_2CO_3 chemically activated cocoyam peel residue	CCYBKCA
K_2CO_3 chemically activated sweet potato peel residue	PTPKCA
K_2CO_3 chemically activated white yam peel residue	YTBKCA

8.1 Characterisation – Ash content, loss on attrition and yield

Chemical activation has been reported by Gautam *et al.,* (2014) as having two important advantages over physical activation for the modification of adsorbents. The first is the lower temperature that is used in the activation process due to the effect of the chemicals during impregnation of the material before thermal treatment. While the second is that the yield of the chemical activation process often tends to be greater since there is less burn of char. Furthermore, the chemical activation procedure used in this study was a single stage activation method after the impregnation of the residues and this method combines the two processes of carbonization and activation. This single step process also saves energy, time, capital and operating cost when compared to physical activation process for residues (Djilani *et al.,* 2012; Gautam *et al.,* 2014). This chemical activation procedure results in adsorbents with different properties such as yield, ash content and these may also be influenced by the nature of the material used for the chemical activation. The yield, ash

content and loss on attrition of the two groups of chemically activated adsorbents obtained in this study are shown in Tables 8.2 and 8.3.

Table 8.2: Ash content, loss on attrition and yield of Na_2CO_3 activated adsorbents

Adsorbent	Ash[e] (%)	Loss on Attrition (%)	Yield (%)
OPFNCA	10.8	13.45	48.7
	±0.033	±1.23	±2.73
CNFNCA	12.1	8.85	49.15
	±0.132	±0.379	±0.291
CCPNCA	10.4	6.1	48.25
	±0.611	±2.43	±3.41
CCYBNCA	8.4	7.7	41.6
	±0.076	±1.54	±2.18
PTHNCA	8.7	7.55	46.6
	±0.78	±1.13	±3.63
PTPNCA	8.4	9.2	42.15
	±0.036	±1.92	±4.87
YTBNCA	10.3	9.1	45.4
	±0.032	±1.78	±4.19

[e] Ash content using AOAC(2000)

From Tables 8.2 and 8.3 it can be seen that the Na_2CO_3 activated adsorbents had yields that were higher than those of the K_2CO_3 adsorbents. For the Na_2CO_3 adsorbents, CNFNCA had the highest yield of 49.1% and the lowest yield was obtained for the CCYBNCA adsorbent. For the K_2CO_3 adsorbents, PTPKCA had the highest yield of 47.8% while OPFKCA had the lowest yield of 40.3%. The variation in activated carbon yield using the same chemical activation agent may be associated with the characteristic properties of each residue used due to their chemical composition and morphology as these would influence the chemical interaction that takes place during impregnation with the Na_2CO_3 and K_2CO_3 chemical activating agents as well as the subsequent thermal treatment leading to the decomposition of the organic components in the residue (Ahmaruzzaman, 2010). The yield values are also comparable with the results obtained for activated carbon from pomegranate peel using 10% HNO_3 reported by El- Ashtoukhy *et al.,* (2008) which had a yield of 46%. Imamoglu and Tekir, (2008) have also reported an activated carbon yield of 37.5% for the chemical activation of hazelnut husk using $ZnCl_2$ at 700°C under N_2 atmosphere for 4 h. Vargas *et al.,* (2011) in their study also reported a yield of 21.5% for

the conversion of flamboyant *Delonix regig* pods into activated carbon using NaOH using a 2 step carbonisation and activation procedure.

Table 8.3: Ash content, loss on attrition and yield of K_2CO_3 activated adsorbents

Adsorbent	Ash [e] (%)	Loss on Attrition (%)	Yield (%)
OPFKCA	11.5	15.85	40.3
	±0.041	±1.73	±3.63
CNFKCA	3.1	13.7	43.4
	±0.429	±0.421	±0.289
CCPKCA	12.8	12.7	42.3
	±0.034	±2.93	±3.83
CCYBKCA	9.7	14.5	45.9
	±0.041	±1.82	±3.58
PTHKCA	11.4	15.8	42.8
	±0.65	±1.93	±3.63
PTPKCA	9.9	13.35	47.8
	±0.042	±3.09	±2.93
YTBKCA	12.3	18.05	40.55
	±0.057	±1.72	±3.98

[e] Ash content using AOAC(2000)

The ash content of the chemically activated adsorbents was determined as described in section 4.3.1 and the results are shown in Table 8.2 for the Na_2CO_3 adsorbents and Table 8.3 for the K_2CO_3 adsorbents. From the results it can be observed that the YTBKCA adsorbent had the highest value of 12.3% while the lowest was 8.4% (CCPNCA & PTPNCA) for the Na_2CO_3 adsorbents. For the K_2CO_3 adsorbents CCPKCA had the highest content of 12.8% while an ash content of 3.1% was obtained for the CNFKCA adsorbent. The implication of ash content for activated carbon adsorbents used in heavy metal removal has generated some debate in literature, some studies report that the presence of a high ash content (inorganic component) may restrict the number of applications for the activated carbon as high as content reduces the mechanical strength and adsorption capacity of activated carbon (Soleimani and Kaghazchi, 2014a; Ahmaruzzaman, 2010). On the other hand, literatures exist on reports that high ash content would favour the application of the activated carbon as adsorbents (Varma *et al.,* 2013).

The ash content of agricultural residues has been reported to be dependent on the amount of inorganic elements such as Ca, K, Na, Si and P in the biomass, type of biomass and type

of cultivation of biomass (Ahmaruzzaman, 2010). In addition to this, the chemical activation procedure used in this study may also contribute inorganic elements such as K and Na from the chemical activating agents into the activated carbon matrix during the impregnation step. From the results of the ash content of the adsorbents prepared from the Na_2CO_3 and K_2CO_3, it was observed that the ash content were comparable to those reported in literature for some chemically activated adsorbents. A 14% ash content of sugar beet pulp activated carbon has been reported Torres-Perez *et al*.,(2012) in their study on the conversion of agricultural residues into activated carbon for water purification. However, El-Ashtoukhy *et al.,* (2008) has reported higher ash content at 32% for the activated pomegranate peel using H_3PO_4: $ZnCl_2$ in a (1:1) ratio. This may be related to the effect of the two activating agents (H_3PO_4 and $ZnCl_2$) on the inorganic content of the activated carbon.

The percentage loss on attrition was another characteristic evaluated for these adsorbents and was determined as described in Section 4.3.11. This characteristic examines the process and degree of generation of fine adsorbent particles during adsorbent contact with the walls of the adsorbent vessel and adsorbent-adsorbent contact arising from intra-particle abrasion (Toles *et al.,* 2000). The trend in this property implies that the higher the percentage of fines generated during contact in a vessel, the less attractive the material will be in a mixing reactor as the fine particles generated has a tendency to cause blockage of reaction systems thereby reducing the efficiency of the sorption process. However, these adsorbents will be well suited for column adsorption processes where contact has a lower frequency. The results in Tables 8.2 and 8.3 indicate that the K_2CO_3 group of adsorbents had higher values for attrition losses with the highest being 18.05% for the YTBKCA adsorbent and the lowest being 12.7% for the CCPKCA adsorbent. On the other hand for the Na_2CO_3 group of adsorbents, the highest attrition loses were obtained for the OPFNCA adsorbent (13.45%), while the least was 6.1% for the CCPNCA adsorbent. This extent of fine generation by these adsorbents may also be related to the effect of the chemical activating agents on the adsorbent particle morphology thereby making them susceptible to degradation on contact. Similar values for chemically activated carbon attrition losses have been reported in literature, Sunanda *et al.,* (2013) reports an attrition loss of 12% for the activated carbon produced through the chemical activation of *sapindus* seed hull using H_2SO_4 in a 1:1 ratio with adsorbent. A phosphoric acid (H_3PO_4) activated hard-shell of apricot stones has also been reported to have an attrition loss of 13.38% (Soleimani and

Kaghazchi, 2008b), while the conversion of *Delonix regia* fruit (DRFP) into activated carbon using H_3PO_4 was reported to yield a carbon adsorbent with attrition losses of 10.20% (Sugumaran *et al.,* 2012). The attrition characteristics of these chemically activated adsorbents may be associated with the nature of the agricultural residue and effect of the chemical activation process on the morphology and microstructure of the final adsorbents (Sugumaran *et al.,* 2012). Toles *et al.,* (2000) reported an attrition percentage of 41% for activated carbon which was prepared from a continuous method thereby confirming that the process of synthesis of the chemical activated carbon adsorbents can influence the extent of losses due to attrition.

8.2 Zeta potential, pH and pHpzc of adsorbents

The surface of activated carbon adsorbents is known to contain different oxygen-containing functional groups such as carboxyl, lactonic, phenolic and hydroxyl (Ahamd *et al.,* 2014) and the concentration of these functional groups (acidic or basic) and other species determine surface charge on the adsorbent. In solution, these functional groups will ionize and the overall charge on the adsorbent surface will depend on their concentration and the pH of the solution. Thus the surface charge of the adsorbent plays a fundamental role on the type of species (such as metal ions) that an adsorbent can remove from solution. The pH of each chemically activated carbon adsorbents that were developed in this study were determined based on the procedure described in Section 4.3.9 and these are shown in Table 8.4. From Table 8.4, it is observed that all the chemically activated adsorbents had values of pH that were in the region between 7.1 and 7.64 indicating that their surface had a higher concentration of basic functional groups that acidic groups. This trend is in contrast to what was reported by Ahmad *et al.,* (2014b) for the KOH activated pomegranate peel using microwave based activation procedure, where the pH of the activated carbon obtained was 3.6 indicating a higher concentration of acidic groups on the surface of the prepared carbon.

This surface acidity or basicity may also arise due to the post treatment regime used after the thermal treatment of the activated carbon. Some protocols in this process may involve either neutralising the chars with an acid if a base was used to activate and the washing off the acid with water until the material is neutral. This process may introduce additional acid functional groups onto the adsorbent.

Table 8.4: pHpzc and pH of Na_2CO_3 and K_2CO_3 activated adsorbents

Adsorbent	pHpzc	Adsorbent pH	Adsorbent	pHpzc	Adsorbent pH
OPFNCA	7.10	7.48	OPFKCA	7.30	7.56
CNFNCA	7.50	7.71	CNFKCA	7.40	7.64
CCPNCA	7.20	7.59	CCPKCA	7.70	7.25
CCYBNCA	7.20	7.34	CCYBKCA	7.30	7.01
PTHNCA	7.90	7.40	PTHKCA	7.60	7.57
PTPNCA	7.20	7.43	PTPKCA	7.80	7.1
YTBNCA	8.00	7.10	YTBKCA	7.90	7.45

Another process if a basic chemical activation was used involves the washing of the char with water until the solution obtained is neutral. This is the procedure that was used in this study and it ensures that the surface functional groups are not altered during this post activation regime by another chemical activating agent during the thermal treatment, washing and drying stages of the adsorbent preparation.

The chemically activated adsorbents were further characterised using photo-correlation spectroscopy (PCS) to determine the zeta potential on the adsorbent surface across a range of pH values from 2 − 12 as described in Section 4.3.3. The plots of the zeta potential vs. pH for these chemically activated adsorbents are shown in Appendix 3 and the pH point of zero charge (pHpzc) of each of the chemically activated adsorbents is shown in Table 8.4. From the plots, it is seen that as the pH of the solution moves from acid to basic there is a reduction in the zeta potential on the adsorbent surface and the pH in which the zeta potential on the adsorbent surface changes from positive values to negative values in zeta potential vs. pH plot is known as the pH point of zero charge (pHpzc). This is the pH at which the amount of negative species (ions) on the adsorbent surface is equal to the positive species resulting in a zero charge at the surface (Nomanbhay and Palanisamy, 2005). At pH values above the pHpzc, the functional groups on the active sites on the adsorbent surface are mainly in the dissociated form and acquire a negative charge, while at pH values lower than the pHpzc, the sites will be in the associated form with a proton thereby becoming positively charged (Ofomaja *et al.,* 2009).

From the plots in Appendix 3 and the results in Table 8.4, it is seen that the pHpzc of the adsorbents were in the range 7.1- 8 and was associated closely with the adsorbent pH. Since the pH of the solution affects the degree of ionisation of the heavy metal ions of interest and based on the pHpzc of these adsorbents, it can therefore be said that the pHpzc an adsorbent material is an important parameter that gives the linear range of pH sensitivity and an indication of the type of surface active sites and sorption probability of a surface to a target pollutant specie. This has made the pHpzc an important parameter that is studied in adsorption literature as it provides insight and better understanding of the adsorption mechanism (Pirbazari *et al.,* 2014).

Furthermore, from the values in Table 8.4 and the trend of association of the pH and pHpzc of the chemically activated adsorbents, the pH of 7 was chosen for the sorption of Cd(II) and Pb(II) from aqueous solution as these positive metal ions will have a higher probability of undergoing sorption on the surface of the chemically activated adsorbents within this pH. It can also be stated that since chemical modification of an adsorbent surface affects the nature and type of chemical species on an adsorbent (Gautam *et al.,* 2014), the K_2CO_3 and Na_2CO_3 used for the activation of the adsorbents in this study played a significant role in the determination of the surface chemistry of these adsorbents, hence the pH and pHpzc of these chemically activated carbon adsorbents are within the basic region. The pHpzc values obtained for these chemically activated carbon adsorbents are similar to those obtained in previous studies reported in literature. Gautam *et al.,* (2014) reported that the pHpzc of coconut shell activated carbon modified with nitric acid (HNO_3), hydrogen peroxide (H_2O_2) and ammonium persulfate ($(NH_4)_2S_2O_8$ were 7.45 (HNO_3 treated coconut shell), 6.76 (H_2O_2 treated coconut shell) and 6.40 ($(NH_4)_2S_2O_8$ treated coconut shell). These values indicate the impact of the chemical used in the activation process on the pHpzc of the resulting adsorbents. The pHpzc of some commercial activated carbon used for adsorption of pharmaceutical active compounds from aqueous solutions have also been reported, for the granular activated carbon the pHpzc was 5.6, while for the powdered activated carbon the pHpzc was 8.7 (Rakic *et al.,* 2015).

8.3 Surface area and porosity of chemically activated carbon adsorbents

The conversion of an agricultural residue into an activated carbon is a transformation that uses either physical or chemical activation techniques to develop or increase certain

characteristics on the precursor. This is carried out so that its carbon content is enriched and its porosity and pore structure increased as a result of the volatilisation of the organic components in the structure leading to the development voids, spaces and pores within the carbon rich product (Gautam *et al.,* 2014). A number of parameters are used to influence the porosity and pore structure of an activated carbon adsorbent thereby improving the metal ion loading of these types of materials. The use of alkaline (basic) reagents for the chemical activation of residues to produce activated carbon has been reported in literature as having significant influence on improving the adsorption performance of activated carbon for both inorganic and organic pollutants (Elnasri *et al.,* 2013). This process of chemical impregnation and activation can induce reactions that lead to the generation of more pores and active functional groups on the surface and bulk of the material which can result in increasing the surface area and porosity of the activated carbon and as a consequence contribute to improving the loading capacity for pollutants of interest (Vargas *et al.,* 2011; Kyzas and Deliyanni, 2014).

The nitrogen adsorption-desorption isotherm plot and pore size distribution of the Na_2CO_3 chemically activated carbon adsorbents (OPFNCA, CNFNCA, CCPNCA, PTHNCA, CCYBNCA, PTPNCA and YTBNCA) are shown in Figures 8.1 − 8.2; while that of the K_2CO_3 chemically activated carbon adsorbents (OPFKCA, CNFKCA, CCPKCA, PTHKCA, CCYBKCA, PTPKCA and YTBKCA) are presented in Figures 8.3 − 8.4. From the plots in Figures 8.1 − 8.4, the surface area and porosity characteristics of the chemically activated adsorbents were obtained and are presented in Tables 8.5 and 8.6 for the Na_2CO_3 and K_2CO_3 activated carbon adsorbents respectively.

From table 8.5, it is observed that for Na_2CO_3 chemically activated adsorbents, the CNFNCA had the highest BET surface area of 827 m^2 g^{-1}, while the PTHNCA adsorbent had the lowest BET surface area of 381 m^2 g^{-1} with the trend in surface area for the adsorbents being CNFNCA > OPFNCA > YTBNCA > CCYBNCA > CCPNCA > PTPNCA > PTHNCA. For the K_2CO_3 chemically activated carbon adsorbents, the BET surface area obtained as shown in Table 8.6 shows that the CNFKCA adsorbent had the highest BET surface area of 553 m^2 g^{-1}, while the OPFKCA adsorbent had the lowest surface area of 267 m^2 g^{-1}. The trend in increasing surface area for the K_2CO_3 chemically activated carbon adsorbents was CNFKCA > PTPKCA > CCPKCA>CCYBKCA > YTBKCA > PTHKCA > OPFKCA.

Table 8.5: Surface area and porosity of Na_2CO_3 chemically activated adsorbents

Adsorbent	BET Surface Area (m^2g^{-1})	Total Pore Volume (cm^3g^{-1})	BJH Desorption Average Pore Diameter (nm)
OPFNCA	670	8.24E-01	8.91
CNFNCA	827	5.67E-01	5.26
CCPNCA	473	4.76E-01	9.62
CCYBNCA	514	4.20E-01	9.66
PTHNCA	381	2.92E-01	5.45
PTPNCA	437	2.82E-02	5.35
YTBNCA	593	5.41E-01	8.02

Table 8.6: Surface area and porosity of K_2CO_3 chemically activated adsorbents

Adsorbent	BET Surface Area (m^2g^{-1})	Total Pore Volume (cm^3g^{-1})	BJH Desorption Average Pore Diameter (nm)
OPFKCA	267	2.75E-01	6.47
CNFKCA	553	3.56E-01	4.03
CCPKCA	361	2.07E-01	4.18
CCYBKCA	354	3.49E-01	8.21
PTHKCA	337	2.01E-01	5.50
PTPKCA	379	4.14E-01	7.44
YTBKCA	339	2.18E-01	4.20

The results of the BET surface area of the chemically activated carbon adsorbents (Na_2CO_3 & K_2CO_3) show that the Na_2CO_3 chemically activated carbon adsorbents had higher surface area than their corresponding K_2CO_3 adsorbents. This may be due to the effect of the Na_2CO_3 during the impregnation and thermal activation stages of the synthesis process.

The results further indicate the trend that has been observed previously with respect to the intrinsic nature of the precursor residue influencing the surface properties of the resulting adsorbents after chemical or thermal conversion. This is also observed in the variation of the BET surface areas of the different adsorbents for the Na_2CO_3 & K_2CO_3 chemically activation processes.

The BET surface area of the Na_2CO_3 & K_2CO_3 chemically activated carbon adsorbents are similar and in some instances higher that those reported in literature for lignocellulosic materials converted to activated carbon using the chemical impregnation route. Lacerda *et al.,* (2015) has reported on the conversion of macauba seed endocarp, carnauba palm leaves and pine nut shell into activated carbon using calcium chloride ($CaCl_2$) and phosphoric acid (H_3PO_4) as chemical activating agents. From their study, the BET surface areas for the chemical activated carbon adsorbents were; 430 $m^2 g^{-1}$ (carnauba palm leaves- $CaCl_2$); 402 $m^2 g^{-1}$ (carnauba palm leaves- H_3PO_4); 371 $m^2 g^{-1}$ (macauba seed endocarp- H_3PO_4); 265 $m^2 g^{-1}$ (macauba seed endocarp- $CaCl_2$); 290 $m^2 g^{-1}$ (pine nut shell- $CaCl_2$) and 296 $m^2 g^{-1}$ (pine nut shell- H_3PO_4). This result indicates that the BET surface areas of these lignocellulosic materials are influenced by the type of chemical activating agent and intrinsic nature of the precursor used for the activation process.

The total pore volume of the Na_2CO_3 & K_2CO_3 chemically activated carbon adsorbents are presented in Tables 8.5 and 8.6 for the Na_2CO_3 & K_2CO_3 chemically activated carbon adsorbents respectively. The results from both tables indicates that for the Na_2CO chemically activated carbon adsorbents, the OPFNCA adsorbent had the largest pore volume of 8.24×10^{-1} $cm^3 g^{-1}$ while the PTPNCA adsorbent had the least (2.82×10^{-3} $cm^3 g^{-1}$). For the K_2CO_3 chemically activated carbon adsorbents, the largest total pore volume was obtained for the PTPKCA adsorbent (4.41×10^{-1} $cm^3 g^{-1}$) and the PTHKCA adsorbent had the least ((2.01×10^{-1} $cm^3 g^{-1}$).
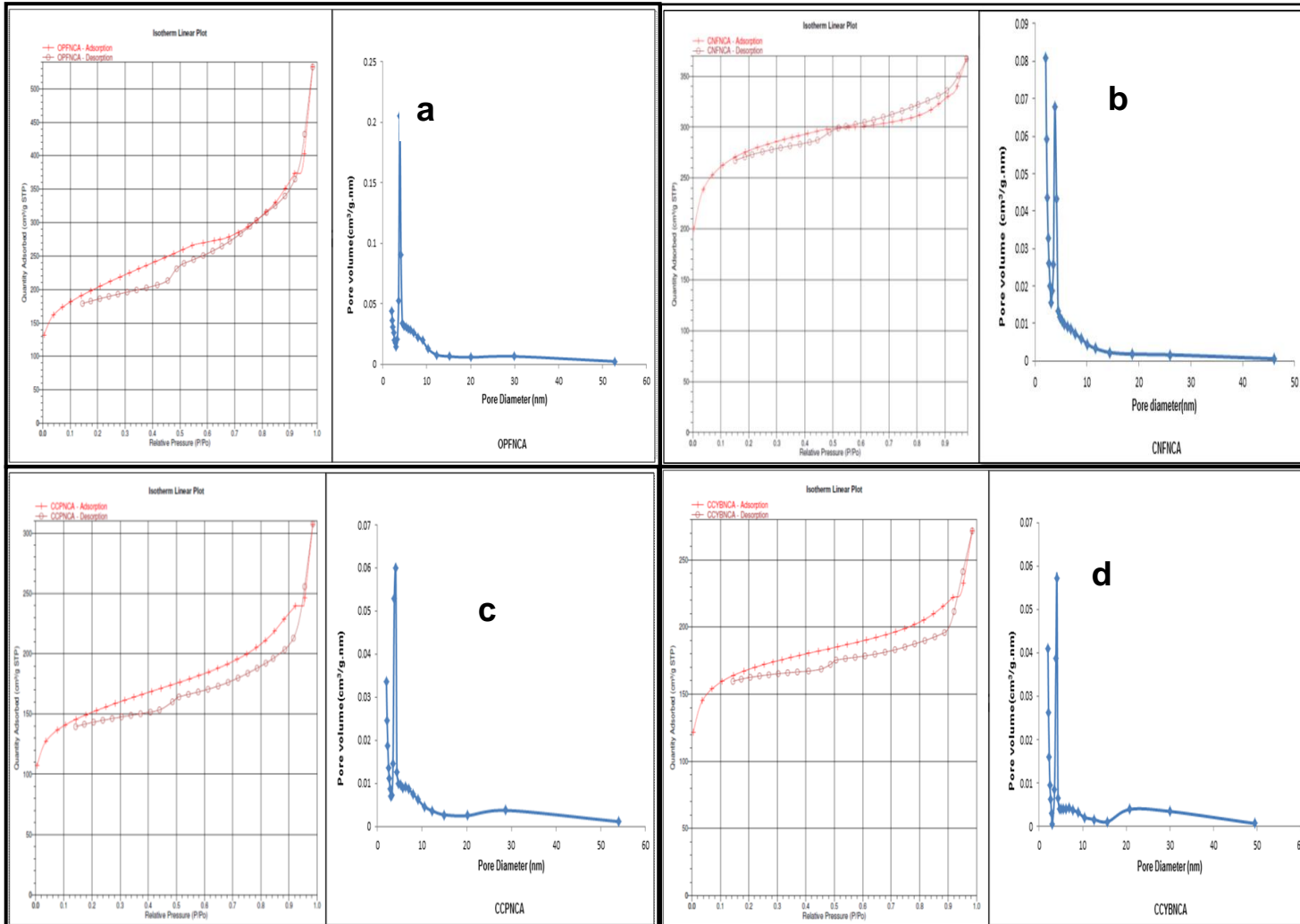
Figure 8.1: N$_2$ adsorption-desorption isotherm and pore size distribution of OPFNCA, CNFNCA, CCPNCA and CCYBNCA adsorbents
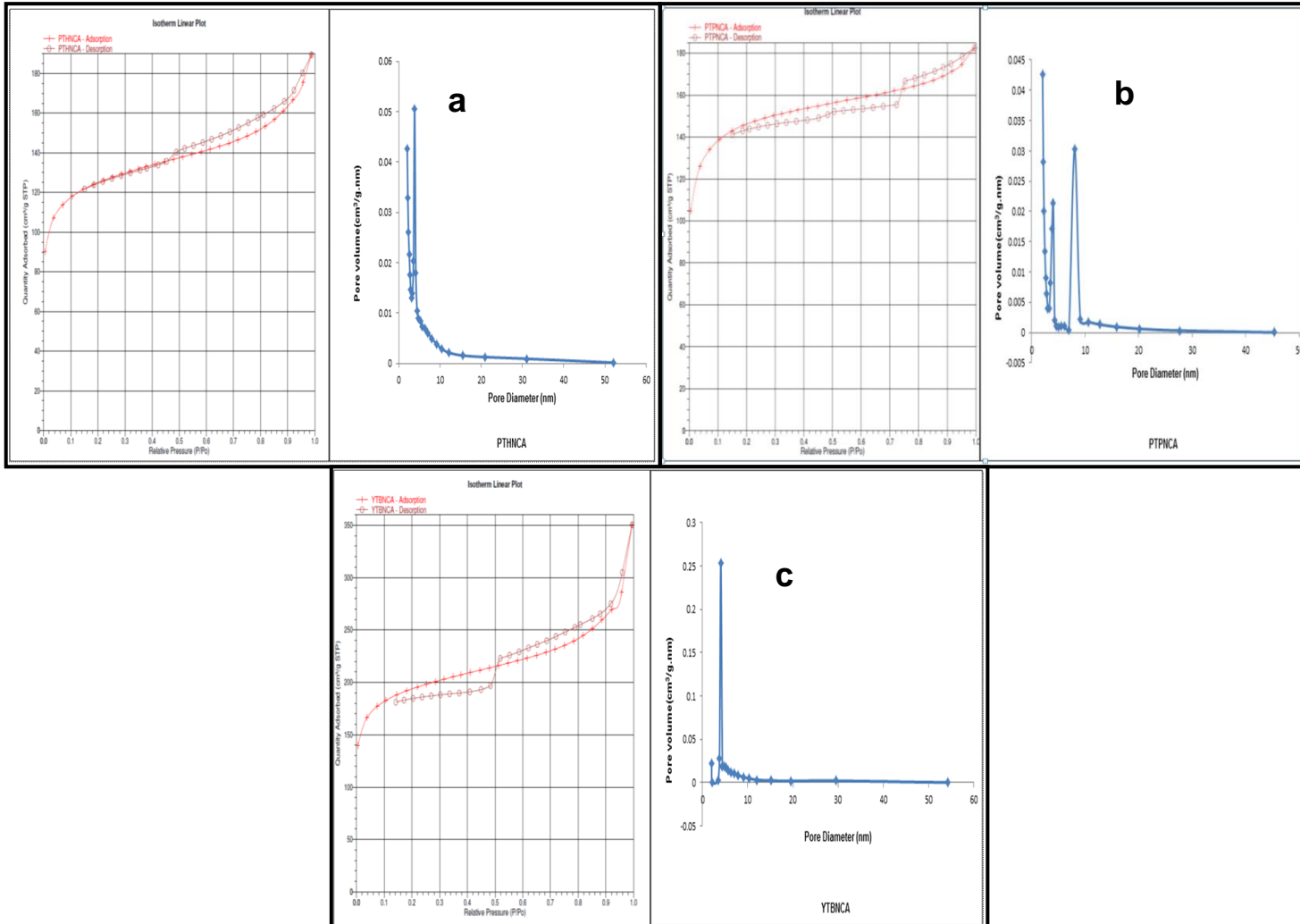
Figure 8.2: N$_2$ adsorption-desorption isotherm and pore size distribution of PTHNCA, PTPNCA and YTBNCA adsorbents
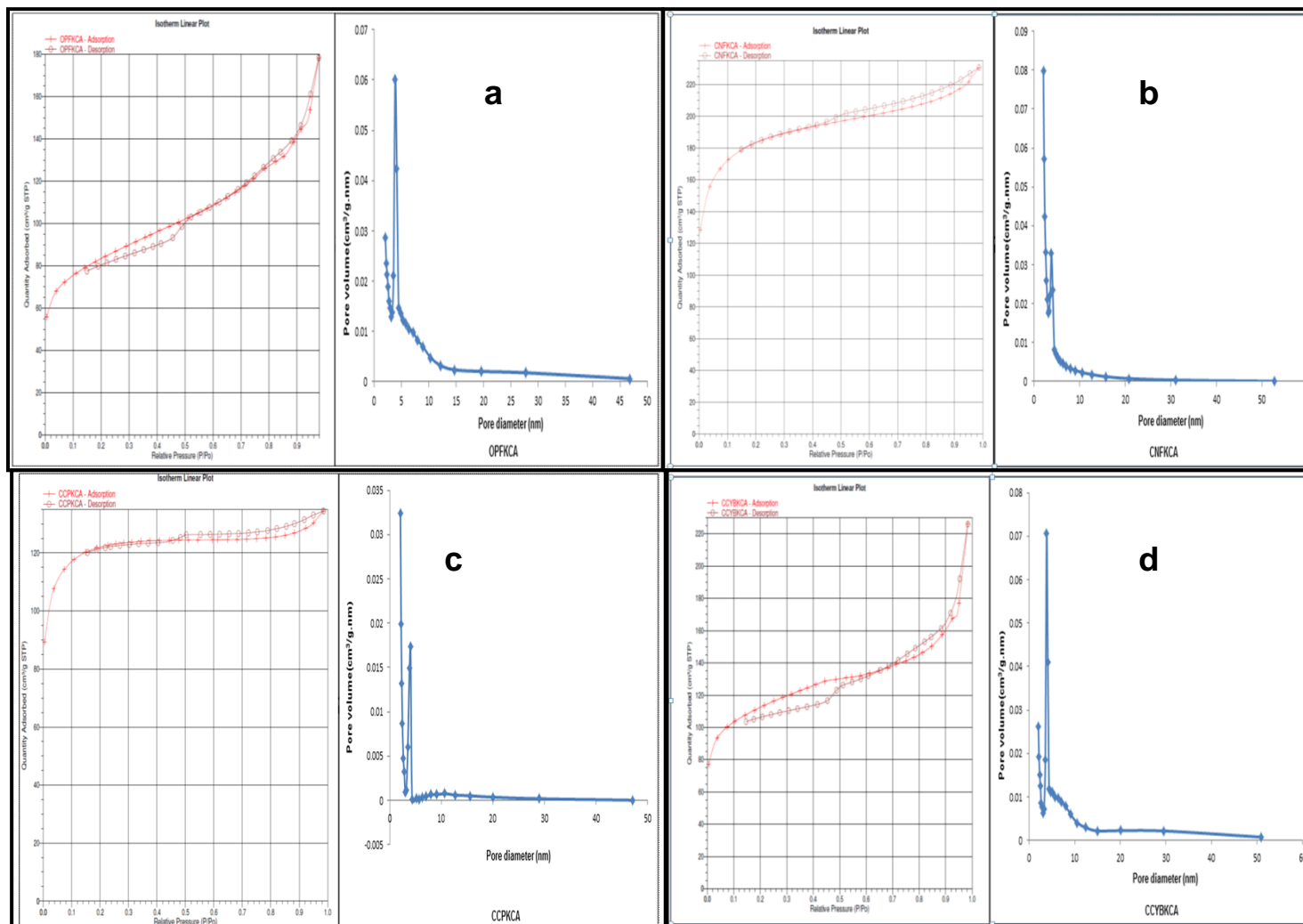
Figure 8.3: N$_2$ adsorption-desorption isotherm and pore size distribution of OPFKCA, CNFKCA, CCPKCA and CCYBKCA adsorbents
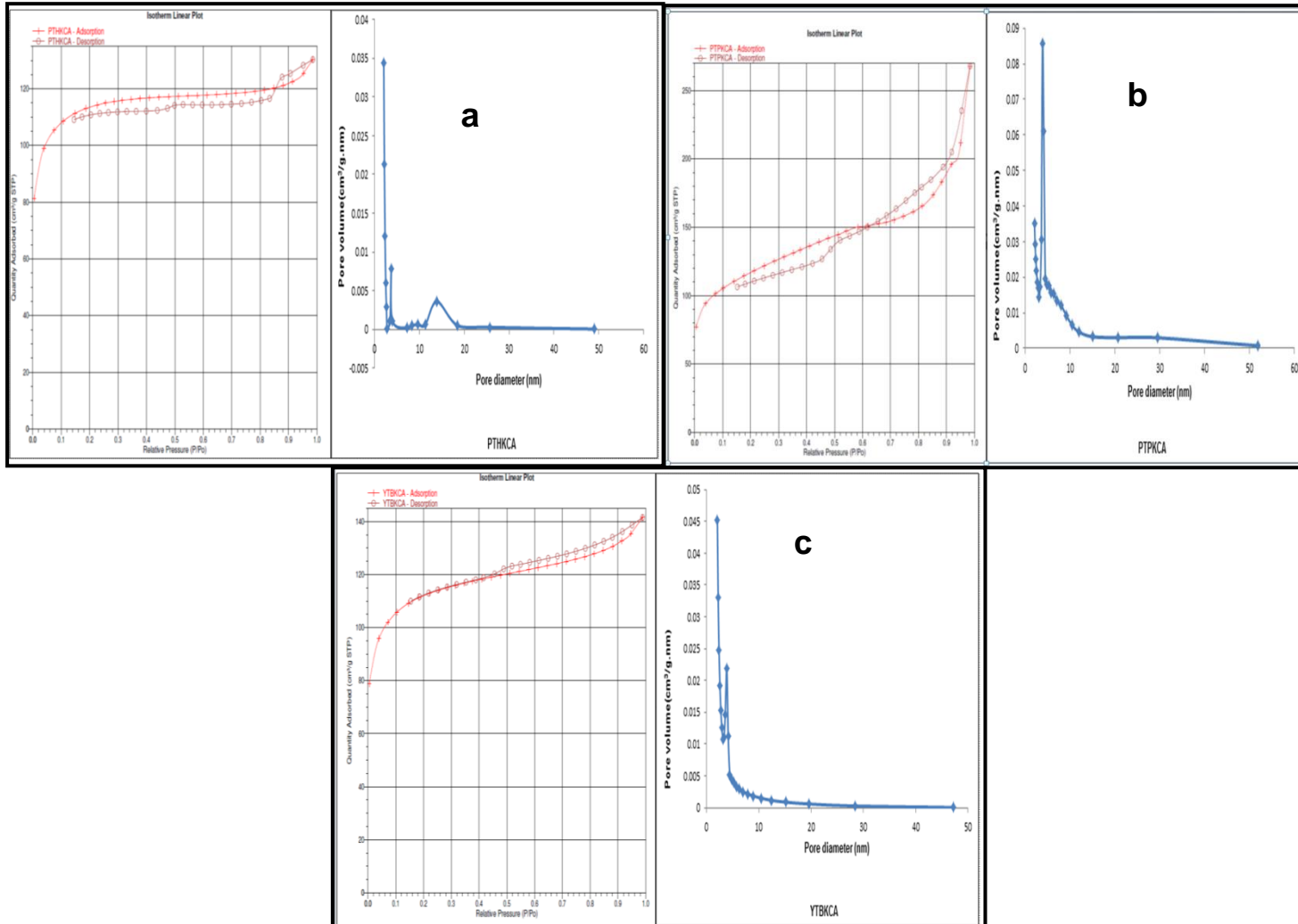
Figure 8.4: N$_2$ adsorption-desorption isotherm and pore size distribution of PTHKCA, PTPKCA and YTBKCA adsorbents

Furthermore, the results presented in tables 8.5 and 8.6 also shows the effect of the chemical activation process on the surface area and porosity of the adsorbents. When a comparison is made between these results (Tables 8.5 & 8.6) and that of the surface area and porosity of the raw residues (Table 5.5), it is observed that the chemical activation process using both Na_2CO_3 and K_2CO_3 as chemical activating agents did affect the BET surface area and porosity of the precursors. This is because the BET and pore characteristics of the Na_2CO_3 and K_2CO_3 activated carbon adsorbents were observed to have substantially increased when compared with the raw agricultural residue, the hydrothermally carbonised adsorbents, as well as the carbonised and pyrolysed adsorbents that have been previously discussed. Furthermore, it was observed that the highest pore diameter (computed based on the desorption branch) using the BJH method was 9.66 nm for CCPPCA, while the least was 5.35 nm for the PTPNCA adsorbent. These pore size distribution are based on the IUPAC classification of adsorbent pores and indicates that the Na_2CO_3 chemically activated adsorbents were mesoporous based on the desorption branch using the BJH method. Similar results were also observed for the K_2CO_3 activated carbon adsorbents which had highest and least pore size distributions of 8.21 nm for CCYBKCA and 4.03 nm for CNFKCA ranking them also as mesoporous materials.

The nitrogen adsorption-desorption isotherms of the chemical activated adsorbents in Figures 8.1 − 8.4 shows increasing adsorption of nitrogen as relative pressure increased and the presence of hysteresis loop in each of the isotherms is used to classify the chemical activated adsorbents according to the Brunauer-Deming-Deming-Teller (BDDT) classification. Based on this method the chemically activated carbon adsorbents can be grouped as mesoporous materials with the type IV N_2 adsorption-desorption isotherm (Brunauer *et al.,* 1940; Ip *et al.,* 2008). These chemically activated carbon adsorbents were all observed to have the H1 type hysteresis loop which indicates the presence of a narrow distribution of pore sizes with characteristic capillary condensation and evaporation processes (Banerjee *et al*., 2015).

The pore size distributions (PSD) of these adsorbents seen in Tables 8.5 and 8.6 essentially show that they are predominantly mesoporous adsorbents and these chemically activated carbon adsorbents also show bimodal pore size distribution with the exception of PTPNCA and PTHKCA adsorbents which showed trimodal distribution appearing in the range 3 − 10 nm. A narrow distribution of pores is observed to occur for each adsorbent

between 3 – 10 nm and wider distribution from the 12 – 50 nm range. This bimodal distribution and the variety in domains of pore distribution has been reported for activated carbon adsorbents obtained from different synthetic waste polymers activated using potassium hydroxide chemical activation (Lian *et al.,* 2011) and the process involved in the activated carbon preparation which results in the creation of porous structure during activation has been used to explain this phenomenon that is commonly reported in carbonaceous adsorbents (Gauden *et al.,* 2007; Lee and Park, 2013).

It has also been observed that the chemically activated carbon adsorbents produced from the use of Na_2CO_3 and K_2CO_3 as chemical activating agents in this study have surface area and porosity characteristics that are similar to some activated carbon manufactured for commercial applications reported in literature as well as those produced using other activation methods such as steam and carbondioxide (CO_2) activation. Ahamd *et al.,* (2012a) has reported on the activation of Cocoa (*Theobroma cacao)* shell based activated carbon using CO_2 at 850$^°$C and the BET surface area obtained was 85.09 $m^2\,g^{-1}$. The total pore volume for this activated carbon was 0.05 $cm^3\,g^{-1}$ with an average pore size of 2.7 nm. The carbon obtained exhibited high microporosity as well as significant mesoporosity. Activated carbon produced from cashew nut shells using KOH activation and CO_2 gasification at 854$^°$C has been reported also in literature and the BET surface area for different KOH/char ratio were determined in the study. These values ranged from 222 to 1120 $m^2\,g^{-1}$, while the pore volume obtained were between 0.11 to 0.57 cm^3g^{-1}. The range of pore sizes for these activated carbon adsorbents were in the mesoporous dimension of 20.11 to 22.57 nm indicating them as mesoporous activated carbon adsorbents (Tangjuank *et al*., 2009).

Almond shell and orange peel have also been converted into activated carbon through carbonisation at temperatures 500 – 1200$^°$C under N_2 atmosphere and activated using carbondioxide according to Hashemian *et al.,* (2014). The BET surface area obtained for the almond shell carbonised at temperatures; 500$^°$C, 700$^°$C and 1200$^°$C were 322, 385 and 342 $m^2\,g^{-1}$ respectively. Those obtained for the activated carbon from orange peels were 225, 248 and 240 $m^2\,g^{-1}$ respectively for the 500$^°$C, 700$^°$C and 1200$^°$C carbonised adsorbents. These adsorbents also had mean pore diameter ranging from 8 – 25 nm implying that they were mesoporous adsorbents, while their total pore volumes were 19.5, 16.9 and 15.5 $cm^3\,g^{-1}$ for the almond shells activated at 500$^°$C, 700$^°$C and 1200$^°$C

respectively. The orange peel activated carbon also had high total pore volumes of 14.5 cm^3g^{-1} (500°C), 15 cm^3g^{-1} (700°C) and 13.5 cm^3g^{-1} (1200°C) (Hashemian *et al.,* 2014). These studies indicate that the activated carbon adsorbents developed in this study had surface area and porosity values that are comparable to what has been reported in literature. In addition, it is also observed that these BET and pore characteristics of the Na_2CO_3 and K_2CO_3 chemically activated carbon adsorbents were not only similar but in some instances higher than those reported using other impregnating agents and activation procedures. The implication of these surface area and porosity characteristics on the metal ion loading will be explained in the subsequent sections.

8.4 Surface morphology and chemical composition

Activated carbon is the product of thermal treatment of organic precursors that eliminates the volatile components with the resulting carbon rich materials possessing void spaces that give characteristic porosity (Hernandez-Ramirez and Holmes, 2008). The morphology of the synthesized activated carbon is often an indication of the pore architecture of prepared adsorbents which may be influenced by: the type and nature of precursors, temperature of activation, type of activation process used and duration of carbonisation or activation. Insight into the morphology of materials such as activated carbon can be obtained using electron microscopy techniques such as scanning electron microscopy (SEM) (Hashemian *et al.,* 2014). SEM gives characteristic morphology of the materials and has been used frequently in the characterisation of adsorbents such as activated carbon. The morphology of the chemically activated adsorbents was obtained using SEM and their chemical composition was determined using the EDAX analysis coupled onto the scanning electron microscope.

8.4.1 Surface morphology of chemically activated adsorbents

In this study SEM was used to characterise the surfaces of the Na_2CO_3 and K_2CO_3 chemical activated carbon adsorbents as described in Section 4.3.2. Electron micrographs obtained for the Na_2CO_3 and K_2CO_3 chemically activated adsorbents are shown in Figures 8.5 to 8.8. Micrographs of the Na_2CO_3 chemically activated carbon adsorbents (Figure 8.5 and 8.6) reveal that the activated OPFNCA adsorbent still had longitudinal fibres as observed in the raw residue although the pores seen are more pronounced. This implies that the activation process did result in more defined pore structure on the adsorbent.

Images of the CCPNCA adsorbent on the other hand show more pores on the surface indicating an increase in surface porosity when compared to the raw residue adsorbent in Chapter 5. This irregular porous structure on the adsorbent that is predominantly mesoporous is a characteristic of the adsorbent that gives rise to the highly developed surface area of the material.
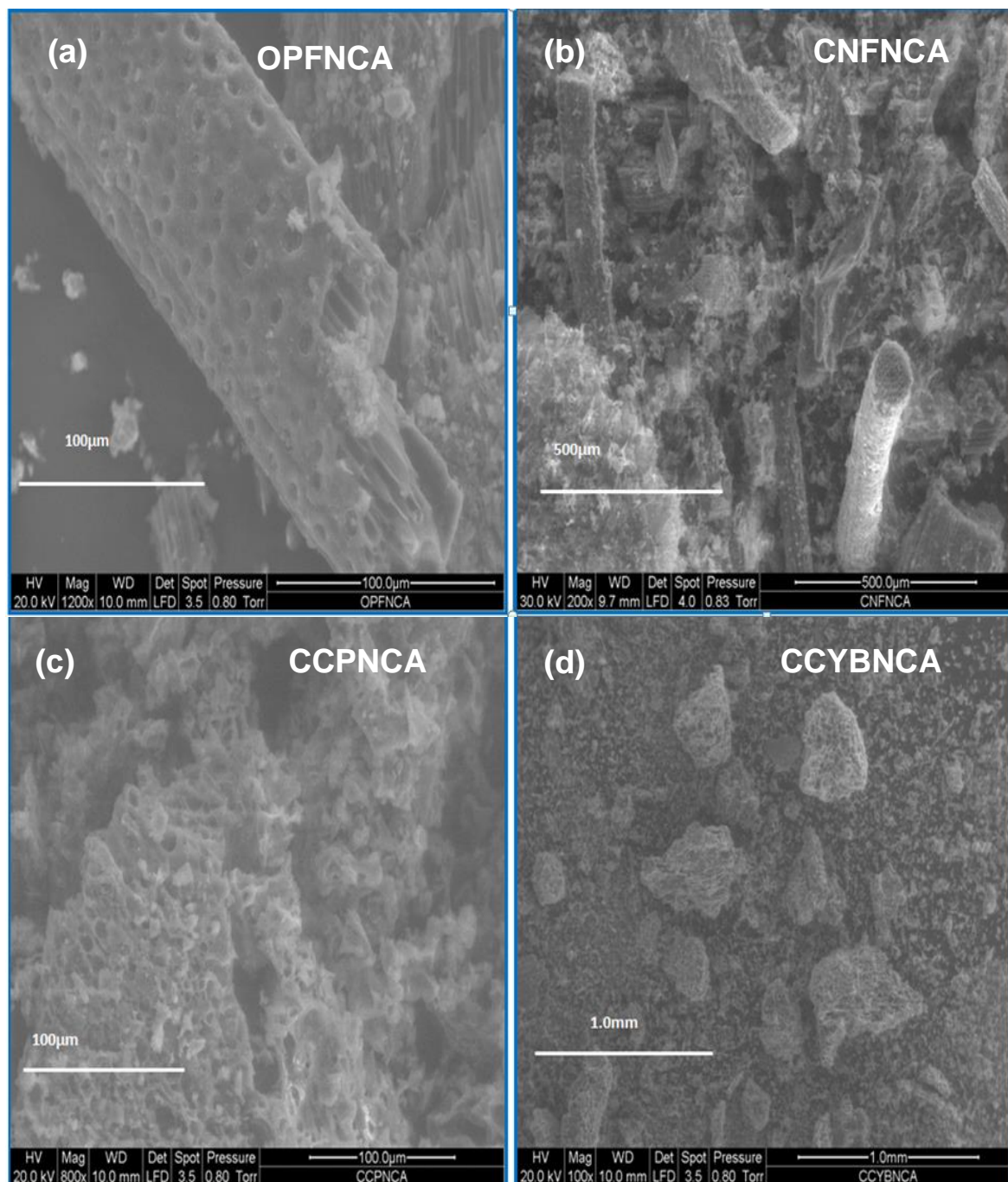
Figure 8.5: SEM micrograph for OPFNCA, CNFNCA, CCPNCA & CCYBNCA adsorbent
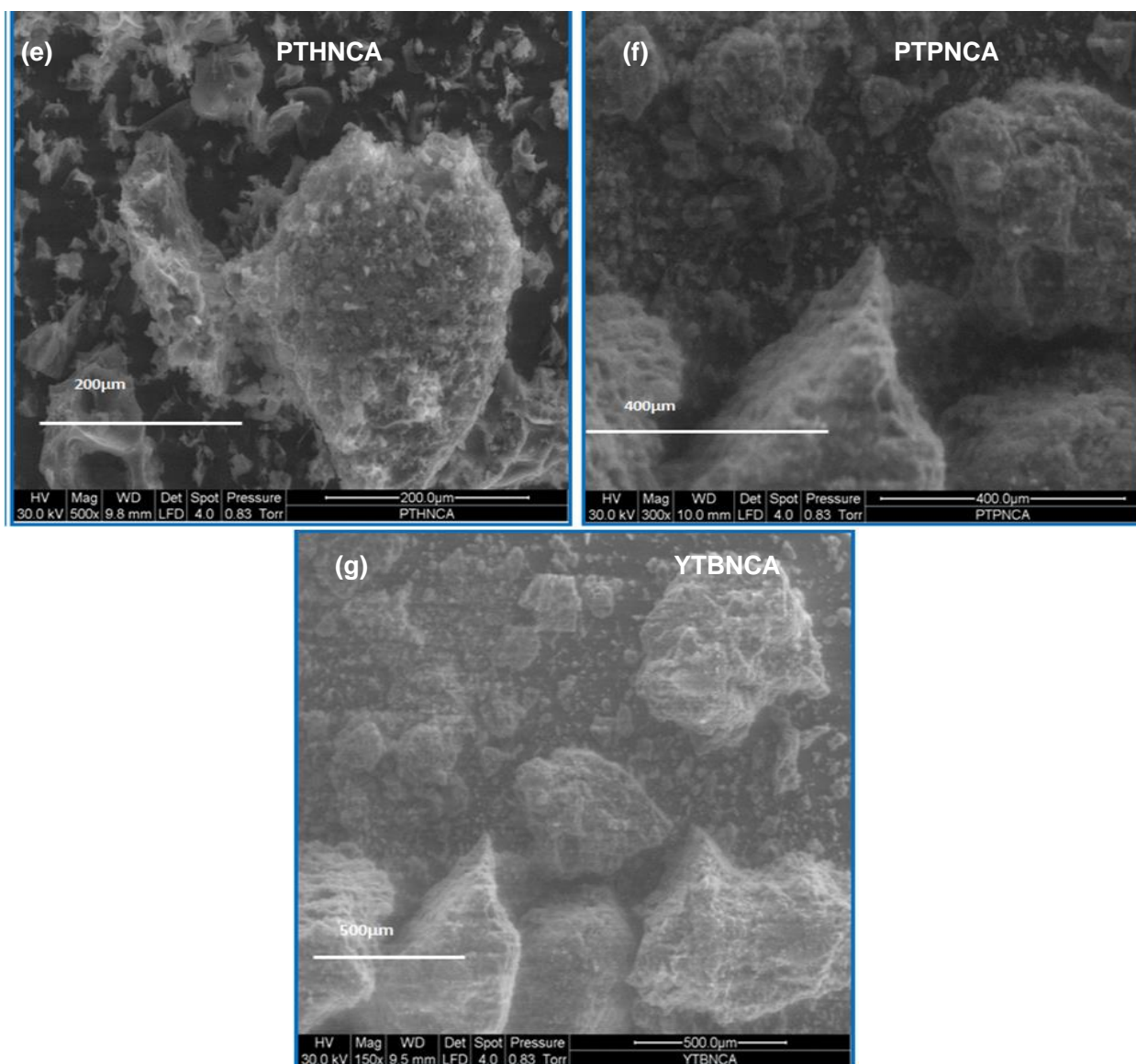
Figure 8.6: SEM micrograph for PTHNCA, PTPNCA and YTBNCA

For the CNFNCA adsorbent, the SEM image shows a well-developed microstructure with honeycomb arrangement resulting from chemical activation of the residue; an improvement from the already existing pore structure of the residue. This pore arrangement may be associated with the processes that occurred during the impregnation of the residue with Na_2CO_3 and the subsequent volatilization of the organic components on the residue matrix. The honeycomb pore microstructures are mainly seen in the longitudinal fibres of the coconut residue and its modified adsorbents. This irregular porous structure on the adsorbent that is predominantly mesoporous is a characteristic of the adsorbent that gives rise to the highly developed surface area of the material. The SEM

image for the CCPNCA adsorbent also shows the development of microstructure although this is not as extensive as the aforementioned in the CNFNCA.

The SEM images of the CCYBNCA, PTHNCA, PTPNCA and YTBNCA adsorbents seen in figure 8.6 shows that these activated carbon adsorbents do not possess the same type of ordered pores observed in the OPFNCA, CCPNCA and CNFNCA adsorbents as their pore arrangement is not well structured. This may be related to the nature of the structure of the residue as it undergoes impregnation and thermal treatment during the chemical activation process. These processes may have led to the decomposition and collapse of the pore arrangement in these adsorbents when the organic and volatile compounds in these residues were eliminated and can be associated with the strength and type of pore structure. The lignin content and type of arrangement existing on the residue may also be responsible for influencing the type of pore structure on these materials. This distinctive characteristic has been observed in some other residues as reported by Suhas *et al.,* (2007) where the agricultural feedstock with high lignin content were found to produce a higher amount of char during activation relating to a better development of micro and mesoporosity within the activated carbon structure. In addition, Deiana *et al.,* (2009) reports that during the preparation of an activated carbon from grape stalk, the chemical activation procedure using phosphoric acid was observed to produce a random distribution of porosity in the activated carbon structure which was attributed to the varying lignin content in the residue which affects the extent of modification of the cellular structure by acid activating agent.

The SEM of the K_2CO_3 chemically activated adsorbents are shown in Figures 8.7 – 8.8 and from these figures, it can be observed that the morphology of the adsorbents are similar to those obtained using the Na_2CO_3 adsorbent although these adsorbents have more enhanced and developed pores and their surface are rough and heterogeneous. This indicates that the process of cavity creation during impregnation and thermal modification was more pronounced in these materials. These pore microstructures are important openings in the adsorbent surface that will facilitate solution transport of adsorbates, enhance sorption probability and are also often used to explain mechanism of sorption kinetics (Zhang, *et al*., 2014). Since the pore structure in the activated carbon adsorbents are irregular leading to some surfaces consisting of agglomerated structures, their development can be seen as characteristic of the nature and kinetics of the thermo-chemical degradation process.
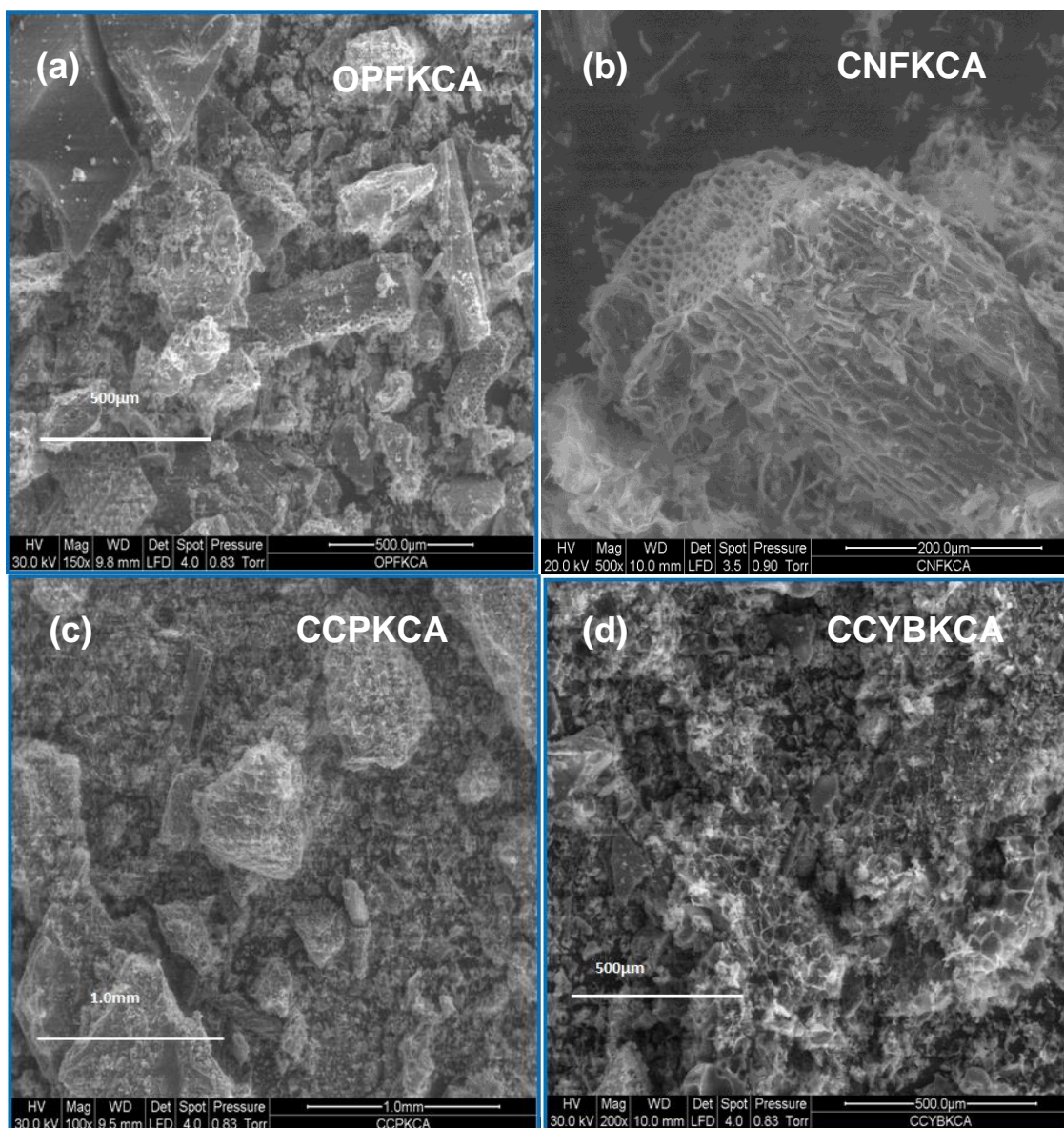
Figure 8.7: SEM micrograph for OPFKCA, CNFKCA, CCPKCA & CCYBKCA adsorbents

Furthermore, as the volatile components on the residues used for chemical activation will have different compositions of lignin, hemicellulose, cellulose, pectin and other extractives, their rate of degradation and extent of volatilization will be different thereby leading to diverse decomposition schemes that result in irregular pore microstructure on the resulting adsorbent. This observation is confirmed by Lian, *et al*., (2011) who notes that a fragmentation of the carbon skeleton on the residue often occurs during the activation of organic precursors for the synthesis of activated carbon resulting in the formation of a "loose sponge" structure after activation.
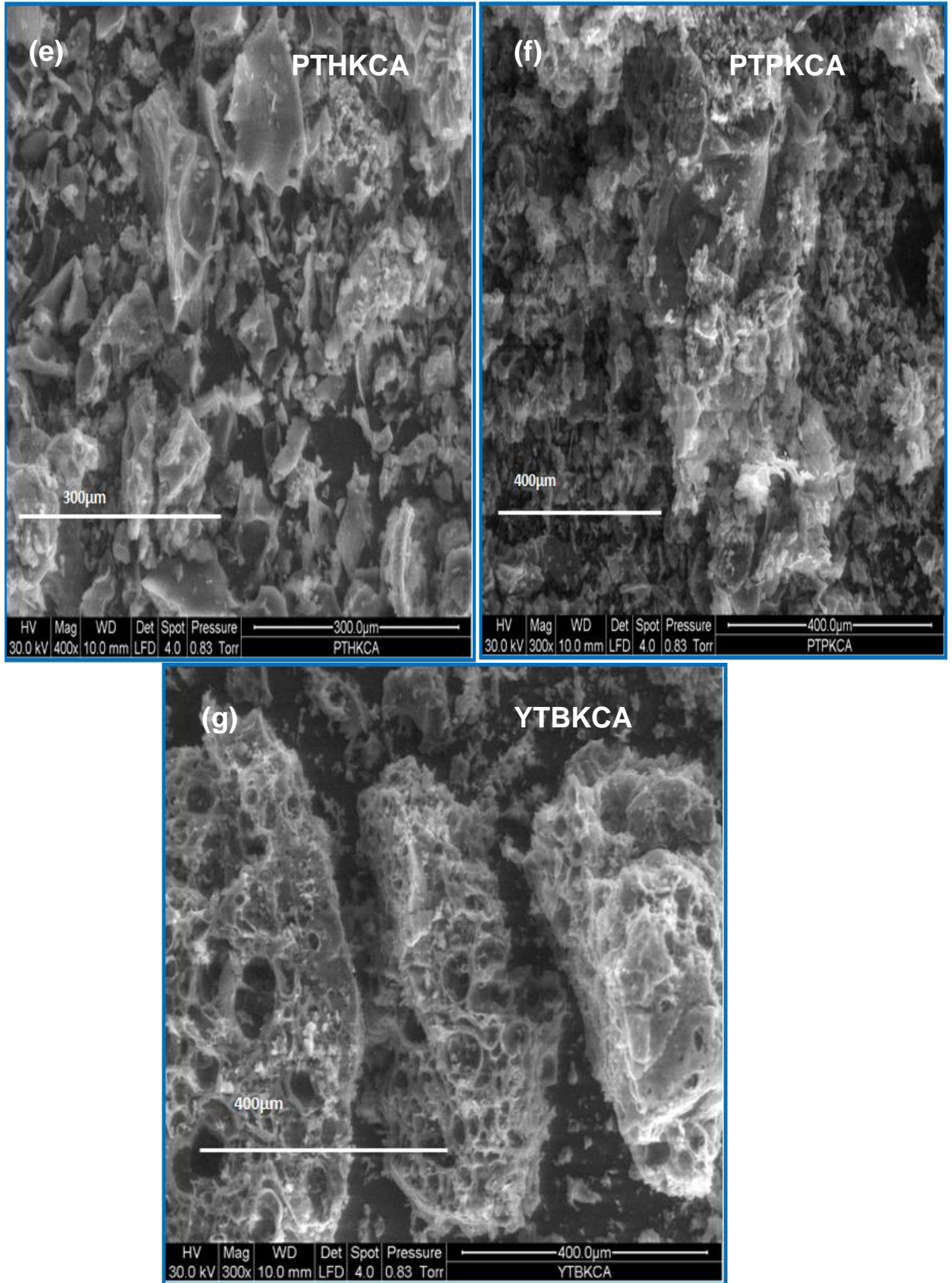
Figure 8.8: SEM micrograph for PTHKCA, PTPKCA & YTBKCA adsorbents

The chemically activated carbon adsorbents prepared in this chapter were subsequently used to study the equilibrium kinetics of the removal Cd(II) and Pb(II) ions from aqueous solutions. These metal ion loaded adsorbents were thereafter subjected to SEM analysis to examine their morphology after sorption. The SEM images of the chemically activated carbon adsorbents after the adsorption of Cd(II) and Pb(II) were also obtained (images not shown) . These images indicate that the adsorption process did not alter the morphology of the used adsorbents as their pore microstructures were still preserved. The unchanged pore microstructure in the used adsorbent suggests stability in the pore architectures which facilitates pore transport of adsorbates or metal ions across the different pore hierarchies in the complex activated carbon structures.

This however contrasts is in contrast with the observation of Hashemian *et al*., (2014) in their study on the preparation of activated carbon from two agricultural wastes (almond shell and orange peel) where the surface of the activated carbon adsorbents prepared before and after adsorption were observed to show significant differences in surface structure. Unlike the unaltered pore microstructure observed in the present study, a modification occurred in the pore structure of the almond shell and orange peel adsorbents of the reported study after sorption resulting in a rough surface with crater-like pores. This difference is presumed to be as result of the intrinsic nature of the lignocellulosic residues used for activated carbon preparation. It is not clear whether this alteration has or would have any impact on the adsorption potential of the adsorbent; however it could be said to contribute to the stability of the adsorbents if regenerated.

8.4.2 EDAX chemical composition of chemically activated adsorbents

The characterisation of the surface morphology of the adsorbent residue also necessitates the determination of the elemental composition of the adsorbent surface. This determination is carried out using the energy dispersive X-ray spectroscopy (EDAX) as previously described in Section 4.3.2 This gives the chemical composition of the material and was used to characterise the adsorbents before and after sorption as well as to confirm the presence of the heavy metal ion of interest. The EDAX analysis was carried out using a spot size of 3.5 and the elemental composition of the spot on the residue was taken as a spectrum using the EDAX genesis software which also gave the composition in percentages (wt %). The elemental composition and EDAX spectrum of the CCPNCA

adsorbents are shown in Figures 8.9 – 8.11. Figure 8.9 indicates that the CCPNCA adsorbent was composed of carbon, oxygen, sodium, silicon, sulphur, phosphorus, potassium and calcium with silicon, phosphorus and sulphur being the elements with most abundance on the adsorbent surface.
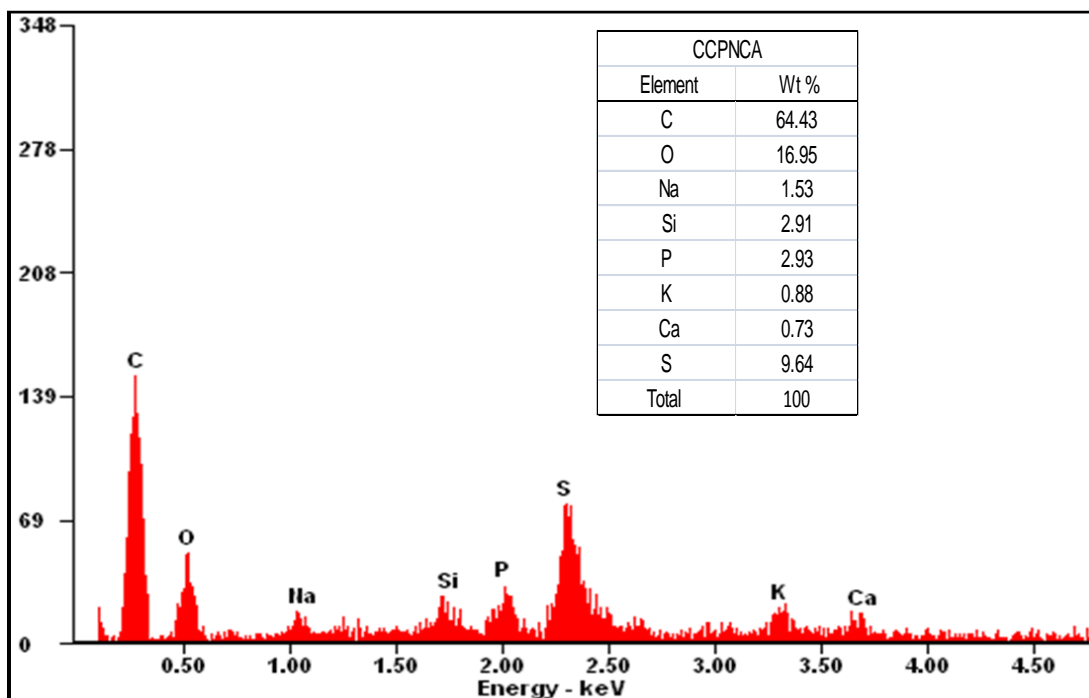
Figure 8.9: EDAX spectrum for CCPNCA

The spectrum of the CCPNCA adsorbent after Cd(II) ion sorption shown in Figure 8.10 also indicates that the adsorbent had lower number of elements within the matrix compared to the fresh adsorbent seen in Figure 8.9. This may be attributed to the removal of these elements from the adsorbent matrix during sorption via processes such as ion exchange or complexation in the adsorption media (Ding *et al.,* 2014).

The presence of Al ions are also detected in the spectrum of Figure 8.10 and this is presumed to be due to the nature of the EDAX spot analysis process; as a different spot was used for the analysis for Figure 8.9 and Figure 8.10 and this could lead to variability in surface composition.

CCPNCA Cd	
Element	Wt %
C	68.21
O	17.36
Na	0.89
Al	3.96
P	0.29
Cd	9.29
Total	100
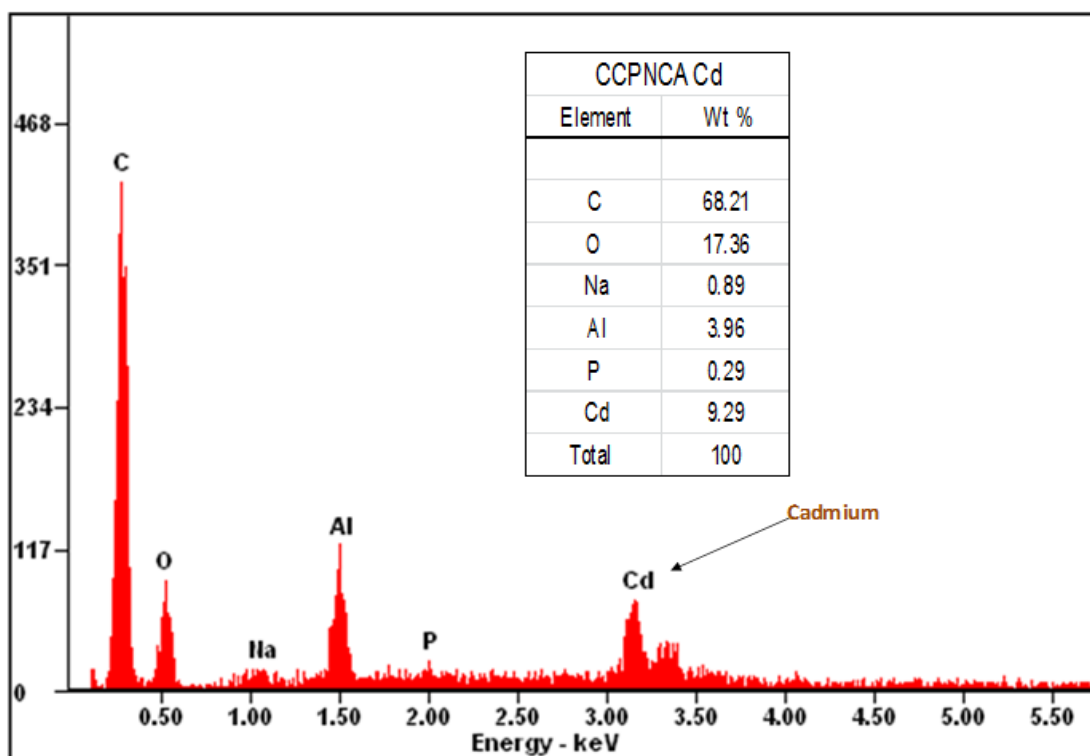
Figure 8.10: EDAX spectrum for CCPNCA after Cd(II) ion adsorption

CCPNCA-Pb	
Element	Wt %
C	64.43
O	16.95
Na	1.53
Si	0.91
P	1.03
Pb	9.54
K	0.85
Ca	0.73
Fe	4.03
Total	100
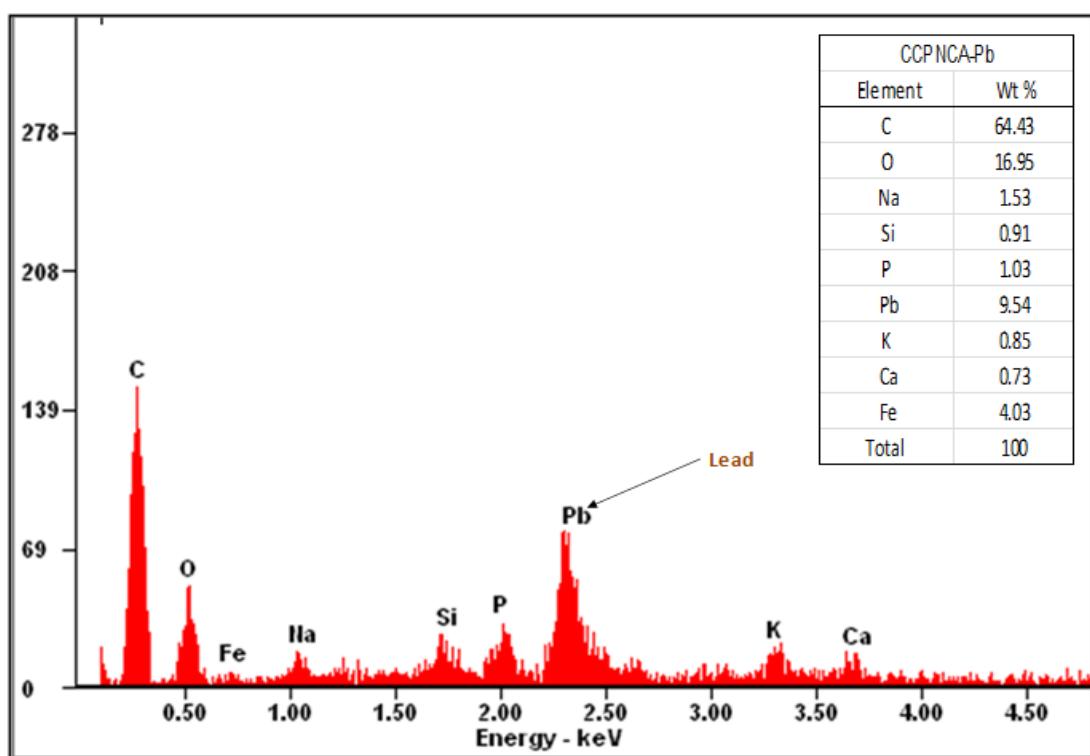
Figure 8.11: EDAX spectrum for CCPNCA after Pb(II) ion adsorption

These spectra also suggests the presence of new peaks associated with Cd(II) ion with a composition of 9.29%. The presence of Pb(II) ion in the adsorbent matrix with an approximate composition of 9.54% can also be confirmed from the EDAX spectrum of the CCPNCA adsorbent after Pb(II) adsorption (Figure 8.11). There was still a distribution of elements present in the fresh adsorbent of the CCPNCA adsorbent matrix after adsorption (Figures 8.9 – 8.11) with a fairly constant composition of carbon and oxygen and this trend was also observed in the other chemically activated adsorbents used for Pb(II) and Cd(II) adsorption. This suggests that these metal ions (Pb and Cd) had been adsorbed onto the surface of the CCPNCA adsorbent. This approach of using EDAX spectrum to confirm the presence of the adsorbed metal ions on the surface of an adsorbent after sorption has also been carried out by Tuna *et al.*, (2013) while investigating the removal of As(V) by activated carbon based hybrid adsorbents.

8.5 Kinetic sorption studies

Kinetics of metal ion sorption for Cd(II) and Pb(II) removal from aqueous solution using the chemically activated adsorbents modified with (K_2CO_3 and Na_2CO_3) were studied at pH 7.5, 25^oC with 500 mgL^{-1} initial metal ion concentration in 100 ml metal ion adsorbent system. Kinetic studies were carried out for the following time intervals – 5, 10, 15, 20, 25, 30, 40, 60, 90, 120 and 180 minutes at 200 rpm. The amount of metal ion adsorbed (q_t) at time t was calculated using eqn. (8.1).

$$qt = \frac{(C_i - C_t)V}{m} \tag{8.1}$$

Where C_t (mgL^{-1}) is the metal ion concentration at time t,

C_i is the initial metal ion concentration

m is the mass of the adsorbent

V is the volume of the aqueous system.

8.5.1 Cadmium (II) ion sorption

The duration of contact between an adsorbent and an adsorbate is a fundamental parameter in a mass transfer phenomenon such as sorption as it gives information regarding the transport properties in an adsorption system (Hashemian *et al.*, 2014). The effect of contact

time on the sorption of Cd(II) ions for the Na_2CO_3 and K_2CO_3 chemically activated carbon adsorbents are shown in Figures 8.12 and 8.13. Figure 8.12 indicates that for all the adsorbents (OPFNCA, CNFNCA, CCFNCA, CCPNCA, CCYBNCA, PTHNCA and YTBNCA), the adsorption of Cd(II) was at first rapid ($5 - 40$ minutes) and thereafter the metal ion removal rate gradually slowed down until the system reached a plateau at 180 minutes. However, for the PTPNCA adsorbent, the initial rapid stage lasted for 60 minutes. The maximum metal ion loading for the adsorbents after 180 minutes were 26.5 mgg^{-1} (OPFNCA), 27.7 mgg^{-1} (CNFNCA), 24.8 mgg^{-1} (CCPNCA), 22.6 mgg^{-1} (CCYBNCA), 24.2 mgg^{-1} (PTHNCA), 27.1 mgg^{-1} (PTPNCA) and 24.8 mgg^{-1} (YTBNCA). This indicates that surface area may be a crucial factor in the rate of uptake as the CNFNCA and OPFNCA adsorbents with the highest BET surface area had the highest metal ion loading.
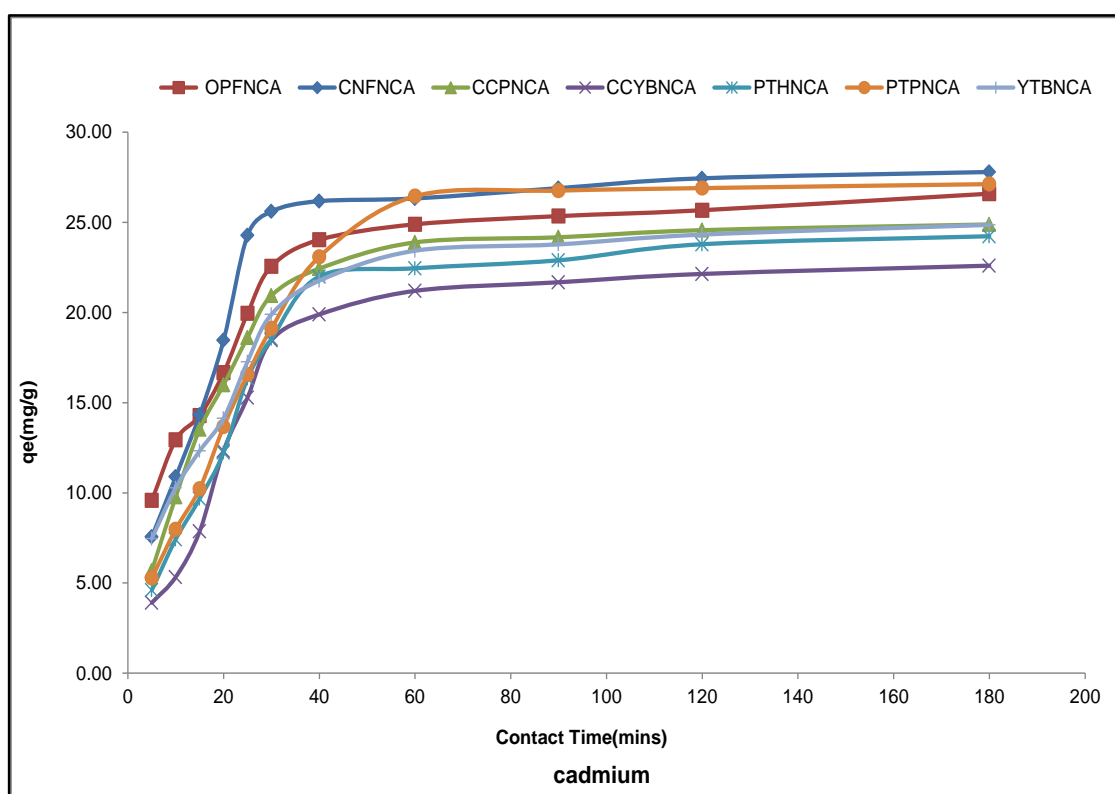
Figure 8.12: Kinetic profile for Cd(II) ion for Na_2CO_3 adsorbents
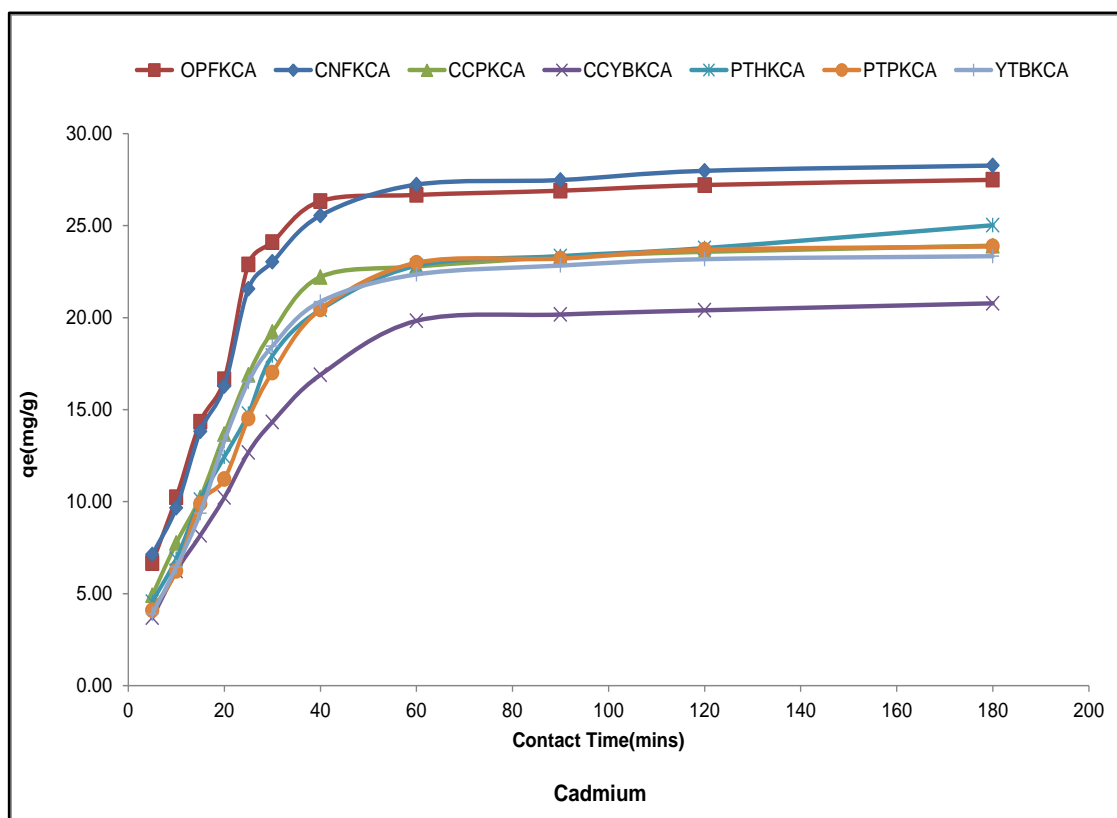
Figure 8.13: Kinetic profile for Cd(II) for K_2CO_3 adsorbents

For the K_2CO_3 chemically modified adsorbents shown in Figure 8.13, the maximum metal ion loading were 27.4 mgg^{-1} (OPFKCA), 28.2 mgg^{-1} (CNFKCA), 23.9 mgg^{-1} (CCPKCA), 20.7 mgg^{-1} (CCYBKCA), 25.0 mgg^{-1} (PTHKCA), 23.8 mgg^{-1} (PTPKCA) and 23.3 mgg^{-1} (YTBKCA). A similar trend of higher metal ion uptake was associated with increasing surface area with respect to the OPFKCA and CNFKCA adsorbents. The values of maximum loading of both metal ions carried out in this study was compared with similar studies reported in literature and this is presented in Table 8.7 for Cd(II) ion. A comparison of the results shows a corresponding trend in the values of Cd(II) removed at time (t) q_t from the adsorbents for both the literature and the present study. The table indicates that the adsorbents prepared in the present study had higher values of metal ion loading than most of those reported in literature.

It was also observed that the K_2CO_3 and Na_2CO_3 chemically activated adsorbents had similar loading capacities for Cd(II) with slight variations. The values also show that CNFKCA adsorbent has the highest loading for Cd(II) while CCYBKCA has the least. The trend of a rapid initial metal ion uptake followed by a gradual slow phase can be linked to the presence of abundant metal ion active sites on the adsorbents at the inception of

sorption. As sorption proceeds gradually, more of these sites become occupied. This results in a slower process because the metal ions in the aqueous phase find it difficult occupying the few remaining vacant sites in the adsorbent surface. The repulsive forces between the metal ions in the occupied sites on the adsorbent surface and those in the aqueous solution may also contribute to the less efficient sorption during the slower phase (Ibrahim *et al.*, 2010; Iqbal *et al.*, 2009a). This two-phase metal ion uptake phenomenon has also been reported by Zhang *et al.*, (2014) for the sorption of Cu(II) by H_3PO_4 treated rice husk where there was a sharp rise in Cu(II) sorption in the first 90 minutes of the process followed by a gradual sorption and reaching a plateau after 180 minutes.

A comparison of the amount of Cd(II) ion removed after180 minutes (q_t) for the Na_2CO_3 chemically activated adsorbents with those reported in literature is presented in Table 8.7. From the table it can be inferred that the chemically activated adsorbents had higher Cd(II) ion loading abilities than those compared from literature thereby implying that the chemical activated carbon adsorbents were effective for metal ion sorption.

Table 8.7: Comparison in adsorbent loading (qt) for Cd(II) ion with literature

Adsorbent	q_t (mgg^{-1})	Reference
Neem oil activated carbon	25.2	Hema and Srinivasan, 2010
Ceiba pentandra hull carbon	7.50	Rao *et al.,* 2006
Arundo donax cane carbon	17.0	Basso *et al.,* 2002
Commercial activated carbon	7.5	Hydari *et al.,* 2012
Nutshell activated carbon	15.9	Tajar *et al.,* 2012
OPFNCA	26.6	This study
CNFNCA	27.7	This study
CCPNCA	24.9	This study
CCYBNCA	22.6	This study
PTHNCA	24.2	This study
PTPNCA	27.1	This study
YTBNCA	24.9	This study

8.5.1.1 Kinetic modelling of cadmium (II) ion sorption

The sorption kinetics often shows a strong dependence on the physical and /or chemical characteristics of adsorbents and this also has been found to influence the mechanism of uptake. To determine the mechanisms which most influence the uptake of adsorbates onto the surface of an adsorbent, kinetic modelling is often used to establish the adsorption parameters (Kolodynska *et al.,* 2012). Based on this the sorption of Cd(II) and Pb(II) ions from the aqueous adsorbates onto the Na_2CO_3 and K_2CO_3 chemically activated adsorbents were modelling using the pseudo-first order (PFO) originally called Lagergren equation (Lagergren, 1898) and the pseudo-second order (PSO) equation adopted by Ho and McKay (1999) which have been previously discussed in this work. To determine the goodness of fit of the kinetic models to the experimental data using non-linear regression, the optimization procedure requires that error functions be defined to enable the fitting of the model parameters with the experimental values. In this study, the coefficient of determination (r^2), the root mean square error (RMSE) and the Chi square test (χ^2) were used as error parameters for each model and these were determined based on eqns. 5.4, 5.5 and 5.6 which have been previously described in section 5.11 of chapter 5 in this study.

Kinetic modelling of Cd(II) ion sorption onto the Na_2CO_3 and K_2CO_3 chemically activated adsorbents were carried out for the pseudo first order (PFO) and pseudo first order (PSO) equations using the solver add-in optimization procedure in Microsoft excel 2010 software. The plots of the PFO are PSO models for Cd(II) are presented in Figures 8.14 and 8.15 for Na_2CO_3 and Figures 8.16 and 8.17 K_2CO_3 chemically activated adsorbents. From these models, the kinetic parameters and their respective error functions obtained are presented in Table 8.8 and 8.9 for the Na_2CO_3 and K_2CO_3 chemically activated adsorbents respectively. These results presented in Figures 8.14-8.17 and Tables 8.8-8.9 confirms that the two models (PFO & PSO) could be used to characterise the kinetics of Cd(II) ion sorption and the prediction of each model for the kinetic parameter ($q_{e,model}$) is close to the result obtained from the experimental analysis of Cd(II) ion sorption.

For the PFO model the $q_{e,cal}$ obtained for the Na_2CO_3 chemically activated adsorbents for Cd(II) ion sorption were in the range $22.9mgg^{-1}$ (CCYBNCA) to 27.9 mgg^{-1}(CNFNCA/PTPNCA) with the order being CNFNCA =PTPNCA > OPFNCA > CCPNCA > YTBNCA > PTHNCA > CCYBNCA, thus implying that the CNFNCA and PTPNCA adsorbents were the highest with the least being the CCYBNCA. For the K_2CO_3 chemically activated adsorbents, the PFO model $q_{e,cal}$ obtained Cd(II) ion sorption were in

the range 21.1mgg^{-1} (CCYBKCA) to 28.4 mgg^{-1}(CNFNCA) with the order being CNFKCA > OPFKCA > PTHKCA > PTPKCA > CCPKCA > YTBKCA > CCYBKCA. From these two different types of chemically activated adsorbents, it can be observed that the CNFKCA had the highest value for q$_{e,cal}$ from the PFO model, while the CCYBKCA adsorbent had the least. The rate constant of the pseudo first order (PFO) reaction (K$_1$) for the Na$_2$CO$_3$ chemically activated adsorbents were in the range 3.70×10^{-2} min^{-1}(PTPNCA) to 6.21× 10^{-2} min^{-1}(OPFNCA), while that of the K$_2$CO$_3$ chemically activated adsorbents were in the range 3.65 ×10^{-2} min^{-1}(PTPKCA) to 5.47 × 10^{-2} min^{-1}(OPFKCA).

The value of the coefficient of determination (r^2) and the two error parameters – the root mean square (RMSE) and Chi square (χ^2) was used to determine the Cd(II) ion uptake kinetics is best described by the PFO model. From Table 8.8 and 8.9, it is observed that for the Na$_2$CO$_3$ chemically activated adsorbents, the YTBNCA, PTPNCA and CCPNCA had the same r^2 value of 0.99, while PTHNCA and OPFNCA adsorbents had r^2 value of 0.98. The lowest r^2 value was 0.97 and was this was for the CNFNCA and CCYBNCA adsorbents. These r^2 values indicates that the experimental data for the kinetics of Cd(II) ion sorption onto the YTBNCA, PTPNCA and CCPNCA adsorbents are in close agreement what that of the PFO model. To further discriminate amongst these three adsorbents, the χ^2 and the RMSE values were used with the lowest values being an indication of best fitting. Based on this assumption, the sorption of Cd(II) ion onto the CCPNCA adsorbent is best described by the PFO model with the lowest χ^2 (0.01) and RMSE (9.90 ×10^{-2}) values. For this adsorbent, the PFO rate constant (K$_1$) obtained was 5.41 ×10^{-2} min^{-1} and the PFO model Cd(II) ion loading (q$_{e,cal}$) was 24.8 mgg^{-1}.

For the K$_2$CO$_3$ chemically activated adsorbents, r^2 value of 0.99 was obtained for the CNFKCA, CCYBKCA, PTHKCA and PTPKCA adsorbents while the OPFKCA, CCPKCA and YTBKCA adsorbents had an r^2 value of 0.98. These r^2 values suggest that the sorption of Cd(II) ion onto these adsorbents were better represented by the PFO model for the CNFKCA, CCYBKCA, PTHKCA and PTPKCA adsorbents. Further evaluation of the values of the error parameters (χ^2 and the RMSE) for these 4 adsorbents were used to determine which one was best described by the PFO model. From Table 8.9, it is observed that the CCYBKCA adsorbent is best described by the PFO model with the lowest χ^2 (0.02) and RMSE (1.42×10^{-1}) values. For this adsorbent, the PFO rate constant (K$_1$) obtained was 3.66 ×10^{-2} min^{-1} and the Cd(II) ion loading (q$_{e,cal}$) for the PFO model was

21.1 mgg^{-1}. Comparing between the Na$_2$CO$_3$ and K$_2$CO$_3$ adsorbents for Cd(II) ion sorption, it is observed that the CCPNCA adsorbent was best described by the PFO model as it had the lowest values for the error parameters (χ^2 and the RMSE) and the highest r^2 value.

The PSO model was also used to evaluate the kinetics of Cd(II) ion sorption onto the Na$_2$CO$_3$ and K$_2$CO$_3$ chemically activated adsorbents and the results are also presented in Tables 8.8 and 8.9. The PSO rate constant (K$_2$) for the Na$_2$CO$_3$ chemically activated adsorbents were in the range 1.18 $\times 10^{-3}$ gmg^{-1}min^{-1}(PTPNCA) to 2.90 $\times 10^{-3}$ gmg^{-1}min^{-1}(OPFNCA), while that of the K$_2$CO$_3$ chemically activated adsorbents were in the range 1.30 $\times 10^{-3}$ gmg^{-1}min^{-1}(PTPKCA) to 2.09 $\times 10^{-3}$ gmg^{-1}min^{-1}(OPFKCA). This indicates a similar tend for the highest and lowest rate constant for the PSO model for both Na$_2$CO$_3$ and K$_2$CO$_3$ chemically activated adsorbents. The initial sorption rate (h) obtained from the PSO model as q$_t$/t$\rightarrow$0 which gives an indication of the intial kinetic rate of sorption for the Na$_2$CO$_3$ chemically activated adsorbents were in the order of OPFNCA > CNFNCA > CCPNCA > YTBNCA > PTHNCA = PTPNCA > CCYBNCA with the OPFNCA adsorbent having the highest value of 2.44mgg^{-1}min^{-1}. For the K$_2$CO$_3$ chemically activated adsorbents, the order for the initial sorption rate (h) was OPFKCA > CNFKCA > CCPKCA > YTBKCA > PTHKCA > PTPNCA > CCYBNCA with the OPFKCA having the highest value of 2.14mgg^{-1}min^{-1}. Comparing the initial adsorption rate for the K$_2$CO$_3$ and Na$_2$CO$_3$ adsorbents shows that the Na$_2$CO$_3$ adsorbents had higher values for the initial adsorption rate than the K$_2$CO$_3$ adsorbents.

The q$_{e,cal}$ obtained from the PSO model for Cd(II) ion sorption onto the Na$_2$CO$_3$ chemically activated adsorbents were in the range 27.5 mgg^{-1} (CCYBNCA) to 33.6 mgg^{-1}(PTPNCA) with the order being PTPNCA > CNFNCA > OPFNCA = PTHNCA > CCPNCA > YTBNCA > CCYBNCA, while that of the K$_2$CO$_3$ chemically activated carbon adsorbents were in the range 25.4 mgg^{-1} (CCYBKCA) to 33.0 mgg^{-1}(CNFKCA) with the order being CNFKCA > OPFNCA > PTHKCA > PTPKCA > CCPKCA > YTBKCA > CCYBKCA, implying that the PTPNCA adsorbent had the highest Cd(II) ion loading.

Table 8.8: PFO & PSO modelling parameters for Cd(II) sorption on Na_2CO_3 activated carbon adsorbents

	Pseudo First Order Model					Pseudo Second Order					
Adsorbent	$q_{e,cal}$(mgg^{-1})	K_1(min^{-1})	r^2	χ^2	RMSE	$q_{e,cal}$(mgg^{-1})	K_2(gmg^{-1}min^{-1})	h(mgg^{-1}min^{-1})	r^2	χ^2	RMSE
OPFNCA	25.8	6.21E-02	0.98	0.07	6.66E-02	29.0	2.90E-03	2.44	0.98	0.07	6.62E-01
CNFNCA	27.9	6.00E-02	0.97	0.10	1.07E+00	31.8	2.38E-03	2.40	0.94	0.22	2.35E+00
CCPNCA	24.8	5.41E-02	0.99	0.01	9.90E-02	28.6	2.32E-03	1.89	0.98	0.08	7.50E-01
CCYBNCA	22.9	4.03E-02	0.97	0.12	9.69E-01	27.5	1.55E-03	1.18	0.94	0.23	1.83E+00
PTHNCA	24.3	4.15E-02	0.98	0.07	6.13E-02	29.0	1.57E-03	1.32	0.96	0.16	1.35E+00
PTPNCA	27.9	3.70E-02	0.99	0.05	4.75E-02	33.6	1.18E-03	1.32	0.97	0.15	1.39E+00
YTBNCA	24.5	5.08E-02	0.99	0.04	3.72E-01	28.2	2.24E-03	1.77	0.98	0.06	5.75E-01

Table 8.9: PFO & PSO modelling parameters for Cd(II) sorption on K_2CO_3 activated carbon adsorbents

	Pseudo First Order Model					Pseudo Second Order					
Adsorbent	$q_{e,cal}(mgg^{-1})$	$K_1(min^{-1})$	r^2	χ^2	RMSE	$q_{e,cal}(mgg^{-1})$	$K_2(gmg^{-1}min^{-1})$	$h(mgg^{-1}min^{-1})$	r^2	χ^2	RMSE
OPFKCA	27.8	5.47E-02	0.98	0.08	8.27E-01	32.0	2.09E-03	2.14	0.95	0.20	2.10E+00
CNFKCA	28.4	4.92E-02	0.99	0.05	5.10E-01	33.0	1.77E-03	1.93	0.97	0.14	1.45E+00
CCPKCA	24.2	4.52E-02	0.98	0.06	4.93E-01	28.5	1.80E-03	1.46	0.96	0.15	1.33E+00
CCYBKCA	21.1	3.66E-02	0.99	0.02	1.43E-01	25.4	1.53E-03	0.99	0.98	0.08	5.62E-01
PTHKCA	24.8	3.79E-02	0.99	0.03	2.62E-01	29.8	1.36E-03	1.21	0.98	0.09	7.72E-01
PTPKCA	24.5	3.65E-02	0.99	0.05	4.25E-01	29.6	1.30E-03	1.14	0.97	0.14	1.16E+00
YTBKCA	23.8	4.22E-02	0.98	0.07	5.69E-01	28.3	1.63E-03	1.31	0.95	0.18	1.15E+00
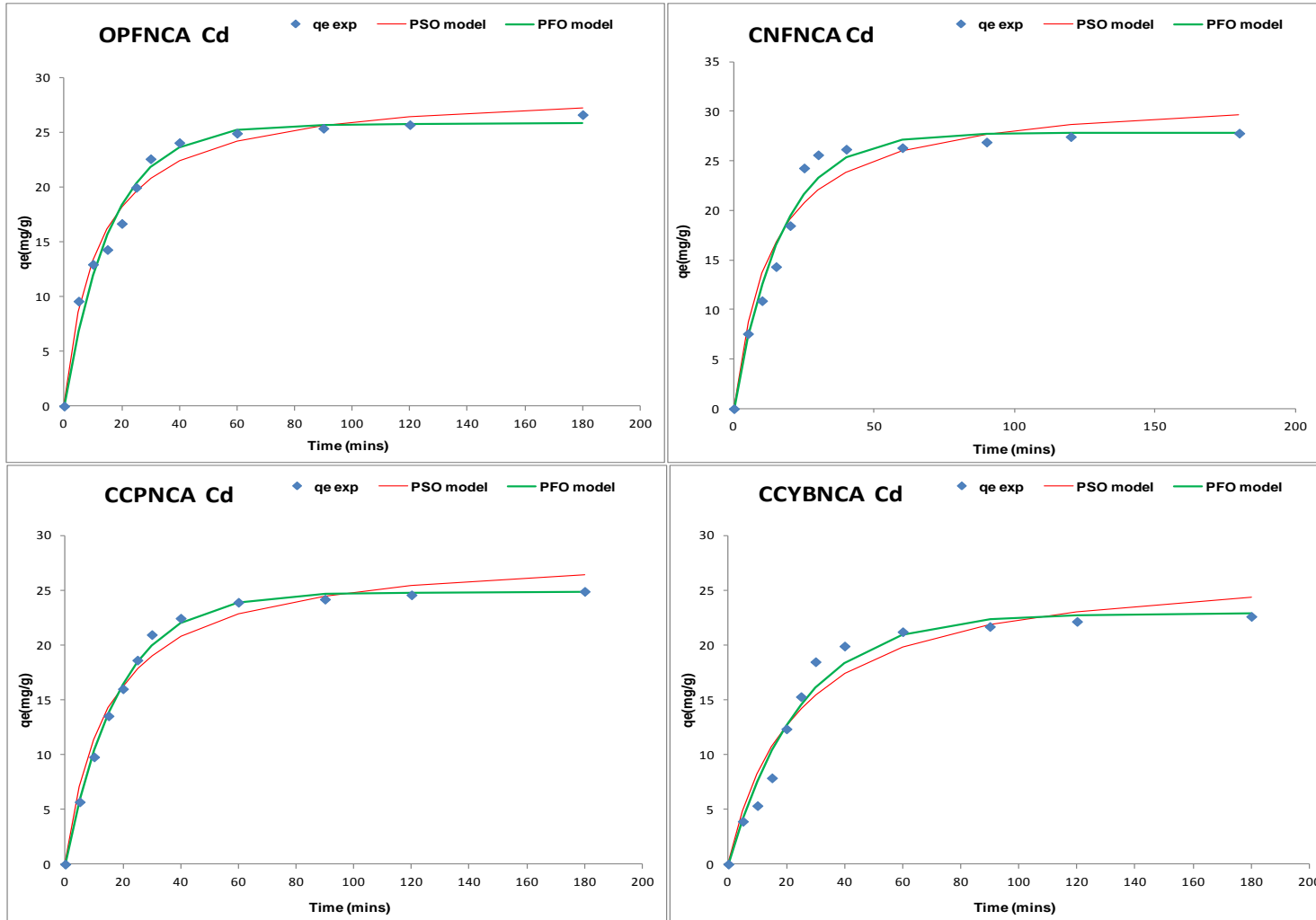
Fig 8.14: Cd(II) ion PFO & PSO sorption kinetic models for OPFNCA,CNFNCA, CCPNCA & CCYBNCA adsorbents
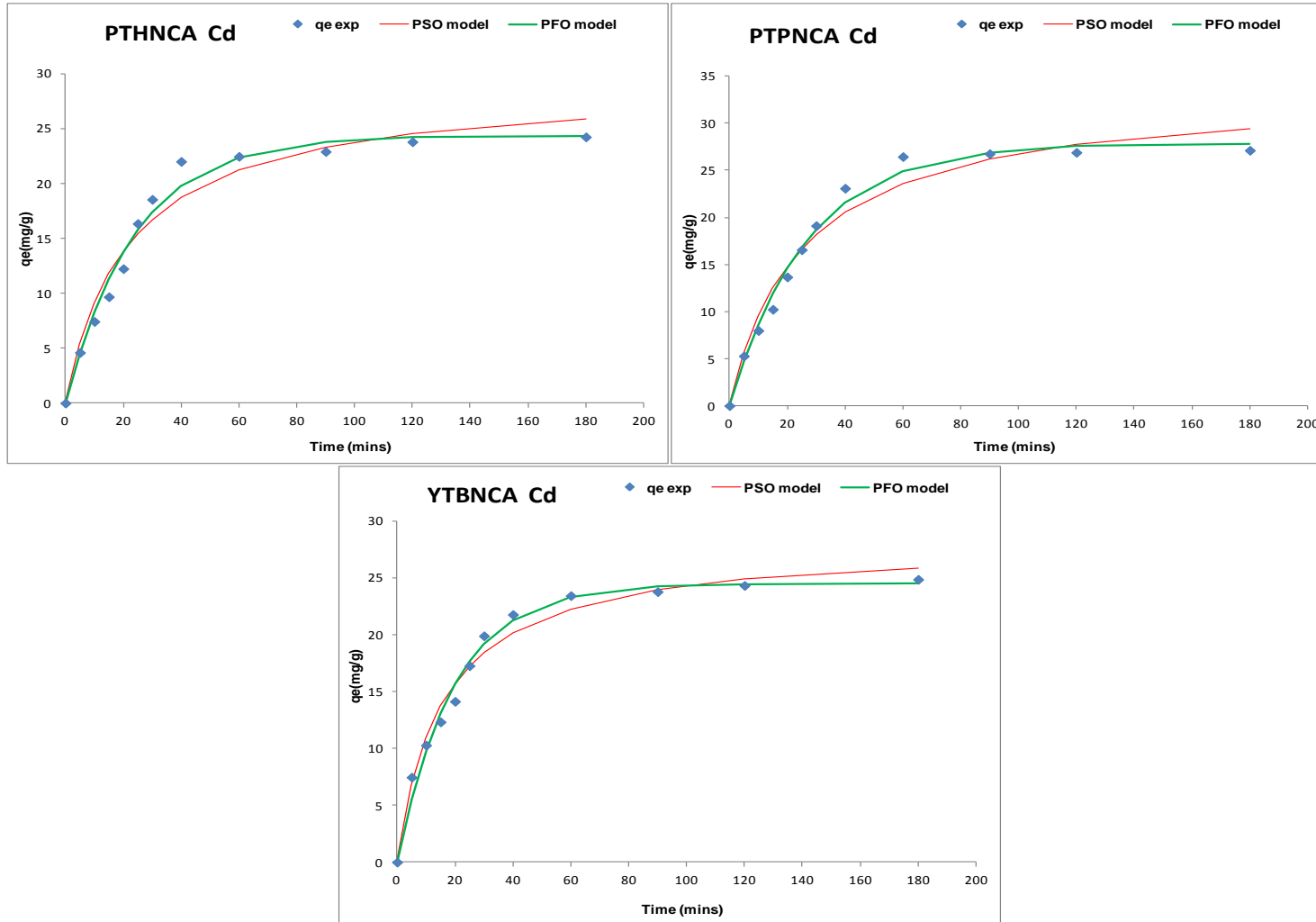
Fig 8.15: Cd(II) ion PFO & PSO sorption kinetic models for PTHNCA, PTPNCA & YTBNCA adsorbents
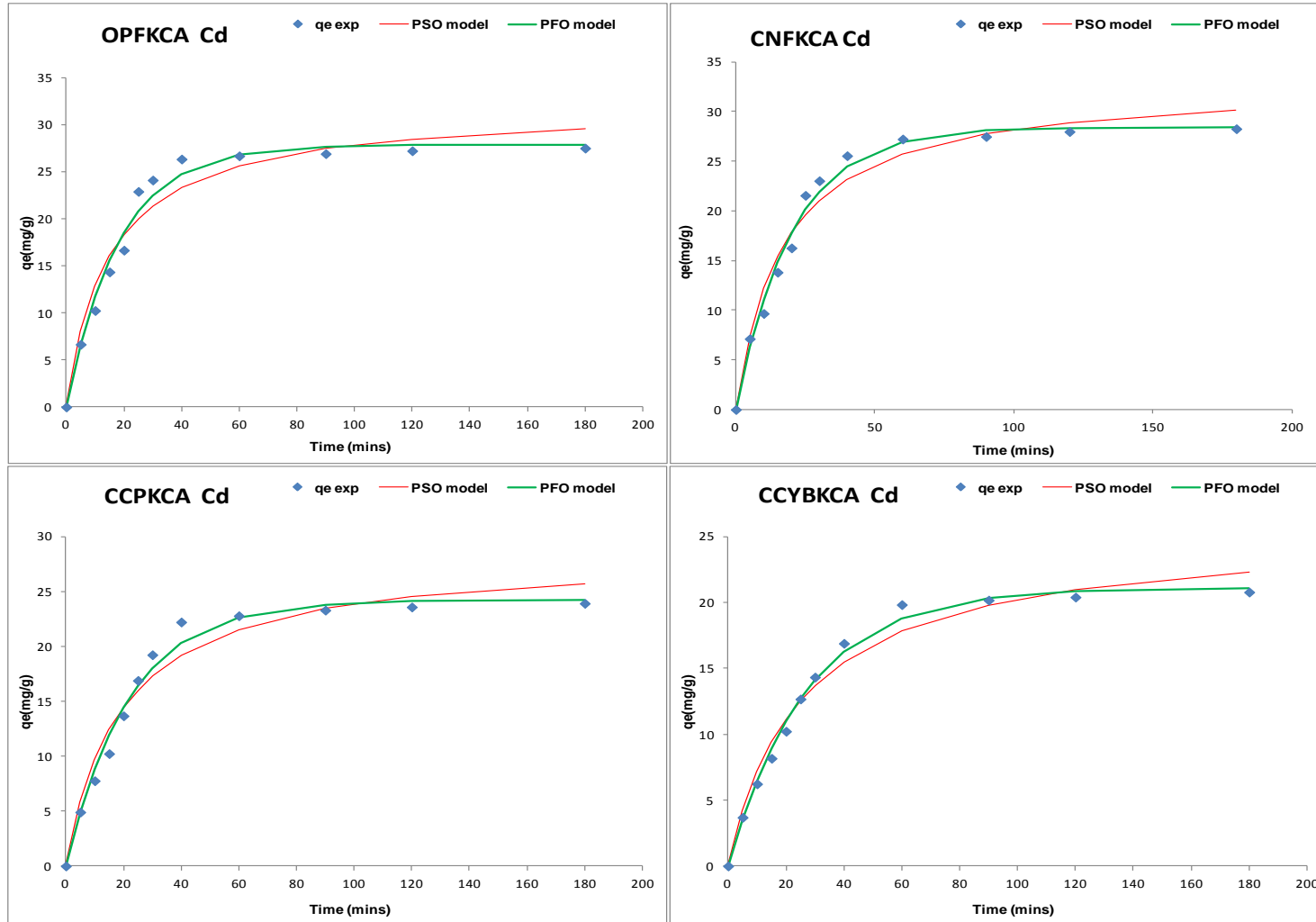
Fig 8.16: Cd(II) ion PFO & PSO sorption kinetic models for OPFKCA,CNFKCA, CCPKCA & CCYBKCA adsorbents
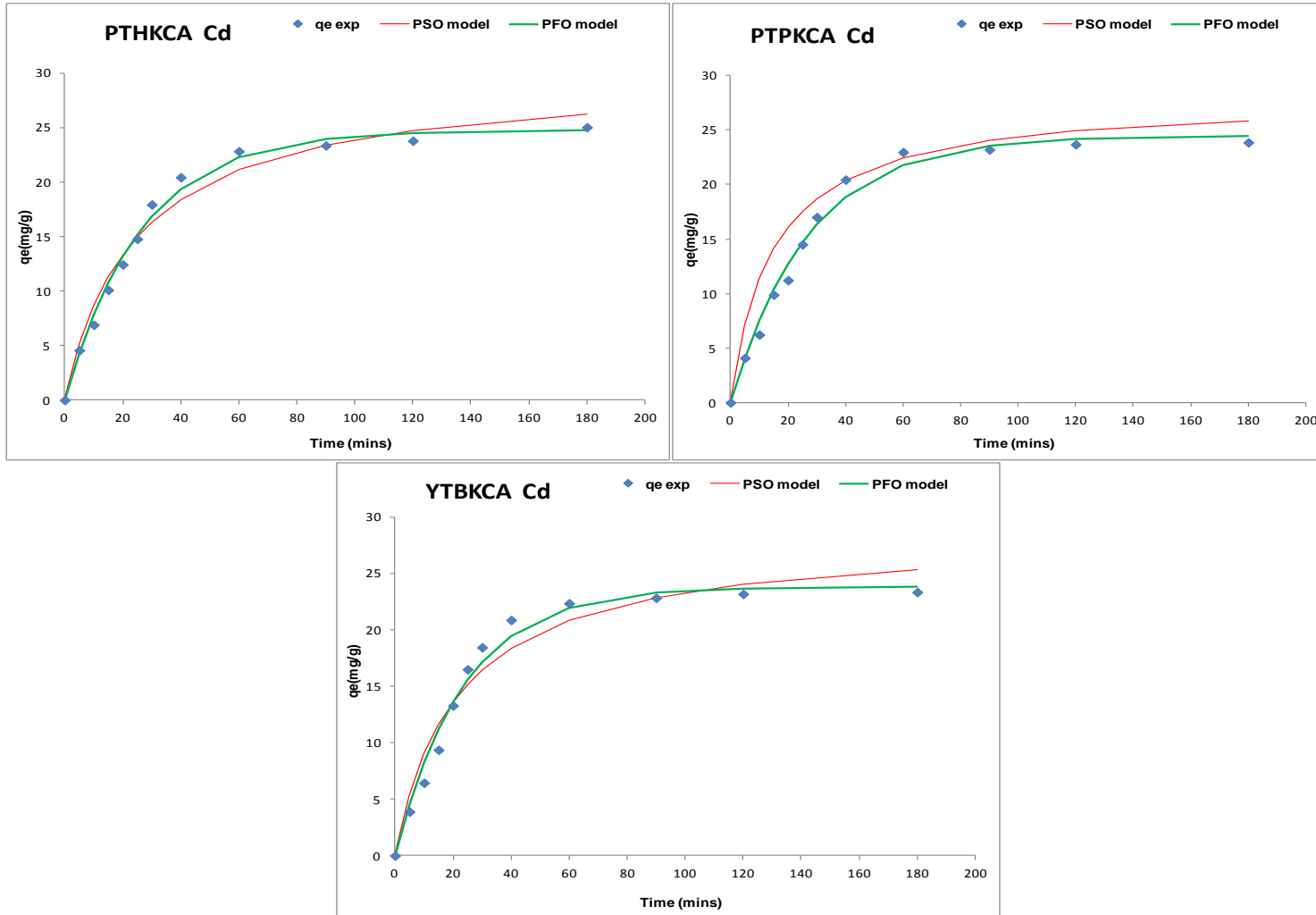
Fig 8.17: Cd(II) ion PFO & PSO sorption kinetic models for PTHKCA, PTPKCA & YTBKCA adsorbents.

The value of the coefficient of determination and the two error parameters – the root mean square (RMSE) and Chi square (χ^2) were used to determine the adsorbent whose kinetics of Cd(II) sorption is best described by the PSO model. The value of these error parameters in Table 8.8 and 8.9 shows that there four different r^2 values for the Na_2CO_3 and K_2CO_3 chemically activated adsorbents. For the Na_2CO_3 adsorbents, the first group which had highest value of 0.98 was for the OPFNCA, CCPNCA and YTBNCA adsorbents. The second and third were 0.97 and 0.96 for PTPNCA and PTHNCA adsorbents respectively, while the final group with the lowest value of 0.94 was for the CNFNCA and CCYBNCA adsorbents. For the K_2CO_3 adsorbents, the first group with the highest value of 0.98 was for the CCYBKCA and PTHKCA adsorbents. The second was 0.97 for the CNFKCA and PTPKCA adsorbents, while the third r^2 was 0.96 for the CCPPNCA adsorbent, while the final set with the lowest r^2 value of 0.95 was for the YTBKCA and OPFKCA adsorbents.

To further discriminate the adsorbent that is best described by the PSO model, consideration was given to the values of the two error parameters- the χ^2 and the RMSE. The adsorbent with the lowest values for these two parameters was thereafter chosen as the best described by the PSO model. For the Na_2CO_3 chemically activated adsorbents, the χ^2 and RMSE values were used to further compare the fitting of the PSO model to the Cd(II) ion experimental sorption data for the OPFNCA, CCPNCA and YTBNCA adsorbents. Based on the values for these two error parameters in Table 8.8, the YTBNCA adsorbent uptake of Cd(II) ion is best described by the PSO model with the lowest χ^2 (0.06) and RMSE (5.75 $\times 10^{-1}$) values. The PSO rate constant (K_2) obtained for this adsorbent was 2.24 $\times 10^{-3}$ $gmg^{-1}min^{-1}$ and the PSO model metal ion loading ($q_{e,cal}$) was 28.2 mgg^{-1}. For the K_2CO_3 chemically activated adsorbents the error parameter comparison was between the CCYBKCA and the PTHKCA adsorbents from which it was observed from the results in Table 8.9 that the CCYBKCA adsorbent uptake of Cd(II) ion is best described by the PSO model with the lowest χ^2 (0.08) and RMSE (5.62 $\times 10^{-1}$) values. The PSO rate constant (K_2) obtained for this adsorbent was 1.53 $\times 10^{-3}$ $gmg^{-1}min^{-1}$ and the PSO model metal ion loading ($q_{e,cal}$) was 25.4 mgg^{-1}. A comparison of the PSO values for r^2 and the two error parameters between the Na_2CO_3 and K_2CO_3 adsorbents for Cd(II) ion sorption, indicates that the YTBNCA adsorbent was best described by the PSO model as it had the lowest values for the error parameters (χ^2 and the RMSE) and the highest r^2 value.

Futhermore, to determine which of the two kinetic models (PFO or PSO) gives the best description of Cd(II) sorption kinetics onto the Na_2CO_3 and K_2CO_3 chemically activated adsorbents an examination of the $q_{e,cal}$ values obtained for the PFO and PSO models is used to compare with the experimental q_e value obtained at the end of sorption (after 180 mins) also called q_t. The assumption is that the model with $q_{e,cal}$ values that are closer to the experimental obtained q_e is the model that describes the Cd(II) ion sorption better. Table 8.10 presents the q_e for both experimental sorption and kinetic models for Cd(II) ion uptake by the Na_2CO_3 and K_2CO_3 chemically activated adsorbents.

Table 8.10: Comparison of q_e values for experiment and model sorption for Cd(II) onto chemically activated adsorbents

Adsorbent	q_e (mgg^{-1})		
	Experiment	PFO model	PSO model
OPFNCA	26.6	25.8	29.0
CNFNCA	27.7	27.9	31.8
CCPNCA	24.9	24.8	28.6
CCYBNCA	22.6	22.9	27.5
PTHNCA	24.2	24.3	29.0
PTPNCA	27.1	27.9	33.6
YTBNCA	24.9	24.5	28.2
OPFKCA	27.5	27.8	32.0
CNFKCA	28.3	28.4	33.0
CCPKCA	23.9	24.2	28.5
CCYBKCA	20.8	21.1	25.4
PTHKCA	25.0	24.8	29.8
PTPKCA	23.9	24.5	29.6
YTBKCA	23.3	23.8	28.3

From Table 8.10, it is observed that the values for qe_{model} for both PFO and PSO models were close to the experimental (q_e) for both Na_2CO_3 and K_2CO_3 chemically activated adsorbents. However, the PFO model for some of the adsorbents gave a closer q_e value to the experimental sorption q_e than the PSO. The PSO mainly gave values that were an overestimate of the experimental qe while that of the PFO was for some adsorbents an underestimation of the experimental q_e. Further evlauation of the values for error parameters (χ^2 and the RMSE) and correlation coefficient (r^2) in Table 8.8 and 8.8 for the two sets of adsorbents indicates that the PFO model had lower values for both error

parameters and higher r^2. Thus, it can be said that the PFO model gave a better approximation of the kinetics of Cd(II) sorption by the Na_2CO_3 and K_2CO_3 chemically activated adsorbents than the PSO order model. This implies that the kinetics supports the assumption that the rate limiting step of Cd(II) ion sorption onto the Na_2CO_3 and K_2CO_3 chemically activated adsorbents is dependent on the concentration of the Cd(II) ions in the adsorbate (Azizian, 2004; Liu and Liu, 2008). However, the closeness of the parameters obtained from the PSO model may also indicate that chemical interactions between the ions in the adsorbate solution and the adsorbent may still influence sorption kinetics but this may depend on the rate of diffusion. This implies that pore diffusivity of the ions onto the active sites may also influence the kinetics as previously discussed in the analysis of the two stage metal uptake (fast and slow) kinetics of Cd(II) ion sorption.

A number of studies have been reported on the application of the PFO and PSO models for the characterisation of the kinetics of Cd(II) ion sorption using chemically activated carbon adsorbents. Alslaibi *et al.,* (2013) has reported on use of microwave activation for the synthesis of potassium hydroxide (KOH) chemically activated Oilve stone adsorbent for Cd(II) ion removal from aqueous solution. In their study, kinetic modelling of Cd(II) ion sorption by the activated carbon adsorbent was carried out using the pseudo-first and second order models. The analysis of the fitting of the two models based on the r^2 value obtained for both PFO and PSO models indicated that the PSO model gave a better fitting for metal sorption with r^2 vlaue of 0.99 while the PFO had an r^2 vlaue of 0.94. Activated carbon derived from steam activated *Ceiba pentandra* hulls has also been used to remove Cd(II) ions from aqueous solutions by Rao *et al.,* (2006). In their study, the kinetics of removal of Cd(II) ions was evaluated using the PFO and PSO models the pseudo-second order model gave a better fitting for the sorption of Cd(II) ions onto the adsorbent than the PFO model.

8.5.2 Lead (II) ion sorption

The effect of contact time on the removal of Pb(II) ions from aqueous solution using both Na_2CO_3 and K_2CO_3 chemically activated carbon adsorbents were also carried out based on the conditions stated in section 8.5. From the kinetic studies shown in the profile plots of K_2CO_3 and Na_2CO_3 (Figures 8.18 and 8.19), it can be seen that Pb(II) ion loading on the different adsorbents were as follows: OPFNCA – 23.8 mgg^{-1}, CNFNCA – 25.3 mgg^{-1}, CCPNCA – 24.3 mgg^{-1}, CCYBNCA – 16.3 mgg^{-1}, PTHNCA – 20.2 mgg^{-1}, PTPNCA -

22.2 mgg^{-1} and YTBNCA – 19.5 mgg^{-1} for the Na$_2$CO$_3$ adsorbents. For the K$_2$CO$_3$ adsorbents, the loading of Pb(II) ions were as follows: OPFKCA – 22.2 mgg^{-1}, CNFKCA – 25.2 mgg^{-1}, CCPKCA – 24.1 mgg^{-1}, CCYBKCA – 18.2 mgg^{-1}, PTHKCA – 20.9 mgg^{-1}, PTPKCA – 23.4 mgg^{-1} and YTBKCA – 23.7 mgg^{-1}. A similar observation made with respect to the influence of the surface area of the chemically activated adsorbents for Cd(II) ion sorption can also be used to explain the trend in loading wherein it was observed that the BET surface area may be a crucial factor in the rate of uptake as the CNFNCA and CNFKCA adsorbents with the highest BET surface area for the Na$_2$CO$_3$ and K$_2$CO$_3$ adsorbents respectively had the highest metal ion loading for Pb(II) ion.

However, this trend was not applicable for all the adsorbents, for the Na$_2$CO$_3$ chemically activated adsorbents the trend in increasing BET surface area is; CNFNCA > OPFNCA > YTBNCA > CCYBNCA > CCPNCA > PTPNCA > PTHNCA, while that of the metal ion loading is CNFNCA > CCPNCA > OPFNCA > PTPNCA > PTHNCA > YTBNCA > CCYBNCA. For the K$_2$CO$_3$ chemically activated adsorbents the trend in increasing BET surface area is; CNFNCA > PTPNCA > CCPNCA > CCYBNCA > YTBNCA > PTHNCA > OPFNCA, while that of the metal ion loading is CNFNCA > OPFNCA > PTHNCA > CCPNCA > PTPKCA > YTBNCA≥ CCYBNCA. The results obtained for the sorption loading of Pb(II) and Cd(II) ions onto these two sets of chemically activated adsorbents indicates that the BET surfaces area is not the only parameter that determines the kinetics of metal ions uptake. The pore volume of these adsorbents may also influence the loading of the metal ions even though the effect of variation in these pore volume may not be as significant in the liquid systems as those observed for gaseous adsorbates. This effect of pore volume of chemically activated carbon adsorbents on metal sorption has also been observed by Gaya *et al.,* (2015) in their study on the sorption Cd(II)and Pb(II) ions onto chemically activated doum palm shell. In their study, it was observed that the pore volume of NaOH- activated doum palm shell (NaOH-AC) was a factor in the high loading of the metal ions onto the adsorbent.

An examination of the kinetic plot for these adsorbents indicates that the removal of Pb(II) ions from the aqueous solution occurred in two steps. This process also followed the trend observed in the Cd(II) sorption process with the first phase involving a rapid metal ion uptake by the adsorbents which occurred during the first 60 minutes of adsorbent-adsorbate contact.
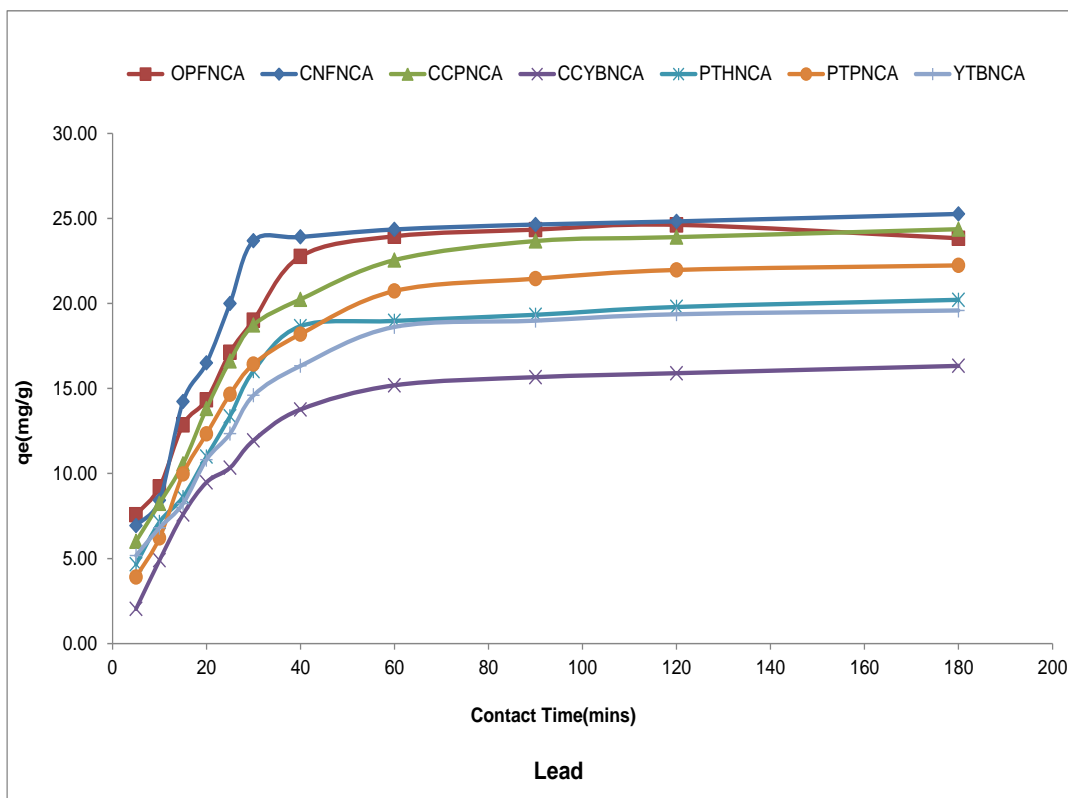
Figure 8.18: Kinetic profile for Pb(II) for Na_2CO_3 chemically activated carbon adsorbents
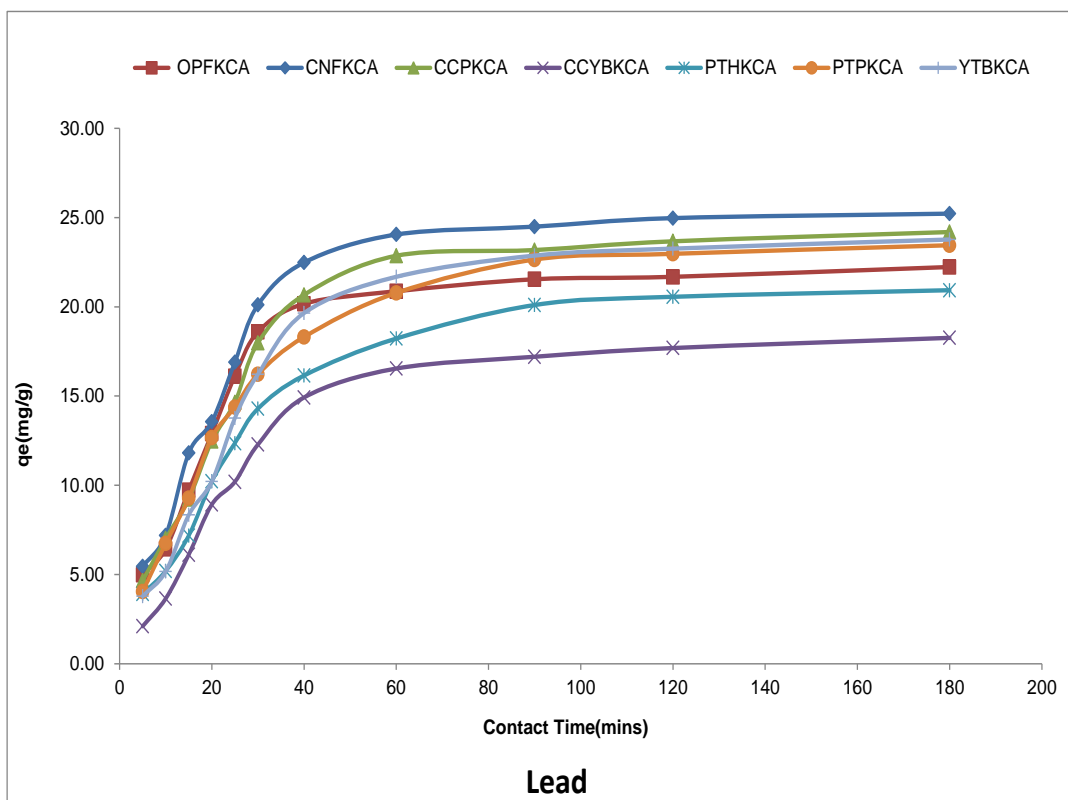
Figure 8.19: Kinetic profile for Pb(II) for K_2CO_3 chemically activated carbon adsorbents

This phase was subsequently followed by a slow phase which involved the gradual uptake of Pb(II) ion that covered a longer period of time (60 – 180 minutes) with a plateau on the kinetic profile indicating the possible attainment of equilibrium at 180 minutes. The observed trend in kinetic profile can also be linked to the vacancy site availability during metal ion loading. At the inception of metal ion loading, the adsorbents have a large number of available sites for metal ion sorption with a rapid uptake of metal ions on these sites. However, as these sites become slowly filled, the number of available sites diminish with time and the accessibility to them also reduce due to the repulsive effect the metal ions on the adsorbent have on the Pb(II) ions in the aqueous solution. This results in a slow but gradual uptake until the sites are completely filled and the system reaches equilibrium. This phenomenon has been reported by Ibrahim *et al*., (2010) on the removal of Pb(II) ions from aqueous solution by a novel agricultural waste adsorbent where the uptake occurred for 60 minutes. The values of the metal ion loading for Pb(II) ion obtained using the chemically activated adsorbents were also compared with the values for Pb(II) in reported literature (Table 8.11). As was the case of the sorption of Cd(II) ions, the result shows a similar trend in the higher loading for the adsorbents prepared in this study than those reported in literature.

Table 8.11: Comparison of adsorbent loading (q_t) for Pb(II) ion with Literature

Adsorbent	q_t (mgg^{-1})	Reference
Coffee residue carbon	10.0	Boudrahem *et al*., 2009
Commercial activated carbon	10.9	Yang *et al.,* 2014
Date palm activated carbon	14.3	El-Shafey and Al-Hashmi, 2013
Phaseolus aureus hull activated carbon	8.4	Rao *et al.,*2009
OPFNCA	23.8	This study
CNFNCA	25.3	This study
CCPNCA	24.4	This study
CCYBNCA	16.3	This study
PTHNCA	20.2	This study
PTPNCA	22.2	This study
YTBNCA	19.6	This study

8.5.2.1 Kinetic modelling for lead (II) ion sorption

To further investigate the kinetics of Pb(II) ion sorption by the Na_2CO_3 and K_2CO_3 chemically activated carbon adsorbents, the Lagergren's pseudo first-order (PFO) and Ho's pseudo second-order (PSO) models were used. The experimental kinetic data for Pb(II) ion sorption for these adsorbents were modelled using the solver add-in optimization procedure in Microsoft excel 2010 software. From this process the plots of the PFO are PSO models obtained for Pb(II) sorption are presented in Figures 8.20 and 8.21 for Na_2CO_3 and Figures 8.22 and 8.23 for the K_2CO_3 chemically activated adsorbents. The kinetic parameters and their respective error functions obtained from the modelling are presented in Table 8.12 and 8.13 for the Na_2CO_3 and K_2CO_3 chemically activated adsorbents respectively. These results presented in Figures 8.20-8.23 and Tables 8.12-8.13 confirms that the two models (PFO & PSO) can be used with a high degree of precision to characterise the kinetics of Pb(II) ion sorption and the prediction of each model for the kinetic parameter ($q_{e,model}$) is close to the result obtained from the experimental analysis of Pb(II) ion sorption.

For the PFO model, the $q_{e,cal}$ obtained for the Na_2CO_3 chemically activated adsorbents for Pb(II) ion sorption were in the range $16.3mgg^{-1}$ (CCYBNCA) to $25.5\ mgg^{-1}$(CNFNCA) with the order being CNFNCA > OPFNCA > CCPNCA > PTPNCA > PTHNCA > YTBNCA > CCYBNCA, thus implying that the CNFNCA adsorbent had the highest loading with the least being the value for the CCYBNCA adsorbent. For the K_2CO_3 chemically activated adsorbents, the PFO model $q_{e,cal}$ obtained Pb(II) ion sorption were in the range $18.5mgg^{-1}$ (CCYBKCA) to $25.5\ mgg^{-1}$(CNFNCA) with the order being CNFKCA > CCPKCA > OPFKCA > YTBKCA > PTPKCA > PTHKCA > CCYBKCA. From these two chemically activated adsorbents, it can be observed that the CNFKCA and CNFNCA adsorbents had the highest value for $q_{e,cal}$ from the PFO model, while the CCYBNCA adsorbent had the least. The rate constant of the pseudo first order (PFO) reaction (K_1) for the sorption of Pb(II) onto the Na_2CO_3 chemically activated adsorbents were in the range $4.07\times10^{-2}\ min^{-1}$(PTPNCA) to $5.74\times10^{-2}\ min^{-1}$(CNFNCA), while that of the K_2CO_3 chemically activated adsorbents were in the range $3.29\times10^{-2}\ min^{-1}$(YTBKCA) to $4.64\times10^{-2}\ min^{-1}$(OPFKCA).

The non-linear kinetic modelling of Pb(II) ions by the Na_2CO_3 and K_2CO_3 chemically activated adsorbents were characterised using the r^2 value and two error parameters the root mean square (RMSE) and Chi square (χ^2) to determine the adsorbent uptake kinetics is best described by the PFO model. From Table 8.12 and 8.13, it is observed that for the Na_2CO_3 chemically activated adsorbents 5 adsorbents- OPFNCA, CCPNCA, YTBNCA, PTPNCA and CCYBNCA had the same r^2 value of 0.99, while PTHNCA and CNFNCA adsorbents had r^2 value of 0.98. These r^2 values indicates that the experimental data for the kinetics of Pb(II) ion sorption onto the OPFNCA, CCPNCA, YTBNCA, PTPNCA and CCYBNCA adsorbents are in close agreement what that of the PFO model. To further discriminate amongst these five adsorbents, the χ^2 and the RMSE values were used with the lowest values being an indication of best fitting. Based on this assumption, the sorption of Pb(II) ion onto the CCYBNCA adsorbent is best described by the PFO model with the lowest χ^2 (0.02) and RMSE (1.00×10^{-2}) values. For this adsorbent, the PFO rate constant (K_1) obtained was 4.14×10^{-2} min^{-1} and the PFO model Cd(II) ion loading ($q_{e,cal}$) was 16.3 mgg^{-1}.

For the K_2CO_3 chemically activated adsorbents, r^2 value of 0.99 was obtained for four adsorbents- CCPKCA, CNFKCA, PTPKCA and PTHKCA adsorbents while the OPFKCA, CCYBKCA and YTBKCA adsorbents all had r^2 values of 0.98. These r^2 values suggest that the sorption of Pb(II) ion onto these adsorbents were better represented by the PFO model for the CCPKCA, CNFKCA, PTPKCA and PTHKCA adsorbents. Further evaluation of the values of the error parameters (χ^2 and the RMSE) for these 4 adsorbents were used to determine which one was best described by the PFO model. From Table 8.13, it is observed that the PTPKCA adsorbent is best described by the PFO model with the lowest χ^2 (0.01) and RMSE (5.97×10^{-2}) values. For this adsorbent, the PFO rate constant (K_1) obtained was 3.72×10^{-2} min^{-1} and the Pb(II) ion loading ($q_{e,cal}$) for the PFO model was 23.4 mgg^{-1}. Comparing between the Na_2CO_3 and K_2CO_3 adsorbents for Pb(II) ion sorption, it is observed that the CCYBNCA adsorbent was best described by the PFO model as it had the lowest values for the error parameters (χ^2 and the RMSE) and the highest r^2 value.

Pseudo-second order (PSO) kinetic modeling of the kinetics of Pb(II) ion sorption onto the Na_2CO_3 and K_2CO_3 chemically activated adsorbents was also carried out in this study and the results are also presented in Tables 8.12 and 8.13. From Tables 8.12 and 8.13, it observed that the PSO rate constant (K_2) for the Na_2CO_3 chemically activated adsorbents

were in the range 1.68×10^{-3} gmg^{-1}min^{-1}(PTPNCA) to 2.44×10^{-3} gmg^{-1}min^{-1}(CNFNCA), while that of the K$_2$CO$_3$ chemically activated adsorbents were in the range 1.36×10^{-3} gmg^{-1}min^{-1}(PTHKCA) to 1.10×10^{-3} gmg^{-1}min^{-1}(YTBKCA). The initial sorption rate (h) of Pb(II) ions onto the chemically activated adsorbents obtained from the PSO model as $q_t/t \to 0$ was also determined. This parameter gives an indication of the rate of sorption and for the Na$_2$CO$_3$ chemically activated adsorbents the values were in the order of CNFNCA >OPFNCA > CCPNCA > PTHNCA > PTPNCA > YTBNCA > CCYBNCA with the CNFNCA adsorbent having the highest value of 2.08mgg^{-1}min^{-1}. For the K$_2$CO$_3$ chemically activated adsorbents, the order for the initial sorption rate (h) was CNFKCA > OPFKCA > CCPKCA > PTPKCA > YTBKCA > PTHNCA > CCYBNCA with the CNFKCA having the highest value of 1.47mgg^{-1}min^{-1}. Comparing the values of the initial sorption rate for the K$_2$CO$_3$ and Na$_2$CO$_3$ adsorbents shows that the Na$_2$CO$_3$ adsorbents had higher values for the initial sorption rate of Pb(II) ions than the K$_2$CO$_3$ adsorbents and this was also observed for the PSO modelling of Cd(II) ion sorption.

The sorption parameter $q_{e,cal}$ obtained from the PSO model for Pb(II) ion sorption onto the Na$_2$CO$_3$ chemically activated adsorbents were in the range 19.4 mgg^{-1} (CCYBNCA) to 29. mgg^{-1}(CNFNCA) with the order being CNFNCA > CCPNCA > OPFNCA > PTPNCA > PTHNCA > YTBNCA > CCYBNCA, while that of the K$_2$CO$_3$ chemically activated carbon adsorbents were in the range 22.9 mgg^{-1} (CCYBKCA) to 30.1 mgg^{-1}(CNFKCA) with the order being CNFKCA > YTBKCA > CCPKCA > PTPKCA > OPFKCA > PTHKCA > CCYBKCA, implying that the CNFKCA adsorbent had the highest Pb(II) ion loading. The value of the coefficient of determination and the two error parameters – the root mean square (RMSE) and Chi square (χ^2) were used to determine the adsorbent's kinetics of Pb(II) sorption that is best described by the PSO model. The value of these error parameters in Table 8.12 and 8.13 shows that there variations in the r^2 values for Pb(II) ion sorption onto the Na$_2$CO$_3$ and K$_2$CO$_3$ chemically activated adsorbents. For the Na$_2$CO$_3$ adsorbents, the first set which had highest value of 0.98 was made up of YTBNCA, PTPNCA and CCPNCA. The second set with a value of 0.97 was composed of the CCYBNCA and OPFNCA adsorbents, while the third and fourth r^2 values were 0.96 and 0.94 was for the PTHNCA and CCFNCA adsorbents respectively.

Table 8.12: PFO & PSO modelling parameters for Pb(II) sorption on Na_2CO_3 activated carbon adsorbents

| | Pseudo First Order Model | | | | | Pseudo Second Order | | | | | |
Adsorbent	$q_{e,cal}$(mgg^{-1})	K_1(min^{-1})	r^2	χ^2	RMSE	$q_{e,cal}$(mgg^{-1})	K_2(gmg^{-1}min^{-1})	h(mgg^{-1}min^{-1})	r^2	χ^2	RMSE
OPFNCA	24.6	5.02E-02	0.99	0.05	4.34E-01	28.3	2.21E-03	1.76	0.97	0.10	9.27E-01
CNFNCA	25.5	5.74E-02	0.98	0.09	8.47E-01	29.1	2.44E-03	2.08	0.94	0.20	1.95E+00
CCPNCA	24.3	4.42E-02	0.99	0.02	1.96E-01	28.5	1.78E-03	1.45	0.98	0.07	5.79E-01
CCYBNCA	16.3	4.14E-02	0.99	0.02	1.00E-01	19.4	2.33E-03	0.88	0.97	0.07	3.72E-01
PTHNCA	20.3	4.48E-02	0.98	0.05	3.58E-01	23.8	2.16E-03	1.22	0.96	0.11	8.09E-01
PTPNCA	22.3	4.07E-02	0.99	0.02	1.18E-01	26.6	1.68E-03	1.19	0.98	0.07	5.75E-01
YTBNCA	19.7	4.20E-02	0.99	0.03	1.87E-01	23.1	2.08E-02	1.11	0.98	0.06	4.15E-01

Table 8.13: PFO & PSO modelling parameters for Pb(II) on K_2CO_3 activated carbon adsorbents

| Adsorbent | Pseudo First Order Model | | | | | Pseudo Second Order | | | | | |
	$q_{e,cal}(mgg^{-1})$	$K_1(min^{-1})$	r^2	χ^2	RMSE	$q_{e,cal}(mgg^{-1})$	$K_2(gmg^{-1}min^{-1})$	$h(mgg^{-1}min^{-1})$	r^2	χ^2	RMSE
OPFKCA	22.3	4.64E-02	0.98	0.07	5.59E-01	26.2	2.02E-03	1.39	0.95	0.16	1.29E+00
CNFKCA	25.5	4.34E-02	0.99	0.05	4.69E-01	30.1	1.62E-03	1.47	0.96	0.14	1.28E+00
CCPKCA	24.4	3.85E-02	0.99	0.05	3.92E-01	29.3	1.41E-03	1.21	0.97	0.13	1.06E+00
CCYBKCA	18.5	3.28E-02	0.98	0.06	3.26E-01	22.9	1.42E-03	0.74	0.96	0.12	7.20E-01
PTHKCA	21.1	3.39E-02	0.99	0.03	1.70E-01	25.7	1.36E-03	0.90	0.98	0.07	4.73E-01
PTPKCA	23.4	3.72E-02	0.99	0.01	5.97E-02	28.2	1.42E-03	1.13	0.99	0.05	3.87E-01
YTBKCA	24.3	3.29E-02	0.98	0.07	5.38E-01	29.9	1.10E-02	0.99	0.96	0.16	1.21E+00
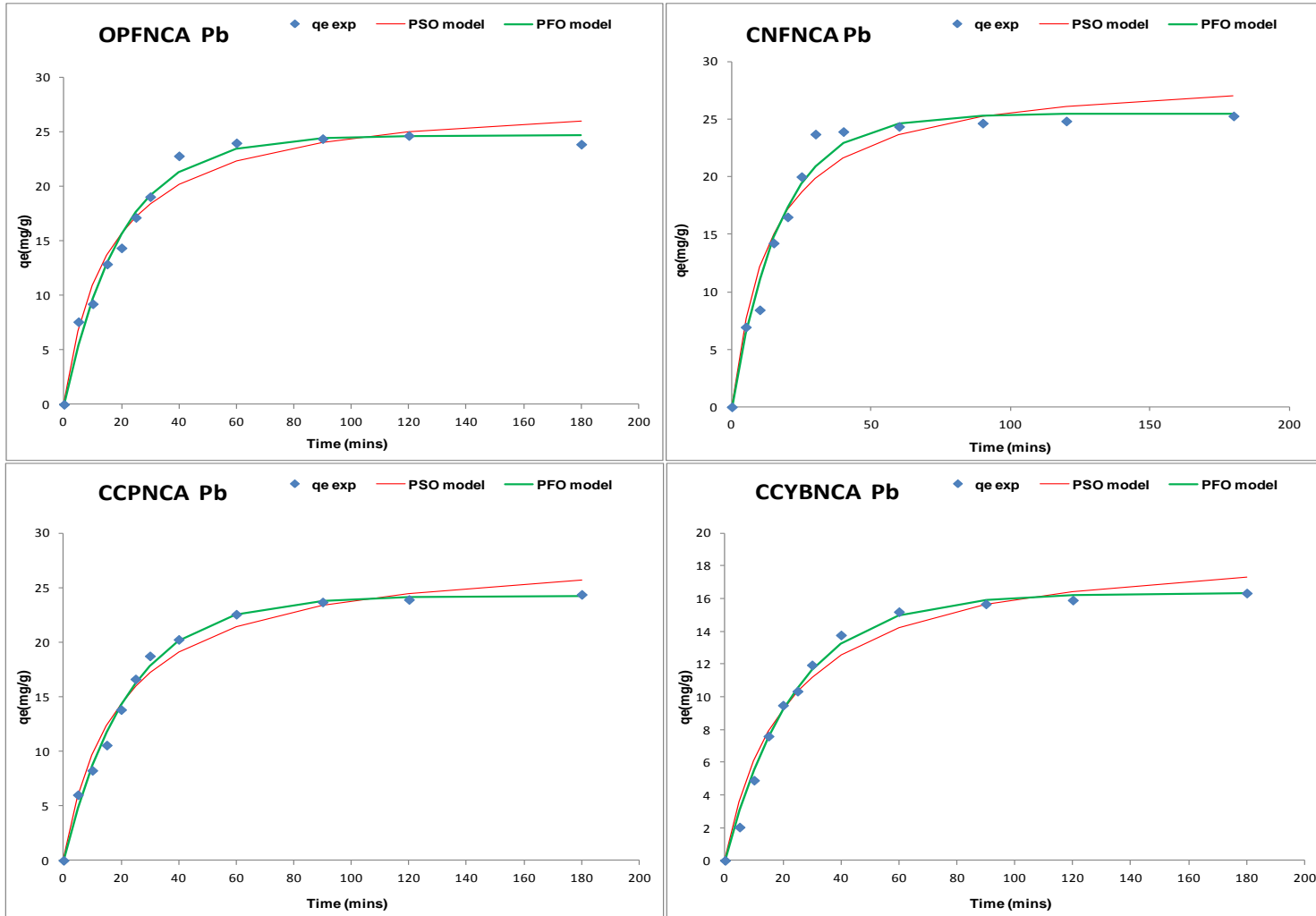
Fig 8.20: Pb(II) ion PFO & PSO sorption kinetic models for OPFNCA,CNFNCA, CCPNCA & CCYBNCA adsorbents
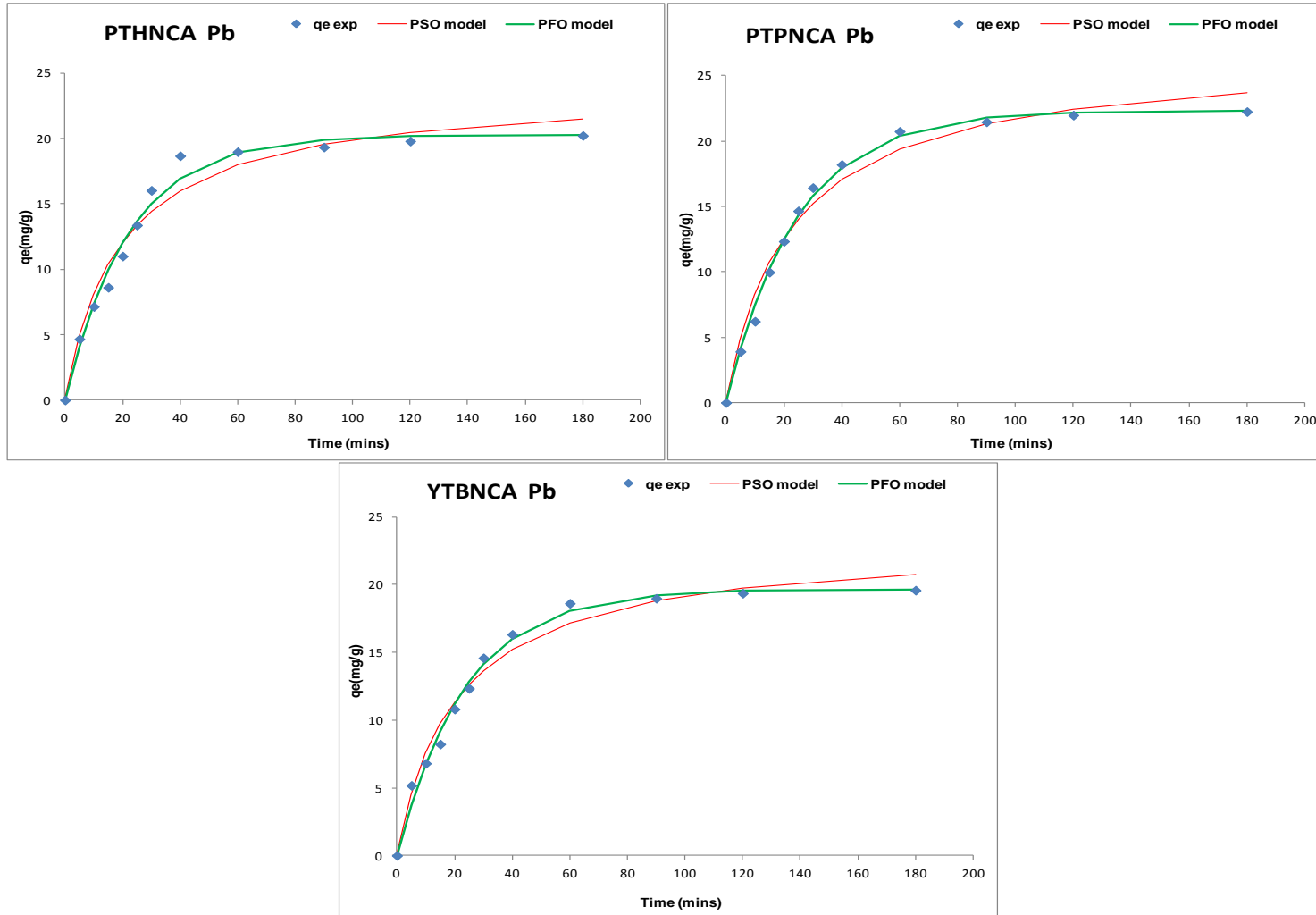
Fig 8.21: Pb(II) ion PFO & PSO sorption kinetic models for PTHNCA, PTPNCA & YTBNCA adsorbents
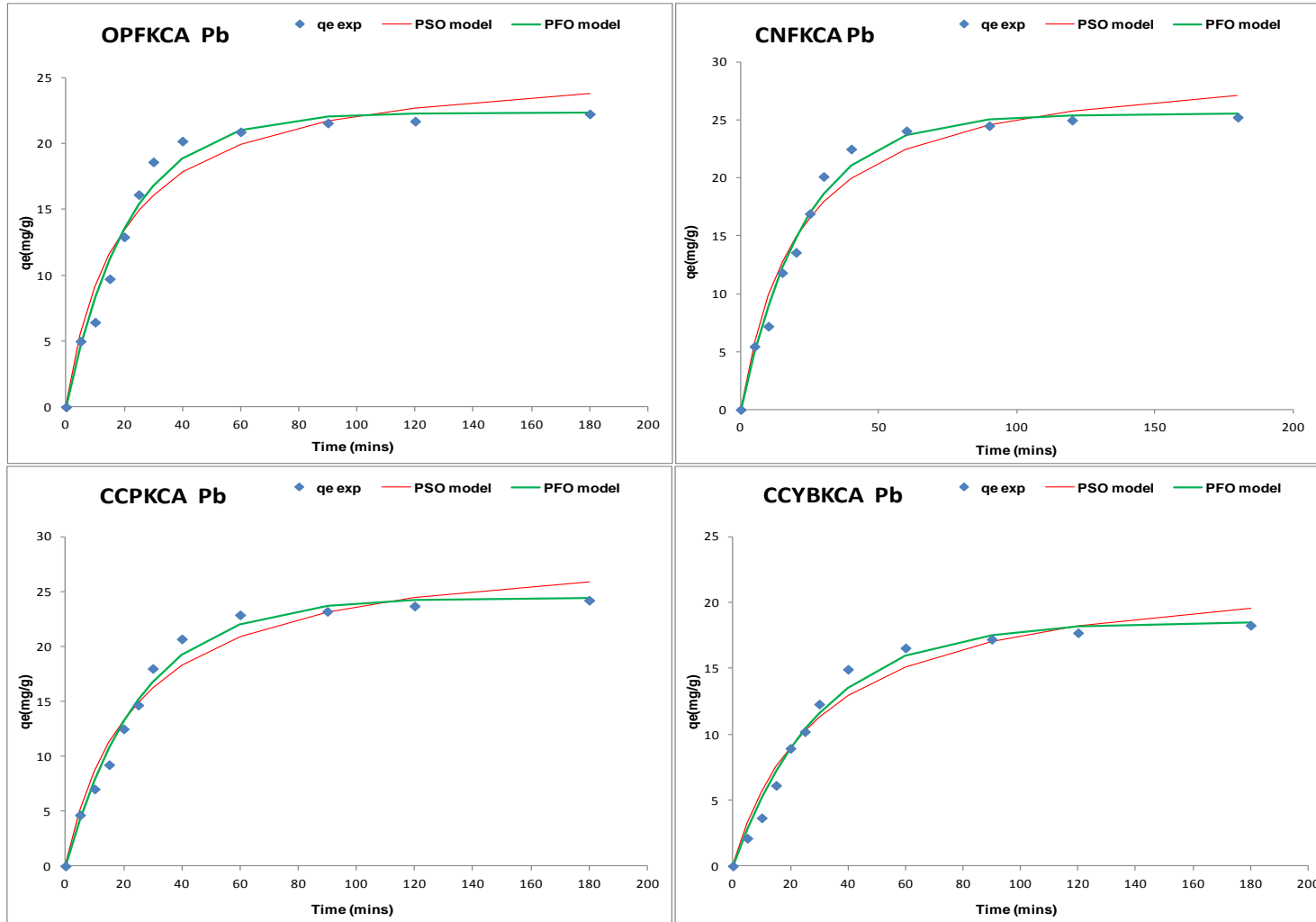
Fig 8.22: Pb(II) ion PFO & PSO sorption kinetic models for OPFKCA,CNFKCA, CCPKCA & CCYBKCA adsorbents
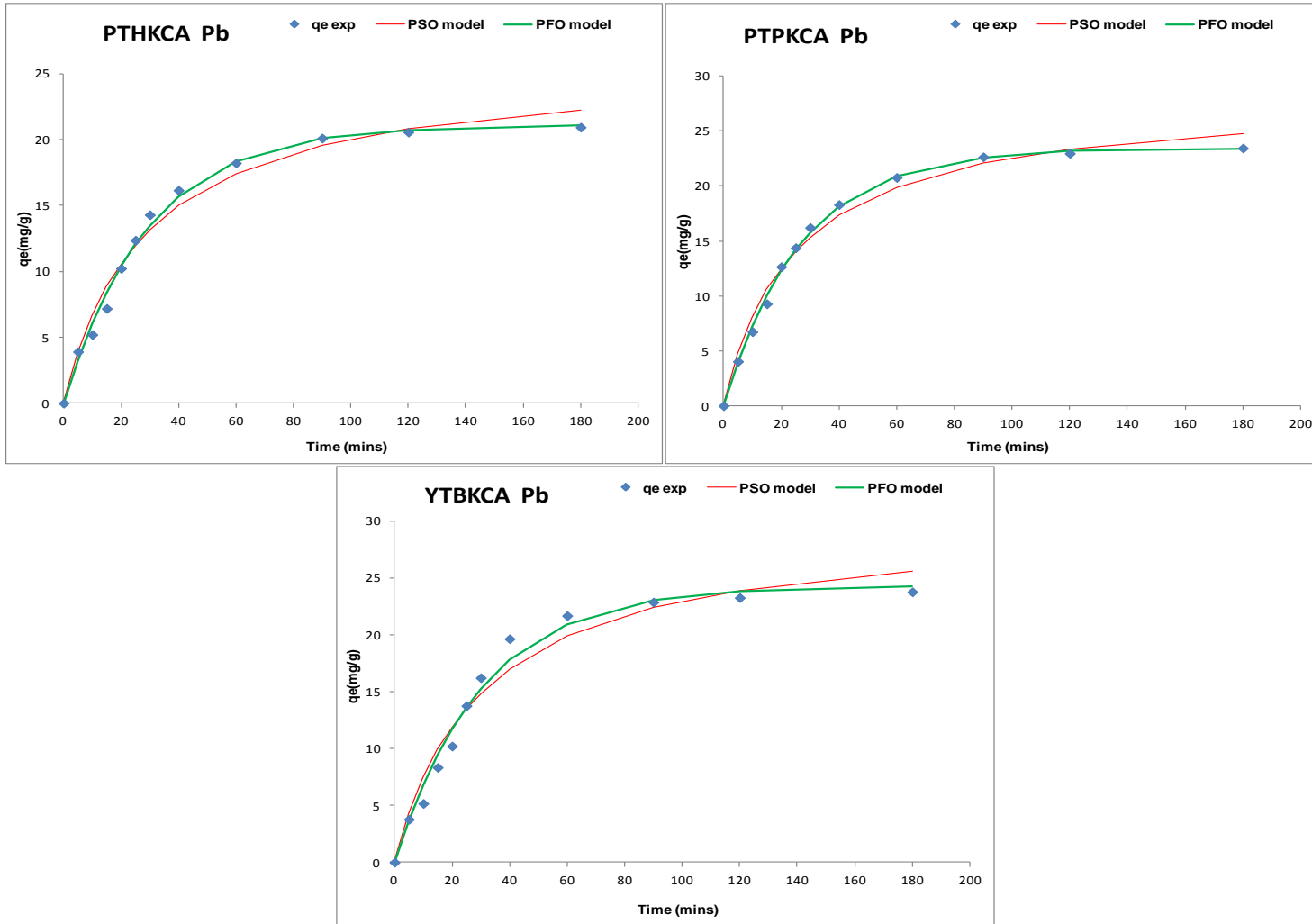
Fig 8.23: Pb(II) ion PFO & PSO sorption kinetic models for PTHKCA, PTPKCA & YTBKCA adsorbents

For the K_2CO_3 adsorbents, five different r^2 values were obtained, the first set with the highest value of 0.99 was for the PTPKCA adsorbent. The second was 0.98 for the PTHKCA adsorbent, the third r^2 was 0.97 for the CCPPKCA adsorbent, the fourth value of 0.96 was for the CNFKC, CCYBKCA and YTBKCA adsorbents while the final set with the lowest r^2 value of 0.95 was for the OPFKCA adsorbent. To further discriminate the adsorbent that is best described by the PSO model, consideration was given to the values of the two error parameters- the χ^2 and the RMSE. The adsorbent with the lowest values for these two parameters was thereafter chosen as the best described by the PSO model. For the Na_2CO_3 chemically activated adsorbents, the χ^2 and RMSE values were used to further compare the fitting of the PSO model to the Pb(II) ion experimental sorption data for the CCPNCA, PTPNCA and YTBNCA adsorbents. Based on the values for these two error parameters in Table 8.12, the YTBNCA adsorbent uptake of Pb(II) ion is best described by the PSO model with the lowest χ^2 (0.06) and RMSE (4.15 $\times10^{-1}$) values. The PSO rate constant (K_2) obtained for this adsorbent was 2.08 $\times10^{-3}$ $gmg^{-1}min^{-1}$ and the PSO model metal ion loading ($q_{e,cal}$) was 23.1 mgg^{-1}.

For the K_2CO_3 chemically activated adsorbents, based on the results in Table 8.13 it is observed that the PTPKCA adsorbent uptake of Pb(II) ion is best described by the PSO model with the lowest χ^2 (0.05) and RMSE (3.87 $\times10^{-1}$) values. The PSO rate constant (K_2) obtained for this adsorbent was 1.10 $\times10^{-3}$ $gmg^{-1}min^{-1}$ and the PSO model metal ion loading ($q_{e,cal}$) was 29.9 mgg^{-1}. A comparison of the PSO values for r^2 and the two error parameters between the Na_2CO_3 and K_2CO_3 adsorbents for Pb(II) ion sorption, indicates that the PTPKCA adsorbent was best described by the PSO model as it had the lowest values for the error parameters (χ^2 and the RMSE) and the highest r^2 value.

Futhermore, to determine which of the two kinetic models (PFO or PSO) gives the best description of Pb(II) sorption kinetics onto the Na_2CO_3 and K_2CO_3 chemically activated adsorbents an examination of the $q_{e,cal}$ values obtained for the PFO and PSO model presented in Tables 8.12 and 8.13 is used to compare with the experimental q_e value obtained at the end of sorption (after 180 mins) also called q_t. The assumption is that the model with $q_{e,cal}$ values that are closer to the experimental obtained q_e is the model that describes the Pb(II) ion sorption better. Table 8.14 presents the q_e for both experimental sorption and kinetic models for Cd(II) ion uptake by the Na_2CO_3 and K_2CO_3 chemically activated adsorbents.

Table 8.14: Comparison of q_e values for experiment and model sorption for Pb(II) onto chemically activated adsorbents

Adsorbent	q_e (mgg^{-1})		
	Experiment	PFO model	PSO model
OPFNCA	23.8	24.6	28.3
CNFNCA	25.3	25.6	29.1
CCPNCA	24.4	24.3	28.5
CCYBNCA	16.3	16.3	19.4
PTHNCA	20.2	20.3	23.8
PTPNCA	22.2	22.3	26.6
YTBNCA	19.6	19.7	23.1
OPFKCA	22.2	22.3	26.2
CNFKCA	25.2	25.5	30.1
CCPKCA	24.2	24.4	29.3
CCYBKCA	18.3	18.5	22.9
PTHKCA	20.9	21.1	25.7
PTPKCA	23.5	23.4	28.2
YTBKCA	23.8	24.3	29.9

From Table 8.14, it is observed that the values for q_{emodel} for both PFO and PSO models were close to the experimental (q_e) for both Na_2CO_3 and K_2CO_3 chemically activated adsorbents. However, the PFO model for some of the adsorbents gave a closer q_e value to the experimental sorption q_e than the PSO. The PSO mainly gave values that were an overestimate of the experimental q_e while that of the PFO was for some adsorbents an underestimation of the experimental q_e. A similar observation wa made for the modelling of Cd(II) ions based on these tow models. Further evaluation of the values for error parameters (χ^2 and the RMSE) and correlation coefficient (r^2) in Table 8.12 and 8.13 for the two sets of adsorbents indicates that the PFO model had lower values for both error parameters and higher r^2. Thus, it can be said that the PFO model gave a better approximation of the kinetics of Pb(II) sorption by the Na_2CO_3 and K_2CO_3 chemically activated adsorbents than the PSO order model.This implies that the kinetics supports the assumption that the rate limiting step of Pb(II) ion sorption onto the Na_2CO_3 and K_2CO_3 chemically activated adsorbents is dependent on the concentration of the Cd(II) ions in the adsorbate (Azizian, 2004; Liu and Liu, 2008). However, as previously observed, the closeness of the parameters obtained from the PSO model may also indicate that chemical interactions between the ions in the adsorbate solution and the adsorbent may still

influence sorption kinetics but this may depend on the rate of diffusion. This implies that pore diffusivity of the ions onto the active sites may also influence the kinetics as previously discussed in the analysis of the two stage metal uptake (fast and slow) kinetics of Pb(II) ion sorption.

Studies have been reported on the application of the PFO and PSO models for the characterisation of the kinetics of Pb(II) ion sorption using chemically activated adsorbents. The kinetics of Pb(II) ion sorption from aqueous solution by zinc chloride ($ZnCl_2$) chemically activated coffee residue has been reported by Boudrahem *et al.,* (2009). In their study, the pseudo-second order (PSO) model gave a better fitting for the sorption of Pb(II) than the pseudo-first order (PFO) model based on higher values of the correlation coefficient(r^2). Huang *et al.,* (2014) has also reported on the kinetics of Pb(II) ion sorption from aqueous solution using phosphoric acid (H_3PO_4) chemically activated water hyacinth. The results from the kinetic modelling of Pb(II) ion sorption indicates that the PFO model did describe the experimental results of sorption better than the PSO based on higher r^2 value of 0.96 (PFO) and 0.91(PSO).

8.6 Equilibrium sorption studies

The effectiveness of the utilization of adsorbents in the removal of contaminants from waste streams is often quantified using different approaches. These approaches are used to determine the quantity of pollutants removed by the adsorbent applied on the effluent. The use of activated carbon for commercial wastewater treatment for heavy metals has been reported in literature (Rao *et al*., 2006). However, the cost of commercial activated carbon has driven the search for use of alternative low cost materials for metal ion removal (Mohan and Sing, 2002). The determination of the amount of pollutants such as heavy metal ions removed from a wastewater system or aqueous solution using an adsorbent is an important parameter for analysing the cost and effectiveness of an adsorbent system with respect to scale up possibilities and commercial applications. In this regard, adsorption isotherms can be employed to obtain heavy metal ion uptake and loading data that can be used to design a specific adsorption process.

Adsorption data when analysed and modelled can describe the relationship between amount of pollutant (such as heavy metal ion) uptake per unit mass of the adsorbent used with respect to the equilibrium concentration of the pollutant in the bulk phase (Ammari *et*

al., 2015). This information can be used to optimize the process design for scale up to determine the volume of effluent, amount of adsorbent and reaction conditions such as temperature, pH and contact time sufficient for maximum uptake of pollutant. It also provides data that would be useful in modelling the maximum loading of a pollutant onto a specific adsorbent (Rao *et al*., 2006).

In this study, the Na_2CO_3 chemically activated adsorbents were used for adsorption study at equilibrium for Cd(II) and Pb(II) ion removal at varying initial concentrations from 50 mgL^{-1} to 500 mgL^{-1} with a step size of 50. The equilibrium uptake data for the Na_2CO_3 activated carbon adsorbents for Cd(II) and Pb(II) were modelled using two isotherm equations (Langmuir and Freundlich). For each chemically activated carbon adsorbent, the applicability of each isotherm for Cd(II) and Pb(II) adsorption was evaluated using the non-linear optimization protocol based on the Excel solver add-in software method – a trial and error procedure in Microsoft excel. The minimization of the error parameter of this non-linear optimization tool in excel provides isotherm constants and co-efficient of determination (r^2) values that best fits the experimental data (Kumar and Sivanesan, 2006). The coefficient of determination, given in Eqn. (8.2) below is one of the most widely used error function for minimizing the error distribution between experimental equilibrium data and the isotherm model data (Kumar *et al*., 2008). Most studies in literature use the linearization process for the isotherm modelling but this technique is fraught with errors as the linearization of the non-linear isotherm equation maximizes the errors. Although it is thought to give a fitting that seems as the best fit, it has fundamental inconsistencies in the approach (Brown, 2001; Foo and Hameed, 2010).

To determine the goodness of fit of the isotherm models to the experimental data using non-linear regression, the optimization procedure requires that error functions be defined to enable the fitting of the model parameters with the experimental values. In this study, the coefficient of determination (r^2), the root mean square error (RMSE) and the Chi square test (χ^2) were used as error parameters for each model and these were determined based on eqns. 5.4, 5.5 and 5.6 which have been previously described in section 5.11 of chapter 5 in this study.

8.6.1 Cadmium (II) ion isotherm modelling

The modelling of the two isotherms used for Cd(II) ion sorption is described in the subsequent sections. These were the Langmuir and Freundlich isotherms.

8.6.1.1 Langmuir isotherm

The Langmuir isotherm assumes the occurrence at a specific homogeneous site within the adsorbent (Langmuir, 1918) and is given in its non-linear form as:

$$qe = \frac{q_m K_L C_e}{1 + K_l Ce} \tag{8.2}$$

Where: q_e is the equilibrium ion uptake (mg g^{-1}), C_e represents the equilibrium concentration of the adsorbate (mgL^{-1}), K_L is the sorption equilibrium constant (Lmg^{-1}) and q_m is the maximum adsorption capacity (mg g^{-1}) (Sari *et al.*, 2008).

For the modelling of the Langmuir isotherm, equilibrium isotherm plots for each adsorbent uptake of Cd(II) ion was carried out. These plots are shown in Figures 8.24 – 8.30 for the Na$_2$CO$_3$ activated adsorbents and Table 8.15 summarizes the isotherm parameters for Cd(II) ion adsorption on the Na$_2$CO$_3$ activated carbon adsorbents. From Figure 8.24, the isotherm plot for OPFNCA shows that the loading of Cd(II) increased with increase in initial ion concentration from 4.44 mgg^{-1} for 50 mgL^{-1} to 18.52 mgL^{-1} for 500 mgL^{-1}. These data were fed into the Excel solver add-in and the optimization procedure generated isotherm shown in Table 8.15. From the values, it can be seen that the Langmuir isotherm constants q$_{max}$ for the OPFNCA activated carbon was 21.4 mgg^{-1}, while K$_L$ was 3.88×10^{-2} Lmg^{-1} and the r^2 value was 0.948. Also, The increase in Cd(II) ion loading with increase in initial concentration was observed for all the Na$_2$CO$_3$ activated carbon adsorbents. The trend in the value of the Langmuir isotherm constant q$_{max}$ for the chemically activated carbon adsorbents shows that CCPNCA had the highest value of 29.3 mgg^{-1} and YTBNCA had the highest value of 15.6 mgg^{-1}.

The Langmuir isotherm model constant q$_{max}$ is a measure of the maximum amount of the metal ion per unit weight of adsorbent that forms a complete monolayer on the surface of an adsorbent at high equilibrium concentration (Ce). The value of q$_{max}$ represents the limiting adsorption loading capacity when the surface of the adsorbent is fully covered with metal ions and gives insight in the determination of adsorption performance,

especially when the adsorbent did not attain its full saturation during contact (Sarada *et al.,* 2014). This q_{max} value is therefore an essential parameter in the design of pilot scale plants for adsorption as it provides information on the maximum loading of an adsorbent for a given volume of waste stream. From the values of q_{max} for the chemically activated adsorbents, it can be said that the CCPNCA adsorbent had the highest loading capacity.

The variation in the q_{max} values for Cd(II) ion loading on the Na_2CO_3 chemically activated adsorbents can be related to the differences in the adsorbent structure, morphology and chemical composition as the combination of these parameters will influence the Cd(II) ion transport and adsorption probabilities. Hence, a single adsorbent characteristic like surface area cannot sufficiently account for this trend in metal ion loading due to the complex nature of the activated carbon adsorbent. A comparison of the values of q_{max} for Cd(II) sorption for the chemically activated adsorbents prepared in this study and those reported in literature for other activated carbon adsorbents is depicted in Table 8.16. These values reflect that the adsorbents compare well with those reported in literature, hence can be used as adsorbents for the removal of Cd(II) ions and other divalent metal ions such as Pb, Cu, Zn and Ni from aqueous systems, wastewater streams and natural water bodies.
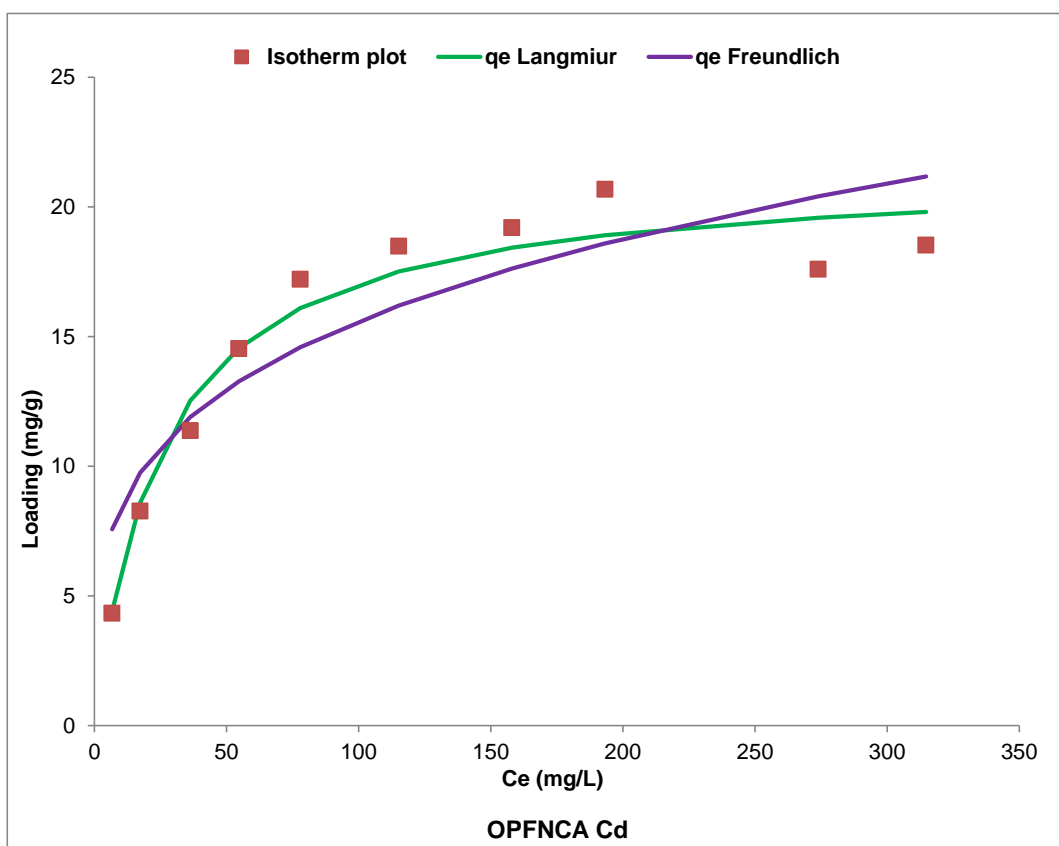
Figure 8.24: Equilibrium isotherm for Cd(II) on OPFNCA
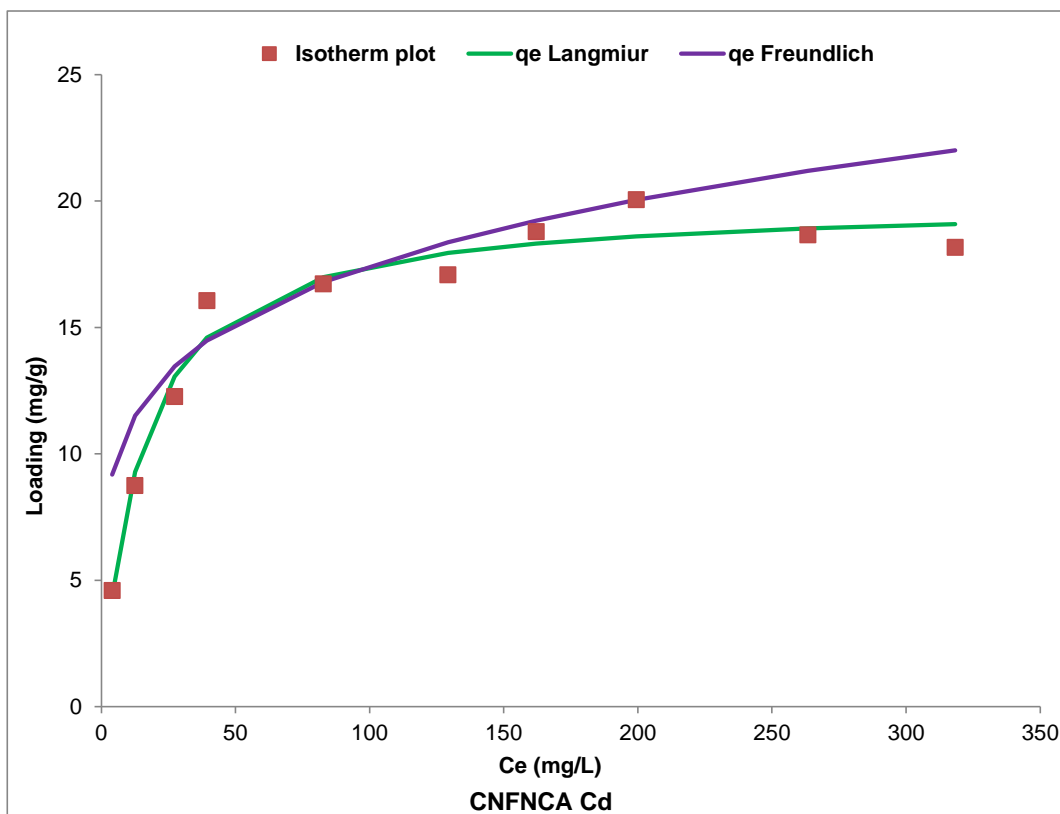
Figure 8.25: Equilibrium isotherm for Cd(II) on CNFNCA
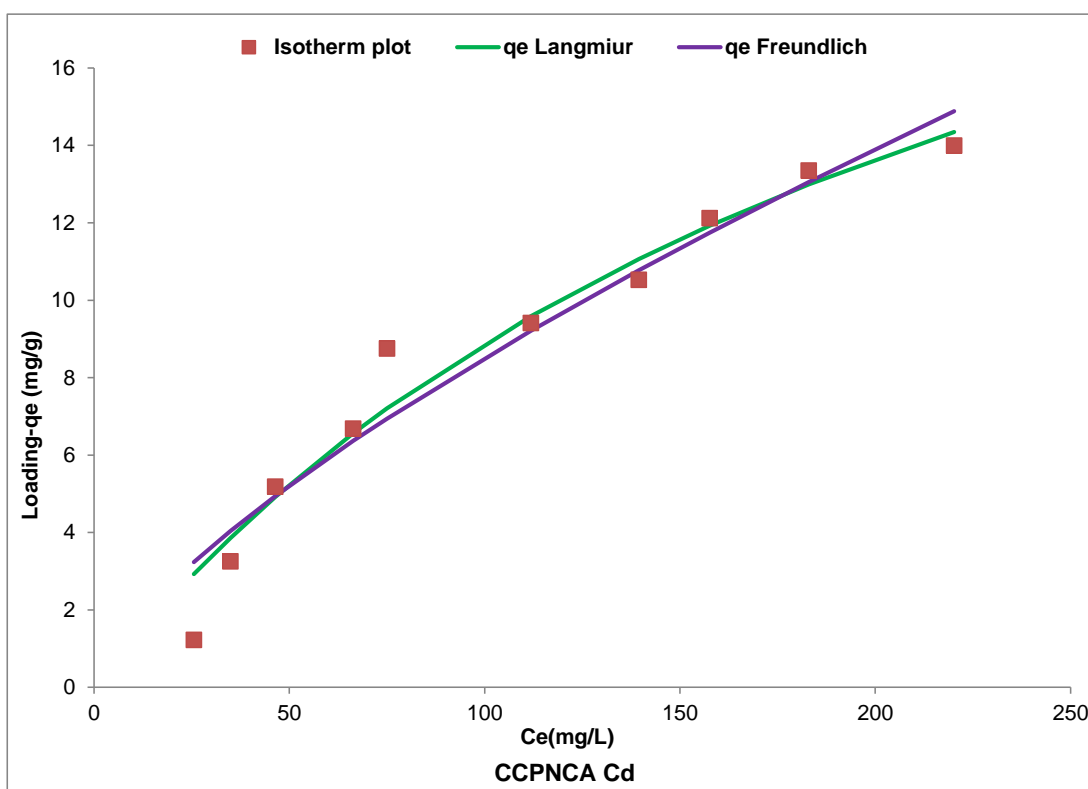
Figure 8.26: Equilibrium isotherm for Cd(II) on CCPNCA
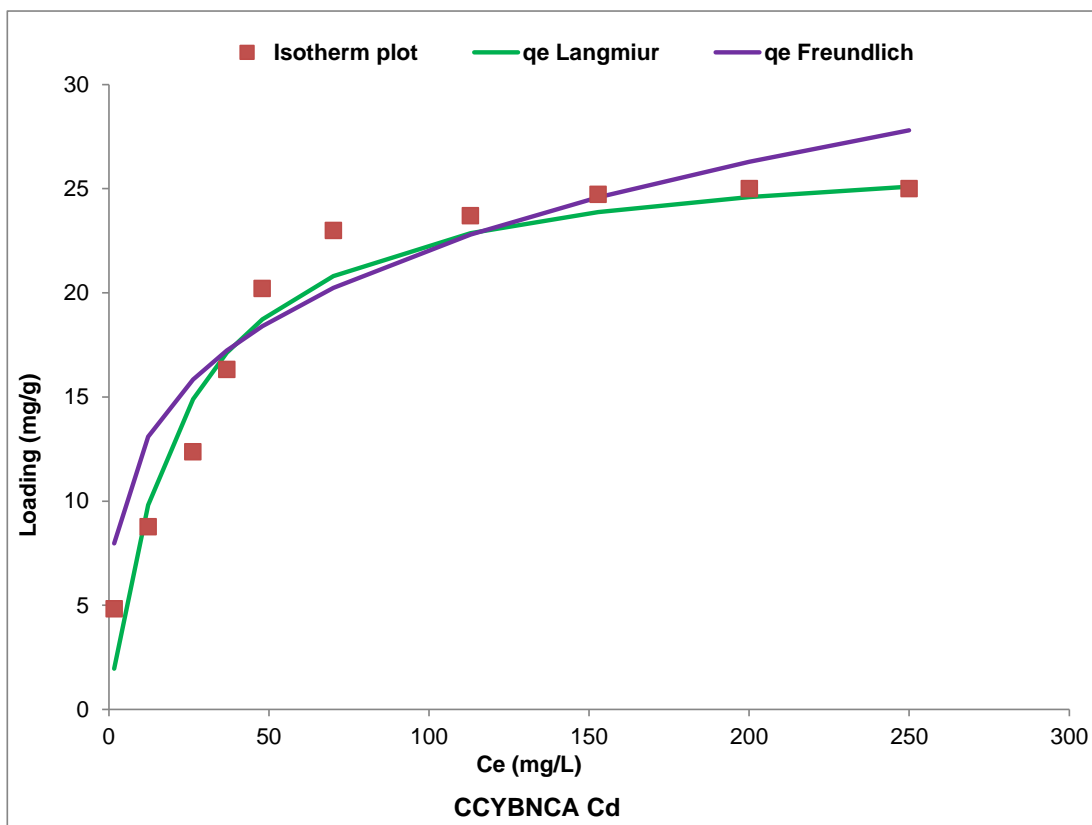
Figure 8.27: Equilibrium isotherm for Cd(II) on CCYBNCA
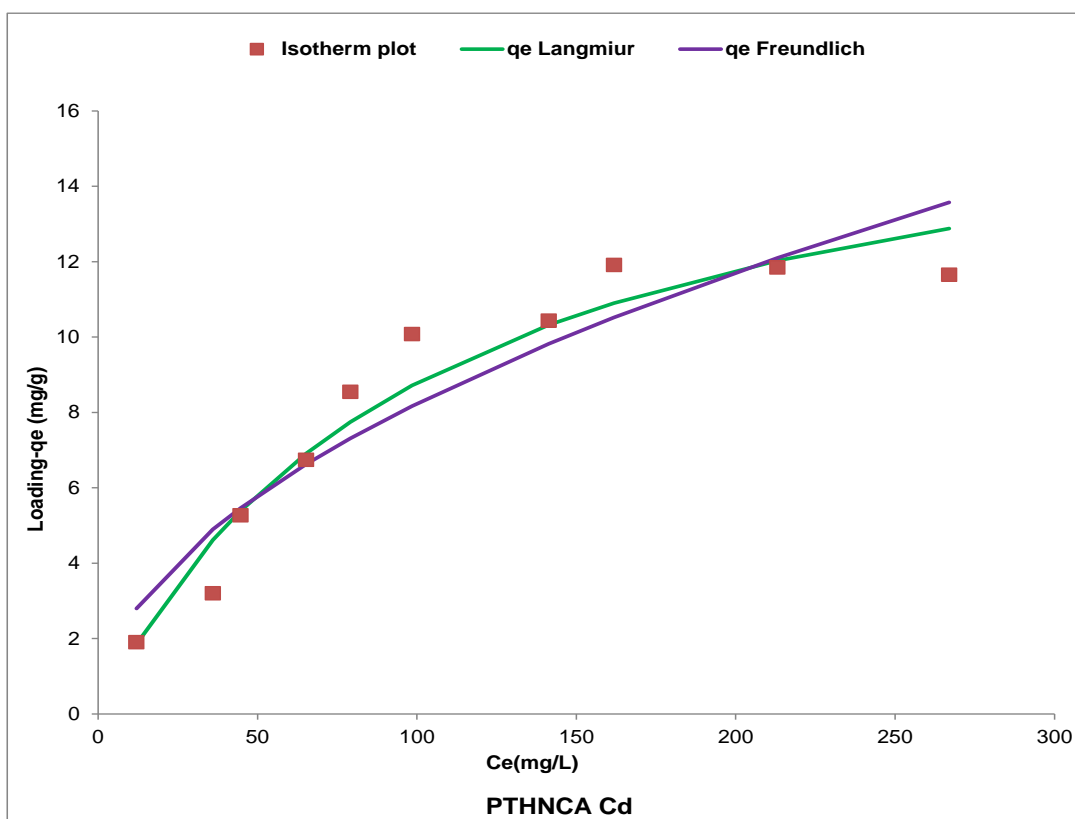
Figure 8.28: Equilibrium isotherm for Cd(II) on PTHNCA

Table 8.15: Isotherm parameters for Cd(II) ion adsorption on Na_2CO_3 activated Adsorbents

| | Langmuir Model | | | | | Freundlich Model | | | | |
Adsorbent	$q_{max}(mgg^{-1})$	$K_L(Lmg^{-1})$	r^2	χ^2	RMSE	$K_F(mgg^{-1})(Lmg^{-1})^{1/n}$	n	r^2	χ^2	RMSE
OPFNCA	21.4	3.88E-02	0.95	8.60E-02	0.81	4.56	3.75	0.79	3.20E-01	3.03
CNFNCA	20.0	6.93E-02	0.97	4.70E-02	0.45	6.93	4.99	0.77	3.35E-01	3.48
CCPNCA	29.4	4.33E-03	0.96	7.46E-02	0.40	0.33	1.41	0.94	1.08E-01	0.58
CCYBNCA	25.3	4.57E-02	0.95	1.38E-01	1.55	6.99	4.00	0.86	3.21E-01	3.91
PTHNCA	17.9	9.67E-03	0.94	8.72E-02	0.44	0.79	1.97	0.87	1.83E-01	0.93
PTPNCA	26.3	1.77E-02	0.95	1.21E-01	1.17	3.17	2.95	0.87	2.10E-01	1.97
YTBNCA	15.7	1.06E-02	0.98	2.38E-02	0.11	0.80	2.05	0.93	8.94E-02	0.43
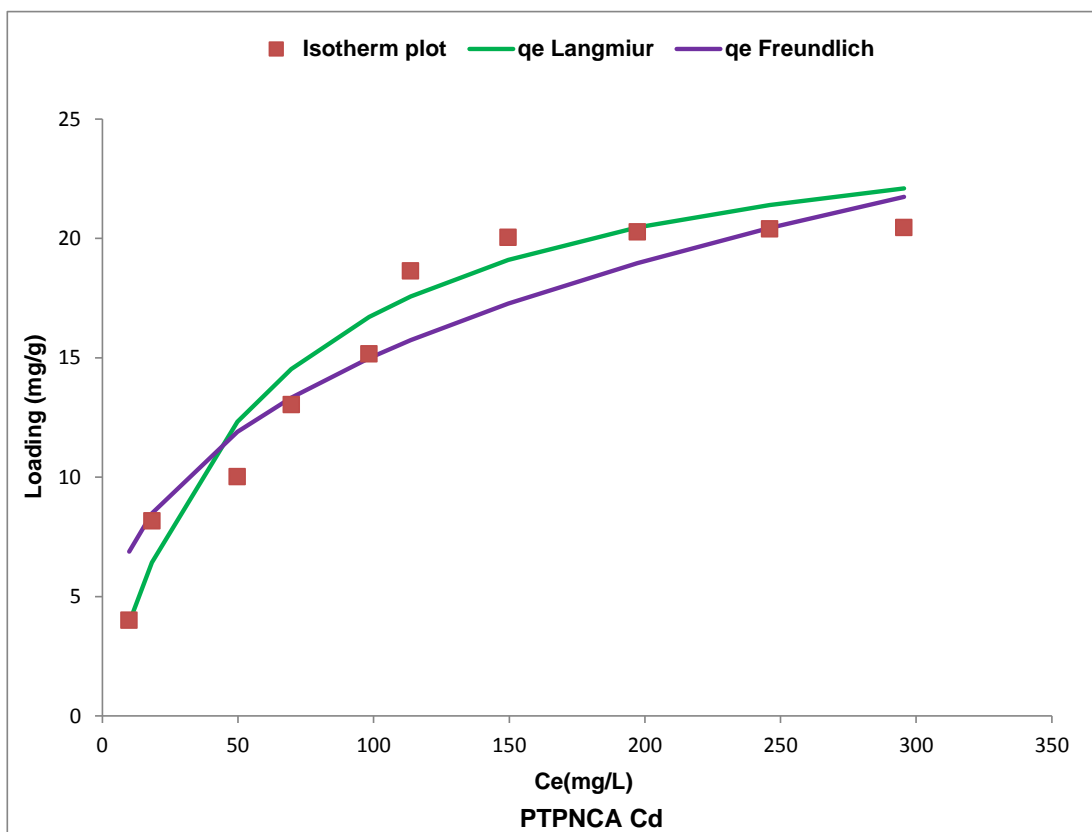
Figure 8.29: Equilibrium isotherm for Cd(II) on PTPNCA
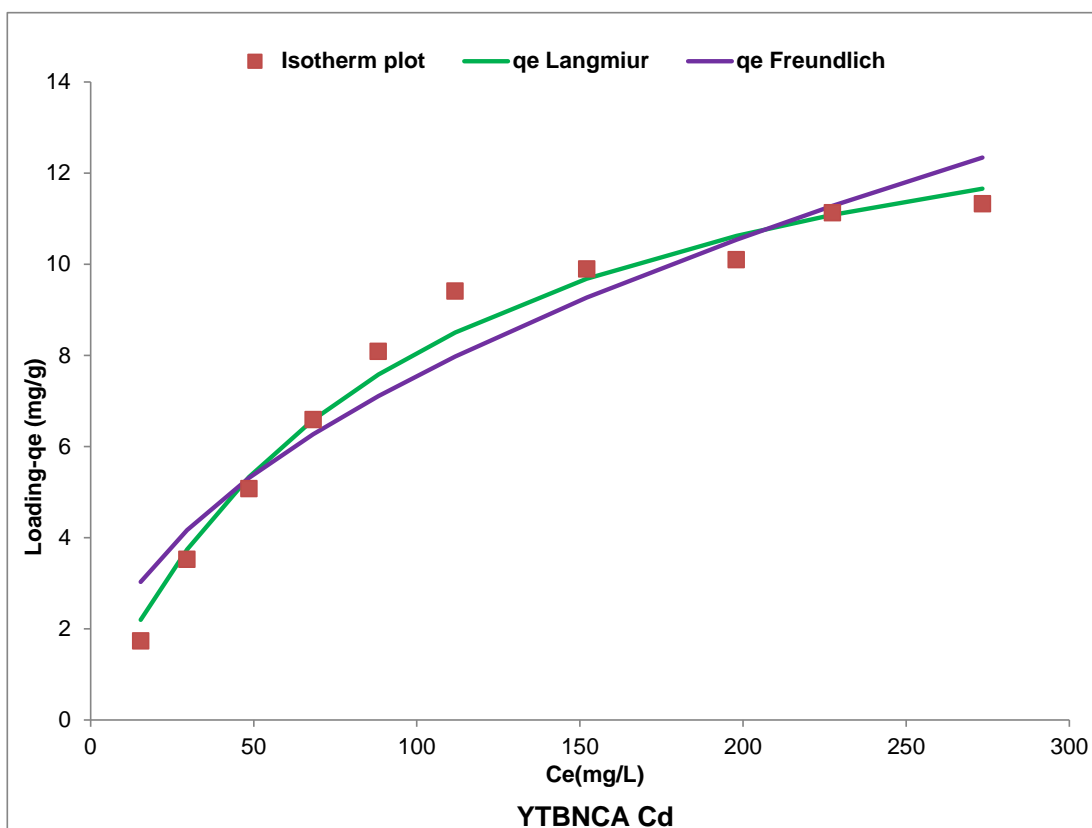
Figure 8.30: Equilibrium isotherm for Cd(II) on YTBNCA

Table 8.16: Comparison of Langmuir constant (q_{max}) for Cd(II) ion with Literature

Adsorbent	q_{max} (mgg^{-1})	Reference
Oil cake activated carbon	23.7	Hema and Srinivasan, 2010
Ceiba pentandra hull activated carbon	19.6	Rao *et al.,* 2006
Chemically activated bagasse pitch	38.0	Mohan and Singh, 2002
Phaseolus aureus hull activated carbon	15.7	Rao *et al.,* 2009
OPFNCA	21.4	This study
CNFNCA	20.0	This study
CCPNCA	29.4	This study
CCYBNCA	25.3	This study
PTHNCA	17.9	This study
PTPNCA	26.3	This study
YTBNCA	15.7	This study

The value of the Langmuir isotherm constant parameter K_L for the Na_2CO_3 chemically activated carbon adsorbents are also shown in Table 8.15. This parameter denotes the affinity of the metal ion Cd(II) to the binding sites on the surface of each chemically activated carbon adsorbent (Ammari *et al.,* 2015). The coefficient of determination (r^2) and the two error parameters- chi square (χ^2) and the root mean square error (RMSE) for each adsorbent in the Langmuir model is also presented in Table 8.15 and the values show a strong correlation between the experimental equilibrium values for the metal ion loading and the predicated values from the isotherm model. The r^2 value for the CCPNCA adsorbent which had the highest qmax was 0.96 while that of YTBNCA with the lowest q_{max} was 0.981 indicating a trend of good model experiment correlation. The χ2 and RMSE values for the isotherm were low thereby for the different adsorbents indicating strong correlation between the experimental values and the Langmuir model.

8.6.1.2 Freundlich isotherm

The Freundlich isotherm model was also used to analyse the equilibrium metal ion sorption for Cd(II) ion using the Na_2CO_3 and K_2CO_3 chemically activated carbon adsorbents.

The Freundlich equation is written in eqn. (8.3)(Sari *et al*.,2008)

$$q_e = K_F (C_e)^{1/n} \qquad\qquad (8.3)$$

Where q_e is the adsorption capacity

Ce is the equilibrium concentration of the adsorbate in solution

K_F and 1/n are Freundlich constants.

The Freundlich model was evaluated based on the excel solver add-in software with the experimental Cd(II) ion loading and the plots are seen in Figure 8.24 – 8.30. From this modelling, the Freundlich isotherm constant parameter and the coefficient of determination (r^2) obtained as well as the values are presented in Table 8.15. The Freundlich constant K_F for OPFNCA was 4.55 mgg^{-1}and the "n" value was 3.745 (1/n = 0.2670). The r^2 value for the Freundlich model was 0.792 indicating that the correlation between experimental values and the Freundlich isotherm was lower than that of the Langmuir isotherm. The values for the Freundlich isotherm constant K_F for the other chemically activated carbon adsorbents ranged from 6.93 (mgg^{-1})(Lmg^{-1})$^{1/n}$ for CNFNCA to 0.32 (mgg^{-1})(Lmg^{-1})$^{1/n}$ for CCPNCA, indicating that the CNFNCA adsorbent had the highest value for K_F while CCPNCA had the least.

The Freundlich parameter K_F is related to the distribution coefficient and loading of metal ions and therefore the degree of Cd (II) ion affinity as well as the mobility on the adsorbent surface. The higher the K_F value, the better the affinity of Cd (II) ions for the adsorbents (Ammari *et al.,* 2015) and the trend in the affinity of the adsorbents to Cd(II) ion was CNFNCA> CCYBNCA> OPFNCA> PTPNCA> YTBNCA> PTHNCA> CCPNCA. A comparison of the K_F values for the adsorbents in this study with previous work reported in literature is presented in Table 8.17 and from the table it can observed that the K_F values for the adsorption of Cd(II) in this study is similar to those reported in literature.

The Freundlich parameter 1/n describes the intensity of the adsorption process and "n" values between 1 and 10 indicate that the adsorption intensity is favourable (Sarada *et al*., 2014). Also, according to Gutierrez-Segura *et al*., (2012), the values of 0.1 < 1/n < 1 show favourable adsorption of Cd(II) ions by adsorbents. The "n" or "1/n" parameter values for the chemically activated carbon adsorbents used in this study are presented in Table 8.15. From the table, it is observed that the values obtained were between 1.412 for CCPNCA to 5.388 for CNFNCA indicating a trend of favourable adsorption intensity for Cd(II) ion by the Na_2CO_3 chemically activated carbon adsorbents.

Table 8.17: Comparison of Freundlich isotherm constant (K_F) for Cd(II) ion with Literature

Adsorbent	$K_F(mgg^{-1})(Lmg^{-1})^{1/n}$	Reference
Ceiba pentandra hull activated carbon	8.32	Rao *et al.*, 2006
Chemically activated bagasse pitch	5.78	Mohan and Singh, 2002
Phaseolus aureus hull activated carbon	4.11	Rao *et al.,* 2009
OPFNCA	4.55	This study
CNFNCA	6.93	This study
CCPNCA	0.32	This study
CCYBNCA	6.88	This study
PTHNCA	0.79	This study
PTPNCA	3.36	This study
YTBNCA	0.79	This study

It also suggests that Cd(II) ions can be well separated from its aqueous solutions using the adsorbents in this study with high adsorption capacity (Sarada *et al.*, 2014). Thus, based on the Freundlich model, the removal of Cd(II) ions by the Na_2CO_3 chemically activated carbon adsorbents was favourable and the affinity parameter from the model indicates that the there was good affinity between the Cd(II) ions and the chemically activated carbon adsorbents used for sorption.

The values of the error functions used in the description of the Freundlich isotherm model are also presented in Table 8.15 for all the adsorbents. The co-efficient of determination (r^2) and two error functions- chi square (χ^2) and the root mean square error (RMSE) for each adsorbent were used in modelling the Freundlich isotherms. The r^2 value ranges between 0-1, with values closer to 1 indicating a favourable correlation between the experimental values for the equilibrium metal ion loading (q_e) and the loading associated with the isotherm model. Normally, error functions are used to minimize the distribution of errors between the experimental equilibrium data and the predicted values from the isotherms in practice. The distribution of the errors between the experimental equilibrium data and the predicted isotherms is reduced either by minimizing the error functions or by maximizing the error functions based on the definition of the error functions. The chi square (χ^2) and the root mean square error (RMSE) values that are lowest indicate favourable fitting between the experimental equilibrium sorption data with those of the

Freundlich isotherm. The coefficient of determination values for the Freundlich isotherm model for the adsorption of Cd(II) ions using the Na_2CO_3 chemically activated carbon adsorbents shown in Table 8.15 indicates a strong correlation between the experimental loading data and the Freundlich model value. From an analysis of the coefficient of determination values for both Langmuir and Freundlich isotherm models for Cd(II) ion removal using the chemical activated adsorbents, it was observed that the Langmuir isotherm described the metal ion process better than the Freundlich for all the adsorbents as its r^2 values were higher than those of the Freundlich model, furthermore the χ^2 and RMSE values for the Langmuir isotherm were lower than those of the Freundlich for all the adsorbents for the sorption of Cd(II) ions.

It has been observed by Mohan and Singh (2002) that the Langmuir isotherm parameter q_{max} and the Freundlich isotherm constant K_F have varying values and meanings even though they lead to the same conclusion about the correlation of the experimental data with the sorption model. This has also been observed in this study for all the Na_2CO_3 chemically activated adsorbents. This can be explained based on the fundamental assumptions from which these models were derived. The Langmuir isotherm assumes that the adsorption free energy is independent of both the surface coverage and the formation of monolayer where the solid surface reaches saturation, whereas Freundlich isotherm does not predict saturation of the solid surface by the adsorbate and therefore the surface coverage is mathematically unlimited as it assumes that the adsorbent has a heterogeneous valence distribution and thus has different affinity for adsorption where the K_F parameter relates to this affinity for adsorption (Mohan and Singh, 2002). However for design and process optimization purposes, the determination of the monolayer saturation point for an adsorbent is crucial as it gives information that is characteristic of the adsorbent material and the forces at play within the adsorption system, hence, the crucial significance of the value of the Langmuir constant q_{max}.

8.6.2 Lead (II) ion isotherm modelling

The removal of Pb(II) ions from aqueous solutions using the Na_2CO_3 chemically activated carbon adsorbents was also studied in this work and the procedure was as described in Section 4.4 of the study. The effect of initial metal ion concentration was studied from an initial concentration of 50 mgL^{-1} of Pb(II) with increment of 50 up to 500 mgL^{-1}. For the OPFNCA adsorbent, the loading of Pb(II) increased from 4.2 mgg^{-1}for 50 mgL^{-1} to 28.52

mgg^{-1}for 500 mgL^{-1}. From the equilibrium data for Pb(II) ion sorption isotherm modelling analysis was carried out using the Langmuir and Freundlich isotherm equations using the excel solver add-in non-linear approximation procedure previously described in section 8.6.1. To determine the goodness of fit of the isotherm models to the experimental data using non-linear regression, the optimization procedure requires that error functions be defined to enable the fitting of the model parameters with the experimental values. In this study, the coefficient of determination (r^2), the root mean square error (RMSE) and the Chi square test (χ^2) were used as error parameters for each model and these were determined based on eqns. 5.4, 5.5 and 5.6 which have been previously described in section 5.11 of chapter 5 in this study.

8.6.2.1 Langmuir isotherm

The Langmuir equation for isotherm equation was used for the modelling of Pb(II) sorption using the Na$_2$CO$_3$ chemically activated carbon adsorbents. From these analysis Langmuir isotherm equilibrium isotherm plots for each Na$_2$CO$_3$ activated carbon adsorbent was obtained as shown in Figure 8.31 – 8.37. From these figures it is seen that the uptake of Pb(II) ion by these adsorbents increased as the initial metal ion concentration increased as the initial metal ion concentration increased up the a maximum value. The isotherm parameters along with the coefficient of determination value for the Langmuir and Freundlich models for Pb(II) ion sorption were obtained from the equilibrium modelling and presented in Table 8.18. The values of the Langmuir isotherm constants and coefficient of determination (r^2) and the two error functions- chi square (χ^2) and the root mean square error (RMSE) for each adsorbent were used to evaluate the isotherm fitting with experimental results. The values of the error parameters-χ^2 & RMSE are low for the adsorbents and this indicates a strong correlation with the experimental data for Pb(II) ion uptake for all the Na$_2$CO$_3$ activated carbon adsorbents. The r^2 values for Pb(II) sorption modelled on the Langmuir isotherm were in the range 0.95 – 0.98 which shows close correlation with the experimental data. The χ^2 values ranged from 7.10×10^{-2} -1.81×10^{-1}, while the RMSE values were in the range 0.17-2.14. The results obtained for these parameters indicates that the Langmuir model closely describes the experimental data for the uptake of Pb(II) ions by the 7 Na$_2$CO$_3$ chemically activated carbon adsorbents.
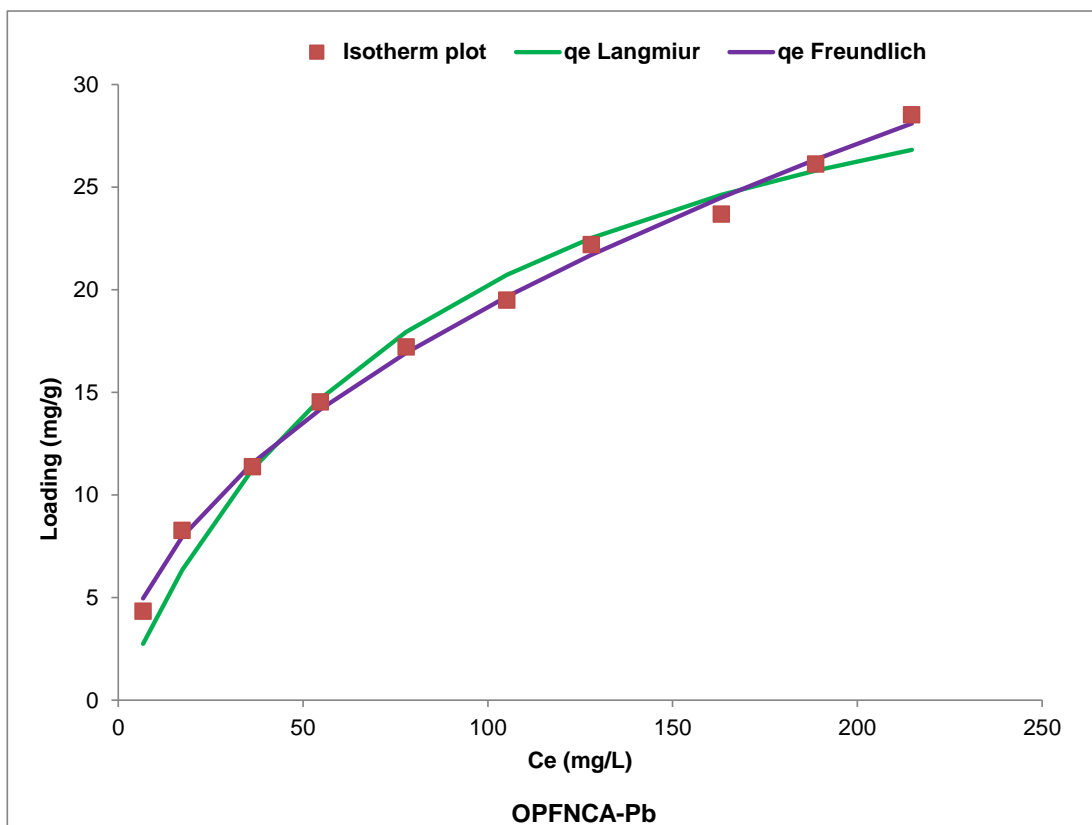
Figure 8.31: Equilibrium isotherm for Pb(II) ion on OPFNCA
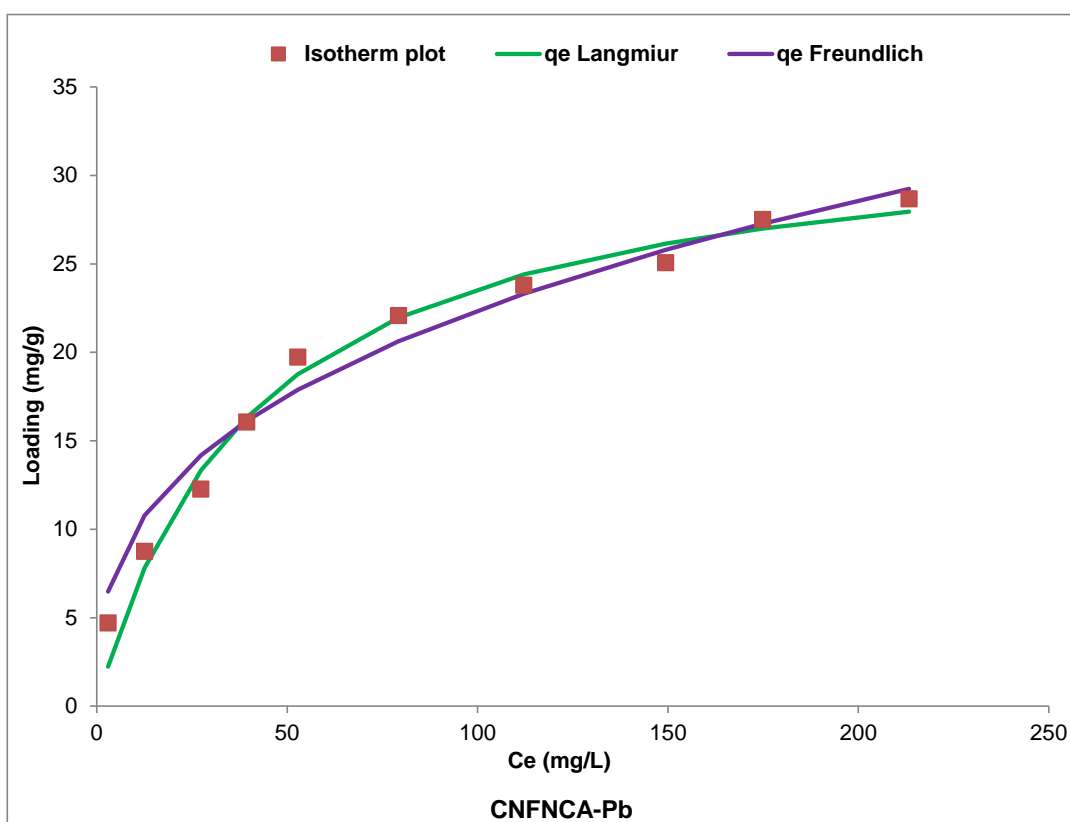
Figure 8.32: Equilibrium isotherm for Pb(II) ion on CNFNCA
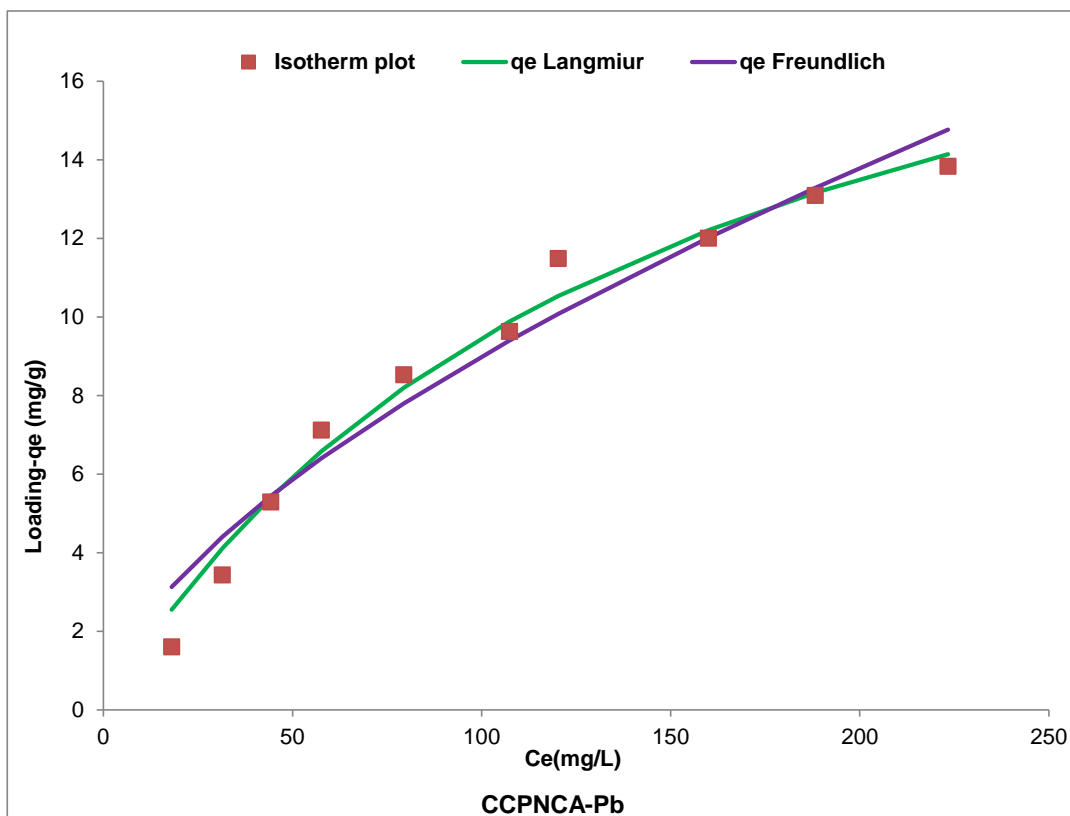
Figure 8.33: Equilibrium isotherm for Pb(II) ion on CCPNCA
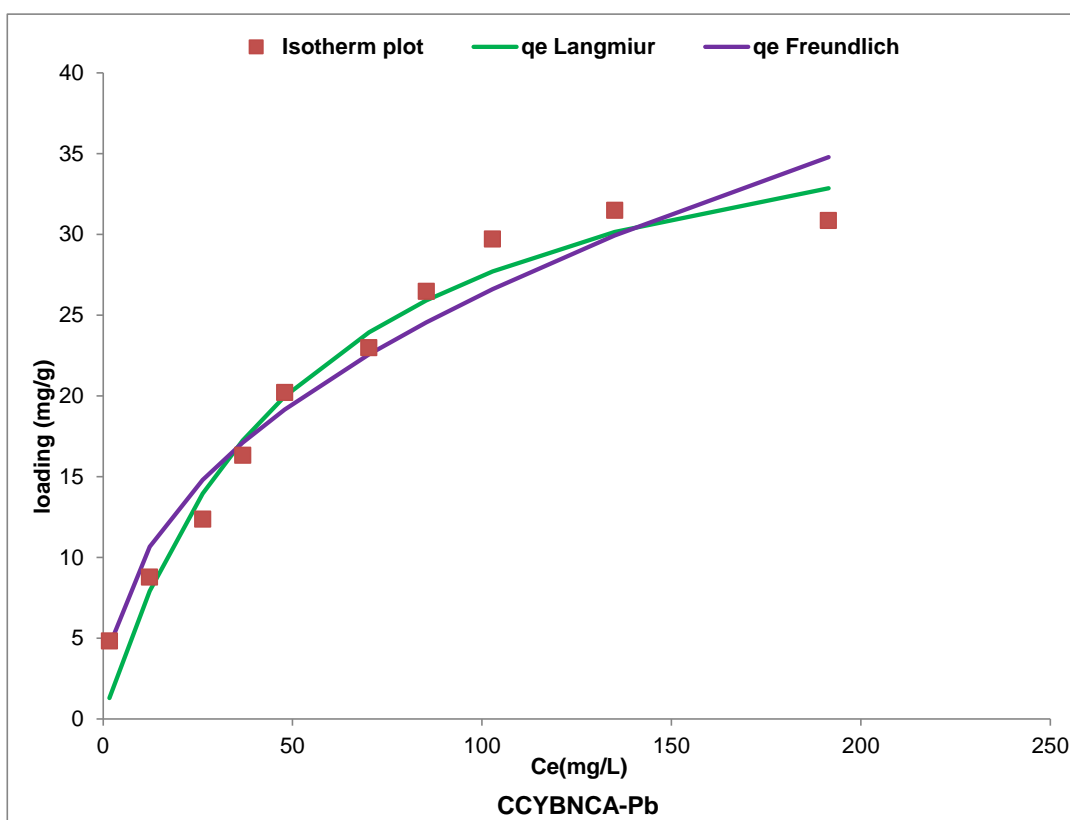
Figure 8.34: Equilibrium isotherm for Pb(II) ion on CCYBNCA
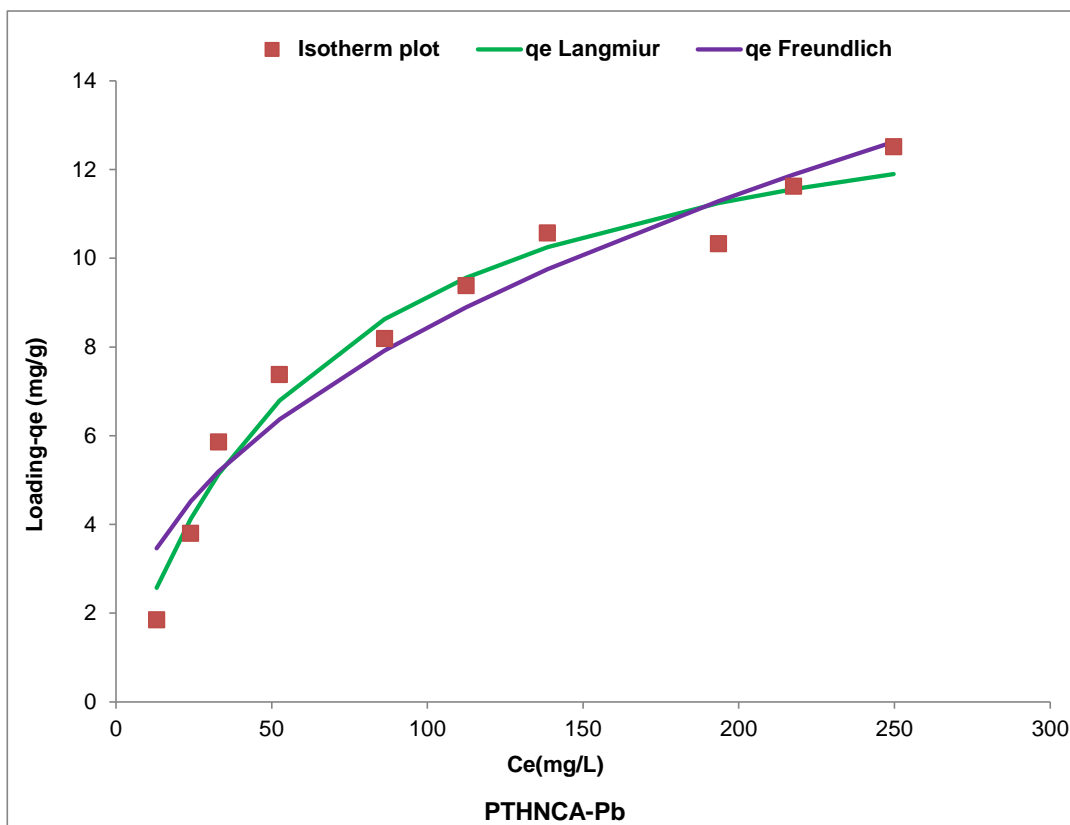
Figure 8.35: Equilibrium isotherm for Pb(II) ion on PTHNCA
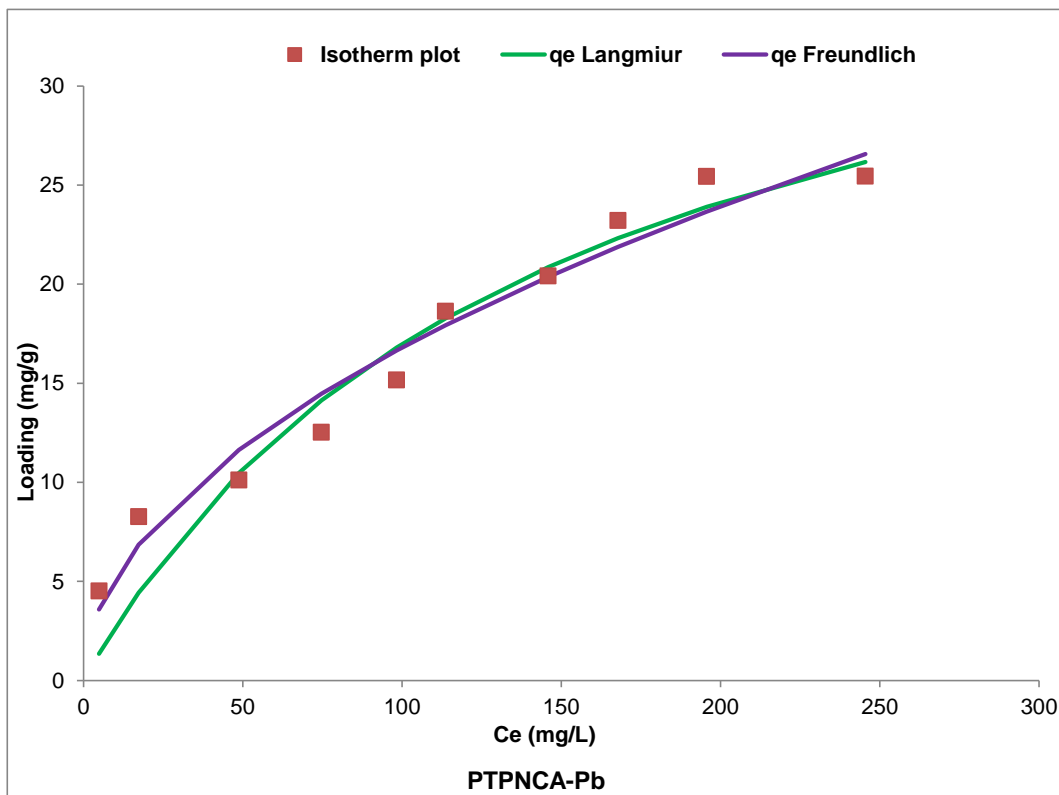
Figure 8.36: Equilibrium isotherm for Pb(II) ion on PTPNCA

Table 8.18: Isotherm parameters for Pb(II) ion adsorption on Na_2CO_3 activated Adsorbents

	Langmuir Model					Freundlich Model				
Adsorbent	$q_{max}(mgg^{-1})$	$K_L(Lmg^{-1})$	r^2	χ^2	RMSE	$KF(mgg^{-1})(Lmg^{-1})^{1/n}$	n	r^2	χ^2	RMSE
OPFNCA	37.3	1.19E-02	0.98	7.10E-02	0.77	1.92	2.00	0.99	1.08E-02	0.12
CNFNCA	33.3	2.44E-02	0.98	6.15E-02	0.72	4.42	2.83	0.97	9.10E-02	1.10
CCPNCA	23.6	6.73E-03	0.98	3.33E-02	0.18	0.53	1.62	0.95	8.40E-02	0.46
CCYBNCA	41.9	1.90E-02	0.97	1.38E-01	1.73	3.62	2.32	0.95	2.08E-01	2.66
PTHNCA	14.9	1.60E-02	0.97	3.70E-02	0.19	1.12	2.28	0.93	8.00E-02	0.41
PTPNCA	41.7	6.87E-03	0.95	1.81E-01	2.14	1.60	1.96	0.96	1.09E-01	1.11
YTBNCA	15.2	2.14E-02	0.98	3.20E-02	0.17	1.58	2.54	0.99	1.10E-01	0.11
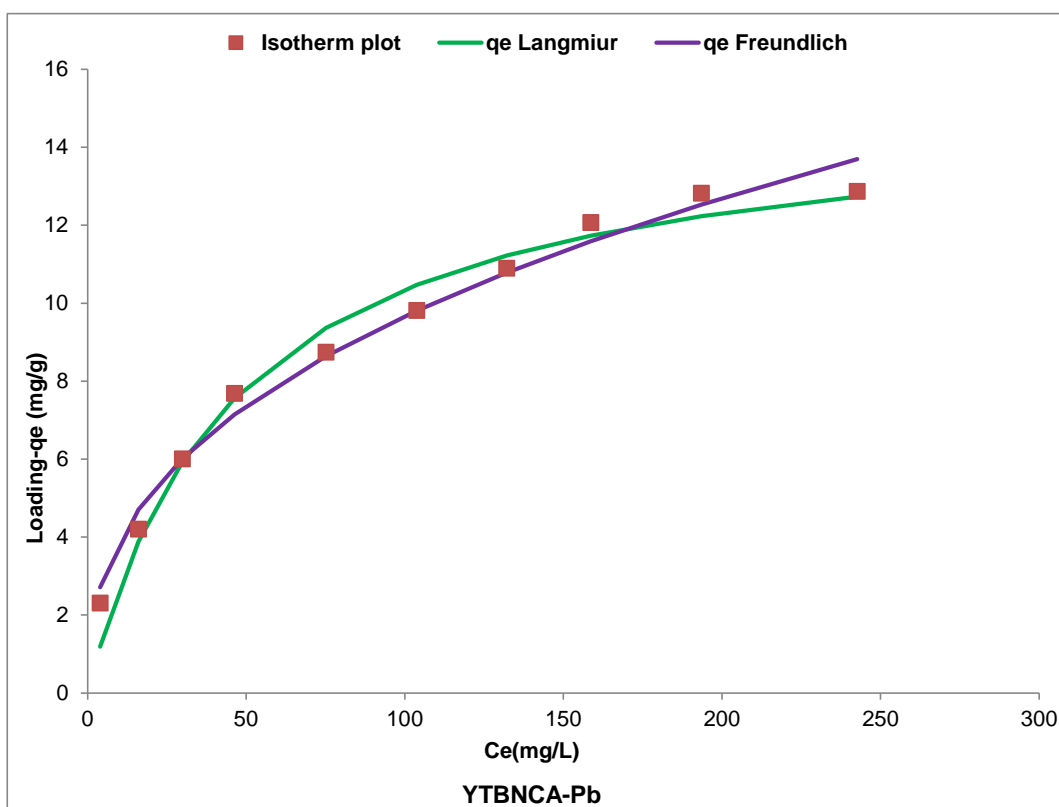
Figure 8.37: Equilibrium isotherm for Pb(II) ion on YTBNCA

The Langmuir isotherm affinity parameters K_L for the adsorbents are also seen Table 8.18 and range from 1.19×10^{-2} Lmg^{-1} for OPFNCA to 6.87×10^{-3} Lmg^{-1} for PTPNCA adsorbent. The Langmuir isotherm constant q_{max} values indicated that the PTHNCA adsorbent had the least maximum loading capacity (14.9mgg^{-1}) while the CCYBNCA adsorbent had the highest loading capacity (41.9 mgg^{-1}) for the Pb(II) ions and the trend in q_{max} for Pb(II) ion was CCYBNCA > PTPNCA > OPFNCA > CNFNCA > YTBNCA > PTHNCA. When compared with that for Cd(II) ion the trend was CCPNCA > PTPNCA > CCYBNCA > OPFNCA > CNFNCA > YTBNCA > PTHNCA. From this it can be observed that the PTHNCA adsorbent had the least q_{max} values for both Cd(II) and Pb(II) ion loading based on the Langmuir isotherm model while the highest q_{max} for Cd(II) was CCPNCA and for Pb(II) the adsorbent with highest q_{max} was CCYBNCA. The high loading of the Cd(II) and Pb(II) ions onto the Na_2CO_3 chemically activated carbon adsorbents implies that these adsorbents have high affinity for these toxic metal ions and can be used to scavenge them from contaminated adsorbate systems with a high level of efficiency. In order to place these materials in the context of current advances in adsorbents a comparison of the values of the q_{max} for the adsorbents in this study and those in reported literature were made as

shown in Table 8.19. From Table 8.19, it is observed that the maximum loading capacity q_{max} value for the adsorbents in this study compared favourably with those reported in literature.

Table 8.19: Comparison of Langmuir maximum loading capacity (q_{max}) for Na_2CO_3 chemical activated carbon and reported literature for Pb(II) ion.

Adsorbent	$q_{max}(mgg^{-1})$	Reference
Coffee residue carbon	63.29	Boudrahem *et al*,2009
Coconut shell activated carbon	21.88	Goel *et al*., 2005
Phaseolus aureus hull activated carbon	21.8	Rao *et al*., 2009
Euphorbia rigida activated carbon	1.23	Gercel and Gercel, 2007
OPFNCA	37.33	This study
CNFNCA	33.32	This study
CCPNCA	23.55	This study
CCYBNCA	41.89	This study
PTHNCA	14.87	This study
PTPNCA	41.68	This study
YTBNCA	15.19	This study

8.6.2.2 Freundlich isotherm

The Freundlich isotherm model plot for Pb(II) removal using the Na_2CO_3 chemically activated carbon adsorbents are shown in Figures 8.31 – 8.37 and the Freundlich isotherm parameter values obtained from these plots are shown in Table 8.18. The error parameter – the coefficient of determination (r^2) values for each isotherm evaluation of the experimental and model uptake data are also shown in Table 8.18. An examination of these r^2 values indicates that the correlation of the experimental values with the Freundlich model were high with values of 0.99 for OPFNCA and YTBNCA while the rest were in the range 0.93-0.97. These r^2 values implies that the Freundlich model for Pb(II) ion sorption had a better fit to the experimental data that what was obtained for Cd(II) ion sorption. Also, the Freundlich isotherm "intensity of adsorption parameter" n obtained from the modelling process showed all values were between 1.62 and 2.83 indicating that the intensity of Pb(II) ion sorption between the Na_2CO_3 chemically activated adsorbents is favourable (Sarada *et al*., 2014). The Freundlich isotherm parameter K_F that is associated with the "affinity and mobility" of the Pb(II) ion for the Na_2CO_3 chemically activated

adsorbents are shown in Table 8.18. This parameter implies that the Na_2CO_3 chemically activated carbon adsorbents had good affinity to the Pb(II) ions in the aqueous solution. From the results, the trend in K_F value is CNFNCA > CCYBNCA > OPFNCA > PTPNCA > YTBNCA > PTHNCA > CCPNCA, indicating the CNFNCA adsorbent had the highest affinity value of 4.42 $(mgg^{-1})(Lmg^{-1})^{1/n}$ while the CCPNCA has the least with a value of 0.52 mgg^{-1}. The trend in K_F value for the Cd(II) ions indicates that CNFNCA had the highest with a value of 6.93 mgg^{-1} while CCPNCA had the least with a value of 0.33 $(mgg^{-1})(Lmg^{-1})^{1/n}$, with the K_F value trend for Cd(II) being CNFNCA > CCYBNCA > OPFNCA > PTPNCA > YTBNCA > PTHNCA > CCPNCA. This indicates that the trend in K_F value for the Cd(II) and Pb(II) ion uptake using the Na_2CO_3 chemical activated carbon adsorbents were similar even though they differed in magnitude.

A comparison between the two isotherm models used to described the sorption of Pb(II) ion can carried using the values of the r^2 and the two error parameters to determine the model that describes the metal uptake process better. The chi square ($\chi2$) and the root mean square error (RMSE) values that are lowest indicate for a particular isotherm model indicates favourable fitting between the experimental equilibrium sorption data. An analysis of the results presented in Table 8.18 indicates a strong correlation between the experimental loading data and the Langmuir model with higher r^2 values that those of the Freundlich model for the Na_2CO_3 chemical activated carbon adsorbents. To further discriminate between the models, the values of the $\chi2$ and RMSE values for the Langmuir isotherm were lower than those of the Freundlich for all the adsorbents for the sorption of Pb(II) ions, thus the Langmuir isotherm described the metal ion process better than the Freundlich for all the adsorbents. Thus, it can be observed that the Langmuir isotherm model can be used as a representative equation that can describe the sorption of Pb(II) ion onto these chemically activated adsorbents. A comparison of the K_F value for Pb(II) ion removal obtained using the Na_2CO_3 chemically activated adsorbent and those reported in literature is shown in Table 8.20. These results indicate that the chemically activated adsorbents were also good adsorbents when compared to previous studies based on the values of the Freundlich isotherm parameter K_F.

Table 8.20: Comparison of K_F value for Pb(II) ion for Na_2CO_3 adsorbents with literature.

Adsorbent	$K_F(mgg^{-1})$	Reference
Phaseolus aureus hull activated carbon	7.5	Rao *et al.*, 2009
Coconut shell activated carbon	11.49	Goel *et al.*, 2005
Sulphur-modified coconut shell activated carbon	12.44	Goel *et al.*, 2005
Nut shell activated carbon	7.96	Tajar *et al.,* 2012
Eucalyptus camaldulensis Dehn bark carbon	0.37	Kongsuwan *et al.,* 2009
OPFNCA	4.55	This study
CNFNCA	6.93	This study
CCPNCA	0.32	This study
CCYBNCA	6.88	This study
PTHNCA	0.79	This study
PTPNCA	3.36	This study
YTBNCA	0.77	This study

8.7 Summary

The removal of Cd(II) and Pb(II) ions from aqueous solution was studied using Na_2CO_3 and K_2CO_3 chemically activated carbon adsorbents. The adsorbents were characterized using a range of physical and chemical characterization protocols. These include ash content, loss on attrition, adsorbent yield, pH and pHpzc, surface area and porosity and surface morphology and chemical composition. These results indicate that the Na_2CO_3 chemically activated carbon adsorbents had higher yields than the K_2CO_3 chemically activated carbon adsorbents. The ash content of the adsorbents was a function of the nature of the residue and the type of chemical activating agent used. The K_2CO_3 chemically activated carbon adsorbents had higher losses due to attrition than the corresponding Na_2CO_3 adsorbents. The values of the pH point of zero charge (pHpzc) of the adsorbents were in the range of 7.1-8 and these were closely associated with the adsorbent pH. The chemical activation process had a remarkable effect on the BET surface areas and pore properties of the resulting adsorbents as the values obtained were in the range of 827 m^2g^{-1} (CNFNCA) to 267 m^2g^{-1} (OPFNCA) and the adsorbents were mesoporous. There was also a considerable increase in total pore volume for these chemically activated carbon

adsorbents. The surface morphology of the adsorbents was also affected by the chemical activation process as the adsorbents had better more pores and these were observed from the results of the SEM imaging.

Effect of contact time and initial concentration on the sorption of Cd(II) and Pb(II) ions were studied for the adsorbents. The kinetics of metal ion sorption for both Cd(II) and Pb(II) ions on the Na_2CO_3 and K_2CO_3 chemically activated carbon adsorbents showed a two-stage kinetic profile- initial quick uptake up to 60 minutes followed by a slow and gradual metal ion removal lasting till 180 minutes. The results of the kinetics of Cd(II) and Pb(II) ion sorption indicated that for the Na_2CO_3 chemically activated carbon adsorbents, optimum uptake for Cd(II) and Pb(II) ions was obtained with the CNFNCA adsorbent with loadings of 27.7 mgg^{-1} for Cd(II) and 25.3 mgg^{-1} for Pb(II) ions. K_2CO_3 chemically activated carbon adsorbents, the CNFKCA adsorbent was the best with loadings of 28.2 mgg^{-1} for Cd(II) and 25.2 mgg^{-1} for Pb(II) ions. The optimum uptake obtained for these adsorbents was associated to the high BET surface area of the CNFNCA and CNFKCA adsorbents which were 827 m^2g^{-1} and 553 m^2g^{-1} respectively. A comparison of the results for the kinetics of Cd(II) and Pb(II) ion sorption indicated that for the chemically activated carbon adsorbents, the CNFKCA adsorbent was the best for Cd(II) ion removal with a loading of 28.2 mgg^{-1}, while for Pb(II) ion removal was best achieved using the CNFNCA adsorbent with a loading of 25.3 mgg^{-1}. Kinetic modelling was also carried out for the uptake of Pb(II) and Cd(II) on the Na_2CO_3 and K_2CO_3 activated adsorbents using the pseudo-first order(PFO) and pseudo-second order(PSO) equations. From the analysis , it was observed that the PFO model gave a better approximation of the kinetics of Cd(II) and Pb(II) sorption by the Na_2CO_3 and K_2CO_3 chemically activated adsorbents than the PSO order model. The quick first stage of cation uptake obtained in this study indicates that these chemically activated carbon adsorbents prepared in this study can be used as adsorbents effectively due to their fast kinetics.

Equilibrium isotherm modelling studies were also carried out using the Na_2CO_3 chemically activated carbon adsorbents. The results obtained for Pb(II) and Cd(II) indicate an increasing metal ion uptake with increasing concentration. The Langmuir and Freundlich isotherm models were used to characterize the metal ion loading. From the values of the fitting parameter (r^2 value) and the two error parameters-chi square (χ^2) and root mean square error (RMSE), the Langmuir isotherm had a better fit to the experimental equilibrium data for the sorption of Cd(II) and Pb(II) ions. The Langmuir isotherm

constant "q_{max}" was computed for the different adsorbents and the results indicates that the value of q_{max} for both Cd(II) and Pb(II) uptake from aqueous solution onto the adsorbents were comparable with that reported in literature. The Langmuir isotherm constant q_{max} values indicated that for Cd(II) ion sorption, the CCPNCA adsorbent had the highest value (29.4 mgg^{-1}), while the YTBNCA adsorbents had the least (15.7 mgg^{-1}). For the Pb(II) ion sorption, the PTHNCA adsorbent had the least maximum loading capacity (14.9mgg^{-1}) while the CCYBNCA adsorbent had the highest loading capacity (41.9 mgg^{-1}). These results were comparable with those reported in previous literature for activated carbon adsorbents obtained from biomass and also implies that the prepared adsorbents developed in this study were effective for Cd(II) and Pb(II) ion removal from aqueous systems. Therefore, these materials are suitable cost effective adsorbents for use in the treatment of heavy metal effluents in the developing countries.

CHAPTER NINE

COMMERCIAL ACTIVATED CARBON

CHAPTER NINE

9.0 Commercial activated carbon adsorbent

The residue adsorbents and prepared carbon adsorbents in this study were examined to explore their capability for metal removal from aqueous systems. Activated carbon has gained widespread use for the treatment for heavy metal ions and other pollutants because of its inherent physical properties such as large surface area, porous structure, high adsorption capacity and large reactive surface (Shrestha *et al.,* 2013). It is widely used due to its exceptional high surface area (ranges from 500 to 1500 m^2g^{-1}), well developed microporosity and wide spectrum of surface functional groups and these properties of activated carbon are generally controlled by the manufacturing process which depends on the nature of raw materials, activating agents and conditions of activation (Rivera- Utilla *et al.,* 2011; Selomulya *et al.,* 1999).

The residues and synthesized carbon adsorbents discussed in the previous chapters of this work were designed as potential candidate adsorbents that can be used as substitutes for commercial activated carbon adsorbents in a developing country (Nigeria) for the treatment of heavy metal polluted effluents and natural water bodies. Thus, to compare the properties and ability of the adsorbents prepared in this work with what is commercially available, a commercially produced activated carbon (Chemviron Carbon sample F-440) was used as described in Section 4.2.6. The characterization of both physical and chemical properties of the commercial activated carbon (CGAC) was carried out. In addition kinetic and equilibrium sorption of Cd (II) and Pb (II) was also studied from which equilibrium and kinetic modelling of the sorption of Pb(II) and Cd(II) ions onto the adsorbent were also carried out.

9.1 Adsorbent characterisation

The commercial activated carbon used for comparison in this study was characterised to determine its surface area and porosity, surface morphology, ash content, loss on attrition, pH and pHpzc based on the methodology reported in chapter 4 of this work and subsequent chapters thereafter and the results are shown in Table 9.1. The N_2 adsorption-desorption

isotherm and pore size distribution of the commercial activated carbon (CGAC) is shown in Figure 9.1.
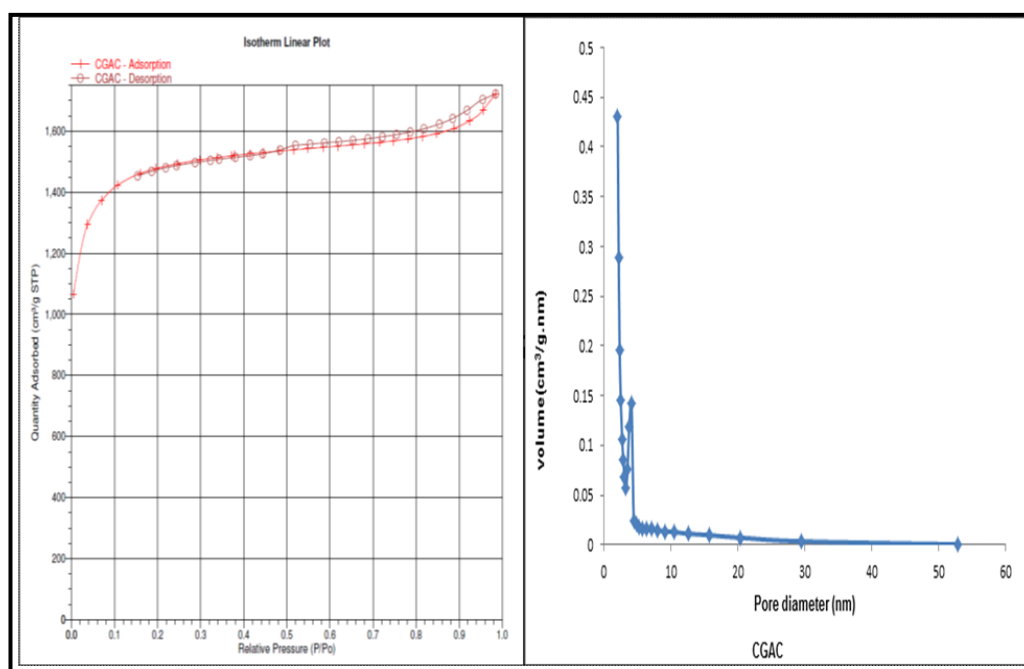
Figure 9.1: N_2 adsorption-desorption isotherm and pore size distribution of CGAC

Figure 9.1 and results from Table 9.1 indicates that the activated carbon has a very high BET surface area of 4273 m^2 g^{-1} as would be expected of commercial prepared activated carbon with an average pore diameter of 4.48 nm and a total pore volume of 2.66 cm^2 g^{-1}. The CGAC activated carbon also exhibits a narrow bimodal pore size distribution between 3-12nm, while a wider distribution is observed from 15-52nm which is similar to what was observed in the Na_2CO_3 and K_2CO_3 chemically activated carbon adsorbents in chapter 8 of this work. Based on the N_2 adsorption-desorption isotherm which indicates a type IV adsorption isotherm and the pore size, the CGAC adsorbent can be classified as a mesoporous adsorbent. The CGAC adsorbent N_2 adsorption-desorption isotherm also indicates the presence of a H1 type hysteresis loop that is present in adsorbents with narrow distribution of pore sizes (Naumov, 2009). The total pore volume of an adsorbent is also used as a measure of adsorption loading since its measurement is based on the amount of adsorbate (liquid nitrogen) adsorbed (Tsai *et al.,* 2001). However, this approach has some limitations in its scope of application. Firstly, this can only be applicable to gaseous adsorbents that would be used at the temperature of the nitrogen adsorption measurement as the extrapolation of this to gaseous adsorption to conditions at different

temperature, pressure and adsorbate composition cannot be directly made (Tsai *et al.,* 2001).

Table 9.1: Characteristics of CGAC adsorbent

Characteristic	CGAC
BET surface area (m^2g^{-1})	4273
Total pore volume (cm^3g^{-1})	2.66
BJH desorption average pore diameter (nm)	4.48
Ash content (%)	10.9
Loss on attrition (%)	4.10
pH	7.80
pHpzc	7.20

However, pore volume is used to give characteristic information on the capability of the material to adsorb molecules which can be extrapolated to liquid systems. Hence its utilisation as a parameter in the characterisation of carbon based adsorbents used in aqueous systems. The high pore volume of the CGAC adsorbent indicates that it has substantial pores to adsorb adsorbates.

The morphology of the CGAC adsorbent before and after adsorption of Cd(II) and Pb(II) ions was determined using a scanning electron microscope as described in Section 4.3.2. EDAX analysis of the chemical composition of the adsorbent was also carried out. SEM micrographs enables the direct observation of changes to surface microstructures of carbons, Goel *et al.,* (2005) and the images of the commercial activated carbon before and after sorption of Cd(II) and Pb(II) ions are shown in Figures 9.2-9.4. From the results, the surface of activated carbon was observed to be rough and coarse with irregular crevices that indicate pore openings for metal ion transport. The SEM micrographs also indicate the presence of corrugated surfaces with boundary edges on the CGAC adsorbent and these were still present in the micrographs of the CGAC adsorbent after metal ion sorption (Fig.9.3 and 9.4)
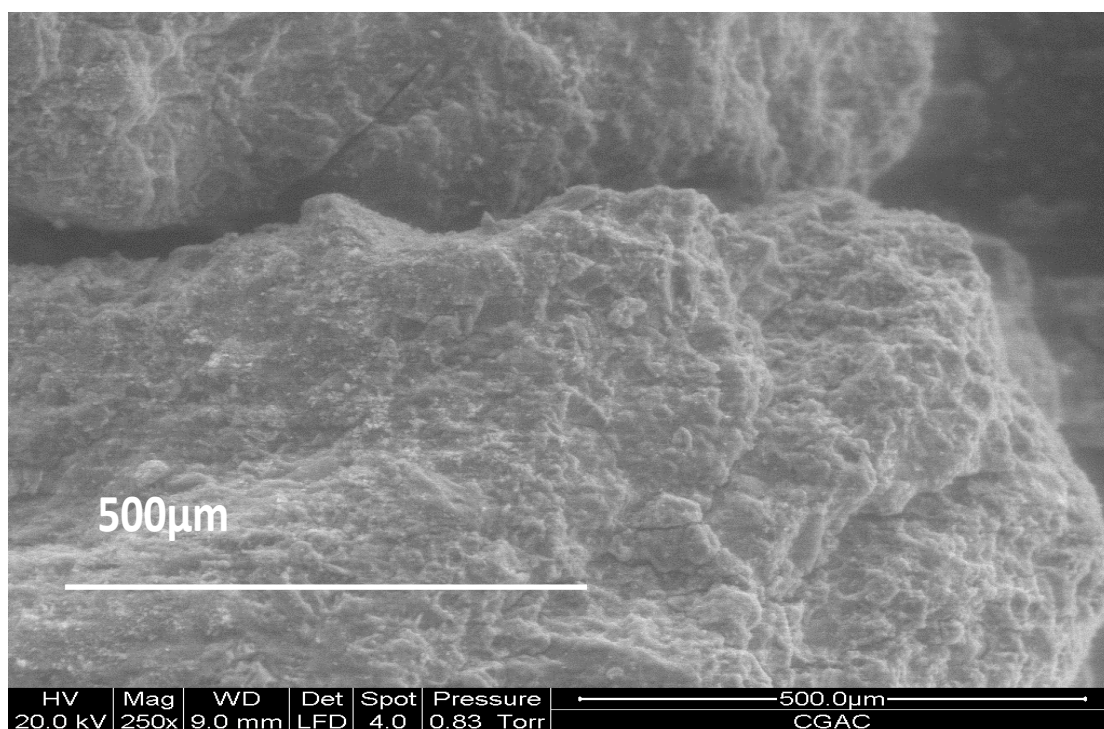
Figure 9.2: SEM micrograph of commercial activated carbon CGAC (Scale bar =500 µm)
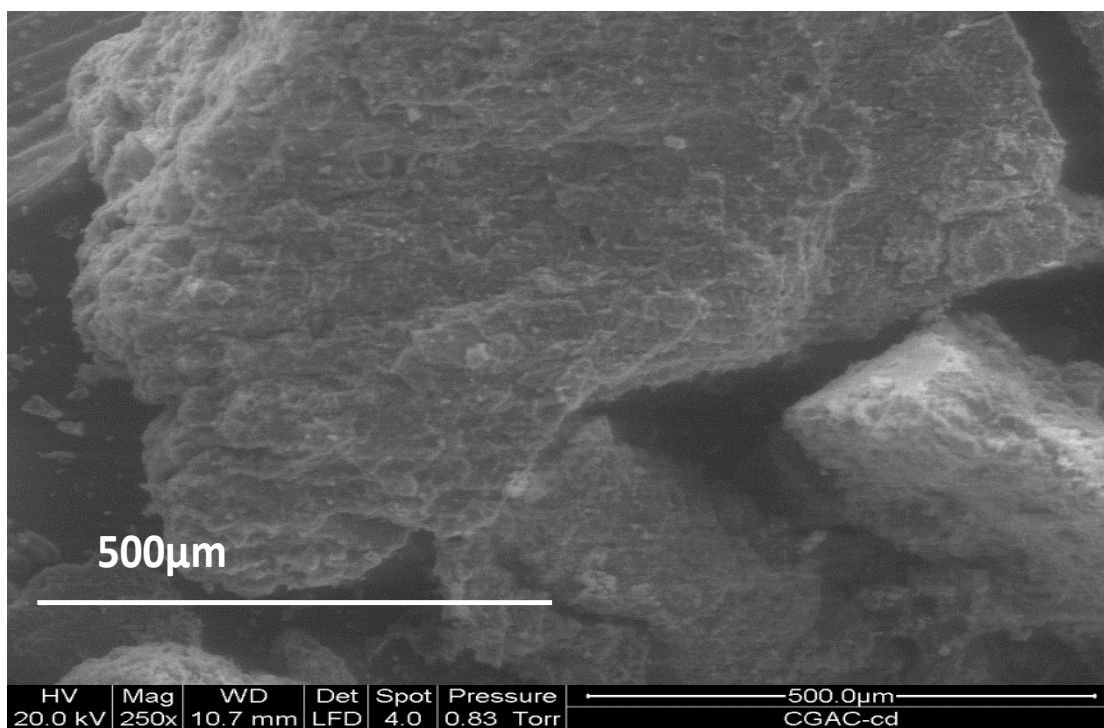
Figure 9.3: SEM micrograph of CGAC after Cd(II) adsorption (CGAC-Cd) (Scale bar = 500 µm).
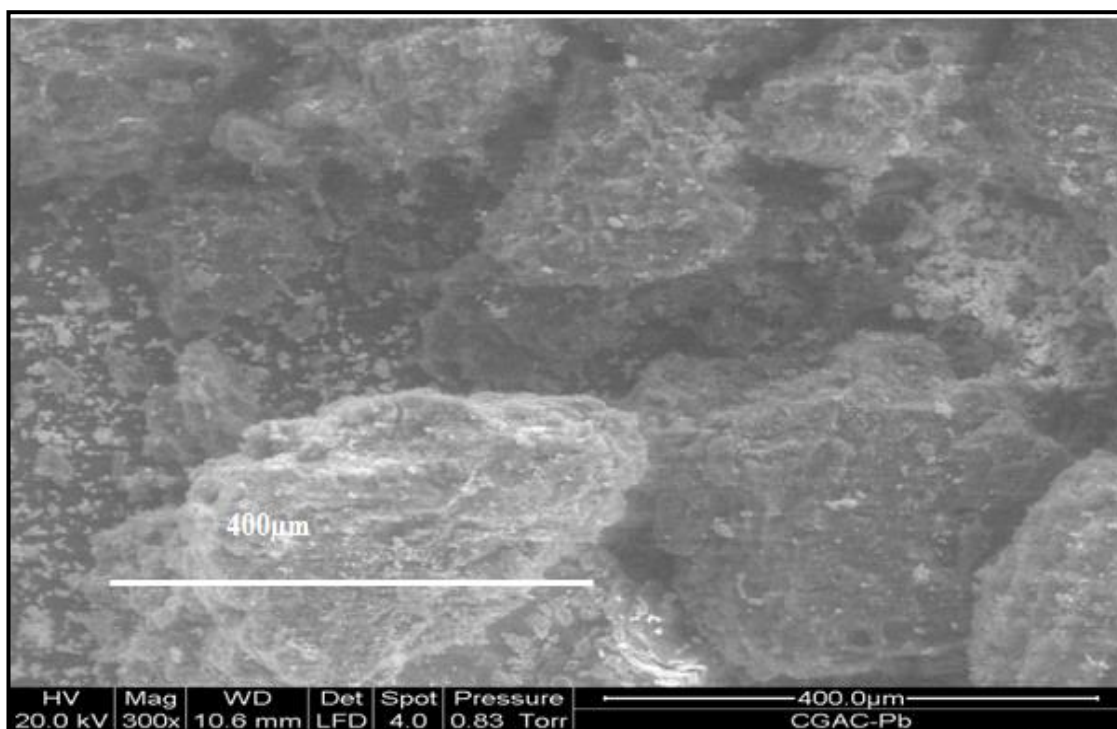
Figure 9.4: SEM micrograph of CGAC after Pb(II) adsorption (CGAC-Pb) (Scale bar = 400 μm)

CGAC	
Element	Wt %
C	89.82
O	5.5
Al	1.16
Si	1.42
Mo	1.87
Ca	0.23
Total	100
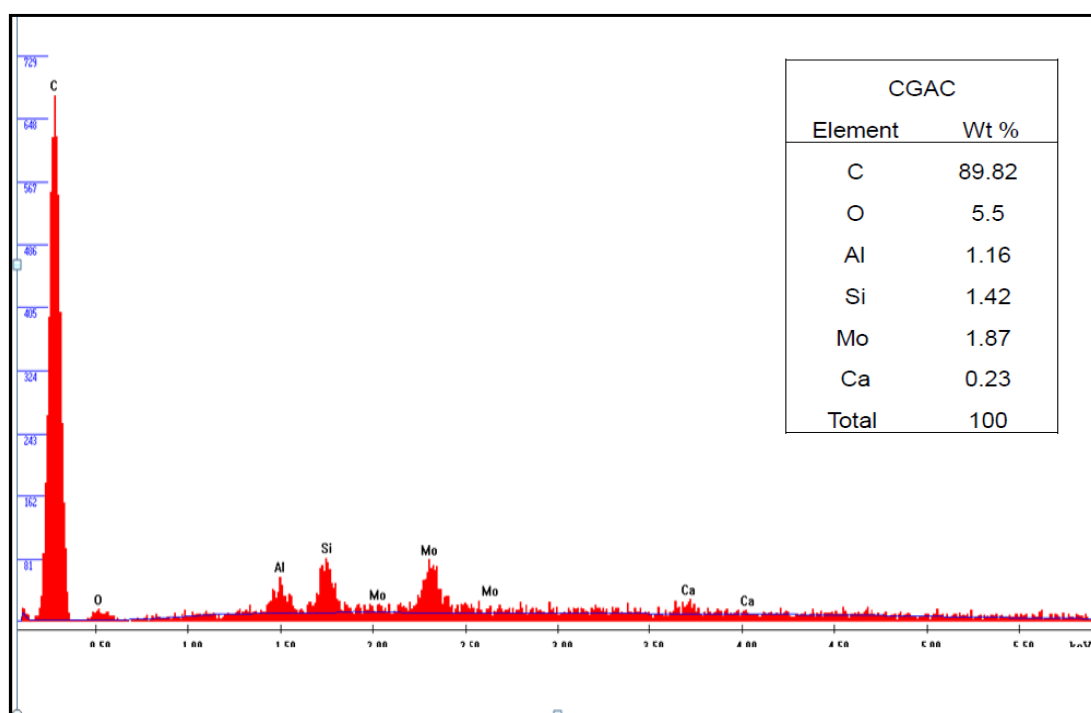
Figure 9.5: EDAX spectrum of CGAC adsorbent
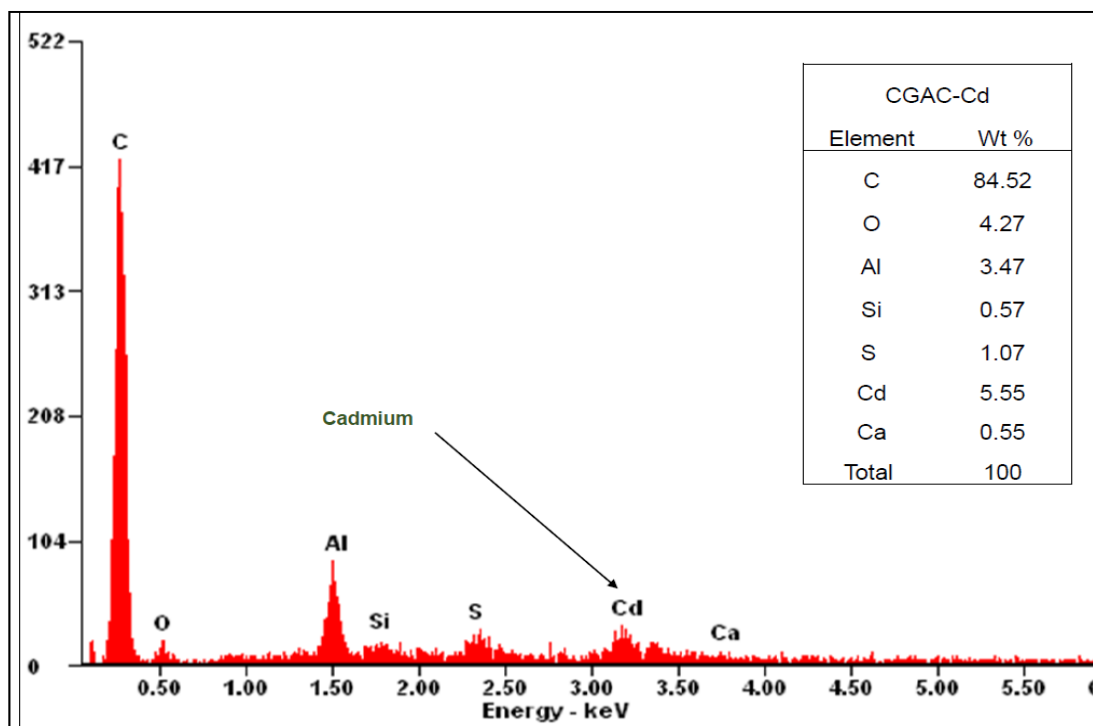
Figure 9.6: EDAX spectrum of CGAC adsorbent after Cd adsorption (CGAC-Cd)
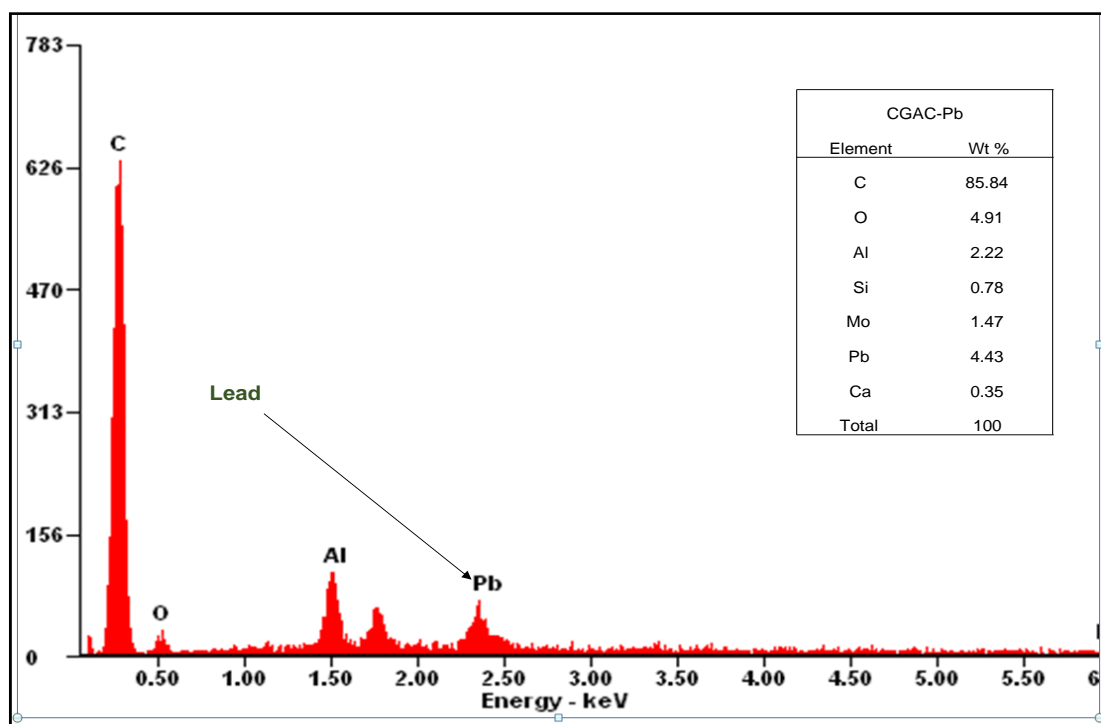
Figure 9.7: EDAX spectrum of CGAC adsorbent after Pb adsorption (CGAC Pb)

The EDAX spectrum of the of the CGAC adsorbent is shown in Figure 9.5 and it indicates that the commercial activated carbon adsorbents had a high carbon content (89.82%), an oxygen content of 5.5% and quantities of aluminium, silicon, molybdenum and calcium

476

which are responsible for its high ash content of 10%. The spectra after metal ion sorption are shown in Figure 9.6 for Cd(II) ion and Figure 9.7 for Pb(II) ion sorption. The EDAX spectrum for each sorption process shows corresponding peaks for the metal ions Cd(II) & Pb(II) confirming their existence on the surface of the activated carbon adsorbent after sorption was carried out. It is also pertinent to observe that the carbon and oxygen content of these used activated carbon adsorbents were lower than that of fresh adsorbent presented in Figure 9.5. This may be associated to the effect of the washing and filtering step of the used adsorbent. The results of the EDAX analysis of the CGAC adsorbent before and after Cd(II) and Pb(II) ion sorption lends credence to the observation that the CGAC adsorbent was able to remove these metal ions from their respective aqueous solutions. This observation has also been reported by Erdem *et al.,*(2013) in their study on the accumulation of Pb(II) onto activated carbon derived from waste biomass, wherein the existence of Pb(II) ion peak on the EDAX spectrum was used to prove the accumulation of the metal ion on the adsorbent.

9.2 Adsorption Kinetics

The study of metal ion sorption kinetics can provide insight on the rate and mechanism of sorption as it gives information that can be used to understand the type of adsorbent-adsorbate interaction and the mechanism of adsorbate removal. Adsorption experiments to study the effect of contact time on the removal of cadmium (II) and lead (II) metal ions from aqueous solutions were carried out at pH7 and a temperature of 25°C using 500mgL^{-1} metal ion concentration using a 100ml metal ion-adsorbent system at 200 rpm. Sorption experiments were carried out for the following time intervals: 5, 10, 15, 20, 25, 30, 40, 60, 90, 120 and 180 minutes.

The kinetic profiles for the sorption of the two metal ions are presented in Figure 9.8 and indicates that for both metal ions {Cd(II) and Pb(II)} sorption took place via two stages namely - a fast sorption uptake that occurred within 30minutes of sorbate–sorbent contact. This was followed by a slow phase of metal ion removal that developed from 40 minutes until 180 minutes when an equilibrium or quasi-stabilised state was presumed to have been reached. The metal ion loadings after 180 minutes were 17.23 mgg^{-1} for Cd(II) ion and 16.84 mgg^{-1} for Pb(II) ion.

The two stage kinetic profile for both Cd(II) and Pb(II) ions can be associated to the nature and types of available surface sites for adsorption. When the sorbent-sorbate contact is

established at the onset of sorption there are a large number of available sites for sorption to occur, hence the fast metal ion uptake observed. However, as the uptake proceeds and readily available sites are occupied, the rate of further adsorption is diminished due a combination of factors such as repulsive forces between the already adsorbed metal ions and the incoming sorbate and the limitation of available sites for occupation. This gradual occupancy of the remaining available sites will thus proceed at a slower rate than when there were abundant sites at the inception of the sorption. This two-phase trend in sorption kinetics has been also reported in literature by a number of studies.
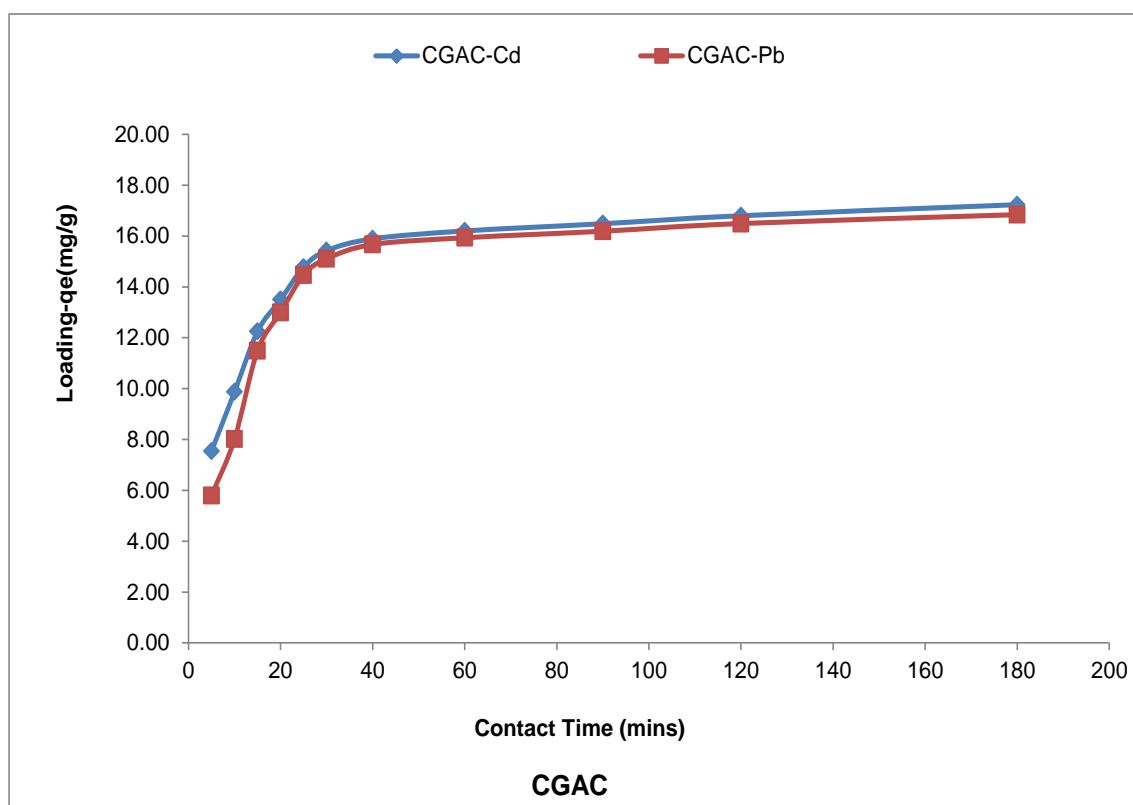
Fig. 9.8 Effect of contact time on metal ion loading on commercial activated carbon

Ibrahim *et al.,* (2010) reported that the adsorption of Pb(II) ions onto a novel agricultural waste adsorbent (modified soda lignin) proceeded via a fast initial stage and a slow second stage until the attainment of equilibrium. A sharp increase in the amount of Cu(II) ion adsorbed by chemically modified orange peel within an initial duration of (0-30minutes) that was followed by a slow sorption until 120 minutes has also been reported by Feng *et al.,* (2009). Similar conclusions on the effect of contact time on sorption of adsorbate onto adsorbents have been proposed by studies reported in literature (El-Ashtoukhy *et al.*, 2008;

478

Iqbal *et al.*, 2009b). According to Liang *et al.,* (2010), this fast and slow two step kinetic sorption regime for the removal of metal ions has significant practical importance in the design of large scale adsorption systems and would imply that if a scale up system is to be designed. The adsorber has to be configured in such a manner that the fast kinetics profile observed for this type of adsorbent is exploited to improve removal efficiency within a short time interval. This may require a system that allows for optimum contact of the adsorbate system with the adsorbent with an efficient mixing cycle.

9.2.1 Kinetic modelling of Cd(II) and Pb(II) ion sorption on CGAC adsorbent

The uptake of Pb(II) and Cd(II) ions by the CGAC adsorbent was also modelled using two adsorption reaction models-the pseudo fist order (PFO) and the pseudo second order (PSO) equations which have been discussed in previous chapters of thesis. The PFO and PSO models were evaluated using the non- linear method, a trial and error procedure. This method is designed to determine isotherm parameters by minimizing the respective coefficient of determination between experimental data and isotherm models using the solver add-in in Microsoft excel (Brown, 2001; Wong *et al.,* 2004). To determine the goodness of fit of the kinetic models to the experimental data using non-linear regression, the optimization procedure requires that error functions be defined to enable the fitting of the model parameters with the experimental values. In this study, the coefficient of determination (r^2), the root mean square error (RMSE) and the Chi square test (χ^2) were used as error parameters for each model and these were determined based on eqns. 5.4, 5.5 and 5.6 which have been previously described in section 5.11 of chapter 5 in this study.

The plots of the PFO and PSO models for Cd(II) sorption by the CGAC adsorbents are presented in Figures 9.9 for Cd(II) ion and 9.10 for Pb(II) ion. From these models, the kinetic parameters and their respective error functions obtained are presented in Table 9.2. An examination of Figures 9.9 and 9.10 indicates that both PFO and PSO could be used to characterise the kinetics of metal ion sorption and their prediction of the parameter $(qe,_{model})$ is close to the result obtained from the experimental analysis of Pb(II) and Cd(II) ion sorption. For the PFO model the $q_{e,cal}$ obtained for the GCAC adsorbent for Cd(II) ion sorption was 16.5 mgg^{-1}, while that for Pb(II) was 16.4 mgg^{-1} indicating a close association of the sorption of both metal ions. The rate constant of the pseudo first order reaction (K_1) for the two metal ions were; 9.43×10^{-2} min^{-1}(CGAC-Cd) and 7.77×10^{-2} min^{-1}(CGAC-

Pb). The value of the coefficient of determination (r^2) and the two error parameters – the root mean square (RMSE) and Chi square (χ^2) can be used to determine the metal ion uptake kinetics is best described by the PFO model.
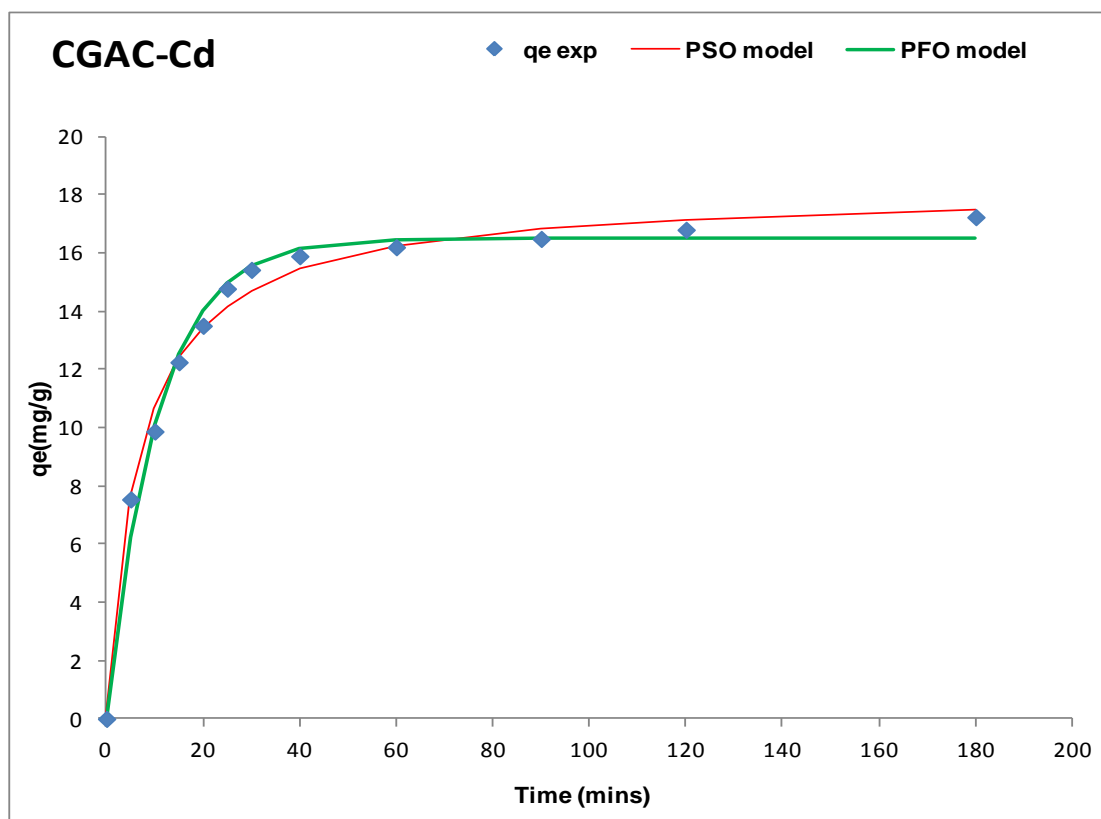
Fig 9.9: PFO & PSO kinetic models for Cd(II) ion sorption onto CGAC adsorbent

From Table 9.2, it is observed that both metal ions had the same r^2 value of 0.99. Hence, to further discriminate amongst them, the χ^2 and the RMSE values are used with the lower values being an indication of a better fitting to the experimental data. Based on this assumption, the sorption of Pb(II) ion onto the CGAC adsorbent is best described by the PFO model with the lower χ^2 (0.01) and RMSE (7.10×10^{-2}) values.
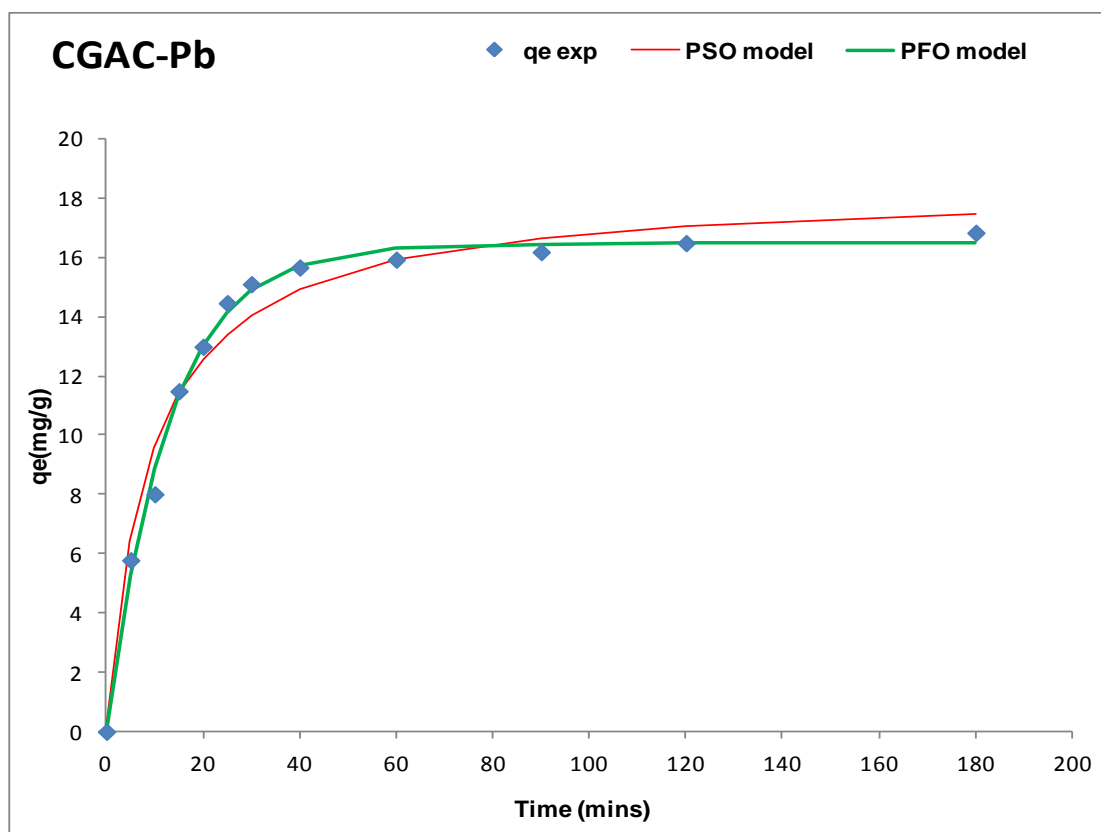
Fig. 9.10: PFO & PSO kinetic models for Pb(II) ion sorption onto CGAC adsorbent

Table 9.2: PFO and PSO kinetic parameters for Cd(II) & Pb(II) sorption on CGAC

Kinetic Models	Parameters	Adsorbent	
		CGAC-Cd	CGAC-Pb
Pseudo First Order (PFO)	$q_{e,cal}(mgg^{-1})$	16.5	16.4
	$K_1(min^{-1})$	9.43E-02	7.77E-02
	r^2	0.99	0.99
	RMSE	1.32E-01	7.10E-02
	χ^2	0.02	0.01
Pseudo Second Order(PSO)	$q_{e,cal}(mgg^{-1})$	18.1	18.4
	$K_2(gmg^{-1}min^{-1})$	7.88E-03	5.88E-03
	$h(mgg^{-1}min^{-1})$	2.59	1.99
	r^2	0.99	0.98
	RMSE	9.22E-02	3.05E-01
	χ^2	0.01	0.04

The PSO model evaluation of the kinetics of CGAC sorption of Pb(II) and Cd(II) ions are presented also presented in Table 9.2. From this table the PSO rate constant (K_2) for Cd(II) ion was 7.80×10^{-3} $gmg^{-1}min^{-1}$(CGAC-Cd) while that for Pb(II) was 5.88×10^{-3} $gmg^{-1}min^{-1}$(CGAC-Pb). From this model, the initial sorption rate (h) obtained from the PSO model as $q_t/t \rightarrow 0$ which gives an indication of the intial kinetic rate of sorption was 2.59 $mgg^{-1}min^{-1}$ (CGAC-Cd) and 2.59 mgg^{-1} min^{-1} (CGAC-Pb). This indicates that the sorption of Cd(II) ions onto the CGAC adsorbent was faster than that of Pb(II) ions. The values of the metal ion loading obtained from the PSO model ($q_{e,cal}$) was 18.1mgg^{-1} (CGAC-Cd) and 18.4 mgg^{-1}(CGAC-Pb) indicating a higher loading of Pb(II) ions onto the commercial activated carbon adsorbent than Cd(II) ions.

The value of the coefficient of determination (r^2) and the two error parameters – the root mean square (RMSE) and Chi square (χ^2) can be used to determine the kinetics of metal ion sorption that is best described by the PSO model. The value of the error parameters and the r^2 value for both metals for the PSO model are presented in Table 9.2. From table 9.2 it is observed that the CGAC-Cd adsorbent had a higher r^2 value (0.998) than the CGAC-Pb adsorbent. Also an evaluation of the two error parameters indicates that the CGAC adsorbent uptake of Cd(II) ion is better described by the PSO model with the lower χ^2 (0.01) and RMSE (9.822×10^{-2}) values. Hence it can be observed that the PFO model described the sorption of Pb(II) ion better, while the PSO described the sorption of Cd(II) ion better. Thus, it can be said that based on the kinetic modelling, the rate limiting step of Pb(II) ion sorption onto the CGAC adsorbent is dependent on the concentration of the Pb(II) ions in the adsorbate, while the sorption of Cd(II) ions onto the CGAC adorbent has a chemisorption rate-controlling mechanism.

9.3 Equilibrium isotherm modelling

The knowledge of sorbate/sorbent interaction at equilibrium is an essential tool in adsorption design and the use of equilibrium isotherm is one of the common methods deployed to obtain this information. According to Yaneva et *al.,* (2013), the essential issue is the understanding of the specific relationship between the pollutant concentration and its uptake degree by the solid phase at constant temperature and this is used to construct adsorption isotherms. Equilibrium studies were carried out for the removal of Cadmium (II) and Lead (II) ions from aqueous system using the commercial activated carbon (CGAC). The range of initial metal ion concentration was from 50 mgL^{-1} to 500 mgL^{-1} as

previously reported in the methodology section (chapter four) of this thesis. The amount of CGAC used was 1 g and 0.2 L solution was used and the experiment was carried out at 25°C and a pH of 7.

From the study, metal ion loading on the adsorbent was calculated and in this study, the Langmuir and Freundlich isotherms were used to characterise the adsorption process. The Langmuir and Freundlich isotherm models were evaluated using the non- linear method, a trial and error procedure. This method is designed to determine isotherm parameters by minimizing the respective coefficient of determination between experimental data and isotherm models using the solver add-in in Microsoft excel (Brown, 2001; Wong *et al.,* 2004). To determine the goodness of fit of the isotherm models to the experimental data using non-linear regression, the optimization procedure requires that error functions be defined to enable the fitting of the model parameters with the experimental values. In this study, the coefficient of determination (r^2), the root mean square error (RMSE) and the Chi square test (χ^2) were used as error parameters for each model and these were determined based on eqns. 5.4, 5.5 and 5.6 which have been previously described in section 5.11 of chapter 5 in this study. The isotherms obtained for the sorption of Cd(II) ions are shown in Figure 9.11 and that for Pb(II) are presented in Figure 9.12. From the isotherm plots, the isotherm parameters were obtained and are presented in Table 9.2.

For Cd(II) ion sorption, an examination of Fig. 9.11 indicates that the metal ion loading on the adsorbent increased from 3.15 mgg^{-1} for an initial metal ion concentration of 50 mgL^{-1} to 20.41mgg^{-1}for 500 mgL^{-1} and from Figure 9.12 it can be observed that the loading of Pb(II) on the CGAC adsorbent increased with increase in initial metal ion concentration from 4.68 mgg^{-1} for 50 mgL^{-1} to 20.32 mgg^{-1} for 500 mgL^{-1} of adsorbate. These equilibrium data were then fed into the Excel solver add-in program to provide an optimisation process for obtaining the isotherm parameters and the results from the process are shown in Table 9.2. The Freundlich isotherm is based on the assumption of an exponential distribution of adsorption sites and energies-heterogeneous surface (Hashemian *et al.*, 2013). The Freundlich constant "K_F" which relates to adsorption capacity for both metal ion loading on CGAC adsorbent were 1.20 (mgg^{-1})(Lmg^{-1})$^{1/n}$ for Cd(II) and 6.63 (mgg^{-1})(Lmg^{-1})$^{1/n}$ for Pb(II). This indicates that based on the Freundlich adsorption assumption model, the loading of Pb(II) was higher than that of Cd(II) on the CGAC adsorbent. Furthermore, the Freundlich constant "n" which relates to the intensity

of adsorption (Hashemian *et al.*, 2013) were 1.99 for Cd(II) and 4.854 for Pb(II) indicating more favourability of the Pb(II) ion sorption on the CGAC adsorbent.

The Langmuir isotherm assumes that the surface has homogeneous binding sites, equivalent sorption energies and no interaction between adsorbed species and its relevant parameters are Langmuir constant "K_L" which refers to the energy constant related to the heat of adsorption capacity and "q_{max}" which represents the maximum loading capacity of the adsorbent (Hashemian *et al.*, 2014). For the two metal ions the Langmuir constant value was 8.8×10^{-3} for Cd(II) and 1.10×10^{-1} for Pb(II) indicating that the Pb(II) loading onto the surface of the CGAC has a lower heat of adsorption. The Langmuir loading capacity constant for Cd(II) was 27.29 mgg^{-1} and that of Pb(II) was 20.30 mgg^{-1}. This indicates the value for the maximum amount of metal ion that can adsorbed on the CGAC adsorbent, thereby implying that the loading of Cd(II) was higher on the adsorbent than that of Pb(II) ion.
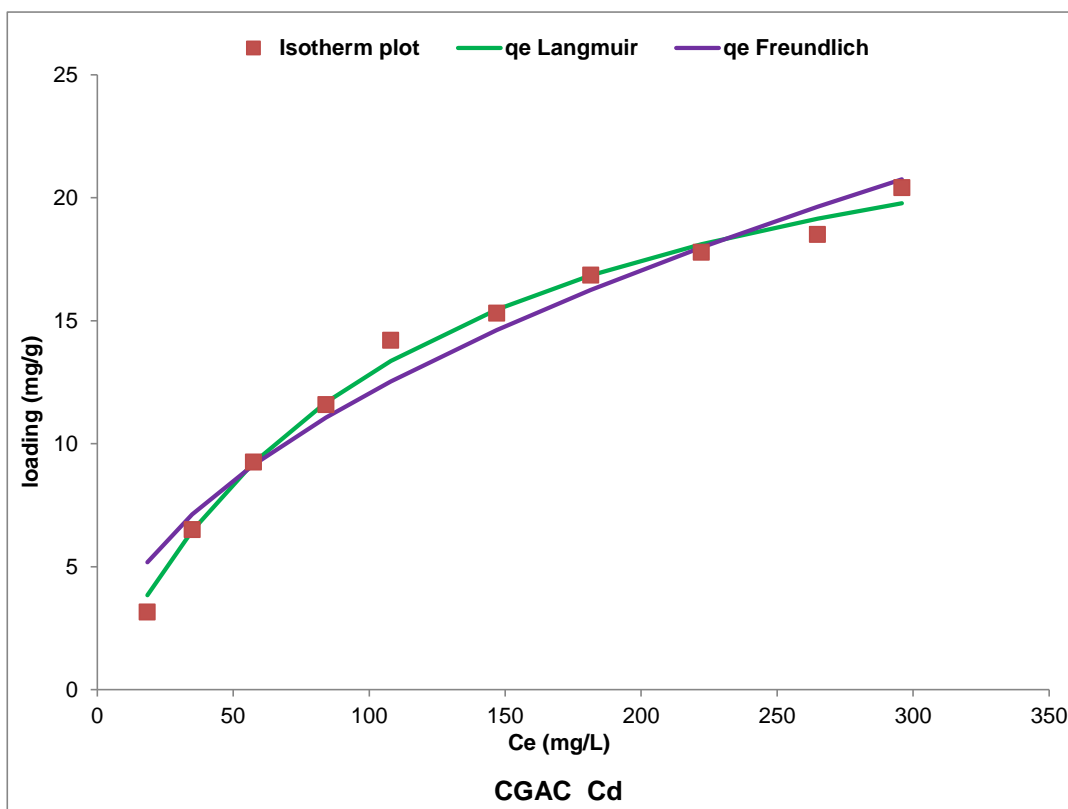
Figure 9.11: Langmuir & Freundlich adsorption isotherms for Cd (II) ions on CGAC

Table 9.3: Isotherm Parameters for Cd (II) and Pb (II) ions on CGAC

Isotherm Models	Parameters	Adsorbent	
		CGAC-Cd	CGAC-Pb
Langmuir	$q_{max}(mgg^{-1})$	27.3	20.3
	$K_L(lmg^{-1})$	4.50E-02	1.10E-01
	r^2	0.95	0.99
	χ^2	1.38E-01	1.10E-02
	RMSE	1.55	0.11
Freundlich	$K_F(mgg^{-1})(Lmg^{-1})^{1/n}$	6.99	6.63
	n	4.00	4.85
	r^2	0.86	0.87
	χ^2	3.21E-01	1.83E-01
	RMSE	3.90	1.86
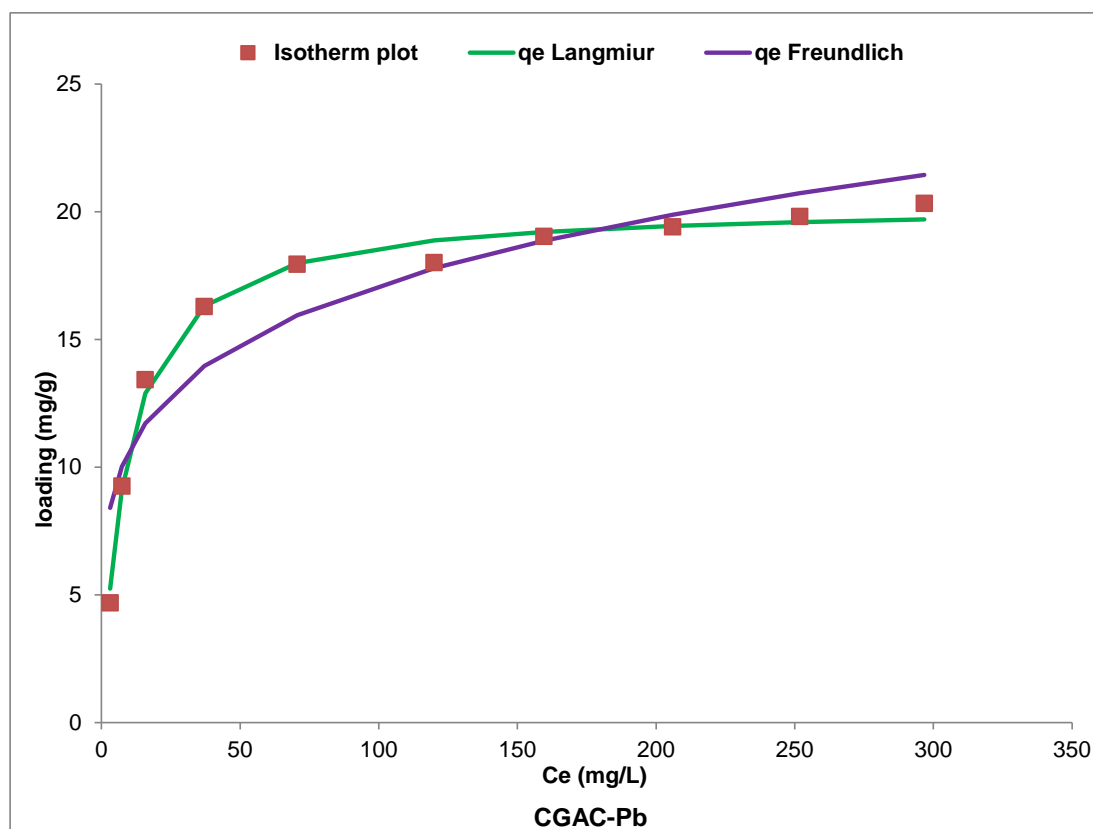
Figure 9.12: Langmuir & Freundlich adsorption isotherms for Pb (II) ions on CGAC

A comparison of the fitting of the two models to the experimental data was also carried out based on the parameters obtained from the two models. The fitting parameters were the co-efficient of determination-r^2, the two error parameters- chi square (χ^2) and root mean square error (RMSE) and these are presented in Table 9.3. From Table 9.3 it can be observed that the Langmuir model describes the uptake of Pb(II) ion by the CGAC adsorbent better than that of the Cd(II) ion as it r^2 value is higher for Pb(II) ion than Cd(II) ion, while the values of RMSE and χ^2 are lower for Pb(II) ion than Cd(II) ion. For the Freundlich model, the same observation can also be made as the isotherm fits the Pb(II) ion better than that of the Cd(II) ion based on the values of r^2, χ^2 and RMSE. Comparison of the isotherm model parameters for the two isotherms indicates that the Langmuir isotherm fits the experimental sorption data better than the Freundlich model as its r^2 values for both Cd(II) and Pb(II) ions sorption are higher than those for the respective ions for the Freundlich. In addition the values for the two error parameters- RMSE and χ^2 are significantly lower for the Langmuir model than for the Freundlich. Hence the Langmuir isotherm is the better isotherm for the description of Cd(II) and Pb(II) ions sorption by the CGAC adsorbent.

Previous studies on the adsorption of Cd(II) ion commercial activated carbon (CAC) has been reported by Kannan and Rengasamy (2005) and the Langmuir loading capacity obtained from the study was 4.29mgg^{-1} and a Langmuir constant "K_L" value of 9.84. In a similar work, Goel et al., (2005) reports on the removal of Pb(II) using granular activated carbon via batch and column sorption and their Langmuir constant "K_L" was 3.5 Lmg^{-1} and the Langmuir maximum loading constant "q_{max}" was 21.88 mgg^{-1}. They also reported Freundlich isotherm constant values of 11.49 (mgg^{-1})(Lmg^{-1})$^{1/n}$ for "K_F" and 2.44 for the "n" Freundlich constant. Thus, it can be inferred that CGAC used in this study was good representative adsorbent for use in this work as its parameters are within the range reported in literature for commercial activated carbon. Thus, it can also serve as a good benchmark for the evaluation of the effectiveness of the adsorbents synthesised via the different thermo-chemical regimes explored in this thesis.

9.4 Summary

The characterisation and use of a commercial activated carbon (CGAC) for Cd(II) and Pb(II) metal ion sorption studies was carried out in this chapter. The activated carbon had high surface area and porosity properties and SEM and EDAX analysis of the fresh and used adsorbents gave insight into the morphology and chemical nature of the adsorbents. The CGAC adsorbent had a high BET surface area of $4273m^2g^{-1}$, with a total pore volume of 2.66 cm^3g^{-1} and it had pores with average diameter of 4.48nm. Thus the CGAC adsorbent can be considered to be a mesoporous activated carbon adsorbent with high surface area and considerable pore volume. The adsorbent morphology showed that the adsorbent surface was rough and coarse with irregular crevices.

Kinetic and equilibrium metal ion sorption studies were carried out and the adsorbent showed a considerable loading of the two metal ions. The kinetics of Cd(II) and Pb(II) ions sorption using the CGAC adsorbent showed a two-stage kinetic profile- initial quick uptake occurring within 30 minutes followed by a slow and gradual removal of the two metal ions until 180 minutes. The kinetics also indicated that optimum loading obtained after 180 minutes of experiment was 17.23 mgg^{-1} and 16.84 mgg^{-1} for Cd(II) and Pb(II) ions respectively. The kinetic modelling using the pseudo first order (PFO) and pseudo second order (PSO) models indicates that the PFO model described the sorption of Pb(II) ion better, while the PSO described the sorption of Cd(II) ion better.

Isotherm modelling was carried out using Langmuir and Freundlich models and it was observed that the Langmuir and Freundlich models describes the uptake of Pb(II) ion by the CGAC adsorbent better than that of the Cd(II) ion. A comparison of between the two models indicates that the Langmuir isotherm is the better isotherm for the description of Cd(II) and Pb(II) ions sorption by the CGAC adsorbent. The maximum loading capacity (q_{max}) obtained from the Langmuir isotherm was 27.3mgg^{-1} and 20.3mgg^{-1} for Cd(II) and Pb(II) ions respectively, thus indicating that CGAC adsorbent had higher affinity for the Cd(II) ion. These metal ion uptake values obtained for the CGAC adsorbent were comparable to those reported in previous literature for Cd(II) and Pb(II) removal using commercial activated carbon adsorbents.

CHAPTER TEN

MECHANISM OF SORPTION, ADSORBENT RANKING AND SPENT ADSORBENT STABILIZATION

CHAPTER TEN

10.0 Mechanism of sorption, adsorbent ranking and spent adsorbent stabilization.

To evaluate the adsorption capability of the commercial activated carbon (CGAC) with those of the prepared adsorbents in this study, a ranking process was carried out to choose a set of adsorbents to be used. For the adsorbent ranking, the commercial activated carbon adsorbent (CGAC) discussed in chapter nine was used as the benchmark for the two different adsorbent ranking carried out. Adsorbent ranking was carried out using the Langmuir isotherm parameter (q_{max}) for the residue, Na_2CO_3 chemically activated carbon adsorbents and the commercial activated carbon adsorbent (CGAC). Two kinetic parameters ($q_{e,\ exp}$ and $q_{e,\ cal}$) obtained from the kinetic sorption studies of all the adsorbents studied in this work were for adsorbent ranking. An examination of the different sorption mechanism that influenced the sorption of the two metal ions onto the different adsorbents used in this study has also been discussed. Stabilization studies on the some of the spent adsorbents used in this study were also carried out via spent adsorbent combustion and the encapsulation of the resulting metal ion saturated ash in a polymeric system.

10.1 Sorption mechanism

The application of adsorbents for the removal of metal ions from aqueous systems is carried out using a wide range of materials however the process by which these adsorbents remove metal ions from aqueous systems is still not fully understood. This is due to the complex nature of adsorbent surfaces and the different interactions that exist between an adsorbent and an adsorbate during sorption. The identification of the mechanism that governs metal ion sorption on sorbents is a challenge as a number of different processes may operate in a sorbent-sorbate system. The different adsorbents used in this study are based on lignocellulosic biomass and thermally and chemically modified carbon adsorbents. For an examination of the mechanism of Cd(II) and Pb(II) sorption, the fresh residue adsorbents (OPFS, CNFS, CCPS, CCYBS, PTHS, PTPS and YTBS) used for the initial sorption analysis were evaluated since data for the characterisation of effect of pH, EDAX and FTIR were available.

These adsorbents are composed of cellulose, lignin, and hemicellulose as major components and to a lesser extent fatty acid bearing functional groups such as alcohol, ketone and carboxylic acids in pectin on the structure of these residues. All these components have functional groups that have been reported as possible sites for reactions with metallic cations during sorption (Dupont and Guillon, 2003; Nurchi and Villaescusa, 2008). A number of possible mechanisms have been proposed in literature and these involve an integrative effect of different interactions such as; electrostatic attraction-hydrogen bonding, ion-exchange, physical adsorption, chemisorption, surface complexation and/or precipitation (Tan *et al.,* 2015; Nguyen *et al.,* 2013). In this study the mechanism through which Cd(II) and Pb(II) ions were sorbed onto the residue adsorbents were examined using EDAX and FT-IR spectroscopy as previously discussed in the characterisation section of the residue adsorbents.

The removal of metal ions from aqueous solutions by adsorption is also highly dependent on the degree of ionization and speciation of the adsorbate. The degree of ionization of an adsorbate also affects the solubility of the metal, since the solubility of many metal salts is due to the polarity of water complexes. The attraction of the negatively charged oxygen atoms in solution allows them to congregate around the positive ions, leading to the formation of an aquo-complex. Solvation of the adsorbate indicates that each ion in solution is surrounded by a sheath of few solute molecules bound to the ion by electrostatic forces, moving through the solution with the ion. When the solution is water, solvation is called hydration (Teker *et al.*, 1999; Kyaynov and Müller, 2011). Cd(II) and Pb(II) ions in aqueous solution may therefore suffer different effects such as solvation, hydrolysis and polymerisation in which a number of reactions as shown in eqns. 10.1-10.3 may take place (Mohan *et al.,* 2007 ; Burgess, 1978; Gomez-Serrano *et al.,*1998).

Hence, when the metal ion is dissolved in water, an aquo complex is formed in the form $\{M\,(H_2O)_x\}^{n+}$.

$$M^{2+} + nH_2O = M(H_2O)_n^{2+} \tag{10.1}$$

$$M(H_2O)_n^{2+} = M(H_2O)^{n-1}(OH)^+ + H^+ \tag{10.2}$$

$$nM^{2+} + mH_2O = M_n(OH)_m^{(2n-m)+} + mH^+ \tag{10.3}$$
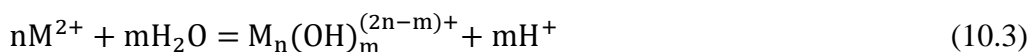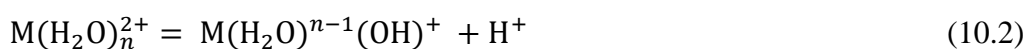
Where; M denotes the metal ion, n+ the net charge on the complex and x, n & m, the co-ordination number (Burgess, 1978; Gomez-Serrano *et al.,* 1998).

The Cd(II) and Pb(II) are thus likely to exist as free ions in equilibrium with the solvated species in the adsorbate system. The hydration numbers for these two metal ions have been estimated to be between 4.6 and 12 for Cd(II) and 4 and 8 for Pb(II) using a number of different physical techniques (Burgess, 1978; Gomez-Serrano *et al.,*1998; Macias-Garcia *et al.,* 2003; Mohan *et al.,* 2007). The stability of the aquo complex is thus dependent on the size of the metal ion and since the displacement of water molecules from the aquo-ion is the basis of adsorption dynamics, the stability of the aquo complex is very essential to the adsorption process (Cotton and Wilkinson, 1972). The initial concentration of the metal ion in the adsorbate also provides an important driving force to overcome the mass transfer resistance of each metal between the aqueous and solid phases. This is also aided by the ionic radius of the metal. The ionic radius of metal ion affects the adsorption process by influencing the diffusion mechanism (Arpa *et al.,* 2000).

Based on the above assumptions a number of approaches have been proposed for the uptake mechanism of metal ions such as Pb(II) and Cd(II) ions in adsorbate solutions. The pH effect and formation of metal complexes with the active sites has been suggested as an important mechanism for metal sorption. According to Krishnan and Anirudhan (2003), during the sorption of the metal ions, the ability of sorption to proceed will depend on the pH, type of species that exist at different pH, ionic radius, presence and effect of anions and stability of complexes. The nature of the species of the metal ions in the adsorbate plays an important role in the mechanism of uptake as interactions between these species and the active sites (functional groups) on the adsorbent surface are dependent on metal ion properties (hydrated ionic radius) and the type of charge on the different species which may influence attractive or repulsive interactions (Arpa *et al.,* 2000). In dilute adsorbate systems that are mildly acidic the Pb(II) species are mainly cations and In the present study the dominant species of the metal ions in solution at pH> 8.0 are the hydroxides {$Cd(OH)_2$ and $Pb(OH)_2$}and $[Pb(OH)_3]^-$. At pH < 8.0 the dominant metal species are of the type Cd^{2+}, $Cd(OH)^+$, Pb^{2+} and $Pb(OH)^+$.

The interaction of these metal ion species with the species in solution and the adsorbent surface will therefore affect the amount that is preferentially adsorbed onto the surface of the adsorbents. The highest loading on the residues was observed to occur at pH 6.0 for Pb(II) and 7.0 for Cd(II) and the pH 6.5 was also chosen based on the zeta potential analysis of the residues; for the other adsorbents (hydrothermal, carbonised, pyrolysed and

chemically activated) the pH of 7 was chosen - also based on the zeta potential characteristics of the surfaces. Thus, the adsorption of the two metal ions in the adsorbate at the pH may be due to the interaction of the species that are dominant at pH < 8, such as Pb^{2+}, Cd^{2+} , $Pb(OH)^+$ and $Cd(OH)^+$ with the functional groups on the adsorbent surface (Kikuchi *et al.,* 2006). This increase in the species of these metal ions that can interact with the functional groups on the adsorbent improves the probability of metal ion removal. Thus due to the multiple-ion-binding sites on the adsorbent surfaces and the variety of metal ion species in the adsorbate a number of metal adsorbent complexes are formed during sorption process. This can be represented according to eqn.10.4 (Akpomie et *al.,* 2015; Rao *et al.,* 2010; Hu *et al.,* 2015):

$$M^{n+} + A - XH \leftrightharpoons M(A - X)_n + H^+ \qquad (10.4)$$
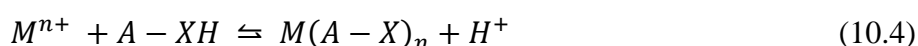
Where M= metal; A-XH (Adsorbent surface); [X=S, O, COO, NH]; $M(A-X)_n$ –metal adsorbent complex and H^+ - Displaced proton.

Hence, the sorption of metals by the adsorbent takes place by ion exchange where the metal ion displaces the proton (H^+) from the adsorption site and becomes attached to the adsorbent forming an adsorbent metal complex. Therefore, speciation plays a significant role in the determination of the amount of metal adsorbed, especially when consideration is given to the ionic radii and ionic charge of the metal. When there is electrical attraction between adsorbates, ions with small ionic radii but higher ionic charge are more strongly attracted to sites of opposite charge (adsorbent). However, for ions of similar charge, the hydrated radius of the hydrated metal ions determines the order of preference and for sorption, metals with ions of smaller ionic radii move closer to potential adsorption sites (Atkinson *et al*., 1998). This mechanism can be used to explain the higher uptake capacity for Cd(II) ion when compared with Pb(II) ions for the different adsorbents investigated in this study. The variation in q_{max}(mgg^{-1}) and q_e(mgg^{-1}) for the respective adsorbents may be attributed to the differences in the ionic sizes of Cd(II) and Pb(II) ions. The ionic radius of Cd(II) is 0.97Å, while that of Pb(II) is 1.20Å. Hence due the smaller ionic size of Cd(II) ion, in the adsorbate system it will exhibit greater affinity to the active sites on the different adsorbents due to its smaller hydrated radius which would increase the rate of diffusion from the adsorbate system onto the adsorbent surface. This trend has also been reported by

Horsfall *et al.,* (2006) in their study on the sorption of Cd(II), Cu(II) and Zn(II) ions from aqueous solutions by cassava (*Manihot sculenta Cranz*) tuber bark waste.

Infra-red spectra evidence of adsorbents after metal ion sorption has been used in a number of studies to confirm the participation of hydroxyl, carbonyl, sulfhydryl, sulfonate, carboxylate phenolic functional groups found on the surface of carbon adsorbents in metal ion sorption (Barka *et al.,* 2013; Ding *et al.,* 2014). According to Bailey *et al.,* (1999), phenolic groups are believed to be accountable for the formation of complexes with heavy metal ions during sorption and evidence from infra-red spectroscopy has been used to confirm this mechanism of sorption. The ability of these groups also called *active sites* to bind metal ions during adsorption have been suggested by El-Kamash *et al,* (2005) to depend on a number of factor such as the quantity of sites, accessibility of sites, chemical state of sites and affinity between metal ion and active sites (Basha *et al.,* 2009). Barkar *et al.,* (2013) in their study on the sorption of Cd(II) and Pb(II) ions using dried cactus observed a decrease in the wave number of asymmetric stretching of the carboxylic double bond in the unloaded dried cactus when compared to those of the metal ion loaded cactus. This shift in band was used to conclude that the carboxylic acid groups were likely responsible for the binding of Cd(II) and Pb(II) by the dried cactus biosorbent.

For the different residue adsorbents (OPFS, CCPS,CNFS, CCYBS, PTHS, PTPS and YTBS) the results obtained from FTIR studies before and after Cd(II) and Pb(II) sorption (Figs.5.27-5.40) shows that a number of carbonyl(-CO), carboxylic acid/esters(-COO) amide (-N-H) and hydroxyl (-O-H) groups may be active sites for metal ion interaction. These functional groups were observed to have decreased intensity or disappeared in the spectrum of the residue adsorbents after Cd(II) and Pb(II) sorption. Cd(II) most stable state is the +II state and it belongs to the transition group metal which has a greater tendency for interaction via coordination bonding. This can be achieved through the coordination bonding using the vacant d-orbital by dative bonding with lone pair of oxygen or nitrogen containing groups and these functional group contain lone pairs of electrons (Chand *et al.,* 2014; Panda *et al.,* 2007). Hence the Cd(II) ions could bond with the hydroxyl and carboxylic acid groups by coordinating bonding as illustrated in Fig. 9.13 as proposed by Vaghetti *et al.,* (2009).

Where M is the metal ion (Cd) and the first step (1) is the deprotonation of the active sites (functional groups) at higher pH and the second stage (2) is the bonding of the deprotonated anions with the metal ion.
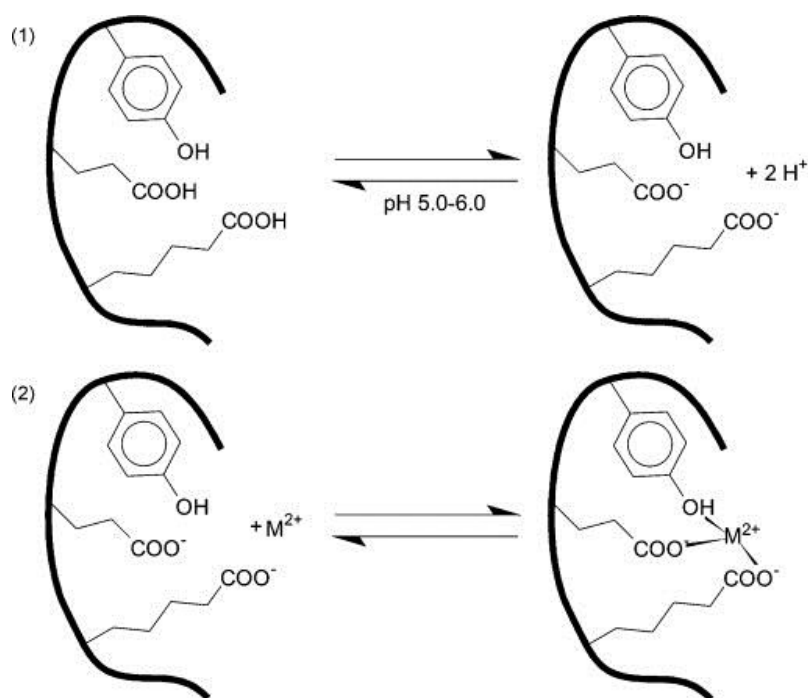
Fig. 10.1: Proposed mechanism of Cd(II) binding onto residue adsorbent surface (Vaghetti *et al.,* 2009).

Based on Fig. 10.1, the higher sorption for Cd(II) at pH 5-7 can also be related to the dissociation of carboxylic acids on the surface of the adsorbent as this cannot occur at low pH since the pka of carboxylic acid ranges from 3.8 to 5.0. Thus at higher pH, the carboxylic acid groups would dissociate leading to the elimination of protons with the subsequent complexation reaction between the carboxylate groups (COO-) and the divalent Cd(II) ion (Vaghetti *et al.,* 2009). This observation of coordination bonding between Cd(II) ion and electron rich nitrogen and oxygen functional groups has also been reported by Chand *et al.,* (2014) in their study on the sorption of Cd(II) ions from aqueous solution using chemically modified apple pomace. In their study, the mechanism of ion uptake by the adsorbent was proposed via coordinating to amine (-NH$_2$) and carbonyl (-CO) groups.

Pb(II) is a p-block element with two oxidation states, the +II and the +IV but the +II state is its most stable state due to the "so-called inert electron pair effect" which describes the tendency of heavier main group elements to adopt an oxidation state two steps below the highest possible oxidation state (Persson *et al.,* 2011). Pb(II) forms a variety of complexes in solution such as Pb^{2+}, $Pb(OH)^{+}$, $Pb_4(OH)_4^{4+}$, $Pb_3(OH)_4^{2+}$ and $[Pb_6(OH)_8]^{4+}$ but most of the complexes are not stable (Kikuchi *et al.,* 2006; Baes and Mesmer, 1976). This process is bound to affect the amount of mononuclear Pb^{2+} aqua ions in solution for adsorption. This is because the complexes formed will reduce the Pb^{2+} species and will also hinder the migration of the more stable Pb(II) species [$Pb(OH)^{+}$ and Pb^{2+}] as these would not be able to migrate easily to adsorption sites due to steric hindrance. Hence the stability and size of the different metal ion species formed in the adsorbate may also be used to explain the higher Cd(II) ions uptake than Pb(II) ions in most of the sorption studies reported in this thesis.

Another approach to explain the metal ion sorption at the pH 6.5 and 7 is that pH window is favourable for interactions between the functional groups on the adsorbents surface especially with interactions that can exist with the sulphur based functional groups that were observed in the EDAX spectra of the residues and the prepared carbon adsorbents. According to the Pearson theory (Pearson, 1988), during acid-base reaction, hard acids prefer to interact with hard bases and soft acids with soft bases. The positively charged metal ion species in this study are soft cations and as a rule, their interaction with the surface groups sulphur groups (soft bases) on the adsorbent matrix is thus favoured. This implies that there may be interactions between the two metal ions with these functional groups thereby promoting uptake probability.

Uptake mechanism can also proceed via ion-exchange due to the interaction of the metal ions on the residue adsorbent surface with the Cd(II) ions in the adsorbate and the examination of the EDAX spectra (Figs.5.21-5.26) indicates that there was a decrease in the percentage composition of some alkali metal ions potassium (K) and calcium (Ca) present in the residue adsorbents when compared to those of the Cd(II) loaded adsorbents after sorption. This may imply that there was ion-exchange between these alkali- metal ions with Cd(II) on the adsorbent surface, thereby making this a possible mechanism for metal ion uptake. This approach has also been reported by Iqbal *et al.,* (2009a) on the use of the EDAX analysis of grapefruit peel to confirm the mechanism of ion-exchange for the removal of Zn (II) from aqueous solutions. The study observed that the calcium (Ca) and

potassium (K) ions identified in the EDAX spectrum of the fresh grapefruit peel were absent in the peel used for Zn(II) ion adsorption, thus suggesting that these ions (Ca, K) may be involved in the ion-exchange with the Zn(II) ions. This ion-exchange mechanism has also been observed by Swiatkowski *et al.,* (2004) for the removal of Pb(II) on activated carbon surfaces, however in their study they reported that the approach of using ion-exchange and acid-based properties of a carbon surface alone to explain the interactions leading to metal ion uptake in an adsorption system is insufficient as there are different interactions that operate in this aqueous system, hence the mechanism by which basic carbon surfaces interact with metal ion adsorbates is still subject to more research.

10.2 Adsorbent ranking

One aspect of the present study was the comparison of the performance of the adsorbents prepared from the agricultural residues using the different modification regimes explored in this work. In addition, it was also necessary that these adsorbents be compared with a commercially available adsorbent used in wastewater treatment for the removal of heavy metal ions, hence the evaluation of the performance of the commercial activated carbon (CGAC) with those of the prepared adsorbents in this work.

Presently, there are no general criteria or tool that is used to evaluate the performance of adsorbents and this has resulted in the use of a variety of criteria for the determination of the suitability of an adsorbent or groups of adsorbents for separation applications (Khurana and Farooq, 2016).The absolute adsorption capacity is one such criterion used to evaluate the potential of new metal−organic framework (MOF) adsorbents used for CO_2 capture (Yazaydin *et al.,* 2009). In a similar manner adsorbents have also been evaluated for their CO_2 capture capacity based on the pure-gas working capacity calculated from the loading difference between the high and low operating pressures (Harlick and Tezel, 2004). Thus it can be observed that adsorbent capacity/loading is an important parameter that can be used to evaluate the performance of adsorbents for separation applications as is the case in this present study.

In this study, kinetic studies for the sorption of Cd(II) and Pb(II) ions were carried out. Thus a ranking based on the kinetic modelling parameter ($q_{e, cal}$) obtained from the pseudo second order (PSO) was used to compare the loading of Cd(II) and Pb(II) ions for all the adsorbents prepared in this work as well as the commercial activated carbon. Equilibrium studies using adsorption isotherms is usually carried out to evaluate the performance of

adsorbent materials (Chen, 2013; Rangabhashiyam *et al.,* 2014) but it was not possible to carry out equilibrium studies for all the sets of adsorbents developed in this study. Thus, this aspect of the work was designed to choose a set of adsorbents that will be used to carry out a comparison study with the commercially activated carbon (CGAC) used in this study. Certain parameters were chosen and the reasons for their choice are outline in the subsequent sections of this chapter.

10.2.1 Parameters for consideration

The evaluation of the performance of adsorbents used for sorption studies often involves the determination of the physical and chemical properties of the adsorbents and an evaluation of how these properties influence the sorption performance of the adsorbents. The major parameters often considered in adsorbents as reported in literature include; surface area and porosity, ash content, fixed carbon, surface acidity or basicity (pH, pHpzc, Boehm titration), elemental composition (XRF, EDAX, CHON elemental analysis), spectroscopic properties (FT-IR, Raman, XPS, UV/Visible, and NMR), thermal properties (TGA& DSC), nature of phases on the adsorbents-crystalline or amorphous (XRD) and surface morphology (SEM, TEM). These characteristic properties are often reported in adsorption studies and used to relate the performance of adsorbents or establish mechanism of sorption (Wu *et al.,* 2012).

An equilibrium study on adsorption often allows the determination of the different parameters that are fundamental in the description and modelling of sorption dynamics. The condition in the equilibrium studies is often allowing sorption to proceed to completion (equilibrium) or a time in which is sufficient to assume completion. However, this assumption of complete sorption does not necessarily mean that the adsorbent surface has completely adsorbed the maximum amount of species hence the utilisation of sorption isotherms to give insight into this process and quantitatively allow for the modelling of the entire sorption system (Chen, 2013; Rangabhashiyam *et al.,* 2014). Thermodynamic modelling of the sorption process is also reported and provides insight into the energetic and driving forces that govern the sorption process (Shon *et al.,* 2013).

Different sorption isotherm models have been reported in literature for the description of sorption such as the Langmuir, Freundlich, Redlich-Peterson, Temkin and Toth. The use of these isotherms is a common approach that describes a vast number of retention/release processes and provides a platform that gives fundamental characteristic of material

interaction that can be used to predict substance mobility (Limousin *et al.,* 2007). Interestingly too some of these isotherms give parameters that are useful in design and scale up of batch adsorption systems (Foo and Hameed, 2010). The Langmuir isotherm provides a constant (q_{max}) that estimates the maximum loading of an adsorbate on an adsorbent and therefore provides a useful parameter for estimation and design purposes.

In this study, the Na_2CO_3 activated adsorbents were selected for comparison with the commercial activated carbon adsorbent (CGAC) so that their performance could be evaluated. Four reasons were behind the choice of this set of adsorbents namely:

- their comparative level of ash,
- their high BET surface area,
- low loss on attrition values and
- high yield

The level of ash in this group of adsorbents (Na_2CO_3) and the K_2CO_3 activated adsorbents is a result two factors- the intrinsic inorganic content of the residue and the chemical used in their activation. The view in activated carbon literature on the significance of ash in activated carbon adsorption performance is diverse as some researchers view the high content as detrimental to performance as a high ash content implies a reduced surface area for adsorption (Soleimani and Kaghazchi, 2014b; Othman, 2008; Ekpete and Horsfall, 2011). Other studies view the influence of the ash constituents (inorganic compounds) as contributing to increasing the adsorption performance (Varma *et al.,* 2013). Sardella *et al.,* (2015) also reports that the ash content is an important parameter that has to be considered for carbon adsorbents because high quantities of ash in their composition have the probability of having higher metal ion retention in adsorption applications due to the effect of the ash in ion-exchange processes. Hence, the ash content was deemed a crucial factor as ash based adsorbents have been reported in adsorption studies with high loading performance. Surface area was another parameter of importance because of its ability to have considerable impact on the utilization of adsorbents for liquid and gaseous phase applications. A high surface area was considered a fundamental characteristic of a good adsorbent. It is generally observed that the higher the surface area, the larger the adsorption capacity of an adsorbent (Guo and Lua, 2002). Thus, their high surface area was also a crucial factor as an increased surface area and porosity implies the probability of more pore channels for the adsorbate to migrate through to facilitate better sorption kinetics. Their low attrition and good yields were also used to choose this set of adsorbents as these

498

parameters are necessary in the development of a useful adsorbent for any commercial application. The ranking of the adsorbents in this work was a comparison of the Langmuir maximum loading capacity parameter (q_{max}).

10.2.2 Ranking of chemically activated adsorbents using Langmuir isotherm parameter (q_{max})

The estimation of the maximum loading on an adsorbent from the Langmuir isotherm determined using the solver-add technique that has been previously discussed in Chapters 5, 8 and 9 of this work was used as the basis for the ranking of the adsorbent performance for the sorption of Cd(II) and Pb(II) ions in this study. The maximum loading (q_{max}) of each sorbent obtained from the Langmuir isotherm modelling is used to estimate the probable sorption capacity of the adsorbent under examination. This property implies that it could be used to estimate what the highest loading the adsorbent can provide when it reaches the theoretical equilibrium.

The determination of the maximum loading on an adsorbent is of crucial importance in the design of an adsorption system and scale up as it plays a fundamental role in determining the capital cost of the process. This is because this parameter is used to determine the amount of adsorbent required and this is used to determine the volume of the absorber vessel (Knaebel, 2008). Hence, the amount of adsorbent for a particular adsorption system and volume of the adsorption vessel for any process can be computed from the data obtained from the Langmuir isotherm for the maximum loading (q_{max}).

The ranking was carried out using this Langmuir parameter for comparing the performance of the Na_2CO_3 activated adsorbents with that of the commercial activated carbon adsorbent (CGAC) and the residue adsorbents for the two cations under equilibrium conditions. The comparison of the three groups of adsorbents based on the q_{max} parameter is presented in Table 10.1. In addition, the effect of surface area on the q_{max} of the different adsorbents examined in this ranking process was also used to gain insight into the influence of an adsorbent physical property on the uptake capacity. Thus the surface areas of the adsorbents are also presented to enable this comparison.

Table 10.1: Residue, Na_2CO_3 chemically activated and CGAC comparison using Langmuir parameter q_{max}

| Adsorbent Class | Adsorbent | Cadmium(II) ion | | Lead (II) ion |
		q_{max} (mgg^{-1})	BET (m^{2}g^{-1})	q_{max} (mgg^{-1})
	OPFS	17.6	1.44	15.1
	CNFS	21.6	12.4	25.3
	CCPS	24.5	0.71	29.2
Residue	CCYBS	21.4	0.45	33.3
	PTHS	16.0	3.98	17.3
	PTPS	18.9	1.91	27
	YTBS	22.4	0.5	25.7
Commercial activated Carbon	CGAC	27.3	4273	20.3
	OPFNCA	21.4	670	37.3
	CNFNCA	20.0	827	33.3
	CCPNCA	29.4	473	23.6
Na_2CO_3 chemically activated	CCYBNCA	25.3	514	41.9
	PTHNCA	17.9	381	14.9
	PTPNCA	26.3	437	41.7
	YTBNCA	15.7	593	15.2

The results presented in Table 10.1 indicates that for the uptake of Cd(II) ions there were increases in the capacity of the adsorbents based on the q_{max} values due to the conversion of the residues into activated carbon using the Na_2CO_3 chemical activation process. This improvement in adsorbent capacity was most significant in the PTPS adsorbent conversion as the q_{max} increased from 17.6mgg^{-1} for the residue to 26.7mgg^{-1} for the PTPNCA chemically activated carbon adsorbent. Improvements in the adsorbent capacity were also observed for the conversion of CCPS, CCYBS, OPFS and PTHS adsorbents into CCPNCA, CCYBNCA, OPFNCA and PTHNCA adsorbents respectively. However, the transformation of the CNFS and YTBS adsorbents into their respective chemically activated carbon adsorbents did not increase the adsorbent capacity of the CNFNCA and YTBNCA adsorbents as their q_{max} parameter was observed to decrease. Comparison of the adsorbent capacity of the residues and their respective chemically activated carbon adsorbents with the commercial activated carbon (CGAC) used to benchmark their performance indicates that for both Cd(II) ion removal the adsorbents prepared in the study had capacities that were comparable to a commercially available product. For Cd(II) ion removal, it was observed that the capacity of the CCPNCA adsorbent (29.4mgg^{-1}) was better than that of the CGAC adsorbent (27.3mgg^{-1}).

For Pb(II) ion sorption the effect of the conversion of the residues into chemically activated carbon adsorbents was very significant on the value of the q_{max} for some adsorbents, while for others the reverse situation was applicable. The increases in adsorbent capacity for Pb(II) ions from the residues to the chemically activated carbon adsorbents was observed for the OPFS, CNFS,CCYBS and PTPS adsorbents which were converted into OPFNCA, CNFNCA, CCYBNCA and PTPNCA adsorbents respectively. The highest improvement in adsorbent capacity was observed in OPFS and PTPS adsorbents which had q_{max} values of 15.1mgg^{-1} and 27.0mgg^{-1} respectively. Upon chemically activation the corresponding adsorbents had significant increases in capacity to 37.3mgg^{-1} (OPFNCA) and 41.7mgg^{-1} (PTPNCA) which could be associated to the effect of the chemical activation process on the porosity and surface properties of the resulting adsorbents The conversion of lignocellulosic residues into activated carbon adsorbents with improve porosity is presumed to play a significant role in the increase in the loading capability of the material. This may be associated with the ease of surface transport that would make uptake of ions by the adsorbent occur at faster rate than in residues with low porosity. However, for the CCPS and PTHS adsorbents, the trend in the value of q_{max}

indicated that there were reductions in the adsorbent loading capacity for their respective chemically activated carbon adsorbents. A comparison of the Pb(II) ion loading capacity (q_{max}) of the residues and chemically activated carbon adsorbents with that obtained for the commercial activated carbon adsorbent (CGAC) indicates that most of the prepared adsorbents in this study had higher capacity of Pb(II) ion than the commercial activated carbon adsorbent. For the residues, the adsorbent capacities of CNFS (25.3mgg^{-1}), CCPS (29.2mgg^{-1}), CCYBS (33.3mgg^{-1}), PTPS (27.0mgg^{-1}) and YTBS (25.7mgg^{-1}) were all higher than that of the CGAC (20.3mgg^{-1}). For the chemically activated carbon adsorbents, the capacities of the OPFNCA (37.3mgg^{-1}), CNFNCA (33.3mgg^{-1}), CCPNCA (23.6mgg^{-1}), CCYBNCA (41.9mgg^{-1}) and PTPNCA (41.7mgg^{-1}) were all higher than that of the commercial activated carbon adsorbent. Thus, it can be stated that based on the ranking of the residue, Na_2CO_3 chemically activated carbon adsorbent and commercial activated carbon adsorbent using the Langmuir qmax parameter, the best adsorbent for Cd(II) and Pb(II) ions are CCPNCA and CCYBNCA respectively and their BET surface areas were 473m^{2}g^{-1} and 514m^{2}g^{-1}.

These results thereby confirm that the adsorbents prepared in this study had loading capacities for Cd(II) and Pb(II) ions that are similar to the materials that are commercially available and can thus be used in eluent and wastewater treatment for these toxic cations in place of commercial activated carbon. However, from the results it was also observed that the effect of surface area on the q_{max} of the adsorbents was noticeable but not very significant as the values of q_{max} obtained from the sorption of Cd(II) and Pb(II) ions using the residues were comparable with those obtained for the Na_2CO_3 chemically activated carbon adsorbents and the commercial activated carbon adsorbent (CGAC) which had higher surface area than the residues.

10.2.3 Ranking of adsorbents using kinetic modelling parameters

A kinetic study describes how the rate sorption proceeds and different models have been used to discriminate between the types of transport that governs the adsorption process (Ho and McKay, 1999; Allen *et al.,* 2005). These models are also used in literature to give insight into sorption dynamics and the parameters' arising from the modelling process gives significant data for compassion with other adsorbents.

Table 10.2: Adsorbent comparison based on kinetic uptake parameter $q_{e,exp}$

Adsorbent Class	Cadmium (II) ion			Lead (II) ion		
	Adsorbent	$q_{e, exp}$ (mgg^{-1})	BET (m^{2}g^{-1})	Adsorbent	$q_{e, exp}$ (mgg^{-1})	BET (m^{2}g^{-1})
Residue	CNFS	16.3	12.4	OPFS	12.5	1.44
HTC-170	CNFS-HTC 170	25.9	75.5	CNFS-HTC 170	19.0	75.5
HTC-200	CNFS-HTC 200	31.1	260	CNFS-HTC 200	26.7	260
Pyrolysed	CCPPCA	29.8	308	YTBPCA	26.9	267
Carbonised	CNFCA	27.0	252	CNFCA	24.7	252
K$_2$CO$_3$ activated	CNFKCA	28.2	553	CNFKCA	25.2	553
Na$_2$CO$_3$ activated	CNFNCA	27.7	827	CNFNCA	25.3	827
Comm. Activated Carbon	CGAC	17.2	4273	CGAC	16.8	4273

Table 10.3: Adsorbent comparison based on kinetic PSO parameter $q_{e,cal}$

Adsorbent Class	Cadmium (II) ion			Lead (II) ion		
	Adsorbent	$q_{e, cal}$ (mgg^{-1})	BET (m^{2}g^{-1})	Adsorbent	$q_{e,cal}$ (mgg^{-1})	BET (m^{2}g^{-1})
Residue	CNFS	18.0	12.4	OPFS	13.1	1.44
HTC-170	CNFS-HTC 170	33.8	75.5	CNFS-HTC 170	24.3	75.5
HTC-200	CNFS-HTC 200	37.1	260	CNFS-HTC 200	34.6	260
Pyrolysed	YTBPCA	36.8	267	YTBPCA	32.4	267
Carbonised	PTHCA	30.8	126	PTHCA	27.8	126
K_2CO_3 activated	CNFKCA	33.0	553	CNFKCA	30.1	553
Na_2CO_3 activated	PTPNCA	33.6	437	CNFNCA	29.1	827
Comm. Activated Carbon	CGAC	18.1	4273	CGAC	18.4	4273

For the kinetic ranking process of the adsorbents, two kinetic parameters were chosen and these were; the kinetic parameter ($q_{e,exp}$) obtained at the end of the kinetic sorption experiment and the maximum loading obtained using the pseudo second order (PSO) kinetic modelling ($q_{e, cal}$). The comparison of the uptake of the prepared adsorbents using the $q_{e,exp}$ parameter is presented in Table 10.2, while that with the $q_{e, cal}$ parameter from the pseudo-second order kinetic model is presented in Table 10.3.

The pseudo second order (PSO model $q_{e, cal}$) was chosen for the ranking of all the adsorbents due to the wide spread application of the PSO model for the characterisation of the kinetic of metal ion sorption in literature (Ho, 2006; Ho *et al.*, 2004; Ho and Ofomaja, 2006). Thus, this model will provide a basis for a wide comparison of the loading of Pb(II) and Cd(II) ions onto the studies adsorbents with results reported in literature for residue, hydrothermal, carbonised, pyrolysed and chemically activated adsorbents. The effect of surface area on the kinetic q_e loadings obtained for the different adsorbents reported in this study were also be evaluated.

For the adsorbent ranking process based on the $q_{e, exp}$ kinetic parameter, the approach was to choose the best adsorbent from each adsorbent modification process for Cd(II) and Pb(II) ions sorption and use this for comparison with the other modifications and the commercial activated carbon (CGAC). The comparison of the loading performance of these adsorbents was also evaluated using their BET surface area as presented in Table 10.2.

An evaluation of the results presented in Table 10.2 using the $q_{e,exp}$ parameter indicates that for the residues, the CNFS adsorbent was the best adsorbent for the removal of Cd(II) ions as it had the highest capacity (16.34 mgg^{-1}), while for Pb(II) ion sorption, the best adsorbent was OPFS with an uptake of 12.5 mgg^{-1}. For the hydrothermal adsorbents, the materials obtained from the CNFS residue were the best for the two different hydrothermal conditions for both Cd(II) and Pb(II) ions. Thus, for the HTC-170 adsorbents, the CNFS-HTC 170 was the best adsorbent for both metals, with loadings of 25.9 mgg^{-1} for Cd(II) and 19.0 mgg^{-1} for Pb(II) ions. In like manner for the HTC-200 adsorbents, the CNFS-HTC 200 adsorbent had the best uptake with $q_{e exp}$ loading values of 31.1 mgg^{-1} and 26.7 mgg^{-1} for Cd(II) and Pb(II) ions respectively. The surface area of the CNFS-HTC 170 and CNFS-HTC 200 adsorbents were presumed to be crucial in their high adsorbent performance based on the $q_{e exp}$ values as can be observed in Table 10.2. For the kinetics of Cd(II) ion sorption using the pyrolysed adsorbents, the best adsorbent for metal removal

was the CCPPCA with a loading of 29.8 mgg^{-1}, while for Pb(II) ion sorption the best adsorbent was YTBPCA with an uptake of 26.9 mgg^{-1}. For the carbonised adsorbents, optimum loading was obtained for the CNFCA adsorbent for both Cd(II) and Pb(II) ion sorption with q$_{e\ exp}$ values of 27.0 mgg^{-1} for Cd(II) and 24.7 mgg^{-1} for Pb(II) ion and the BET surface area of this adsorbent was 252 m^{2}g^{-1}.

For the K$_2$CO$_3$ chemically activated carbon adsorbent, the best adsorbent was the CNFKCA as it had the highest uptake capacity for both cations examined in this study. The q$_{e\ exp}$ values obtained for this adsorbent was 28.2 mgg^{-1} for Cd(II) and 25.2 mgg^{-1} for Pb(II) ion and its surface area was 553m^{2}g^{-1}. The adsorbent with the best sorption capacity based on the q$_{e\ exp}$ values for the Na$_2$CO$_3$ chemically activated carbon adsorbent was the CNFNCA with a BET surface area of 827 m^{2}g^{-1}. This adsorbent had the highest surface area amongst all the prepared adsorbents in this study. The loading for Cd(II) ion was 27.7 mgg^{-1}, while that of Pb(II) was 25.3 mgg^{-1}. The q$_{e\ exp}$ values obtained for the kinetics of Cd(II) and Pb(II) ion sorption using the commercial activated carbon (CGAC) adsorbent were 17.2 mgg^{-1} and 16.8 mgg^{-1} and this adsorbent had a BET surface area of 4273 m^{2}g^{-1}. Based on the results in table 10.2 and the above discussion, the different adsorbents evaluated in this study can be ranked accordingly as follows; CNFS-HTC200 > CCPPCA > CNFKCA > CNFNCA > CNFCA > CNFS-HTC170 > CGAC > CNFS for Cd(II) sorption based on their adsorbent capacity using the kinetic parameter q$_{e\ exp}$. For Pb(II) ion uptake the adsorbents can be ranked as follows; CCPPCA > CNFS-HTC200 > CNFNCA > CNFKCA > CNFCA > CNFS-HTC170 > CGAC > OPFS. This comparison indicates that the adsorbents based on the transformation of the coconut fibre residue-CNFS have the best potential as adsorbents for Cd(II) and Pb(II) ion from aqueous systems and effluents. The capacity of this residue may be associated to a certain extent to the surface properties of the resulting materials especially the BET surface area and porosity.

The pseudo second order (PSO) kinetic modelling parameter q$_{e,cal}$ was also used to compare the sorption capacity of the different adsorbents prepared in this work. The values of the q$_{e,cal}$ and the BET surface area used for the comparison are presented in Table 10.3. For the adsorbent ranking process based on the q$_{e,\ cal}$ kinetic parameter, the approach was to choose the best adsorbent from each adsorbent modification process for Cd(II) and Pb(II) ions sorption and use this for comparison with the other modifications and the commercial activated carbon (CGAC). The comparison of the loading performance of

these adsorbents was also evaluated using their BET surface area as presented in Table 10.3.

From Table 10.3, it observed that the CNFS was the best adsorbent amongst the residues for Cd(II) ion uptake with a $q_{e, cal}$ loading of 18.0 mgg^{-1}, while the OPFS was the best for Pb(II) ion removal with a capacity of 13.1 mgg^{-1}. The BET surface areas of the two adsorbents were 12.4m^{2}g^{-1}(CNFS) and 1.44m^{2}g^{-1}(OPFS). For the hydrothermally carbonised adsorbent-HTC-170, the CNFS-HTC 170 adsorbent with a BET surface area of 75.5 m^{2}g^{-1} was the best adsorbent for the sorption of both metals. The $q_{e, cal}$ loading for Cd(II) and Pb(II) were 33.8 mgg^{-1} and 24.3 mgg^{-1} respectively. For the HTC-200 adsorbents, the CNFS-HTC 200 adsorbent with a BET surface area of 260 m^{2}g^{-1} had the best uptake for both cations with $q_{e, cal}$ values of 37.1 mgg^{-1} and 34.6 mgg^{-1} for Cd(II) and Pb(II) ions respectively. The evaluation of the $q_{e, cal}$ values for the pyrolysed adsorbents indicated that the YTBPCA adsorbent with a BET surface area of 267 m^{2}g^{-1} was the best adsorbent for both metals. The uptake capacity was 36.8 mgg^{-1} and 32.4 mgg^{-1} for Cd(II) and Pb(II) ions respectively. For the carbonised adsorbents, optimum loading capacity was obtained for the PTHCA adsorbent which had a BET surface area of 126 m^{2}g^{-1} and the values were 30.8 mgg^{-1} and 27.8 mgg^{-1} respectively.

For the Na$_2$CO$_3$ chemically activated carbon adsorbents, the best adsorbent for Cd(II) ion was the PTPNCA with a BET surface area of 437 m^{2}g^{-1}, with a $q_{e, cal}$ uptake value of 33.6 mgg^{-1}. For Pb(II) ion sorption, the best Na$_2$CO$_3$ chemically activated adsorbent was the CNFNCA with a surface area of 827 m^{2}g^{-1} and $q_{e, cal}$ loading of 29.1 mgg^{-1}. For the K$_2$CO$_3$ chemically activated carbon adsorbents the CNFKCA adsorbent with a BET surface area of 553 m^{2}g^{-1}, was the best adsorbent for both Cd(II) and Pb(II) ions. The $q_{e, cal}$ loadings obtained for the two ions were 33.0 mgg^{-1}and 30.1 mgg^{-1} for Cd(II) and Pb(II) ions respectively. The commercial activated carbon adsorbent (CGAC) had a BET surface area of 4273 m^{2}g^{-1} and the $q_{e, cal}$ loading for Cd(II) ion was for this adsorbent was 18.1 mgg^{-1}, while that of Pb(II) was 18.4 mgg^{-1}.

From an evaluation of the results in table 10.3 and the discussions presented above, the different adsorbents evaluated in this study can be ranked accordingly as follows; CNFS-HTC200 > YTBPCA > CNFS-HTC170 > PTPNCA > CNFKCA > PTHCA > CGAC > CNFS for Cd(II) sorption based on their adsorbent capacity using the kinetic parameter $q_{e, cal}$ obtained from the pseudo second order model. The ranking of the adsorbents for Pb(II) ion uptake is as follows; CNFS-HTC 200 > YTBPCA > CNFKCA > CNFNCA > PTHCA >

CNFS-HTC170 > CGAC > OPFS. This comparison indicates that the adsorbents based on the transformation of the coconut fibre residue (CNFS) have the best potential as adsorbents for Cd(II) and Pb(II) ion from aqueous systems and effluents. The capacity of this residue may be associated to a certain extent to the surface properties of the resulting materials especially the BET surface area and porosity.

10.3 Spent adsorbent stabilization studies

The adsorption of Cd(II) and Pb(II) ions onto the different adsorbents prepared and utilized in this study also gives rise to issues regarding the desorption and disposal of adsorbent saturated with heavy metal ions. Since sorption of these metal ions is a reversible process, in which the adsorbed ions may be desorbed from the adsorbent in acidic or basic media, proper disposal of the used adsorbents is fundamental due to the increasing incidence of metal pollution of the environment. This is because if these metal saturated adsorbents are not properly disposed, contamination issues may arise as these ions can be liberated upon contact with acid rain causing pollution to natural water receivers and groundwater (Papandreou *et al.,* 2007). It has also been observed that the leaching of heavy metal ions is increasingly becoming a cause of concern due to the increasing number of abandoned industrial sites (brownfields) in many developing countries. This has led to these toxic metal ions leaching into the soil and natural water around these sites due to improper management of these types of polluted areas (Voglar and Lestan 2013). Thus, it is important that appropriate pre-treatment methods be utilized for the stabilization of the metal ion saturated adsorbents obtained from this study as the safe disposal of these materials is an important component of the adsorption system being designed so as to make it more environmentally sustainable.

A number of methods have been reported for use in the stabilization of heavy metal saturated waste materials. Most of these methods involve solidification and stabilization (S/S) procedures using cement matrices. These include: calcium aluminate cement matrices (Navarro-Blasco *et al.,* 2013); matrices from treated clay powder and lime (Habib *et al.,* 2012); polyphosphate-calcium aluminate cement matrices (Fernandez *et al.,* 2014). These materials have been used to encapsulate and stabilize a number of heavy metal ions in cement based and non-cement based matrices. Based on the aforementioned materials, the approach in this study was to examine a polymer based stabilization procedure that can

be used to confine these toxic materials prior to their disposal in industrial landfills with appropriate protection against metal ion leaching into the environment.

A polymer encapsulation procedure was designed using polydimethylsiloxane (PDMS) to encapsulate the metal saturated ash obtained after the carbonisation of the Cd(II) and Pb(II) adsorbents. The nomenclature of the adsorbents for the disposal studies have been reported in section 4.4.1 of this thesis. Three sets of samples were used for the adsorbent disposal studies and these were adsorbents obtained after Cd(II) and Pb(II) sorption. The results were obtained in triplicates and the mean values of each concentration determined are presented. The standard deviation values for each set of concentration were used to determine the error values.

The first set were the metal ion loaded adsorbents that were only subjected to ash digestion prior to direct analysis to determine metal ion concentration and these were labelled used ash (UA). These were; CCYBNCA-Cd-UA; CCYBNCA-Pb-UA; OPFNCA-Cd-UA; PTHNCA-Pb-UA; CCPNCA-Cd-UA; CCPNCA-Pb-UA; YTBNCA-Cd-UA; YTBNCA-Pb-UA; CGAC-Cd-UA and CGAC-Pb-UA. The second set of used adsorbents analysed were those obtained from the leaching of the metal loaded adsorbent ash in deionized water. These were labelled deionized water leached ash (DWA). These included; CCYBNCA-Cd-DWA; CCYBNCA-Pb-DWA; OPFNCA-Cd-DWA; PTHNCA-Pb-DWA; CCPNCA-Cd-DWA; CCPNCA-Pb-DWA; YTBNCA-Cd-DWA; YTBNCA-Pb-DWA; CGAC-Cd-DWA and CGAC-Pb-DWA.

The third set of used adsorbents evaluated for adsorbent disposal were those obtained from metal loaded ash encapsulated in polydimethylsiloxane (PDMS) matrix as shown in Figure 10.2. These PDMS encapsulated samples were subjected to leaching in deionzed water. The samples were labelled encapsulated deionized water leached ash (EWA) and these were; CCYBNCA-Cd-EAW; CCYBNCA-Pb-EAW; OPFNCA-Cd-EAW; PTHNCA-Pb-EAW; CCPNCA-Cd-EAW; CCPNCA-Pb-EAW; YTBNCA-Cd-EAW; YTBNCA-Pb-EAW; CGAC-Cd-EAW and CGAC-Pb-EAW. Images of the Cd(II) and Pb(II) encapsulated samples shown in Figures 10.3 and 10.4. The DWA and EAW samples were leached in deionized water for 60 days after which the deionized water were analysed for Cd(II) and Pb(II) ions. The UA sample was analysed immediately after acid digestion as described in section 4.4.1of this thesis.
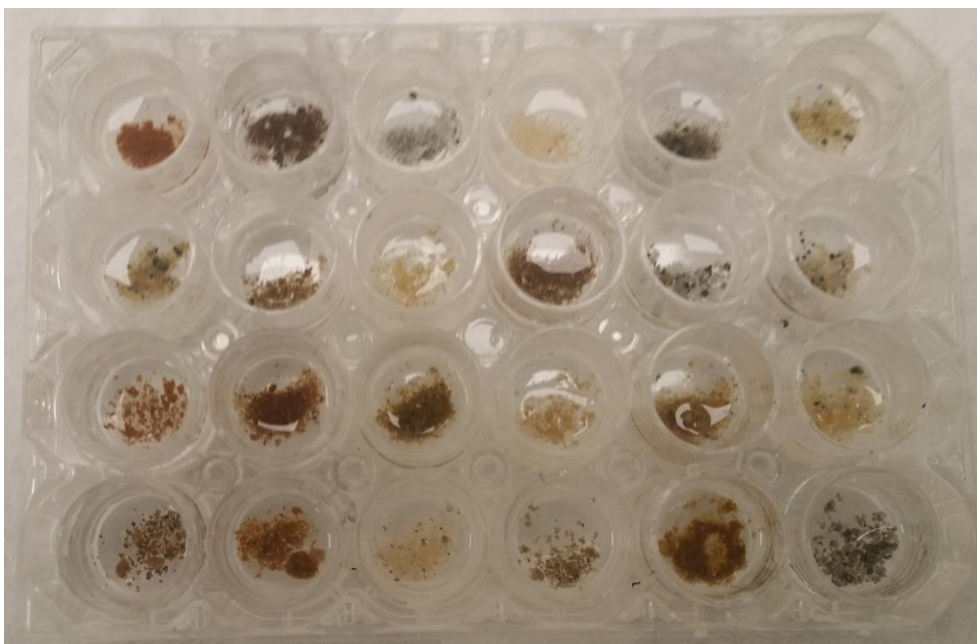
Figure 10.2: Photographs of PDMS encapsulated samples in mould

The concentration of these two metal ions in the UA samples gave an indication of the amount of metal ions in the used adsorbents after carbonisation. The results of the analysis of the different used adsorbent and leached adsorbents are presented in Table 10.4 and Figures 10.5 for Cd(II) adsorbents and 10.6 for Pb(II) adsorbents.

Examination of the results in Table 10.4 indicates that the concentration of the Pb(II) loaded adsorbent for the UA samples were higher than those of the Cd(II) loaded adsorbents and this may be associated with the degree of thermal stability of the two metal ions as the temperature of decomposition of Pb(II) precursor is higher than that of Cd(II) ion (401°C for $Cd(NO_3)_2.4H_2O$ and 470°C for $Pb(NO_3)_2$ (Fisher Scientific, 2014; Wojciechowski and Malecki, 1999).

Figure 10.3: Photographs of Cd(II) PDMS encapsulated samples

Figure 10.4: Photographs of Pb(II) PDMS encapsulated samples
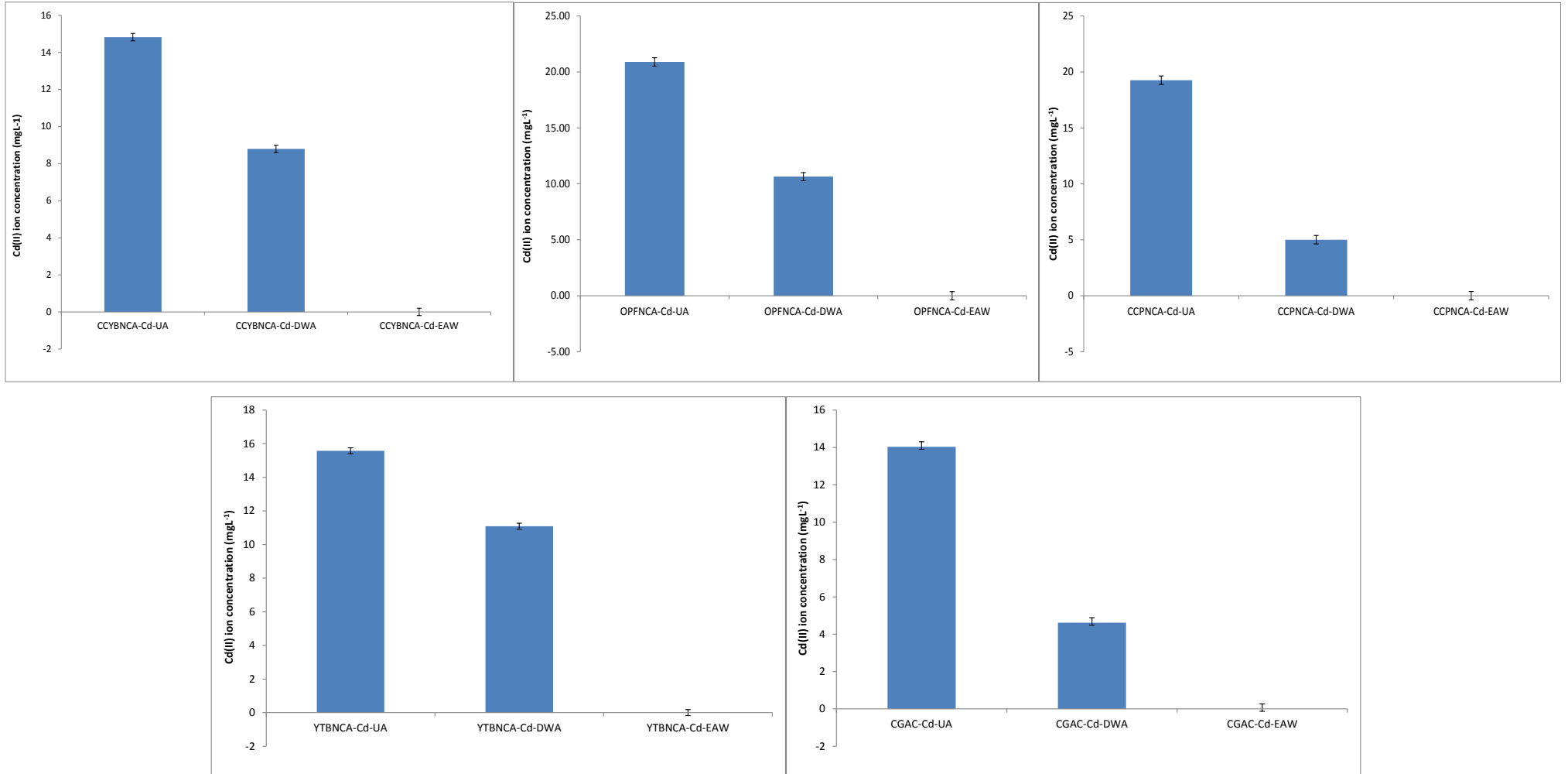
Fig.10.5: Cd(II) ion solution concentration in ash, leached and encapsulated adsorbents
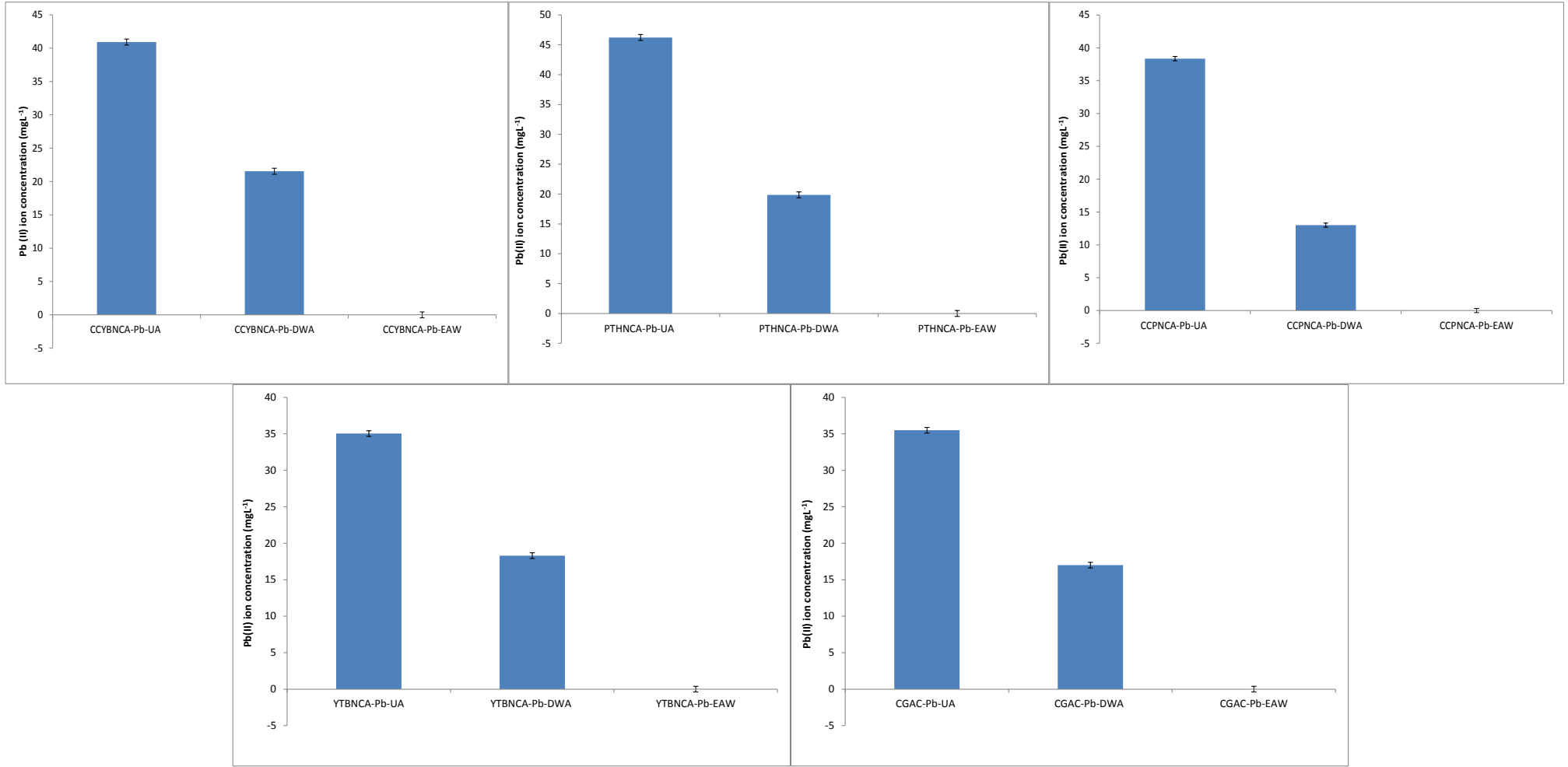
Fig.10.6: Pb(II) ion solution concentration in ash, leached and encapsulated adsorbents

Table 10.4: Metal ion concentration in spent adsorbent ash and leached systems

Cadmium	mgg^{-1}	Lead	mgg^{-1}
CCYBNCA-Cd-UA	14.82	CCYBNCA-Pb-UA	40.91
CCYBNCA-Cd-DWA	8.80	CCYBNCA-Pb-DWA	21.54
CCYBNCA-Cd-EAW	<0.005	CCYBNCA-Pb-EAW	<0.005
OPFNCA-Cd-UA	20.89	PTHNCA-Pb-UA	46.22
OPFNCA-Cd-DWA	10.64	PTHNCA-Pb-DWA	19.86
OPFNCA-Cd-EAW	< 0.002	PTHNCA-Pb-EAW	< 0.004
CCPNCA-Cd-UA	19.26	CCPNCA-Pb-UA	38.36
CCPNCA-Cd-DWA	5.01	CCPNCA-Pb-DWA	13.00
CCPNCA-Cd-EAW	<0.003	CCPNCA-Pb-EAW	<0.007
YTBNCA-Cd-UA	15.58	YTBNCA-Pb-UA	35.04
YTBNCA-Cd-DWA	11.09	YTBNCA-Pb-DWA	18.31
YTBNCA-Cd-EAW	< 0.005	YTBNCA-Pb-EAW	<0.002
CGAC-Cd-UA	14.04	CGAC-Pb-UA	35.49
CGAC-Cd-DWA	4.61	CGAC-Pb-DWA	17.00
CGAC-Cd-EAW	< 0.006	CGAC-Pb-EAW	<0.004

From Table 10.4 and Figs 10.5-10.6, it can be observed that the concentration of the two metal ions {Cd(II) and Pb(II)} in the used ash (UA) samples for all the examined adsorbents were higher than the ash leached in deionized water (DWA) for 60 days. In addition, the concentration of the two metal ions in the third set of samples (ash encapsulated in PDMS) denoted as (EAW) was negligible after 60 days of leaching in deionized water as seen in Table 10.4 for all the adsorbents. This indicates that the encapsulation of the spent adsorbent ash in a polymer (PDMS) can be a promising measure and an important component for the disposal of used adsorbents after sorption. This is because for the sorption of Pb(II) and Cd(II) ions using lignocellulosic carbon materials as adsorbents in this work, the option of subjecting the spent adsorbents to regeneration processes using acidic or alkaline solutions is not a straight forward process in most cases (Verbinnen *et al.,* 2015). This is due to the generation of heavy metal loaded sludge during the regeneration process which invariably recreates the problem again. Hence, for the study under consideration, the better approach of encapsulation using a polymer would serve as an effective means of stabilizing the toxic Cd(II) and Pb(II) saturated ashes obtained from the combustion of the used adsorbents and prevent their ease of leaching in an industrial landfill site.

The results encapsulation of the spent adsorbent ash in the PDMS polymeric matrix also has implications with respect to the strength of the polymer system to maintain the heavy metal ash under different conditions of disposal such as landfilling. This aspect of the study was not examined in this work as it was only focused on evaluating the leaching of the metal ions from the polymeric system if the disposal is into a liquid medium such as natural water bodies. Furthermore, the carbonisation and encapsulation process can also serve as means of reducing the volume of the used adsorbent prior to disposal. This process was observed to reduce the final volume of the used adsorbent prior to encapsulation by 80% for all the used adsorbents due to the thermal decomposition of the organic constituents if the different adsorbents with the evolution of carbondioxide and water. The disposal of these encapsulated adsorbents in the environments under consideration can be effected by the use of properly designed landfill sites with appropriate cementing procedures to avoid leaching on toxic compounds (Papandreou *et al.,* 2007).

10.4 Summary

The mechanisms that may influence the loading of the metal ions onto the different adsorbents used in this work were also highlighted using the uptake of Cd(II) ions onto the residue adsorbents as models. Based on the examination of the EDAX spectra uptake mechanism for the metal ions can proceed via ion-exchange due to the interaction of the metal ions on the residue adsorbent surface with the adsorbate system. Infra-red (IR) spectra evidence of the residue adsorbents after metal ion sorption were used infer the participation of hydroxyl, carbonyl, carboxylate, phenolic functional groups found on the surface of the residue adsorbents in metal ion sorption. Based on the IR spectra it was presumed that the Cd(II) ions in the adsorbate system could bond with the hydroxyl and carboxylic acid groups on the residue adsorbents by coordinating bonding.

The ranking of the commercial activated carbon (CGAC) with the Na_2CO_3 chemical activated adsorbents studied in Chapter 8 was carried using the Langmuir isotherm maximum loading capacity (q_{max}). All the adsorbents studied in this work were further ranked based on the kinetic modelling parameter to determine the adsorbents with optimum loading for the two metal ions. The comparison of the ranking parameter values obtained for the different adsorbents prepared in this study with that of the commercially obtained activated carbon adsorbent (CGAC) used as a benchmark for the adsorbents also

gave insight into the effectiveness of the different adsorbent modification regimes utilised in this study. The implications of the ranking of some of the absorbents based on the Langmuir isotherm parameter (q_{max}) and the complete ranking of all the adsorbents used in this study with the kinetic parameters ($q_{e, exp}$ & $q_{e, cal}$) showed that these adsorbents could be used as substitute materials for commercial activated carbon in water treatment applications for the removal of toxic cations. Based on these ranking the unmodified, Na_2CO_3 chemically activated carbon adsorbents and the commercial activated carbon adsorbent (CGAC) using the Langmuir isotherm parameter (q_{max}). It was observed that the adsorbent that is most effective for the removal of Cd(II) ion was CCPNCA with loading of $29.4 mgg^{-1}$, while for Pb(II) ion uptake, the best adsorbent was CCYBNCA with a loading of $41.9 mgg^{-1}$. Evaluating the performance of all the adsorbents examined in this study based on the kinetics of metal sorption, it was found that the best adsorbent for the removal of Cd(II) ion using the kinetic parameter $q_{e,exp}$ obtained at the end of the sorption experiment was CNFS-HTC 200 with a loading of $31.9 mgg^{-1}$, while for Pb(II) the most effective adsorbent was YTBPCA with a loading of $26.9 mgg^{-1}$. In addition to this, the pseudo second order (PSO) kinetic parameter $q_{e,cal}$ was also used to compare the adsorbents and the results indicated that the best adsorbent for Cd(II) and Pb(II) ion sorption was the CNFS-HTC 200 with a loadings of $33.8 mgg^{-1}$ and $34.6 mgg^{-1}$ respectively. The effect of adsorbent surface area on the kinetic q_e loadings obtained for the different adsorbents reported in this study were found to be significant but this was observed to have a less significant effect on the value of the Langmuir parameter q_{max}.

Adsorbent stabilization studies were conducted using some of the metal ion saturated adsorbents using a combustion process which was followed by polymeric encapsulation of the resulting ash. Leaching studies was carried out using the PDMS encapsulated ash and spent adsorbent ash in deionized water for 60 days. The results obtained indicated that the PDMS encapsulated spent ash were well stabilized within the polymeric system as the Cd(II) and Pb(II) ions did not leach into the deionized water.

CHAPTER ELEVEN

CONCLUSION & RECOMENDATIONS

CHAPTER ELEVEN

11.0 Conclusion and recommendations

Adsorption technology has been applied in the removal of a variety of pollutants from wastewater. The use of activated carbon for the treatment of municipal and industrial wastewaters in many countries has also developed quite rapidly and on a much larger scale than ever before. However in developing countries, the use of activated carbon mainly produced from developed countries, for the treatment of wastewater has huge financial implications thus limiting its use especially in small scale industries where the cost of the treatment process is fundamental to the wastewater treatment process deployed. This comes with the attendant consequences of dumping wastewater in natural streams, rivers and land with huge environmental implications for these countries. Due to this constraint, the utilisation of readily available materials such as agricultural residues and municipal waste as precursors for the production of carbon based adsorbents for use in wastewater treatment in these developing countries has become the focus of research.

Thus, this technology is expanding in scope and application more so, due to the types of wastewater and nature of adsorbents used. To reduce the environmental pollution incidences associated with wastewater in developing countries, the utilisation of low cost materials as adsorbents for wastewater treatment has been highlighted as an effective and economical approach to the problem. In line with this, there is a growing interest in the use of agricultural residues. The lack of appropriate waste management techniques for these agricultural residues results in indiscriminate disposal actions leading to environmental and health consequences. The utilisation of agricultural residues as a source of raw materials for the development of low cost carbon adsorbents is, therefore, an interesting area with environmental and economic benefits to developing economies in that most of these countries are agro-based and generate lots of agricultural substrates with potential properties as adsorbents.

The conversion of these agricultural residues into carbon based adsorbents induces certain physical and chemical properties which can affect their use as adsorbent for heavy metal removal. Thus, the need to study some of the techniques used to transform these materials into adsorbents and characterise the resulting sorbents. This would give insight into the

nature and transformations that take place during the synthesis of these adsorbents as well as the effect of these properties on the nature of the sorption process. The efficiency of adsorption depends on factors such as temperature, contact time, initial adsorbate concentration, adsorbent dosage and pH. Some of these variables were examined during the course of the study to understand their effect on the removal of the two metal ions of interest, Pb(II) and Cd(II) using some selected adsorbents from the pool of synthesised carbon based adsorbents.

HTC process is known to generate more oxygen-containing groups on the surface of the resulting hydrochar adsorbent. This property contributes to the improvement of the loading of these materials for metal ions from aqueous streams. Due to this increased functionality on the surface of the resulting biochar, the process has gained widespread use as a well-established thermo chemical synthesis alternative to produce a range of functional carbon materials with tunable chemical structure from different carbohydrate or lignocellulosic biomass. The properties and yield of the final products (solid, liquid and gas) depends strongly on the process conditions with the reaction temperature as the main governing process parameter. Thus, two temperature regimes were utilized in this study to characterise this effect on the properties and adsorption capability of the resulting hydrochars. Carbonisation, pyrolysis and chemical activation were the other methods deployed in the transformation of these residues into useful adsorbents in this study for the removal of Cd(II) and Pb(II) ions from aqueous systems.

The use of isotherm modelling to further describe the adsorption of an adsorbate onto the surface of an adsorbent has become one of the key features in adsorption literature. The isotherms give information on parameters that can be used to characterize the nature and mechanism of adsorption. The Langmuir model describes homogeneity of the surface with monolayer coverage of a fixed saturation capacity (q_{max}) while the Freundlich model characterizes the description of a heterogeneous surface with multilayer adsorption. The accuracy of an isotherm model to describe an adsorbent surface is generally a function of the number of independent parameters. However, the widespread application of these models is due mainly to their mathematical simplicity and the use of error parameters to describe the level of association of the models with experimental data makes them attractive in adsorption studies. In addition, the use of kinetic modelling for the examination of the rate of uptake of the two ions onto the different adsorbents prepared

was also evaluated. Finally, an examination of a measure to stabilise the spent adsorbents that were obtained in this study was also carried out.

11.1 Conclusion

The characterization and utilisation of some tropical agricultural residues (palm fruit fibre, coconut shell fibre, cocoa pod, plantain husk, cocoyam peel, sweet potato peel and white yam peel) obtained from Nigeria for the removal of Cd(II) and Pb(II) metal ions from aqueous system was examined in this work. The study was designed to evaluate the potential of some agricultural residues that are readily available in a developing country (Nigeria) as precursors for the preparation of adsorbents for use in wastewater removal as an alternative to the use of imported commercial activated carbon. These residues are generated in huge quantities, which make their efficient disposal challenging with their localities. Hence, the approach of using them for the production of adsorbents would provide an alternative route for these waste materials to be recycled in a sustainable manner. Two metal ions – Cd(II) and Pb(II) were chosen for the study due to their toxicity and prevalence in the Nigerian environment. The raw residues were characterised and used for adsorption studies. These residues were subsequently subjected to a number of thermo-chemical and hydrothermal treatments such as hydrothermal carbonisation, pyrolysis, carbonisation and chemical activation to improve their adsorption potential. The adsorbents obtained from these transformation were also characterised and use for sorption studies. The following conclusions can be made from the studies carried out:

- Results of the characterization studies indicates that the different agricultural residues used in the study had high ash content, low porosity and were acidic in nature. Their surface was characterize with rough fissures, no obvious pore arrangement except for the CNFS and OPFS residues and were amorphous nature. The residues had inorganic constituents including potassium, sulphur, iron, calcium and phosphorus which could be related to the nature of the soil of their cultivation. Hydroxyl, carboxylic, phenolic and amine functional groups were observed on their surface from infra-red spectroscopy and these are the presumed to be the main active sites that are responsible for metal ion sorption.
- From the sorption studies carried out, these residues were discovered to have low loading capacity and slow rate of metal uptake (kinetics) when utilized without treatment as adsorbents for adsorption of Cd(II) and Pb(II) ions. To improve their

metal ion loading potential, the residues were thereafter subjected to a number of modification process and these were; hydrothermal carbonisation, pyrolysis, carbonisation and chemical activation. From the equilibrium modelling studies carried out for Cd(II) ion and Pb(II) using agricultural residues, the Langmuir isotherm described the experimental data better than the Freundlich. The trend in the maximum Langmuir monolayer adsorption constant (q_{max}) for Pb(II) ion sorption was CCYBS > CCPS > PTPS >YTBS > CNFS > PTHS > OPFS with the maximum q_{max} of 33.mgg^{-1} obtained for the CCYBS adsorbent. For Cd(II) this trend was CCPS > YTBS > CNFS >CCYBS > PTPS > OPFS > PTHS with the maximum q_{max} of 24.5mgg^{-1}obtained from the CCPS adsorbent.

- The hydrothermal carbonization of the agricultural residue when compared with the other biomass treatment regimes (that have been studied in this work) is the only process that would involve the least capital outlay. This makes it a feasible process for adoption in developing economies where cost of production of materials is very high. Another advantage of the use of hydrothermal carbonization for the conversion of residue into useful adsorbents is the nature of the process and the requirement on type of biomass. The hydrothermal process is carried out in the presence of water and is not limited by high moisture content feedstock. This eliminates the cost of drying biomass before it is subjected to HTC treatment as is the ease in pyrolysis, carbonization and chemical activation. The biomass drying process eliminates or reduces the moisture content of these materials but the cost of drying before thermal treatment is higher than for a process that does not include drying (HTC Process).

- The physical and chemical characteristics of the prepared carbon adsorbents from the various thermo-chemical processes were evaluated using a range of characterisation techniques and these techniques gave insight into the chemical composition, porosity and morphology of the synthesized carbon adsorbents. Some of the characteristics of these carbon based adsorbents were observed to be temperature dependent while others were less sensitive to temperature. The prepared carbon adsorbents as well as the agricultural residues had poor mechanical strength when compared to the commercial activated carbon evaluated in this study; hence these materials would have higher performance when applied in adsorption columns rather than agitated reactor vessels. The adsorbate pH was an

important parameter in the determination of appropriate windows where the adsorbents will have optimum metal loading capabilities. All the adsorbents synthesized in this study and the agricultural residues used for adsorption were mesoporous in nature with bimodal or trimodal pore size distributions. The nature of the precursor used for hydrothermal carbonization and pyrolysis was observed to have a significant influence on the yield of the resulting hydrochar or biochar in addition to the temperature of treatment.

- The loss on attrition was a characteristic that was investigated due to its effect on the type of reaction systems that the synthesized adsorbent can be used in. The attrition characteristics of these adsorbents may be associated with the nature of the agricultural residue and effect of the synthesis conditions such as- thermal, hydrothermal and chemical activation processes on the morphology and microstructure of the final adsorbents. From this study, it was observed that hydrothermal carbonisation resulted in the highest percentage loss on attrition for the respective adsorbents (20-37%). The process of pyrolysis was found to produce adsorbents with the least attrition losses (5-7%). For the carbonised adsorbents, the loss on attrition was in the range of 10-13%, while those obtained from the process of chemical activation was between 7-18%. As a point of perspective, the loss on attrition for the commercial activated carbon adsorbent (CGAC) was 4%. This implies that the pyrolysed adsorbents are best suited for use in batch reactor systems and those obtained from the hydrothermal carbonisation are the least suited.

- Surface area was a crucial factor in the determination of the rate of metal ion uptake as the higher surface area chemically activated carbon adsorbents and pyrolysed adsorbents had the highest metal ion uptake. However, there was an exception to this trend as the optimum uptake for Cd(II) ions for all the prepared adsorbents was obtained using the CNFS-HTC 200 adsorbent (31.1mgg^{-1}) with a surface area of 260 m^{2}g^{-1}. The prepared adsorbent with the highest surface area in this study was the CNFNCA with a BET surface area of 827 m^{2}g^{-1} and its optimum uptake for Cd(II) ion was 27.71mgg^{-1}. Quiet interestingly these two loadings for Cd(II) were higher that what was obtained using the commercial activated carbon (CGAC) which had an optimum loading for Cd(II) of 17.23 mgg^{-1}. This result implies that the surface area alone is not the only criterion for determining optimum

adsorbents as uptake of metal ions will also depend on chemical interactions between the adsorbate and the adsorbent.

- The kinetics of Cd(II) and Pb(II) sorption was also studied for the residues and the different carbon based adsorbents. For the residues the kinetics was studied from 5-1440 minutes and the optimum contact time 180 minutes was obtained and used for the kinetic studies of the hydrothermal, carbonised, pyrolysed, chemically activated carbon and commercial activated carbon (CGAC) adsorbents. The optimum contact time for these adsorbent were different, the commercial activated carbon (CGAC) had an optimum contact time of 30 minutes, for the Na_2CO_3 chemical activated carbon adsorbents this was 40 minutes, for the hydrothermal carbonised HTC-200, pyrolysed, carbonised and K_2CO_3 chemically activated adsorbents this was 60 minutes, while for the hydrothermal carbonised HTC-170 this was achieved after 90 minutes. This result indicated that based on rate of ion uptake, the Na_2CO_3 chemically activated adsorbents was the best adsorbent due to its fast kinetics which was comparable that the commercial product (CGAC). The fast kinetic profile for the prepared carbon adsorbents indicates that they can be effective for heavy metal ion removal with short residence intervals.

- Kinetic modelling for the sorption of Cd(II) and Pb(II) ions using the developed and the CGAC adsorbents indicated that the pseudo-first order (PFO) model described the sorption better than the pseudo second order (PSO) for both ions, implying that the rate limiting step of sorption is dependent on the concentration of the ions in solution. However, the closeness of the parameters obtained from the PSO model for all the adsorbents may also indicate that chemical interactions between the ions in the adsorbate solution and the adsorbent may also influence the rate of sorption but this may depend on the rate of diffusion as indicated in the two stage metal uptake (fast and slow) profiles obtained for all the adsorbents. This implies that pore diffusivity of the ions onto the active sites may also influence metal sorption kinetics.

- The results of the kinetics of Cd(II) and Pb(II) ion sorption indicated that for the unmodified residues, the highest uptake was observed for the OPFS adsorbent for Pb(II) ion ($12.5 mgg^{-1}$) and CNFS for Cd(II) ion ($16.3 mgg^{-1}$). For the hydrothermal carbonised adsorbents, optimum uptake for Cd(II) and Pb(II) ions was obtained using CNFS-HTC 200 adsorbent with loadings of $31.2 mgg^{-1}$ for Cd(II) and 26.8

mgg^{-1} for Pb(II). The uptake for the pyrolysed and carbonised adsorbents indicated that for Cd(II) ion sorption, the CCPPCA adsorbent was the best with loading of 29.8 mgg^{-1}, while for Pb(II), the best adsorbent was YTBPCA with a loading of 26.7 mgg^{-1}. For the chemically activated carbon adsorbents, the CNFKCA adsorbent was the best for Cd(II) ion removal with a loading of 28.3 mgg^{-1}, while for Pb(II) ion removal was best achieved using the CNFNCA adsorbent with a loading of 25.2 mgg^{-1}. For the commercial activated carbon adsorbent (CGAC), the loading for Cd(II) and Pb(II) ions were 17.23 mgg^{-1} and 16.84 mgg^{-1} respectively. The adsorbent surface area is presumed to play an important role in the facilitation of metal ion sorption but this was not always the case for these adsorbents as the uptake for the commercial activated carbon adsorbent was lower than what was obtained for most of the adsorbents developed in this study with the exception of the residue adsorbents. The prepared adsorbents also had higher values of metal ion loading than most of those reported in literature based on a comparison of both. The uptake capacity obtained from the kinetic study of the sorption of Cd(II) and Pb(II) for these chemically activated adsorbents prepared in this study were also higher than that obtained for the commercial activated carbon adsorbent (CGAC).

- Equilibrium isotherm modelling studies were also carried out using the Na$_2$CO$_3$ chemically activated carbon adsorbents. The results obtained for Pb(II) and Cd(II) indicate an increasing metal ion uptake with increasing concentration. The Langmuir and Freundlich isotherm models were used to characterize the metal ion loading. The coefficient of determination r^2, the chi-square (χ^2) and the root mean square error (RMSE) values were used as fitting parameter to determine which of the isotherm best describes the sorption of the two heavy metal ions. From the value of the fitting parameter, the Langmuir isotherm had a better fit to the experimental equilibrium data metal ion sorption. The Langmuir isotherm constant "q$_{max}$" was computed for the different adsorbents and the results indicates that the value of q$_{max}$ for both Cd(II) and Pb(II) uptake from aqueous solution onto the adsorbents were comparable with that reported in literature. The Langmuir isotherm constant q$_{max}$ values indicated that the PTHNCA adsorbent had the least maximum loading capacity while the CCYBNCA adsorbent had the highest loading capacity for the Pb(II) ion with a loading of 41.9 mgg^{-1} and the trend in q$_{max}$ for Pb(II) ion was CCYBNCA > PTPNCA > OPFNCA > CNFNCA > YTBNCA >

PTHNCA. When compared with that for Cd(II) ion the trend was CCPNCA > PTPNCA > CCYBNCA > OPFNCA > CNFNCA > YTBNCA > PTHNCA, where the highest loading was 29.4mgg^{-1}(CCPNCA).

- The 7 residue adsorbents and the Na_2CO_3 chemically activated adsorbents were ranked with the commercial activated carbon based on the Langmuir isotherm constant (q_{max}). From this comparison, it was observed that the adsorbent that is most effective for the removal of Cd(II) ion was CCPNCA with a loading of 29.4mgg^{-1}, while for Pb(II) ion uptake, the best adsorbent was CCYBNCA with a loading of 41.9mgg^{-1}. The performances of all the adsorbents prepared in this study were also compared based on the kinetics of metal sorption. From the results of the ranking it was found that the best adsorbent for the removal of Cd(II) ion using the kinetic parameter $q_{e,exp}$ obtained at the end of the sorption experiment was CNFS-HTC 200 with a loading of 31.9mgg^{-1}, while for Pb(II) the most effective adsorbent was YTBPCA with a loading of 26.9mgg^{-1}. In addition to this, the pseudo second order (PSO) kinetic parameter $q_{e,cal}$ was also used to compare the adsorbents and the results indicated that the best adsorbent for Cd(II) and Pb(II) ion sorption was the CNFS-HTC 200 with a loadings of 33.8mgg^{-1} and 34.6mgg^{-1} respectively. The effect of adsorbent surface area on the kinetic q_e loadings obtained for the different adsorbents reported in this study were found to be significant but this was observed to have a less significant effect on the value of the Langmuir parameter q_{max}. The implications of the ranking of some of the absorbents based on the Langmuir isotherm parameter (q_{max}) and the complete ranking of all the adsorbents used in this study with the kinetic parameters ($q_{e, exp}$ & $q_{e, cal}$) showed that these adsorbents could be used as substitute materials for commercial activated carbon in water treatment applications for the removal of toxic cations.

- The $q_{e exp}$ values obtained from the kinetics of Cd(II) and Pb(II) ion sorption were used to evaluate the different adsorbents in this study and the trend was as follows; CNFS-HTC200 > CCPPCA > CNFKCA > CNFNCA > CNFCA > CNFS-HTC170 > CGAC > CNFS for Cd(II) sorption. For Pb(II) ion uptake the adsorbents were ranked also using the $q_{e exp}$ values as follows; CCPPCA > CNFS-HTC200 > CNFNCA > CNFKCA > CNFCA > CNFS-HTC170 > CGAC > OPFS. Ranking of the best adsorbents from each set of preparation method evaluated in this study was also carried out based on the pseudo-second order (PSO) kinetic parameter $q_{e,cal}$

and the results showed the trend as; CNFS-HTC200 > YTBPCA > CNFS-HTC170 > PTPNCA > CNFKCA > PTHCA > CGAC > CNFS for Cd(II) sorption, while that for Pb(II) ion uptake is as follows; CNFS-HTC 200 > YTBPCA > CNFKCA > CNFNCA > PTHCA > CNFS-HTC170 > CGAC > OPFS. This comparison indicates that the adsorbents based on the transformation of the coconut fibre residue (CNFS) have the best potential as adsorbents for Cd(II) and Pb(II) ion from aqueous systems and effluents. The capacity of this residue may be associated to a certain extent to the surface properties of the resulting materials especially the BET surface area and porosity.

- Consideration was also given to discriminate the possible mechanisms that can affect the loading of the two metal ions onto the different adsorbents used in study using Cd(II) ion as the model case. Ion-exchange, surface complexation, physical and chemical adsorption may be the interactions that determine the loading of these two metal ions on the surface of the different types of adsorbents used in this work. This was based on the characteristics of the materials studied before and after metal ion sorption using techniques such as solution pH, EDAX and infrared spectroscopy. Based on the examination of the EDAX spectra, uptake mechanism for the metal ions is presumed to proceed via ion-exchange due to the interaction of the metal ions on the residue adsorbent surface with the adsorbate system. Infra-red (IR) spectral evidence of the residue adsorbents after metal ion sorption were used infer the participation of hydroxyl, carbonyl, carboxylate and phenolic functional groups found on the surface of the residue adsorbents in metal ion sorption. Also, based on the results of the Infrared spectra of the residue adsorbents, it was suggested that the Cd(II) ions in the adsorbate system could bond with the hydroxyl and carboxylic acid groups on the residue adsorbents by coordinating bonding.

- Adsorbent stabilization studies were also carried out with some of the metal ion saturated adsorbents using a combustion process which was followed by polymeric encapsulation of the resulting ash. Leaching studies was carried out using the PDMS encapsulated ash and spent adsorbent ash in deionized water for 60 days. The results obtained indicated that the PDMS encapsulated spent ash was well stabilized within the polymeric system as the Cd(II) and Pb(II) ions did not leach into the deionized water.

Thus, the results obtained in this work implies that the prepared adsorbents obtained using different modification regimes were effective for Cd(II) and Pb(II) ions removal from aqueous systems. Comparisons were also made with similar adsorbents based on waste biomass and these materials had metal ion loadings that were similar and better in some instances than those obtained in previous literature and commercially available activated carbon adsorbent. Hence these adsorbents can be used for treatment of effluents within the location of interest. The results of this study also highlight the potential of using agricultural waste as precusors for the development of useful adsorbents for metal ion sorption especially in developing economies.

11.2 Recommendations

From the above conclusion, the issues that relate to conversion of agricultural residues into useful adsorbents that can have industrial wastewater applications converge on the conclusion that a variety of processes needs to be carried out before an agricultural residue can meet the industrial criteria of for wastewater treatment as high metal binding capacity is not a sufficient factor to judge a material's suitability. Insight into the mechanism of metal ion sorption is still not well understood and this is an important area that is crucial in the design of optimum sorbents.

Hence the following recommendations can be made:

- The sorption process requires further research into the mechanism of metal ion transport and their effect of the adsorbent structure. In addition the discrimination of metal ion binding mechanism should be investigated in more detail using instrumental techniques such as X-ray photoelectron spectroscopy (XPS) and solid-state and liquid nuclear magnetic resonance spectroscopy (NMR) to give insight into the actual chemical environment and species in the adsorption system. The advancement in insitu methods using these techniques would contribute significantly to the understanding of these mechanisms.

- The degree of technical applicability of the system to be designed, plant simplicity and cost effectiveness are important factors that have to be taken into consideration in the selection of the modes of application of these low cost adsorbents in these developing economies. Thus, the cost implications of the adsorbent development have to be investigated so that a broad view of the overall implication of the technology can be evaluated.

- Multi-metal ion sorption on the adsorbents in the presence of some organic compounds and other contaminants should be investigated. This is because the wastewater systems that these low-adsorbents will be used to treat often have multiple pollutants as these species can influence the nature of adsorbent-adsorbate interactions.

- Research into the evaluation of the environmental impacts of these low cost residues in terms of using life cycle approach (LCA) should be carried out as this will generate important data that will be useful in predicting the benefits or problems of using these materials in their target areas.

- Column adsorption studies should be carried out so as to generate data that can be used in the scale-up of the technology to give insight into their feasibility on a commercial scale. This would be important as the adsorbents prepared in this study had high attrition losses, hence would be best applied in column adsorption systems where there is less agitation of the column bed.

- Research into the synthesis and application of composite adsorbents using these agricultural residues can also be carried out to give insight into extent to which these materials can be modified to improve their adsorption performance especially in the synthesis of multi-functional composites and their regeneration.

- Studies into the modelling of the process of regeneration of the used sorbents and the recovery of the metal ions and the immobilisation of the waste material or recovery of the adsorbent after complete use should be carried out to give insight into the approaches that can enhance efficiency and environmental sustainability.

REFERENCES

Abdullah, S. S.; Yusup, S.; Ahmad, M. M.; Ramli, A. and Ismail, L. (2010) Thermogravimetry study on pyrolysis of various lignocellulosic biomass for potential hydrogen production. *International Journal of Chemical and Biological Engineering,* 3:3: 137-141.

Abdus-Salam, N. and Adekola, F. A. (2005)The influence of pH and adsorbent concentration on adsorption of Lead and Cadmium. *African Journal of Science and Technology,* 6(2): 55-66.

Abollino, O.; Aceto, M.; Malandrino, M.; Sarzanini, C. and Mentasti, E. (2003) Adsorption of heavy metals on Na-montmorillonite- Effect of pH and organic substances. *Water Research,* 1619-1627.

Adamafio, N.A. (2013). Theobromine Toxicity and Remediation of Cocoa By-products: An Overview. *Journal of Biological Sciences,* 13: 570-576.

Acharya, J.; Sahu, J. N.; Mohanty, C. R. and Meikap, B. C. (2009) Removal of lead(II) from wastewater by activated carbon developed from Tamarind wood by zinc chloride activation. *Chemical Engineering Journal,* 149: 249-262.

Adediran, G. O.; Tella, A. C. and Mohammed, H. A. (2007) Adsorption of Pb, Cd, Zn, Cu and Hg ions on formaldehyde and pyridine modified Bean Husk, *Journal of Applied Science and Environmental Management,* 11(2): 153-158.

Adekunle, A.S.; Oyekule, J.A.O.; Baruwa, S.O; Ogunfowokan, O.A. and Ebenso, E.E.(2014) Speciation study of the heavy metals in commercially available recharge cards coatings in Nigeria and the health implications. *Toxicology Reports*, 1: 243-251.

Adelekan, B. A. (2012) An Evaluation of the Global Potential of Cocoyam (*Colocasia and Xanthosoma species*) as an Energy Crop. *British Journal of Applied Science &Technology,* 2((1): 1-15.

Ademiluyi, F. T; Amadi, S. A.; Amakama, N. J. (2009) Adsorption and Treatment of Organic Contaminants using Activated Carbon from Waste Nigerian Bamboo. *Journal of Applied Science and Environmental Management,* 13(3): 39-47.

Ademoroti, C. M. A. (1996) *Environmental Chemistry and Toxicity: Pollution by Heavy Metals*. Foludex Press Ibadan pp: 152-173.

Adeolu A.T and Enesi D.O. (2013) Assessment of proximate, mineral, vitamin and phytochemical compositions of plantain (*Musa paradisiaca*) bract – an agricultural waste. *International Research Journal of Plant Science,* 4(7):192-197.

Adewumi, I.K. (2009) Activated Carbon Water treatment in Nigeria: Problems and Prospects. In: *Appropriate Technologies for Environmental Protection in the Developing World*. Yanful, E.K (ed), Springer Science+ Business Media. B.V. Netherlands. pp 115-122.

Adie, G. U. and Osibanjo, O. (2009) Assessment of Soil-pollution by slag from an automobile battery manufacturing plant in Nigeria. *African Journal of Environmental Science and Technology,* 3(9): 239-250.

Ahmad, F.; Daud, W. M. A. W.; Ahmad, M. A. and Radzi, R. (2012a) Cocoa (*Theobroma cacao*) shell-based activated carbon by CO_2 activation in removing of cationic dye from aqueous solution. Kinetics and equilibrium studies. *Chemical Engineering Research and Design,* 9-0: 1480-1490.

Ahmad, M.; Anushka, R. U. Paskska, A. U.; Lim, J. E. Zhang, M.; Bolan, N.; Mohan, D.; Vithanage, M.; Lee, S. S. and Ok, Y. S. (2014a) Biochar as a sorbent for contaminant management in soil and water: A Review. *Chemosphere,* 99: 19-33.

Ahmad, M. A.; Puad, N. A. A. and Bello, O. S. (2014b) Kinetic, equilibrium and thermodynamic studies of synthetic dye removal using pomegranate peel activated carbon prepared by microwave-induced KOH activation. *Water Resources and Industry,* 6: 18-35.

Ahmad, M.; Lee, S. S.; Dou, X.; Mohen, D.; Sung, J. K; Yang, J. Y. and Sung, J. (2012b) Effects of pyrolysis temperature on soybean stove-and peanut shell-derived biochar properties and TCE adsorption in water. *Bioresource Technology,* 118: 536-544.

Ahmadzadeh, A. and Zakaria, S. (2009) Preparation of Novolak resin by liquefaction of oil palm empty fruit bunches (EFB) and characterisation of the EFB residue. *Polymer-Plastics Technology and Engineering*, 48:10-16.

Ahmaruzzaman, M. (2010) A Review on the utilization of fly ash. *Progress in Energy and Combustion Science,* 36: (3) 327-363.

Ajimal, M.; Rao, R. A. K.; Anwar, S.; Ahmad, J.; Ahmad, R. (2003) Adsorption studies on rice husk: removal and recovery of Cd(II) from wastewater. *Bioresource Technology,* 86: 147-149.

Akpomie, K.G.; Dawodu, F.A. and Kayode O. Adebowale, K.O. (2015) Mechanism on the sorption of heavy metals from binary-solution by a low cost montmorillonite and its desorption potential. *Alexandria Engineering Journal*, 54(3): 757-767.

Aksu, Z. (2002) Determination of the equilibrium, kinetic and thermodynamic parameters of the batch biosorption of nickel(II) ions onto Chlorella vulgaris. *Process Biochemistry*, 38:89-99.

Alhawas, M.; Alwabel, M.; Ghoneim, A.; Alfarraj, A. and Sallam, A. (2013) Removal of Nickel from Aqueous Solution by Low-Cost Clay Adsorbents. *Proceedings of the International Academy of Ecology and Environmental Sciences*, 3(2): 160-169. Available Internet: http://www.iaees.org/publications/journals/piaees/articles/2013-3(2)/removal-of-nickel-from-aqueous-solution.pdf   Accessed on 20/07/2013

Ali, I. and Gupta, V. K. (2007) Advances in water treatment by adsorption technology. *Nature Protocols,* 1(6): 2661-2667.

Ali, R.M.; Hamad, A.A.; Hussein, M.M. and Malash, G.F. (2016) Potential of using green adsorbent of heavy metal removal from aqueous solutions: Adsorption kinetics, isotherm, thermodynamics, mechanisms and economic analysis. *Ecological Engineering,* 91:317-332.

Ali, M.; Al-Hashimi, I. and Al- Safar, M. M. (2013) Removal of cadmium from synthetic water using agricultural wastes. ACTA TECHNICA CORVINIENSIS – *Bulletin of Engineering Tome,* VI -FASCICULE 2: 131-138.

Al-Lagtah, N.M.A.; Al-Muhtaseb, A.H.; Ahmad, M.N.M and Salameh, Y. (2016) Chemical and physical characteristics of optimal synthesised activated carbons from grass-derived sulfonated lignin versus commercial activated carbons. *Microporous and Mesoporous Materials*, 225: 504-514.

Alkan, M., Demirbaş, Ö. and Doğan, M. (2007) Adsorption kinetics and thermodynamics of an anionic dye onto sepiolite. *Microporous and Mesoporous Materials*, 101(3): 388-396.

Alkan, M.; Karadas, M.; Dogan, M. and Demirbas, O. (2009) Zeta potentials of perlites samples in various electrolyte and surface media. *Colloids and Surfaces A: Physicochemical and Engineering Aspects,* 259(1-3): 155-166.

Allen, S. J.; Gan, Q.; Matthews, R. and Johnson, P. A. (2005) Kinetic modelling of the adsorption of basic dyes by kudzu. *Journal of Colloid and Interface Science* 286: 101-109.

Al-Maydama, H.; El-Shekeil, A.; Khalid, M. A.; Al-Karbouly, A. (2006) Thermal degradation behaviour of some polydithiooxamide metal complexes. *Ecletica Quimica,* 31 (1): 45-52.

Alslaibi, T.M.; Abustan, I.; Ahmad, M.A. and Foul, A.A. (2013) Cadmium removal from aqueous solution using microwaved olive stone activated carbon. *Journal of Environmental Chemical Engineering*, 1: 589-599.

Alo B.I and Olanipekun, A. (2006) Heavy metal pollution in different environmental media in Africa: Problems and prospects (with case studies from Nigeria). A Presentation by the Pollution Control Department, Federal Ministry of Environment, Abuja, Nigeria. Available internet: http://www.who.int/ifcs/documents/forums/forum5/olanipekun_alo.pdf Accessed on 12/10/2010.

Aluko, O. B. and Koya, O. A. (2006) Some Engineering Properties of Yam setts from two species of yams, *Journal of Food Engineering,* 76: 396-401.

Alva-Argaez, A.; Kokossis, A. C.; Smith, R. (2007) The design of water using systems in petroleum refining using a water pinch decomposition. *Chemical Engineering Journal,* 128*:* 33- 46.

Alvarez-Ayuso, E.; Garcia-Sanchez, A.; Querol, X. (2003) Purification of metal electroplating wastewaters using zeolites. *Water Research,* 37: 4855-4862.

Amir, M. H.; Dariush, N.; Fourgh, V.; Shakrokh, N. (2005) Teawaste as an adsorbent for heavy metal removed from industrial wastewaters. *American Journal of Applied Science,* 2(1): 372-375.

Ammari, T. G.; Al-Labadi, I.; Tahboub, A. and Ghrair, A. (2015) Assessment of unmodified wetland bio-waste: Shoots of *Cyperus laevigatus*, for cadmium adsorption from aqueous solutions. *Process Safety and Environmental Protection,* 95: 77-85.

Amuda, O. S.; Ojo, O.; Edewor, J. I. (2007) Biosorption of lead from industrial wastewater using *chrysophyllum albidum* seed shell. *Bioremediation Journal,* 11 (4) 183-194.

Amusa, N. A.; Adegbite, A. A.; Muhammed, S. and Baiyewu, R. A. (2003) Yam Diseases and its Management in Nigeria. *African Journal of Biotechnology,* 2(12): 497-502.

Anandhan, S. (2008) Thermal Analysis. Available internet: http://www.nitk.ac.in/static/assets/files/MetMat/Dr.AS/TGA.pdf Accessed on 17/10/2012.

Antonio-Cisneros, C. M. and Elizalde-Gonzalez, M. P. (2010) Characterization of manihot residues and preparation of activated carbon. *Biomass and Bio-energy,* 34: 389-393.

Antunes, W.M.; Luna, A.S.; Henriques, C.A. and Costa, A.C.A. (2003) An evaluation of copper biosorption by a brown seaweed under optimized conditions. *Electronic Journal of Biotechnology*,6(3).Available internet: Available from Internet: http://www.ejbiotechnology.info/content/vol6/issue3/full/5/index.html. Accessed on 12/10/2012.

Anyakora, C.; Nwaeze, K.; Awodele, O.; Nwadike, C.; Arbabi, M. and Coker, H.(2011) Concentrations of heavy metals in some pharmaceutical effluents in Lagos, Nigeria. *Journal of Environmnetal Chemistry and Ecotoxicology*, 3(2): 25- 31.

AOAC (2000) *Official Methods of Analysis*. Horwitz, W(ed), 17th Ed. Association of Official Analytical Chemist. Gaithersburg MD. Publishers, Virginia, USA.

APIS (2014) Air Pollution Information System. Available internet: http://www.apis.ac.uk/overview/pollutants/overview_HM.htm Accessed on 12/12/2015.

Appenroth, K. J. (2010) Definition of "heavy metals" and their role in the biological systems. In: *Soil Heavy Metals, Soil Biology*. I. Sherameti and A. Varma (eds), vol.19.DOI 10.1007/978-3-642-02436-8.Springer-Verlag, Berlin Heidelberg.

Arief, V. O.; Trilestari, K; Sunarso, J.; Indraswati, N.; and Ismadji, S. (2008) Recent Progress on Biosorption of Heavy Metals from Liquids using Low Cost Biosorbents: Characterisation, Biosorption Parameters and Mechanism Studies. *Clean*, 36(12): 937-962.

Arpa, C., Say, R., Satiroglu, N., Bektas, S., Yurum, Y. and Genc, O. (2000). Heavy Metal Removal from Aquatic Systems by Northern Anatolian Smectites. *Turkish Journal of Chemistry,* 24:209 – 215

Arvanitoyannis, I. S.; Ladas, D.; Mavromatis, A. (2006) Potential uses and applications of treated wine waste: a review. *International Journal of Food Science and Technology,* 41: 475- 487.

Askarieh, G.; Hedhammar, M.; Nordling, K.; Saenz, A.; Cristina Casals, C.; Rising, A.; Johansson, J. and Knight, S.D. (2010) Self-assembly of spider silk proteins is controlled by a pH-sensitive relay. *Nature*, 465 (7295):236-239.

Asuquo, E. D. (2005) Sorption of some heavy metal ions on modified and unmodified oil palm (*Elaeis guineensis*) fruit fibre. Unpublished MSc Thesis, University of Port Harcourt, Nigeria.

Athar, M.; Farooq, V.; Aslam, M. and Salam, M. (2013) Adsorption of Pb(II) ions onto biomass from *Trifolium resupinatum*: equilibrium and kinetic studies. *Applied Water Science,* 3: 665-672.

Akhtar, N.; Iqbal, J. and Iqbal, M. (2004) Removal and recovery of nickel (II) from aqueous solution by Ioofa sponge-immobilized biomass of *Chlorella sorokiniana*: characterisation studies. *Journal of Hazardous Materials*, 108(1-2): 85-94.

ATSDR (2008) Agency for Toxic Substances and Disease Registry-Case Studies in Environmental Medicine (CSEM) Cadmium Toxicity. Available Internet: http://www.atsdr.cdc.gov/csem/cadmium/docs/cadmium.pdf Accessed on 20/12/2012

ATSDR (2010) Agency for Toxic Substances and Disease Registry-Case Studies in Environmental Medicine (CSEM) Lead Toxicity. Available Internet: http://www.atsdr.cdc.gov/csem/lead/docs/lead.pdf Accessed on 20/12/2012.

Awoyale, A.A; Eloka-Eboka, A.C. and Odubiyi, O.A.(2013) Production and experimental efficiency of activated carbon from local waste bamboo for wastewater treatment. *International Journal of Engineering and Applied Sciences*,3 (2):8-17.

Ayenimo, J.G.; Adeeyinwo, C.E. and Amoo, I.A. (2005) Heavy metal pollutants in Warri river, Nigeria. *Kragujevac Journal of Science*, 27: 43-50.

Ayoola P.B; Adeyeye A (2009) Proximate Analysis and Nutrient Evaluation of Some Nigerian Pawpaw Seeds Varieties. *Sci. Focus*. 14(4): 554-558.

Azargohar, R.; Nanda, S.; Kozinski, J. A; Dalai, A.K. and Sutarto, R. (2014) Effects of temperature on the physicochemical characteristics of fast pyrolysis bio-chars derived from Canadian Waste biomass *Fuel,* 125: 90-100.

Aziz, A. A.; Husin, M. and Mokhtar, A. (2002) Preparation of Cellulose from Oil Palm empty Fruit bunches via ethanol digestion: Effect of Acid and Alkali catalysts. *Journal of Oil Palm Research,* 14(1): 9-14.

Azizian, S. (2004) Kinetic models of sorption: a theoretical analysis. *Journal of Colloid and Interface Science*, 276: 47-52.

Babayemi, J. O.; Dauda, K. T.; Kayode, A. A. A.; Nwude, D. O.; Ajiboye, J. A.; Essien, E. R., and Abiona, O. O. (2010) Determination of Potash Akali and Metal content of ashes obtained from peels of some varieties of Nigerian Grown Musa Species. *BioResources* 5(3)1384-1392.

Babel, S. and Kurniawan, T. A. (2003a) Low-cost adsorbents for heavy metal uptake form contaminated water: a review. *Journal of Hazardous Materials,* B97: 219-243.

Babel, S. and Kurniawan, T. A. (2003b) A research study on Cr (VI) removal from contaminated wastewater using natural zeolite. *Journal of Ion Exchange,* 14: 289-292.

Babel, S. and Kurniawan, T. A. (2004) Cr(VI) removal from synthetic wastewater using coconut shell charcoal and commercial activated carbon modified with oxidizing agents and/ or chitosan. *Chemosphere*, 54:951-97.

Baes, G. B. and Mesmer, R. E. (1976) *Hydrolysis of Cations*. John Wiley and Sons Ltd. New York. P.365.

Bagajewicz, M. (2000) A review of recent design procedures for water networks in refineries and process plants. *Computers and Chemical Engineering,* 24(9): 2093-2115.

Bailey, S. E.; Olin, T. J.; Bricka, M. R.; Adrian, D. D. (1999) A review of potentially low-cost sorbents for heavy metals. *Water Research,* 3(11): 2469-2479.

Balkaya, N. and Cesur, H. (2008) Adsorption of Cadmium from aqueous solution by phosphogypsum. *Chemical Engineering Journal,* 140: 247 – 254

Banerjee, S.; Gautam R. K.; Jaiswal, A.; Chattopadhyaya, M. C. and Sharma, Y. C (2015) Rapid scavenging of methylene blue dye form a liquid phase by adsorption on alumina nanoparticles. *RSC Advances,* 5: 14425-14440.

Barkar, N.; Abdennouri, M.; El Makhfouk, M. and Qourzal, S. (2013) Biosorption characteristics of cadmium and lead onto eco-friendly dried cactus (*opuntia ficus indica*) cladodes. *Journal of Environmental Chemical Engineering,* 1: 144-149.

Barontini, F.; Rocchi, M.; Tugnolo, A.*;* Cozzani, V.; Tetteh, J.; Jarriault, M. and Zinovik, I. (2013) Quantitative analysis of evolved gas in the thermal decomposition of a Tobacco substrate. *Chemical Engineering Transactions*, 32:703-708.

Bartczak, P; Norman, M.; Klapiszewski, L.; Karwańska, N.; Kawalec, M.; Baczyńska, M.; Wysokowski, M.; Zdarta, J.; Ciesielczyk, F. and Jesionowski, T. (2015) Removal of nickel(II) and lead(II) ions from aqueous solution using peat as a low-cost adsorbent: A kinetic and equilibrium study, *Arabian Journal of Chemistry*, In Press: http://dx.doi.org/10.1016/j.arabjc.2015.07.018

Basha, S.; Murthy, Z.V.P and Jha, B. (2009) Sorption of Hg(II) onto *Carica papaya*; Experimental studies and design of batch sorber. *Chemical Engineering Journal*, 147:226-234.

Basso, M. C.; Cerrella, E. G. and Cukierman, A. L. (2002). Lignocellulosic materials as potential biosorbents of trace toxic metals from wastewater. *Industrial Engineering Chemistry Research,* 41: 3580-3585.

Benaissa, H. (2006) Screening of new sorbent materials for cadmium removal from aqueous solutions. *Journal of Hazardous Materials,* B132: 189 – 195.

Benavente, M. (2008) Adsorption of Metallic Ions onto Chitosan: Equilibrium and Kinetic Studies, Licentiate Thesis of Royal Institute of Technology- Department of Chemical Engineering and Technology, Division of Transport Phenomena, Stockholm, Sweden. Available internet: http://www.diva-portal.org/smash/get/diva2:13755/FULLTEXT01.pdf Accessed on 12/12/2010.

Betiku, E. and Ajala, S.O. (2014) Modeling and optimization of *Thevetia peruviana* (yellow oleander) oil biodiesel synthesis via *Musa paradisiacal* (plantain) peels as heterogeneous base catalyst: A case of artificial neural network vs. response surface methodology. *Industrial Crops and Products*, 53:314–322.

Bhatnagar, A. and Sillanpaa, M. (2010) Utilization of agro-industrial and municipal waste materials as potential adsorbents for wastewater- A Review. *Chemical Engineering Journal,* 157: 277-296.

Bhattacharyya, K. G.; Sharma, G. (2005) Kinetics and thermodynamics of methylene blue adsorption on Neem (*Azadirachta indica*) leaf powder. *Dyes and Pigments,* 65: 51-59.

Bindell, J, B. (2000) Scanning Electron Microscopy. In: *Encyclopedia of Material characterisation, Brundle*, C. R.; Evans, C.A and Wilson, S.C. (eds), Butterworth-Heinemann, USA.

Blacksmith Institute (2012) The World's Worst Pollution Problems: Assessing Health Risk at Hazardous Waste Sites. Available Internet: http://www.worstpolluted.org/files/FileUpload/files/2012%20WorstPolluted.pdf Accessed on 2/01/2013.

Blazquez, G.; Martin-Lara, M. A.; Tenorio, G. and Calero, M. (2011) Batch biosorption of lead (II) from aqueous solutions by olive tree pruning waste: Equilibrium, kinetics and thermodynamics study. *Chemical Engineering Journal,* 168: 170 – 177.

Bodirlau, R.; Teaca, C.A. and Spiridon, I. (2009) Preparation and characterisation of composites comprising modified hardwood and wood polymers/poly (vinyl chloride). *Bioresources*, 4(4):1285-1304.

Boss, C. B. and K. J. Fredeen (1997) *Concepts, Instrumentation and Techniques in Inductively Coupled Plasma Optical Emission Spectrometry.* Perkin. Elmer Corporation, USA.

Boudrahem, F.; Aissani-Benissad, F. and Ait-Amar, H. (2009) Batch sorption dynamics and equilibrium for the removal of lead ions from aqueous phase using activated carbon developed from coffee residue activated with zinc chloride. *Journal of Environmental Management,* 90: 3031-3039.

Boudrahem, F.; Aissani-Benissad, F. and Soualah, A.(2011) Adsorption of Lead (II) from aqueous solution by using leaves of Date Trees as an adsorbent. *Journal of Chemical Engineering Data,* 56:1804-1812.

Brouwer, P. (2010) *Theory of XRF - Getting Acquainted with the Principles*. 3rd ed. PANalytical B.V. Almelo, Netherlands. pp10-18.

Bowen, J. H. (1991). Sorption Processes. In: *Chemical Engineering*. 2nd ed. Vol. 3 Coulson, J. M. and Richardson, J. F. (eds). Pergamon Press, Oxford.

Brown, A. M. (2001) A step-by-step guide to non-linear regression analysis of experimental data using a Microsoft Excel Spreadsheet. *Computer Methods and Programs in Biomedicine,* 65: 191-200.

Brunauer, B.; Deming, L. S.; Deming, W. E. and Teller, E. (1940) On a Theory of the van der Waals Adsorption of Gases. *Journal of American Chemical Society*, 62: 1723-1732.

Brunauer, S.; Emmett, P. H and Teller, E. (1938) Adsorption of gases in multimolecular layers. *Journal of American Chemical Society,* 60: 309-319.

Burgess, J. (1978) Metal ions in Solution. John Wiley & Sons, New York.

Busch, D.; Stark, A. Kammann, C. I and Glaser, B. (2013) Genotoxic and phytotoxic risk assessment of fresh and treated hydrochar from hydrothermal carbonization compared to biochar from pyrolysis. *Ecotoxicology and Environmental Safety,* 9759-66.

Cechinel, M. A. P.; Souza, S. M. A. G. U.; Souza, A. A.; Augusto, A. and Souza, U. (2014) Study of lead (II) adsorption onto activated carbon originating from cow bone. *Journal of Cleaner Production,* 65: 342-349.

Ceribasi, H.I. and Yetis, U. (N 2001) Biosorption of Ni (II) and Pb(II) by *Phanaerochate chrysosporium* from binary metal system-kinetics. *Water SA*, 27(1):15-20.

Chakravarty, P.; Sarma, N.S. and Sarma, H.P.(2010) Removal of lead(II) from aqueous solution using heartwood of Areca catechu powder. *Desalination*, 256(1-3):16-21.

Chand, P.; Shil, A.K.; Sharma, M. and Pakade, Y.B. (2014) Improved adsorption of cadmium ions from aqueous solution using chemically modified apple pomace: mechanism, kinetics and thermodynamics. *International Biodeterioriation & Biodegradation*, 90:8-16.

Chandumpai, A.; Singhpibulporn, N.; Faroongsarng, D. and Sornprasit, P. (2004) Preparation and Physico-chemical characterisation of chitin and chitosan from the pens of

the squid species, Loligo *lessoniana* and Loligo *formosana. Carbohydrate Polymers,* 58: 467-474.

Chang, Y. M.; Tsai W.T.; Li, M. H. and Chang, S.H. (2015) Preparation and characterization of porous carbon material from post-extracted algal residue by a thermogravimetric system. *Algal Research*, 9: 8-13.

Chen, B.; Hui, C.W.H. and McKay, G. (2001) Film-pore diffusion modeling and contact time optimization for the adsorption of dyestuffs on pith. *Chemical Engineering Journal*, 84: 77-94.

Chen, C. (2013) Evaluation of Equilibrium Sorption Isotherm Equations. *The Open Chemical Engineering Journal* 7: 24-44.

Chen, H. (2014) *Biotechnology of Lignocellulose-Theory and Practice*. Springer-Netherlands, pp25-71.

Chen, X.; Chen, G.; Chen, L.; Chen, Y.; Lehmann, J.; McBride, M. B. and Hay, A.C. (2011) Adsorption of copper and Zinc by biochars produced from pyrolysis of hardwood and corn straw in aqueous solution. *Bioresource Technology,* 102: 8877-8884.

Cheng, G.; Varanasi, P. ; Chenlin, L.; Liu, H.; Melnichenko,Y. B.; Blake, A. S.; Kent, M. S. and Seema, S. (2011) Transition of cellulose crystalline structure and surface morphology of biomass as a function of ionic Liquid Pretreatment and its Relation to Enzymatic Hydrolysis. *Bio-macromolecules* .dx.doi.org/10.1021/bm101240z.

Chi, Y; Geng, W.; Zhao, L.; Yan, X,; Yuan, Q.; Li, N. and Li, X (2012) Comprehensive study of mesoporous carbon functionalized with carboxylate groups and magnetic nano particles as a promising adsorbent *Journal of Colloid and Interface Science,* 369: 366-372.

Chindah, A. C.; Braide, A. S. and Sibeudu, O. C. (2004) Distribution of hydrocarbons and heavy metals in sediment and a crustacean (Shrimps—*Penaeus notialis*) from the Bonny/New Calabar River Estuary, Niger Delta. *AJEAM-RAGEE* 9: 1–17

Chiou, M. S.; Ho, P. Y. and Li, H. Y. (2004) Adsorption of anionic dyes in acid solution using chemically cross-linked chitosan beads. *Dyes and Pigments,* 60: 69-84.

Chojnacka, K.; Chojnacki, A. Gorecka, H. (2004) Trace element removal by *Spirulina sp.* from copper smelter and refinery effluents. *Hydrometallurgy,* 73: 147-153.

Chowdhury, Z. Z.; Zain, S. M.; Khan, R. A, Arami-Niya, A and Khalid, K. (2012) Process variables optimization for preparation and characterization of novel adsorbent form lignocellulosic waste. *BioResources,* 7(3): 3732-3784.

Chunfeng, W.; Jiansheng, L.; Xia, S.; Lianjun, W. and Xiuyun, S. (2009) Evaluation of zeolites synthesized from fly ash as potential adsorbents for wastewater containing heavy Metals. *Journal of Environmental Science,* 21: 127-136.

Ciolacu, D.; Ciolacu, F. and Popa, V.I. (2011) Amorphous cellulose-structure and characterisation. *Cellulose Chemistry and Technology*, 45(1-2): 13-21

Clearfield, A.; Reibenspies, J. H. and Bhuvanesh, N. (2008) *Principles and Applications of Powder Diffraction*. Blackwell Publishing Ltd, West Sussex.

Coelho, A.; Castro, A. V.; Dezotti, M.; Sant'Anna Jr, G. L. (2006) Treatment of petroleum refinery source water by advanced oxidation process. *Journal of Hazardous Materials,* B137: 178-184.

Coelho, G. F.; Goncalves, A.C.; Tarley, C. R. T.; Casarin, J.; Nacke, H. and Francziskowski, M. A. (2014) Removal of metal ions Cd (II), Pb (II) and Cr (III) from water by the cashew nut shell *Anacardium occidentale* L. *Ecological Engineering,* 73: 514 – 525.

Connolly, J. R. (2010) Introduction to X-Ray Powder Diffraction. Available internet: http://epswww.unm.edu/xrd/xrdclass/01-XRD-Intro.pdf Accessed on 03/04/2012.

Cordero, D. J.; Heras, F.; Alonso-Morales, N.; Gilarranz, M. A. and Rodriguez, J. J. (2013) Porous structure and morphology of granular chars from flash and conventional pyrolysis of grape seeds. *Biomass and Bioenergy* 54: 123-132.

Cotton, F. A. and Wilkinson, G. (1972). *Advanced Inorganic Chemistry* 3rd ed. John Wiley & Sons Inc. New York.

Crini, G. (2005) Recent Development in Polysaccharide-based Materials used as Adsorbents in Wastewater Treatment. *Progress in Polymer Science,* 30: 38-70.

Cruz-Olivares, J.; Perez –Alonso, C; Barrera-Diaz, C.; Natividad, R. and Chaparro-Mercado, M. C. (2011) Thermodynamical and analytical evidence of lead ions chemisorption onto *Pimenta dioica. Chemical Engineering Journal,* 166: 814 – 821.

Cruz, G.; Pirila, M.; Huuhtanen, M.; Carrion, L.; Alvarenga, E. and Keiski, R. (2012) Production of activated carbon from Cocoa (*Theobroma cacao*) Pod Husk. *Journal of Civil Environmental Engineering,* 2(2): 109 – 114.

Cuenot, F.; Meyer, M.; Bacaille, A.; Guilard, R. (2005) A molecular approach to remove lead form drinking water. *Journal of Molecular Liquids*, 118: 89 – 99.

Cullity, B. D. and Stock, S. R. (2001) *Elements of X-ray Diffraction*, Vol.3, Prentice Hall, New Jersey.

Dabrowski, A. (2001) Adsorption-from theory to Practice. *Advances in Colloid and Interface Science,* 93: 135-224

Danish, M.; Hashim, R.; Ibrahim, M. M. N.; Rafatullah, M,; Ahmad, T and Sulaiman, O. (2011) Characterisation of *Acacia Mangium* wood based Activated Carbon Prepared in the Presence of Basic Activating Agents. *BioResources,* 6(3): 3019-3033.

Davydov, A.(2003) *Molecular Spectroscopy of Oxide Catalyst Surfaces*. John Wiley & Sons, Ltd.

Dean, J. G. ; Bosqul, F. L and Lanouette, K. H. (1972) Removing Heavy Metals from Wastewater, *Environmental Science and Technology*, 6(6): 518-521.

De Haro-Del Rio, D.A; Al-Joubori, S.; Kontogiannis,O.; Papadatos-Gigantes, D.; Ajayi, O.; Li, C. and Holmes, S.M. (2015) The removal of caesium ions using supported clinoptilolite. *Journal of Hazardous Materials*, 289:1-8.

Deiana, A. C..; Sardella, M. F.; Silva, H.; Amaya, A. and Tancredi, N. (2009) Use of grape stalk, a waste of the viticulture Industry to obtain activated carbon. *Journal of Hazardous Materials,* 172: 13 -19.

Deliyanni, E.A.; Kyzas, G. Z.; Triantafyllidis, K.S. and Matis, K.A. (2015) Activated carbons for the removal of heavy metal ions: A systematic review of recent literature focused on lead and arsenic. *Open Chemistry*, 13:699-708.

Demirbas, A. (2000) Mechanism of liquefaction and Pyrolysis is reaction of biomass. *Energy Conversion and Management,* 1(6): 633-646.

Demirbas, A. (2006) Effect of temperature on pyrolysis products from four nut shells. *Journal of Analytical and Applied Pyrolysis,* 76: 285-289.

Demirbas, A. (2007) Heavy metal adsorption onto agro based waste materials: A review. *Journal of Hazard Material,* 157(2-3): 220-229.

Demirbas, E.; Kobja, M.; Senturk, E.; Ozkan, T. (2004) Adsorption kinetics for the removal of chromium (VI) from aqueous solution on the activated carbons prepared from agricultural wastes. *Water SA,* 30 (4): 533-540.

Deraman, M.; Zakaria, S.; Husin, M.; Aziz, A.A.; Ramli, R. ;Mokhtar, A.; Yusof, M.N.M. and Sahri, M.H. (1999) X-ray Diffraction Studies on Fiber of Oil Palm Empty Bunch and Rubberwood for Medium–density Fiberboard. *Journal of Materials Science Letters,* 18(3):249-253.

Diaz-Teran, J.; Nevskaia, D, M.; Fierro, J. L. G.; Lopez-Peinado, A. J. and Jerez, A. (2003) Study of chemical activation process of a lignocellulosic material with KOH by XPS and XRD. *Microporous and Mesoporous Materials,* 60: 173-181.

Ding, S. (2014) Overview of Lignocellulose: Structure and Chemistry. In: *Biological Conversions of Biomass for Fuels and Chemicals: Explorations from Natural Utilization Systems.* Sun, J; Ding, S. and Doran-Peterson, J. (eds). RSC Energy and Environmental Series No. 10. The Royal Society of Chemistry, Cambridge. pp14-25.

Ding, W.; Dong, X.; Ime, I. M.; Gao, B and Ma, L. Q. (2014) Pyrolytic temperatures impact lead sorption mechanism by bagasse biochars. *Chemosphere,* 105: 68-74.

Djilani, C.; Zaghoudi, R.; Modarressi, A.; Rogalski, M. and Djazi, F. (2012) Elimination of organic micro pollutants by adsorption on activated carbon prepared from agricultural waste. *Chemical Engineering Journal,* 189-190: 203-213.

Dodd, J. W.; Tonge, K. H. (1987) Thermal method. John Wiley and Sons, London.

Dubey, S. P. and Gopal, K. (2006) Adsorption of Chromium (VI) on low-cost adsorbents derived from agricultural materials: a comparative study. *Journal of Hazardous Materials,* 145: 467-470.

Duffus, J.H.(2002) "Heavy metal"-a meaningless term? *Pure and Applied Chemistry*, 74:793-807.

Duong, D.D.(1998) *Adsorption Analysis: Equilibria and Kinetics.* Series on Chemical Engineering. Vol.2. Imperial College Press, London.

Duru, C. C. and Uma, N .U (2003) Protein Enrichment of solid waste from cocoyam (*Xanthosoma sagittifolium* (L) Schott) cormel processing using *Aspergillus oryzae* obtained from Cormel Flour. *African Journal of Biotechnology,* 2(8): 228-232.

Duruibe, J.O.; Ogwuegbu, M.O.C. and Egwurugwu, J.N. (2007) Heavy metal pollution and human biotoxic effects. *International Journal of Physical Sciences*, 2(5); 112-118.

EAG (2013) Inductively Coupled Plasma Spectroscopy (ICP-OES) ICP Analysis. Available internet: http://www.eaglabs.com/mc/inductively-coupled-plasma-spectroscopy.html Accessed on 12/02/2013.

Ekiye, E. and Zejiao, L. (2010) Water quality monitoring in Nigeria; Case study of Nigeria's industrial cities. *Journal of American Science*, 6(4): 22-28.

Egbe, M. O.; Afuape, S. O. and Idoko, J. A. (2012) Performance of Improved Sweet Potato (*Ipomea batatas* L.) Varieties in Makurdi, Southern Guinea Savanna of Nigeria. *American Journal of Experimental Agriculture,* 2(4): 573-58.

Ekpete, O. A. and Horsfall, M. Jnr (2011) Preparation and Characterization of Activated Carbon derived from Fluted Pumpkin Stem Waste (*Telfairia occidentalis Hook F*). *Research Journal of Chemical Sciences,* 1(3): 10-17.

El-Ashtoukhy, E-S. Z.; Amin, N. K. and Abdelwahab, O. (2008) Removal of lead (II) and copper (II) from aqueous solution using pomegranate peel as a new adsorbent. *Desalination,* 223(2008): 162-173.

Elaigwu, S.E.; Rocher, V.; Kyriakou, G. and Greenway, G.M. (2014) Removal of Pb^{2+} and Cd^{2+} from pyrolysis and microwave-assisted hydrothermal carbonisation of *Prosopis africana* shell. *Journal of Industrial and Engineering Chemistry*, 20:3467-3473.

El-Khaiary, M.I; Malash, G.F, Ho,Y.S (2010) On the use of linearized pseudo-second-order kinetic equations for modeling adsorption systems. *Desalination,* 257; 93-101.

El-Shafey E.I.A and Al-Hashmi, H.R. (2013) Sorption of lead and silver from aqueous solution on phosphoric acid dehydrated carbon. *Journal of Environmental Chemical Engineering*, 1(4): 934-944.

Elizalde-Gonzalez M. P. and Hernandez-Motoya, V. (2009) Guava seed as an adsorbent and a precursor of carbon for the adsorption of acid dyes. *Bioresource Technology,* 100: 2111-2117.

Elnasri, N. A.; Elshiek, M. A. and Eltayeb, M. A. (2013) Physico-chemical characterization and Freundlich Isotherm Studies of Adsorption of FE (II) from aqueous solution by using Activated carbon prepared from Doum fruit waste. *Archives of Applied Science Research,* 5:149 -158.

Emoyan, O. O.; Ogban, F. E. and Akarah, E. (2006) Evaluation of heavy metals loading of river Ijana in Ekpan-Warri, Nigeria. *Journal of Applied Science & Environmental Management,* 10: 121–127.

EPS (2015) Engineering Performance Solutions-Powdered Activated Carbon Test & Services. Available internet: http://www.epslabs.com/powdered_activated_carbon_services Accessed on 12/01/2016.

Erdem, M.; Ucar, S.; Karagoz, S. and Turgay, T. (2013) Removal of Lead(II) ions from aqueous solutions onto activated carbon derived from waste biomass. *The Scientific World Journal*, article ID 146092, 7 pages. http://dx.doi.org/10.1155/2013/146092

Etchie, A. T.; Etchie, T. O.; Adewuyi, G. O.; Krishnamurthi, K.; Devi, S. S and Wate, S. R. (2013) Prioritizing Hazardous Pollutants in Two Nigerian Waters Supply Schemes; A Risk-based Approach. *Bulletin of the World Health Organisation,* 91: 553-561.

Eziashi, E. and Omamor, I.(2010) Lethal yellowing disease of the coconut palms (*cocos nucifera* l.): An overview of the crisis. *African Journal of Biotechnology*, 9(54): 9122-9127.

Falco, C.; Macro-Lozar, J. P.; Salinas-Torres, D.; Morallon, E.; Cazorla- Amors, D.; (2013) Tailoring the porosity of chemically activated hydrothermal carbons: Influence of the precursor and hydrothermal carbonization temperature. *Carbon,* 62: 346-355

Fang, J.; Gao, B.; Chen, J. and Zimmerman, A. R. (2015) Hydrochars derived from plant biomass under various conditions: Characterization and Potential application and impacts. *Chemical Engineering Journal,* 267: 253-259.

FAO, (1997) African Oil Palm- Food and Agricultural Organisation. Available internet: http://www.fao.org/docrep/003/w3647e/W3647E04.htm Accessed on 12/02/2013

FAO (2013) Food and Agricultural Organisation- Analysis of Incentives and disincentives for cocoa in Nigeria. Available internet: http://www.fao.org/3/a-at586e.pdf. Accessed 12/8/2014

FAOSTAT (2015) Food and Agricultural Organisation of the United Nations Statistics Division. Available internet: http://faostat3.fao.org/browse/Q/QC/E Accessed 12/4/2015.

Fakayode, S.O. and Onianwa, P.C.(2002) Heavy metal contamination of soil and bioaccumulation in guinea grass (*Panicum maximum*) around Ikeja Industrial estate, Lagos Nigeria. *Environmnetal Geology*, 43:145-150.

Fasinu, P.S. and Orisakwe, O.E. (2013) Heavy metal pollution in sub-Saharan Africa and possible implications in Cancer Epidemiology. *Asian Pacific Journal of Cancer Prevention*, 14: 3393-3402.

Feng, D.; van Deventer, J.S.J. and Aldrich, C. (2004) Removal of pollutants from acid mine wastewater using metallurgical by-product slags, *Separation and Purification Technology*, 40, (1): 61-67.

Feng, N.; Guo, X. and Liang, S. (2009) Adsorption study of copper (II) by chemically modified orange peel. *Journal of Hazardous Materials* 164: 1286-1292.

Fernandes, M. E.; Ledesma, B.; Roman, S.; Bonelli, P. R. and Cukierman, A. L. (2015) Development and characterization of activated hydrochars from orange peels as adsorbents for emerging organic contaminants. *Bioresource Technology*, 183: 221-228.

Fernandez, J.M.; Navarro-Blasco, I.; Duran, A.; Sirera, R. and Alvarez, J.I. (2014) Treatment of toxic metal aqueous solutions: Encapsulation in a phosphate calcium aluminate matrix. *Journal of Environmental Management*, 140: 1-13.

Fierro V.; Torne-Fernandez V.; Montane D.; Celzard A. (2008) Adsorption of phenol onto activated carbons having different textural and surface properties. *Microporous and Mesoporous Materials,* 111, 276– 284.

Fiol, N.; Villaescusa, I.; Martinez, M. Miralles, N.; Poch, J. and Serarols, J. (2006) Sorption of Pb(II), Ni(II), Cu(II) and Cd(II) from aqueous solution by olive stone waste. *Separation and Purification Technology,* 50: 132-140.

Fisher Scientific (2014) Material Safety Data Sheet-Lead (II) nitrate. Available internet: http://www.fishersci.com/msds?productName=AC193320100&productD.Accessed on 12/12/2015.

Foo, K.Y. and Hameed B. H. (2010) Insights into the modelling of adsorption isotherm systems. *Chemical Engineering Journal,* 156: 2-10.

Funke, A. and Ziegler, F. (2010) Hydrothermal Carbonization of biomass: A summary and discussion of chemical mechanism for process engineering. *Biofuels, Bioproduct & Biorefining,* 4: 160-177.

Flegler, S. L.; Heckman, J. W. Jr., and Klomparens, K. L (1993) *Scanning and Transmission Electron Microscopy*: An Introduction, W. H. Freeman and Company, New York.

Freundlich, H. M. F. (1906) Over the Adsorption in Solution. *Journal of Physical Chemistry,* 57: 385-471.

Fu, P.; Hu, S.; Xiang, J.; Li, Peisheng, Huang, D.; Jiang, L.; Zhang, A and Zhang, J. (2010) FTIR study of pyrolysis products evolving from typical agricultural residues. *Journal of Analytical and applied pyrolysis,* 88(2):117-123.

Galwey, A. K and Brown, M. E. (1998) Kinetic background to thermal analysis and calorimetry. In: *Handbook of Thermal Analysis and Calorimetry*. Brown, M. E. (Ed) vol. 1: Principles and Practices, 1st ed. Elsevier Science, Amsterdam pp: 147-224.

Garg, U.; Kaur, M. P.; Jawa, G. K.; Sud, D. and Garg, V. K. (2008) Removal of cadmium (II) from aqueous solutions by adsorption on agricultural waste biomass. *Journal of Hazardous Materials,* 154 (1-3): 1149-1157.

Gaspard, S.; Passé-Coutrin, N.; Durimiel, A.; Casaire, T. and Jaenne-Rose, V. (2014) Activated carbon from biomass for water treatment. In: *Biomass for sustainable application: Pollution remediation and energy.* Gaspard, S. and Ncibi, M, C, (eds). The Royal Society of Chemistry, Cambridge: 46-60

Gauden, P. A.; Terzyk, A. P.; Jaroniec, M. and Kowalczyk, P. (2007) Bimodal pore size distributions for carbons: Experimental results and computational studies. *Journal of Colloid and Interface Science,* 310: 205-216.

Gautam, R. K.; Mudhoo, A.; Lofrano, G.; Chattopadhyaya, C. M. (2014) Biomass-derived biosorbents for metal ions sequestration: Adsorbent modification and activation methods and adsorbent regeneration. *Journal of Environmental Chemical Engineering,* 2: 239-259.

Gaya, U.I.; Otene, E. and Abdullah, A.H. (2015) Adsorption of aqueous Cd(II) and Pb(II) on activated carbon nanopores prepared by chemical activation of doum palm shell. *Springer Plus*, 4:458. DOI:10.1186/s40064-015-1256-4.

Gercel, O. and Gercel, H. F. (2007) Adsorption of lead (II) ions from aqueous solutions by activated carbon prepared from biomass plant material of *Euphorbia rigida*. *Chemical Engineering Journal,* 132: 289-297.

Ghasemi, M.; Naushad, M.; Ghasemi, N. and Khosravi-fard, Y. (2014) Adsorption of Pb(II) from aqueous solution using new adsorbent prepared from agricultural waste:

Adsorption isotherm and kinetic studies. *Journal of Industrial Engineering Chemistry,* 20(4): 2193-2129.

Ghodbane, I.; Nouri, L.; Hamdaoui, O. and Chiha, M. (2008) Kinetic and equilibrium study for the sorption of cadmium (II) ions from aqueous phase by eucalyptus bark. *Journal of Hazardous Materials,* 152: 148-158.

Ghorbani, F.; Younesi, H.; Mehraban, Z.; Celik, M.S.; Ghoreyshi, A.A and Anbia, M. (2013) Preparation and characterisation of highly pure silica from sedge as agricultural waste and its utilisation in the synthesis of mesoporous silica. *Journal of the Taiwan Institute of Chemical Engineers*, 44:821-828.

Giraldo, I and Moreno-Pirajan, J. C. (2012) Synthesis of activated carbon mesoporous form coffee waste and its application in adsorption of zinc and mercury ions from aqueous solutions. *Journal of Chemistry,* 9(2): 938-948

Goel, J.; Kadirvelu, K.; Rajagopal, C. and Garg, V. K. (2005) Removal of lead (II) by adsorption using untreated granular activated carbon: batch and column studies. *Journal of Hazardous Materials,* 125(1-3): 211-20.

Gomez-Serrano, V.; Macias-Garcia, A.; Espinosa-Mansilla, A. and Valenzuela-Calahorro, C. (1998) Adsorption of mercury, cadmium and lead from aqueous solution on heat-treated and sulphurised activated carbon. *Water Research*, 32(1):1-4.

Gong, X. (2013) Kinetic and Equilibrium Studies on the Adsorption of Pb(II), Cd(II) and Cu(II) by Rape Straw. *Adsorption Science and Technology,* 31(6): 559-571.

Gonzalez-Navarro, M. F. Giraldo, L. and Moreno-Pirajan, J. C. (2014) Preparation and characterization of activated carbon for hydrogen storage form waste African oil- palm by microwave-induced LiOH basic activation. *Journal of Analytical and Applied Pyrolysis,* 107: 82-86.

Goodhew, P. J; Humphreys, J. and R Beanland, R. (2001) *Electron Microscopy and Analysis.* 3rd Ed. CRC Press, pp 16-213.

Goyal, P.; Sharma, A.; Srivastava, S and Srivastava, M.M. (2008) *Saraca indica* leaf powder for decontamination of Pb: removal, recovery, adsorbent characterisation and equilibrium modelling. *International Journal of Environmental Science and Technology,* 5(1)27-34.

Goyer, R. A. (1993) Lead Toxicity: Current Concerns. *Environmental Health Perspectives*, 100: 177-187

Grassi, M.; Kaykioglu, G.; Belgiorno, V. and Lofrano, G. (2012) Removal of Emerging Contaminants from Water and Wastewater by Adsorption Process. In: *Emerging Compounds for Wastewater*. Lofrano, G. (ed) SpringerBriefs in Green Chemistry for Sustainability. Springer, USA.

Greenwood, N. N. and Earnshaw, A. (2006) *Chemistry of the Elements*. 2nd Ed, Elsevier Ltd, Oxford.

Guo, J. and Lua, A. C. (2002) Characterization of adsorbent prepared from oil-palm shell by CO_2 activation for removal of gaseous pollutants. *Material Letters,* 55: 334-339.

Guo, J. and Lua, A. (1998) Characterisation of Chars Pyrolysed from Oil Palm Stones for the Preparation of Activated Carbons. *Journal of Analytical and Applied Pyrolysis,* 46: 113-125.

Guo, J.; Xu, W.S.; Chen, Y.L. and Lua, A.C.(2005) Adsorption of NH_3 onto activated carbon prepared from palm shells impregnated with H_2SO_4. *Journal of Colloid and Interface Science,* 281: 285-290.

Gurses A., Hassani A., Kıransan M., Acıslı O. and Karaca S. (2014) Removal of methylene blue from aqueous solution using by untreated lignite as potential low-cost adsorbent: Kinetic, thermodynamic and equilibrium approach, *Journal of Water Process Engineering*, 2 10–21.

Gutierrez-Segura, E.; Solache-Rios, M.; Colin-Cruz, A. and Fall, C. (2012) Adsorption of cadmium by Na and Fe modified zeolitic tuffs and carbonaceous material from pyrolyzed sewage sludge. *Journal of Environmental Management*, 97: 6-13.

Guyer, H. H. 1998 *Industrial processes and waste streams management*. John Wiley and Sons, Inc. New York. pp 24-157.

Haber, J. Manual on catalyst characterization (Recommendations 1991). *Pure & Applied Chemi*stry,63(9): 1227-1246.

Habib, M. A.; Bahadur, N.M.; Mahmood, A.J. and Islam, M.A. (2012) Immobilization of heavy metals in cementitious matrices. *Journal of Saudi Chemical Society*, 16:263-269.

Hameed, B.H. and El-Khaiary, M.I. (2008a) Sorption kinetics and isotherm studies of a cationic dye using agricultural waste: Broad bean peels. *Journal of Hazardous Materials*, 154: 639-648.

Hameed, B.H. and El-Khaiary, M.I. (2008b) Malachite green adsorption by rattan sawdust: Isotherm, kinetic and mechanism modeling. *Journal of Hazardous Materials*, 159(2-3): 574-579.

Hameed, B.; Salman, J. and Ahmad, A. (2009) Adsorption isotherm and kinetic modelling of 2,4-D pesticide on activated carbon derived from date stones. *Journal of Hazardous Materials,* 163(1): 121-126.

Hammond, C. (1992) *Introduction to crystallography.* Royal Microscopical Society microscopy handbooks, Oxford, Rev Ed,

Han, J. S. (1999). Stormwater filtration of Toxic Heavy Metal Ions using Lignocellulosic Materials: Selection Process, Fiberization, Chemical Modification and Mat Formation. Proceedings of 2nd Inter Regional Conference on Environment-Water.Emerging Technologies for sustainable Land Use and Water Management. Available Internet: *http://www.fpl.fs.fed.us/documnts/pdf1999/han99a.pdf?* Accessed on: 12/12/2014

Hanafiah, M. A. K. M.; Ngah, W. S. W.; Ibrahim, S. C.; Zakaria, H. and Ilias, W. A. H. W. (2006) Kinetics and thermodynamics study of lead adsorption from aqueous solution onto rubber (*Hevea brasiliensis*) leaf powder. *Journal of Applied Science,* 6(13): 2762-2767.

Hanif, M.A.; Nadeem, R.; Bhatti, H.N.; Ahmad, N.R.; Ansari, T.M.(2007) Ni(II) biosorption by *Cassia fistula* (Golden Shower) biomass*, Journal of Hazardous Materials*,139(2):345-355.

Harja, M.; Rusu, L.; Bucur, D.; Munteanu, C. and Ciocinta, R. C. (2012) Fly-ash derived Zeolites as Adsorbents for Ni removal from Wastewater. *Revue Roumaine de Chime*, 57(6): 587-597.

Harlick, P.J.E and Tezel, F.H (2004) An experimental adsorbent screening study for CO_2 removal from N_2. *Microporous and Mesoporous Materials*, 76(1-3):71-79.

Hashem, M. A. (2007) Adsorption of lead ions from aqueous solution by okra wastes. *International Journal of Physical Sciences,* 2(7): 78-184.

Hashemian, S.; Salari, K..; Hamila S.; and Zahra A. Y. (2013) Removal of Azo Dyes (Violet B and Violet 5R) from Aqueous Solution Using New Activated Carbon Developed from Orange Peel. *Journal of Chemistry,* 2013: 1-10.

Hashemian, S.; Salari, K. and Yazdi, Z. A. (2014) Preparation of activated carbon from agricultural wastes (almond shell and orange peel) for adsorption of 2-pic from aqueous solution. *Journal of Industrial and Engineering Chemistry,* 20: 1892-1900.

Hema, M. and Srinivasan, K. (2010) Uptake of toxic metals from wastewater by activated carbon from agro industrial by-product. *Indian Journal of Engineering and Materials Science,* 17: 373-381.

Hernandez-Ramirez, O. (2009) Hierarchical bio-structures incorporating zeolite Y for wastewater treatment applications. A thesis submitted to the University of Manchester for the degree of Doctor of Philosophy in the Faculty of Engineering and Physical Sciences.

Hernandez-Ramirez, O. and Holmes, S. M. (2008) Novel and modified materials for wastewater treatment applications. *Journal of Material Chemistry*, 18: 2751-2761.

Hill, J. W. (1984) *Chemistry for Changing Times*. 4[th]ed Burgess Publishing Company, Minneapolis.

Hill, J. W.; Kolb, D. K. and Mccreary, T. W. (1998) *Chemistry for changing times*. 12th ed, Pearson International, Paris.

Hirunpraditkoon, S.; Tunthong, N.; Ruangchai, A. and Nuithitkul, K. (2011). Adsorption capacities of activated carbons prepared from Bamboo by KOH activation. *World Academy of Science, Engineering and Technology,* 5: 06-25.

Ho, Y.S. (2004a) Citation review of Lagergren kinetic rate equation on adsorption reactions. *Scientometrics*, 59(1):171-177.

Ho, Y.S. (2004b) Selection of optimum sorption isotherm. Carbon 42 (2004) 2115–2116.

Ho, Y. S. (2006) Review of second-order models for adsorption systems. *Journal of Hazardous Materials B,* 136: 681-689.

Ho, Y. S. and Chiang, C. C. (2001) Sorption studies of acid dye by mixed sorbents. *Adsorption,* **7**: 139-147.

Ho, Y.S.; Huang, C.T. and Huang, H.W (2002) Equilibrium sorption isotherm for metal ions on tree fern. *Process Biochemistry*, 37(12):1421-1430.

Ho, Y. S. and McKay, G. (1998) A comparison of chemisorption kinetic models applied to pollutant removal on various sorbents. *Trans IChemE*, 76(B): 332- 340.

Ho, Y. S. and McKay, G. (1999) Pseudo-second order model for sorption processes. *Process Biochemistry,* 34: 451- 165.

Ho, Y. S. and McKay. (2000) The Kinetics of sorption of divalent metal ions onto sphagnum moss peat. *Water Research* 34: 735-742.

Ho, Y. S.; Chiu, W. T.; Hsu, C. S.; Huang, C. T. (2004) Sorption of lead ions form aqueous solution using tree fern as a sorbent. *Hydrometallurgy,* 73: 55-61.

Ho, Y. S. and Ofomaja, A. E. (2006) Biosorption thermodynamics of Cadmium on coconut copra meal as biosorbent. *Biochemical Engineering Journal,* 30: 117-123.

Ho, Y. S. and Ofomaja, A. E. (2005) Kinetics and thermodynamics of lead ion sorption on palm kernel fibre from aqueous solution. *Process Biochemistry,* 40: 3455-3461.

Hoekman, K. S; Broch, A. and Robbins, C. (2011) Hydrothermal Carbonization (HTC) of Lignocellulosic Biomass, *Energy and Fuels,* 25: 1802-1810.

Hooi, K. K.; Alimuddin, Z. and Ong, L. K. (2009) Laboratory scale Pyrolysis of Oil Palm pressed fruit fibres. *Journal of Oil Palm Research,* 21: 577-587.

Horsfall, M. and Abia, A. A. (2003) Sorption of Cadmium (II) and Zinc (II) ions from aqueous solutions by cassava waste biomass (*Manihot Sculenta Cranz*). *Water Research,* 37: 4913-4923.

Horsfall, M.; Abia, A. A and Spiff, A. I. (2006) Kinetic studies on the adsorption of Cd^{2+}, Cu^{2+} and Zn^{2+} ions from aqueous solutions by cassava (*Manihot sculenta Cranz*) tuber bark waste. *Bioresource Technology*, 97: 283-291.

Horsfall, M.; Spiff, A. I. (2005) Sorption of lead, cadmium and zinc on sulphur-containing chemically modified wastes of fluted pumpkin (*Telfairia Occidentalis Hook f*.). *Chemistry and Biodiversity,* 2(3): 373-385.

Hou, X. and James, B. T. (2000) Inductively Coupled Plasma/Optical Emission Spectrometry. In: *Encyclopedia of Analytical Chemistry*. Meyers, R.A. (ed) John Wiley and Sons, Ltd, Chichester pp. 9468-9485.

His, H.; Tsai, C.; Kuo, T and   Chiang, C.(2011) Development of low concentration mercury adsorbents from biohydrogen-generation agricultural residues using sulphur impregnation. *Bioresource Technology*, 102(16): 7470-7477.

Hu, B.; Wang. K.; Wu, L.; Yu, S. H.; Antonietti, M and Titrici, M. M. (2010) Engineering Carbon Materials from the Hydrothermal Carbonization Process of Biomass. *Advanced Materials,* 22: 813-828.

Hu, H.; Jiang, B.; Zhang, J. and Chen, X. (2015) Adsorption of perrhenate ion by bio-char produced from *Acidosasa edulis* shoot shell in aqueous solution. *RSC Advances*,5: 104769–104778.

Huang, Y.; Li, S.; Chen, J.; Zhang, X. and Chen, Y. (2014) Adsorption of Pb(II) on mesoporous activated carbons fabricated from water hyacinth using H_3PO_4 activation: Adsorption capacity, kinetic and isotherm studies. *Applied Surface Science*, 293:160-168.

Hubbe, M. A; Hasan, S. H. and Ductose, J. J. (2011) Cellulosic substrates for removal of pollutants from aqueous systems: A Review.1. Metals. *BioResources* 6(2); 2161-2287.

Hughes, M. F. (2002) Arsenic toxicity and potential mechanism of action. *Toxicology Letters,* 133: 1-16

Hydari, S.; Sharififard, H.; Nabavinia, M.and Parvizi, M.R.(2012) A comparative investigation on removal performances of commercial activated carbon, chitosan biosorbent and chitosan/activated carbon composite for cadmium, *Chemical Engineering Journal*, 193-194: 276-282

Ibrahim, M. N. M.; Ngah, W. S. W.; Norliyana, M. S.; Daud, W. R. W.; Rafatullah, M.; Sulaiman, O. and Hashim, R. (2010) A novel agricultural waste adsorbent for the removal of lead (II) ions from aqueous solutions. *Journal of Hazardous Materials*, 182: 377-385.

ICO (2012) International Cocoa Organization- Production of cocoa beans. Quarterly Bulletin of Cocoa Statistics, Vol. 37, No. 4, Cocoa Year 2011/2012. Available internet: http://www.icco.org/about-us/international-cocoa-agreements/cat_view/30-related-documents/46-statistics-production.htm Accessed 10/06/2013.

Igwe, J. C. and Abia, A. A. (2007) Adsorption kinetics and intraparticulate diffusivities for bioremediation of Co (II), Fe (II) and Cu (II) ions from wastewater using modified and unmodified maize cob. *International Journal of Physical Science,* 2(5): 119-127.

Imamoglu, M. and Tekir, O. (2008) Removal of Copper (II) and Lead (II) ions form aqueous solutions by adsorption on activated carbon from a new precursor hazelnut husk. *Desalination,* 228: 108-113.

Inyang, M.; Gao, B.; Yao, Y.; Xue, Y.; Zimmerman, A.R.; Pullammanappallil, P. and Cao, X. (2012) Removal of heavy metals from aqueous solution by biochars derived from anaerobically digested biomass. *Bioresource Technology*, 110:50-56.

Ioannidou, Q. A.; Zabanoitou, A. A.; Stavropoulos, G. G.; Islam, M. A. and Albanis, T. A. (2010) Preparation of activated carbons from agricultural residues for pesticide adsorption. *Chemosphere,* 80: 1328-1336

Ioannidou, O. and Zabaniotou, A. (2007) Agricultural residues as precursors for activated carbon production - A review. *Renewable and Sustainable Energy Reviews,* 11: 1966-2005.

Ip, A. W. M.; Barford, J. P. and McKay, G. (2008) Production and comparison of high surface area bamboo derived active carbons. *Bioresource Technology*, 99: 8909-8916.

Ipeaiyeda, A.R. and Onianwa, C. P. (2011) Pollution effects of food and beverages effluents on the Alaro River in Ibadan city, Nigeria. *Bulletin of the Chemical Society of Ethiopia*, 25(3): 347-360.

Iqbal, M.; Saeed, A. and Zafar, S. I. (2009a) FTIR Spectrophotometry- kinetics and adsorption isotherms modelling, ion exchange and EDX analysis for understanding the mechanism of Cd^{2+} and Pb^{2+} removal by mango peel. *Journal of Hazardous Materials*,164: 161-171.

Iqbal, M.; Schiewar, S. and Cameron, R. (2009b) Mechanistic elucidation and evaluation of biosorption of metal ions by grapefruit peel using FTIR spectroscopy, kinetics and

isotherms modeling, cations displacement and EDX analysis. *Journal of Chemical Technology &. Biotechnology*, 84 (10): 1516-1526.

Isa, N. B.; Wahab, N. A. A. and Haris, M. R. H. (2010) Cd(II) removal from aqueous solution by unmodified sugarcane bagasse and coconut coir: Adsorption equilibrium and kinetics. *2010 International Conference on Science and Social Research (CSSR 2010)*, December 5-7, 2010. Kuala Lumpur, Malaysia.

Islam, M.A. ;Benhouria, A.; Asif, M. and Hameed, B.H. (2015) Methylene blue adsorption on factory-rejected tea activated carbon prepared by conjunction of hydrothermal carbonisation and sodium hydroxide activation process. *Journal of Taiwan Institute of Chemical Engineers*, 000:1-8. doi:10.1016/j.jtice.2015.02.010

Israel, U. A.; Ogali, R. E.; Akaranta, O. and Obot I. B. (2011) Extraction and Characterisation of coconut (*Cocos nucifera* L). *Songklanakarin Journal of Science & Technology,* 33(6): 717-724.

IUPAC (1991) International Union of Pure and Applied Chemistry -Manual on catalyst characterization. *Pure & Applied Chemistry*, 63(9):1227-1246.

Iza, M.; Woerly, S.; Danumah, E.; Kaliaguine, S. and Bousmina, M. (2000) Determination of pore size distribution for mesoporous materials and polymeric gels by means of DSC measurements: thermoporometry. *Polymer,* 41: 5885-5893.

Jagtoyen, M. and Derbyshire, F. (1998) Activated carbons from yellow popular and white oak by H$_3$PO$_4$ activated. *Carbon,* 36(7-8): 87-93.

Jain, A; Jayaraman, S.A; Balasubrmanian, R. and Srinivasan, M. P (2014) Hydrothermal pre-treatment for mesoporous carbon synthesis: enhancement of chemical activation. *Journal of Materials Chemistry, A* 2: 520-528.

Jekayinfa, S. and Omisakin, O. (2005) The Energy potentials of some agricultural wastes as local fuel materials in Nigeria. *International Commission of Agricultural Engineering (CIGR, Commission Internationale du Genie Rural) E-Journal*, 7.

Jin, X. J.; Yu, Z. M and Wu, Y. (2012) Preparation of activated carbon from lignin obtained by straw pulping by KOH and K$_2$CO$_3$ chemical activation. *Cellulose Chemical Technology,* 46(1-2): 79-85.

Joseph, P. (2009) Mechanism of cadmium carcinogenesis. *Toxicology and Applied Pharmacology*, 238:272-279.

Jun, T.Y.; Arumugam, S.D.; Hidayah, N.; Latip, A.; Abdullah,A.M. and Latif, P.A. (2010) Effect of activation temperature and heating duration on physical characteristics of activated carbon prepared from agricultural waste. *Environment Asia*, 3:143-148.

Kafia, M. and Surchi, S. (2011) Agricultural Wastes as Low Cost Adsorbent for Pb Removal: Kinetics, Equilibrium and Thermodynamics: *International Journal of Chemistry,* 3(3) 103-112.

Kakalanga, S.J.; Jabulani, X.B.; Olutoyin, O.B. and Uteiyin, O.O.(2012) Screening of agricultural waste for Ni(II) adsorption: kinetics, equilibrium and thermodynamic studies. *International Journal of Physical Sciences*, 7(17):2525-2538.

Kalut, S. A. (2008) Enhancement of Degree of Deacetylation of Chitin in Chitosan Production, Thesis of Universiti Malaysia Pahang, Faculty of Chemical Engineering and Natural Resources, Malaysia. Available internet: http://umpir.ump.edu.my/650/1/Stephenie_Ak_Kalut.PDF Accessed on 10/12/2010 Accessed on 19/06/2012

Kambo, H.S. and Dutta, A. (2005) A comparative review of biochar and hydrochar in terms of production, physico-chemical properties and applications. *Renewable and Sustainable Energy Reviews*, 45: 359-378.

Kamrin, M. and Leader, R. W. (2012) "Toxicology," in Access Science, McGraw-Hill Education, 2012. Available Internet: http://.accessscience.com Accessed on 12/01/2011

Kamrin, M. and Leader, R. W. (1997). Toxicology. In: *Mc-Graw Hill Encyclopedia of Science and Technology*. 8th ed vol. 18 Parker, S. P. (ed) Mc-Graw Hill Inc, New York.

Kannan, N. and Rengasamy, G. (2005) Comparison of Cadmium ion adsorption on various activated carbon. *Water, Air and Soil Pollution,* 163: 185-201.

Karnitz, O.; Gurgel, l. V. A.; Melo, J. C. P.; Botaro, V. R.; Melo, J. M. S.; Gil, R. P. F.; Gil, L. F. (2007) Adsorption of heavy metal ion form aqueous single metal solution by chemically modified sugarcane bagasse. *Bioresource Technology,* 98: 1291-1297.

Kaszuba, M.; Corbett, J. and Watson, F.M. (2010) High-concentration zeta potential measurements using light-scattering techniques. *Philosophical Transactions of the Royal Society of London A,* 368: 4439–4451.

Kavitha, D. and Namasivayam, C. (2007) Experimental and Kinetic studies on methylene blue/adsorption by coir pith carbon. *Bioresource Technology,* 98: 14-21.

Kazantzis, G. (2004) Cadmium osteoporosis and calcium metabolism. *Biometals,* 17:493-498.

Kazemipour, M.; Ansari, M.; Tajrobehkar, S.; Majdzadeh, M. and Kermani, H. R. (2008) Removal of lead, Cadmium, zinc and copper for industrial wastewater by carbon developed from walnut, hazelnut, almond, pistachio shell and apricot stone. *Journal of Hazardous Materials,* 150: 322-327.

Kellner, R. Mermet, J. M.; Otto, M; Valcarcel, M.; Widmer, H. M. (2004) *Analytical Chemistry: A Modern Approach to Analytical Science*. 2nd Ed. Wiley-VCH VerlagGmbH & Co KGaA, Weinheim.

Khan, T. A.; Chaudhry, S. A and Ali, I. (2015) Equilibrium uptake, isotherm and kinetic studies of Cd(II) adsorption onto iron oxide activated red mud for aqueous solution. *Journal of Molecular Liquids,* 202: 265-175.

Khor, K. H.; Zainal, A. and Lim, K. O. (2009) Laboratory-Scale Pyrolysis of Oil Palm Pressed Fruit Fibres. *Journal of Oil Palm Research*, 21: 577-587.

Khurana, M. and Farooq, S. (2016) Adsorbent screening for post combustion CO_2 capture: A method relating equilibrium isotherm characteristics to an optimum vacuum swing adsorption process performance. *Industrial and Engineering Chemistry Research*, 55(8):2447-2460.

Kikuchi,Y.; Qian, Q.; Machida, M. and Tatsumoto, H.(2006) Effect of ZnO loading to activated carbon on Pb(II) adsorption from aqueous solution. *Carbon,* 44(2):195-202.

Kim, W. K.; Shim, T.; Kim, Y. S, Hyun, S.; Ryu, C.; Pork, Y. K and Jung, J (2013) Characterization of cadmium removal form aqueous solution by biochar produced from a giant *Miscanthus* at different pyrolytic temperatures. *Bioresource Technology,*138: 266-270.

Knaebel, K. S. (2008) Adsorbent Selection. Adsorption Research, pp 1-21. Available Internet: http://www.adsorption.com/publications/adsorbentsel1b.pdf Accessed on 12/6/2014.

Kolodynska, D.; Wnetrzak, R.; Leahy, J.J.; Hayes, B.B.; Kwapinski, W. and Hubicki, D. (2012) Kinetic and adsorptive characterization of biochar in metal ions removal. *Chemical Engineering Journal*, 197; 295-305.

Kondo, K. (2000) Congenital Minamata disease: Warnings from Japan's experience. *Journal of Child Neurology,* 15(7): 438-464.

Kongsuwan, A.; Patnukao, P and Pavasant, P. (2009) Binary component sorption of Cu(II) and Pb(II) with activated carbon from *Eucalyptus camaldulensis* Dehn Bark. *Journal of Industrial Engineering Chemistry,* 15(4): 465-470.

Kraynov, A. and. Müller, T.E. (2011) Concepts for the Stabilization of Metal Nanoparticles in Ionic Liquids. In: Applications of Ionic Liquids in Science and Technology. Scott Handy (Ed.), InTech, Available internet:

http://www.intechopen.com/books/applications-of-ionic-liquids-in-science-andtechnology/concepts-for-the-stabilization-of-metal-nanoparticles-in-ionic-liquids. Accessed 12/10/2014.

Krishnan, K. A.; Anirudhan, T. S. (2003) Removal of cadmium (II) from aqueous solution by steam-activated sulphurised carbon prepared from sugar-cane bagasse pith: kinetics and equilibrium studies. *Water SA,* 29(2): 147-156.

Krishnani, K. K.; Meng, X.; Christodoulatos, C.; Boddu, VM. (2008) Biosorption mechanism of nine different heavy metals onto biomatrix from rice husk. *Journal of Hazardous Materials,* 153: 1222-1234.

Krotz, L. and Giazzi, G. (2012) Organic Elemental Analysis for Carbon Characterisation by Flash Combustion Method. Thermo Fisher, Italy. Available internet: http://tecnofrom.com/moduloNotas/noti_9/archivosAdjuntos/flash_oea_flipbook_274.pdf Accessed on 12/01/2013.

Kumar, K. V. (2006) Linear and non-linear regression analysis for the sorption kinetics of methylene blue one activates carbon. *Journal of Hazardous Materials,* B137: 1538-1544.

Kumar, K. V. and Sivanesan, S. (2006) Equilibrium data, isotherm parameters and process design for partial and complete isotherm of methylene blue onto activated carbon. *Journal of Hazardous Materials,* B134: 237- 244.

Kumar, K. V.; Porkodi, K. and Rocha, F. (2008) Comparison of various error functions in predicting the optimum isotherm by linear and non-linear regression analysis for the sorption of basic red 9 by activated carbon. *Journal of Hazardous Materials,* 150: 158-165.

Kumar, P.S.; Ethiraj, H.; Venkat, A.; Deepika, N.; Nivedha, S.; Vidhyadevi,T.; Ravikumar, L. and Sivanesan,S.(2015) Adsorption kinetic equilibrium and thermodynamic investigations of Zn(II) and Ni(II) ions removal by poly(azomethinethioamide) resin with pendent chlorobenzylidine ring. *Polish Journal of Chemical Technology*, 17(3):100-109.

Kumar, P. S.; Ramakrishnan, K.; Kirupha, D. S. and Sivanesan, S. (2010) Thermodynamic and Kinetic Studies of Cadmium Adsorption from Aqueous Solution onto Rice Husk. *Brazilian Journal of Chemical Engineering,* 27(2): 437-355.

Kumar, P. S.; Ramalingam, S.; Sathyaselvabala, V.; Kirupha, S. D.; Murugesan, A. and Sivanesan, S. (2012) Removal of cadmium from aqueous solution by agricultural waste cashew nut shell. *Korean Journal of Chemical Engineering*, 29(6) 756-768.

Kumar, S.; Loganathan, V.A; Gupta, R.B. and Barnett, M.O. (2011) An assessment of U(VI) removal from groundwater using biochar produced from hydrothermal carbonisation. *Journal of Environmental Management*, 92:2504-2512.

Kumar, V. and Bandyopadhyay, M. (2006) Sorption of cadmium from aqueous solution using pre-treated rice husk. *Bioresource Technology,* 97: 104-109.

Kung, C. C.; Kung, F. and Choi, Y. (2015) Pyrolysis and biochar potential using crop residues an agricultural wastes in china. *Ecological Indicators,* 51:139-145

Kurniawan, T. A.; Chan, G. Y. S.; Lo, W. H.; Babel, S. (2006) Comparisons of Low-cost adsorbents for treating wastewaters laden with heavy metals. *Science of the Total Environment,* 366: 409-426.

Kyzas, G. Z. and Deliyanni, E. A. (2014) Modified activated carbons from potato peels as green environmental-friendly adsorbents for the treatment of pharmaceutical effluents. *Chemical Engineering Research and Design,* 97:135-144.

Lacerda, V.S.; Lopez-Sotelo, J.B.; Correa-Guimaraes, A.; Hernandez-Navarro, S.; Sanchez-Bascones, M.; Navas-Gracia, L.M.; Martin-Ramos, P. and Martin-Gil, J. (2015) Rhodamine B removal with activated carbons obtained from lignocellulosic waste. *Journal of Environmental Management*, 155:67-76.

Lagergren, S. (1898) About the theory of so-called adsorption of soluble substances. Kungliga Svenska Vetenskapsakademiens. *Handlingar*, Band 24, No. 4, 1-39.

Laidler, K. J.; Meiser, J. H. (1982). Physical Chemistry. The Benjamin / Cummings Publishing Company Inc. California.

Langmuir, I. (1918) The adsorption of gases on plane surfaces of glass, mica and platinum. *Journal of American Chemical Society* 40: 1361-1403.

Leddy, N. (2012) Surface area and porosity. CMA Analytical Workshop-Centre for Microscopy and Analysis. Available internet: http://cma.tcd.ie/misc/Surface_area_and_porosity.pdf Accessed on 12/07/2013.

Lee, S. H. and Yang, J. W. (1997) Removal of Copper in aqueous solution by apple wastes. *Separation Science and Technology,* 32(8): 1371-1387.

Lee, S. Y. and Park, S. J. (2013) Determination of the optimal pore size for improved CO2 adsorption in activated carbon fibres. *Journal of Colloid and Interface Science,* 389: 230-235.

Lenntech Water Treatment and Air Purification (2004) Water Treatment. Lenntech BV, Rotterdamseweg 402, Netherlands. Available internet: http://www.lenntech.com/processes/heavy/heavy-metals/heavy-metals.htm. Accessed on 12/10/2014.

Leofanti, G.; Padovan, G.; Tozzola, G.; Venturelli, B.(1998) Surface area and pore texture of catalyst. *Catalysis Today*, 41:207-

Lewin, M.(1991) *Wood structure and composition*. Marcel Dekker Inc., New York. pp 49-139.

Lian, F.; Xing, B. and Zhu, L. (2011) Comparative study of the composition, structure and adsorption behaviour of activated carbons derived from different synthetic waste polymers. *Journal of colloid and Interface Science* 360(2): 725-730.

Liang, S.; Guo, X., Feng, N. and Tian, Q. (2009) Adsorption of Cu^{2+} and Cd^{2+} from aqueous solution by mercapto-acetic acid modified orange. *Colloids and Surface B: Biointerfaces,* 73: 10-14.

Liang, S.; Guo, X.; Feng, N. and Tian, Q. (2010) Isotherms, kinetics and thermodynamic studies of adsorption of Cu^{2+} from aqueous solutions by Mg^{2+}/K^{+} type orange peel adsorbents. *Journal of Hazardous Materials,* 174: 756 -762.

Libra, J.A. ; Ro, S.K.; Kammann.; Funke, A.; Berge, N.D.; Neubauer, Y.; Titirici, M.M.; Fuhner, C.; Bens, C.; Kern. J. and Emmerich, K.H. (2011) Hydrothermal carbonisation of biomass residuals: a comparative review of the chemistry, processes and application of wet and dry pyrolysis. *Biofuels*, 2(1): 89-124.

Li, H.; Dai, Q.; Ren, J.; Jian, L.; Peng, F. and Sun, R. (2016) Effect of structural characteristics of corncob hemicelluloses fractionated by graded ethanol precipitation on furfural production. *Carbohydrate Polymers*, 136:203-209.

Li, T.; Shen, J.; Huang, S., Li, N and Ye M. (2014) Hydrothermal carbonization synthesis of a novel montmorillonite supported carbon nanosphere adsorbent for removal of Cr (VI) form waste water. *Applied Clay Science,* 93-94: 48- 55

Li, N. and Bai, K. (2006) Development of chitosan-based granular adsorbents for enhanced and selective adsorption performance in heavy metal removal. *Water Science and Technology,* 54 (10): 103-113.

Li, X.; Tang, Y.; Cao, X.; Lu, D.; Luo, F. and Shao, W. (2008) Preparation and evaluation of orange peel cellulose adsorbents for effective removal of cadmium, zinc, cobalt and nickel. *Colloids and Surfaces A: Physicochemical & Engineering Aspects* 317: 512-521.

Lim, L.; Priyantha, N.; Tennakoon, D.; Chieng, H.; Dahri, M.; Suklueng, M. (2014) Breadnut peel as a highly effective low-cost biosorbent for methylene blue: equilibrium, thermodynamic and kinetic studies. *Arabian Journal of Chemistry*. In Press: http://dx.doi.org/10.1016/j.arabjc.2013.12.018

Lima, L. and Marshall, W. E. (2005) Utilization of turkey manure as granular activated carbon; physical, chemical and adsorptive properties. *Waste Management*, 25: 726-732.

Limousin, G.; Gaudet, J. P.; Charlet, L.; Szenknect, S.; Barthes, V. and Krismissa, M. (2007) Sorption isotherms: A review on physical bases, modelling and measurement. *Applied Geochemistry,* 22: 249-275.

Lin, J. and Wang (2009) Comparison between linear and non- linear forms of first-order and pseudo-second order adsorption kinetic models for the removal of methylene blue by activated carbon. *Frontiers of Environmnetal Science & Engineering in China*, 3(3): 320-324.

Liu, C.F.; Xu, F.; Sun, J.X.; Ren, J.L.; Curling, S.; Sun, R.C.; Fowler, P and Baird, M.S. (2006) Physicochemical characterization of cellulose from perennial ryegrass leaves (*Lolium perenne*). *Carbohydrate Research*, 340: 2376-2391.

Liu, S. X. (2014) *Agricultural Wastewater Utilization and Treatment*. 2nd Ed. John Wiley & Sons, UK.

Liu, Y. and Liu, Y. (2008) Biosorption isotherms, kinetics and thermodynamics. *Separation and Purification Technology*, 61: 229-242.

Liu, Z. and Zhang, F.S. (2009) Removal of lead from water using biochars prepared from hydrothermal liquefaction of biomass. *Journal of Hazardous Materials*, 167:933-939.

Liu, Z. and Zhang, F.S. (2011) Removal of copper (II) and phenol from aqueous solution using porous carbons derived from hydrothermal chars. *Desalination,* 267: 101-106

Liu, Z.; Zhang, F.S. and Wu, J. (2010) Characterisation and application of chars produced from pinewood pyrolysis and hydrothermal treatment. *Fuel*, 89:510-514.

Lopez, F. A.; Centeno, T. A; Garcia-Diaz, I. and Alguacil, F. J. (2013) Textual and fuel characteristics of the chars produced by the pyrolysis of waste wood and the properties of activated carbons prepared from them. *Journal of Applied Pyrolysis* 104: 551-558.

Lowell, S. and Shields, J. E. (1991) *Powder Surface Area and Porosity*. 3rd Ed. Chapman & Hall, London.

Low, K.S.; Lee, C.K. and Leo, A.C.(1995) Removal of metals from electroplating waste using banana pith. *Bioresource Technology,*51: 227-231.

Low, K. S. Lee, C. K. and Lee, K. P. (1993) Sorption of Copper by Dye-treated Oil palm Fibres. *Bioresource Technology,* 44(2): 109-112.

Luangkiattikhun, P.; Tangsathitkulchai, C. and Tangsathitkulchai, M. (2008) Non-isothermal thermogravimetric analysis of oil palm solid wastes. *Bioresource Technology*, 99: 986-997.

Lydersen, A. L.; Dahlq, I. C. (1992) *Dictionary of Chemical Engineering*. John Wiley and Sons. New York.

Lynan, J. G.; Coronella, C. J.; Yan, W.; Reza, M. T.; Vasofuez, V. R. (2011) Acetic acid and lithium chloride effects on hydrothermal carbonization of lignocellulosic biomass. *Bioresource Technology,* 102: 6192-6199.

Ma, J. and Zhu, L. (2006) Simultaneous sorption of phosphate and phenanthrene to inorgano-organo-bentonite from water. *Journal of Hazardous Materials,* B136: 982-988.

Macias-Garcıa, A; Gómez-Serrano, V. Alexandre-Franco, M.F. and Valenzuela-Calahorro, C.(2003) Adsorption of cadmium by sulphur dioxide treated activated carbon, *Journal of Hazardous Materials*, 103 (1–2): 141-152.

Mafra, M.R.; Igarashi-Mafra, L.; Zuim, D.R.; Vasques, E.C. and Ferreira, M.A. (2013) Adsorption of Remazol brilliant blue on an orange peel adsorbent. *Brazilian Journal of Chemical Engineering*, 30(3):657-665.

Malvern Instrument (2004) Zetasizer Nano Series User Manual. MANO 317, Issue 2.1 July, Available Internet:

http://www.biophysics.bioc.cam.ac.uk/files/Zetasizer_Nano_user_manual_Man0317-1.1.pdf Accessed on 12/10/2012

Malvern Instrument (2014) Zeta Potential-An Introduction in 30 minutes. Zetasizer nano series technical note MRK654-01. Available Internet: https://www.caliscc.org/images/presentations/Morante_Zeta_Potential.pdf Accessed on 20/5/2014

Mane, V.; Mall, I. D and Srivastava, V. C. (2007) Use of bagasse fly ash as an adsorbent for the removal of brilliant green dye from aqueous solution. *Dyes and Pigments,* 73: 269-278.

Manning, T. J. and Grow, W. R. (1997) Inductively coupled plasma-atomic emission spectrometry. *The Chemical Educator,* 2(1): 1-19

Mannino, D.M.; Helguin, F.; Greves, H. M.; Savage-Brown, A.; Stock. A. L.; Jones,R.L.(2004) Urniary cadmium levels predict lower lung function in current and former smokers: data from the Third National Health and Nutrition Examination Survey. *Thorax*, 59: 919-924.

Markovic, J.P.; Radovic, J,B.; Strbanovic, R.T. ; Bajic, D.S. and Vrvic, M.M. (2009) Changes in the infra red attenuated total reflectance (ATR) spectra of lignins from alfalfa stem with growth and development. *Journal of Serbian Chemical Society*, 74(8-9): 885-892.

Marshall, W.E. and Champagne, E.T. (1995) Agricultural by-products as adsorbents in laboratory prepared solutions and in manufacturing wastewater. *Journal of Environmental Science and Health. Part A: Environmental Science and Engineering and Toxicology,* 30(2):241-261.

Mattison, K.; Morfesis, A.; Kaszuba, M.(2003) "A Primer on Particle Sizing Using Dynamic Light Scattering" American Biotechnology Laboratory. Available internet: https://www.researchgate.net/publication/237663975_A_Primer_on_Particle_Sizing_Using_Dynamic_Light_Scattering Accessed on 12/10/2015.

Mason, G. (1982) The effect of pore space connectivity on the hysteresis of capillary condensation in adsorption-desorption isotherms. *Journal of Colloid and Interface Science*, 88(1)36-46.

Matrix Metrologies (2012) Technology Guide- X-ray Fluorescence Metrology Tools, Available internet: http://www.matrixmetrologies.com/sitebuildercontent/sitebuilderfiles/matrixmetrologiesXRFtechguide.pdf Accessed on 12/01/2013.

Meitei, M. D. and Prasad, M. N. V. (2013) Lead (II) and Cadmium (II) biosorption on Spirodela polyrhiza (L.) Schleiden biomass. *Journal of Environmental Chemical Engineering,* 1: 200-207.

Menendez-Diaz, J.A and Martin-Gullon, I.(2006) Types of carbon adsorbents and their production. Activated carbon surfaces in environmental remediation. *Interface Science and Technology*, 7:1-47.

Meszaros, E.; Jakab, E.; Varhegyi, G.; Bourke, J.; Manley-Heris, M.; Nunoura, T and Antal, M.J. (2007) do all carbonised charcoals have the same chemical structure. 1. Implications of thermogravimetry-mass spectrometry measurements. *Industrial & Engineering Chemistry Research,* 46: 5943-5953.

Micromeritics, (2001) Tristar 3000 Surface Area and Porosimetry Analyzer. Available internet: http://www.importecnical.com/IMG/PDF/maspdf/TriStarBrochure.pdf Accessed on 12/12/2012.

Miralles, N.; Valderrama, C.; Casas, I.; Martinez, M. and Florido, A. (2010) Cadmium and lead removal from aqueous solution by grape stalk wastes: Modelling of a fixed bed. *Journal of Chemical Engineering Data,* 55: 3548-3554.

Miska, V.; Gorter, K. Menkveld, H. W. H.; Neef, R.; Vander Graaf, J. H. J. M. (2006) Behaviour of heavy metals during tertiary bio-filtration. *Water Science and Technology,* 54 (10): 209-216.

Mohan, D. and Singh, K. P. (2002) Single and multi-component adsorption of cadmium and zinc using activated carbon derived from bagasse – an agricultural waste. *Water Research,* 36: 2304-2318.

Mohan, D.; Pittman, C. U. (2007) Arsenic removal from water/wastewater using adsorbents - A critical review. *Journal of Hazardous Materials,* 142**:** 1-53.

Mohan, D.; Pittman, C.U.; Bricka, M. ;Smith, F.; Yancey, B.; Mohammad, J.; Steele, P.H.; Alexandre-Franco, M.F.; Gómez-Serrano, V. and Gong, H. (2007) Sorption of arsenic, cadmium, and lead by chars produced from fast pyrolysis of wood and bark during bio-oil production. *Journal of Colloid and Interface Science*, 310(1): 57-73

Mohanty, K.; Das, D.; Biswas, M. N. (2006) Preparation and Characterisation of activated carbons from *sterculia alata* nutshell by chemical phenol form wastewater. *Adsorption,* 12:119-132.

Mohapatra, M; Mohapatra, L.; Singh, P.; Anand, S. and Mishra, B. K. (2010) A Comparative study on Pb (II), Cd(II), Cu(II) and Co(II) adsorption from single and binary aqueous solutions on additive assisted nano-structured goethite. *International Journal of Engineering, Science and Technology,* 2(8): 89-103.

Moubarik, A. and Grimi, N. (2015) Valorization of olive stone and sugar cane bagasse by-products as biosorbents for the removal of cadmium from aqueous solution. *Food Research International*, 73:169-175.

Moyo, M.; Chirinda,A, A.; Nharingo, T. (2016) Removal of copper from aqueous solution using chemically treated potato (*Solanum tuberosum*) leaf powder. *Clean- Soil, Air ,Water* 43(9999):1-8.

Nadeem, M.; Mahmood, A.; Shahid, S. A.; Shan, S. S.; Khalid, A. M. and McKay, G. (2006) Sorption of Lead from Aqueous Solution by Chemically Modified Carbon Adsorbents, *Journal of Hazardous Materials,* 138(3): 604-613.

Nadeem, V. (2013) Bioremediation of Cadmium (II) from aqueous solution using agricultural waste: Zea maize leaves. *European Chemical Bulletin*, 2(12): 993-998.

Naiya, T. K.; Bhahacharya, A. K.; Mandal, S. and Das, S. K. (2009) The sorption of lead (II) ions on rice husk ash. *Journal of Hazardous Materials,* 163: 1254-1264.

Naiya, T.K.; Singha, B. and Das, S.K.(2011) FTIR study for the Cr(VI) removal from aqueous solution using rice waste. International Conference on Chemistry and Chemical Process-*IPCBEE*, 10:114-119.

Namasivayam, C and Kadirvelu, K. (1999) Uptake of mercury (II) from wastewater by activated carbon from unwanted agricultural solid by-product: coir pith. *Carbon* 39: 79-84.

Naraine, P. (1998). Removal of Inorganic Contaminants by Activated Carbon. Available Internet: *http://www.ceevtedu / program – areas/ environment / teach / gwprimer / groups 23 / sorption. html.* Accessed on: 31/8/2008.

Nascimento, R.F; Sousa, F.W.; Neto, V.O.S.; Fechine, P.B.A ;Pereira Teixeira, R.N.P; Tarso, P.; C. Freire, C. and Araujo-Silva, M.A. (2012) Biomass Adsorbent for Removal of Toxic Metal Ions from Electroplating Industry Wastewater. *Electroplating*. D. Sebayang and S.B.H Hasan (eds.), ISBN: 978-953-51-0471-1, InTech Open Science. DOI: 10.5772/32670. Available internet: http://www.intechopen.com/books/electroplating/biomass-adsorbent-for-removal-of-toxic-metal-ions-from-electroplating-industry-wastewater Accessed 12/07/2014.

Nasernejad, B.; Zedeh, T. E.; Pour, B. B.; Bygi, M. E.; Zamani, A. (2005) Comparison of or Biosorption modelling of heavy metals (Cr (III), Cu (II), Zn (II) adsorption from wastewater by carrot residues. *Process Biochemistry,* 40: 1319-1322.

Naumov, S. (2009) Hysteresis Phenomena in Mesoporous Materials, Dissertation of Universitat Leipzig, Available Internet: http://www.uni-leipzig.de/~gfp/sites/default/files/27-dr._sergej_naumov/dissertation.pdf Accessed on 23/12/2012.

Navarro-Blasco, I.; Duran, A.; Sirera, R.; Fernandez, J.M. and Alvarez, J.I. (2013) Solidification/stabilization of toxic metals in calcium aluminate cement matrices. *Journal of Hazardous Materials*, 260; 89-103.

Nayak, P. G.; Singh, B. K.; Nayak, S. (2007) Equilibrium, kinetic and thermodynamic studies on phenol sorption to clay. *Journal of Environmental Protection Science,* 1: 83-91.

Ncibi, M. C.; Ranguin, R.; Pinsor, M. J.; Jeanne-Rose, V.; Sillanpaa, M. and Gaspard, S. (2014) Preparation and characterization of chemically activated carbons derived from Mediterranean. *Posidonia Oceanica* (L.) fibres. *Journal of Analytical and Applied Pyrolysis,* 109: 205-214.

Ngah, W. S. W and Hanafiah, M. A. K. M. (2008) Removal of metal ions from wastewater by chemically modified plant wastes as adsorbents: A Review. *Bioresource Technology,* 99: 3935-3948.

Nguyen, T. A. H.; Ngo, H. H.; Guo, W. S.; Zhang, J.; Liang, S. Yue, Q. Y.; Li, Q. and Nguyen, T. V. (2013) Applicability of agricultural waste and by-products for adsorptive removal of heavy metals from wastewater. *Bioresource Technology,* 148: 574-583.

Niu, C.; Wu, W.; Wang, Z.; Li, S.; Wang, J. (2007) Adsorption of heavy metal ions from aqueous cross linked carboxymethyl konjac glucomannan. *Journal of Hazardous Materials,* 141: 209-214.

Niemantsverdriet, J.M.(2007) *Spectroscopy in Catalysis-An Introduction.*3rd Ed. Wiley-VCH Verlag GmbH & Co. KGaA, Weinheim.

Nomanbhay, S. M.; and Palanisamy, K. (2005) Removal of Heavy Metal from industrial Wastewater using chitosan coated oil palm shell charcoal. *Electronic Journal of Biotechnology,* 8(1): 43-53.

Nouri, L.; Ghodbane, I.; Hamadoui, O. and Chiha, M. (2007) Batch sorption dynamics and equilibrium for the removal of cadmium ions from aqueous phase using wheat bran. *Journal of Hazardous Materials,* 149: 115 – 125.

Nurchi, V. M. and Villaescusa, I. (2007) Agricultural biomass as sorbents of some trace metals. *Coordination Chemistry Reviews,* 252: 1178-1188.

Obahiagbon, F. I. (2012) A Review: Aspects of the African oil palm (*Elaeis guineensis jacq*) and the Implications of its Bioactive in Human Health. *American Journal of Biochemistry and Molecular Biology,* 2(3): 106-119.

Obute, G. O.; Osuji, L. C.; Kalio, C. (2004) Genotoxicity of Petroleum Refining Wastewater in Nigeria. *Global Journal of Environmental Science,* 3: 55-58.

O'Connell, D. W.; Birkinshaw, C.; O'Dwyer, F. T. (2006) A modified cellulose adsorbent aqueous solutions. *Journal of Chemical Technology and Biotechnology,* 81**:** 1820-1828.

O'Connell, D. W.; Birkinshaw, C.; O'Dwyer, F. T. (2008) Heavy metal adsorbents prepared from the modification of cellulose: A review. *Bioresource Technology,* 99: 6709-6724.

Official Journal of the European Economic Communities (1974) Dangerous substances Directive -76/464/EEC, Brussels, Belgium.

Official Journal of the European Communities (1999) Directive on the Landfill of Waste, L182/2, p1-19, Brussels, Belgium.

Official Journal of the European Communities (2000) Directive on Water Framework, L327/1, P 1.72, Brussels, Belgium.

Official Journal of the European Communities (2006) Directive on pollution caused by certain dangerous substances discharged into the aquatic environment of the Community, L64, p52-59, Brussels, Belgium.

Ofomaja, A. E.(2008) Kinetic study and sorption mechanism of methylene blue and methyl violet onto mansonia (*Mansonia altissima*) wood sawdust. *Chemical Engineering Journal*, 143:85-95.

Ofomaja, A. E.(2010) Intraparticle diffusion process for lead (II) biosorption onto mansonia wood sawdust. *Bioresource Technology,* 101:5868-5876.

Ofomaja, A. E. and Unuabonah, E.I.(2011) Adsorption kinetics of 4-nitrophrenol onto a cellulosic material, mansonia wood sawdust and multistage batch adsorption process optimization. *Carbohydrate Polymers*, 83: 1192-1200.

Ofomaja, A. E.; Ho, Y.S. (2007) Effect of pH on cadmium biosorption by coconut copra meal. *Journal of Hazardous Materials,* 139: 356-362.

Ofomaja, A. E.; Naidoo, E. B. and Modise, S. J. (2009) Removal of copper (II) from aqueous solution by pine and base modified pine cone powder as biosorbent. *Journal of Hazardous Materials,* 139: 356-362.

Oh, S.Y.; Yoo, D.I.; Shin, Y.; Kim, H.C.; Kim, H.Y.; Chung,Y.S.; Park, W.H. and Youk, J.H.(2005) Crystalline structure analysis of cellulose treated with sodium hydroxide and carbondioxide by means of X-ray diffraction and FTIR spectroscopy. *Carbohydrate Research*, 340:2376-2391.

Ohimain, E., Jonathan, G. and Abah, S. O. (2008) Variations in heavy metal concentrations following the dredging of an oil well access canal in the Niger Delta. *Advances in Biological Research,* 2(5-6): 97–103

Ohler, J. C. (1999) Modern Coconut Management-Palm Cultivation and Products. Food and Agriculture Organisation, ITDG Publishing, Rome, pp 2-67.

Okafor, P. C.; Okon, P. U.; Daniel, E. F. and Ebenso, E. E. (2012) Adsorption Capacity of Coconut (*Cocas mucifera L.*) Shell for Lead, Copper, Cadmium and Arsenic from Aqueous Solutions. *International Journal of Electrochemical Science*, 7: 12354-12369.

Okeoghene, E. S.; John, E. and Ose, O. O. (2013) Profitability Analysis of Yam Production in Ika South Local Government Area of Delta State, Nigeria, *Journal of Biology, Agriculture and Healthcare,* 3(2): 118-129.

Okieimen, F.E.; Maya, A.O.; Oriakhi, C.O. (1998) Sorption of cadmium and zinc ions on sulphur containing chemically modified cellulosic materials. *International Journal of Environmental Analytical Chemistry*, 32(1):23-27.

Olafadehan, O.A.; Jinadu, O.W.; Salami, L. and Popoola, O.T. (2012) Treatment of brewery wastewater effluent using activated carbon prepared from coconut shell. *International Journal of Applied Science and Technology*, 2(1):165-178.

Olagunju, F. I.; Fakayode, S. B.; Babatunde, R.O. and Ogunwole-Olapade, F. (2013) Gender Analysis of Sweet Potato Production in Osun State, Nigeria. *Asian Journal of Agricultural Extension, Economics & Sociology,* 2(1): 1-13.

Olade, M.A.(1987) Heavy metal pollution and the need for monitoring: Illustrated for developing countries in West Africa. In: *Lead, mercury, cadmium and arsenic in the environment*. T.C. Hutchinson and K.M. Meema (eds). John Wiley and Sons Ltd. pp. 335-341.

Oladayo, A.(2010) Proximate composition of some agricultural wastes in Nigeria and their potential use in activated carbon production. *Journal of Applied Sciences and Environmental Management*, 14(1):55-58.

Oladeji, J.T. (2011) Agricultural and forestry wastes and opportunities for their use as an energy source in Nigeria- An overview. *World Rural Observation*, 3(4):107-112.

Onsoyen, E. and Skaugrud, O. (1990) Metal Recovery using Chitosan. *Journal of Chemical Technology and Biotechnology,* 49: 395-404.

Onwu, F.K. and Ogah, S.P.I.(2010) Studies on the effect of pH on the sorption of cadmium(II), nickel(II), lead(II) and chromium(VI) from aqueous solutions by African white star apple (*Chrysophyllum albidium*) shell. *African Journal of Biotechnology*, 9(42):7086-7093.

Onyeka, J. (2014) Status of Cocoyam (Colocasia esculenta and Xanthosoma spp) in West and Central Africa: Production, Household Importance and the Threat from Leaf Blight. Lima (Peru). CGIAR Research Program on Roots, Tubers and Bananas (RTB). Available internet: Available internet: http://www.rtb.cgiar.org/publication/view/status-of-cocoyam-colocasia-esculenta-and-xanthosoma-spp-in-west-and-central-africa-production-household-importance-and-the-threat-from-leaf-blight/ Accessed on 12/01/2015.

Opara, L. U. (2003) Edible Aroids: Post Harvest Operation. Food & Agriculture Organisation (FAO). Available internet: http://www.fao.org/fileadmin/user_upload/inpho/docs/Post_Harvest_Compendium_-_Edible_aroids.pdf Accessed on 12//09/2012.

Opeolu, B.O.; Bamgbose, O.; Arowolo, T.A. and Adetunji, M.T.(2009) Utilization of maize (*Zea mays*) cob as an adsorbent for lead(II) removal from aqueous solutions and industrial effluents. *African Journal of Biotechnology,* 8(8): 1567-1573.

Orisakwe, O.E.; Nwachukwu, E.; Osadolor, H.B.; Afonne, O.J. and Okocha, C.E.(2007) Liver and kidney function tests amongst paint factory workers in Nkpor, Nigeria. *Toxicology and Industrial Health,* 23: 161–165.

Orisakwe, O.E. (2014) Lead and Cadmium in Public Health in Nigeria: Physicians Neglect and Pitfall in Patient Management. *North American Journal of Medical Science*, 6(2): 61–70.

Osuji, L. C.; Udoetok, I. A.; Ogali, R. E. (2006) Attenuation of Petroleum hydrocarbons by weathering: A case study. *Chemistry and Biodiversity,* 3: 422-433.

Osuji, L. C. and Uwakwe, A. A. (2006) Petroleum industry effluents and other oxygen demanding wastes in Niger Delta, Nigeria. *Chemistry and Biodiversity*, 3: 705-717.

Othman, A. M. (2008) Preparation of Sulfurized granular activated carbon from Beji Asphalt using concentrated H_2SO_4. *Tikrit Journal of Pure Science*,13 (3): 1-7.

Otokunefor, T. V.; Obiukwu, C. (2005) Impact of refinery effluent on the physiochemical properties of a water body in the Niger Delta. *Applied Ecology and Environmental Research,* 3(1): 61-72.

Otti, V.I.; Ifeanyichukwu, H.I.; Nwaorum, F.C. and Ogbuagu, F.U. (2014) Sustainable Oil Palm Waste Management in Engineering Development. *Civil and Environmental Research*, 6(5): 121-125.

Oviasogie, P.O.; Odewale, J.O. ; Aisueni, N.O. ; Eguagie, E.I.; Brown, G. and Okoh-Oboh, E. (2013) Production, utilization and acceptability of organic fertilizers using Palms and Shea tree as sources of biomass. *African Journal of Agricultural Research*, 8(27): 3483-3414.

Oyaro, N.; Juddy, O.; Murago, E.N.M. and Gitonga, E. (2007) The contents of Pb, Zn, and Cd in meat in Nairobi, Kenya. *International Journal of Food Agricultural Environ*ment, 5:119-121.

Ozarcar, M. and Sengil, I.A.(2006) A two stage batch adsorber design for methylene blue removal to minimize contact time. *Journal of Environmental Management*,80:372-379.

Padervand, M.; Gholami, M. R. (2013) Removal of toxic heavy metal ions from Wastewater by functionalized magnetic core-zeolite shell nanocomposites as adsorbents. *Environmental Science and Pollution Research* 20: 3900-3909.

Padmavathy, V. V.; Vasudevan, P. and Dhingra, S. C. (2003) Thermal and Spectroscopic studies on sorption of nickel(II) ion on protonated baker's yeast, *Chemosphere,* 52: 1807-1817.

Paduraru, C.; Tofan, L.; Teodosiu, C.; Bunia, I.; Tudorachi, N. and Toma, O. (2015) Biosorption of Zinc(II) on rapeseed waste: Equilibrium studies and thermogravimetric investigations. *Process Safety and Environmental Protection*, 94: 18-25.

Pagliuca, A. and Mufti, G.J. (1990) Lead poisoning: an age-old problem. *British Medical Journal*, 300:830.

Pamukoglu, Y.; Kargi, F. (2007) Biosorption of Copper (II) ions onto powdered waste sludge in a completely mixed fed-batch reactor: Estimation of design parameters. *Bioresource Technology,* 98: 1155-1162.

Pandey, R.; Prasad, R.L.; Ansari N.G. and Murthy, R.C. (2015) utilization of NaOH modified *Desmostachya bipinnata* (Kush grass) leaves and *Bambusa arundinacea* (bamboo) leaves for Cd(II) removal from Aqueous solution. *Journal of Environmental Chemical Engineering*, 3: 593-602

Pansamut, V.; Pongrit, V. and Intarangsi, C. (2003) The Oil Palm. Department of Alternative Energy Development and Efficiency. Ministry of Energy, Thailand. http://weben.dede.go.th/webmax/content/energy-crops-biogas-production Accessed 12/10/2013.

Papandreou, A.; Stournaras, C.J. and Panias, D. (2007) Copper and cadmium adsorption on pellets made from fired coal fly ash. *Journal of Hazardous Materials*, 148:538-547.

Park, Y. J., Yang, J. K and Choi, S. L. (2008) The Application of reused powdered waste as adsorbent for treating arsenic containing mine drainage. *Journal of Environmental Science and Health Part* A, 43: 1093-1099.

Park, D.; Yun, Y. S.; Jo, J. H. Park, J. M. (2006) Biosorption process for treatment of electroplating wastewater containing Cr (IV): Laboratory-scale feasibility Test. *Industrial and Engineering Chemistry Research,* 45: 5059-5065.

Parshetti, G.K.; Hoekman, K.S. and Balasubramanian, R. (2013) Chemical, a structural and combustion characteristic of carbonaceous products obtained by hydrothermal carbonization of empty fruit bunches. *Bioresource Technology,* 135: 683-689.

Paulino, A.T.; Minasse, F.A.S.; Guilhere, M.R. Reis, A.V.; Muniz, E.C. (2006) Novel adsorbent based on silkworm chrysalides for removal of heavy metals from wastewaters. *Journal of Colloid Interface Science*, 301; 479-487

Pavasant, P.; Apiratikul, R.; Sungkhum, V.; Suthiparinyanont, P.; Wattanachira, S.; Marhaba, T. F. (2006) Biosorption of Cu^{2+}, Cd^{2+}, Pb^{2+} and Zn^{2+} using marine green macroalga *Caulerpa lentillifera. Bioresource Technology,* 97: 2321-2329.

Pearson, R. G. (1988). Absolute electronegativity and hardness: application to inorganic chemistry. *Inorganic Chemistry,* 27(4): 734-740.

Percival-Zhang, Y. H. (2008) Reviving the carbohydrate economy via multi-product Lignocellulose biorefineries. *Journal of Industrial Microbiology and Biotechnology,* 35: 367-375.

Perez, N. A.; Rincon, G.; Delgado, L, A.; Gonzales, N. (2006) Use of biopolymers for the removal of heavy metals produced by the oil industry *Adsorption,* 12: 279-286.

Periasamy, K.; Namasivayam, C. (1995) Removal of Nickel (II) from aqueous solution and Nickel plating industry wastewater using an agricultural waste: Peanut Hulls. *Waste Management,* 15(1): 63-68.

PerkinElmer, (2011) Award Winning Results-2400Series II CHNS/O Elemental Analyser. Available internet: http://www.perkinelmer.co.uk/CMSResources/Images/44-74386BRO_2400_SeriesII_CHNSO_Elemental_Analysis.pdf Accessed on 09/03/2011.

PerkinElmer (2005) FT-IR Spectroscopy-Attenuated Total Reflectance (ATR), Technical Note. Available internet: http://www.utsc.utoronto.ca/~traceslab/ATR_FTIR.pdf Accessed on 12/02/2012.

PerkinElmer, (2010) Thermogravimetric Analysis (TGA) A Beginner's Guide. Available internet: http://www.perkinelmer.co.uk/CMSResources/Images/44-74556GDE_TGABeginnersGuide.pdf Accessed on 30/04/2013.

Persson, I.; Lyczko, K.; Lundberg, D.; Eriksson, L. and Placzek, A.(2011) Coordination chemistry study of hydrated and solvated Lead(II) ions in solution and solid state. *Inorganic Chemistry*, 50:1058-1072.

Pirbazari, A. E.; Saberikhan, E.; Badrouh, M. and Emami, M. S. (2014) Alkali treated Foumanat tea waste as an efficient adsorbent for methylene blue adsorption from aqueous solution. *Water Resources and Industry,* 6: 64-80.

Poletto, M.; Ornaghi, H.L and Zattera, A.J.(2014) Native cellulose: structure, characterisation and thermal properties. *Materials*, 7:6105-6119.

Prola, L.D.T.; Acayanka, E.; Lima, E.C.; Umpierres, C.S.; Vaghetti, J.C.P.; Santos, W.O.; Laminsi, S. and Djifon, P.T.(2013) Comparison of *Jatropha curcas* shells in natural form and treated by non-thermal plasma as biosorbents for removal of Reactive Red 120 textile dye from aqueous solution. *Industrial Crops and Products*, 46:328-340.

Purdue (2010) Scanning Electron Microscope. Available internet: http://www.purdue.edu/rem/rs/sem.htm Accessed on 01/02/2012.

Puri, B. R., Sharma, L. R. and Pathania, M. S. (2002) *Principles of Physical Chemistry.* Visual Publishing Co, Jalandar India.

Qaiser, S.; Saleemi, A. R.; Ahmed, M. M. (2007) Heavy metal uptake by agro-based waste materials. *Environmental Biotechnology,* 10: 409-416.

Qiu, H.; Lu, L. V.; Pan, B.; Zhang, Q.; Zhang, W. and Zhang, Q. (2009) Critical Review in Adsorption Kinetic Models. *Journal of Zhejiang University of Science A,* 10(5): 716-724.

Qureshi, K., Inamulla, B.; Razi, R. and Ansari, A. K. (2008) Physical and Chemical Analysis of Activated carbon prepared from sugarcane bagasse and use of sugar decolorisation. *International Journal of Chemical and Biological Engineering,* 1(3): 144-148.

Rafatullah, M.; Sulaiman, O.; Hashim, R. and Ahmad, A. (2009) Adsorption of copper (II) chromium, nickel (II) and lead (II) ions from aqueous solutions by meranti sawdust. *Journal of Hazardous Materials*, 170: 969-977.

Rakic, V.; Rac, V.; Krmar, M.; Otman, O. and Auroux, A. (2015) The adsorption of pharmaceutically active compounds from aqueous solutions onto activated carbons. *Journal of Hazardous Materials,* 282: 141-149.

Ramos, M. E.; Bonelli, P. R. and Cukierman, A. L. (2008) Physico-chemical and electrical properties of activated carbon cloths: Effect of inherent nature of fabric precursor. *Colloids and Surfaces A Physicochemical & Engineering Aspects,* 324: 86-92

Rangabhashiyam, S.; Anu, N.; Nandagopal, G. and Selvaraju, N. (2014) Relevance of isotherm models in biosorption of pollutants by agricultural by products. *Journal of Environmental Chemical Engineering,* 2: 398-414.

Rao, K. S.; Anand, S. and Venkateswarlu, P. (2010a) Adsorption of cadmium (II) ions from aqueous by *Tectona grandis* L. F. (Teak leaves powder) *BioResources* 5(1): 438-454.

Rao, K. S.; Mahapatra, M.; Anand, S. and Venkateswarlu, P. (2010b) Review on Cadmium Removal from Aqueous Solutions. *International Journal of Engineering, Science and Technology,* 2(7): 81-103.

Rao, M. M.; Ramana, D. K.; Seshaiah, K. ; Wang, M. C. and Chien, S. W. C. (2009) Removal of some metal ions by activated carbon prepared from *Phaseolus aureus* hulls, *Journal of Hazardous Materials,* 166(2-3):1006-1013.

Rao, M. M.; Ramesh, A.; Rao, P. C.; Seshaiah, K. (2006) Removal of Copper and Cadmium from the aqueous solutions by activating carbon derived from *ceiba_pentandra* hulls. *Journal of Hazardous Materials,* 129: 123-129.

Reeves, G. G. (2000) Wastewater minimization with chemical free water treating. *Environmental Progress,* 19(4): 292-298.

Rivera-Utrilla, J.; Sanchez-Polo, M.; Gomez-Serrano, V.; Alvarez, P.M.; Alvim-Ferraz, M.C.M. and Dias, J.M. (2011) Activated carbon modifications to enhance its water treatment applications. An overview. *Journal of Hazardous Materials*, 187:1-23.

Roman, S; Valente-Nabais, J. M.; Ledesma, B.; Gonzalez, J. F; Laginhas, C and Titirici, M. M. (2013) Production of low-cost adsorbents with tunable surface chemistry by conjugation of hydrothermal carbonization and activation process. *Microporous and Mesoporous Materials,* 165: 127-133.

Run, C.S.; Jeremy, T.; Gwynn, L. J. (2000) Fractional characterization of ash AQ lignin by successive extraction with organic solvents from oil palm EFB fibre. *Polymer Degradation and Stability*, 68: 111-119.

Rusten, B. and Odegaard, H.(2006) Evaluation and testing of fine mesh sieve technologies for primary treatment of municipal wastewater. *Water Science and Technology,* 54(10): 31-38.

Ruthven, D. M. (1991) Adsorption In: *Kirk-othmer Encyclopedia of Chemical Technology* 4 ed. Vol. 1 Kroschwitsz, J. I. and Howe-Grant, M. (eds.). John Willey and Sons, Inc. New York.

Sabo, A.; Gani, A. and Ibrahim, A. Q. (2013) Pollution status of heavy metals in water and bottom sediments of River Delimi in Jos, Nigeria. *American Journal of Environmental Protection*, 1(3): 47-53.

Sadeek, S.A.; Negm, N.A.; Hefni, H.H.H; and Wahab, M.M.A.(2015) Metal adsorption by agricultural biosorbents: Adsorption isotherm, kinetic and biosorbents chemical structures. *International Journal of Biological Macromolecules*, 81: 400-409.

Sahu, J. N.; Acharya, J and Meikap, B. C. (2010) Optimization of production conditions for Activated carbons from Tamarind wood by Zinc Chloride using Response Surface Methodology. *Bioresource Technology,* 101: 1974-1982.

Saien, J. and Nejati, A. (2007) Enhanced photocatalytic degradation of pollutants in petroleum refinery wastewater under mild conditions. *Journal of Hazardous Materials,* 148: 49-498.

Saleh, N. B.; Pfefferie, L. D. and Elimelech, M. (2008) Aggregation Kinetics of Multiwalled Carbon Nanotubes in Aquatic Systems: Measurements and Environmental Implications. *Environmental Science & Technology,* 42: 7963-7969.

Salem, N. M.; Farham, A. M.; Awwad, A. M. (2012) Biosorption of Cadmium (II) from aqueous solution by Prunus Avium Leaves. *American Journal of Environmental Engineering* 2(5) 123-127.

Salopek, B.; Krasic, D. and Filipovic, S. (1992) Measurement and application of zeta potential. *Rudarsko-geolsko-naftni zbornik* 4: 147-151.

Sanchez-Silva, L.; Lopez-Gonzalez, D.; Villasenor, J.; Sanchez, P. and Valverde, J. L. (2012) Thermogravimetric-mass spectroscopic analysis of lignocellulosic and marine biomass pyrolysis. *Bioresource Technology,* 109: 163-172.

Santhy, K. and Selvapathy, P. (2006) Removal of reactive dyes from wastewater by adsorption on coir pith activated carbon. *Bioresource Technology,* 97: 1329-1336.

Sarada, B.; Prasad, M. K.; Kumar, K. K. and Murthy, Ch. V. R. (2014) Cadmium removal by macro algae *Caulerpa fastigiata*: characterization, kinetic, isotherm and thermodynamic studies. *Journal of Environmental Chemical Engineering,* 2: 1533- 1542.

Sardella, F.; Gimenez, M.; Navas, C.; Morandi, C.; Deiana, C. and Sapag, K. (2015) Conversion of viticultural industry wastes into activated carbon for removal of lead and cadmium. *Journal of Environmental Chemical Engineering*, 3(1): 253-260

Sari, A.; Mendil, D.; Tuzen, M. and Soulak, M. (2008) Biosorption of Cd (II) and Cr (III) from aqueous solution by moss (*Hylocomium splendens*) biomass: Equilibrium, kinetic and thermodynamic studies. *Chemical Engineering Journal,* 144: 1-9.

Schwartz, G.G. and Reis, I.M. (2000) Is cadmium a cause of human pancreatic cancer? *Cancer Epidemiology Biomarkers & Prevention,* 9(2): 139-145.

Šćiban, M.; Kukić, D. and Prodanović, J. (2013) Potential of agrobased waste materials as adsorbents of heavy metal ions from water. *Reporting for Sustainability: Proceedings of the International Science Conference*, 7th -10th of May, 2013, Montenegro.

Seader, J. D.; Henley, E. J. and Roper, D. K. (2011) *Separation Process Principles-Chemical and Biochemical Operations*. 3rd Ed. John Wiley & Sons, New Jersey, USA.

Segal, L.; Creely, L. Martin, A. E. and Conrad, C. M. (1959) An empirical method for estimating the degree of crystallinity of native cellulose using X-ray diffractometer. *Textile Research Journal*, 29(10): 786-794.

Selomulya, C.; Meeyoo, V. and Amal, R. (1999) Mechanism of Cr (VI) removal from Water by various types of Activated Carbon. *Journal of Chemical Technology & Biotechnology,* 74:111-122.

Senthilkumar, P.; Ramalingam, S.; Abhinaya, R. V.; Kirupha, D. S.; Vidhyadevi, T. and Sivanesan, S. (2012) Adsorption Equilibrium, thermodynamics, kinetics, mechanism and process design of Zinc(II)ions onto cashew nutshell. *Canadian Journal of Chemical Engineering*, 90: 973-982.

Sen, T. K and Sarzali, M. V. (2008) Removal of Cadmium metal ion (Cd^{2+}) from its aqueous solution by aluminium oxide (Al_2O_3): A Kinetic and Equilibrium Study. *Chemical Engineering Journal,* 142: 91-102.

Sevilla, M.; Macia-Agullo, J. A and Fuertes, A. B. (2011) Hydrothermal carbonization of business as a route for the sequestration of CO_2: Chemical and structural properties of the carbonized products. *Biomass and Bioenergy,* 35(7): 3152-3159

Sevilla, M. and Furetes, A. B. (2009) The production of carbon materials by hydrothermal carbonization of cellulose *Carbon,* 47: 2281-2289.

Shang, S. K., Reedijk, J. (1984) Co-ordination chemistry of chelating resins and ion-exchangers. *Coordination Chemistry Review,* 59: 1-139.

Sharp, D. W. A. (1990) Dictionary *of Chemistry*. 2nd ed. Penguim Books, London.

Shen, J. and Duvnjak, Z. (2004) Effects of temperature and pH on adsorption isotherms for cupric and cadmium ions in their single and binary solutions using corncob particles as adsorbent. *Separation Science and Technology*, 39(13):3023-3041.

Shimadzu (2010) Shimadzu X-ray Diffractometer-A General Purpose X-ray Diffractometer to fulfil your varying analytical needs. Available Internet: http://www.shimadzu.com.br/analitica/produtos/difratometros/catalogos/xrd-6100.pdf Accessed on 21/12/2012.

Shodehinde, S.A. and Oboh, G. (2013) Antioxidant properties of aqueous extracts of unripe *Musa paradisiaca* on sodium nitroprusside induced lipid peroxidation in rat pancreas in vitro. *Asian Pacific Journal of Tropical Medicine*, 3(6):449-457.

Sherman-Hsu, C.P (1997) Infrared Spectroscopy. *Handbook of Instrumental Techniques for Analytical Chemistry*. Settle, F.A(ed). Prentice Hall PTR, New Jersey.pp247-263.

Shon, H. K.; Phuntsho, S.; Chaudhary, D. S.; Vigneswaran, S. and Cho, J. (2013) Nanofiltration for water and wastewater treatment − a mini review. *Drinking Water Engineering Science* 6: 47-53.

Shrestha, S.; Son, G.; Lee, S. H. and Lee, T. G. (2013) Isotherm and thermodynamic studies of Zn (II) adsorption on lignite and coconut shell-based activated carbon fibre. *Chemosphere,* 92: 1053-1061.

Simonescu, M.C. (2012) Application of FTIR Spectroscopy in Environmental Studies. In: *Advanced Aspects of Spectroscopy*. Farrukh, A. M. (ed). Intech Publishers, New York, pp 49-84.

Sing, K. (2001) The use of nitrogen adsorption for the characterisation of porous materials. *Colloids and Surfaces A: Physicochemical and Engineering Aspects*, 187-188: 3-9.

Sing, K. S. W. (1982) Reporting Physisorption Data for Gas/Solid Systems with Special Reference to the Determination of Surface Area and Porosity. *Pure & Applied Chemistry,* 54: 2201-2218.

Sing, K. S. W. (2014) Adsorption by active carbons. *In Adsorption by powders and porous solids. Principles, methodology and application.* Rouquerol, F. Rouquerol, J. Sing, K. S. W. Llewellyn, P. Maurin G. (eds). Elsevier ltd, Oxford. pp.321-391

Sing, K. S. W.; Everett, D. H.; Haul, R. A. W.; Moscou, L.; Pierotti, R. A.; Rouquerol, J. and Siemieniewska, T. (1985) Reporting physisorption data for gas/solid systems with special reference to the determination of surface area and porosity. *Pure & Applied Chemistry,* 57: 603-619.

Sing, K. S. W. and Williams, R.T. (2004) Physisorption Hysteresis loop and the characterisation of Nanoporous Materials. *Adsorption Science and Technology,* 22(10): 7773-782.

Slack, R. A.; Gronow, J. R.; Voulvoulis, N. (2005) Household hazardous waste in municipal landfills: contaminants in leachate. *Science of the Total Environment,* 337: 119-137.

Sobamiwa, O. and Longe, O. G. (1994) Utilization of cocoa-pod pericarp fractions in broiler chick diets. *Animal Feed Science and Technology,* 47: 237-244.

Sokan-Adeaga, A.A. and Ana, G.R.E.E. (2015) A comprehensive review of biomass resources and biofuel production in Nigeria: potential and prospects. *Reviews on Environmental Health*, 30(3):143-162.

Soleimani, M. and Kaghazchi, T. (2008) Activated Hard Shell of Apricot Stones: A Promising Adsorbent in Gold Recovery. *Chinese Journal of Chemical Engineering,* 16 (1): 112-118.

Soleimani, M. and Kaghazchi, T. (2014a) Agricultural Waste Conversion to Activated Carbon by Chemical Activation with Phosphoric Acid. *Chemical Engineering & Technology,* 30(5): 649-654.

Solemani, M. and Kaghazchi, T. (2014b) Low-Cost Adsorbents from Agricultural By-Products Impregnated with Phosphoric Acid *Advanced Chemical Engineering Research,* 3: 34-41.

Sonune, A. and Ghate, R. (2004) Developments in wastewater treatment methods. *Desalination,* 167: 55- 63.

Speakman, S. A. (2012) Basics of X-Ray Powder Diffraction. Available Internet: http://prism.mit.edu/xray/Basics%20of%20X-Ray%20Powder%20Diffraction.pdf Accessed on 16/02/2013.

Srinivas, T. (2009) Economics of Sweetpotato production and marketing. In: *The Sweet potato*. G.Loebenstein and G. Thottappilly (eds). Springer Science+Business Media,B.V. Netherlands. pp235-267.

Srivastava, V. C.; Mall, I. D. and Indra, M. M. (2006) Characterization of mesoporous rise husk ash (RHA) and adsorption kinetics of metal ions from aqueous solution onto RHA. *Journal of Hazardous Materials,* 134: 257-267.

Srivastava, V.; Weng, C. H. and Sharma, Y. C. (2013) Application of a thermally modified agrowaste material for an economically viable removal of Cr(VI) from aqueous solutions. *Journal of Hazardous, Toxic and Radioactive Waste,* 17: 125-133.

Sricharoenchaikul, V.; Pechyen, C. C.; Aht-ong, D. and Atong, D. (2008) Preparation and Characterisation of Activated Carbon from the Pyrolysis of Physics Nut (*Jatrophacuras L.*) Waste, *Energy and Fuels,* 22: 31-37.

Stefany, P. M.; Garcia, D.: Lopez, J. and Jimenez, A. (2005) Thermogravimetric Analysis of Composite obtained from sintering of Rice Husk scrap tire Mixtures. *Journal of Thermal Analysis and Calorimetry* 81: 315-320.

Stodghill, S.P. (2010) Thermal Analysis-A review of techniques and applications in the pharmaceutical Sciences. *American Pharmaceutical Review,* 13(2): 29-36.

Storck, S.; Bretinger, H. and Maier, W. F. (1998) Characterization of micro and mesoporous solids by physisorption methods and pore-size analysis. *Applied catalysis A: General,* 174: 137-146.

Sud, D.; Mahajan, G.; Kaur, M. P. (2008) Agricultural waste material as potential adsorbent for sequestering heavy metal ions from aqueous solutions. A review. *Bioresource Technology,* 99(14): 6017-6027.

Sugumaran, P.; Susan, V..; Ravichandran, P. and Seshadri, S. (2012) Production and Characterization of Activated Carbon from Banana Empty Fruit Bunch and *Delonix regia* Fruit Pod. *Journal of Sustainable Energy and Environment* 3: 125-132.

Suhas, P. J. M.; Carroh, M. and Ribeiro Carrott, M. M. (2007) Lignin from natural adsorbent to activities carbon: A review. *Bioresource Technology,* 98(12): 2301-12.

Sunanda, T. D. P.; Sharma, D. N. and Kumar, R. J. S. (2013) Sapindus Based Activated Carbon by Chemical Activation. *Research Journal of Materials Sciences,* 1(17): 9-15.

Sun, G. and Xu, X. (1997). Sunflower stalks as adsorbents for colour removal from textile wastewater. *Industrial and Engineering Chemistry Research,* 3: 808-810.

Sun, K.; Tang, J.; Gong, Y. and Zhang, H.(2015) Characterization of potassium hydroxide (KOH) modified hydrochars from different feedstocks for enhanced removal of heavy metals from water. *Environmental Science and Pollution Research*, 22:16640-16651.

Sun, X.; and Li, Y. (2004) Colloidal carbon spheres and their core/shell structures with noble-metal nanoparticles. *Angewante Chemie International Edition,* 43(5): 597-601

Sun, Y and Webley, P. A. (2011) Preparation of Activated Carbons with Large Specific Surface Areas from Biomass Corncob and their Adsorption Equilibrium for Methane, Carbondioxide, Nitrogen and Hydrogen. *Industrial Engineering & Chemical Research,* 50: 9286-9294.

Sushrut Chemicals (2006) Activated Carbon. Available internet: http://www.sushrutchemicals.com/activatedCarbon.html Accessed on 12/03/2016.Swiatkowski, A.; Pakula, M. P.; Biniak, S. and Walczyk, M. (2004) Influence of the surface Chemistry of modified activated carbon on its electrochemical behaviour in the presence of Lead (II) ions. *Carbon,* 42: 3057-3069.Syamsiro, M.; Saptoadi, H.; Tambunan, B.H. and Pambudi, N.A.(2012) A preliminary study on use of cocoa pod husk as a renewable source of energy in Indonesia. *Energy for Sustainable Development,*16: 74-77.

Tan, X.; Liu, Y.; Zeng, G.; Wang, X.; Hu, X. and Gu, Y. (2015) Application of biochar for the removal of pollutants from aqueous solutions *Chemosphere,* 125: 70-85.

Tajar, A. F.; Kaghazchi, T. and Soleimani, M. (2009) Adsorption of cadmium from aqueous solutions on sulfurized activated carbon prepared from nut shells. *Journal of Hazardous Materials*, 165(1-3): 1159-1164.

Tangjuank, S.; Insuk, N.; Tontrakoon, J.; and Udeye, V. (2009) Adsorption of Lead(II) and Cadmium(II) ions from aqueous solutions by adsorption on activated carbon prepared from cashew nut shells. *World Academy of Science, Engineering and Technology,* 28: 110-116.

Tarawou, T. and Horsfall, M. Jr. (2007) Adsorption of methylene blue dye on pure and carbonized water weeds. *Bioremediation Journal,* 11(2): 77-84.

Tarley, T.C.R. and Arruda, M.A.Z. (2004) Biosorption of heavy metals using rice milling by-product-Characterisation and application for removal of metal from aqueous effluents. *Chemosphere*, 54: 987-995.

Taty-Costodes, V. C.; Fauduet, H.; Porte, C.; Ho, Y. S. (2005) Removal of lead(II) ions from synthetic and real effluents using immobilized *Pinus Sylvestris* sawdust: Adsorption on a fixed-bed column. *Journal of Hazardous Materials,* 123: 135-144.

Teker, M.; Imamoglu, M and Saltasbas, O.(1999) Adsorption of copper and cadmium ions by activated carbon from rice hulls. *Turkish Journal of Chemistry*, 23(2): 185-191.

Terinte, N.; Ibbett, R. and Schuster, C. (2011) Overview of native cellulose and microcrystalline cellulose I structure studied by X-ray diffraction (WAXD): Comparison between measurement techniques. *Lenzinger Berichte,* 89: 118-131.

Temkin, M.I. and Pyzhev,V. (1940) Kinetics of ammonia synthesis on promoted iron catalyst, *Acta Physiochim.* URSS 12: 327–356.

Tertian, R. and Claisse, F. (1982) *Principles of Quantitative X-ray Fluorescence Analysis.* Heyden & Sons Ltd, London. pp 3-56.

Thermo Fisher Scientific (2008) Flash 2000 Series CHN/CHNS /Oxygen Automatic Elemental Analyzer. Available internet: https://static.thermoscientific.com/images/D13580~.pdf Accessed on 06/02/2010

Thirumavalavan, M.; Lai, Y. L. and Lee, J. F. (2011) Fourier transform infrared spectroscopic analysis of fruit peels before and after the adsorption of heavy metal ions from aqueous solution. *Journal of Chemical Engineering Data,* 56:2249-2255.

Thomas, A.; Kuhn, P.; Webber, J.; Titirici, M and Antonietti, M. (2009) Porous polymers: Enabling solutions for energy applications. *Macromolecular Rapid Communications,* 30: 221-236.

Thompson, M. (2008) CHNS Analysers Royal Society of Chemistry Analytical Methods Committee (AMC) Technical Briefs, AMCTB No.29 April, 2008. Available internet: http://www.rsc.org/images/CHNS-elemental-analysers-technical-brief-29_tcm18-214833.pdf Accessed on 12/10/2011.

Thomas, R. (2008) *Practical Guide to ICP-MS: A Tutorial for Beginners. Practical Spectroscopy Series*, Vol. 37. Boca Raton: CRC Press. 376.

Thommes, M. (2010) Physical Adsorption Characterisation of Nanoporous Materials, *Chemie Ingenieur Technik,* 82(7): 1059-1073.

Titiloye, J.O., Abu Bakar, M.S., Odetoye, T.E.(2013) Thermochemical Characterisation of Agricultural Wastes from West Africa. *Industrial Crops and Products,* 47: 199-203.

Titirici, M; Funke, A and Kruse, A (2015a) Hydrothermal carbonization of biomass. In *Recent Advances in Thermochemical Conversion of Biomass*. Pandey, A.; Bhaskar, T.; Stocker, M. and Sukumaran, R. (Eds) Elsevier science Ltd, Amsterdam.

Titirici, M.; Thomas A. and Antonietti, M. (2007a) Back in the black: hydrothermal carbonization of plant material as an efficient process to treat CO_2 problem? *New Journal of Chemistry*, 31: 787-789

Titirici, M.; Thomas A; Yu, S. H. ; Muller, J. and Antonietti, M. (2007b) A direct synthesis of mesoporous carbons with biocontinuous pore morphology from crude plants material by hydrothermal carbonization. *Chemistry of Materials,* 19(17): 4205-4212.

Titirici, M.; White, R.J.; Brun, N.; Budarin,V.L.; Su, D.S.; Del Monte, F. Clark, J.H. and MacLachlan, M.J.(2015b) *Sustainable Carbon Materials*, Chemical Society Reviews, 44:250-290.

Toles, C. A; Marshall, W. E. and Johns, M. M. (1999) Surface functional groups on acid-activated nutshell carbons, *Carbon*, 37: 1207-1214.

Toles, C. A.; Marshall, W. E.; Johns, M. M.; Wartelle, L. H. and McAloon, A. (2000) Acid-activated carbons from almond shells: physical, chemical and adsorptive properties and estimated cost of production. *Bioresource Technology,* 71: 87-92.

Tong, S.; Schirnding, Y. E. V. and Prapamontol, T. (2000) Environmental Lead Exposure: A Public Health Problem of Global Dimensions, *Bulletin of the World Health Organisation* 78(9): 1068-1077.

Torres-Perez, J.; Gerente, C. and Andres, Y. (2012) Conversion of agricultural residues into activated carbons for water purification: Application to arsenate removal. *Journal of Environmental Science and Health Part A* 47: 1173-1185.

Tsai, W. T.; Chang, C. V.; Lin, M. C.; Chien, S. F.; Sun, H. F. and Hsieh, M. F. (2001) Adsorption of acid dye onto activated carbons prepared from agricultural waste bagasse by $ZnCl_2$ activation. *Chemosphere,* 45: 51-58.

Tserki, V.; Matzinos, P.; Kokkou, S. and Panayiotou, C. (2005) Novel biodegradable composites based on treated lignocellulosic waste flour as filler. Part 1: Surface Chemical Modification and Characterization of waste flour. *Composites*, Part A, 36: 965 – 974.

Tuna, A. O. A.; Ozdemir, E.; Simsek, E. B. and Beker, V. (2013) Removal of As(V) from aqueous solution by activated carbon-based hybrid adsorbents: Impact of experimental conditions. *Chemical Engineering Journal,* 223: 116-128.

Uchimiya, M.; Wartelle, L. H.; Klasson, T.; Fortier, C. A.; Lima, I. M. (2011) Influence of pyrolysis temperature on biochar property and function as a heavy metal sorbent in soil. *Journal Agricultural and Food Chemistry*, 59(6): 2501-2510.

Udosen, E. D., Udoessien, E.I. and Ibok, U.J. (1990) Evaluation of Some Metals in the Industrial Wastes from a Paint Industry and their Environmental Pollution Implications. *Nigerian Journal of Technology & Research.,* 2:71-77.

Udosen, E.D.; Ukpong, G.E. J. E. Asuquo, J.E. and Etim, E.E. (2012) Trace Metal Levels in Soils within an Abandoned Steel Industry Environment. *International Journal of Modern Analytical and Separation Sciences,* 1(1): 1-12

Uhegbu, F. O., Akubugwo, E. and Iweala, E. E. J. (2012) Effect of Garri Processing effluents wastewater on the cyanide Level of some root tubers commonly consumed in the South East of Nigeria. *African Journal of Food Agriculture and Nutrition and Development,* 12(6): 6748-6758.

UNCTAD (2012) United Nations Conference on Trade and Development. Infocom Commodity Profile-Sweet Potato. Available internet:
http://www.unctad.info/en/Infocomm/AACP-Products/COMMODITY-PROFILE---Sweet-potato Accessed on 10/11/2013.

Unuabonah, E.I; Gunter, C.; Weber, J.; Lubahn, S. and Taubert, A. (2013) Hybrid clay: A new highly efficient adsorbent for water treatment. *ACS Sustainable Chemistry and Engineering*, 1:966-973.

Unur, E. (2013) Functional nanoporous carbons from hydrothermally treated biomass for environmental purification. *Microporous and Mesoporous Materials* 168: 92-101

US EPA (2013) United States Environmental Protection Agency-Drinking Water Contaminants-National Primary Drinking Water Regulations. Available Internet: http://water.epa.gov/drink/contaminants/index.cfm Accessed on 30/7/13.

Uwubanmwen, I.O; Nwawe, C.N.; Okere, R.A.; Dada, M. and Eseigbe, E. (2011) Harnessing the Potentials of the Coconut Palm in the Nigerian Economy. *World Journal of Agricultural Sciences*, 7 (6): 684-691.

Vaghetti, J. C. P; Lima, E. C.; Royer, B.; Cunha, B. M. C. and Cardoso, N. F. (2009) Pecan nutshell as biosorbent to remove Cu (II), Mn (II), and Pb (II) from aqueous solutions, *Journal of Hazardous Materials*, 162: 270-280.

VanLoon, G and Duffy, S.J.(2010) *Environmental Chemistry: A Global Perspective*. 3rd Ed. Oxford University Press, Oxford.

Varma, G.; Singh, R. K. and Saha, V. (2013) A comparative study of the removal of heavy metals by adsorption using fly ash and sludge. A Review. *International Journal of Application of Innovation in Engineering and Management,* 2(7): 45-56.

Vargas, A. M. M.; Cazetta, A. L.; Garcia, C. A.; Moraes, J. C. G.; Nogami, E. M. (2011) Preparation and characterization of activated carbon from a new raw lignocellulosic material: Flamboyant (*Delonix regia)* pods. *Journal of Environmental Management,* 92: 178-184.

Varshney, K, V. And Naithani, S. (2011) Chemical Functionalization of cellulose Derived From nonconventional Sources. *In: Cellulose Fibres: Bio-and Nano-Polymer Composites,* Kalia, S. *et al*., (eds) Springer-Verlag Berlin Heidelberg. pp. 43- 60.

Verbinnen, B.; Block, C.; Caneghem, J.V. and Vandecasteele, C. (2015) Recycling of spent adsorbents for oxyanions and heavy metals ions in the production of ceramics. *Waste Management,* 45:407-411.

Villaescusa, I.; Fiol, N.; Martinez, M.; Miralles, N.; Poch, J.; Serarols, J. (2004) Removal of Copper and Nickel ions from aqueous solutions by grape stalks wastes. *Water Research,* 38: 992-1002.

Vivien, C.; Caleb, A. I and Lekwot, V. E. (2012) Public Health Effects of Effluent Discharge of Kaduna Refinery into River Romi. *Greener Journal of Medical Sciences,* 23: 064-069.

Volesky, B. (1990) *Biosorption of heavy metals*. CRC Press, Boca Raton, Florida

Vriesmann, L. C.; Teofilo, R. F.; and Petkowicz, C. L. O. (2012) Extraction and Characterisation of Pectin from Cacao pod husk (*Theobroma Cacao L*) with citric acid. *LWT- Food Science and Technology* 49:108-116.

Voglar, G.E. and Lestan, D. (2013) Equilibrium leaching of toxic elements from cement stabilized soil. *Journal of Hazardous Materials*, 246-247: 18-25.

Wahab, M.A.; Boubakri, H,; Jellai, S. and Jedial, N.(2012) Characterisation of ammonium retention processes onto cactus leaves fibres using FTIR, EDX and SEM analysis. *Journal of Hazardous Materials*, 241-242: 101-109.

Wan, S.; Ma, Z.; Xue, Y.; Ma, M.; Xu, S.; Qian, L. and Zhang, Q. (2014) Sorption of Lead (II), cadmium and Copper (II) ions from aqueous solution using tea waste. *Industrial & Engineering Chemistry Research,* 53: 3629-3635.

Wang, G.; Zhang, S.; Yao, P.; Chen, Y.; Xu, X.; Li ,T. and Gong, G.(2015a) Removal of Pb(II) from aqueous solutions by *Phytolacca americana* L. biomass as a low cost biosorbent, *Arabian Journal of Chemistry*. In Press: http://dx.doi.org/10.1016/j.arabjc.2015.06.011

Wang, J.; Chen, C. (2006) Biosorption of heavy metals by *Saccharomyces cerevisine*: A review. *Biotechnology Advances,* 24: 427-451.

Wang, K.; Jiang, J. X.; Xu, F. and Sun, R. C. (2009) Influence of streaming pressure on steam explosion pre-treatment of Lespedeza stalks (*Lespedeza crytobotrya*): Part1. Characteristics of degraded cellulose. *Polymer degradation and Stability,* 94: 1379-1388.

Wang, S.; Mulligan, C. N. (2006) Occurrence of arsenic contamination in Canada: Sources, behaviour and distribution. *Science of the Total Environment* 366: 701-721.

Wang, Y.; Yang, R.; Li, M. and Zhao, Z. (2015b) Hydrothermal preparation of highly porous carbon spheres from hemp (*Cannabis sativa* L.) stem hemicelluloses for use in energy related application. *Industrial Crops and Products*, 65: 216-226

Wang, Z.; Cao, J. and Wang, J. (2009) Pyrolytic characteristics of pine wood in a slowly heating and gas sweeping fixed-bed reactor. *Journal of Analytical and Applied Pyrolysis,* 84: 179-184.

Weber, W.J and Morris, J.C. (1963) Kinetics of adsorption on carbon from solution. *Journal of the Sanitary Engineering Division*, 89(2); 31-60

Weiss, B. and Landrigan, P. J. (2000) The developing brain and the environment: an introduction. *Environmental Health Perspectives*, 108:373-374.

Weng, C. H. (2002) Removal of nickel (II) from dilute aqueous solution by sludge-ash. *Journal of Environmental Engineering,* 128: 716-722.

Weng, C. H.; Pan, Y. F. (2007) Adsorption of a cationic dye (methylene blue) onto spent activated clay. *Journal of Hazardous Materials,* 144: 335-362.

White, J. E.; Catallo, W. J. and Legendre, B. L. (2011) Biomass pyrolysis kinetics: A competitive critical review with relevant agricultural residue case studies. *Journal of Analytical and Applied Pyrolysis,* 91:1-33

White, R. J.; Budrin, Y. L and Clark, J. H (2010) Pectin-derived porous materials. *Chemistry- A European Journal,* 16: 1326-1335

WHO (2010) Exposure to cadmium: a major public health concern. Preventing disease through healthy environments. Available internet: http://www.who.int/ipcs/features/cadmium.pdf Accessed on 06/10/2010.

Wickramaratne, N. P.; Xu, J.; Wang, M.; Zhu, L. Dai, L and Mietek, J. (2014) Nitrogen enriched porous carbon spheres: Attractive materials for supercapacitor electrodes and CO_2 adsorption. *Chemistry of Materials,* 26(9): 2820-2828

Wilson, K.; Yang, H.; Seo, C. W. and Marshall, W. E. (2006) Select metal adsorption by activated carbon made from peanut shells. *Bioresource Technology,* 97: 2266-2270.

Wojciechowski, K.T and Malecki, A.(1999) Mechanism of thermal decomposition of cadmium nitrate $Cd(NO_3)_2.4H_2O$. *Thermochimica Acta*, 331:73-77.

Wong, Y. C.; Szeto, V. S.; Cheung, W. H. and McKay, G. (2004) Adsorption of acid dyes on Chitosan-equilibrium isotherm analysis. *Process Biochemistry,* 39: 693-702.

Wu, D.; Gu, Z and Li, Y. (2015) Attrition of catalyst particles in a laboratory-scale fluidized-bed reactor. *Chemical Engineering Science*, 135:431-440.

Wu, F. C.; Tseng, R. L. and Juang, R. S. (2000) Comparative Adsorption of Metal and Dye on Flake- and Bead-types of Chitosans Prepared from Fishery Wastes. *Journal of Hazardous Materials,* 73: 63-75.

Wu, J. (2004) Modelling adsorption of Organic Compounds on Activated Carbon - A multivariate Approach. Thesis of the Umea University, Sweden. Available internet: http://umu.diva-portal.org/smash/get/diva2:142987/FULLTEXT01.pdf   Accessed on 10/01/2011.

Wu, X.; Ma, H.; Zhang, L. and Wang, F. (2012) Adsorption properties and mechanism of mesoporous adsorbents prepared with fly ash for removal of Cu(II) in aqueous solution. *Applied Surface Science*, 261: 902-907.

Xiao, L. P.; Zhao, J. S.; Shi, Z. J.; Xu, F. and Sun, R. C. (2011) Impact of hot compressed water pre-treatment on the structural changes of woody biomass for bioethanol production. *BioResources,* 6(2): 1576-1598.

Xu, Q.; Qian, Q.; Quek, A.; Ai, N.; Zeng, G. and Wang, J. (2013) Hydrothermal carbonization of microalgae and the effects of experimental parameters on the properties of hydrochars. *ACS Sustainable Chemistry and Engineering*, 1: 1092-1101

Xu, Y.; Lou, Z.; Yi, P.; Chen, J.; Ma. X. and Wang, Y. (2014) Improving abiotic reducing ability of hydrothermal biochar by low temperature oxidation under air. *Bioresource Technology,* 172: 212-218.

Xuan, Z.; Tang, Y.; Li, X.; Liu, Y. and Luo, F. (2006) Study on the equilibrium, kinetics and isotherm of Biosorption of lead ions onto presented chemically modified orange peel. *Biochemical Engineering Journal,* 31: 160-164.

Xue, Y.; Gao, B.; Yao, Y.; Inyang, M.; Zhang, M.; Zimmerman, A.R. and Ro, K.S. (2012) Hydrogen peroxide modification enhances the ability of biochar (hydrochar) produced from hydrothermal carbonization of peanut hull to remove aqueous heavy metals: Batch and column tests. *Chemical Engineering Journal*, 200-202: 673-680.

Yabe, J.; Ishizauka, M. and Umemura, T. (2010) Current levels of heavy metal pollution in Africa. *Journal of Veterinary Medical Science*, 72(10): 1257–1263, 2010

Yamasaki, H.; Makihata, Y.; Fukunaga, K. (2006) Efficient phenol removal of wastewater form phenolic resin plants using cross linked cyclodextrin particles. *Journal of Chemical Technology and Biotechnology,* 81: 1271-276.

Yaneva, S. L.; Koumanova, B. K. and Georgieva, N. K. (2013). Linear and Nonlinear Regression Methods for Equilibrium modelling of *p*-Nitrophenol Biosorption by *Rhizopus oryzae*: Comparison of Error Analysis Criteria. *Journal of Chemistry*: Article ID 517631, pp 10. http://dx.doi.org/10.1155/2013/517631

Yang, H.; Yan, R.; Chen, H.; Lee, D. H.; Zheng, C. (2007) Characteristics of hemicellulose, cellulose and lignin pyrolysis. *Fuel,* 86: 1781-1788.

Yang, R. T. (2003) *Adsorbents: Fundamentals and Applications.* John Wiley & Sons, Inc, New Jersey. pp 79-111.

Yang, X. and Cui, X. (2013) Adsorption characteristics of Pb(II) on alkali treated tea residue. *Water Resources and Industry*, 3:1-10.

Yang, Y.; Wei, Z.; Xu, C.; Yue, D.; Yin, Q.; Xiao, L. and Yang, L.(2014) Biochar from Alternanthera philoxeroides could remove Pb(II) efficiently. *Bioresource Technology,* 171: 227-232.

Yavuz, O.; Altunkayak, Y.; Guzel, F. (2003) Removal of Copper, Nickel, Cobalt and Manganese from aqueous solution by kaolinite. *Water Research,* 37: 948-952.

Yazaydın, A.O.; Snurr, R.Q.; Park, T.; Koh, K.; Liu, J.; LeVan, M. D; Benin, A.I; Jakubczak, P.; Lanuza, M.; Galloway, D. B.; Low, J.J. and Willis, R.R. (2009) Screening of Metal−Organic Frameworks for Carbon Dioxide Capture from Flue Gas Using a Combined Experimental and Modeling Approach. *Journal of the American Chemical Society, 131* (51): 18198-18199.

Yeneneh, M. A.; Maitra, S. and Eldemerdash, U. (2011) Study on Biosorption of Heavy Metals by Modified Lignocellulosic Waste, *Journal of Applied Sciences,* 11(21): 3555-3562.

Yousef, R.I.; El-Eswed, B. and Al-Muhtaseb, A.H (2011) Adsorption characteristics of natural zeolites as solid adsorbents for phenol removal from aqueous solutions: Kinetics, mechanism, and thermodynamics studies, *Chemical Engineering Journal*, 171(3):1143-1149.

Yu, X.; Tong, S.; Ge, M.; Wu, L.; Zuo, J.; Cao, C. and Song, W.(2013) Adsorption of heavy metal ions from aqueous solution by carboxylated cellulose nanocrystals. *Journal of Environmental Sciences*, 25(5): 933-943.

Yuan, J. H.; Xu, R. and Zhang, H. (2011) The forms of alkalis in the biochar produced from crop residues at different temperatures. *Bioresource Technology,* 102: 3488-3497

Zhao, G.; Wu, X.; Tan, X. and Wang, X. (2011) Sorption of Heavy Metal ions from Aqueous Solutions: A Review. *The Open Colloid Science Journal,* 4: 19-31.

Zhang, V.; Zheng, R.; Zhao, J.; Ma, F.; Zhang, Y. and Meng, Q. (2014) Characterization of H_3PO_4-treated rice husk adsorbent and adsorption of copper (II) from aqueous solution. *BioMed Research International,* 496878.

Zhao, J.; Zhu, Y. J.; Zheng, J. Q.; Zhao, X. Y.; Lu, B. Q. and Chen, F. (2014) Chitosan-coated mesoporous microspheres of calcium silicate hydrate: environmentally friendly synthesis and application as a highly efficient adsorbent for heavy metal ions. *Journal of Colloid Interface Science,* 15(418): 208-15.

Zhou, Y.; Hu, X.; Xinhai, Q. J.; Wang, X. and Ma, T. (2013) Adsorption of Cd(II) from aqueous solutions by cellulose modified with maleic anhydride and thiourea. *Adsorption Science and Technology*, 31(7): 583-598.

Zhu, X.; Liu, Y.; Qian, F.; Zhou, C.; Zhang, S. and Chen, J. (2014) Preparation of magnetic porous carbon from waste hydrochar by simultaneous activation and magnetisation for tetracycline removal. *Bioresource Technology,* 154:209-214.

Zouboulis, A. I.; Kydros, K. A. (1993) Use of red mud for toxic metal removal: the case of nickel. Journal of Chemical *Technology Biotechnology* 58: 95-101.

APPENDICES

APPENDIX 1

N₂ adsorption-desorption isotherm and pore size distribution of residue adsorbents
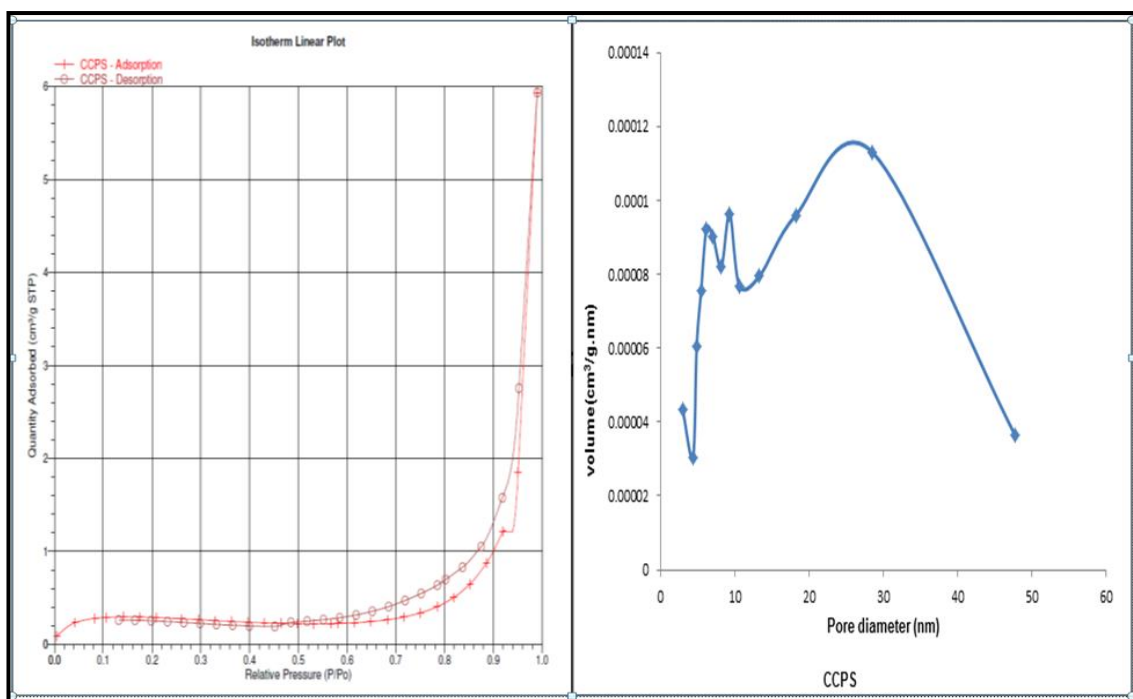
N₂ adsorption-desorption isotherm and pore size distribution of CCPS residue adsorbent
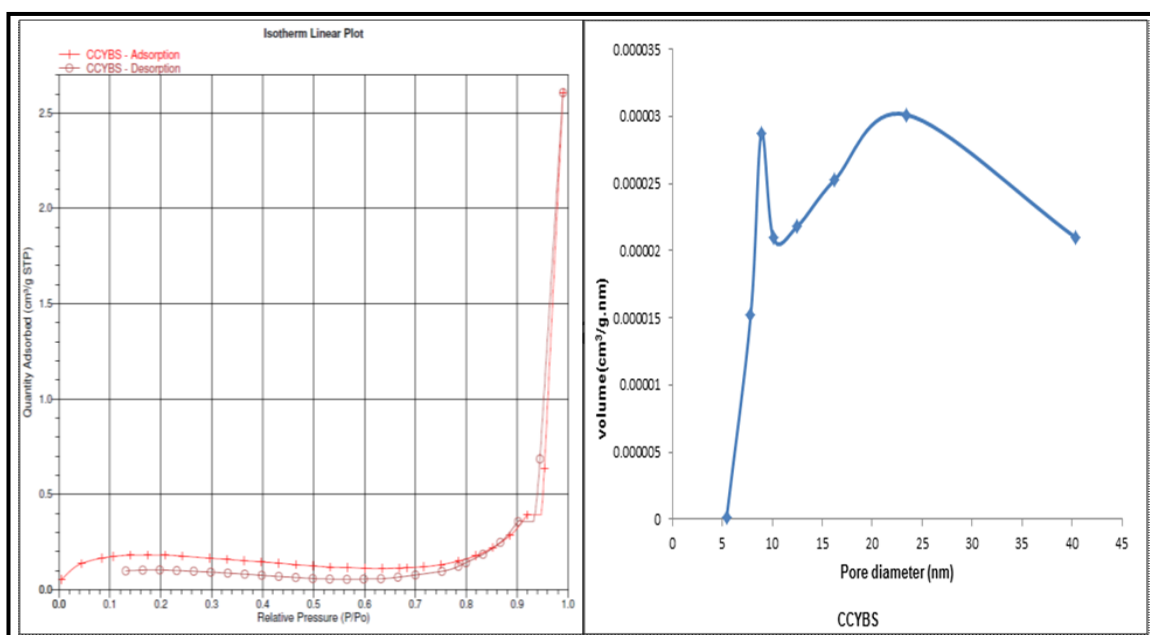
N₂ adsorption-desorption isotherm and pore size distribution of CCYBS residue adsorbent
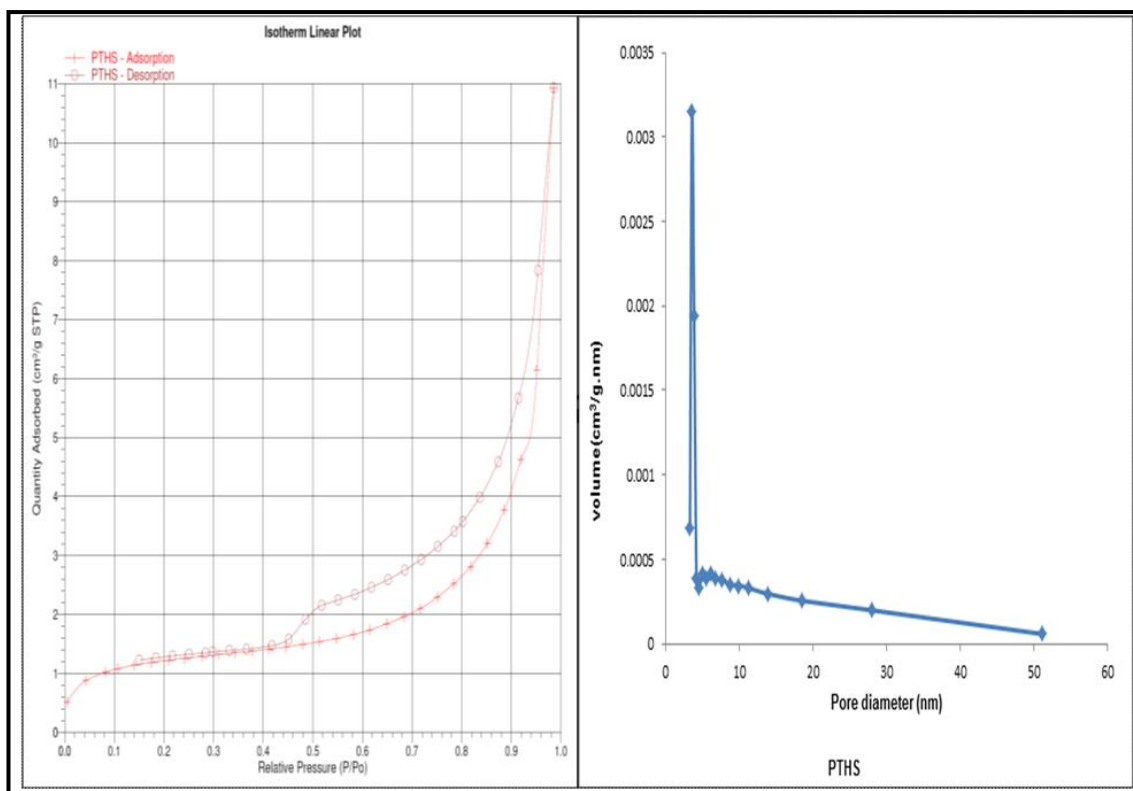
N$_2$ adsorption-desorption isotherm and pore size distribution of PTHS adsorbent
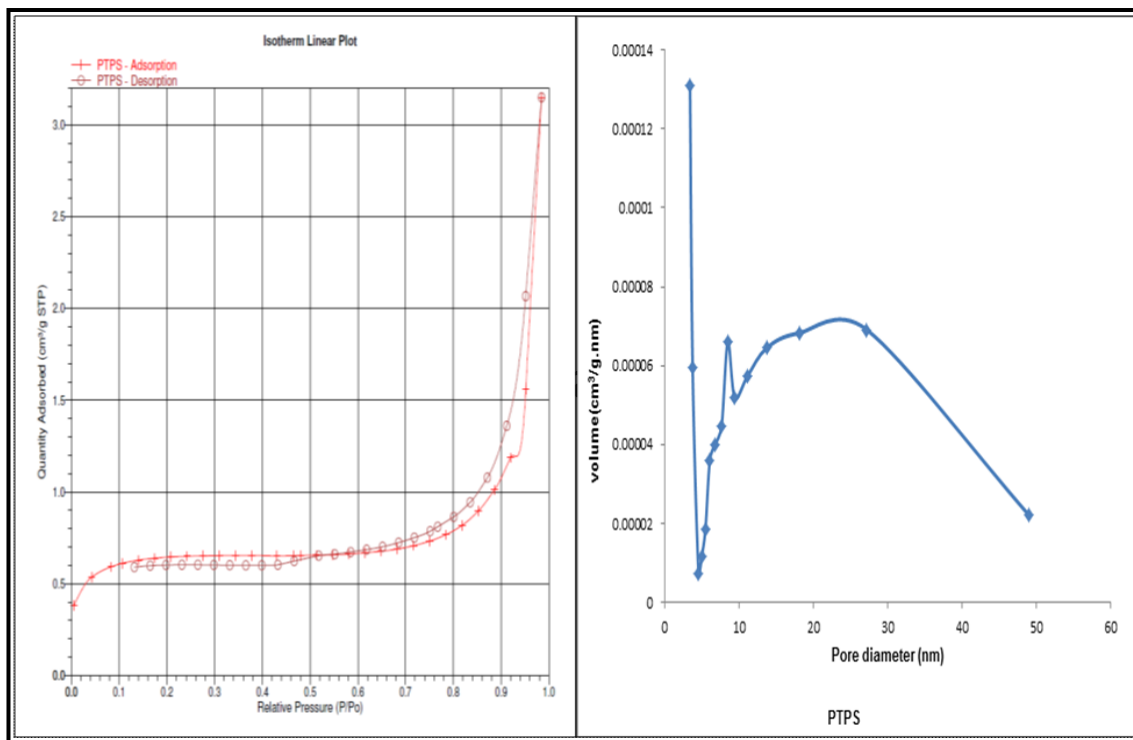
N$_2$ adsorption-desorption isotherm and pore size distribution of PTPS residue adsorbent
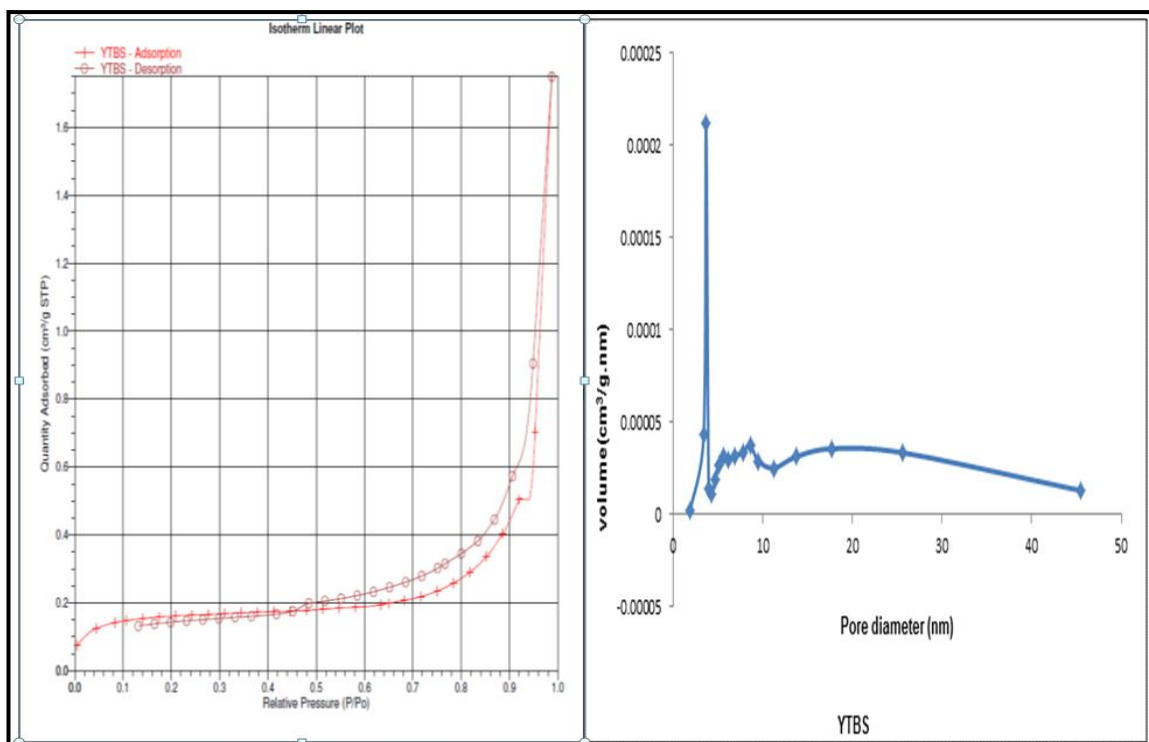
N$_2$ adsorption-desorption isotherm and pore size distribution of YTBS adsorbent

APPENDIX 2

Thermogravimetric Analysis of Residue Adsorbents
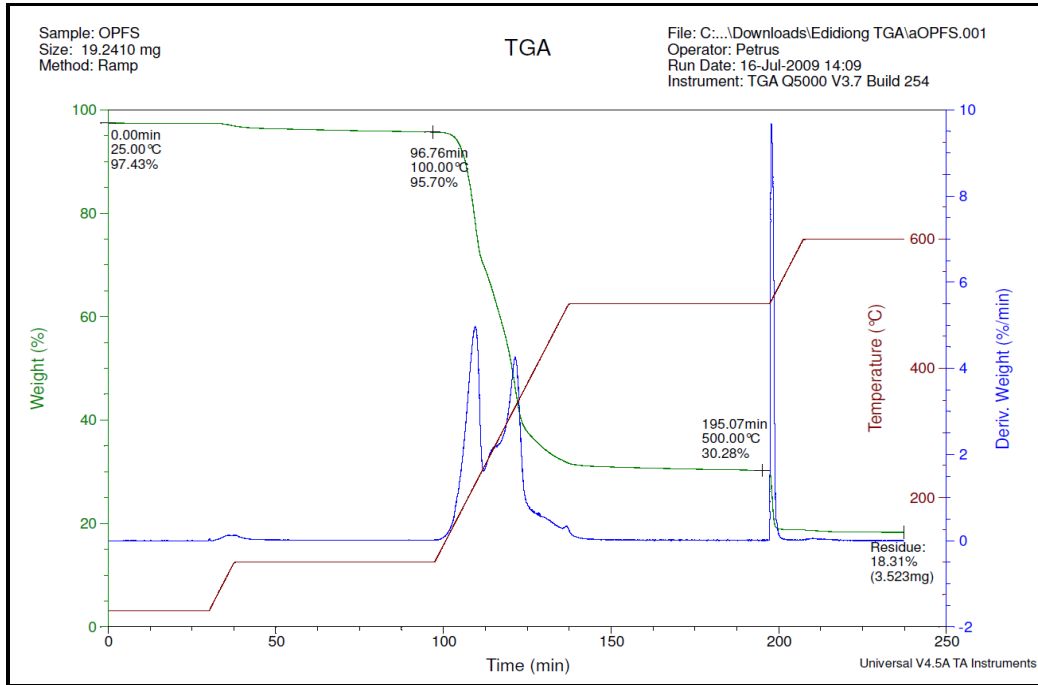
Thermogravimetric Analysis of OPFS
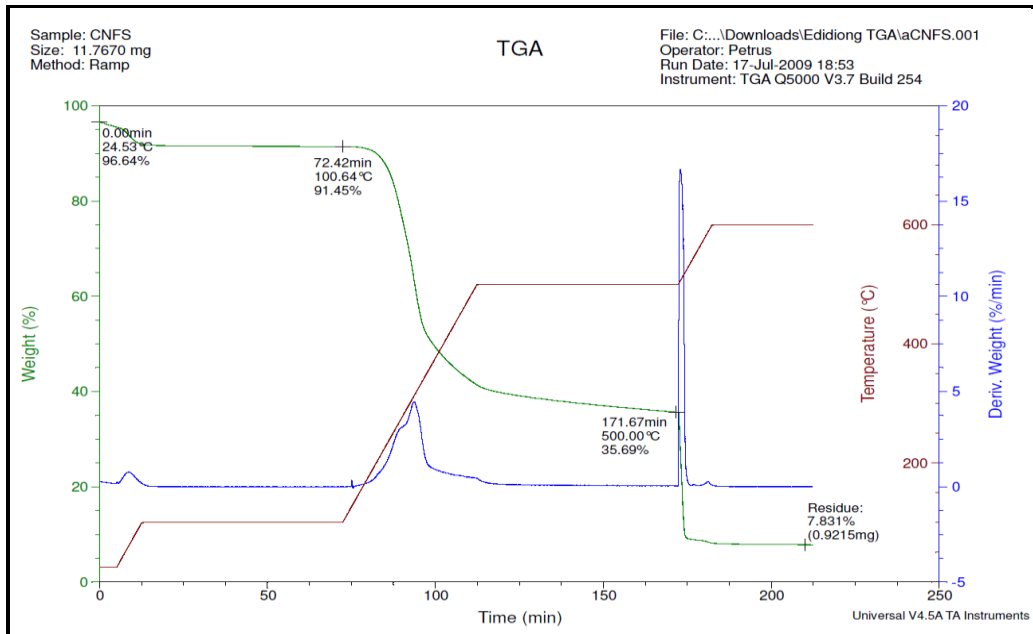
Thermogravimetric Analysis of CNFS
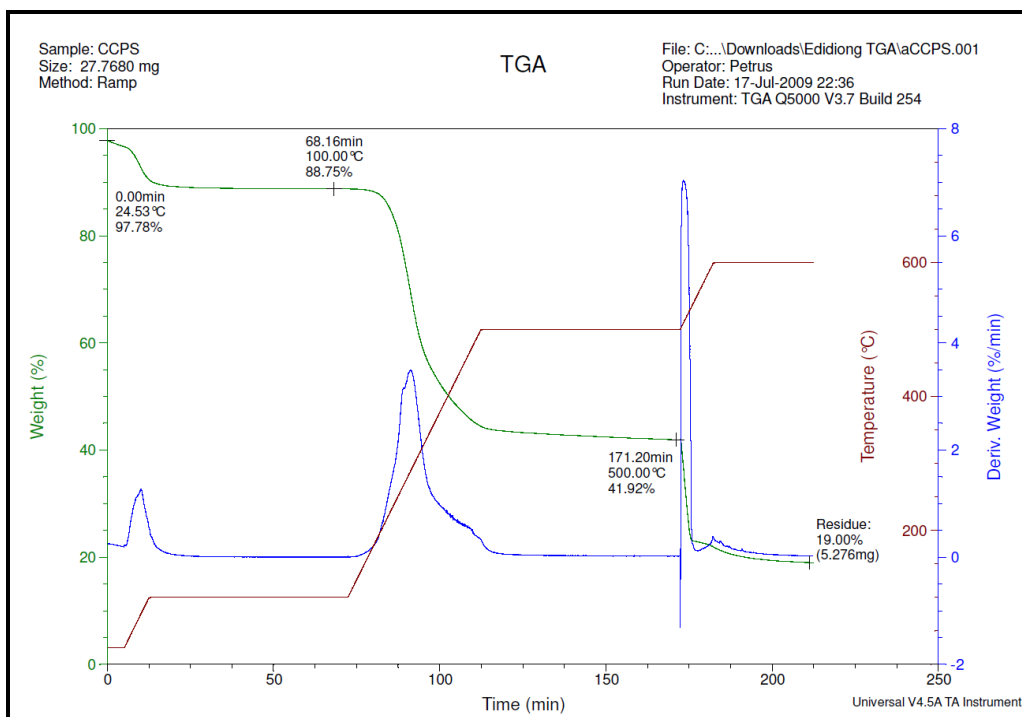
Thermogravimetric Analysis of CCPS
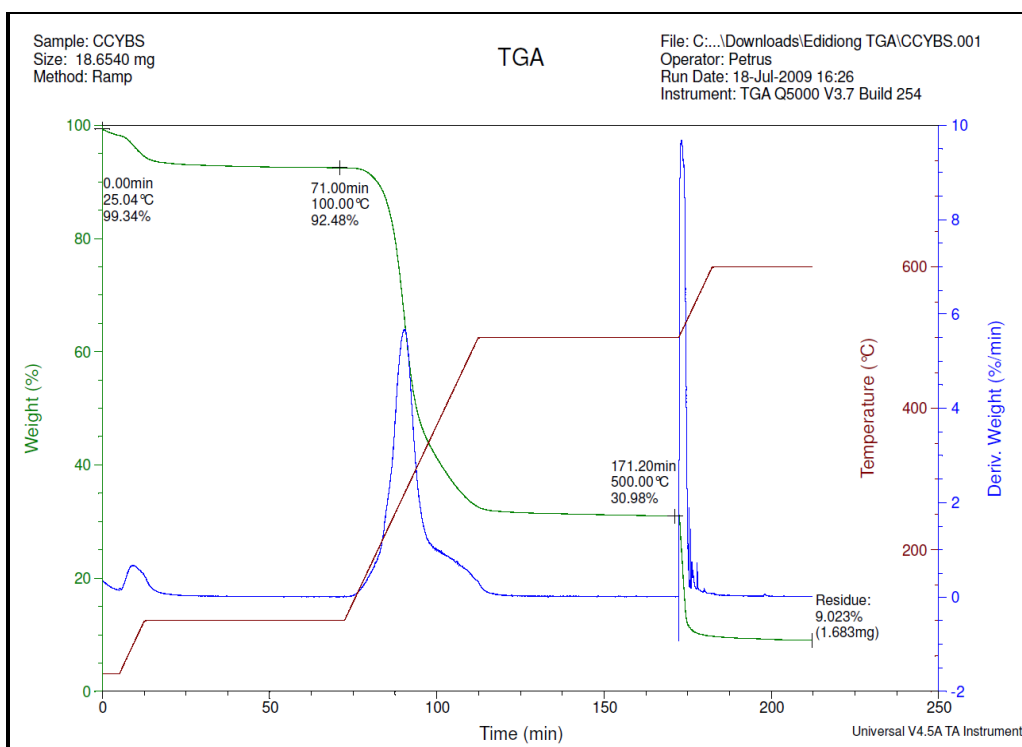
Thermogravimetric Analysis of CCYBS
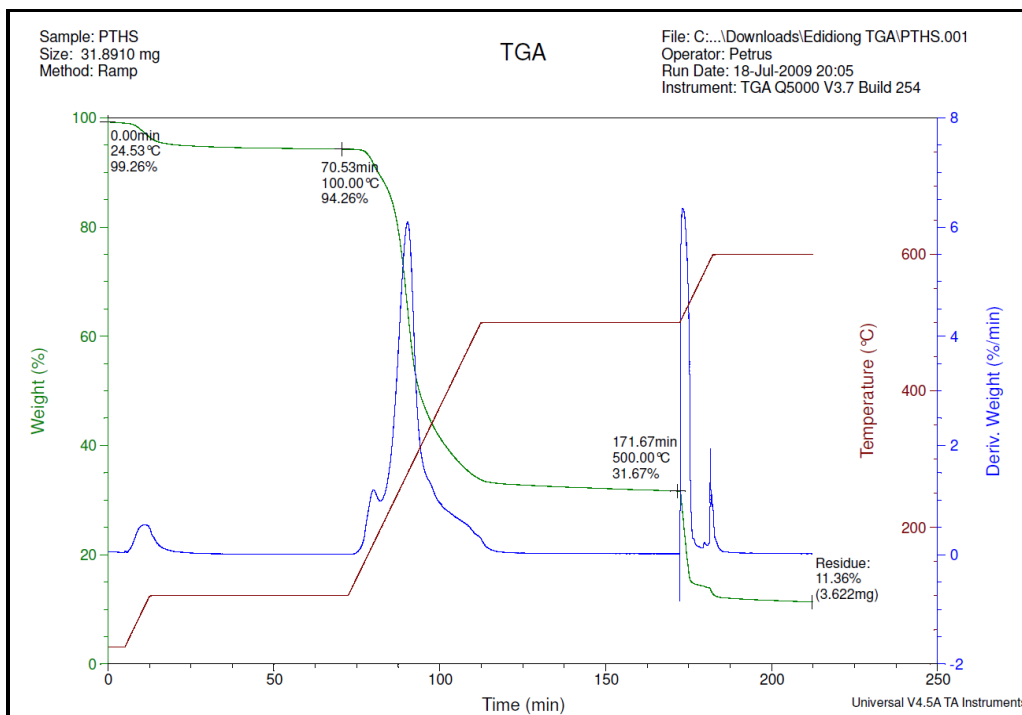
Thermogravimetric Analysis of PTHS
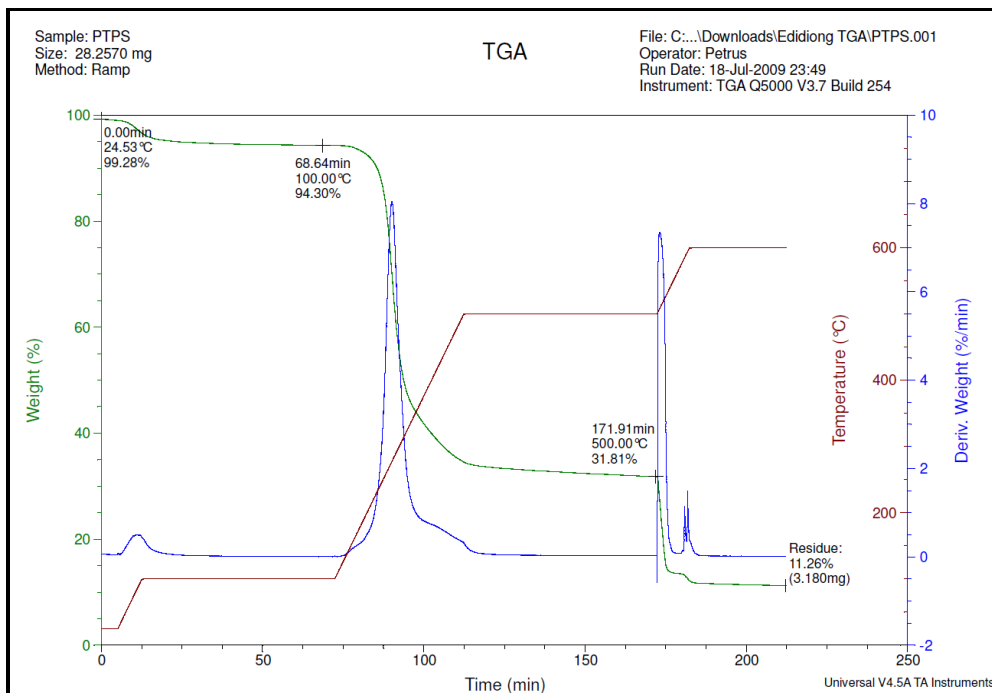
Thermogravimetric Analysis of PTPS
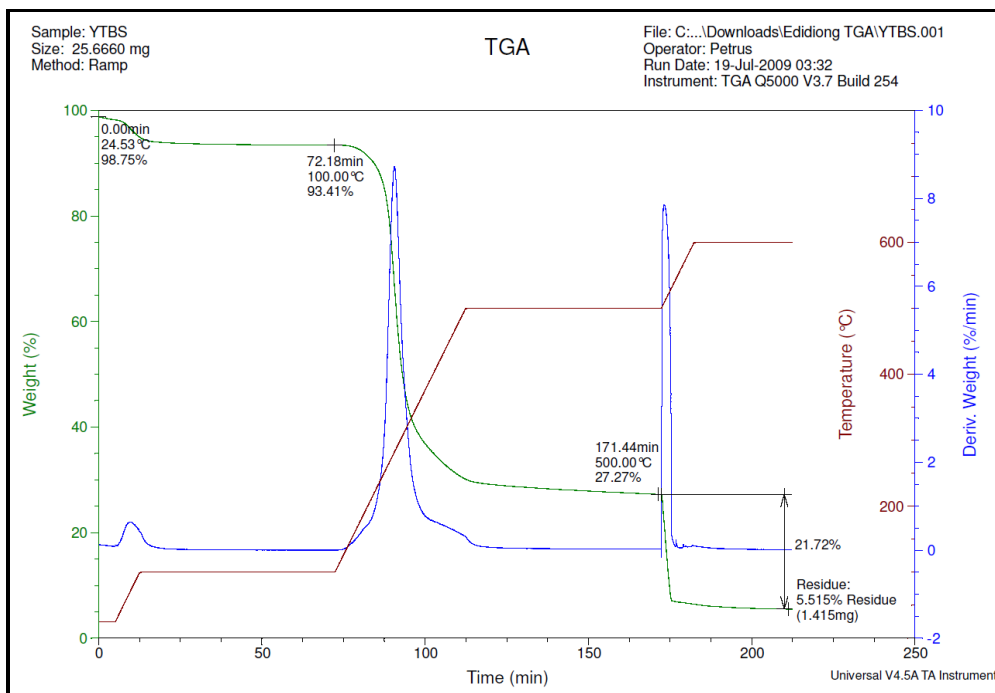
Thermogravimetric Analysis of YTBS

APPENDIX 3

ZETA POTENTIAL PLOT FOR ADSORBENTS
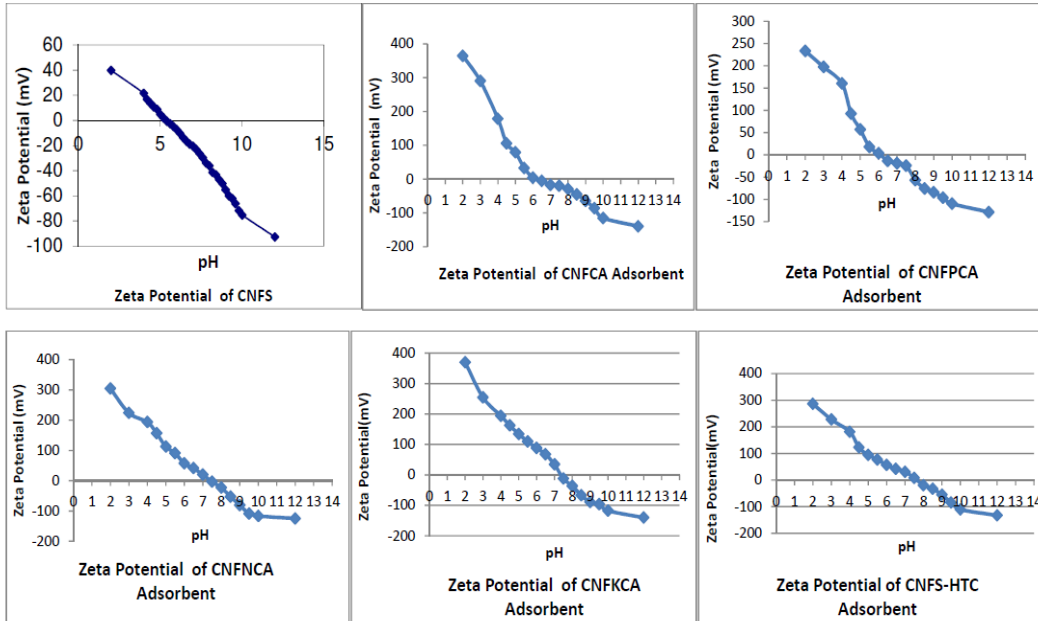
Zeta Potential of Coconut fibre adsorbents
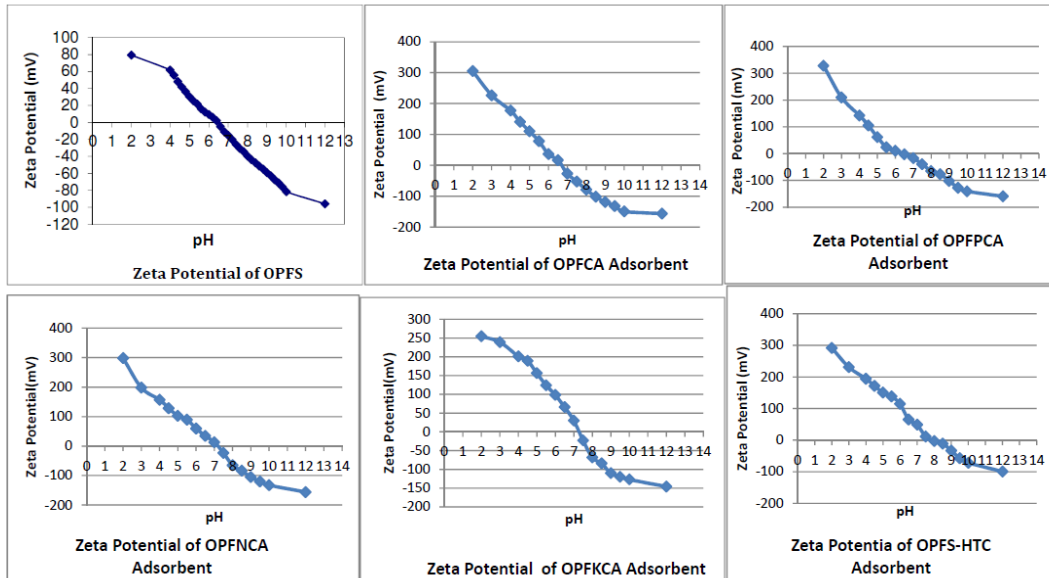
Zeta Potential of Oil Palm fibre adsorbents
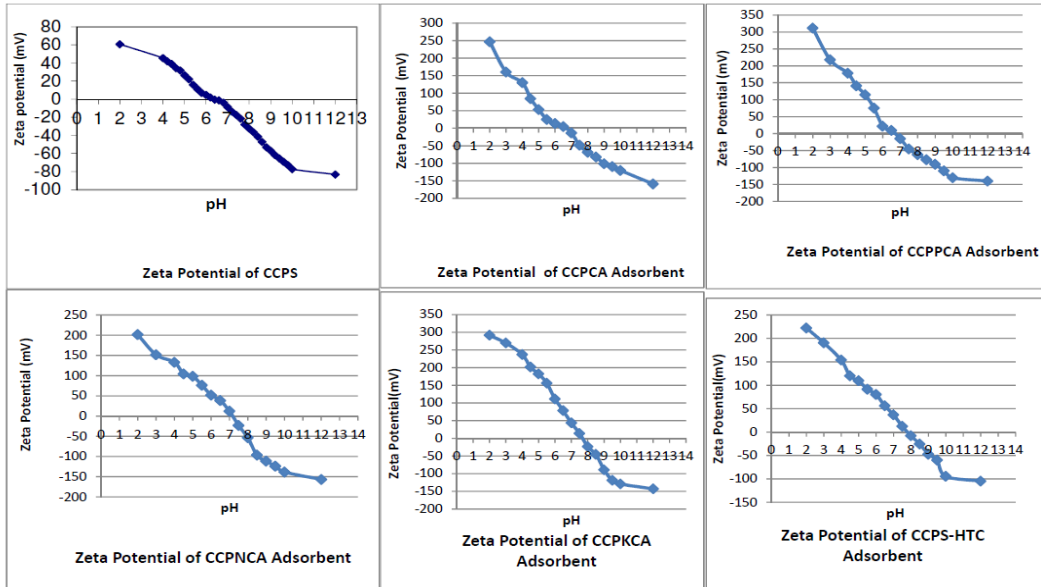
Zeta Potential of Cocoa pod adsorbents
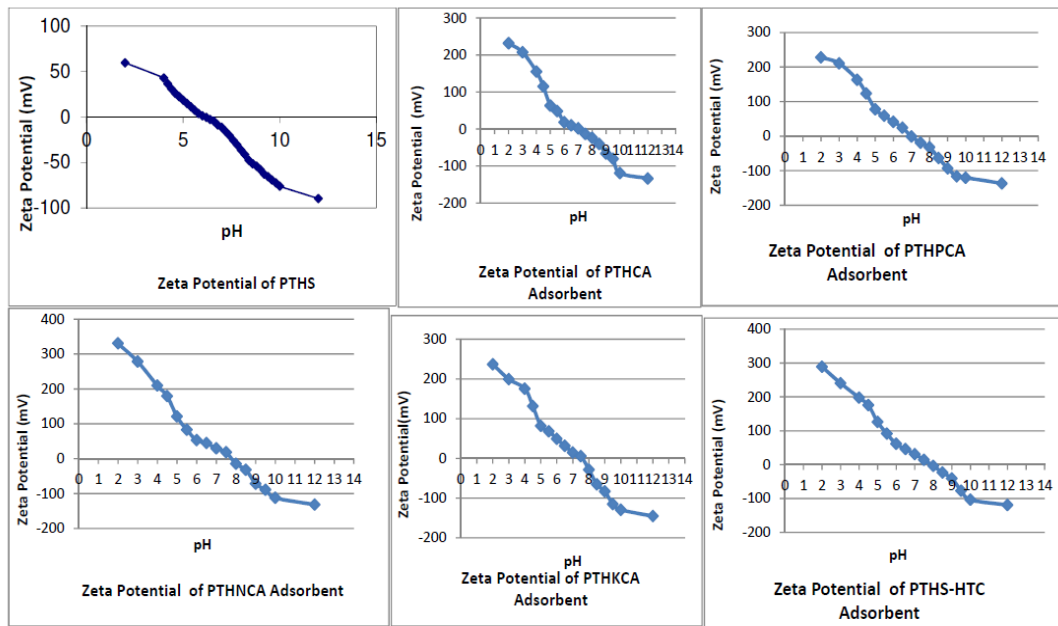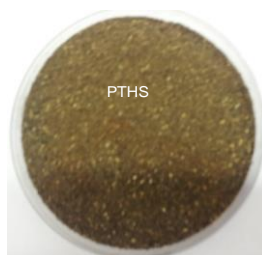

Zeta Potential of plantain peel adsorbents
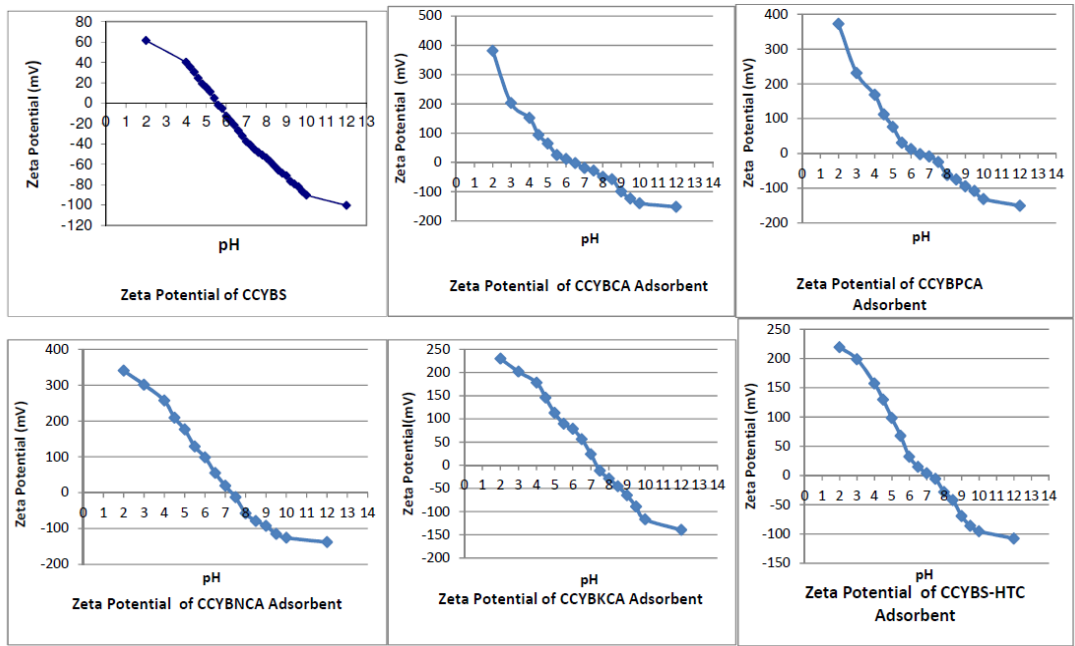
Zeta Potential of cocoyam peel adsorbents
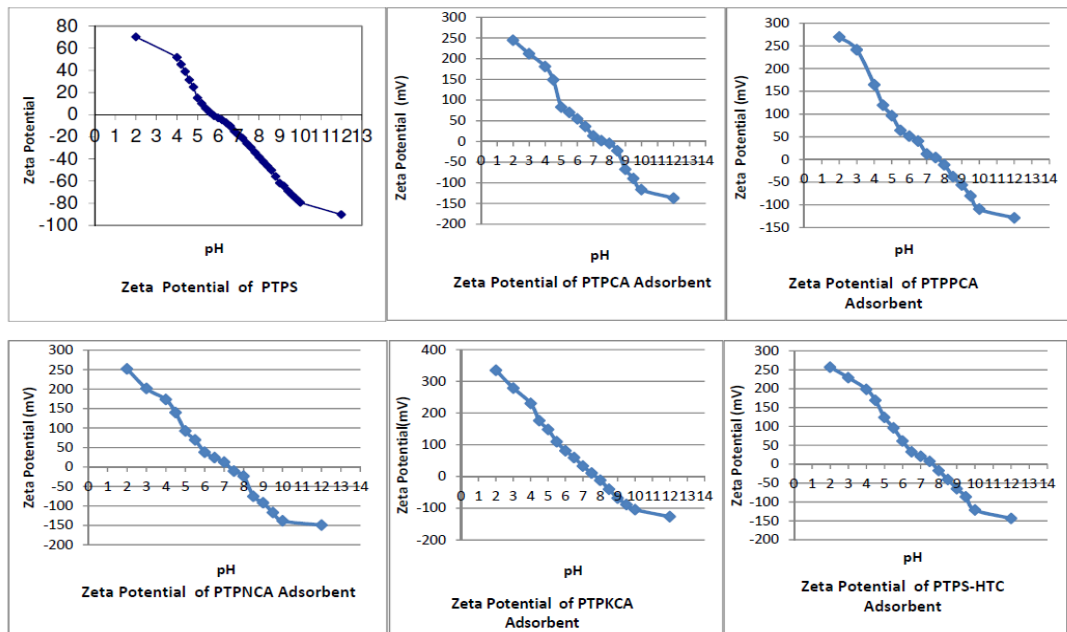
Zeta Potential of sweet potato peel adsorbents
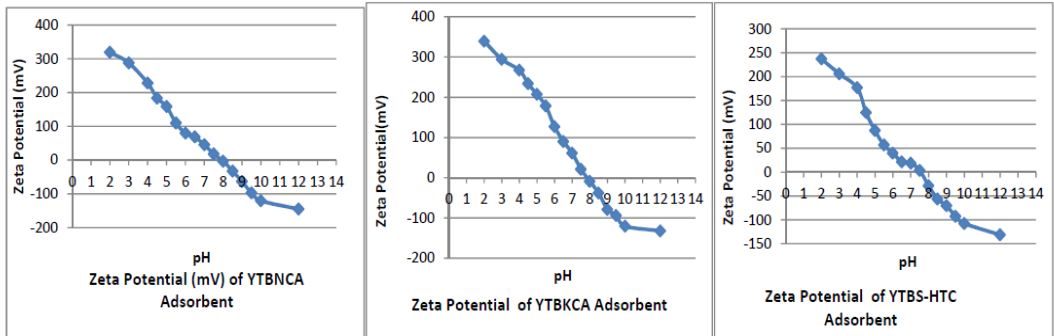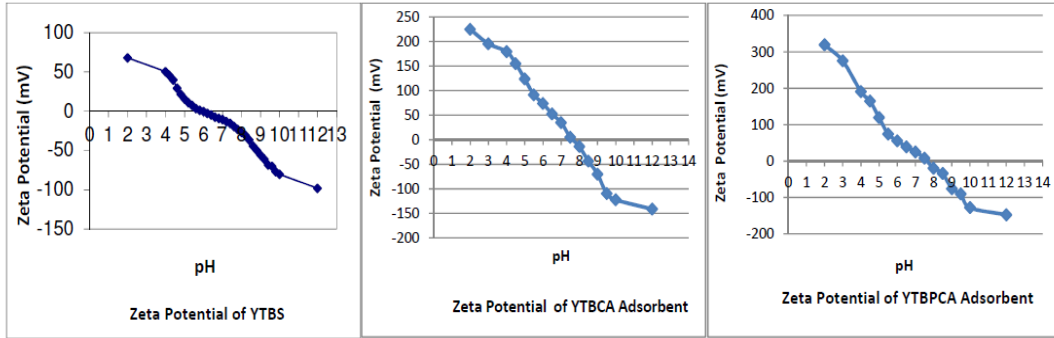
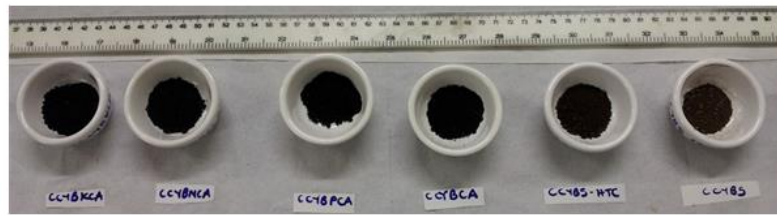Zeta Potential of white yam tuber adsorbents
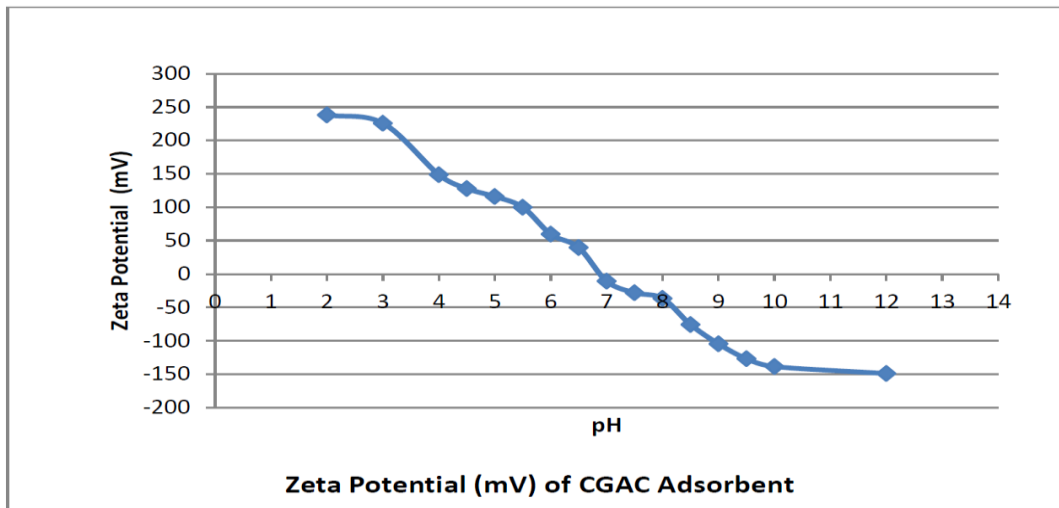
Zeta Potential CGAC adsorbent

APPENDIX 4

Photographs of Residue and Prepared Adsorbents
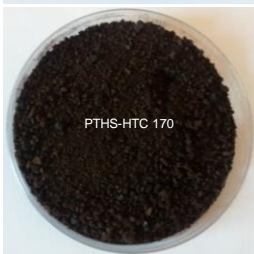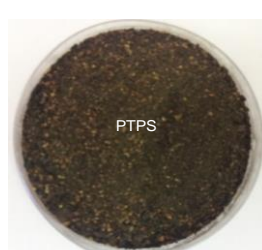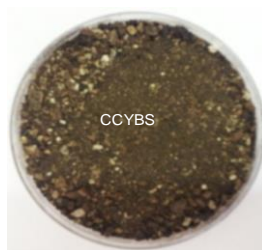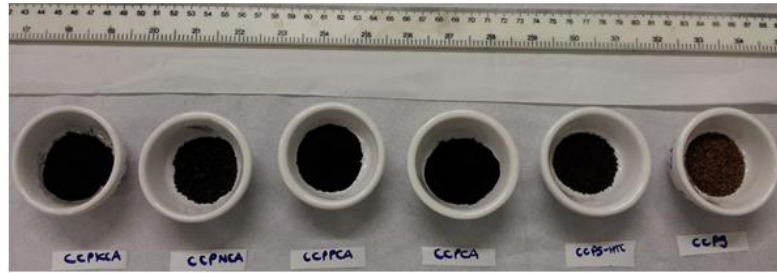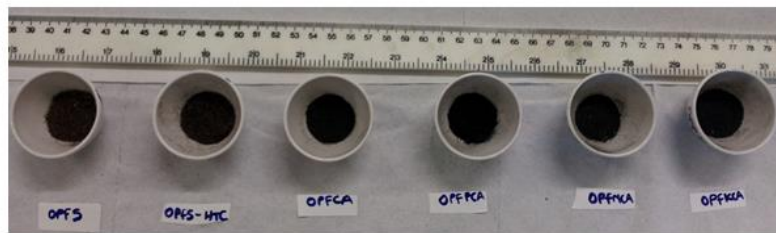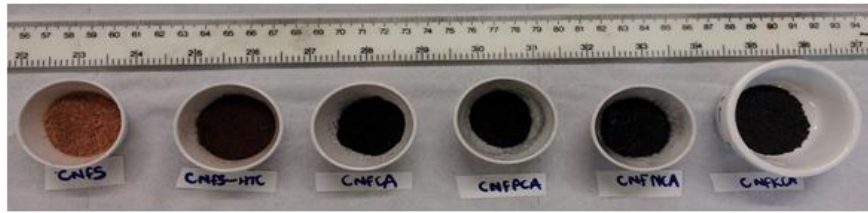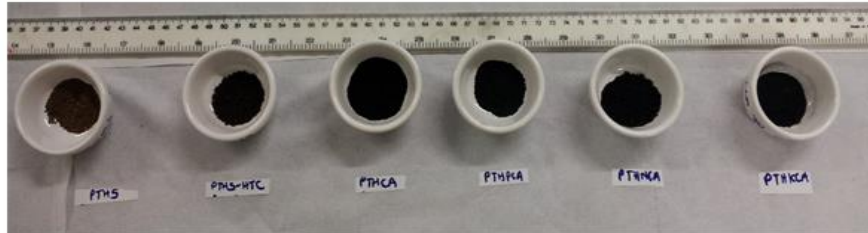
Cocoa Pod Adsorbents

Cocoyam Adsorbents

Oil Palm Fruit Fibre Adsorbents

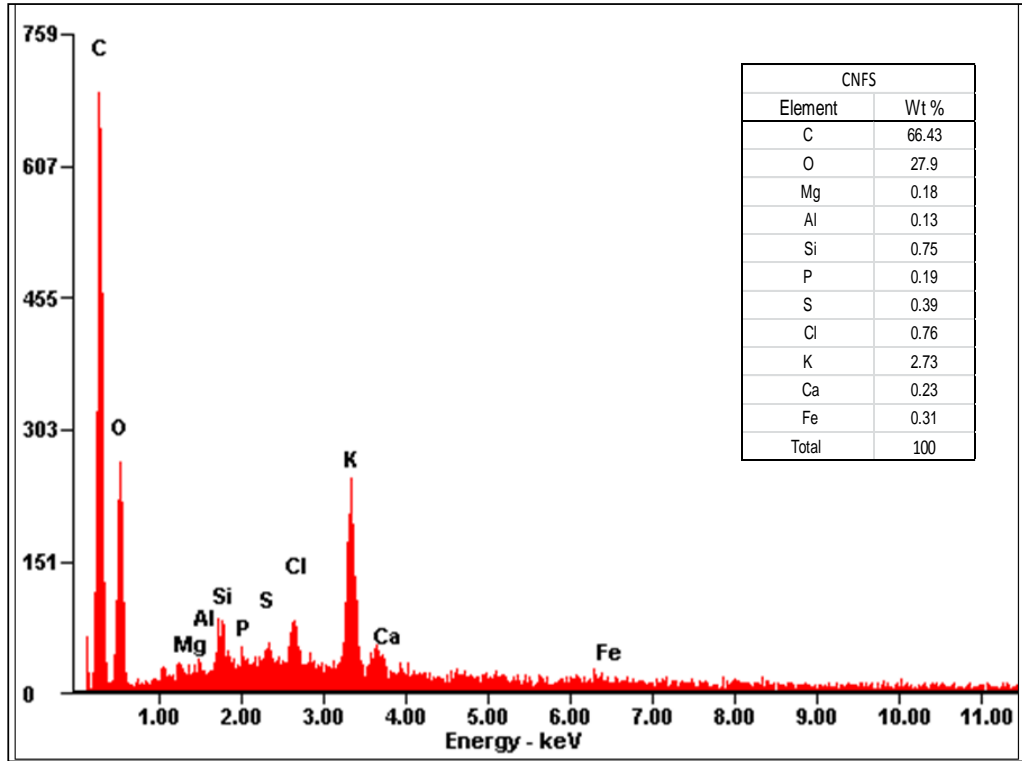Coconut Shell Fibre Adsorbents
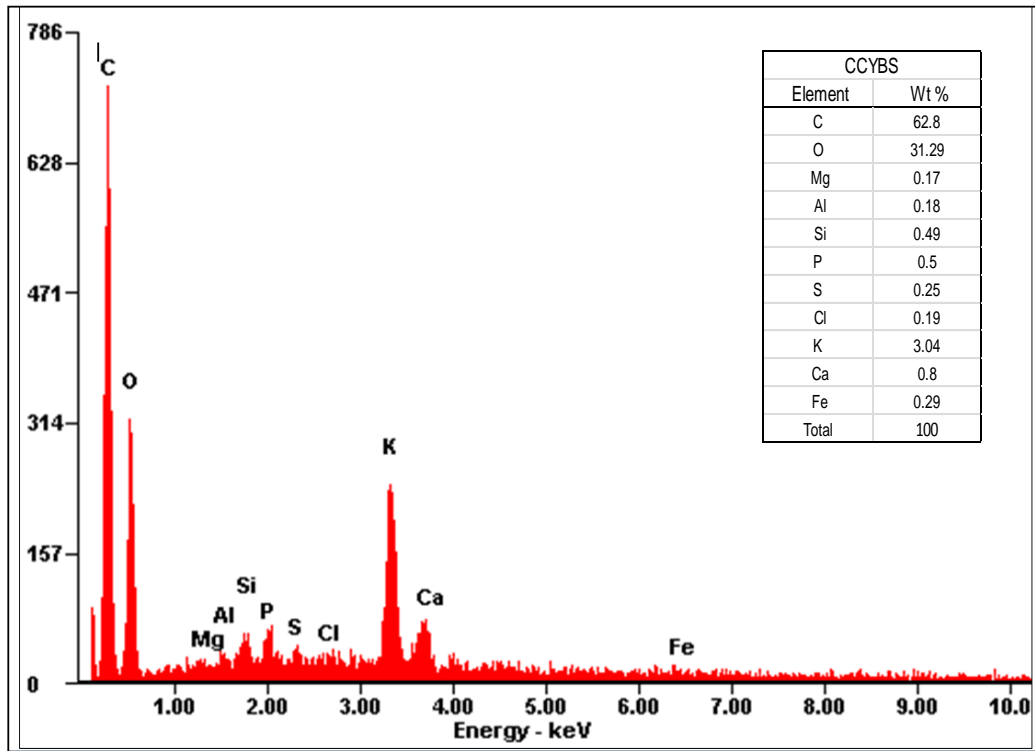

Plantain Peel Adsorbents

Sweet Potato Peel Adsorbents

Commercial Granular Activated Carbon (CGAC)

APPENDIX 5

EDAX Spectra of Residues adsorbents

CNFS	
Element	Wt %
C	66.43
O	27.9
Mg	0.18
Al	0.13
Si	0.75
P	0.19
S	0.39
Cl	0.76
K	2.73
Ca	0.23
Fe	0.31
Total	100

EDAX spectrum for CNFS

CCYBS	
Element	Wt %
C	62.8
O	31.29
Mg	0.17
Al	0.18
Si	0.49
P	0.5
S	0.25
Cl	0.19
K	3.04
Ca	0.8
Fe	0.29
Total	100

EDAX spectrum for CCYBS

EDAX spectrum for PTHS

PTHS	
Element	Wt %
C	70.05
O	24.09
Mg	0.24
Al	0.09
Si	0.07
P	0.25
S	0.15
Cl	0.41
K	4.47
Ca	0.06
Fe	0.12
Total	100

EDAX spectrum for PTPS

PTPS	
Element	Wt %
C	58.72
O	32.94
Mg	0.51
Al	0.79
Si	2.1
P	0.2
S	0.26
Cl	0.36
K	2.89
Ca	0.45
Fe	0.78
Total	100